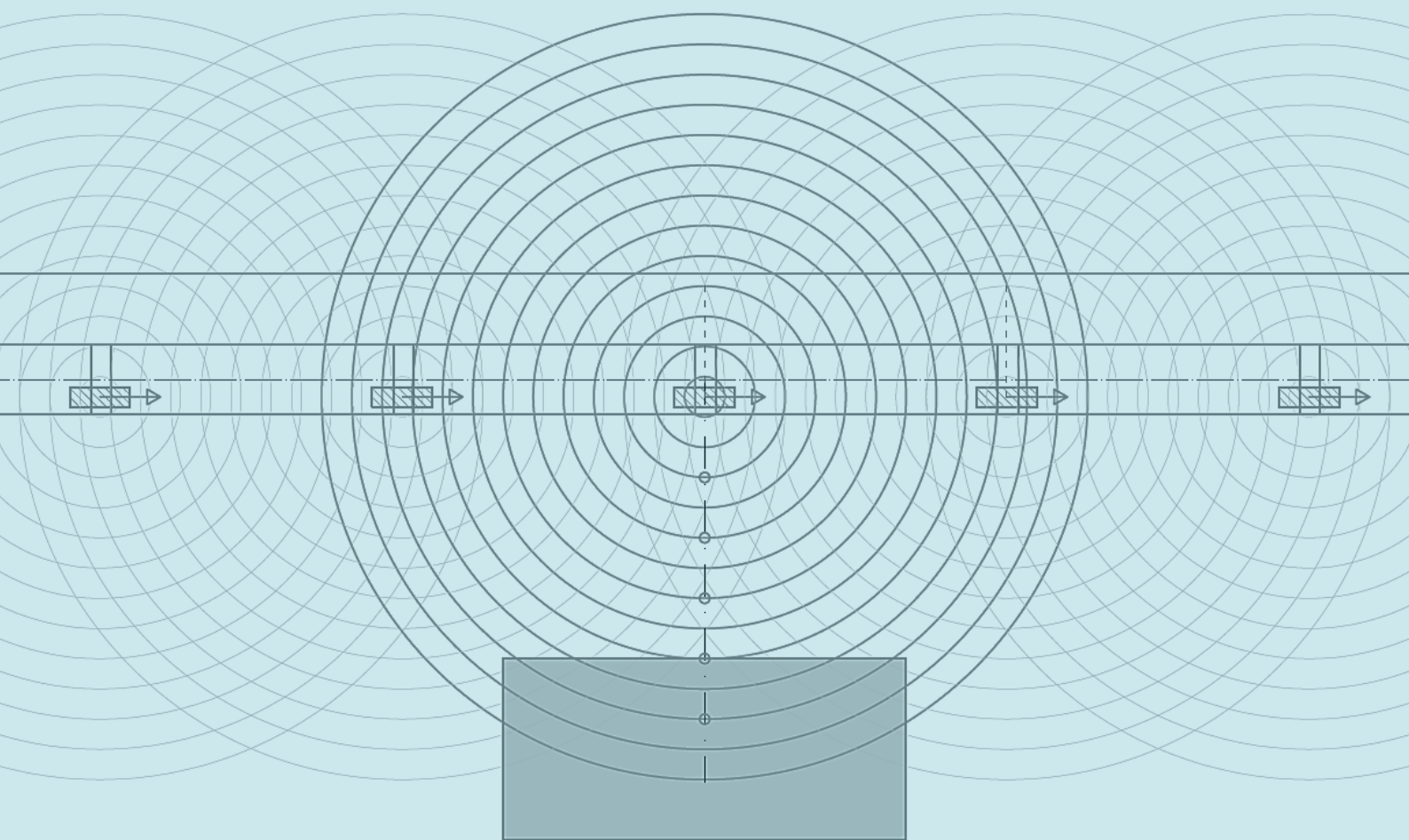


Practical Engineering Design Tool for Vibration Sensitive Laboratory Building Structures

EDDABuS_{GS}



Gerwin Schut



Delft University of Technology
Faculty of Civil Engineering and Geosciences
Department of Building Engineering
Section Structural Design

Practical Engineering Design Tool for Vibration Sensitive Laboratory Building Structures

*Development of a practical design tool based on a scientific model for an early
design of vibration sensitive laboratory building structures excited by traffic
induced vibrations for use in engineering practice*

For the degree of Master of Science in Building Engineering at Delft University of Technology

Author

G. Schut
Student ID: 4376692
E: gerwin.schut@outlook.com
T: +31 6 15 30 22 23

Graduation Committee

Prof. ir. R. Nijse (TU Delft)
Dr. ir. J.M. Barbosa (TU Delft)
ir. S. Pasterkamp (TU Delft)
ir. M.J. Koekoek (Pieters Bouwtechniek)

September 23, 2019

An electronic version of this report is available at: <http://repository.tudelft.nl/>.

*Everything is energy and that's all there is to it.
Match the frequency of the reality you want
and you cannot help but get that reality.
It can be no other way.
This is not philosophy.
This is physics.*

Darryl Anka

Preface

This report is the graduation thesis of me, Gerwin Schut, student at the Technical University in Delft, The Netherlands. The report documents the Master thesis research that I have performed in fulfilment of the Master Civil Engineering, master track Building Engineering with specialization Structural Design at the Technical University in Delft.

Five years ago, I finished the Bachelor programme Building Engineering at the Hogeschool Utrecht. I started the master programme at the Technical University in Delft to increase my theoretical knowledge about structural designing. The courses I have followed were mainly focussed on Building Engineering, however when I got closer to end of the Master programme, my interest in Structural Dynamics increased and therefore my ambition was to perform my Master thesis research in the field of Structural Dynamics. At that time, I had already worked for three years as structural engineer at a part-time basis at Pieters Bouwtechniek in Delft. Ir. Jan Versteegen, partner at Pieters Bouwtechniek, had the idea of realizing a practical engineering tool for designing vibration sensitive laboratory structures. This problem statement included my ambition of performing research on Structural Dynamics, which made me very enthusiastic about implementing the subject in my Master thesis research. As I gained more knowledge about the problem statement, it appeared that I needed a lot of theory about field of practices that were relatively new for me: soil dynamics, moving dynamic loads, numerical programming and the dynamic interrelation between structures and the soil. However, this great challenge made that I was even more driven to bring this thesis research to a success.

Now, at the end of the thesis research, I have managed to tackle all the problems that I have encountered which makes me proud of the eventual end result. In order to come at this end, I have received the support of several persons that I would like to thank for participating in my Master thesis research.

First, I would like to thank my entire graduation committee; my daily supervisor, ir. Maarten Koekoek (Pieters Bouwtechniek) for assisting me with the development of the research and for making time for discussions; dr. ir. Joao Manuel de Oliveira Barbosa (TU Delft) for assisting me with all theoretical and practical problems that I have encountered concerning the soil- and structural dynamics; prof. ir. Rob Nijssse (TU Delft) and ir. Sander Pasterkamp (TU Delft) for guiding me through the master thesis process, while maintaining a critical attitude, which helped me in the development of the research and the eventual tool that has been created.

I would also like to thank dr. ir. Paul Hölscher (Deltares), ir. Basjan Snoeij (Peutz), ing. Reinoud Fennema (DGMR) and prof. ir. Geert Degrande (KU Leuven) for making time to discuss the practical- and theoretical problems relating to the research subject. In addition, I would like to thank all my colleagues at Pieters Bouwtechniek who showed continued interest in the research I was doing, and especially ir. Rob Doomen and ir. Jan Versteegen who made it possible for me to perform this Master thesis research in a pleasant working environment.

And finally, a special thank you goes to my parents and my sister who have followed and supported me on a daily basis since the very beginning. Without you I could never have realized my ambitions. Your guidance, support and unconditionally love means a lot to me.



Gerwin Schut
Delft, September 2019

Abstract

Introduction

The prediction of structural vibrations in vibration sensitive laboratory structures is a complex problem involving heavy computational models with long computational times. However, in the early design phases of a project the structural engineer prefers to perform multiple iterations to see what choices should be made for the structural design to meet the vibration requirements of the building. A long computational time is undesirable, therefore the wish of Pieters Bouwtechniek is the development of a practical engineering tool that can be used in the early design phases of such a project. This led to the initiation of the current Master thesis research about the development of a practical engineering design tool for an early design of vibration sensitive laboratory building structures.

Scope of research

From a comprehensive literature study to this complex dynamic problem it appeared that for many projects, vibrations induced by heavy traffic driving over a nearby road irregularity, is one of the dominant excitations for vibration sensitive laboratory structures. Therefore, the main focus of this Master thesis is about structural vibrations induced by heavy traffic at geological locations with soft soils. Computational iterations are made for one specific geological location: Amsterdam, The Netherlands.

The dynamic problem is split up into the four consecutive parts: source of vibrations, transmission of vibrations, soil-structure interaction and the vibration receiving structure.

Source of vibrations

The source of vibrations (heavy traffic) is implemented as a moving load, which excites the soil underneath the road. The loading on the soil depends on the vehicle characteristics, the road irregularity profile, the vehicle speed and the stiffness of the road. The dominant frequency content of the loading (the frequencies at which the moving harmonic loads are applied) is generally in-between the ranges 0.8 – 3 Hz (1st mode) and 8 – 15 Hz (2nd mode) with peaks in the mid-region of these ranges.

Transmission of vibrations

The transmission of vibration is implemented as a layered semi-infinite halfspace (a soil medium with perfectly horizontal layers and a free surface). Three important types of waves exist in a semi-infinite homogeneous halfspace: the compressional wave, the shear wave and the Rayleigh wave. The Rayleigh wave contains the largest portion of energy and is only present near the soil surface. The wavelengths of Rayleigh waves, and thus their influence zone in the soil, depend on the frequency of excitation and the soil layering, but can be approximated for soft soils to be around 15 m. The layering of the soils causes reflections and refractions of the incident wavefield and therefore makes the predictions of the soil response a challenging task, especially because in reality soil layers are hardly ever perfectly horizontal. The soil layering determines at which frequencies the soil amplifies or attenuates the dynamic moving loads and mainly depends on the stiffness of the layers. Stiff soils excited by heavy traffic have a responsive frequency spectrum generally in-between 10 and 40 Hz, while the responsive frequency spectrum of soft soils is generally in-between 3 and 15 Hz. Wave barriers can be used to mitigate the vibrations before they reach the receiving structure.

Vibration receiving structure

The vibration receiving structure is simplified to a very stiff and rigid 2D structure, which makes that the global structural vibrations can be computed by considering a 3DoF system.

The assumption here is that the dominant vibrations occur in a 2D (x,z)-plane and that the building is not vulnerable to torsion. The dominant eigenfrequencies of a large and rigid concrete building structure are generally below 3 Hz. Additionally to the global structural response the local flexible floor response of the foundation slab or first floor is considered in the form of an analytical expression of the Euler-Bernoulli beam (EB-beam). The surrounding elements of this floor of interest (adjacent walls and floor) which cause deformation resistance of the floor are also taken into account as EB-beams. This results in a frame of eight flexible Euler-Bernoulli beam elements. The frequency content of the local floor response in case of stiff concrete floors is generally in-between 8 and 12 Hz.

Soil-structure interaction

The soil-structure interaction affects the incident wavefield, and thus the excitation on the 3DoF structure, and affects the vibrations of the structure. Due to the presence of the structure, the incident wavefield is reflected and refracted which may cause either amplification or attenuation of the soil response near the structure. The flexibility of the supporting soil surrounding the structure partly determines the eigenfrequencies of the 3DoF system. Different approaches exist for taking into account the soil-structure interaction. In this thesis the sub-structuring approach is implemented, based on the research of Gazetas et al. (Gazetas G. , 1991).

Numerical method

The software FEMIX is used for computing the moving loads and the soil response. FEMIX is an already existing Beta-version software and uses the Thin-Layer Method and 2.5D BEM-FEM coupling in the computations.

Python is used for the development of the computational script of the practical engineering tool 'EDDABuS_{GS}' (Early Design Dynamic Analysis of Building Structures by Gerwin Schut). The script takes the computed soil response by FEMIX as input and determines the global-(3DoF) and local (EB-beam) structural response based on the input parameters (for the supporting soil and the structure) given by the user.

Verification of results

Verification projects are used to verify the results computed by FEMIX and EDDABuS_{GS}. The available verification projects are scarce, however prof. Degrande et al. of the KU Leuven have performed measurements for projects in Belgium to verify their own prediction model (Degrande & Lombaert, 2002). Despite the fact that these projects are not in The Netherlands, they are used as verification projects for this thesis research. The source and transmission stage have been verified and agree very well with the verification projects. The receiving stage could only partly be verified because the type of building (flexible and dominant floor spans parallel to the length of the road) is not suitable for the EDDABuS_{GS}-tool (rigid buildings with dominant floor spans perpendicular to the length of the road).

A confined amount of modelling information is available for a vibration sensitive project of Pieters Bouwtechniek in Amsterdam. The information is extended with the knowledge gained from the literature study and with the verification projects in Belgium to approximate the soil response for a location in Amsterdam. This soil response is used as input excitation for the final EDDABuS_{GS}-tool.

Research iterations

After verification of the tool several iterations have been performed by changing the structural parameters and the supporting soil in EDDABuS_{GS}. A design chart has been developed based on these iterations and the literature research. It appears that, in general, it cannot be said in advance whether changing a certain parameter is conservative or not. It depends on the

interrelations of all the parts of the problem. However for soft soils, excited by heavy traffic, it generally holds that the eigenfrequencies of the global building response should be made relatively low (< 3 Hz), while the eigenfrequencies of the local structural elements (e.g. floors) should be made relatively high (> 12 Hz). Additionally, the resistance against vibrations (impedances) of the structural elements need to be as large as possible, which might sometimes contradict the preferred shift of the eigenfrequencies.

Conclusion

The EDDABuS_{GS}-tool together with the design chart give an extensive overview of the influence of the structural parameters and the supporting soil. The verification of EDDABuS_{GS} and the observations from the computed iterations show that the outcomes of the tool are well in line with general known theory about structural dynamics. Therefore the goal of this thesis, to develop a practical engineering tool for an early design phase of a project concerning vibration sensitive laboratory structures, is accomplished.

The influence factors that can be determined from changing certain parameters should be reliable, however it is advised not to use the tool to predict the vibration amplitudes in absolute sense. Too many unknowns remain in the modelling parameters, but also some simplifications made for the EDDABuS_{GS}-tool need to be verified. These simplifications mainly concern the implementation of the supporting soil impedances, the supporting pile foundation impedances and the consideration of the floor element as a simple one-span EB-beam. Therefore the recommendations stated for future research mainly focus on these aspects. Also, extending the applicability of the tool for more possible situations (e.g. different loading, different soil layering, different vehicle characteristics and speeds) is recommended to consider in future research.

Contents

Preface	6
Abstract	7
List of Figures	14
List of Tables.....	25
Acronyms	26
Symbols.....	28
Part I Introduction	32
1. Introduction	34
1.1. Background	34
1.2. Scope	34
1.2.1. Aim	34
1.2.2. Approach.....	35
1.2.3. Limitations.....	36
1.3. Outline	37
Part II Literature Study	40
2. In Practice	42
2.1. Vibration Level Criteria	42
2.2. Vibration Sources.....	43
2.3. Transfer of Vibrations and Measurements	43
2.3.1. TNW Zuid	43
2.3.2. VU Amsterdam	44
2.4. Vibration Mitigation Measures	45
3. Source of Vibrations	48
3.1. Road Traffic Induced Vibrations – Measurements in Practice	48
3.2. Road Traffic Induced Vibrations - Empirical Prediction Model	50
3.3. Road Traffic Induced Vibrations – Scientific Prediction Model	51
4. Transmission of Vibrations.....	55
4.1. Homogeneous Elastic Soil	55
4.1.1. Waves in a three-dimensional infinite body	55
4.1.2. Waves in a three-dimensional semi-infinite body	57
4.1.3. Wave attenuation	59
4.2. Layered Elastic Soil Halfspace	60
4.2.1. Three-dimensional wave propagation	60
4.2.2. Conclusion layered soil medium.....	61
4.3. Dominant Frequencies Soil Medium	62

4.4.	Wave Barriers.....	62
4.4.1.	Optimization of wave barriers in layered soils by A. de Zeeuw.....	62
4.4.2.	Conclusion wave barrier.....	65
5.	Structural System (Receiver of Vibrations).....	66
5.1.	Simplification Laboratory Structure	66
5.2.	Single Degree of Freedom system	66
5.2.1.	Governing equations	67
5.2.2.	Undamped free vibration	67
5.2.3.	Undamped forced vibration.....	67
5.2.4.	Damped free vibration	68
5.2.5.	Damped forced vibration	69
5.3.	Two Degrees of Freedom system	70
5.3.1.	Undamped forced vibration.....	70
5.4.	Multi-Degrees of Freedom system	71
5.4.1.	Differential equations (undamped case)	71
5.4.2.	Undamped free vibration of a n MDoF system.....	72
5.4.3.	Harmonic loads for a n MDoF system.....	72
5.4.4.	Viscous damped systems with n degrees of freedom.....	73
5.5.	Continuous Systems	73
5.5.1.	Bending beam (Euler-Bernoulli beam model).....	73
5.5.2.	Governing differential equations	73
5.5.3.	Free vibration.....	74
5.5.4.	Boundary conditions	74
6.	Soil-Structure Interaction	76
6.1.	Effect of Soil-Structure Interaction on the Response of Structures.....	76
6.2.	Modelling of the Soil-Foundation System	77
6.3.	Modelling of the Soil-foundation System	79
6.4.	Conclusion Soil-Structure Interaction	80
Part III Method		82
7.	Numerical Method for Computations	84
7.1.	FEMIX.....	84
7.1.1.	Thin Layer Method in FEMIX	84
7.1.2.	Perfectly Matched Layer in FEMIX.....	85
7.1.3.	Possibilities of FEMIX.....	85
7.2.	Python	88
7.2.1.	Numerical programming of input files.....	88
7.2.2.	Computing structural response	88

8.	Verification Projects.....	89
8.1.	Projects KU Leuven.....	89
8.1.1.	Verification Project Degrande et al. (1) – Free Field.....	89
8.1.2.	Verification Project Degrande et al. (2) – Soil Building.....	90
8.1.3.	Verification Project Degrande et al. (3) – Building Response.....	91
8.2.	VU Amsterdam.....	92
9.	Source Modelling and Results in FEMIX.....	93
9.1.	2D Vehicle Model.....	93
9.2.	Road Unevenness.....	93
9.3.	Generated Moving Loads.....	94
9.3.1.	Loads in the frequency domain.....	94
9.3.2.	Loads in the time domain.....	95
10.	Transmission Modelling and Results in FEMIX.....	96
10.1.	Road Layering.....	96
10.2.	Soil Layering.....	96
10.3.	Receiver Points and Verification of Soil Response.....	97
10.3.1.	Soil response verification project Degrande et al. (1) – Free Field.....	97
10.3.2.	Soil response verification project Degrande et al. (2) – Soil Building.....	99
10.3.3.	Soil response in Amsterdam.....	101
10.3.4.	Soil response attenuation by wave barrier in soil of Amsterdam.....	102
11.	Soil-Structure Interaction Modelling in EDDABuS_{GS}.....	104
11.1.	Background and Structural Simplifications in the Tables of Gazetas.....	104
11.2.	Derivation of Impedances.....	105
11.3.	Practical Use of the Tables.....	105
12.	Receiving Structural System Modelling and Results in EDDABuS_{GS}.....	109
12.1.	Global Dynamic Response of the 3DoF Rigid Building.....	109
12.1.1.	Structural parameters.....	109
12.1.2.	Excitation.....	110
12.1.3.	Computation of the building response due to a harmonic loading term.....	110
12.2.	Local Dynamic Response of Flexible Floor.....	113
12.2.1.	The composition of the flexible frame.....	113
12.2.2.	Finding the response of the floor in the same form as the VC-curves.....	114
12.3.	Verification of the Local Dynamic Response of the Flexible Floor.....	115
12.4.	Consequences for soil response and structural response when changing the Belgium soil into the Amsterdam soil.....	118
Part IV Results & Conclusion.....		120
13.	Results from Iterations by EDDABuS_{GS} and Design Chart.....	122

13.1.	Observations from Iterations	122
13.2.	Design Chart for Vibration Sensitive Laboratory Structures	126
14.	Conclusions and Recommendations	128
14.1.	Discussion of Results	128
14.2.	Recommendations for Designing, Using EDDABuS _{GS}	132
14.3.	Recommendations for Future Research.....	133
	References	134
	Appendices	138
A.	Appendix: application and interpretation of VC-curves	139
B.	Appendix: Additions to Chapter 3 ‘Source of Vibrations’	140
C.	Appendix: Extensive overview of Chapter 4 ‘Transmission of Vibrations’	143
D.	Appendix: Extensive overview of Chapter 5 ‘Structural System (Receiver of Vibrations)’	169
E.	Appendix: Additions to Chapter 6 ‘Soil-Structure Interaction’	190
F.	Appendix: Additions to Chapter 7 ‘Numerical Method for Computations’	193
G.	Appendix: Extensive overview of Chapter 8 ‘Verification Projects’	198
H.	Appendix: Additions to Chapter 9 ‘Source Modelling and Results’	214
I.	Appendix: table of computed vehicle axle load-frequency spectrums for changing parameter values	217
J.	Appendix: PPV with- and without wave barrier in soil Amsterdam.....	223
K.	Appendix: Additions to Chapter 11 ‘Soil-Structure Interaction Modelling’	224
L.	Appendix: Additions to Chapter 12 ‘Receiving Structural System Modelling and Results’	229
M.	Appendix: Maple sheet for determining 3DoF eigenfrequencies.....	239
N.	Appendix: Input parameters for Verification Project Degrande et al. (3) – Building Response	243
O.	Appendix: Results for Verification Project Degrande et al. (1) – Free Field and (3) – Building Response with layered soil of Amsterdam	257
P.	Appendix: Boundary- and Interface conditions of the three Model_{x, z, φ}	259
Q.	Appendix: Maple sheet for determining dynamic EB-beams response Model_x	261
R.	Appendix: Maple sheet for determining dynamic EB-beams response Model_z	280
S.	Appendix: Maple sheet for determining dynamic EB-beams response Model_φ	300
T.	Appendix: Iterations of structural parameters to compute structural response.....	318
U.	Appendix: User manual of EDDABuS _{GS}	349

List of Figures

1.	Diagram representation of the practical engineering design tool.....	35
2.	Illustrative figure to make clear the approach of this thesis: In the total overview, the source and the soil response will be calculated. The soil response is implemented as excitation and as soil-structure interaction-springs and -dashpots for the rigid MDoF structure. Locally the floor response (vibrations) will be determined using a frame composed of Euler-Bernoulli bending beams.....	38
3.	Generic vibration criterion (VC) curves for vibration-sensitive equipment (Amick, Gendreau, Busch, & Gordon, 2005).....	42
4.	Execution of experiment for determining transfer function of vibrations from soil to floor: a falling Bigbag at a certain distance from the building (Eilders, 2015).....	44
5.	Passive vibration isolation table (PES Ltd, 2019).....	46
6.	Structural design of (left) the Faculty of Applied Sciences of the TU Delft (Janssen & Ku, 2014) and (right) VU Amsterdam (Versteegen & Koekoek, 2018).....	47
7.	Comparison between vibration levels induced by an empty transit bus (air-bag suspension) and a loaded truck (multi-leaf steel spring suspension) (Hunaidi, 2000)....	48
8.	Frequency spectrum of a truck with leaf suspension or air suspension (Singh, Singh, & Joneson, 2006) and for reference of soil vibration amplification, also the frequency content of a specific site is included	49
9.	Vertical response obtained by the drop weight device in summer and winter for the ground in front of the building at a particular site (Hunaidi & Tremblay, Traffic-induced buiding vibrations in Montréal, 1997).....	49
10.	2D 4 DoF model for a truck with two axles (Lombaert, Degrande, & Clouteau, 2000).....	51
11.	The longitudinal road profile of a traffic plateau with sinusoidal slopes as a function of the coordinate y along the road (Lombaert, Degrande, & Clouteau, 2000).....	52
12.	Eigenmodes of the 2D 4-DoF model for a truck: (a) pitch and bounce mode; (b) axle hop mode.....	52
13.	Results of the calculated front axle load (Lombaert, Degrande, & Clouteau, 2000).....	52
14.	Time history and frequency content of the vertical soil velocity for a vehicle speed v equal to 8, 12, 16 and 20 m/s (Lombaert, Degrande, & Clouteau, 2000)	53
15.	Time history of the predicted rear axle load for the passage of a truck on (left) a traffic plateau and (right) a joint in a road surface (Lombaert & Degrande, 2001)	54
16.	Cartesian coordinate system	55
17.	Representation of a P-wave. Alternating compression and dilation particle motion and parallel to direction of propagation (Braile, 2019).....	56
18.	Representation of a S-wave. Alternating transverse particle motion in any plane (here in vertical plane) and perpendicular to the direction of propagation (Braile, 2019).....	57
19.	Geometrical attenuation for body waves (left) and surface waves (right) (Persson, 2016)	57
20.	Variation of Rayleigh wave and body wave propagation velocities with poisson's, ratio relating to the shear wavespeed v_s (Kramer, 1996).....	58

21.	Representation of a Rayleigh wave. Elliptical particle motion in vertical plane and parallel to direction of propagation. Amplitude decreases with depth (Braile, 2019)	58
22.	Horizontal and vertical motion of Rayleigh waves. A negative amplitude ratio indicates that the displacement deeper underneath the surface is in the opposite direction of the surface displacement (Kramer, 1996) after (Richart, Hall, & Woods, 1970)	59
23.	Complete wavefield predicted by Lamb (1904) for a surface point source on an elastic halfspace (a) horizontal radial motion; (b) vertical motion; (c) particle path of Rayleigh waves (Foti, 2000)	60
24.	Refraction principle of an SH-wave ray path (reflected waves are not shown) (Kramer, 1996)	61
25.	Simplified representation of possible paths along which energy is transferred (Spijkers, Vrouwenvelder, & Klaver, 2005)	61
26.	Illustrative soil response for soft soil deposits (e.g. Amsterdam, The Netherlands) excited by a passing truck at a particular distance from the road	62
27.	Inner FEM domain of the two-layered soil profiles. Left: shallow upper layer. Right: deep upper layer (de Zeeuw, 2018)	63
28.	Displacement amplitude <i>ureal</i> ($\mu\text{m}/\text{kN}$) for wave barriers optimized for 50 Hz. Left: <i>ureal</i> for an optimized wave barrier in homogeneous soil. Middle: <i>ureal</i> for a homogeneous-soil-optimized wave barrier in layered soil. Right: <i>ureal</i> for an optimized wave barrier in layered soil model (de Zeeuw, 2018)	63
29.	Inner FEM domain of the three-layered soil profile (de Zeeuw, 2018)	64
30.	Displacement amplitude <i>ureal</i> ($\mu\text{m}/\text{kN}$) for wave barrier optimized for 50 Hz. The embedded softer soil layer is used as a waveguide (de Zeeuw, 2018)	64
31.	The shape of optimized wave barriers in a two-layered soil with increasing level of manufacturability with the soil interface at 10 m depth (de Zeeuw, 2018)	65
32.	The shape of optimized wave barriers in a three-layered soil with increasing level of manufacturability (de Zeeuw, 2018)	65
33.	Idealization of horizontal motion of an offshore platform, excited by waves, by a mass-spring system with a translational degree of freedom (in x – direction) (Metrikine, 2018)	67
34.	(left) Amplitude-frequency characteristic (magnification factor) and (right) phase-frequency characteristic (Metrikine, 2018)	68
35.	A mass-spring-dashpot system with a translational degree of freedom (in x – direction) (Metrikine, 2018)	68
36.	Free vibration of the mass-spring-dashpot system in the case $n < \omega n$ (Metrikine, 2018)	69
37.	(left) Magnification factor and (right) Phase lag of the damped SDoF steady-state solution (Metrikine, 2018)	69
38.	Undamped two degrees of freedom system with spring coupling (Metrikine, 2018)	70
39.	Forced two degrees of freedom system. The vibrations absorber k - m is attached to the main system K - M (Metrikine, 2018)	70
40.	Displacement-frequency curves for the two degrees of freedom system (Metrikine, 2018)	71

41.	Foundation block with three degrees of freedom (Spijkers, Vrouwenvelder, & Klaver, 2005).....	71
42.	Frequency-response function for an undamped five degrees of freedom system for the degree of freedom $xq(t)$ (Spijkers, Vrouwenvelder, & Klaver, 2005)	72
43.	Example of a frequency response function for the degree of freedom $xq(t)$ when a harmonic loading is applied in the point xp (Spijkers, Vrouwenvelder, & Klaver, 2005)..	73
44.	Sign convention and indication of the meaning of the symbols used for the prismatic beam (Spijkers, Vrouwenvelder, & Klaver, 2005)	74
45.	First three eigenmodes of the simply supported Euler-Bernoulli bending beam (Spijkers, Vrouwenvelder, & Klaver, 2005).....	75
46.	Derivation of the third column of the flexibility matrix, including all cross-coupling dynamic stiffness's (Tsouvalas, 2018).....	77
47.	Effect of embedment depth D of the structure when excited horizontally at the structure's base. The response amplitude at the top of the building (U_b) is normalized by the excitation amplitude at the surface of the free field (U_g) (Miura, 2016)	78
48.	Input parameters for the tables considering SSI for foundation piles (Tsouvalas, 2018) ..	79
49.	Levels of modelling the effect of the soil on the structure: (a) fixed support, (b) elastic support, (c) substructure approach, (d) direct approach (Pap & Kollár, 2018)	80
50.	Discretization into thin-layers (left) and a thin-layer as a free body in space with the order of the interpolation function equal to 3 (Barbosa J. , 2013).....	85
51.	Principle of the Fourier expansion (representing any arbitrary function by a summation of continuous sines and cosines) (MathIsFun.com, 2019)	86
52.	Principle of influence of the repetition period P in the Fourier expansion (snapshots taken at different time instances). In case P is taken too small the wave fields at the receiver points are influenced by multiple repetitive unevenness profiles.....	87
53.	Example of the numerical Python scripts that computes the data-files needed as input for FEMIX. The current part of the script defines a function that is used for the computation of the coefficients of the Fourier expansion of the road irregularity.....	88
54.	Frequency content (left) and time history (right) of the predicted front axle load of the Volvo FL6 truck when passing the artificial profile at a vehicle speed $v = 58$ km/h (Degrande & Lombaert, 2002).....	90
55.	Predicted (solid line) and measured (dash-dotted line) soil response in the z-direction of point FF4 (at 16 m from the middle of the road) in the frequency- (left) and time (right) domain (Degrande & Lombaert, 2002)	90
56.	Frequency content (left) and time history (right) of the predicted front axle load of the Volvo FL6 truck when passing the artificial profile at a vehicle speed $v = 50$ km/h (Degrande, Pyl, Lombaert, & Haegeman, 2004).....	91
57.	Predicted soil response in the z-direction of point FF3 (at 16 m from the middle of the road) in the frequency- (left) and time (right) domain (Degrande, Pyl, Lombaert, & Haegeman, 2004).....	91
58.	Measured structural response in the z-direction of point F11 (on the ground floor of the building) in the frequency- (left) and time (right) domain (Degrande, Pyl, & Clouteau, 2004).....	91

59.	Soil response at the top left measurement point from Figure 172 at the VU Amsterdam site, taken from the documents of TNO (Koopman, 2012)	92
60.	MAN TGS 10x8 WSA sandtruck used for the measurements at the VU Amsterdam site (modderaandebanden.nl, 2019).....	92
61.	2D 4 DoF dynamical vehicle model for the implementation in the FEMIX software (left) and a representation of the mass-dashpot-spring systems in a more reality-based representation in the form of the vehicle body, a spring-dashpot for the primary suspension, a mass for the axle and a spring-dashpot system for the tyre (right).....	93
62.	Representation of the road irregularity with specified variable input parameters (LTirreg, LBirreg, Hirreg and P) for computing the road irregularity profile.....	94
63.	Representation of the road irregularity by means of a Fourier expansion with period 'P' = 50 m and deviating values for the number of summations 'N'. Note that the height of the irregularity is equal to 0.054 m, the length at the bottom of the bump is equal to 1.9 m and the length at the top of the bump is equal to 1.3 m.....	94
64.	Computed front axle frequency spectrum by FEMIX (top left, blue) and the frequency spectrum of Verification Project Degrande et al. (1) – Free Field (top right, black) (Degrande & Lombaert, 2002). In the bottom figure the differences between both spectrums can be observed	95
65.	Computed front axle loading in the time domain by FEMIX (top left, blue) and the loading in the time domain of Verification Project Degrande et al. (1) – Free Field (top right, black) (Degrande & Lombaert, 2002). In the bottom figure the differences between both graphs can be observed.....	95
66.	Representation of the vehicle on the layered FEM-model of the road which is connected to the soil surface by means of a BEM-FEM coupling. The order of the node-numbers is from left to right and from the bottom of the road to the top of the road	96
67.	Computed frequency spectrum of the Free Field soil response (from left to right: x-,y-,z-direction) at 16 m from the middle of the road by FEMIX (top, blue) and of Verification Project Degrande et al. (1) – Free Field (middle, black) (Degrande & Lombaert, 2002), where the solid line is the predicted soil response and the dashed line is the measured soil response. In the bottom figure the differences between both spectrums of the vertical soil response can be observed	97
68.	Computed time history of the Free Field soil response (from left to right: x-,y-,z-direction) at 16 m from the middle of the road by FEMIX (top) and of Verification Project Degrande et al. (1) – Free Field (middle) (Degrande & Lombaert, 2002), where the solid line is the predicted soil response and the dashed line is the measured soil response. In the bottom figure the differences between both time histories of the vertical soil response can be observed.....	98
69.	Difference of the frequency spectrums (top) and time histories (bottom) of the Free Field soil response (from left to right: x-,y-,z-direction) at 16 m from the middle of the road between the computation by FEMIX for the road embedded in the soil (blue lines) and the computation by FEMIX for the road on top of the soil surface (red lines).....	99
70.	Difference of the frequency spectrum (left) and time history (right) of the vertical Free Field soil response between the computation by FEMIX (blue lines) and the results of the Verification Project Degrande et al. (2) – Soil Building (black lines) (Degrande, Pyl, Lombaert, & Haegeman, 2004)	100
71.	Picture taken from Google Maps (Google, 2019) at the specific site	100

72.	Factorizing functions for the computed soil response for Verification Project Degrande et al. (2) – Soil Building in the frequency domain for the soil response in the horizontal x-direction (left), the horizontal y-direction (middle) and the vertical z-direction (right)	101
73.	Difference of the frequency spectrum (left) and time history (right) of the vertical Free Field soil response between the modified computation by FEMIX (blue lines) and the results of the Verification Project Degrande et al. (2) – Soil Building (brown lines) (Degrande, Pyl, Lombaert, & Haegeman, 2004).....	101
74.	Frequency spectrums of the Free Field soil response for the soil similar to VU Amsterdam (from left to right: x-,y-,z-direction) at 30 m from the middle of the road, computed by FEMIX.....	101
75.	Time histories (bottom) of the Free Field soil response for the soil similar to VU Amsterdam (from left to right: x-,y-,z-direction) at 30 m from the middle of the road, computed by FEMIX.....	102
76.	Frequency spectrum (left) and time history (right) of the Free Field soil response velocities for the approximated homogeneous halfspace for Amsterdam (z-direction) at 30 m from the middle of the road, computed by FEMIX	102
77.	Frequency spectrum of soil response (velocities in vertical direction at soil surface) at 52 m from the middle of the road (or 24 m behind the wave barrier). Left: no wave barrier, right: wave barrier at 28 m from the middle of the road	103
78.	Effect on PPV (m/s) of the free field soil response with the realization of a wave barrier (width = 1.6 m, depth = 4 m) at 28 m from the middle of the road (represented by the two black vertical lines) for the 3 directions x (U_1), y (U_2) and z (U_3) at the soil surface (top) and at a depth of 3 m	103
79.	Rigid foundation block with its six degrees of freedom (Gazetas G. , 1991)	104
80.	Graph a accompanying table 15.1, left: Gazetas (Gazetas G. , 1991), middle: extrapolated, right: both graphs in one	106
81.	Graph k_y , $L/B = \infty$ accompanying table 15.2, left: Gazetas (Gazetas G. , 1991), middle: extrapolated, right: both graphs in one	106
82.	Distribution of displacement amplitudes of the soil along the shaft of an oscillating (active) pile and of a neighbouring (passive) pile (Gazetas & Dobry, 1988)	107
83.	Principle of the assumptions made for the pile-group impedance terms based on the graphs accompanying the paper of Gazetas et al. (Gazetas & Dobry, 1988)	107
84.	Simplified model for the computation of the parameters needed for the dynamic response of the 3DoF building	110
85.	Simplified dynamical model which is used to set up the equations of motion for the rigid 3DoF building.....	110
86.	Typical representation of an EB-beam element	113
87.	Principles for the flexible frame for computation of the local dynamic response of w_1 . Left: displaced flexible frame due to rigid building movement of 3DoF system. Right: flexible frame composed of four flexible Euler-Bernoulli beam floor elements w_1, w_2, w_3, w_4 and four flexible Euler-Bernoulli beam wall/column elements u_1, u_2, u_3, u_4	113
88.	Principle of the computation of the excitation for the 3DoF rigid building system (displaced springs and dashpots).....	116

89.	Principle of maximum building length which can be assumed to be rigid for a given wavelength of the soil response	116
90.	Structural response in the time domain (top) and the frequency domain (bottom) for all three DoF (x, z, φ) of the 3DoF system modelled for verification project Degrande et al. (3) – Building Response	117
91.	Predicted local EB-beam- (top) and measured- (bottom) structural response of the first floor in the time domain (left) and frequency domain (right) for verification project Degrande et al. (3) – Building Response	117
92.	Principal of the effect on the amplitude of the structural response due to an increased impedance (left) and increased eigenfrequency (right) caused by a higher spring stiffness k_s . Green arrow: effect of increased impedance is greater than effect of increased eigenfrequency. Red arrow: effect of increased impedance is smaller than effect of increased eigenfrequency	124
93.	Test profiles used at the Transport and Road Research Laboratory (Watts, 1990)	140
94.	Transfer function for vertical PPV at 12 Hz by distance (Watts, 1990)	140
95.	Propagation of waves in the soil ($m / m/s / m/s^2$) induced by a 2-axle vehicle driving over a traffic plateau at different distances from the plateau in the time domain (Hölscher, Soil Dynamics, 2014)	142
96.	A thin rod (a) with co-ordinate x and displacement u of a section and (b) the stresses acting on element Δx of the rod (Metrikine & Vrouwenvelder, Part 2 Wave Dynamics, 2018).....	143
97.	Particle displacement (a) as a function of time, and (b) as function of position along the rod (Kramer, 1996).....	145
98.	Cartesian coordinate system	146
99.	Representation of a P-wave. Alternating compression and dilation particle motion and parallel to direction of propagation (Braile, 2019).....	147
100.	Representation of a S-wave. Alternating transverse particle motion in any plane (here in vertical plane) and perpendicular to direction of propagation (Braile, 2019)	148
101.	Geometrical attenuation for body waves (left) and surface waves (right) (Persson, 2016)	149
102.	Variation of Rayleigh wave and body wave propagation velocities with poisson's ratio (Kramer, 1996)	150
103.	Representation of a Rayleigh wave. Elliptical particle motion in vertical plane and parallel to direction of propagation. Amplitude decreases with depth (Braile, 2019)	150
104.	Horizontal and vertical motion of Rayleigh waves. A negative amplitude ratio indicates that the displacement deeper underneath the surface is in the opposite direction of the surface displacement (Kramer, 1996) after (Richart, Hall, & Woods, 1970).....	151
105.	Complete wavefield predicted by Lamb (1904) for a surface point source on an elastic halfspace (a) horizontal radial motion; (b) vertical motion; (c) particle path of Rayleigh waves (Foti, 2000)	152
106.	Harmonic vertical point source acting on the surface of a homogeneous, isotropic, linear elastic halfspace: (a) Complete displacements wave field; (b) partition of energy between different types of waves (Foti, 2000) from (Woods, 1968)	153

107.	Incident (σ_i), reflected (σ_r) and transmitted (σ_t) stress waves at the junction of two rods ($Z_2 > Z_1$) (Metrikine & Vrouwenvelder, 2018).....	154
108.	Ray path, ray, and wavefront for (a) plane wave and (b) curved wavefront (Kramer, 1996)	156
109.	Reflected and refracted rays resulting from incident (a) p-wave, (b) SV-wave, and (c) SH-wave (Kramer, 1996)	156
110.	Refraction principle of an SH-wave ray path (reflected waves are not shown) (Kramer, 1996)	156
111.	Simplified representation of possible paths along which energy is transferred (Spijkers, Vrouwenvelder, & Klaver, 2005).....	157
112.	Representation of a Love wave (a horizontal S-wave). Particle motion perpendicular to direction of propagation. Amplitude decreases with depth (Braile, 2019).....	157
113.	Illustrative soil response for soft soil deposits excited by a passing truck at a particular distance from the road.....	158
114.	Schematic diagram of the problem studied: Passive vibration isolation by rectangular trenches in a viscoelastic halfspace (AI-Hussaini & Ahmad, 1991)	160
115.	Influence of normalized trench depth and width for concrete (infilled) trench (AI-Hussaini & Ahmad, 1991)	161
116.	Influence of D/W ratio in the vibration screening by a concrete trench (AI-Hussaini & Ahmad, 1991)	161
117.	Inner FEM domain of the two-layered soil profiles. Left: shallow upper layer. Right: deep upper layer (de Zeeuw, 2018).....	162
118.	Displacement amplitude <i>ureal</i> ($\mu\text{m}/\text{kN}$) for wave barrier optimized for 50 Hz. Left: <i>ureal</i> for optimized wave barrier in homogeneous soil. Middle: <i>ureal</i> for homogeneous-soil-optimized wave barrier in layered soil. Right: <i>ureal</i> for optimized wave barrier in layered soil model (de Zeeuw, 2018).....	163
119.	Inner FEM domain of the three-layered soil profile (de Zeeuw, 2018).....	164
120.	Displacement amplitude <i>ureal</i> ($\mu\text{m}/\text{kN}$) for wave barrier optimized for 50 Hz. The embedded softer soil layer is used as a waveguide (de Zeeuw, 2018)	164
121.	The shape of optimized wave barriers in a two-layered soil with increasing level of manufacturability with the soil interface at 10 m depth (de Zeeuw, 2018).....	164
122.	The shape of optimized wave barriers in a three-layered soil with increasing level of manufacturability (de Zeeuw, 2018).....	165
123.	Reduction ratio A_r for an open trench as a function of the distance from the source. The different lines represent different calculation methods, but appear to be very similar (Barbosa J. , 2013)	166
124.	Reduction ratio A_r as a function of the stiffness of the in-fill material over the stiffness of the soil (Barbosa J. , 2013)	167
125.	Typical figure for the insertion loss (IL) of the 3D analyses for different in-fill materials and depths of the trench (Barbosa J. , 2013).....	168
126.	Idealization of horizontal motion of an offshore platform, excited by waves, by a mass-spring system with a translational degree of freedom (in x – direction) (Metrikine, 2018)	170

127.	The free vibration of the undamped mass-spring system (Metrikine, 2018).....	171
128.	The resonance diagram of the forced single degree of freedom system (Metrikine, 2018)	172
129.	(left) Amplitude-frequency characteristic (magnification factor) and (right) phase- frequency characteristic (Metrikine, 2018)	173
130.	Development of resonance of the undamped forced single degree of freedom system in time (Metrikine, 2018)	173
131.	A mass-spring-dashpot system with a translational degree of freedom (in x – direction) (Metrikine, 2018).....	174
132.	Free vibration of the mass-spring-dashpot system in the case $n < \omega n$ (Metrikine, 2018)	175
133.	(left) Magnification factor and (right) Phase lag of the damped SDoF steady-state solution (Metrikine, 2018)	176
134.	Response of a (damped) SDoF system to suddenly applied constant force (Metrikine, 2018).....	176
135.	Undamped two degrees of freedom system with spring coupling (Metrikine, 2018)	177
136.	Normal modes of the undamped two degrees of freedom system. In mode 1, the two masses move in-phase with each other (k_3 is not stretched, nor compressed). In mode 2, the two masses move out-of-phase with each other (k_3 is stretched or compressed from both sides at the same time). (Metrikine, 2016)	178
137.	Normal modes of the undamped two degrees of freedom system: the shear frame (Blauwendraad, 2016).....	178
138.	Forced two degrees of freedom system. The vibrations absorber k - m is attached to the main system K - M (Metrikine, 2018).....	179
139.	Displacement-frequency curves for the two degrees of freedom system (Metrikine, 2018)	179
140.	Foundation block with three degrees of freedom (Spijkers, Vrouwenvelder, & Klaver, 2005).....	180
141.	Frequency-response function for an undamped five degrees of freedom system for the degree of freedom $x_q(t)$ (Spijkers, Vrouwenvelder, & Klaver, 2005)	183
142.	Frequency response function $H_{iFP\Omega}$ for particular values of i and p (Spijkers, Vrouwenvelder, & Klaver, 2005).....	185
143.	Example of a frequency response function for the degree of freedom $x_q(t)$ when a harmonic loading is applied in the point x_p (Spijkers, Vrouwenvelder, & Klaver, 2005)	186
144.	Sign convention and indication of the meaning of the symbols used for the prismatic beam (Spijkers, Vrouwenvelder, & Klaver, 2005)	186
145.	First three eigenmodes of the simply supported Euler-Bernoulli bending beam (Spijkers, Vrouwenvelder, & Klaver, 2005).....	188
146.	First three eigenmodes of the cantilever Euler-Bernoulli bending beam (Spijkers, Vrouwenvelder, & Klaver, 2005).....	189
147.	Physical representation of soil-structure interaction (Miura, 2016).....	190
148.	Levels of modelling the effect of the soil on the structure: (a) fixed support, (b) elastic support, (c) substructure approach, (d) direct approach (Pap & Kollár, 2018).....	191

149.	Finite Element mesh. As representation of the TLM the element width 'h' is infinitesimal small (Lysmer, 1970)	193
150.	Discretization into thin-layers (left) and a thin-layer as a free body in space with the order of the interpolation function equal to 3 (Barbosa J. , 2013)	194
151.	Example of a 2D structure (trench) in the soil (embedded) which is invariant in the longitudinal (3 rd) direction (Barbosa J. , 2013)	195
152.	Example of a 3D structure on the soil (not embedded) for which the BEM-FEM coupling can be considered by FEMIX (Barbosa J. , 2013)	195
153.	Weak coupling between track and structure (Barbosa J. , 2013).....	196
154.	Example of data-file for the geometry in the (x,z)-plane, needed as input for the FEMIX software	196
155.	Example of computing the command 'prefemix' of FEMIX for the data-file 'soilprofile' in the command prompt which describes the soil layering of the problem to be considered	197
156.	The Volvo FL6 truck in front of the artificial road unevenness installed at the test site (Degrande & Lombaert, 2002).....	200
157.	Artificial road unevenness with sizes indicated (Degrande, Pyl, Lombaert, & Haegeman, 2004).....	200
158.	Road-soil interface at the bottom of the top soil layer (Lombaert & Degrande, 2001)....	201
159.	Position of the measurement points of the verification project (1) (Degrande & Lombaert, 2002).....	202
160.	Frequency content (left) and time history (right) of the predicted front axle load of the Volvo FL6 truck when passing the artificial profile at a vehicle speed $v = 58$ km/h (Degrande & Lombaert, 2002).....	202
161.	Frequency content of the predicted (solid line) and the measured (dash-dotted line) free field velocity at 8, 16 and 24 m for a vehicle speed $v = 58$ km/h (Degrande & Lombaert, 2002).....	203
162.	Time history of the predicted (solid line) and the measured (dash-dotted line) free field velocity at 8, 16 and 24 m for a vehicle speed $v = 58$ km/h (Degrande & Lombaert, 2002)	204
163.	Position of the measurement points of the verification projects (2) and (3) (Degrande, Pyl, Lombaert, & Haegeman, 2004)	206
164.	Frequency content (left) and time history (right) of the predicted front axle load of the Volvo FL6 truck when passing the artificial profile at a vehicle speed $v = 50$ km/h (Degrande, Pyl, Lombaert, & Haegeman, 2004).....	206
165.	Time history and frequency content of the measured soil particle velocity in point FF3 for the passage of the truck at a speed $v = 50$ km/h on the plywood unevenness (Degrande, Pyl, Lombaert, & Haegeman, 2004)	207
166.	Time history and frequency content of the predicted soil particle velocity in point FF3 for the passage of the truck at a speed $v = 50$ km/h on the plywood unevenness (Degrande, Pyl, Lombaert, & Haegeman, 2004)	207
167.	Embedded concrete box foundation with sizes (left) of the single-family dwelling (right) (Degrande, Pyl, & Clouteau, 2004).....	209

168.	Cross section of the storey floors of verification project (3) (Degrande, Pyl, & Clouteau, 2004).....	209
169.	Position of the measurement points of the verification project (3) (Degrande, Pyl, & Clouteau, 2004).....	209
170.	Frequency content (left) and time history (right) of the measured structural response (velocity) in point F ₁₁ for the passage of the truck at a speed $v = 50$ km/h on the plywood unevenness (Degrande, Pyl, & Clouteau, 2004)	210
171.	Frequency content (left) and time history (right) of the predicted structural response (velocity) in point F ₁₁ for the passage of the truck at a speed $v = 50$ km/h on the plywood unevenness (Degrande, Pyl, & Clouteau, 2004)	210
172.	Situation of measurements at the VU Amsterdam site, taken from the documents of TNO (Koopman, 2012). The red arrows indicate the travelling path of the sand truck. The top left measurement point (x,y,z) and the top three measurement points on the right (z) are used to verify the result computed by FEMIX.....	211
173.	Soil response at the top left measurement point from Figure 172 at the VU Amsterdam site, taken from the documents of TNO (Koopman, 2012)	212
174.	MAN TGS 10x8 WSA sandtruck used for the measurements at the VU Amsterdam site (modderaandebanden.nl, 2019).....	212
175.	Exact representation of the functions $f(y)$ of the road irregularity for the ranges of the longitudinal coordinate 'y' for which the height of the road irregularity is larger than zero	214
176.	A frequency spectrum of an arbitrary heavy vehicle with steel leaf suspension vehicle characteristics (left) and frequency spectrums for deviating values of the vehicle characteristics (right)	215
177.	Frequency spectrum of the truck with steel leaf suspension of the verification project (left) and the approximated bus with air suspension (right). See Appendix I 'Appendix: table of computed vehicle axle load-frequency spectrums for changing parameter values' for frequency spectrums for deviating vehicle characteristics one-by-one.....	216
178.	Vertical response (frequency spectrum) obtained with the drop weight device in summer and winter for the ground in front of a building at a particular site in Montreal (Hunaidi & Tremblay, Traffic-induced buiding vibrations in Montréal, 1997).....	216
179.	Geometrical assumptions for computing the SSI impedances for left: table 15.1, middle: table 15.2, right: table 15.6 (Gazetas G. , 1991)	225
180.	Graphs accompanying table 15.1, illustrating the frequency dependency (horizontal axes) of the stiffness- and dashpot coefficients (vertical axes) (Gazetas G. , 1991).....	225
181.	Structure with variable embedment in a soil layer overlaying a bedrock, left: table 15.3, right: table 15.4 (Gazetas G. , 1991)	227
182.	Part of the graphs accompanying table 15.3 for computing the dynamic stiffness coefficient in the vertical (z-) direction including the consideration of a bedrock underneath the soil layer with height H (Gazetas G. , 1991)	227
183.	Graph a accompanying table 15.1, left: Gazetas (Gazetas G. , 1991), middle: extrapolated, right: both graphs in one	228
184.	Graph k_y , $L/B = \infty$ accompanying table 15.2, left: Gazetas (Gazetas G. , 1991), middle: extrapolated, right: both graphs in one	228

185.	Simplified model for the computation of the parameters needed for the dynamic response of the 3DoF building	229
186.	Simplified dynamical model which is used to set up the equations of motion for the rigid 3DoF building.....	229
187.	Typical representation of an EB-beam element	233
188.	Principles for the flexible frame for computation of the local dynamic response of w_1 . Left: displaced flexible frame due to rigid building movement of 3DoF system. Right: flexible frame composed of four flexible Euler-Bernoulli beam floor elements w_1, w_2, w_3, w_4 and four flexible Euler-Bernoulli beam wall/column elements u_1, u_2, u_3, u_4	234
189.	Combination of most interesting Interface- and Boundary Conditions of the flexible EB-beam frame, excited by the prescribed time dependent rigid building motion of the 3DoF system. The ICs and BCs per rigid body excitation (x, z, φ) , as implemented in the Python script, can be found in Appendix P	235
190.	Some examples for determining whether the rocking motion generates a positive or negative horizontal and vertical displacement of a particular node in the frame based on the position of the centre of gravity (CG).....	236
191.	Frequency spectrum (top) and time history (bottom) of the Free Field soil response (from left to right: x -, y -, z -direction) at 16 m from the middle of the road by FEMIX.....	257
192.	Structural response in the time domain (top) and the frequency domain (bottom) for all three DoF (x, z, φ) of the 3DoF system modelled for verification project Degrande et al. (3) – Building Response with the layered soil of Amsterdam.....	258
193.	Predicted local EB-beam structural response of the first floor in the time domain (left) and frequency domain (right) for verification project Degrande et al. (3) – Building Response with the layered soil of Amsterdam	258
194.	Reference system and lever-arms within the EB-beam frame	259
195.	Model x representing the BCs and ICs for computing the dynamic response due to all horizontal excitations	259
196.	Model z representing the BCs and ICs for computing the dynamic response due to all vertical excitations	260
197.	Model φ representing the BCs and ICs for computing the dynamic response due to all rotational excitations.....	260

List of Tables

1.	First five natural frequencies and eigenmodes of Euler-Bernoulli beams with constant $EI\rho A$ (Spijkers, Vrouwenvelder, & Klaver, 2005).....	75
2.	Simplification of the layered soil of Amsterdam into a homogeneous halfspace used for computing the dynamic soil impedances for the computational tool EDDABuS _{GS}	102
3.	Application and interpretation of the generic vibration criterion (VC) curves (Amick, Gendreau, Busch, & Gordon, 2005).....	139
4.	Effect of ground characteristics on transmission of vibration (Watts, 1990).....	141
5.	Approximate values of the coefficient of absorption of wave energy (damping constant) obtained as a result of investigations of wave propagation in different soils (Barkan, 1962)	154
6.	First five natural frequencies and eigenmodes of Euler-Bernoulli beams with constant $EI\rho A$ (Spijkers, Vrouwenvelder, & Klaver, 2005).....	189
7.	Specified vehicle characteristics for modelling the Volvo FL6 truck of the verification project (1) (Degrande & Lombaert, 2002)	201
8.	Specified road parameters of the verification project (1) (Degrande & Lombaert, 2002)	201
9.	Specified soil parameters of the verification project (1) (Degrande & Lombaert, 2002)..	201
10.	Specified vehicle characteristics for modelling the Volvo FL6 truck of the verification projects (2) and (3) (Degrande, Pyl, Lombaert, & Haegeman, 2004)	205
11.	Specified road parameters of the verification projects (2) and (3) (Degrande, Pyl, Lombaert, & Haegeman, 2004)	205
12.	Specified soil parameters of the verification projects (2) and (3) (Degrande, Pyl, Lombaert, & Haegeman, 2004)	205
13.	Simplification of the layered soil into a homogeneous halfspace used for computing the dynamic soil- and structural response of the verification projects (2) and (3) (Degrande, Pyl, Lombaert, & Haegeman, 2004)	205
14.	Specified structural parameters of the verification project (3) (Degrande, Pyl, & Clouteau, 2004).....	208
15.	Dynamic specification of layered soil at the VU Amsterdam site as presented by DGMR (Fennema, May 2018).....	211
16.	Assumed specified vehicle characteristics for modelling the MAN TGS 10x8 WSA truck	213
17.	Computed load-frequency spectrums of the 2D truck vehicle model when driving over the road unevenness as described in the verification project of Degrande et. al. for changing parameter values (Figures (a). – (h).)	217

Acronyms

2D	Two-dimensional
2.5D	Two-and-a-half-Dimensional
3D	Three-Dimensional
3DoF	Three Degrees of Freedom
BC	Boundary Condition
BE	Boundary Element
BEM	Boundary Element Method
CG	Centre of Gravity
CPT	Cone Penetration Test
D/W	Depth divided by Width
DoF	Degree of Freedom
EB-beam	Euler-Bernoulli beam
EDDABuS _{GS}	<i>Computational tool (Early Design Dynamic Analysis of Building Structures by Gerwin Schut) developed through the research of this thesis</i>
EOM	Equation(s) Of Motion
FE	Finite Element
FEM	Finite Element Method
FEMIX	<i>Particular software, used in this thesis for wave propagation in the soil</i>
FFT	Fast Fourier Transform or Forward Fourier Transform
Frequency content	<i>The frequencies at which the summation of harmonic loads are applied (every dynamic loading can be decomposed into a summation of harmonic loads)</i>
FRF	Frequency Response Function
FT	Fourier Transform
Half-space	<i>Semi-infinite domain. In this thesis: the soil with a horizontal surface plane</i>
HGV	Heavy Good Vehicle
HVAC	Heat Ventilation and Air Conditioning system
IC	Interface Condition
Impedance	<i>Resistance against vibrations (a combination of mass, damping and stiffness)</i>
IL	Insertion Loss
KU	Katholieke Universiteit (<i>translates to "Catholic University"</i>)
L/B	Length divided by Width
LC	Loading Case
MDoF	Multi-Degrees of Freedom
P-wave	Primary wave (or compressional wave, dilatational wave)
PDE	Partial Differential Equation
PML	Perfectly Matched Layer
PPV	Peak Particle Velocity (<i>m/s or $\mu\text{m/s}$</i>)
PSD	Power Spectral Density
Python	<i>Particular software, used in this thesis for numerical programming</i>
R-wave	Rayleigh wave
RHDHV	<i>Royal Haskoning and DHV (Dwars, Heedrik, Verhey), an internationally operating organization (with Dutch roots) specialised in engineering</i>
RMS	Root-Mean-Square
RRMS	Running Root Mean Square
S-wave	Shear wave

SASW	Spectral Analysis of Surface Waves
SCPT	Seismic Cone Penetration Test
SDoF	Single-Degree of Freedom
SH-wave	Shear Horizontal wave (<i>particle motion of S-wave in horizontal plane</i>)
SSI	Soil-Structure Interaction
SV-wave	Shear Vertical wave (<i>particle motion of S-wave in vertical plane</i>)
TLM	Thin-Layer Method
TNO	‘Toegepast-Natuurwetenschappelijk Onderzoek,’ a Dutch organization for Research in Applied Sciences
TNW	Technische Natuurwetenschappen (<i>translates to “Applied Sciences”</i>)
TRRL	Transport and Road Research Laboratory (<i>in Berkshire, England</i>)
TU	Technische Universiteit (<i>translates to “Technical University”</i>)
VC-curves	Vibration Criteria curves
VU	Vrije Universiteit (<i>translates to “Liberal University”</i>)
WIB	Wave Impeding Block

Symbols

Meaning of the symbols used in this thesis (unless described differently in the text). The meaning of double mentioned signs should become clear from the context in which the sign is used.

Sign	Description	Unit
A	Area	m^2
A_b	Effective surface area of the foundation basemat	m^2
A_r	Amplitude reduction ratio	—
A_w	Side wall-soil contact surface	m^2
C	Parameter used for the determination of the natural frequencies of EB-beams by means of equivalent masses	—
$C_j(\omega)$	Frequency-dependent damping impedance term of the 3DoF system (in 2D, $j = x, z, \varphi$)	Ns/m or Nms/rad
C_p	Damping of the vehicle's primary suspension in a MDoF model	Ns/m
C_s	Shear wave speed of vibrations through a specific material	m/s
C_t	Damping of the vehicle's tyre in a MDoF model	Ns/m
\mathbf{C}	Global damping matrix	—
\mathbf{C}^*	Modal damping matrix	—
$\widehat{\mathbf{C}}(\omega)$	Frequency-dependent radiation damping matrix	—
D	Depth of embedment	m
E	Young's modulus	N/m^2
\mathbf{E}	Eigenmatrix	—
\mathbf{E}^T	Transposed eigenmatrix	—
F	Force	N
F_{wAVG}	Vibration level reduction based on AVG	—
$F_{i,j,avg}(t, \omega)$	Frequency dependent average excitation load on the 3DoF system ($i = u, v$) ($j = x, z, \varphi$)	N or Nm
G	Shear modulus	N/m^2
H	Height	m
$H_j(\Omega)$	Frequency response function for the subject 'j,' depending on the loading radial frequency ' ω ' or ' Ω '	—
$H_j(f)$	Modulus of the transfer function for the subject 'j,' depending on the frequency ' f '	—
I	Second moment of area	m^4
I_b	Moment of inertia of the vehicle's body in a MDoF model or moment of inertia of the building	kgm^2
$Im(g)$	Imaginary part of the function g	—
J	Mass Moment of inertia	kgm^2
J_{CG}	Mass Moment of inertia around the centre of gravity	kgm^2
K_p	Stiffness of the vehicle's primary suspension in a MDoF model	N/m
K_t	Stiffness of the vehicle's tyre in a MDoF model	N/m
$K_j(\omega)$	Frequency-dependent stiffness impedance term of the 3DoF system (in 2D, $j = x, z, \varphi$)	N/m or Nm/rad
$\mathbb{K}_j(\omega)$	Frequency-dependent impedance terms (in 2D, $j = x, z, ry$)	<i>variable unities</i>

$\mathbb{K}_j^G(\omega)$	Frequency-dependent impedance terms (in 2D, <i>variable unities</i> $j = x, z, ry$) of a foundation pile-group	
$\mathbb{K}_{j,i}^S(\omega)$	Frequency-dependent impedance terms (in 2D, <i>variable unities</i> $j = x, z, ry$) of a single foundation pile (i)	
\mathbf{K}	Global stiffness matrix	–
\mathbf{K}^*	Modal stiffness matrix	–
$\tilde{\mathbf{K}}(\omega)$	Frequency-dependent stiffness matrix	–
L	Length	m
L_b	Length of building	m
M	Moment	Nm
M_a	Mass of the vehicle's axle in a MDoF model	kg
M_b	Mass of the vehicle's body in a MDoF model or Mass of the building in the 3DoF system	kg
\mathbf{M}	Global mass matrix	–
\mathbf{M}^*	Modal mass matrix	–
N	Normal force (<i>should become clear from the context</i>)	N
N	Number of summation terms (<i>should become clear from the context</i>)	–
$N(z)$	Interpolation function in the vertical direction	–
P	Period of the Fourier expansion	m
Q	Shear force	N
$Re(g)$	Real part of the function g	–
T	Period of a vibration	s
	$T = \frac{1}{f}$	
T_n	Natural period	s
$U_{j,avg}(t)$	Average prescribed excitation motion on the 3DoF system ($j = x, z, \varphi$)	m or rad
V	Volume	m^3
V_r	Rayleigh wave velocity	m/s
V_s	Shear wave velocity	m/s
W	Width	m
X_1	Horizontal translation of the 3DoF system response	m
X_2	Vertical translation of the 3DoF system response	m
X_3	Rotational motion of the 3DoF system response	rad
Z	Impedance (resisting against vibrations)	Ns/m
a	Acceleration	m/s^2
a_0, a_n, b_n	Coefficients of the Fourier expansion	–
c	Wave speed (<i>should become clear from the context</i>)	m/s
c	Damping coefficient of a dashpot (<i>should become clear from the context</i>)	Ns/m
c_1	Damping coefficient of the primary suspension in a quarter truck vehicle model	Ns/m
c_2	Damping coefficient of the tyre in a quarter truck vehicle model	Ns/m
c_p	Wave speed of the P-wave	m/s
c_r	Wave speed of the R-wave	m/s
c_s	Wave speed of the S-wave (or shear wave speed)	m/s
d	Depth	m
f	Frequency	Hz
$f_{dom,load}$	Dominant frequency of the loading (the excitation)	Hz

$f_{n,str}$	Natural frequency of the structure	Hz
h	Height	m
k	Wavenumber (<i>should become clear from the context</i>)	m^{-1}
k	Spring stiffness (<i>should become clear from the context</i>)	N/m
k_1	Stiffness of the primary suspension in a quarter truck vehicle model	N/m
k_2	Stiffness of the tyre in a quarter truck vehicle model	N/m
k_j	Wavenumber for subject 'j'	m^{-1}
l	Length	m
m	Mass	kg
m_s	Mass of part of the body in a quarter truck vehicle model	kg
m_u	Mass of the axle in a quarter truck vehicle model	kg
n	Damping parameter $n = \frac{1}{2}c/m$	Ns/m ²
q	Distributed load	kN/m
r	Distance from a reference point	m
s	Position along a Cartesian coordinate	m
s_n	Characteristic exponent	–
t	Time (<i>should become clear from the context</i>)	s
t	Traction (<i>should become clear from the context</i>)	N/m ²
u	Displacement	m
\dot{u}	First time derivative of displacement u (speed):	m/s
	$\dot{u} = \frac{\delta u}{\delta t} = a$	
\ddot{u}	Second time derivative of displacement u (acceleration):	m/s ²
	$\ddot{u} = \frac{\delta^2 u}{\delta t^2} = v$	
$u_{b,i,j}$	3DoF motion (displacements or rotations) (in 2D, $i = x, z, \varphi$) ($j = 1^{st}, 2^{nd}, \dots N^{th}$ harmonic loading term)	m or rad
$u_{0,i,j}$	3DoF prescribed motion (displacements or rotations), i.e. the excitation on the 3DoF system	m or rad
u_i	EB-beam wall element ($i = 1,2,3,4$)	–
v	Speed or velocity (<i>should become clear from the context</i>)	m/s
ν	Poisson's ratio (<i>should become clear from the context</i>)	–
v_0	Initial velocity (at $t = 0$)	m/s
v_{RMS}	RMS-value of the vibration level velocity	m/s
$v_{w1}(x, t)$	Vibration velocities of EB-beam element w_1 at a particular x -coordinate along the length of the element	m/s
w	Width	m
w_i	EB-beam floor element ($i = 1,2,3,4$)	–
x	Cartesian coordinate (generally horizontal)	m
\dot{x}	First time derivative of Cartesian coordinate x :	m/s
	$\dot{x} = \frac{\delta x}{\delta t}$	
\ddot{x}	Second time derivative of Cartesian coordinate x :	m/s ²
	$\ddot{x} = \frac{\delta^2 x}{\delta t^2}$	
\underline{x}	Vector of variable x	–
$\underline{\hat{x}}$	Eigenvector (the solution to the homogeneous set of equations for a multi-degrees of freedom system)	–
	$(-\omega^2 \mathbf{M} + \mathbf{K}) \underline{\hat{x}} = \underline{0}$	
x_0	Initial translation (at $t = 0$)	m

y	Cartesian coordinate (generally horizontal)	m
z	Cartesian coordinate (generally vertical)	m
χ	Dimensionless frequency	—
Ω	Angle of rotation (<i>should become clear from the context</i>)	rad
Ω	Radial frequency (<i>should become clear from the context</i>)	rad/s
$\mathbf{\Omega}^2$	Diagonal matrix	—
β	Material damping ratio (<i>should become clear from the context</i>)	—
β	Parameter used for solving continuous systems: $\beta^4 = \frac{\rho A \omega^2}{EI}$ (<i>should become clear from the context</i>)	—
γ	The amount of damping $\gamma = 2n/\omega_n$ with $n = \frac{1}{2}c/m$	$\frac{Ns}{m^2 rad}$
Δ	Delta, i.e. difference between two values of the same parameter	—
δ	Partial derivative	—
ε	Strain	—
ε_0	Volumetric Strain ($\varepsilon_{xx} + \varepsilon_{yy} + \varepsilon_{zz}$)	—
ϵ	Strain	—
ϵ_0	Volumetric Strain ($\epsilon_{xx} + \epsilon_{yy} + \epsilon_{zz}$)	—
θ	Angle	rad
λ	Wavelength (<i>should become clear from the context</i>)	m
λ	Lamé's first parameter (<i>should become clear from the context</i>)	N/m^2
λ_j	Wavelength for subject 'j'	m
λ_R	Rayleigh wavelength	m
μ	Lamé's second parameter	N/m^2
μm	Micrometer	$10^{-6} m$
ξ_i	Modal damping ratio per uncoupled degree of freedom 'i' of a damped multi-degrees of freedom system: $\xi_i = \frac{1}{2\omega_i} * \frac{\hat{x}_i^T \mathbf{C} \hat{x}_i}{\hat{x}_i^T \mathbf{M} \hat{x}_i}$	—
φ	Phase lag	rad
ρ	Density	kg/m^3
σ	Stress	N/m^2
ω	Radial frequency	rad/s
ω_1	Modified representation of the natural frequency ω_n in combination with the damping parameter n : $\omega_1 = \sqrt{\omega_n^2 - n^2}$	0
ω_n	Natural frequency (a property of a system)	rad
∇^2	Laplace operator: $\left(\frac{\partial}{\partial x^2} + \frac{\partial}{\partial y^2} + \frac{\partial}{\partial z^2}\right)$	—

Part I

Introduction

1. Introduction

1.1. Background

Structural vibrations are always present and even the smallest vibrations can give rise to hindrance of experiments taking place in research laboratories. Since the research industry keeps on evolving and needs to do more and more accurate experiments, the vibration level requirements for such research facilities are expected to increase in strictness. For the research industry one can think of research to medicines, developing new antibiotics, computer chips, optics, or other industries in which work is taking place on nanoscale.

The vibrations are induced by loadings within or outside the building and, among other things, may be caused by walking, machinery, wind, traffic, etc. Each type of loading has its own frequency (range) at which the vibration waves propagate. It appears that low-frequency loading is hard to mitigate due to their large wavelength and low damping rate along their traveling path. Heavy traffic is one of those loadings which generally have a low-frequency content (the frequencies at which the harmonic loads are applied).

Since research facilities need to be easily accessible by the organizations which use them, for example a university, the laboratory is preferably built close to these organizations. Unfortunately this often happens to be in a big, crowded, city, where heavy traffic can drive by at any moment of the day, which means that the vibration sensitive laboratory building is exposed to heavy vibrations. The structure of the building needs to be designed such that vibrations from inside and outside the building are reduced to such an extent that research can be done without obstructing disturbances. Here the structural engineer comes into play who designs the structure of the building. However vibration mitigation is not the main aspect of the structural engineer's work. Very often a specific vibration expert is involved to make statements about the vibration level reduction of a certain (structural) design and to help in further mitigating the vibration level when necessary.

It appears that, in practice, very heavy computational models with long computational times are often needed to get insight into the vibration levels for a structure in a certain situation. This way of working is less desired when the building is still in the initial design phases. In the initial design phase it should be possible to make a lot of iterations and see what the influences of changing certain parameters are. If each iteration takes a long computation time, the feasibility to make a lot of iterations is obstructed. To overcome this problem, Pieters Bouwtechniek (Dutch advising company for structural engineering and design) has the wish for a practical engineering design tool for vibration sensitive laboratory structures. This tool should give the structural engineer / designer insight into the consequences of changing a certain parameter in a specific environmental situation on the vibration levels in the building structure without the need for long computational times. This thesis lays the foundation for such a practical engineering design tool, called 'EDDABuS_{CS}' (Early Design Dynamic Analysis of Building Structures by Gerwin Schut).

1.2. Scope

1.2.1. Aim

The aim of this research is to increase the ability of a structural engineer, who is not specialized in soil dynamics and structural dynamics, to make fundamental choices for a vibration sensitive laboratory building structure, which is excited by traffic induced vibrations (e.g. road traffic, trams or trains), in the early design phase of a project. This requires a practical computational design tool which is relatively simple to use and requires a (limited) number of parameters as input and gives the response of the structure (in m and m/s (because the vibration criteria are given in m/s), in both the time domain and the frequency domain) as output.

In addition to this computational tool (EDDABuS_{GS}) a static tool in the form of a design chart will be presented which states what steps the engineer should go through and what types of mitigation measures one can think of when designing a vibration sensitive laboratory structure. Together the EDDABuS_{GS}-tool and the design chart form the desired practical engineering design tool (Figure 1). The design decisions based on the practical engineering tool should always be verified by a building physics/vibrations expert.

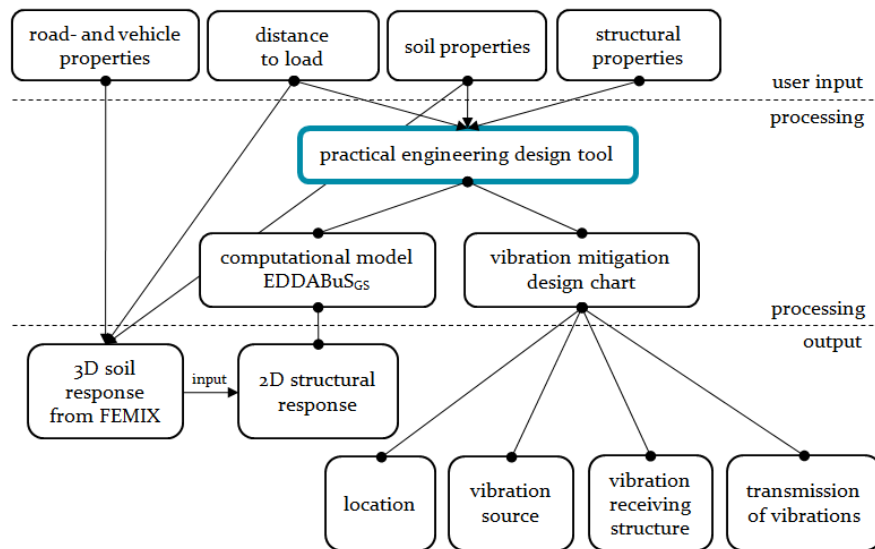


Figure 1. Diagram representation of the practical engineering design tool

Central research question

How can a scientific model be created as the basis of a practical engineering tool for the design of vibration sensitive laboratory building structures, excited by traffic induced vibrations, which is sufficiently accurate for an early design phase of a project?

Key research questions

1. How can a 2D model give reliable predictions for the 3D problem?
2. How do the properties of the structure (e.g. mass distribution, stiffness, embedment depth, foundation piles) influence its vibrations?
3. In what ways do variations in built-ups of different soil layers influence the design of the structure?
4. How do sensitivities in the used models influence the structure's design and how can these sensitivities be minimized?
 - 4.1. What are the sensitivities influencing the structural design?
 - 4.2. How can a robust model be made?
5. What is the influence of external interventions (e.g. a wave barrier and cavities) on the structure's design?

1.2.2. Approach

For approaching the development of this design tool the computational model will be split into four interrelating and consecutive parts: source, transmission, interaction, receiver. The source describes the source of the loading and what kind of loading types are applicable. The transmission describes the soil through which waves, initiated by the source, propagate

towards the structure. The interaction describes the dynamic soil-structure-interaction (SSI) between the soil surrounding (and supporting) the structure and the structure itself. And finally the receiver describes the structure and more in particular the bottom- or first storey floor of the structure on which the laboratory activities take place (or on which vibration isolating islands stand on).

The literature study and the development of the computational model will be done in a similar separated sense. Eventually the computational model (EDDABuS_{GS}) will combine all the four consecutive parts into one integrated tool which should be easy to use and only requires the input of (a limited amount of) certain parameters. The tool will be verified with measurements performed for real projects. After verifying the output of the EDDABuS_{GS}-tool, the tool will be used to perform iterations by changing the parameters of the soil and the structure.

Finally, the thesis is concluded with comprehensive answers to the research questions and the possibilities and shortcomings of the EDDABuS_{GS}-tool created. Also, recommendations will be given for possible future research to enhance the product delivered by this thesis.

1.2.3. Limitations

Model dimensions

The dimensions of the computational model for computing the soil response (FEMIX) are bounded to a 2.5D model, which represents the 3rd dimension as an aggregate of 2D solutions, i.e. a moving load can be implemented, but the model geometry is invariant in the 3rd dimension.

The dimensions of the EDDABuS_{GS}-tool for the structural response will be limited to a 2D model. A 2D model (vertical cross section of soil and structure) should compute the influence of changing a model parameter sufficiently reliable in order to be used as a design tool for an early design phase of a project. The 3rd dimension is assumed to be invariant.

Soil model wave propagation

The research part of the thesis concerning the wave propagation in the soil (linear elastic half-space with free surface (Figure 2)) will be done with the aid of already available FEM software: FEMIX.

The eventual EDDABuS_{GS}-tool will not use FEM software, but instead uses the results computed by the FEM software (.csv-files) for one particular geological situation as input for the computational script for the structural response. Focus is on the built-up of soil layers in the Western part of The Netherlands where softer soil layers are overlying stiffer soil layers deeper in the ground (e.g. Amsterdam).

Loading

The literature study about the loading source will focus on several kinds of sources (e.g. a traffic road with cars, lorries, or rail tracks for trams or trains etc.). However, to narrow the scope of this thesis research the loading of the vibrations source in the eventual EDDABuS_{GS}-tool will be limited to only one particular loading condition: heavy traffic driving over a road irregularity. This load appears to be one of the governing loading types for several projects Pieters Bouwtechniek is working on (see 2.3 ‘Transfer of Vibrations and Measurements’).

It is assumed that the internal vibration sources of the building are completely separated from the laboratory structure, i.e. they are placed in a building part that is completely separated from the laboratory structure. It is assumed that the vibrations caused by internal vibration sources inside the remaining part of the building do therefore not influence the vibrations in the laboratory structure.

Soil-Structure Interaction

In the EDDABuS_{GS}-tool soil-structure interaction (SSI) is assumed to act on the (embedded) structure and on the pile foundation (if applicable). However, the loading is assumed to act on the (embedded) structure only and not on the foundation piles.

Structure

The global structural response computed by EDDABuS_{GS} is limited to a rigid 3DoF system in a 2D (x,z)-plane of which the structural parameters (total mass, mass moment of inertia, soil- and pile impedances) are determined for a 3D building model. The 3D building model is assumed to be symmetrical around the vertical (x,z)- and the (y,z)-plane but can be invariant around any horizontal (x,y)-plane. The structure can be placed on top of the soil or (partly) embedded into the soil (implemented as a variable model parameter) and can either be supported by a pile foundation or not (implemented as a variable model parameter).

The local structural response computed by EDDABuS_{GS} is limited to the bottom slab or the first storey floor of the structure. A flexible 2D frame, composed of (the analytical descriptions of) Euler-Bernoulli beam elements, is used in the (x,z)-plane.

Scientific model

The central research question mentions the terms ‘scientific model’. In this thesis a ‘scientific model’ entails that the computations and possible approximations in the tool (and therefore also the results given by the tool) are based on (/ argued by) scientific laws, formulations and researches as they can be found in the scientific literature of the TU Delft, other universities, productions of professors, papers, experiments, in-situ measurements, realized projects in practice etc.

Illustrative figures

Figure 2 presents some illustrative figures to make clear the intended approach and limitations for this thesis. The assumptions made in these figures (rigidity, excitation, global and local structural response), are explained in Part II ‘Literature Study’ and in Part III ‘Method’ of this thesis.

1.3. Outline

Part II ‘Literature Study’ starts with chapter 2 ‘In Practice’ and gives a description of design aspects of vibration sensitive laboratory structures in practice, what kind of vibration level requirements exist and what the generally known vibration mitigation measures are. Thereafter more theory is gathered about the four main aspects of the computational model which describes the source of the vibration (chapter 3), the transmission of the vibration waves through the soil medium (chapter 4) towards the vibration receiver which is the laboratory structure (chapter 5). Chapter 6 describes how the vibrations are altered due to the interaction between the soil medium and the receiving structure and how the flexible soil and pile foundation support the receiving structure.

All theory is then used for implementation into the actual parts of the computational model (FEMIX and EDDABuS_{GS}). This is described in part III ‘Method’, consisting of chapters 7 to 12, with again the elements source, transmission, interaction and receiver. Eventually the computational tool EDDABuS_{GS} is created and verified by comparing the results with measurements performed in situ for already realized projects. EDDABuS_{GS} is then used in part IV ‘Results & Conclusion’ in which chapter 13 ‘Results from Iterations by EDDABuS_{GS} and Design Chart’ describes iterations performed by using the EDDABuS_{GS}-tool and combines the observations of the computed results and of the literature study in a design chart. Eventually chapter 14 ‘Conclusions and Recommendations’ will discuss the findings of all the preceding chapters by answering the research questions and will give recommendations for using the EDDABuS_{GS}-tool and for future research.

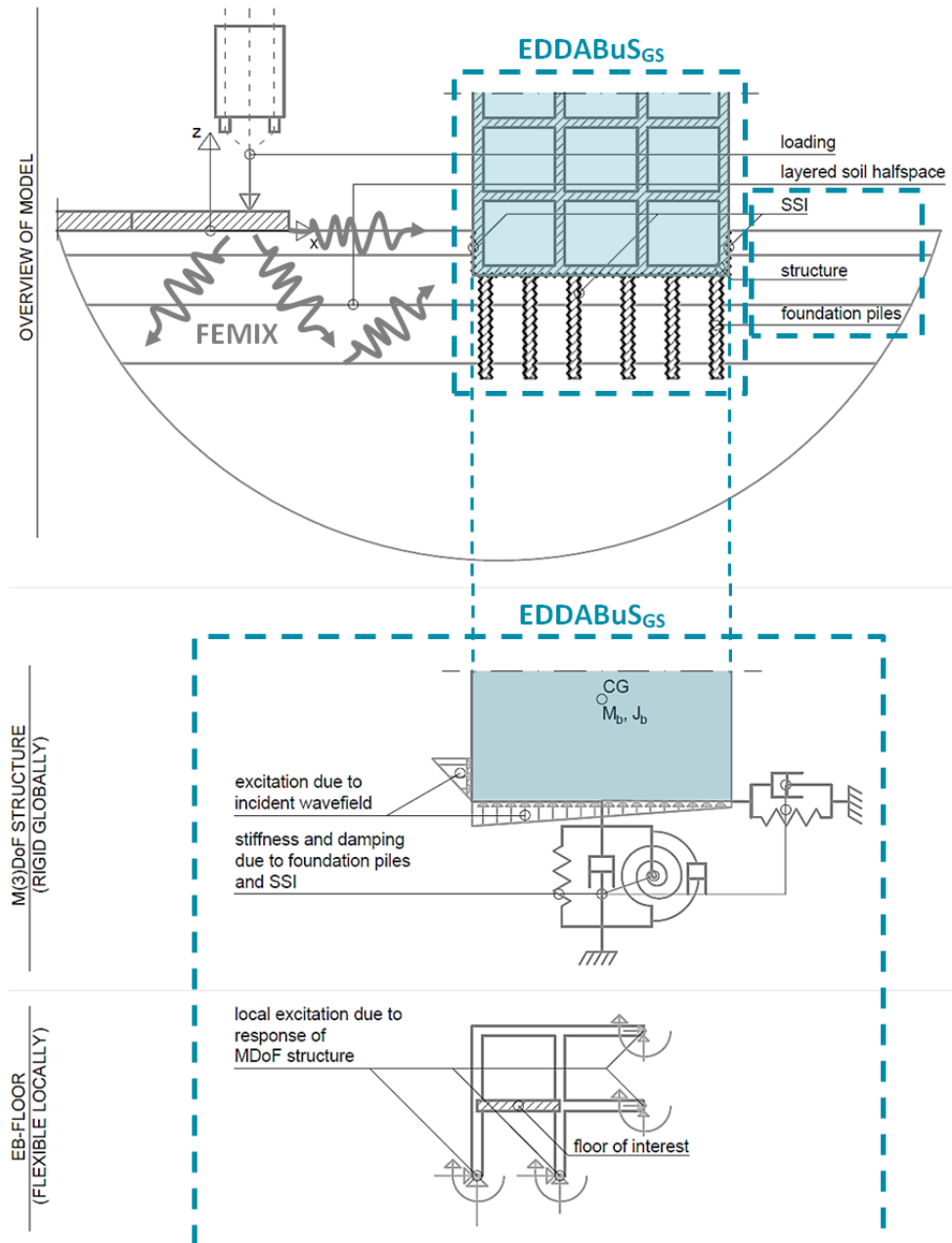


Figure 2. Illustrative figure to make clear the approach of this thesis: In the total overview, the source and the soil response will be calculated. The soil response is implemented as excitation and as soil-structure interaction-springs and -dashpots for the rigid MDoF structure. Locally the floor response (vibrations) will be determined using a frame composed of Euler-Bernoulli bending beams



Part II

Literature Study

2. In Practice

For a better understanding of the problem statement, research has been done to the vibration level criteria for vibration sensitive buildings and what kind of sources might be causing these vibrations. The research also considered already realized- and on-going projects of Pieters Bouwtechniek.

This section will first describe the vibration level criteria which are generally used for laboratory buildings (2.1. ‘Vibration Level Criteria’), thereafter a brief overview will be given for the sources that should be considered when predicting whether these vibration criteria are within the limits (2.2. ‘Vibration Sources’). In practice the vibration levels at a particular site are often determined by means of measurements and the vibration transfer to the building is approximated by measuring similar building situations. This procedure is described briefly in 2.3. ‘Transfer of Vibrations and Measurements’. Eventually possible mitigation measures used in practice are discussed in 2.4. ‘Vibration Mitigation Measures’.

2.1. Vibration Level Criteria

The vibration level requirements for buildings are applicable for the surfaces at which the vibration sensitive equipment is placed, for example the structural floor. The requirements are generally applicable for all the three translational degrees of freedom: x-, y- (two horizontal), and z- (one vertical) translational direction of the supporting surface. Nowadays VC-curves (velocities $\mu\text{m/s}$ in the frequency range 1 – 80 Hz) are used very often as general criteria for vibration sensitive setups. These curves were created in the early 1980’s (Amick, Gendreau, Busch, & Gordon, 2005) and have since then been developed into the most recent criteria shown in Figure 3. Table 3 in Appendix A describes the usage-type for these criteria.

The requirements for VC-C to VC-E have become stricter over the years, because the allowed rms-velocities are now constant for all frequencies while before the criteria for frequencies < 8 Hz were higher in a similar linear manner as for the VC-B requirements. This change is due to the fact that nowadays some equipment often have internal pneumatic vibration isolation which shifts the frequency of greatest vibration sensitivity down to the range of 1 to 4 Hz, while before the lowest resonance frequencies of equipment were higher than 8 Hz (Amick, Gendreau, Busch, & Gordon, 2005).

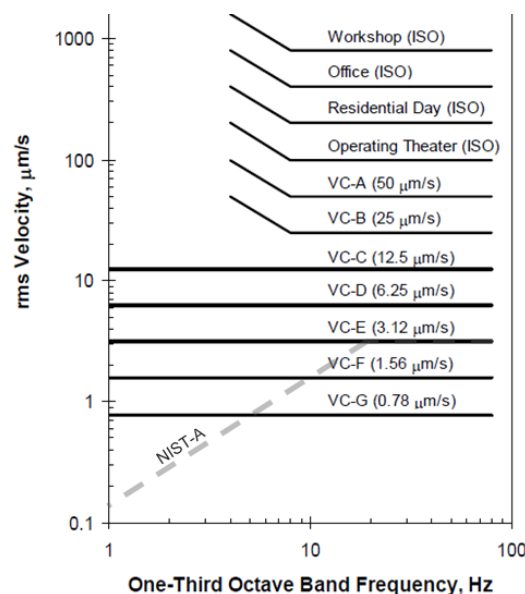


Figure 3. Generic vibration criterion (VC) curves for vibration-sensitive equipment (Amick, Gendreau, Busch, & Gordon, 2005)

Relating to Figure 3:

$$\text{rms Velocity } [\mu\text{m/s}] = v_{RMS,i}(f) \approx \frac{v_{Peak,i}(f)}{\sqrt{2}}$$

with $i = (1, 2, \dots, N)$, where N is the last $1/3$ -octave band
(every octave band is split up into three smaller ' $1/3$ -octave bands'. For every $1/3$ -octave band the $v_{RMS,i}$ is computed in the frequency (f) domain)

(2.1)

While the vibration level criteria are a good indication of the preferred vibration-less environmental demands of the users, still the chance of exceedance of this vibration level is hardly ever zero. Exceedance could be caused for example by a vibration source that was not accounted for in the design of the building and may produce vibrations for a limited amount of time, only a couple of times per year (i.e. 'incidents'). Whether this exceedance is bad or not should be weighed against the consequences of this exceedance (e.g. availability and costs for a new experiment are high or low) and how often the exceedance is possible to take place. In case experimental activities are bounded by long processes, an exceedance of the vibration criteria could have large consequences compared to short term experimental activities.

2.2. Vibration Sources

Many kinds of vibration sources exist. A short summary based on already realized projects is listed here to give an indication of what kind of sources one should think of when encountering a structural design of a vibration sensitive laboratory structure:

- Environmental traffic (busses, trucks, cars, etc. on roads and trams, trains etc. on rails).
- Vibration generating equipment of neighbouring sites (compressors, wind tunnel, emptying of containers, local logistics, pumps).
- Hot-and-cold storage and corresponding pumps in the soil.
- Internal vibration generating equipment (heat-, ventilation- and air conditioning systems (HVAC), elevators, pumps, aggregates, hoisting installations, etc.).
- Personal logistics (walking, sports, dancing) inside the building.
- Wind loading on the building.
- Construction works (e.g. pile driving).
- Earthquakes.

2.3. Transfer of Vibrations and Measurements

For information about how the transfer of vibrations are predicted and measured in practice, two example projects of Pieters Bouwtechniek will be considered in this section. The principles of both projects are similar and other known projects at Pieters Bouwtechniek underline the same kind of approach.

2.3.1. TNW Zuid

For the project Faculty of Applied Sciences of the Technical University in Delft the vibration level of the floor is determined by the multiplication of the excitation spectrum with the relevant transfer function of the soil (dependent on distance from the source) and with the relevant transfer function of the structure (from soil to structure). In formula form this looks like (Snoeijs B., 2011):

$$V_{floor}(f) = H_{structure}(f) \cdot H_{soil}(f) \cdot V_{source}(f)$$
(2.2)

where:

- $H_{structure}(f)$ = transfer function of soil to floor structure
- $H_{soil}(f)$ = transfer function of soil over a certain distance
- $V_{source}(f)$ = spectrum vibration source, velocity in the soil

$V_{floor}(f)$ = spectrum vibrations at the topside of the floor, velocity
 f = frequency

A similar kind of approach can also be found in other literature (e.g. the lectures of Soil Dynamics at the TU Delft (Hölscher, 2017)). This approach generally consists of the partition into the parts: source, transmission, interaction and receiver. This partition will also be used as guidance through this thesis research.

For this particular project the transfer function from soil to vibration sensitive floor is determined by measuring the vibrations, caused by a falling Bigbag filled with sand (Figure 4), in the soil and on the floor at the same time. The measurements are then compared to the results of a predictive FEM calculation. A normalized method for determining the vibration transfer from soil to floor does not exist, however the method with the falling Bigbag is a method that is used more often for similar kind of researches.



Figure 4. Execution of experiment for determining transfer function of vibrations from soil to floor: a falling Bigbag at a certain distance from the building (Eilders, 2015)

The prediction by the FEM calculations for the vibration sensitive floors appeared to be conservative compared to the measured values (much more reduced vibrations were measured). The fact that the FEM calculations are conservative is most presumable due to the shielding effect of the foundation of the building volumes surrounding the vibration sensitive floors (the surrounding structures make that the vibrations cannot reach the vibration sensitive floors (directly)). This shielding effect was taken into account conservatively in the FEM calculations (Eilders, 2015).

2.3.2. VU Amsterdam

For the project Research facility VU Amsterdam an analytical model is used by TNO to approximate the vibration transfer from the soil to the foundation of the structure. This analytical model is first validated by comparing the results with measurements performed by TNO at the nearby Medical Faculty (similar soil and building situation). The second validation is done by comparing the results with the predictive FEM computations performed by RHDHV for the vibration-less block (Pruiksma, 2015).

Without validation of the model the results of the calculations will not be sufficiently accurate for determining the actual vibration levels of the laboratory floors. However, the ratio of the influence of certain parameters can still be determined. It is advised to perform actual measurements to validate the model in absolute sense. The model can then be tuned with realistic values and can therefore make a much better prognosis of the actual vibration levels of the laboratory floors (Fennema, 2018). After the validation the analytical model is used to determine the vibration transfer from the soil to the foundation of the vibration sensitive building.

The measurements performed by TNO show large values for the vibration amplitudes, indicating the presence of a very soft soil. These large values can be the result of reflections of vibrations at deeper soil layer interfaces or a strong wave propagation in relatively thin soil layers which lay on a soft soil. In both of the situations it is expected that there will also be a great amount of vibration reduction at the transfer of vibrations from soil to the building. This vibration reduction will be greater in case the building is heavy (a great mass) and has a foundation with piles which are supported by a deeper stiff soil layer (sand) (Fennema, Definitief Ontwerp bouwfysica, akoestiek, energiezuinigheid en trillingstechniek, 2018).

The following conclusions were made based on the measurements (Koopman, 2012):

- Road traffic is the most important source for vibrations
- There is proper damping through the soil by distance
- Very strong vibrations within 30 m due to soft soil

Similar to the project Faculty of Applied Sciences of the Technical University in Delft the loading of heavy traffic driving over a road unevenness is implemented in the model for determining the maximum vibration levels of the structure in Amsterdam.

Based on the analytical model of TNO the following prognosis has been made for the achievable vibration levels of the structure in Amsterdam (without taking into account the influence of the shielding effect of the building in front):

Trams: vibration prognosis façade/basement-floor/ground floor: $3 \mu\text{m/s} = \text{VC-E}$

Heavy traffic: vibration prognosis façade/basement-floor/ground floor: $8 \mu\text{m/s} = \text{VC-C/D}$

The storey floors are excited by amplification of the foundation vibrations due to the flexibility of the superstructure (which is placed on top of the foundation) and by sources inside the building itself. The vibration levels of the storey floors are therefore believed to be one vibration level class lower than the vibration level class of the façade/basement floor/ground floor (Fennema, February 2018).

As the above studies about the vibration generating sources for laboratory buildings point out the vibrations induced by road traffic (and trams) is generally the governing loading type of such kind of laboratory building structures. This is partly due to the fact that these types of buildings are rarely placed nearby train rail tracks, because of the general conception that train rail tracks can produce significant vibration levels. Therefore, the loading type concerning heavy vehicles driving over an unevenness in the road will be the focus of the research performed in this thesis.

2.4. Vibration Mitigation Measures

Several mitigation measures are possible to reduce the influence of environmental vibrations in the building. The standard strategy for mitigating vibrations considers, among other things:

- I. Choice of location / area and control environmental aspects.
- II. Spatial separation of source and receiver.
- III. Structural separation of source and receiver.
- IV. Vibration separation of source and receiver (isolate).

The measures are further elaborated in the following text. It must be noted that the mitigation measures that need to be chosen for a specific project can differ for different situations.

I. Choice of location

Most of the (high frequency) vibration sources (e.g. pumps and subways) are damped out over a distance of 200 m to 300 m such that a vibration level class VC-E is achievable. However heavy traffic needs 400 m to be damped out to a similar extent. All locations in an urban environment are therefore disadvantageous for a vibration-less building (Hermens, 2012). Note

that these distances hold as approximate maxima, i.e. in case no other mitigation measures can be realized. The values can differ for every specific project and depend, among other things, on the soil (stiffness and damping).

II. Spatial separation of source and receiver

Generally known measures taken close to (or at) the vibration generating source are:

- Smoothen traffic roads (asphalt) and lower traffic speed
- No spots where traffic has to stop or accelerate.
- Arrange a plan with other parties for certain time-windows in which vibration generating activities (e.g. emptying containers, arrivals of goods, etc.) may take place.
- Place vibration generating equipment on vibration isolators.

III. Structural separation of source and receiver

Generally known measures taken around the building are:

- Realization of a wave barrier in the form of diaphragm walls in the soil surrounding the close proximity of the building.
- Support roads by foundation piles.
- High frequency operation of equipment in the soil (high frequencies are hard to transfer through the soil and are easier to reduce in the isolation set-up of the vibration sensitive equipment).

V. Vibration separation of source and receiver (isolate):

Generally known measures taken in the building design are:

- Heavy mass and great stiffness of building.
- Limited length of spans and no cantilevers.
- Minimize the number of floor openings (if needed, surround the opening by stiffening beams).
- An active or passive vibration isolation table, to support the vibration sensitive equipment (Figure 5) (Snoeijs B. , 2011).
- Eigenfrequencies of floors above dominant frequencies of excitation. For traffic excitation the eigenfrequencies of the floors should be high in bending (> 8 Hz) (Fennema, 2017).
- Isolate vibration generating installations and components and maximize distance to laboratory rooms.

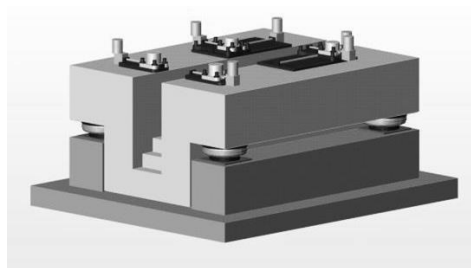


Figure 5. Passive vibration isolation table (PES Ltd, 2019)

The resistance against vibrations (impedance, see 12.1.3 ‘Computation of the building response due to a harmonic loading term’) of a structure can be increased by adding mass, damping and/or stiffness. When increasing the floor stiffness, the resistance against vibrations is increased, however the vibration transfer to other structural components will remain the same. When increasing the floor mass locally (e.g. with a poured concrete part on top) the generation of vibrations will be decreased and (with similar floor stiffness) the vibration transfer to other structural components will be decreased. Therefore, adding a poured concrete layer on top of floors is an effective measure to reduce the generation and transmission of vibrations from a floor with vibration generating equipment to adjacent structural elements. (Fennema, 2017).

TNW Zuid

For the project Faculty of Applied Sciences of the Technical University in Delft the following specific mitigation measures have been applied (Figure 6 (left)):

- Separation of floor islands on the ground floor from the surrounding building volume.
- Floor islands (min. size in preliminary design $W \times L \times H: 10 \times 10 \times 0.8 \text{ m}^3$), completely dilatated from the rest of the building, on a dense grid ($2 \times 2 \text{ m}^2$) of (partly) inclined foundation piles.

VU Amsterdam

For the project Research Facility of the VU Amsterdam the following specific mitigation measures have been applied (Figure 6 (right)):

- Separation of building volumes: all vibration generating equipment is placed in a taller building volume closest to the road. A lower building volume which contains all vibration-sensitive equipment is structurally separated from the taller building volume. The taller building volume has a shielding effect to ground- and wind vibrations for the lower building volume.
- The lower building volume is designed as a stiff and heavy structure consisting of multiple floor levels. Due to the great inertia of the structure, it should be harder to dynamically excite the structure.
- The basement is designed as a very stiff and heavy box volume supported by a dense grid of foundation piles.

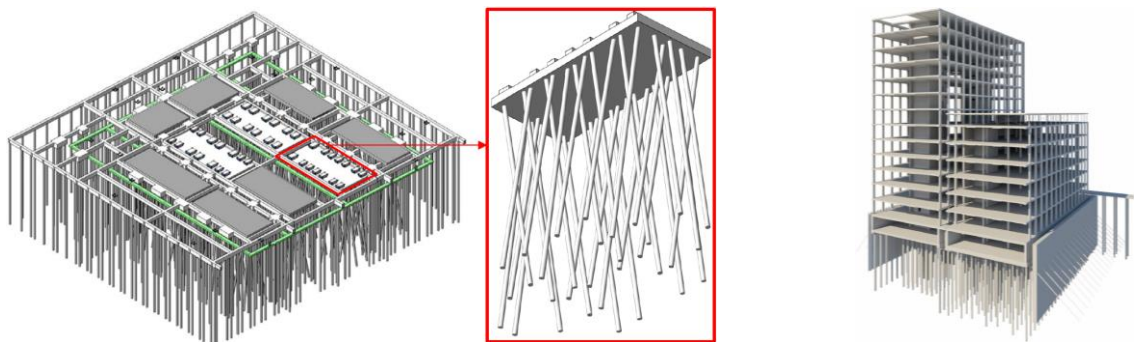


Figure 6. Structural design of (left) the Faculty of Applied Sciences of the TU Delft (Janssen & Ku, 2014) and (right) VU Amsterdam (Versteegen & Koekoek, 2018)

Note that both projects have a different approach for reducing the vibration levels in the building. The design of the more recent building in Amsterdam makes use of great mass, stiffness and inertia while the building in Delft makes use of more elaborated vibration separation. Experience from a number of already realized projects indicates that the application of large vibration-less volumes gives a higher vibration reduction than multiple smaller vibration-less islands. However which vibration mitigation measures should be chosen best is project specific and depends, among other things, on the excitation intensity and characteristics (e.g. vibration amplitude and -frequencies), demands of the building users and design freedom/(im)possibilities.

Measures taken at the vibration source are much more effective than measures taken in the building design. Isolating the source generally is much quicker and simpler than measures to be taken at the vibration receiver / the building. Therefore, it is recommended to first explore the possibilities to reduce the vibration generation at the source and only if these possibilities are not sufficient, the building design might be taken into consideration.

3. Source of Vibrations

As described in chapter 2 'In Practice' vibration levels caused by passing by traffic at a relative close distance is the governing loading condition for the projects Pieters Bouwtechniek was involved in. Since buildings (in which Pieters Bouwtechniek is specialized in) are placed in densified city locations, the focus of the remaining part of this thesis will be on traffic induced building vibrations. The predominantly traffic type appears to be heavy traffic in the form of busses or trucks (or trams) that drive over an unevenness in the road. Also, other studies aiming at environmental building vibrations show that heavy traffic like busses and trucks are the predominant traffic type as vibration source. Hereafter this type of traffic will be referred as 'truck,' but implies all similar heavy traffic vehicles, including e.g. busses.

In this section the specifics of this type of loading (heavy traffic) will be briefly discussed and the dominant influencing parameters of the loading will be stated. Several additions to this chapter are included in Appendix B 'Appendix: Additions to Chapter 3 'Source of Vibrations',' explaining more thoroughly several topics of this section, consisting of the empirical prediction model and the influence of the road stiffness and the vehicle speed on the vertical soil velocity.

3.1. Road Traffic Induced Vibrations – Measurements in Practice

Several studies have been performed concerning the measurements of traffic induced vibrations in the underlying soil. One of these studies, performed by Osama Hunaidi (Hunaidi, 2000) and Martin Tremblay (Hunaidi & Tremblay, 1997) shows measurements performed in front of nine different houses which are situated nearby a traffic road in Montreal, Canada. The soil conditions differed from silty clay to sand or silty sand. Both a transit bus (empty approx. 10 000 kg and loaded approx. 14 000 kg) and a truck (loaded approx. 14 000 kg) were used to perform the measurements. When the vehicles both drive at 50 km/h a difference in the generated vibration levels can be observed: for the truck the vibration level is 33 mm/s^2 , while for the transit bus the vibration level is 65 mm/s^2 .

A part of the measurements is presented in Figure 7 with the unit velocity (mm/s) (instead of acceleration). The difference in vibration level is caused by differences in the suspension systems of both vehicles (bus had air-bag suspension, which are more complicated but provide a smoother ride and prevents sensitive cargo for getting damaged; truck had multi-leaf steel spring suspension, which is cheaper and applicable for heavy duty where ride isn't as important and cargo is not as sensitive (FE Staff, 2017)). This indicates the importance of considering the suspension type of vehicles driving nearby a vibration sensitive building.

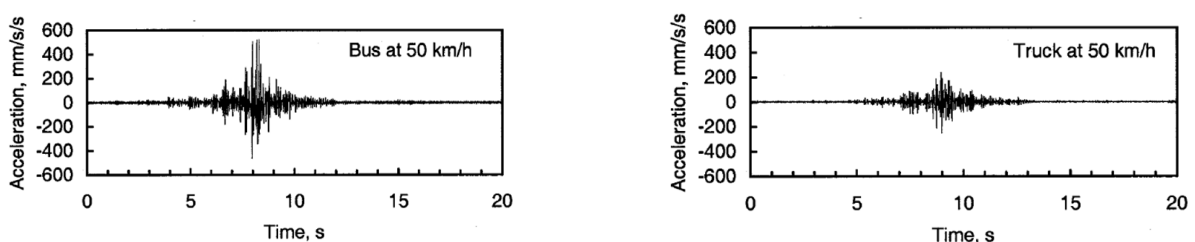


Figure 7. Comparison between vibration levels induced by an empty transit bus (air-bag suspension) and a loaded truck (multi-leaf steel spring suspension) (Hunaidi, 2000)

However, the fact that busses generate higher vibration levels than trucks is contradicted by another research, performed by the Transportation Association of Canada (Woodrooffe, LeBlanc, & LePiane, 1986). In this study the dynamic loads induced by a test truck fitted with air-bag suspension is about 60% of the dynamic loads induced by the same truck but fitted with steel multi-leaf suspension. This contradiction between the two researches can be explained by the differences in frequency content of a vehicle with a steel leaf suspension or air

suspension and how these suspension frequency contents compare to the frequency content of the specific site. According to the research by J. Sing, S.P. Sing and E. Joneson (Singh, Singh, & Joneson, 2006) the frequency contents of the vehicle suspensions deviate per manufacturer. However a global difference between leaf suspensions and air suspension can be recognized (Figure 8). The frequency content of the vehicle with air suspension is somewhat shifted to the left compared to the vehicle with leaf suspension, due to the smaller stiffness (but higher damping) of the air suspension.

Also the axle mass plays an important role in the shift of the natural frequencies: for a higher axle mass, the eigenfrequencies shift to the left (decrease). The soil in Montreal has a dominant frequency range between 10 and 20 Hz. This frequency range corresponds to one of the natural frequencies of the vehicle with air suspension. Therefore, for this particular site the vehicle with air suspension (the bus) generates higher vibration levels than the vehicle with leaf suspension (the truck).

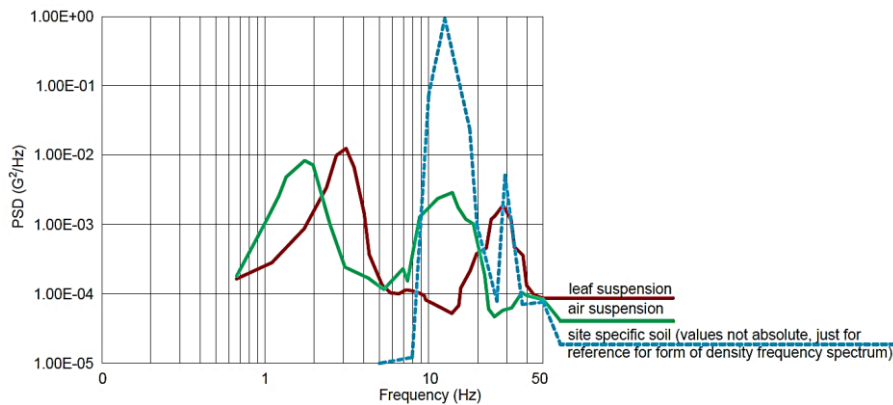


Figure 8. Frequency spectrum of a truck with leaf suspension or air suspension (Singh, Singh, & Joneson, 2006) and for reference of soil vibration amplification, also the frequency content of a specific site is included

Additionally, the research in Montreal compared the vibration levels in case the soil was frozen or not (summer versus winter conditions) (Figure 9). Measured vibration levels caused by road traffic (frequency range < 20 Hz) while the top soil was frozen in winter were about one half of those measured while the soil was not frozen (Hunaidi & Tremblay, 1997). However, another study (referred by (Hunaidi & Tremblay, 1997) as 'Private communication' with Bracken, M. 1994. Aercoustics Engineering Limited) showed that vibration levels, induced by subways in Toronto, were higher in winter. This observation can also be substantiated from Figure 9 since the dominant frequency range for subways is between 40 and 50 Hz.

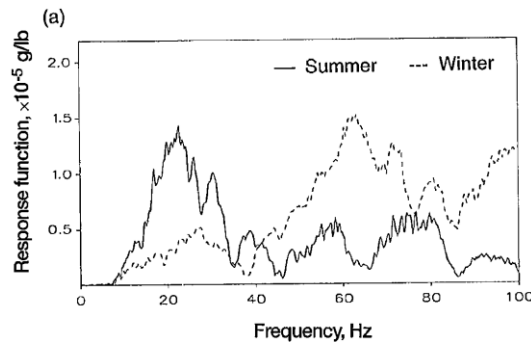


Figure 9. Vertical response obtained by the drop weight device in summer and winter for the ground in front of the building at a particular site (Hunaidi & Tremblay, Traffic-induced buiding vibrations in Montréal, 1997)

3.2. Road Traffic Induced Vibrations - Empirical Prediction Model

According to the research performed by G.R. Watts (Watts, 1990) about traffic induced vibrations in buildings (in the United Kingdom, which has stiffer soils than in The Netherlands), ground-borne traffic vibrations have dominant frequencies in a relative low frequency band, ranging from 8 Hz to 20 Hz.

Ground vibrations are dependent on a number of factors which include the vehicle characteristics such as axle load, suspension design and operating speed, the road surface profile and the nature of the ground between the road base and the building foundations. All these factors make that a practical prediction method is hard to determine. However, a relatively simple prediction technique has been developed in order to make a first estimate on the peak vertical vibration levels at the foundation of buildings.

The method is based on making predictions of vertical peak particle velocities (PPV) at 6 m from the source using the observed trends with amplitude of road surface irregularity and speed, and the most appropriate ground scaling factor. By combining these factors the expected value of the maximum vertical PPV at a building foundation can be calculated as (also see Appendix B ‘Appendix: Additions to Chapter 3 ‘Source of Vibrations’’):

$$PPV_{foundation} = 0.028 \cdot a \cdot \frac{v}{48} \cdot t \cdot p \cdot \left(\frac{r}{6}\right)^x \quad (3.1)$$

where:

PPV	= peak particle velocity of the soil at the foundation	(m/s)
a	= maximum height or depth of surface defect	(mm)
v	= maximum expected speed of heavy good vehicles (HGVs)	(km/h)
t	= ground scaling factor (see Table 4)	(-)
p	= 0.75 in case surface defect occurs in one wheel path only	(-)
	= 1.00 in case surface defect occurs in both wheel path	(-)
r	= distance of foundation from the defect	(m)
x	= power factor for most appropriate soil type	(-)

Generally, peak particle velocities increase with speed for all vehicles.

As stated before the predictive empirical model is only suited for a very rough estimate of the PPV at a particular site. Some of the shortcomings of this model are:

- No incorporation of building characteristics (mass, inertia, stiffness, damping).
- Difficult to determine soil characteristics as one particular ground type.
- The dominant frequency is approximated to be 12 Hz, however this depends on the frequency of excitation and the soil stratification and can thus deviate significantly.
- Non-transparent about the underlying wave propagation theory and occurring mechanisms.
- Applicable for significant irregularity in the road surface and not so much for small irregularities.
- Applicable for great magnitude of vibration levels (not so much for sensitive equipment).
- No incorporation of possible mitigation measures (e.g. a wave barrier).

Because of the major uncertainties in such kind of empirical models a more scientific model has to be developed which can take these factors into account more accurately. Hereafter, first a scientific approach which has been developed within the KU Leuven will be described for the vibration source. In the following chapters the propagation of ground vibrations through the soil and the response of the building structure are considered.

3.3. Road Traffic Induced Vibrations – Scientific Prediction Model

As already stated in the previous section some particularities about traffic loading exist which govern the type, magnitude and frequency of the loading applied at the soil surface. A more scientific determination of these factors follows from the scientific model presented in this section, developed by G. Degrande and G. Lombaert from the KU Leuven (Lombaert, Degrande, & Clouteau, 2000).

First, a simplified dynamical model of a truck is considered. The truck can be modelled as a 2D multi-degrees of freedom (MDoF) system consisting of a rigid body (the chassis and/or bodywork of the truck), mass-spring-dashpot elements for the suspension, rigid masses for the axles and another mass-spring-dashpot element for the tire (Lombaert, Degrande, & Clouteau, 2000) (Figure 10). The stiffness of the road is much larger than the stiffness of the tyre, therefore the solutions of the equations of motion of the vehicle and the road can be uncoupled.

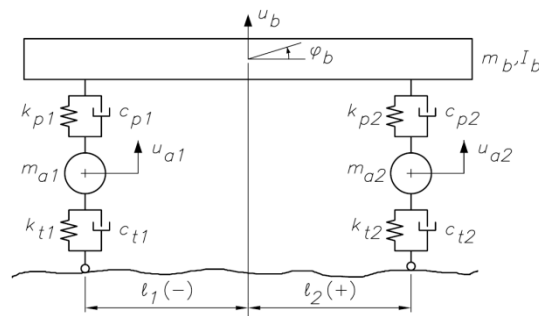


Figure 10. 2D 4 DoF model for a truck with two axles (Lombaert, Degrande, & Clouteau, 2000)

After solving the equation of motion of the vehicle 2D model the dynamic axle loads can be computed. The dynamic axle loads impose the dynamic loading on the surface of the road and are determined by the vehicle dynamics, the profile of the road (the road unevenness), the road flexibility and the vehicle speed. Loss of contact cannot be modelled with this simplified model.

Each longitudinal road profile is characterized by unevenness, which subjects the vehicle to vertical oscillations that cause dynamic axle loading. A profile of a traffic plateau or a kink/dent in the road with a particular length, height and slope is implemented by a mathematical expression, for example as the equation (Lombaert, Degrande, & Clouteau, 2000):

$$u_{w/r}(y) = \begin{cases} H & |y| < \frac{L}{2} \\ H \left[1 - \cos\left(\frac{2\pi(|y| - L/2 + l)}{2l}\right) \right] & \frac{L}{2} < |y| < \frac{L}{2} + l \\ 0 & |y| > \frac{L}{2} + l \end{cases} \quad (3.2)$$

The physical representation of this unevenness is given in Figure 11 in which $L = 5$ m.

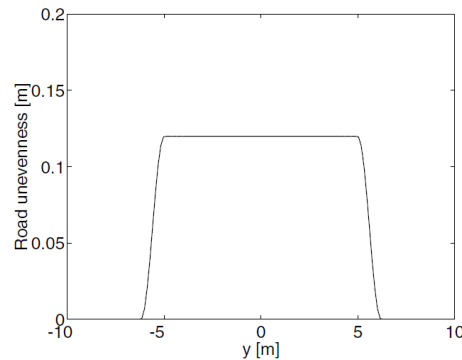


Figure 11. The longitudinal road profile of a traffic plateau with sinusoidal slopes as a function of the coordinate y along the road (Lombaert, Degrande, & Clouteau, 2000)

The dynamic axle loads

Two groups of eigenmodes dominate the frequency content of the axle loads: the pitch and bounce modes at relatively low eigenfrequencies between 0.8 Hz and 3 Hz and the axle hop modes at frequencies between 8 Hz and 15 Hz (Figure 12) (Lombaert & Degrande, 2001).

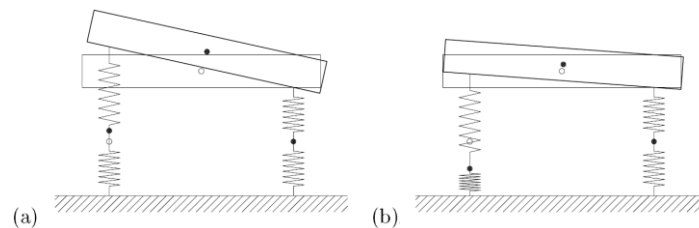


Figure 12. Eigenmodes of the 2D 4-DoF model for a truck: (a) pitch and bounce mode; (b) axle hop mode

The pitch and bounce frequencies are determined by the weight of the vehicle body and the stiffness of the suspension and the tire, while the axle hop frequencies are determined primarily by the weight of the axle and the tire stiffness (Lombaert & Degrande, 2001).

An example of the time history of the front axle load clearly shows the impact at the ascending ($t = -0.3$ s) and the descending ($t = 0.4$ s) slope of the traffic plateau (Figure 13). An analogous observation can be made for the rear axle loads.

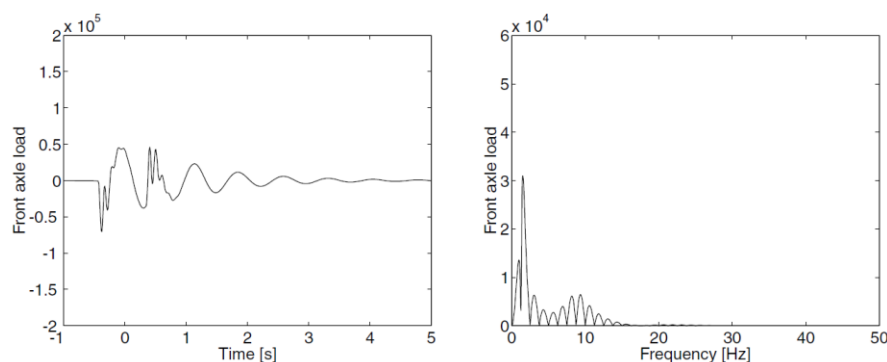


Figure 13. Results of the calculated front axle load (Lombaert, Degrande, & Clouteau, 2000)

Influence of road stiffness on the vertical soil velocity

The road stiffness can influence the generated soil vibrations significantly. A stiffer road reduces the vibration levels of the dynamic axle loads, but when a soft road is applied the dynamic axle loads are hardly influenced. If one wants to incorporate this influence into the model the road-soil interaction needs to be taken into account.

Influence of vehicle speed on the vertical soil velocity

Several literature (e.g. (Watts, 1990), (Lombaert, Degrande, & Clouteau, 2000), (Hunaidi & Tremblay, Traffic-induced building vibrations in Montréal, 1997)) indicate that the vehicle speed is a very important factor for the magnitude of the dynamic axle loads. An increase in vehicle speed shifts the frequency content to the axle hop modes, resulting in a higher PPV. From the model of Degrande and Lombaert (Lombaert, Degrande, & Clouteau, 2000) one can observe that as the vehicle speed increases, the time delay between the impact at the ascending and the descending of plateau decreases and the PPV increases (Figure 14). It also follows that the frequency content of the axle loads widens for increasing vehicle speeds. This illustrates that the relationship between vehicle speed and vibration levels is a function of the suspension system, the condition of the road surface and the dynamic properties of the underlying soil. This has also been observed during in-situ measurements.

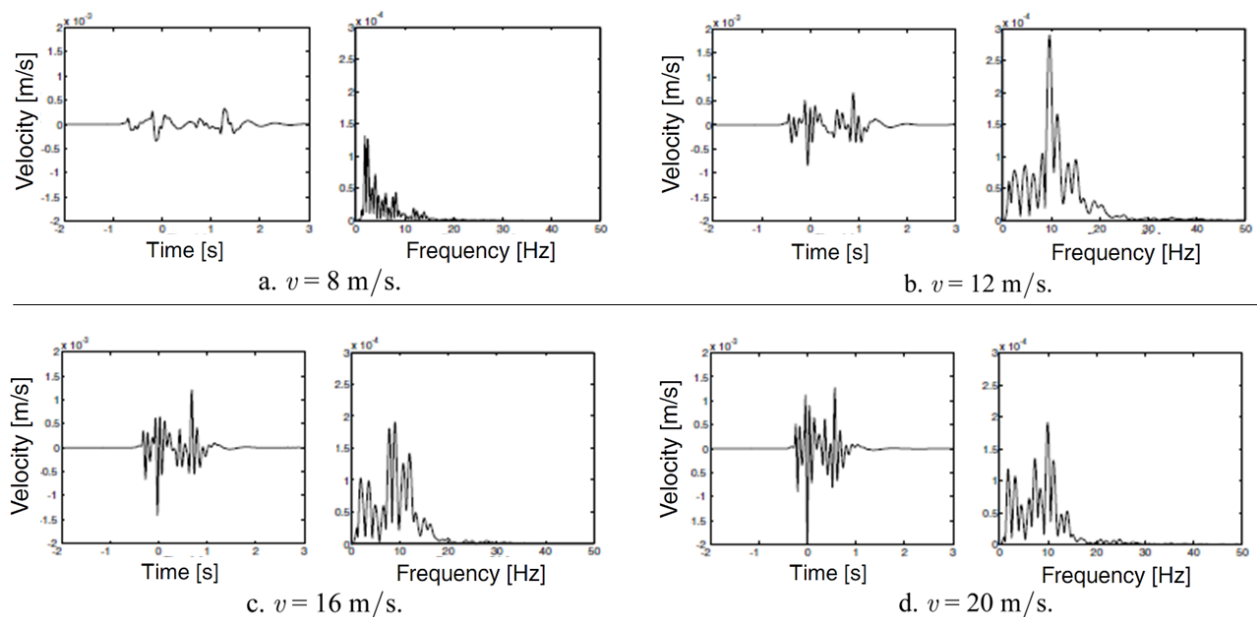


Figure 14. Time history and frequency content of the vertical soil velocity for a vehicle speed v equal to 8, 12, 16 and 20 m/s (Lombaert, Degrande, & Clouteau, 2000)

Concluding key factors influencing the free field traffic induced vibrations

Lombaert and Degrande also performed an elaborative parametric study to identify the key factors for the generation of free field traffic induced vibrations (Lombaert & Degrande, 2001). This study is related to parameters that determine the road unevenness, the vehicle dynamics and characterize the road and the soil. The influence of the vehicle speed is also discussed extensively. According to Lombaert and Degrande (Lombaert & Degrande, 2001) the following conclusions can be drawn from the parametric study:

- The relevant content of wavenumbers k_y of the longitudinal unevenness road profile in the wave domain is situated between 2.5 rad/m and 12 rad/m, corresponding to wavelengths between 0.5 m and 2.5 m. In this range, the wavenumber content of a joint in the road surface with a limited height has the same order of magnitude as the profile of a traffic bump with a much larger height. As a result, the free field vibrations generated by the passage of a vehicle on a traffic plateau and a joint in the road surface have the same order of magnitude (Figure 15).
- The height and the slope of the ramps are the predominant factors. The wavenumber content increases linearly with the height H . Steep ramps result in a disadvantageous high wavenumber content. The shape of the ramps is only of secondary importance.

- For the passage of a vehicle on a traffic plateau with sine shaped slopes, the free field vibration levels can increase with a factor 3 when the vehicle speed increases from 8 m/s to 20 m/s. However, in case of a passage on a joint in the road surface, the vehicle speed has no large influence on the generated vibrations.
- An excitation of the axle hop modes is responsible for the generation of the free field vibrations in the frequency range between 8 Hz and 15 Hz. A study of the vehicle FRF shows that, more than the gross vehicle weight, the masses of the individual axles are important. Vehicles with high axle masses will therefore generate the largest vibrations, both in laden and unladen state. The stiffness of the tires and the damping of the suspension system are parameters that affect the FRF's in an equally important way.
- At large distance from the source, the soil's material damping is very important. In the case of a stratified soil the nature of stratification determines at which frequencies the response is attenuated or amplified. The dynamic soil properties have to be determined up to a sufficiently large depth in order to accurately predict the low frequency content (large wavelengths) of the response.
- The results suggest that the gross vehicle weight does not play a large role in the generation of traffic induced vibrations. However, the experiment of Watts (Watts, 1990) showed that an unladen vehicle with steel leaf suspension generates larger vibrations than the laden vehicle. This is due to the loss of contact between the road and the vehicle, a non-linear effect that is not taken into account in the present study. Although the difference between the vibrations generated by unladen and laden vehicles is not always clear, the heavier vehicle types are still responsible for the generation of the highest vibration levels.

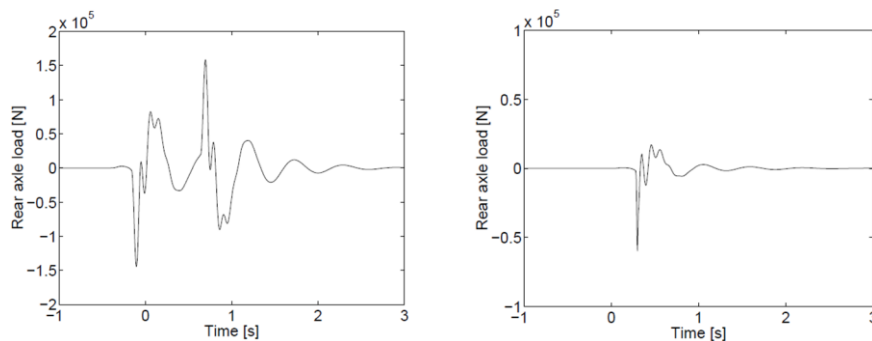


Figure 15. Time history of the predicted rear axle load for the passage of a truck on (left) a traffic plateau and (right) a joint in a road surface (Lombaert & Degrande, 2001)

4. Transmission of Vibrations

The vibrations generated by a source like road traffic can only reach a building's structure once it is transmitted through a medium. This medium consists of the soil which is different for every site and can even differ within 1 m^2 at one site. The soil is often layered and consists of soil types of different densities and stiffness laying over each other. Also, in the Netherlands the soil is often layered where typically softer layers overly stiffer soil layers. The wavespeeds and the depth of the different layers influence the frequencies of the generated waves in the soil medium.

In the previous sections it was already discussed that determining the wave propagation for a certain soil layering is difficult. However, several models have been created over the past half century which enables the prediction of wave propagation in layered media in a simplified manner. These approaches will be discussed in section 4.2. 'Layered Elastic Soil Halfspace'. However first a simpler case will be discussed concerning a non-layered homogenous soil (4.1. 'Homogeneous Elastic Soil') to give a more general introduction to the soil dynamics of the transmission path. A more extensive overview of this chapter is given in Appendix C: 'Appendix: Extensive overview of Chapter 4 "Transmission of Vibrations"'

4.1. Homogeneous Elastic Soil

Among many other authors (Verruijt, 2008), (Kramer, 1996), (Hölscher, 2016) and (Metrikine & Vrouwenvelder, 2018) give a comprehensive overview of the elastodynamics of a homogeneous elastic soil medium. A brief overview will be given in the present section, which is a confinement of the work of the previous mentioned authors. First let us consider waves in an infinite medium, in other words: a medium that has no bounds.

4.1.1. Waves in a three-dimensional infinite body

The derivation of the three-dimensional equations of motion follows the same steps as those used for one-dimensional propagation (see Appendix C: 'Appendix: Extensive overview of Chapter 4 "Transmission of Vibrations"'). However, in the three-dimensional case the various relationships are more complex and the derivation is more cumbersome. The three-dimensional case will be briefly discussed.

In the derivation a Cartesian coordinate system is used (x, y, z) with corresponding displacements u, v, w (Figure 16).

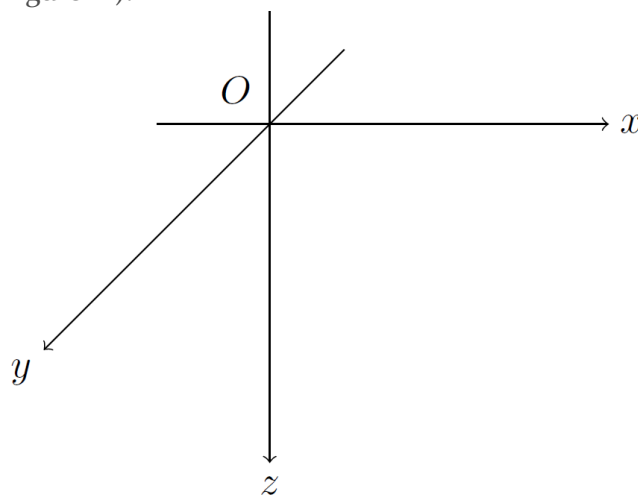


Figure 16. Cartesian coordinate system

The equilibrium equations, neglecting the body forces X give the three-dimensional equations of motion for an isotropic, linear elastic solid:

$$\rho \frac{\delta^2 u}{\delta t^2} = (\lambda + \mu) \frac{\delta \epsilon_0}{\delta x} + \mu \nabla^2 u \quad (4.1)$$

$$\rho \frac{\delta^2 v}{\delta t^2} = (\lambda + \mu) \frac{\delta \epsilon_0}{\delta y} + \mu \nabla^2 v \quad (4.2)$$

$$\rho \frac{\delta^2 w}{\delta t^2} = (\lambda + \mu) \frac{\delta \epsilon_0}{\delta z} + \mu \nabla^2 w \quad (4.3)$$

with:

$$\epsilon_0 = \frac{\delta u_x}{\delta x} + \frac{\delta u_y}{\delta y} + \frac{\delta u_z}{\delta z} \quad (4.4)$$

and the Laplacian operator ∇^2 represents:

$$\nabla^2 = \frac{\delta^2}{\delta x^2} + \frac{\delta^2}{\delta y^2} + \frac{\delta^2}{\delta z^2} \quad (4.5)$$

These equations can be manipulated to produce two wave equations. Consequently, only two types of waves can travel through such an unbounded solid: the compressional waves and the shear waves.

Compressional waves (P-waves)

The irrotational- or dilatational wave propagates through the body at a velocity:

$$c_p = \sqrt{\frac{\lambda + 2\mu}{\rho}} \quad (4.6)$$

This wave is called a P-wave (or primary wave) and c_p is referred to as the P-wave velocity of the material. The particle displacements are parallel to the direction of wave propagation (Figure 17).

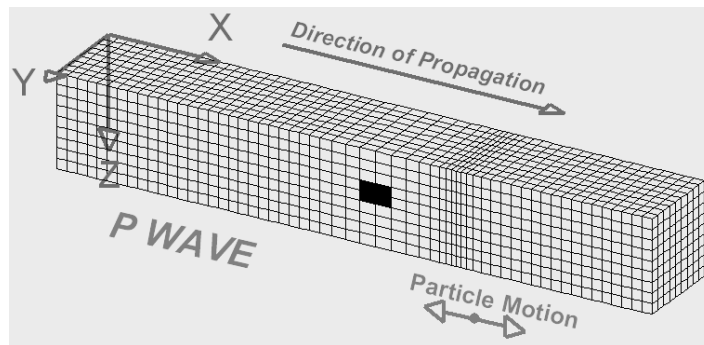


Figure 17. Representation of a P-wave. Alternating compression and dilation particle motion and parallel to direction of propagation (Braille, 2019)

Shear waves (S-waves)

The other type of waves is the equivoluminal- or distortional wave. The particle motion is described as a rotation about either the x-, y- or z-axis. The distortional wave will propagate through the solid at a velocity

$$c_s = \sqrt{\frac{\mu}{\rho}} = \sqrt{\frac{G}{\rho}} \quad (4.7)$$

This type of wave is commonly known as a S-wave (or shear wave) and c_s is referred to as shear wave velocity of the material. The particle motion is constrained to a plane perpendicular to the direction of wave propagation.

S-waves are often divided into two types: SH-waves, having particle motion occurring only in a horizontal plane and SV-waves, having particle motion occurring only in a vertical plane (Figure 18).

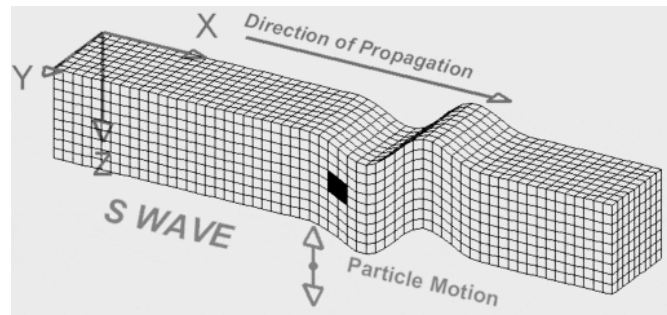


Figure 18. Representation of a S-wave. Alternating transverse particle motion in any plane (here in vertical plane) and perpendicular to the direction of propagation (Braile, 2019)

For comparison of the wavespeeds of the different kind of waves in an unbounded solid the ratio between the wavespeeds is computed as:

$$\frac{c_p}{c_s} = \sqrt{\frac{2-2\nu}{1-2\nu}} \quad (4.8)$$

It becomes obvious that the Poisson's ratio ν is the only factor that affects the ratio. For a typical Poisson's ratio of 0.3 for geologic materials, the ratio $c_p/c_s = 1.87$ and for a Poisson's ratio of 0.49, the ratio $c_p/c_s = 7.14$. This shows that, depending on the soil material, the P-wave can arrive at a certain location much earlier than the S-wave.

4.1.2. Waves in a three-dimensional semi-infinite body

Till now it was assumed that the body had infinite dimensional length. However, a realistic soil body cannot be assumed to be infinitely long in all directions. One dimension is restricted to the soil's surface (Figure 19) where, generally speaking, no stresses occur. This surface is often referred to as the planar free surface and introduces two new types of surface waves that are of primary importance for buildings: the Rayleigh wave and the Love wave. The Love wave can only exist when the soil is layered and is discussed in Appendix C: 'Appendix: Extensive overview of Chapter 4 "Transmission of Vibrations" Other types of surface waves also exist but are much less significant for excitation to buildings at the free surface (Kramer, 1996).

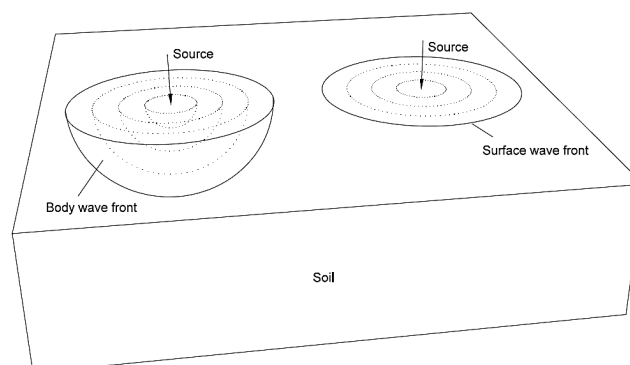


Figure 19. Geometrical attenuation for body waves (left) and surface waves (right) (Persson, 2016)

Rayleigh waves (R-waves)

The existence of elastodynamic waves propagating along the surface of an elastic half space was first considered by Rayleigh (Lord Rayleigh, 1885). This wave propagates near the free surface of an elastic halfspace and it strongly decreases exponentially with depth. The Rayleigh wave is generated by the interaction between the two body waves and the surface itself. A brief overview will be given of the characteristics of the Rayleigh wave.

The Rayleigh wavespeed c_r can be approximated by an analytical expression depending on the Poisson's ratio ν of the soil and the S-wave velocity c_s by the following expression (Bergmann & Hatfield, 1938):

$$c_r = \frac{0.87 + 1.12\nu}{1 + \nu} c_s \quad (4.9)$$

and thus, varies between $0.87c_s$ and $0.95c_s$ (Figure 20).

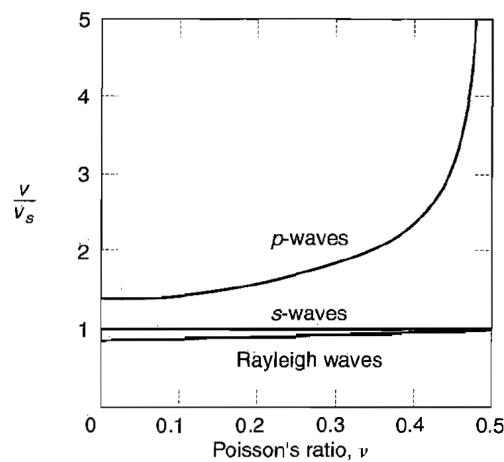


Figure 20. Variation of Rayleigh wave and body wave propagation velocities with Poisson's ratio relating to the shear wavespeed v_s (Kramer, 1996)

Rayleigh waves can be thought of as combinations of P- and S-waves (SV-waves in the case of a vertical (x,z)-plane). In isotropic solids, the individual particles move in ellipses parallel to the direction of propagation (Figure 21).

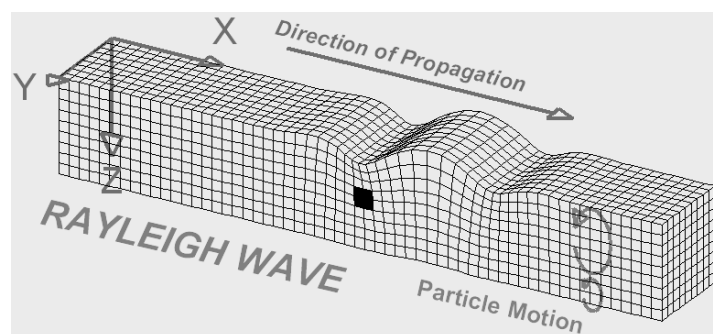


Figure 21. Representation of a Rayleigh wave. Elliptical particle motion in vertical plane and parallel to direction of propagation. Amplitude decreases with depth (Braille, 2019)

Also, the displacement amplitudes of the Rayleigh wave can be derived from the expression obtained when considering the velocity of the Rayleigh wave. The horizontal and vertical displacement amplitudes are illustrated for several values of Poisson's ratio (Figure 22) (Kramer, 1996).

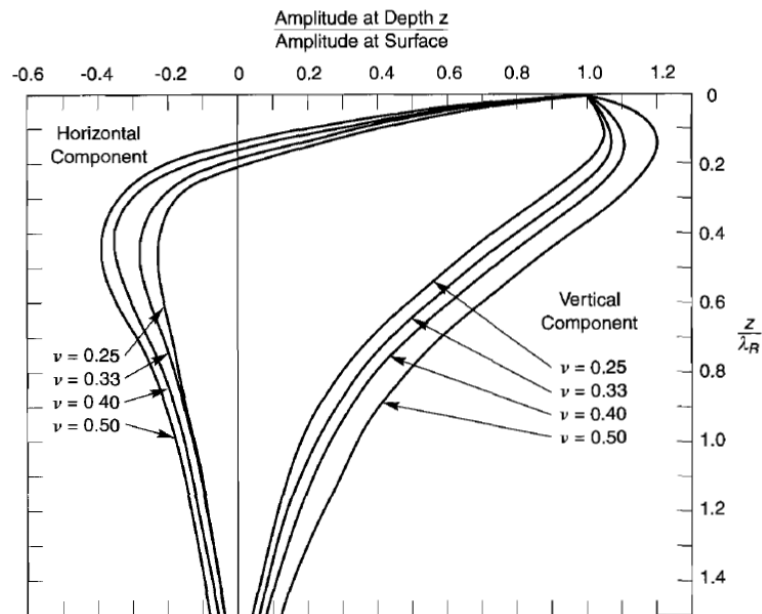


Figure 22. Horizontal and vertical motion of Rayleigh waves. A negative amplitude ratio indicates that the displacement deeper underneath the surface is in the opposite direction of the surface displacement (Kramer, 1996) after (Richart, Hall, & Woods, 1970)

From Figure 22 it appears that the horizontal displacement will be zero when the vertical displacement reaches its maximum (or minimum), and vice versa. Despite the fact that the amplitude decrease of the Rayleigh wave with depth is exponential, the superficial zone is still influenced by the soil material up to a depth of about a wavelength. In practice an absolute number for this wavelength is hard to determine since the soil is layered and all soil layers influence the wavelength. Also, the excitation frequency influences the (Rayleigh) wave frequency, and thus the wavelength. To give an impression of this Rayleigh wavelength one can do a very rough estimate for road traffic induced vibrations by assuming an excitation frequency of 8 Hz (road traffic induced vibrations in The Netherlands are usually within the range of $3 \text{ Hz} < f < 15 \text{ Hz}$) and a Rayleigh-wave velocity of the soil about 120 m/s (approximation for soft soil, taken from (Deltares, 2019)). The wavelength would then be: $\lambda = c_r/f = 120/8 = 15 \text{ m}$.

4.1.3. Wave attenuation

The amplitude of a wave decreases as the wave travels through the soil medium. There are two primary mechanisms that cause this attenuation of wave amplitude: radiation damping and material damping.

Radiation damping

Radiation damping is the result from the spreading of wave energy over a larger volume of material as it travels away from its source. In the case of a point source the surface waves exhibit radiational damping in the form of plane surface circles in the direction away from the source (an annular wave field) (Figure 19). However, body waves (P- and S-waves), generated by a point source attenuate in all three-dimensional directions in the form of volumetric spheres in the direction away from the source (Figure 19).

In summary for a linear elastic homogeneous halfspace, excited by a point source, a simple power law of the following type can express the radiation damping consequences on waves amplitude (Foti, 2000):

$$\frac{1}{r^n} \text{ with } n = \begin{cases} 2 & \text{for longitudinal and shear waves on the surface} \\ 1 & \text{for body waves (P – and S – waves) in the solid} \\ 1/2 & \text{for Rayleigh waves} \end{cases} \quad (4.10)$$

where r is the distance from the point source. However, these radiation damping terms are for the far field only. Close to the source, the terms are more in line with $1/r^2$ for Rayleigh waves and $1/r^3$ for body waves in the solid.

Due to the much slower attenuation of the Rayleigh wave, most vibration energy at a particular distance from the source is carried by the Rayleigh wave. Lamb has predicted the wavefield for a surface point source on an elastic homogeneous halfspace which can be observed in Figure 23.

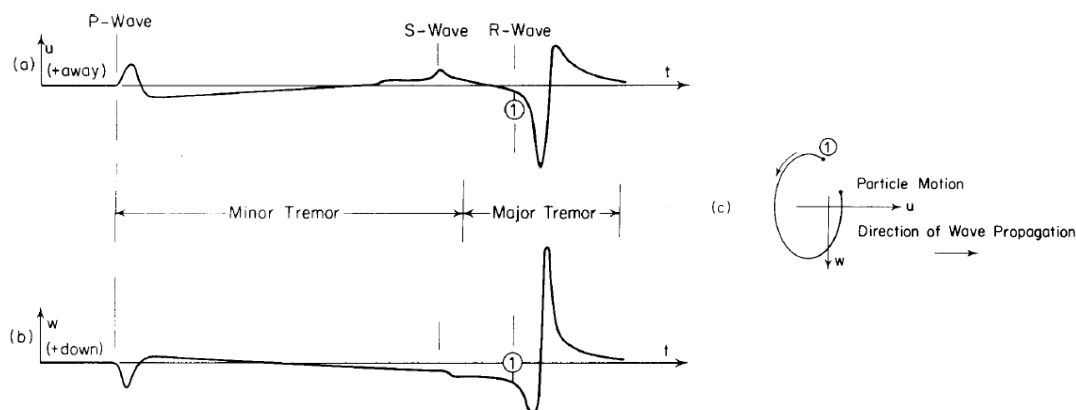


Figure 23. Complete wavefield predicted by Lamb (1904) for a surface point source on an elastic halfspace (a) horizontal radial motion; (b) vertical motion; (c) particle path of Rayleigh waves (Foti, 2000)

Material damping

Next to radiation damping the waves amplitudes also decay over distance because of material damping. Material damping occurs due to the absorption of energy by the materials the wave is travelling through. In the materials, part of the elastic energy of a travelling wave is converted to heat. The conversion is accompanied by a decrease in the amplitude of the wave.

4.2. Layered Elastic Soil Halfspace

The existing waves just described were found for a homogeneous soil halfspace. However, this is rarely a realistic situation. The soil is composed of layers, e.g. softer layers near the surface and stiffer layers deeper down into the soil. The composition of the layers is different for every region and can even deviate significantly within one particular building site.

The waves that were found in the previous section still exist in the realistic stratified soil, however the differences between the layer properties causes the incident waves to reflect and refract at the interface between two layers. This makes that predicting the vibration propagation in a stratified soil becomes a difficult task. However, many studies have been done to this problem and several approaches exist for theoretical prediction models (see Part III Method).

This section will briefly describe the mechanisms that occur in a stratified soil halfspace.

4.2.1. Three-dimensional wave propagation

In a layered soil the incident waves are partly reflected and transmitted due to the difference in stiffness between the soil layers and also due to the existence of the free surface. In general, the incident waves in a layered soil halfspace will not approach the interfaces at 90° angles. In

addition, the soil layers have different wave propagation speeds, depending on their material characteristics. As a consequence, both the reflected and transmitted waves have another propagating angle relative to the horizontal than the incident wave. Therefore, the transmitted waves are called refracted waves instead.

The direction of propagation of a wave is generally called a 'ray path'. Snell considered the change of direction of ray paths at interfaces between materials with different wave propagation velocities. Using Fermat's principle, Snell showed that

$$\frac{\sin i}{c} = \text{constant} \quad (4.11)$$

where i is the angle between the ray path and the normal to the interface and c is the velocity of the wave of interest. Snell's law indicates that waves travelling from higher-velocity material into lower-velocity material will be refracted closer to the normal to the interfaces (Figure 24).

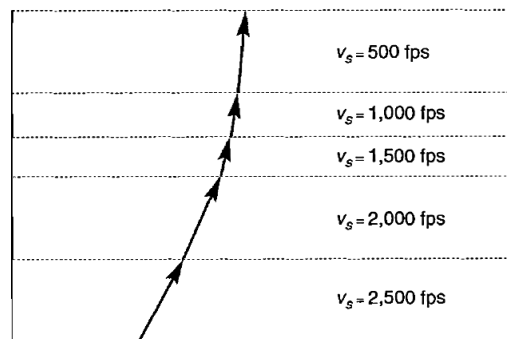


Figure 24. Refraction principle of an SH-wave ray path (reflected waves are not shown) (Kramer, 1996)

The creation of new waves and the reflection and refraction of the waves by these heterogeneities cause traffic induced vibration to reach a building by many different (ray) paths (Figure 25). Since the paths have different lengths and wavespeeds, the motion of the soil is spread out in time by this scattering effect.

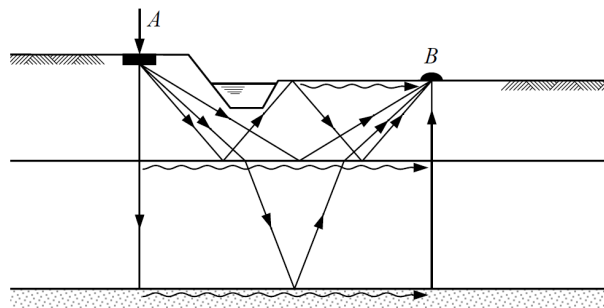


Figure 25. Simplified representation of possible paths along which energy is transferred (Spijkers, Vrouwenvelder, & Klaver, 2005)

4.2.2. Conclusion layered soil medium

In a realistic stratified soil, a complex wave field is present, consisting of different kind of waves, propagating with different wavespeeds and different particle motions. For a prediction model which should give quite accurate results for the soil response a complex mathematical model is required. Several models have been created by different authors, relying on different kind of mathematics but all with the same aim: to predict the soil response in a stratified soil halfspace. In the next part of the thesis, 'Part III Method,' one method will be chosen for implementation into the practical engineering design tool EDDABuS_{GS}.

4.3. Dominant Frequencies Soil Medium

As waves propagate through soil media, their amplification or attenuation is mainly dependent on the fundamental natural period of the soil deposit. This fundamental natural period depends on mechanical and geometrical characteristics of the layered soil deposit.

Figure 26 presents an illustrative example of the soil response for a soil in Amsterdam, The Netherlands, due to the passage of a truck at a distance of approximately 30 m from the receiver. The figure clearly shows an amplification of the soil response for the frequency range $4 \text{ Hz} < f < 7 \text{ Hz}$. This frequency range is generally within the frequency range of the eigenmodes of a truck, which are in the frequency range $1 \text{ Hz} < f < 15 \text{ Hz}$ (see 3.3 Road Traffic Induced Vibrations – Scientific Prediction Model). However, the strong peak at $f = 5 \text{ Hz}$ indicates some sort of resonance behaviour of the soil. This can be explained by the fact that for that particular frequency, the excitation frequency and the dominant frequency of the soil deposit are very close to each other, resulting in a strong magnification of the soil response. It is interesting to see in advance of the design process of a structure at which frequency the soil response is likely to be amplified strongly. The designer should then make sure that the eigenfrequencies of the structural system are far away from that dominant frequency (or frequencies) of the soil deposit.

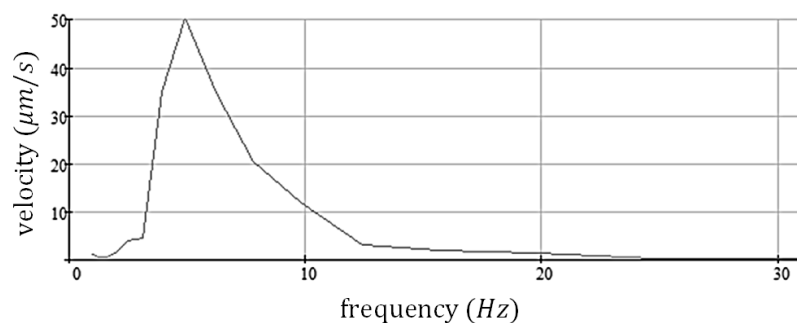


Figure 26. Illustrative soil response for soft soil deposits (e.g. Amsterdam, The Netherlands) excited by a passing truck at a particular distance from the road

4.4. Wave Barriers

The rectangular wave barrier (open or infilled trenches), frequently used in engineering practice, reduces the ground vibration by interception, scattering and diffraction of the surface (Rayleigh) waves of relatively small wave lengths. Properly designed open or infilled trenches can be used for an effective vibration isolation (or screening) system.

This section describes the results of one particular Master thesis research by A. de Zeeuw concerning wave barriers in layered soils. Two other researches concerning the effectiveness of wave barriers are included in Appendix C: ‘Appendix: Extensive overview of Chapter 4 ‘Transmission of Vibrations’.

4.4.1. Optimization of wave barriers in layered soils by A. de Zeeuw

A. de Zeeuw performed a research for his Master thesis in Civil Engineering at the TU Delft concerning the effectiveness of wave barriers in 2D layered soils when excited by a vertical harmonic point load at the surface. The soil is considered to be undamped.

Wave barrier in a two-layered soil

The 2D two-layered soils consist of a soft upper layer and a stiffer underlying halfspace (Figure 27 and Figure 28).

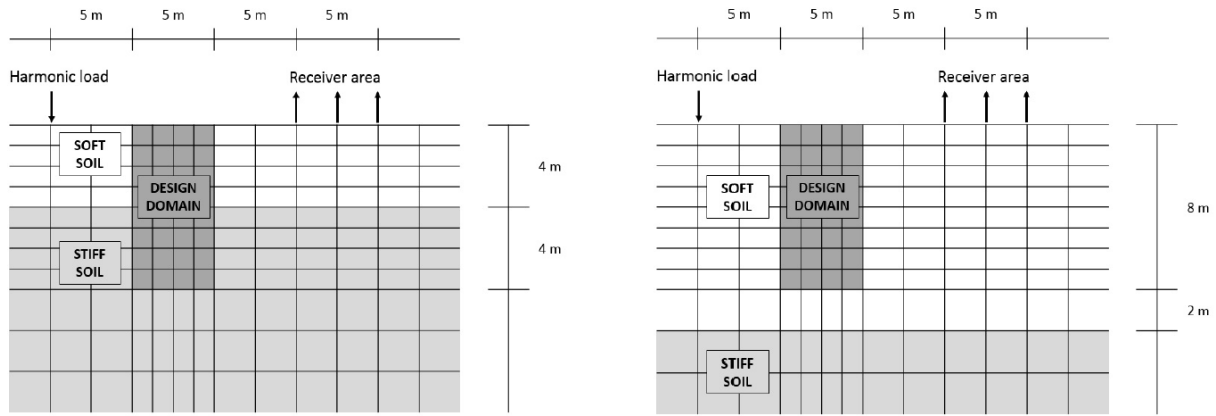


Figure 27. Inner FEM domain of the two-layered soil profiles. Left: shallow upper layer. Right: deep upper layer (de Zeeuw, 2018)

According to the research the following conclusions can be made regarding the effectiveness of wave barriers in 2D two-layered soils when excited by a vertical harmonic point load at the surface:

- The effectiveness of the wave barrier was sensitive to changes of the interface depth.
- Most of the energy from the loading is propagated in two wave types: a Rayleigh wave and a shear wave.
- The Rayleigh wave is propagating along the surface.
- Most energy of the shear wave is propagating at an angle of around 40 to 45 degrees.
- Much of the energy propagating as a shear wave is reflected from the interface upwards.
- The barrier shows a diminished effectiveness resulting from deviations in the interface depth.

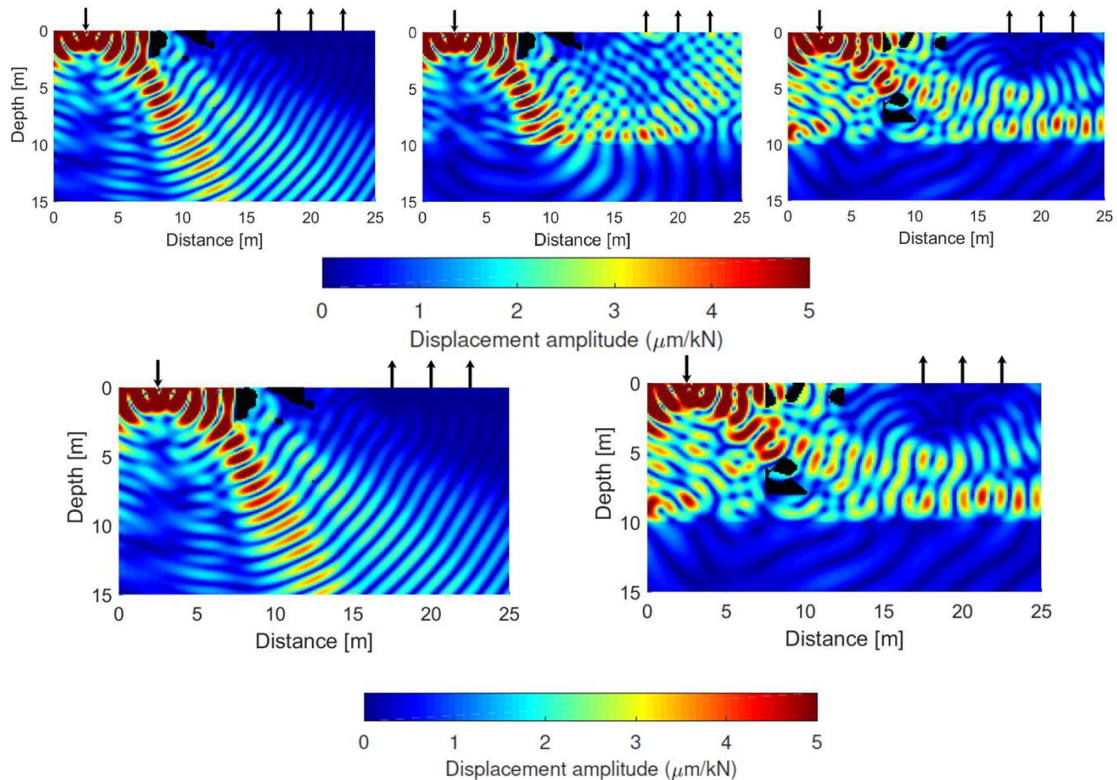


Figure 28. Displacement amplitude $\hat{u}_{real}(\mu\text{m}/\text{kN})$ for wave barriers optimized for 50 Hz. Left: \hat{u}_{real} for an optimized wave barrier in homogeneous soil. Middle: \hat{u}_{real} for a homogeneous-soil-optimized wave barrier in layered soil. Right: \hat{u}_{real} for an optimized wave barrier in layered soil model (de Zeeuw, 2018)

Wave barrier in a three-layered soil

The 2D three-layered soils consist of a stiff top soil layer on a soft intermediate layer and a stiffer underlying halfspace (Figure 29 and Figure 30).

According to the research the following conclusions can be made regarding the effectiveness of wave barriers in 2D three-layered soils when excited by a vertical harmonic point load at the surface:

- An optimization objective function for a receiver at the surface only can result in a wave barrier that decreases the energy at the surface, while increasing the energy below the surface.
- For the optimized wave barrier, much of the energy appears to be continuously reflected within the softer layer, never reaching the surface (Figure 30). This is possible for shear waves approaching the interface at an angle lower than the critical angle, resulting in a full reflection as a shear wave.
- The diminishing effect of the barrier in a three-layered soil with deviation of the interface depth is larger than for a two-layered soil.

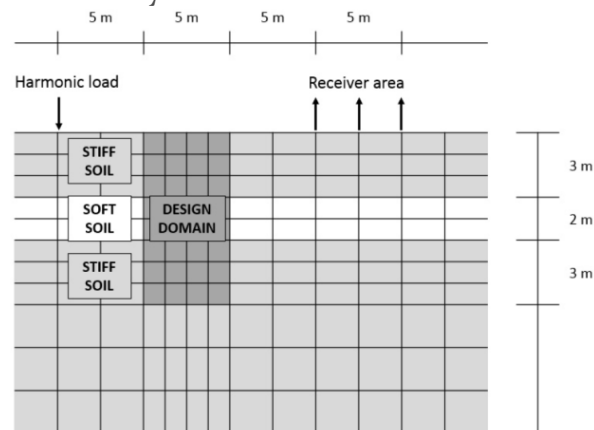


Figure 29. Inner FEM domain of the three-layered soil profile (de Zeeuw, 2018)

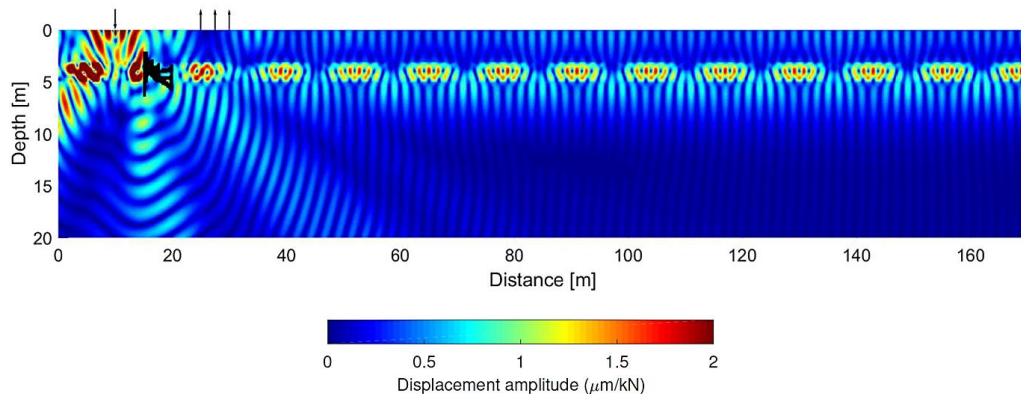


Figure 30. Displacement amplitude \hat{u}_{real} ($\mu\text{m}/\text{kN}$) for wave barrier optimized for 50 Hz. The embedded softer soil layer is used as a waveguide (de Zeeuw, 2018)

Optimized wave barrier in layered soil

Several optimization algorithms have been used to come to a new form of a wave barrier, optimized for the particular two-layered soil as described before. The final simplified wave barrier, which also takes manufacturability into account, has a relatively simple design while still providing a significant reduction of the vibration level at the receiver (factor 0.31). The design is essentially a combination of two straight vertical barriers connected horizontally at the surface, see Figure 31, where F_{wAVG} indicates the vibration level reduction at receivers at the soil surface due to that specific wave barrier.

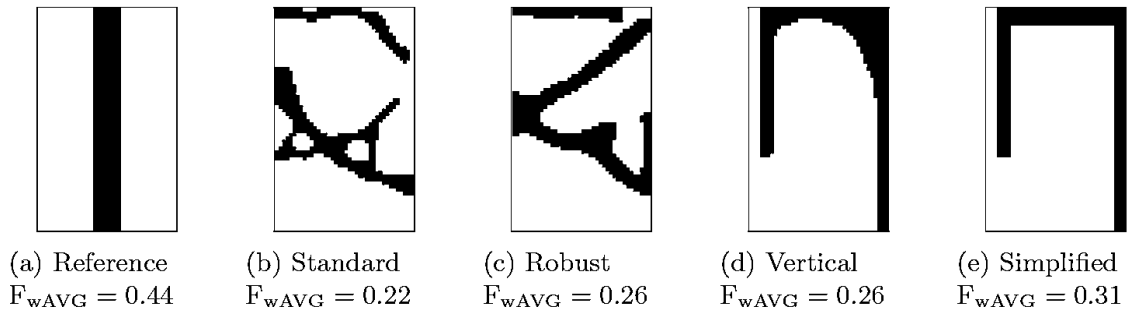


Figure 31. The shape of optimized wave barriers in a two-layered soil with increasing level of manufacturability with the soil interface at 10 m depth (de Zeeuw, 2018)

However, for the three-layer soil case it appears that, when taking into account the vertical optimization constraints, the reference barrier is in fact the optimal topology (Figure 32).

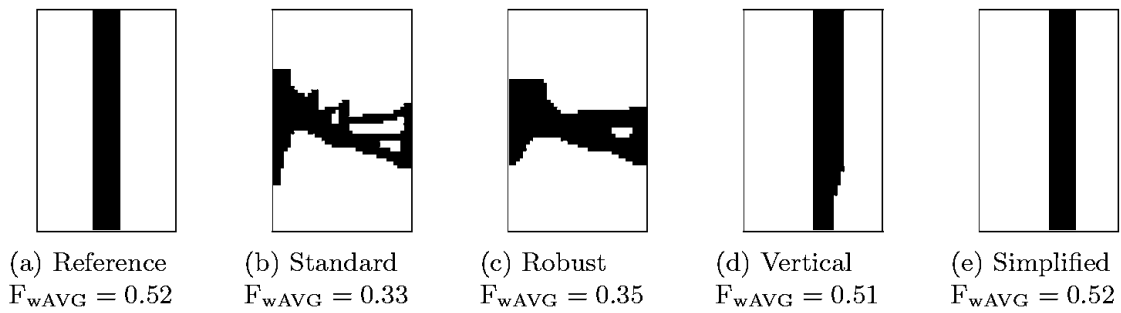


Figure 32. The shape of optimized wave barriers in a three-layered soil with increasing level of manufacturability (de Zeeuw, 2018)

4.4.2. Conclusion wave barrier

The stratification of the soil makes that a wave barrier can perform very differently from the case in which a wave barrier is used in a homogeneous soil halfspace. However, in all studies it is observed that the wave barrier does decrease the vibration levels in the soil in the close proximity behind the wave barrier. However, the soil surrounding this ‘shadowed’ region can exhibit amplified vibration levels. A general reduction factor created by the wave barrier cannot easily be determined and depends on every specific situation.

5. Structural System (Receiver of Vibrations)

The system to be considered for this thesis is a system with multiple degrees of freedom (MDoF) (e.g. the global dynamic response of the entire building). However, to remind the reader of the particularities of the dynamic response of a system, first a brief overview of the simple case of a single degree of freedom (SDoF) is presented. Thereafter the simple single degree of freedom case is extended to the case of a two degree of freedom system (which is already a multi-degrees of freedom system). After this introduction of a multi-degrees of freedom system, the two degrees of freedom system is extended to a n -multi-degrees of freedom system. Finally, the case of continuous systems (e.g. a local floor element) is briefly discussed. This system may be referred to as a n -multi-degrees of freedom system where n goes to infinity. All systems discussed in this thesis are supposed to be linear. This is justified by the fact that the vibration levels considered for vibration sensitive laboratory structures are relatively small so that all materials remain in their linear elastic state.

An extensive overview of this chapter is given in Appendix D: 'Appendix: Extensive overview of Chapter 5 'Structural System (Receiver of Vibrations)',' while the text in this chapter only highlights the most important particularities.

5.1. Simplification Laboratory Structure

The laboratory structure is simplified to a system that can be solved by established methods for structural dynamics. Since a laboratory structure has such strict vibration level criteria, the structure is often made very heavy and stiff in order to realize a system with a great resistance against vibrations (impedance) and natural frequencies as far away as possible from the fundamental excitation frequencies. The most straightforward approximation one can make for such a structure is, therefore, a rigid slab or a rigid building volume (depending on the design) which has only three degrees of freedom: two translational (horizontal and vertical) and one rotational (rocking). This system is often referred to as a multi-degrees of freedom system (MDoF system).

However, due to this simplification, only the global modal shapes of the system can be determined. In reality, the floors and walls are not infinitely rigid, but are flexible, which causes these elements to undergo local modal shapes. These local modal shapes of for example the floors and the walls are neglected by the simplification of rigidity, while the natural frequencies of these local elements are often different than the natural frequencies of the global rigid system. Therefore, in order to make a proper estimation of the vibration levels of a local floor, on which the laboratory equipment is placed, the local modal shapes should also be taken into account. Since these local modal shapes makes the interaction (chapter 6 Soil-Structure Interaction) between the structure and the soil mathematically very complicated, the interaction is only based on a rigid slab or rigid building volume. Once the response of the rigid structure is known, the local elements, e.g. the floors are analysed separately. The excitation of these local elements consists of the global response of the rigid structure.

5.2. Single Degree of Freedom system

Before hopping into the mathematics of the multi-degrees of freedom system (MDoF system), the simpler case of a single degree of freedom is briefly discussed to explain the fundamentals of the dynamic characteristics of a structure. The reader is expected to have some knowledge about the mathematical approach to such kind of systems, therefore only a brief explanation is given here. In case the reader wants to know more in-depth theory, he or she is kindly referred to the lecture notes of the Technical University Delft about Structural Dynamics, with course codes CT4140 (Spijkers, Vrouwenvelder, & Klaver, 2005), CT4145 (Metrikine, 2018) and CIE

5260 (Tsouvalas, 2018). The following text is a brief summary of the theory explained in these lecture notes.

5.2.1. Governing equations

To determine the dynamic response of a structural system, first the governing equations should be determined. For this thesis the Displacement Method is used for obtaining these equations.

5.2.2. Undamped free vibration

First the most simple case of a single degree of freedom (SDoF) will be considered: the free vibration of an undamped system (Figure 33) where the loading term $F(t)$ is zero.

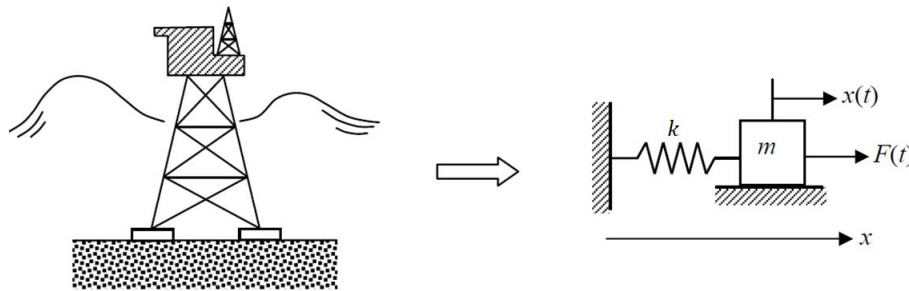


Figure 33. Idealization of horizontal motion of an offshore platform, excited by waves, by a mass-spring system with a translational degree of freedom (in x – direction) (Metrikine, 2018)

By applying the Displacement Method (displace the mass in the direction of the degree of freedom and write the equilibrium equations for the dynamic forces), the following equation of motion for the mass-spring system, which is a second ordinary linear differential equation, is obtained:

$$m\ddot{x} + kx = 0 \quad (5.1)$$

The natural frequency of the mass-spring system is equal to:

$$\omega_n = \sqrt{k/m} \quad (5.2)$$

This is the frequency, at which the mass-spring system would vibrate given arbitrary initial conditions and no loading.

5.2.3. Undamped forced vibration

The previously considered case was a state of free vibration, i.e. the loading term was zero. The obtained results indicate the characteristics of the system, independent of any loading applied. However, when a force is applied the dynamic response of the system is altered. The case of a harmonic loading is considered, since any time-dependent force can be represented as a superposition of harmonic forces with different amplitudes and phases.

Harmonic loading

Assume the external harmonic loading to be applied at the single degree of freedom as illustrated in Figure 33. The obtained equation of motion then is:

$$m\ddot{x} + kx = F_0 \cos(\omega t) \quad (5.3)$$

The general solution for this equation of motion is in the form of a homogeneous solution (the solution for the free vibration) plus a particular solution. The mass-spring system vibrates at

two frequencies, one being the natural frequency ω_n and the other being the frequency ω of the external force. The amplitude- and phase-frequency dependencies are shown in Figure 34.

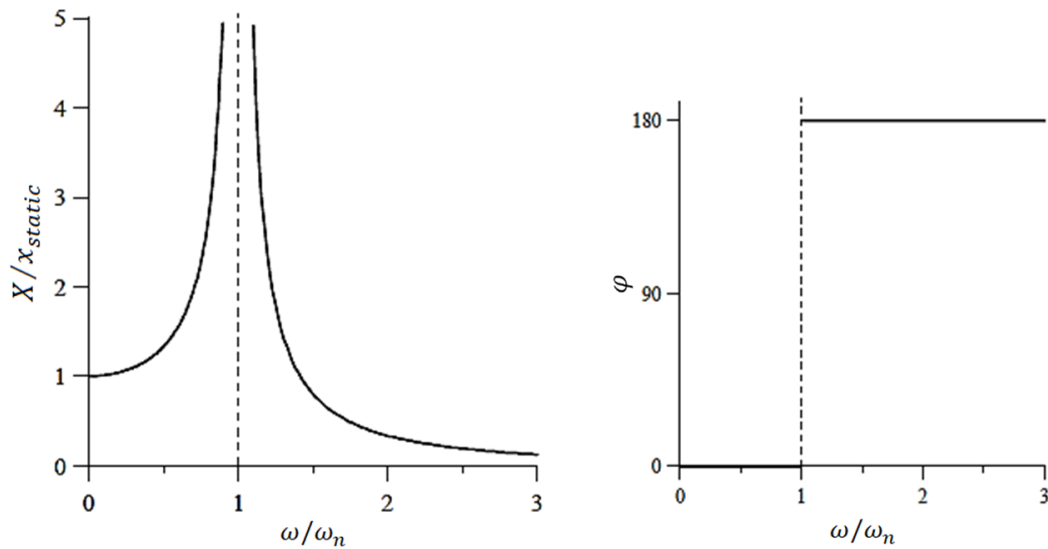


Figure 34. (left) Amplitude-frequency characteristic (magnification factor) and (right) phase-frequency characteristic (Metrikine, 2018)

These figures indicate that for ω close to $\omega = 0$, the loading frequency is extremely slow, and the mass will deflect by the force to its static deflection only. For very high frequencies $\omega/\omega_n \gg 1$, the force changes its direction so fast that the mass simply has no time to follow and the amplitude of the response is very small. At $\omega/\omega_n = 1$, the amplitude of the response becomes infinitely large. The frequency of the force coincides exactly with the natural frequency of the system, therefore, the force can push the mass always in the direction in which the mass moves itself, thereby increasing the amplitude of vibrations indefinitely. This phenomenon is known as resonance. The amplitude of resonant vibrations grows in time linearly and the displacement of the mass-spring system increases to infinity (note that this holds only in the undamped case).

5.2.4. Damped free vibration

Every engineering system experiences damping that dissipates the energy of vibrations. Now the mass-spring system is considered to be subject to viscous damping (Figure 35), which is proportional to the velocity of the mass.

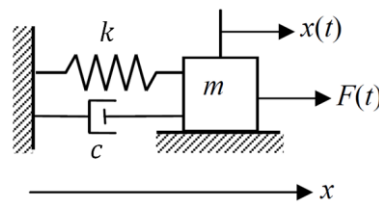


Figure 35. A mass-spring-dashpot system with a translational degree of freedom (in x – direction) (Metrikine, 2018)

Again, by applying the Displacement Method, and writing the balance of forces, one obtains the following scalar equation, which has one additional term compared to the undamped case:

$$m\ddot{x} + c\dot{x} + kx = F(t) \quad (5.4)$$

Due to the damping, the vibrations are attenuated over time (Figure 36). Thus, damping extracts energy from the system leading to a decay of the amplitude of vibrations.

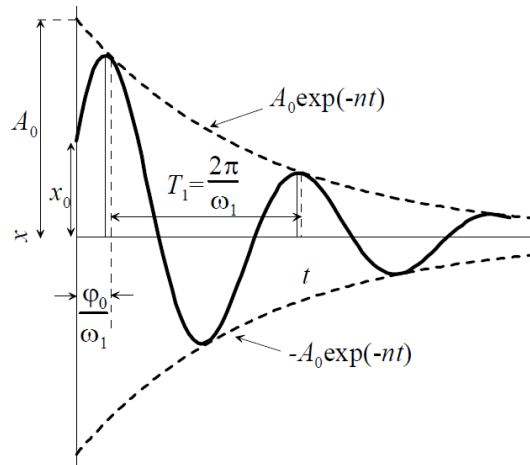


Figure 36. Free vibration of the mass-spring-dashpot system in the case $n < \omega_n$ (Metrikine, 2018)

The period of vibration T and its reciprocal, the frequency of vibration f_1 , depend also on the damping parameter n :

$$f_1 = f_n \left(1 - \frac{n^2}{2\omega_n^2} \right), \quad \text{where } f_n = \frac{\omega_n}{2\pi} \quad (5.5)$$

5.2.5. Damped forced vibration

When taking into account the loading term, a similar approach is followed as for the undamped mass-spring system.

Harmonic loading

Again, the case of harmonic loading is considered, and the equation of motion is:

$$m\ddot{x} + c\dot{x} + kx = F_0 \cos(\omega t) \quad (5.6)$$

The magnification factor of the vibration amplitude and the phase lag can be plotted as function of ω/ω_n for different amounts of damping (Figure 37).

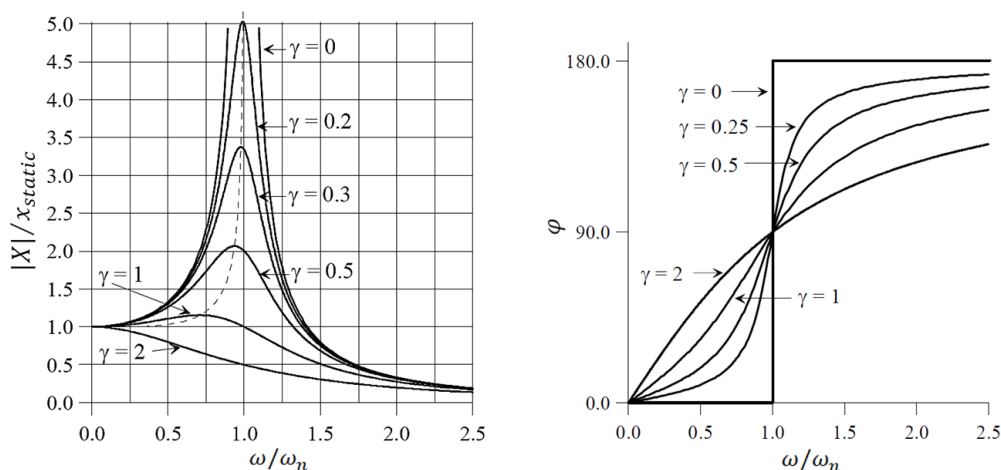


Figure 37. (left) Magnification factor and (right) Phase lag of the damped SDoF steady-state solution (Metrikine, 2018)

Note that, compared to the undamped SDoF-case (Figure 34), the peak at $\omega/\omega_n = 1$ for the damped SDoF system does not go towards infinity anymore, but is finite.

5.3. Two Degrees of Freedom system

Previously, only single degree of freedom systems have been discussed. These systems enable us to explain the resonance phenomenon and to calculate the natural frequencies of a number of structures. However, most realistic structures have multiple degrees of freedom. In order to explain additional phenomenon that occur in case of multiple degrees of freedom, the theory is developed to more complicated systems. As a first step, a system with two degrees of freedom is considered, which will yield the explanation of most 'vibration dampers' applied in practice. The most general undamped two degree of freedom system can be schematized as in Figure 38.

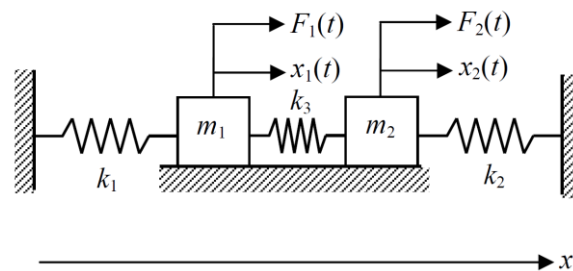


Figure 38. Undamped two degrees of freedom system with spring coupling (Metrikine, 2018)

Following the same principle as before, by applying the Displacement Method, two scalar equations are obtained:

$$\begin{aligned} m_1 \ddot{x}_1 + k_1 x_1 + k_3 (x_1 - x_2) &= F_1(t) \\ m_2 \ddot{x}_2 + k_2 x_2 + k_3 (x_2 - x_1) &= F_2(t) \end{aligned} \quad (5.7)$$

5.3.1. Undamped forced vibration

Now the case is considered in which a harmonic load is applied at one mass and the spring at the right-hand-side is not taken into account (Figure 39). The forced steady-state vibrations are considered. This vibration takes place at the frequency of the force.

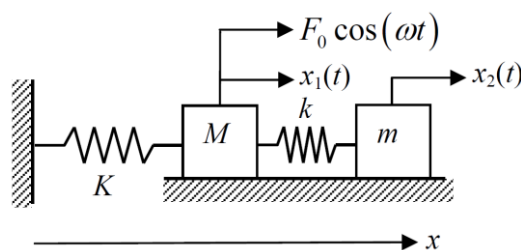


Figure 39. Forced two degrees of freedom system. The vibrations absorber k-m is attached to the main system K-M (Metrikine, 2018)

Since no damping is considered in this steady-state-case, the masses vibrate with infinite amplitudes when the frequency of the force becomes equal to one of the two natural frequencies of the system (Figure 40). Furthermore, if the frequency of the force becomes equal to the natural frequency of the auxiliary system (ω_b), the amplitude of the main system (A_1) becomes zero.

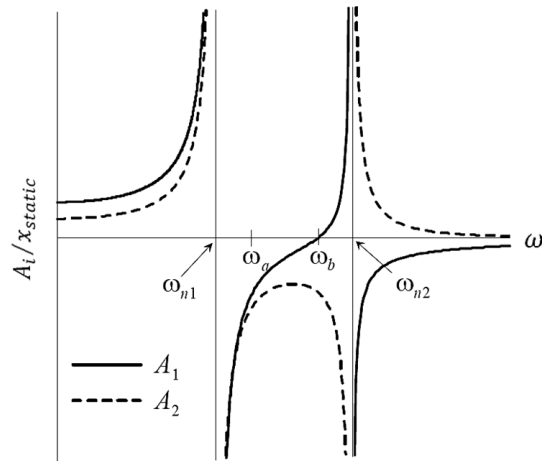


Figure 40. Displacement-frequency curves for the two degrees of freedom system (Metrikine, 2018)

5.4. Multi-Degrees of Freedom system

According to (Spijkers, Vrouwenvelder, & Klaver, 2005), many technical structures are so complicated that the dynamic behaviour of it cannot be described accurately with merely one or two degrees of freedom. Also, the structure to be considered in this thesis cannot be described by only one or two degrees of freedom. Therefore, in this section the two degrees of freedom system is expanded to the more general case of a n -multi-degrees of freedom system (n MDoF system). The text is a brief summary of the very comprehensive explanation, given in the lecture notes ‘Structural Dynamics CT 4140 – Part I Structural Vibrations’ of the Technical university Delft (Spijkers, Vrouwenvelder, & Klaver, 2005).

5.4.1. Differential equations (undamped case)

Again, the Displacement Method is used. As an example, a 2D block foundation with three degrees of freedom (3DoF, in the plane of the drawing) is considered (Figure 41). The degrees of freedom are two translations and a rotation about the centre of gravity, all three measured with respect to the state of static equilibrium, so that the deadweight load (mg) does not play a role in the dynamic analysis.

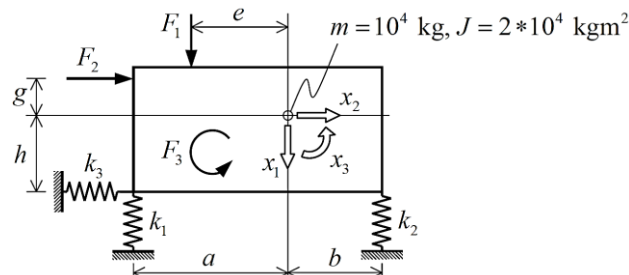


Figure 41. Foundation block with three degrees of freedom (Spijkers, Vrouwenvelder, & Klaver, 2005)

The equations of motion can be noted down in matrix notation:

$$\begin{bmatrix} m & 0 & 0 \\ 0 & m & 0 \\ 0 & 0 & J \end{bmatrix} \begin{bmatrix} \ddot{x}_1 \\ \ddot{x}_2 \\ \ddot{x}_3 \end{bmatrix} + \begin{bmatrix} k_1 + k_2 & 0 & ak_1 - bk_2 \\ 0 & k_3 & hk_3 \\ ak_1 - bk_2 & hk_3 & a^2k_1 + b^2k_2 + h^2k_3 \end{bmatrix} \begin{bmatrix} x_1 \\ x_2 \\ x_3 \end{bmatrix} = \begin{bmatrix} F_1 \\ F_2 \\ F_3 + eF_1 - gF_2 \end{bmatrix} \quad (5.8)$$

or symbolically:

$$\underline{M}\ddot{\underline{x}} + \underline{K}\underline{x} = \underline{F} \quad (5.9)$$

For this 3DoF-case the mass and stiffness matrices are both symmetrical (3 x 3) matrices in which the mass matrix is a diagonal matrix. However, for a n MDoF system, the matrices are of the size ($n \times n$).

5.4.2. Undamped free vibration of a n MDoF system

In the case the loading terms are zero, the n MDoF system undergoes only free vibrations. As homogeneous solution, a synchronic harmonic motion is assumed:

$$\underline{x}(t) = \underline{\hat{x}} \sin(\omega t + \varphi) \quad (5.10)$$

This solution implies that all degrees of freedom vary in time in the same manner. The free vibration is called a principal mode (or normal mode) of vibration. The unknown amplitude vector $\underline{\hat{x}}$ is called an eigenvector.

After substituting the proposed solution into the homogeneous system of equations, the generalized eigenvalue problem is obtained. A non-trivial solution will be found if the set of equations proves to be dependent, thus the determinant of the system should be equal to zero:

$$\det[-\omega^2 \mathbf{M} + \mathbf{K}] = 0 \quad (5.11)$$

with ω^2 representing the so-called eigenvalue. This leads to a polynomial of degree n in ω^2 , which is called the characteristic polynomial. The determination of the roots of the characteristic equation is often not possible without numerical methods. By the aid of the computer the n natural frequencies and n associated eigenvectors of the system with n degrees of freedom can be found, but are only determined up to scalar multiples (Spijkers, Vrouwenvelder, & Klaver, 2005). The eigenvectors represent the principal modes of vibration and are therefore often displayed graphically. So for linear systems with n degrees of freedom, there appear to be n principal modes of vibration (eigenmodes). The free vibration of the system is the summation of all possible eigenmodes. The remaining unknown constant can be found from the prescribed initial conditions.

5.4.3. Harmonic loads for a n MDoF system

The frequency response function of one specific degree of freedom $x_q(t)$ possesses vertical asymptotes at the position of the (n) natural frequencies, showing some kind of resonance phenomenon when the loading frequency is equal to one of the natural frequencies of the system (Figure 42). This phenomenon is similar to the previously described SDoF system (Figure 34 in 5.2.3 ‘Undamped forced vibration’).

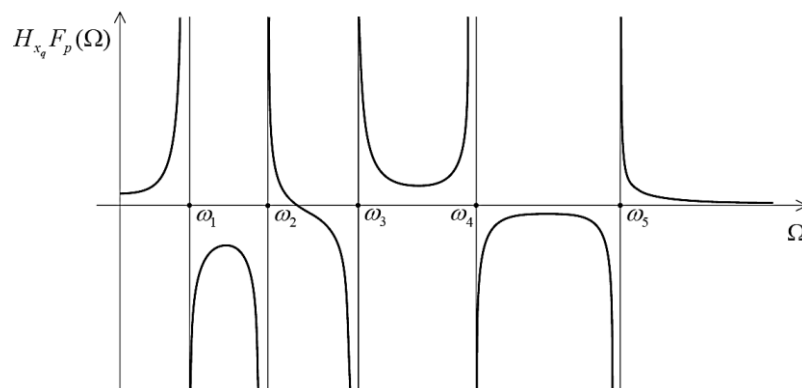


Figure 42. Frequency-response function for an undamped five degrees of freedom system for the degree of freedom $x_q(t)$ (Spijkers, Vrouwenvelder, & Klaver, 2005)

5.4.4. Viscous damped systems with n degrees of freedom

In case damping is taken into account for a n MDoF system, the equations of motions have an additional term:

$$\mathbf{M}\ddot{\underline{x}} + \mathbf{C}\dot{\underline{x}} + \mathbf{K}\underline{x} = \underline{F}(t) \quad (5.12)$$

In the case we are interested in one specific degree of freedom, for example the degree of freedom $x_q(t)$, the frequency response function (absolute values only) for this degree of freedom due to a harmonic loading in the point x_p has the form as in Figure 43. Similar to the damped SDoF system (5.2.5 'Damped forced vibration'), the resonance peaks are now finite due to the damping in the system.

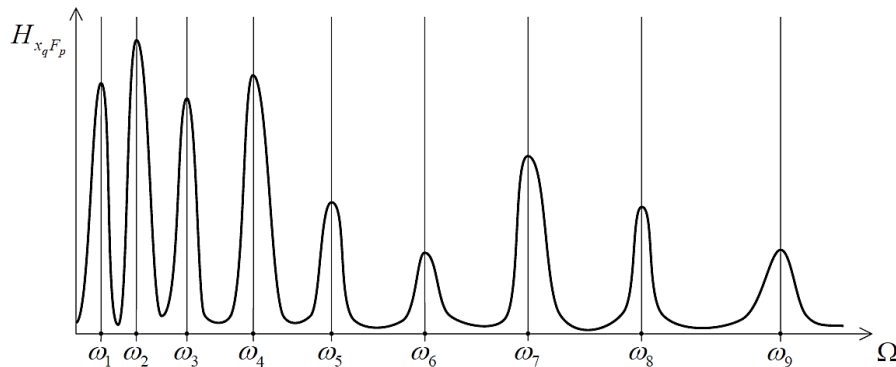


Figure 43. Example of a frequency response function for the degree of freedom $x_q(t)$ when a harmonic loading is applied in the point x_p (Spijkers, Vrouwenvelder, & Klaver, 2005)

5.5. Continuous Systems

The multi-degrees of freedom systems discussed before are classified as discrete systems. They are described by means of a coupled set of ordinary differential equations. However, when a system is analysed of which the mass is continuously distributed along a line, plane or volume, then also a continuous function should be chosen for the degree of freedom. These systems are typified as continuous systems. Their dynamic behaviour is described by means of partial differential equations (Spijkers, Vrouwenvelder, & Klaver, 2005). The soil, subject of the previous chapters, and described by an elastic half-space, is an example of a three-dimensional continuous system. In a linear structure two dimensions are small with regard to the third dimension, which is for example the case for the bending beam.

5.5.1. Bending beam (Euler-Bernoulli beam model)

An example of linear structures which can be described by a continuous system is the bending beam. The bending beam is described by means of a fourth-order partial differential equation. The way a beam is supported (clamped, hinged, free, guided or movable end) is essential for its dynamic behaviour. The supports are not expressed in the differential equations describing its dynamic behaviour, but they are introduced by means of so-called boundary conditions, which are needed when solving the differential equations.

5.5.2. Governing differential equations

The displacement in the positive z -direction is indicated by the symbol $w(x,t)$ and it represents the degree of freedom, which is a continuous function of the position variable x , and naturally is a function of the time variable t too. The beam has a flexural stiffness EI (Nm^2), a cross-sectional area A (m^2) and a mass density ρ (kg/m^3). The Displacement Method is used for the derivation of the equation of motion of an infinitesimal element dx of the beam (Figure 44).

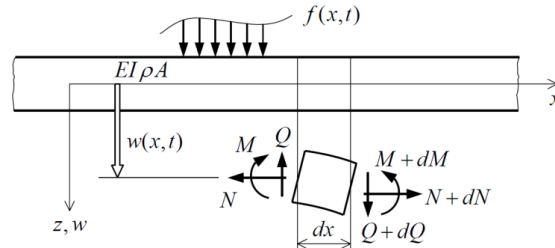


Figure 44. Sign convention and indication of the meaning of the symbols used for the prismatic beam (Spijkers, Vrouwenvelder, & Klaver, 2005)

The complete derivation of the problem is not included here. The reader is kindly referred to the lecture notes on Structural Vibrations ‘CT 4140 part I’ of the Technical University Delft (Spijkers, Vrouwenvelder, & Klaver, 2005). Only a very brief overview is given of the governing equations.

After substitution of the kinematic relations and the constitutive relation into Newton’s second law, the following inhomogeneous partial differential equation of the fourth order is obtained:

$$EI \frac{\delta^4 w(x, t)}{\delta x^4} + \rho A \frac{\delta^2 w(x, t)}{\delta t^2} = f(x, t) \quad (5.13)$$

This is commonly referred to as the Euler-Bernoulli beam.

5.5.3. Free vibration

In case the free vibrations are considered, again a solution $w(x)$ is sought for the eigenvalue problem. This solution is referred to as the eigenfunction. Eventually the solution is of the form:

$$\begin{aligned} w(x) &= C_1 e^{\beta x} + C_2 e^{-\beta x} + C_3 e^{i\beta x} + C_4 e^{-i\beta x} \\ &\text{or} \\ w(x) &= A \cosh(\beta x) + B \sinh(\beta x) + C \cos(\beta x) + D \sin(\beta x) \end{aligned} \quad (5.14)$$

in which:

$$\beta^4 = \frac{\rho A \omega^2}{EI} \quad (5.15)$$

This parameter β appears to be convenient for the further elaboration of the problem. The unknown constants are depending on the manner the beam is supported: the applied boundary conditions.

5.5.4. Boundary conditions

For the five unknown constants, only four boundary conditions exist: two at each end of the beam, thus one equation is missing. It appears that, apart from an unknown constant, the modal shapes of the structural system can be derived.

Boundary conditions concerning the deflection or slope are called kinematic boundary conditions. The boundary conditions concerning the bending moment and shear force are called dynamic boundary conditions. One types of in practice often applied boundary conditions will be briefly considered to illustrate the obtained results by applying the method for continuous systems: the simply support beam.

Simply supported beam

The bending beam appears to have an infinite number of natural frequencies. For each natural frequency there appears to be a corresponding eigenfunction $w_n(x)$. The three lowest eigenfunctions are displayed in Figure 45, each with an arbitrary (still undetermined) amplitude D_n .

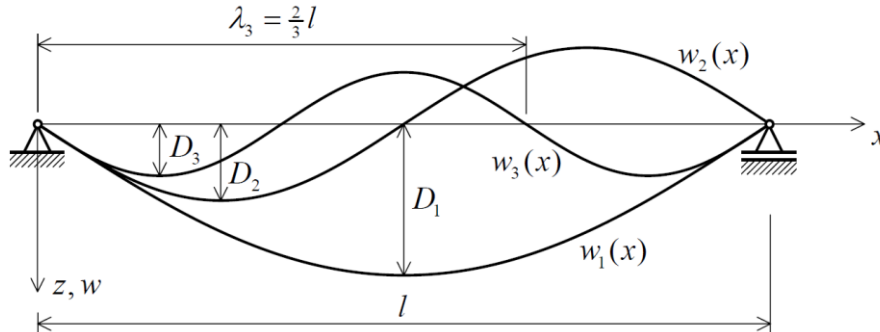


Figure 45. First three eigenmodes of the simply supported Euler-Bernoulli bending beam (Spijkers, Vrouwenvelder, & Klaver, 2005)

The remaining unknown constants are determined from the initial conditions at $t = 0$. This procedure is completely analogous with the way this occurs in discrete systems (the systems with a finite number of degrees of freedom described before). The eigenfunctions do have orthogonal properties with regard to the mass and the stiffness.

Natural frequencies beams - equivalent masses

The method of equivalent masses enables to find only the fundamental natural frequency in a simplified and approximate manner. Table 1 has been realized with which the first five natural frequencies of the Euler-Bernoulli beam can be approximated for specific boundary conditions. The natural frequencies can be determined, based on the value C (given in Table 1) by the formula:

$$\omega_n = C\sqrt{EI/(\rho A l^4)} \tag{5.16}$$

Table 1. First five natural frequencies and eigenmodes of Euler-Bernoulli beams with constant $EI/\rho A$ (Spijkers, Vrouwenvelder, & Klaver, 2005)

		$n = 1$	$n = 2$	$n = 3$	$n = 4$	$n = 5$
clamped	free	$C = 3.52$	$C = 22.4$	$C = 61.7$	$C = 121.0$	$C = 200.0$
simply supported	simply supported	$C = 9.87$	$C = 39.5$	$C = 88.9$	$C = 158.0$	$C = 247.0$
clamped	clamped	$C = 22.4$	$C = 61.7$	$C = 121.0$	$C = 200.0$	$C = 296.0$
free	free	$C = 22.4$	$C = 61.7$	$C = 121.0$	$C = 200.0$	$C = 298.0$
clamped	simply supported	$C = 15.4$	$C = 50.0$	$C = 104.0$	$C = 178.0$	$C = 272.0$
simply supported	free	$C = 15.4$	$C = 50.0$	$C = 104.0$	$C = 178.0$	$C = 272.0$

6. Soil-Structure Interaction

In the case of static design, fixed foundations can be assumed, however, in case of designing a structure excited dynamically, the effect of the soil must be taken into account. The interaction between the structure and the soil causes altering effects to the structural system and the soil vibrations near the structure. This interaction is called dynamic soil-structure interaction (SSI). Many studies have already been performed concerning SSI, however the description of it remains still a challenging task.

This chapter will briefly discuss the effects of soil-structure interaction on both the structure and the soil near the structure. The focus of this explanation will be on the dynamics problem considered for this thesis: a (partly embedded) structure, supported by foundation piles, and excited by an incident wave field propagating through the soil.

This section is greatly derived from the lecture notes ‘Structural Response to Earthquakes,’ written by A. Tsouvalas for the similar-named course at the Technical University Delft (Tsouvalas, 2018). Among other things, these lecture notes give a very comprehensive and understandable explanation of the SSI problem, which is summarized in the current chapter. Additional explanatory text for this chapter can be found in Appendix E: ‘Appendix: Additions to Chapter 6 ‘Soil-Structure Interaction’,’ concerning the effect of energy dissipation, non-linear soil response and the approaches for modelling of the soil-foundation system.

6.1. Effect of Soil-Structure Interaction on the Response of Structures

According to (Tsouvalas, 2018) the primary effects of SSI in the structural response can be summarized as follows:

Effects on the incident wavefield

The presence of the structure, resting on top of the soil, alters the free-field ground motion to some other (unknown) incident wavefield. This is usually referred to as kinematic interaction and it is caused by the fact that the equilibrium that needs to be satisfied at the structure-soil interface is not the same as for a stress-free surface, while the stress-free surface was the basis for the determination of the original site response spectra. Therefore, the engineer should consider the dynamic SSI to modify the site response spectra accordingly (Tsouvalas, 2018).

Effect on structural periods of vibration and energy dissipation

The presence of the soil can alter the structure’s vibration characteristics considerably. The amount of influence depends on the dynamic properties of both the structure and the soil. It also depends on the type of foundation (resting on the ground surface or embedded in the soil). The original structure, founded on a rigid base, is substituted by a new one, founded on an elastic (or visco-elastic) soil continuum. The effect is usually an elongation of the structural periods (and thus a decrease in natural frequencies) and an increased energy dissipation due to the radiation of waves into the soil during structural vibrations. However, there are cases in which the presence of a soft soil deposit can amplify the structural response significantly due to local site amplification and energy trapping (soil resonances) (Tsouvalas, 2018).

According to A. Tsouvalas (Tsouvalas, 2018) engineers usually neglect SSI in engineering practice, arguing that this yields generally conservative results (the radiation damping is not taken into account). However, this commonly shared opinion is not always justified due to a number of reasons:

- Structural period elongation, thus a decrease of the natural frequencies of the structural system, is not always beneficial, as it depends very much on the frequency content of the excitation input. In case the (fundamental) natural frequency of the structural system gets

closer to the dominant frequency of the excitation, the vibration response might even be amplified. In that case, neglecting SSI results in a non-conservative simplification.

- In a complex dynamic system, the actual response cannot possibly be known without first modelling the soil (in a coupled manner to the structure).
- Soil amplification effect may be overlooked.

6.2. Modelling of the Soil-Foundation System

The most comprehensive approach to solve SSI problems is through a full Finite Element (FE) analysis. However, such models are computationally expensive, therefore this approach is less convenient at the initial stages of the design of a structure. For this reason, several simplified methods have been developed, which allow for an equivalent representation of the soil reaction.

Shallow foundations

The consideration of the SSI effects can be greatly simplified by assuming rigid foundations. Since, for this thesis problem, the structure is indeed very rigid, this assumption is expected to give reliable results. First the shallow foundation on top of the soil surface is regarded.

Several theories exist to describe the dynamic reaction of a shallow rigid foundation block from generally applicable frequency dependent dynamic impedance matrices. Eventually the goal is to derive an equivalent (frequency-dependent) spring-dashpot representation of the soil reaction to a rigid foundation block. To do this, one of the methods is to separate the coupled soil-structure system in two substructures (subsystems): the rigid foundation block and the stratum beneath. Subsequent application of a unit amplitude (harmonic) force at each of the six degrees of freedom of a massless rigid foundation on the soil (Figure 46), provides each column of the so-called flexibility matrix. Inversion of the flexibility matrix yields the dynamic stiffness matrix. Instead of applying an unit force or moment to obtain first the flexibility matrix and then invert it, one can apply directly unit displacements and rotations to derive column-by-column the elements of the (frequency-dependent) stiffness matrix (Tsouvalas, 2018).

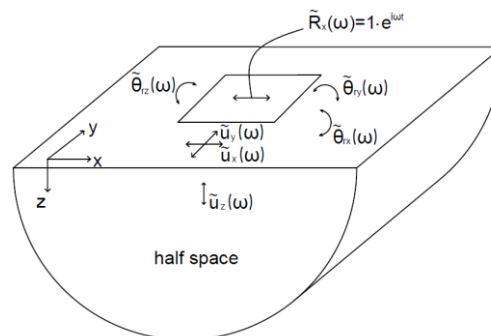


Figure 46. Derivation of the third column of the flexibility matrix, including all cross-coupling dynamic stiffness's (Tsouvalas, 2018)

The frequency-dependent stiffness matrix depends on:

- The shape of the foundation-soil system (circular, rectangular, etc.);
- Amount, or depth, of embedment;
- Characterization of the soil profile (variable layered soil);
- Mode of vibration and excitation frequency;
- Flexibility of the foundation block (rigid or flexible).

The frequency-dependent stiffness matrix $\tilde{K}(\omega)$ is a complex-valued matrix, which can be expressed as:

$$\tilde{\mathbf{K}}(\omega) = \text{Re}(\tilde{\mathbf{K}}(\omega)) + i\text{Im}(\tilde{\mathbf{K}}(\omega)) = \hat{\mathbf{K}}(\omega) + i\omega\tilde{\mathbf{C}}(\omega) \quad (6.1)$$

with:

$$\tilde{\mathbf{C}}(\omega) = \hat{\mathbf{C}}(\omega) + 2\beta/\omega\hat{\mathbf{K}}(\omega) \quad (6.2)$$

The real part of the complex-valued stiffness ($\hat{\mathbf{K}}(\omega) = \text{Re}(\tilde{\mathbf{K}}(\omega))$) reflects the inertia and stiffness of the supporting soil. It's dependence on frequency reflects solely the influence of the inertia of the soil.

The imaginary component of the complex-valued stiffness ($i\omega\tilde{\mathbf{C}}(\omega)$) reflects two types of damping: radiation damping ($\hat{\mathbf{C}}(\omega)$) and material damping ($2\beta/\omega\hat{\mathbf{K}}(\omega)$). Radiation damping is due to the energy carried away by waves from the structure into the soil (also see 6.1 Effect of Soil-Structure Interaction on the Response of Structures) and the material damping is due to the energy dissipation from hysteric soil behaviour. When multiple soil layers are present, numerical techniques are needed to derive the frequency-dependent stiffness matrix per excitation frequency.

Tables can be used in engineering design to obtain the dynamic stiffness coefficients and radiation dashpot coefficients for the evaluation of the soil impedance in each direction (Gazetas G. , 1991). However, these tables are only applicable for rigid foundation blocks and for the assumption of a homogeneous soil halfspace. The tables provide expressions for equations (6.1)-(6.2) which depend on the input parameters:

- Soil-foundation contact surface: area (A_b) and area moments of inertia about different axes (I_{bx}, I_{by}, I_{bz}).
- Half-width (B) and half-length (L) of the circumscribed rectangle.
- Shear modulus (G) and Poisson's ratio (ν) of the soil
- Depth of embedment (D)
- Side wall-soil contact surface (A_w) and depth (d), which should be smaller than the nominal contact surface to account for slippage and separation near the ground surface (this can deviate per mode of oscillation)

Effect of embedment

Embedment of the structure is investigated in the research computed by K. Miura (Miura, 2016), where tests were carried out using test specimen, first standing on the soil surface, and then partly embedded in the soil. According to the research the embedment increases the resonance frequency, but the specimen response amplitude is also more damped. A simplified building with basement and variable basement depth D was modelled, excited horizontally at the base of the building by an incident horizontal wavefield. The results show a similar phenomenon as the tests (Figure 47).

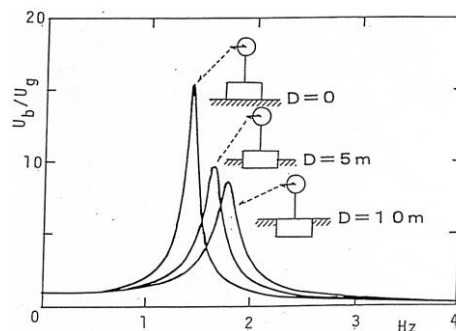


Figure 47. Effect of embedment depth D of the structure when excited horizontally at the structure's base. The response amplitude at the top of the building (U_b) is normalized by the excitation amplitude at the surface of the free field (U_g) (Miura, 2016)

When increasing the embedment depth, the resonance frequency of the coupling system is shifted towards the natural frequency of the building under the fixed-base condition (2 Hz), indicating a stiffening (increased restraint) effect. But also the amplitude of the system's vibration is more damped due to larger embedment depth (Miura, 2016).

Foundation on piles

To complete the elements that exhibit soil-structure interaction within this thesis research, foundation piles are considered. The formulations for pile foundations focus on the dynamic impedance matrix at the level of the pile-head alone and assume a pile of length L embedded in a homogeneous soil of depth $H = L$. With these formulations the impedances in case of swaying, cross swaying-rocking and rocking at the pile head are computed.

Again, tables can be used in engineering design to obtain the dynamic stiffness coefficients and radiation dashpot coefficients, used for the evaluation of the pile-soil impedance at the head of the pile in each direction (Gazetas G. , 1991). However, these tables are only applicable for simplified soil models (such as a homogeneous soil halfspace or a soil halfspace with linearly increasing stiffness with depth). The tables provide expressions for equations (6.1)-(6.2) which depend on the input parameters (Figure 48):

- Diameter of the pile (d);
- Length of the pile (L);
- Active length of the pile (L_c);
- Height from ground surface to bedrock (H);
- Characteristic soil profile (soil modulus profile with depth: linear, parabolic or constant);
- Shear wave velocity of soil (V_{SH}) at depth $z = H$.

Also the pile-to-pile interaction factors can be taken into account by these tables for assessing the response of floating pile groups. A more elaborate explanation is given in chapter 11 'Soil-Structure Interaction Modelling in EDDABuSGS'.

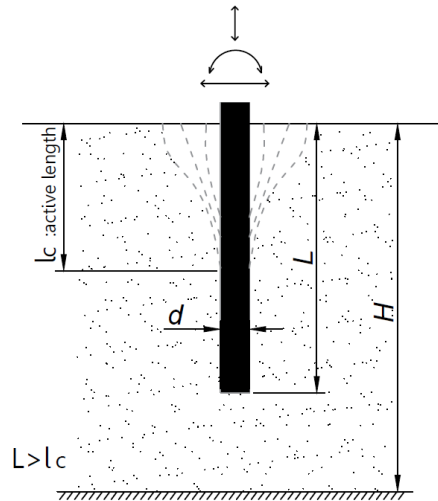


Figure 48. Input parameters for the tables considering SSI for foundation piles (Tsouvalas, 2018)

6.3. Modelling of the Soil-foundation System

At the initial stages of the design of a structure, simplified approaches are desired for taking into account SSI. When foundations are relatively rigid and/or of simple geometry, several methods exist to overcome the need for a full detailed description of the foundation-soil system. In principal, there are two main ways to solve dynamic SSI problems (Figure 49):

- Direct approach (suitable for both linear and non-linear formulations)
- Sub-structuring approach (limited to linear formulations)

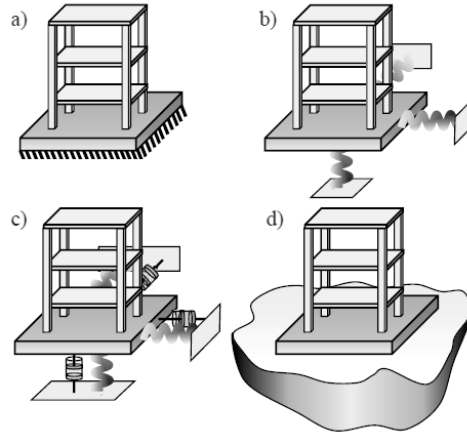


Figure 49. Levels of modelling the effect of the soil on the structure: (a) fixed support, (b) elastic support, (c) substructure approach, (d) direct approach (Pap & Kollár, 2018)

Due to the large computational effort of the direct approach and the computational efficiency of the sub-structuring approach in case of linear systems, the sub-structuring approach is the most practical approach for the initial design stages.

6.4. Conclusion Soil-Structure Interaction

In general, the soil-structure interaction can be rather significant for stiff structures resting on soft soil sites, while it may not be that significant for soft (flexible) structures founded on stiff soil deposits. The natural periods ($T = \frac{1}{f}$) of the soil-structure system are longer (the natural frequencies decrease) compared to a fixed-base structure. The ground motions due to SSI may be amplified or de-amplified due to the presence of the structure, and their estimation is important for attaining dedicated designs for structures excited by dynamical loading (Jia, 2018).

Basically the difference between the fixed base structure and the coupled soil-structure system in mathematical terms is as follows (Papadopoulos, 2018): The modal characteristics of structures, disregarding any interaction with the soil and any source of damping, are obtained as the solution of the generalized eigenvalue problem:

$$\det[-\omega^2 \mathbf{M} + \mathbf{K}] = 0 \quad (6.3)$$

If viscous damping is included inside the structure, the modal characteristics are obtained as the solution of the following quadratic eigenvalue problem:

$$\det[-\omega^2 \mathbf{M} + i\omega \mathbf{C} + \mathbf{K}] = 0 \quad (6.4)$$

When dynamic SSI is taken into account, the computation of the modal characteristics of the coupled soil-structure system generally requires the solution of the following eigenvalue problem:

$$\det[-\omega^2 \mathbf{M} + i\omega \mathbf{C} + \mathbf{K} + \tilde{\mathbf{K}}(\omega)] = 0 \quad (6.5)$$

Thus, now the determinant has a frequency dependent stiffness component which requires numerical solution methods to compute the modal characteristics of the structural system.

Part III

Method

7. Numerical Method for Computations

The literature study has given sufficient insight in the complex problem at hand so that the computational script of the practical engineering tool ‘EDDABuS_{GS}’ can be developed in the numerical programming software Python. First the loading generation phase is considered by the aid of the software FEMIX. This software uses input data-files and computes the characteristics of the moving loads and the soil response at any desired location in the layered soil stratum due to these moving loads. Python is used for computing the data-files needed by FEMIX and to implement the output of FEMIX as input to EDDABuS_{GS} which computes the dynamic structural response of the excited building. Both software packages (FEMIX and Python) will be briefly discussed in the following sections. Additional explanatory text for the section about FEMIX can be found in Appendix F: ‘Appendix: Additions to Chapter 7 ‘Numerical Method for Computations’’, concerning the Thin-Layer Method, material assumptions, the possibility of the inclusion of a structure on or in the soil, the input files needed by FEMIX and a brief overview of the interface of the software.

7.1. FEMIX

According to the website of FEMIX (Azevedo, 2019): “FEMIX is a non-commercial (Beta Version) Finite Element Analysis software which can be used for static and dynamic analysis of structures. Both linear and nonlinear material behaviour can be considered.” The development of FEMIX was initiated by Alvaro Azevedo in 1991, currently Assistant Professor at the University of Porto, Portugal, and has since then been further developed by Alvaro Azevedo and, among others, Joaquim Barros (1991-), Jose Sena Cruz (1996-), Ventura Gouveia (1999-), Sergio Neves (2005-), Rajendra Varma (2006-) and João Barbosa (2008-).

The version of the software FEMIX that is used for this Master Thesis considers soil- and structural vibrations only. The soil vibrations are computed based on the Thin Layer Method with Perfectly Matched Layers at the boundaries of the half-space (Boundary Element Method or BEM). The structural vibrations are computed based on a Finite Element Model (FEM). The soil and the structure are coupled by means of a BEM-FEM coupling. This section will briefly discuss some particularities of FEMIX.

7.1.1. Thin Layer Method in FEMIX

The Thin Layer Method (TLM) is a semi-discrete numerical technique used for the analysis of wave motion in layered media (Barbosa J. , 2013). The TLM discretizes the soil in perfect horizontal layers which are continuous in the horizontal direction but are discretized in several layers in the vertical direction (similar to a FEM-mesh, but only in the vertical direction). The horizontal directions are therefore described by analytical solutions, along which the material properties are assumed to be constant.

The stresses (or tractions t) at the layer boundaries / interfaces need to be in equilibrium and the displacements (u) at the interfaces need to be compatible. Interpolation functions $N(z)$ in the vertical direction are used for accommodating these requirements. If the order of the interpolation function is equal to 2, the interpolation function is linear and thus gives a linear relation between the displacements at the top interface and the bottom interface of the Thin Layer. In case the interpolation order is higher than 2, inner surfaces are created inside one Thin Layer. Figure 50 presents an interpolation order $m = 3$, which corresponds to a quadratic interpolation with one internal nodal surface. FEMIX uses interpolation functions with order $m = 3$. A system of linear partial differential equations is the result (Barbosa J. , 2013). The obtained results are exact for all three Cartesian coordinate directions (x, y, z).

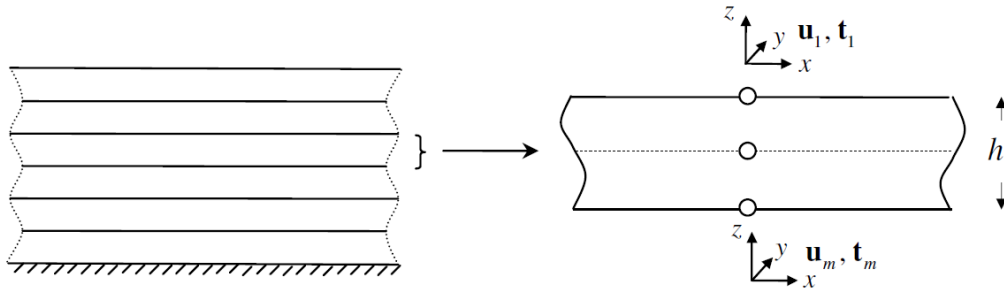


Figure 50. Discretization into thin-layers (left) and a thin-layer as a free body in space with the order of the interpolation function equal to 3 (Barbosa J., 2013)

7.1.2. Perfectly Matched Layer in FEMIX

Due to the discrete character of the TLM, the analyses are limited to bounded domains. However, soil is often represented as a half-space, which has two of the three coordinate directions that or not bounded (i.e. the domain goes to infinity). To simulate the infinite domains, the Perfectly Matched Layer (PML) has been successfully coupled to the TLM by Barbosa et al. (Barbosa, Park, & Kausel, 2012). As described in the work of Barbosa (Barbosa J., 2013), the PML is a numerical technique used for purposes similar to those of absorbing or transmitting boundaries, namely to suppress undesirable echoes and reflections of waves in infinite media modelled with discrete finite systems. In FEMIX, the PML is formulated based on the coordinate stretching approach. This approach causes the waves within the PML to attenuate exponentially. Also, since there is no impedance contrast at the PML boundary, no reflections take place no matter what the angle of propagation of the waves entering the PML is (while this was a problem with techniques involving the Paraxial Boundaries as were used before).

7.1.3. Possibilities of FEMIX

The part of FEMIX that is used for this Master Thesis particularly considers the wave propagation in layered soils. The waves are induced by moving vehicles which drive in the direction that is considered to be invariant for the geometry. FEMIX can compute the soil response for every given point coordinate in the (x, y, z) -domain. This section will briefly discuss the (im)possibilities of FEMIX.

Any vehicle model and road irregularity

Any 3D or 2D vehicle model can be implemented in the software, for example a train or a truck. For this Master Thesis, a heavy road vehicle (truck) is considered only and it will be implemented as a 2D multi-degrees of freedom system.

Instead of a perfectly horizontal track or road, which will barely induce soil vibrations, an irregularity can be implemented by means of a continuous function (the y -direction is assumed to be invariant, i.e. the 2.5D fundamental solution, therefore a continuous function is needed in the (y,z) -plane). In order to be able to consider all possible irregularity profiles, a Fourier expansion is most suitable. The Fourier expansion is a summation of sines and cosines, which, with a sufficient amount of summation terms ' N ,' can approximate the irregularity profile quite accurately. The Fourier expansion ' $f(x)$ ' can be represented as follows (note that N is taken equal to ∞):

$$f(x) = a_0 + \sum_{n=1}^{\infty} a_n \cos(nx\pi/L) + \sum_{n=1}^{\infty} b_n \sin(nx\pi/L) \quad (7.1)$$

$$a_0 = \frac{1}{2L} \int_{-L}^L f(x) dx$$

$$a_n = \frac{1}{L} \int_{-L}^L f(x) \cos(n\pi x/L) dx$$

$$b_n = \frac{1}{L} \int_{-L}^L f(x) \sin(n\pi x/L) dx$$

where:

- $f(x)$ = the function that is wanted
(over the range of x in-between the bounds of the integral)
- L = half of the period P of the function
- a_0, a_n, b_n = coefficients of the Fourier expansion

The greater the number N , the more the Fourier expansion $f(x)$ looks like the actual desired function. See for example the explanation of the Fourier expansion by the website 'mathisfun.com' (MathIsFun.com, 2019), where a square wave is created by a Fourier expansion with an increasing value of N (Figure 51):

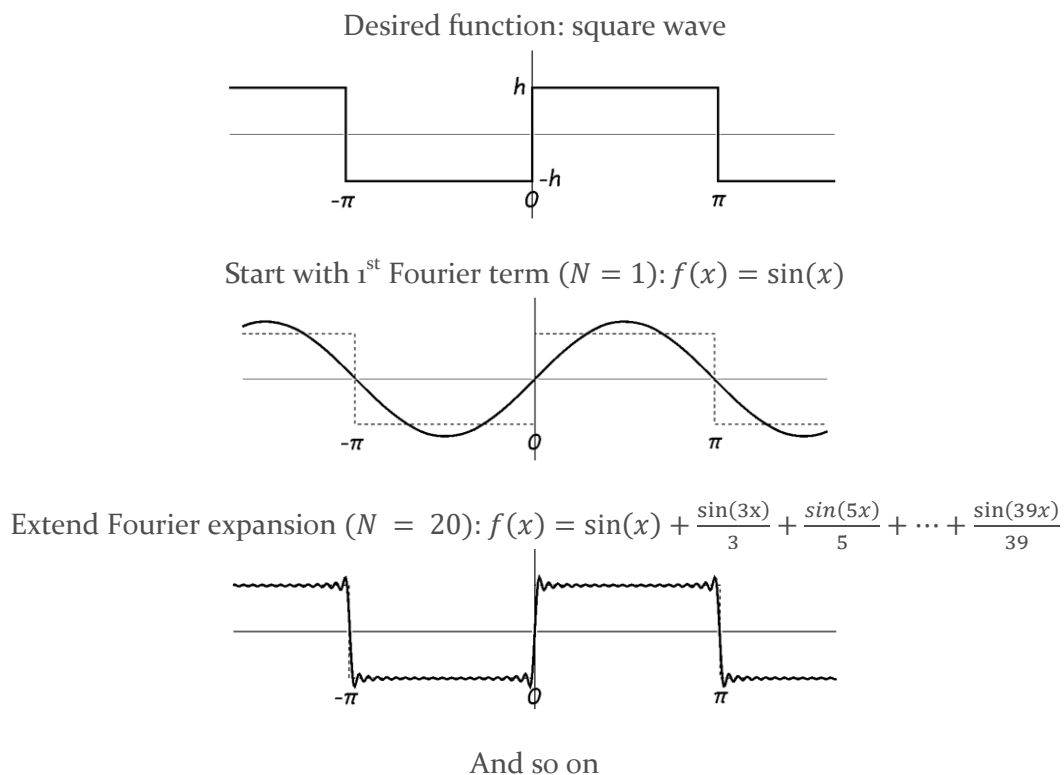


Figure 51: Principle of the Fourier expansion (representing any arbitrary function by a summation of continuous sines and cosines) (MathIsFun.com, 2019)

Since the Fourier expansion is continuous, there is always a repetition, i.e. there exists a period ' P ' at which the irregularity repeats itself. Since for this Master Thesis only one irregularity at a particular spot will be considered, the value of P should be large enough. The distance P should be taken such that for the receiver point $A(x, y, z)$ at an arbitrary location of interest in

the soil, the propagating waves initiated by the vehicle driving over the bump at longitudinal distance $y = s$ (m) are not influenced by the propagating waves initiated by the vehicle driving over the next bump at longitudinal distance $y = s + P$ (m) or over the previous bump at longitudinal distance $y = s - P$ (m) (Figure 52).

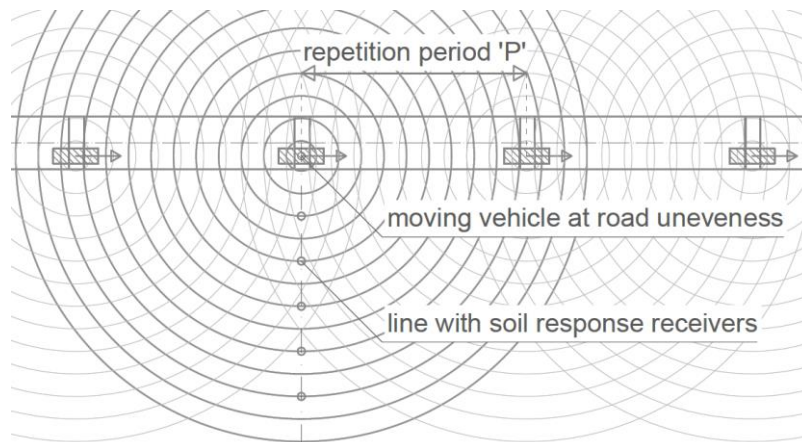


Figure 52. Principle of influence of the repetition period P in the Fourier expansion (snapshots taken at different time instances). In case P is taken too small the wave fields at the receiver points are influenced by multiple repetitive unevenness profiles

After implementing the vehicle model and the road irregularity in the form of a Fourier expansion in FEMIX, it is possible to investigate the dynamic vehicle behaviour by means of visualizing the load-frequency spectrums and the load-time representation for the different axles of the vehicle.

Any track- or road layering

The layering of the track or the road is implemented as a FEM model which can contain any elastic isotropic material for each element in the mesh. The FEM-model is coupled to the soil (BEM) by means of a BEM-FEM coupling, which takes into account the soil-structure interaction. This makes it possible to take into account the affected moving loads when the road and the soil underneath the road deform and therefore influence the generated loads. In other words: because the road material and the soil deform due to the loading, the irregularity takes a different shape and therefore affects the loading (similar to a second-order effect).

Any soil layering

Since the soil is modelled with the thin-layer method the soil layers must be perfectly horizontal, which is, in many cases, not very realistic. However, this assumption has shown for other experimental modelling (e.g. (Degrande & Lombaert, 2002)) that it can still produce reliable results. Apart from the soil layers being 100 % perfectly horizontal, any soil layering can be implemented with any material and depth of the soil desired.

The soil response can be computed for any given coordinate point in the layered soil. The soil response as a result of the moving loads can be computed for both the frequency- and time domain.

2D structure embedded in the soil or 3D structure on the soil

It is also possible to implement a structure in or on the soil, next to or at some distance from, the track/road. This structure is implemented as a FEM-model and is coupled to the soil by means of a BEM-FEM coupling that takes into account the soil-structure interaction. A numerical script (e.g. Matlab or Python) is needed for this coupling.

7.2. Python

Python is an open source programming language (Python Software Foundation, 2019) and is used for this Master Thesis research to compute the data-files which are needed as input for the FEMIX software. It will also be used to compute the structural response (EDDABuS_{GS}) to the excitation from FEMIX. The topics will be briefly addressed in the following subsections in order to give some insight into how Python works.

7.2.1. Numerical programming of input files

The data-files for the input of the software FEMIX require a lot of lines and repetitive actions. Therefore, it is much more convenient to write a numerical script that computes these data-files automatically based on a limited amount of input parameters. The input parameters for the computation of the data-files are gathered in one Excel-file. The Python script reads these input parameters and mainly uses definitions (assigning functions), for-loops and if/else-statements to compute all the lines of the data-files. The 'running' of such a Python script only takes a couple of seconds. An example of part of the script is presented in Figure 53.

```

13 # Fourier expansion of the road irregularity
14
15 # defining functions for the intervals between abrupt changes of the continuity of the road irregularity
16 # (abrupt change in the derivative of z(y) of the road profile)
17 def f1(y):
18     if coslike == 0:
19         f1 = 0
20     elif coslike == 1:
21         f1 = h1*( math.cos( (y+sb) * math.pi/2 * 1/(1/2*(L-sb)) ) - 1 )
22     return f1
23 s11 = -L
24 s12 = -sb
25
26 def f2(y):
27     if coslike == 0:
28         f2 = h/(sb-st)*(y+sb)
29     elif coslike == 1:
30         f2 = h2*( math.cos( (y-(sb-st)+st) * math.pi/2 * 1/(sb-st) ) + 1 )
31     return f2
32 s21 = -sb
33 s22 = -st

```

Figure 53. Example of the numerical Python scripts that computes the data-files needed as input for FEMIX. The current part of the script defines a function that is used for the computation of the coefficients of the Fourier expansion of the road irregularity

Every Python script is programmed such that after the computation of the script the text 'computation of sheet complete' is printed to the screen of the user. If this message appears, the computation of the script ran smoothly, otherwise the script could not be computed entirely but was interrupted by an error. If the latter is the case one should check whether the input of the Excel-file is correct. If so, the user should contact the script writer (the author of this Master Thesis) in order to find where the error could originate from.

7.2.2. Computing structural response

FEMIX will be used to compute the soil response due to the passage of a specified vehicle over a specified road unevenness with specified road layering, on top of a specified layered soil medium. That soil response is used as input for the calculation of the structural response, which will be computed by writing another Python script: EDDABuS_{GS}. EDDABuS_{GS} will include all numerical computations for computing and analysing the dynamical structural response and is the main part of the final computational tool.

8. Verification Projects

The numerical software described in the previous chapter will be used to write a computational script for obtaining results for the soil response (soil vibrations in the free field by FEMIX) and for obtaining results for the structural response (vibrations in the structural elements by EDDABuS_{GS}). The results should be reliable in order to be used as indication of an educated guess about the vibration levels in the soil but mainly for the structure. Therefore, the results should be verified with experimental computed vibration levels for both the free field soil and the structural elements. Verification projects are needed for this verification work. Since the design tool is aimed to be used for projects in The Netherlands at first, or more particularly, for projects of Pieters Bouwtechniek, it is desired to verify the design tool with experimental measurements performed for locations in The Netherlands. However, the projects of Pieters Bouwtechniek appear to be considered in a very practical sense and not all information is provided that is needed for modelling the dynamic problem. Therefore, a more scientific approach is considered: after performing additional literature study, the scientific and experimental work of prof. Degrande et al. of the KU Leuven seemed to be promising. Their work will be summarized in 8.1 'Projects KU Leuven' together with figures to which the results of the design tool can be compared, and eventually to which the results of the design tool can be verified. An extensive overview of this chapter is given in Appendix G: 'Appendix: Extensive overview of Chapter 8 'Verification Projects'.

8.1. Projects KU Leuven

The KU Leuven has performed experimental measurements to validate their own numerical prediction model. Several projects were used to validate their numerical model.

The paper 'The experimental validation of a numerical model for the prediction of the vibrations in the free field produced by road traffic' (Degrande & Lombaert, 2002) describes the project concerning the validation of the predicted free field soil response due to the passage of a truck driving over an artificial road unevenness. This project will be referred to as 'verification project Degrande et al. (1) – Free Field' from hereon.

The paper 'Validation of a Source-Receiver Model for Road Traffic-Induced Vibrations in Buildings. I: Source Model' (Degrande, Pyl, Lombaert, & Haegeman, 2004) describes the project concerning the validation of the predicted soil response in front of a building due to the passage of a truck driving over an artificial road unevenness. This project will be referred to as 'verification project Degrande et al. (2) – Soil Building' from hereon.

The paper 'Validation of a Source-Receiver Model for Road Traffic-Induced Vibrations in Buildings. II: Receiver Model' (Degrande, Pyl, & Clouteau, 2004) describes the project concerning the validation of the predicted structural response of a building due to the passage of a truck driving over an artificial road unevenness. This project will be referred to as 'verification project Degrande et al. (3) – Building Response' from hereon.

A brief summary will be given in the following subsections. The computed results by FEMIX and EDDABuS_{GS} will be verified by comparison with the results of the verification projects Degrande et al. (1) to (3).

8.1.1. Verification Project Degrande et al. (1) – Free Field

The verification project 'The experimental validation of a numerical model for the prediction of the vibrations in the free field produced by road traffic' (Degrande & Lombaert, 2002) will be used to verify the computed results by FEMIX for the free field soil response.

Results

The generated loads due to the passage of the truck (modelled as a 2D 4DoF dynamical model) over the artificial unevenness are given in both the frequency- and time domain (Figure 54).

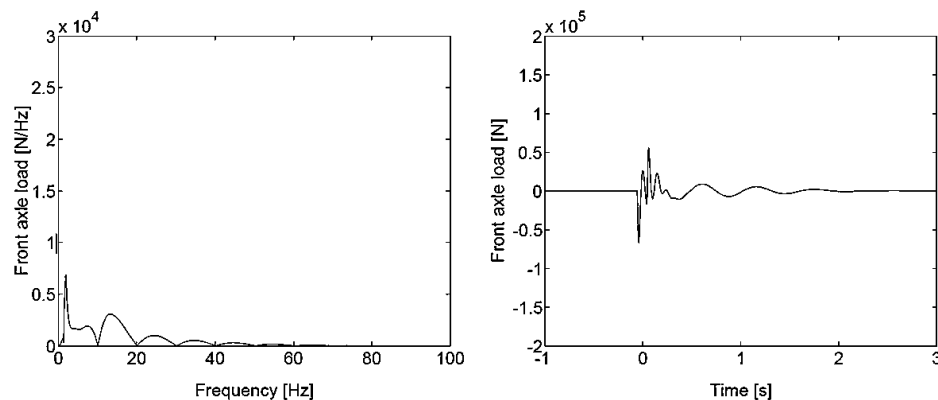


Figure 54. Frequency content (left) and time history (right) of the predicted front axle load of the Volvo FL6 truck when passing the artificial profile at a vehicle speed $v = 58$ km/h (Degrande & Lombaert, 2002)

The vibration levels (speed of the soil particle motion) have been determined for several receiver points. The most interesting points to verify with are points FF2, FF4 and FF5 since these are the points that are measured in all three directions. In this way the results of FEMIX can be compared for all three (x-, y- and z-) directions. Figure 55 shows the soil response of point FF4 (at 16 m from the middle of the road) for the z-direction. The soil response results for the other directions and the other points are given in Appendix G: ‘Appendix: Extensive overview of Chapter 8 ‘Verification Projects’.

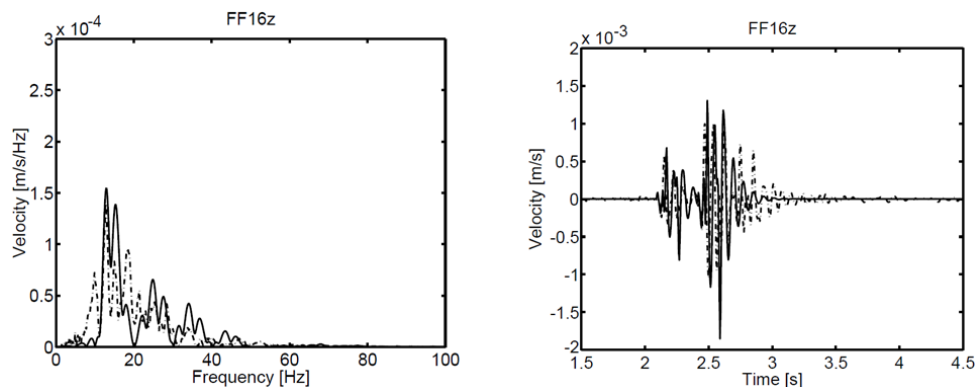


Figure 55. Predicted (solid line) and measured (dash-dotted line) soil response in the z-direction of point FF4 (at 16 m from the middle of the road) in the frequency- (left) and time (right) domain (Degrande & Lombaert, 2002)

8.1.2. Verification Project Degrande et al. (2) – Soil Building

The verification project ‘Validation of a Source-Receiver Model for Road Traffic-Induced Vibrations in Buildings. I: Source Model’ (Degrande, Pyl, Lombaert, & Haegeman, 2004) will be used to verify the computed results by FEMIX for the soil response. Note that this project cannot be used for the verification of the free field soil response because the presence of the building (reflection of vibrations) has to be taken into account for this project.

Results

The generated loads due to the passage of the truck over the artificial unevenness are given in both the frequency- and time domain (Figure 56).

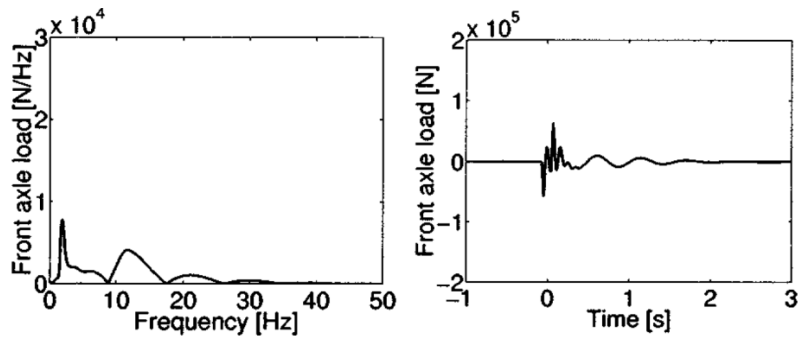


Figure 56. Frequency content (left) and time history (right) of the predicted front axle load of the Volvo FL6 truck when passing the artificial profile at a vehicle speed $v = 50$ km/h (Degrande, Pyl, Lombaert, & Haegeman, 2004)

The vibration levels (speed of the soil particle motion) for point FF3 can be found in Appendix G: ‘Appendix: Extensive overview of Chapter 8 ‘Verification Projects’’. Figure 57 shows the soil response of point FF3 for the z-direction.

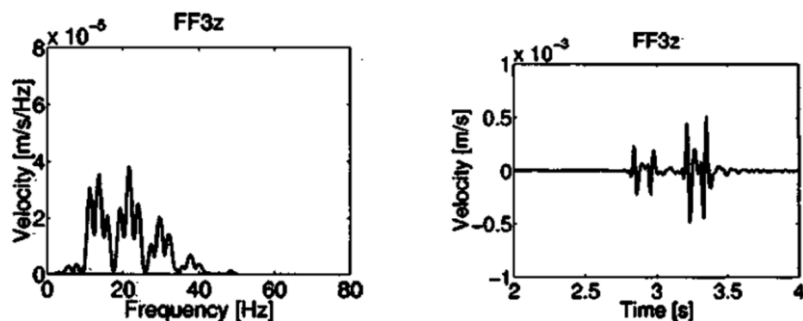


Figure 57. Predicted soil response in the z-direction of point FF3 (at 16 m from the middle of the road) in the frequency- (left) and time (right) domain (Degrande, Pyl, Lombaert, & Haegeman, 2004)

8.1.3. Verification Project Degrande et al. (3) – Building Response

The verification project ‘Validation of a Source-Receiver Model for Road Traffic-Induced Vibrations in Buildings. II: Receiver Model’ (Degrande, Pyl, & Clouteau, 2004) will be used to verify the computed results of the structural response by EDDABuSGS. For the source and transmission characteristics, see the Verification Project Degrande et. al. (2) – Soil Building, as described before.

Results

The structural response / vibration levels for point F11 (located at the first floor of the building, closest to the road) can be found in Appendix G: ‘Appendix: Extensive overview of Chapter 8 ‘Verification Projects’’. Figure 58 shows the predicted structural response (velocity) of point F11 for the z-direction.

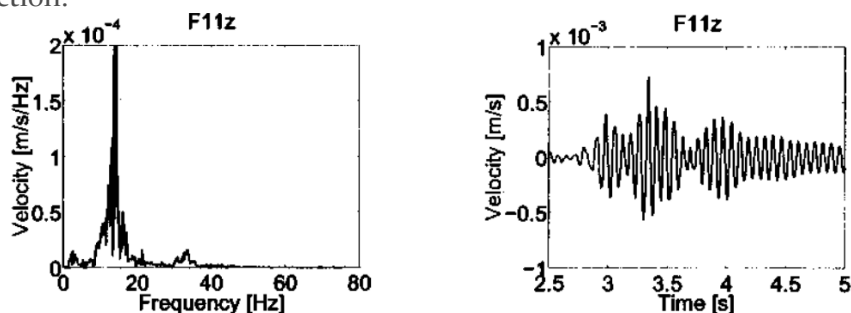


Figure 58. Measured structural response in the z-direction of point F11 (on the ground floor of the building) in the frequency- (left) and time (right) domain (Degrande, Pyl, & Clouteau, 2004)

8.2. VU Amsterdam

EDDABuS_{GS} eventually considers the dynamic response of the soil for locations in The Netherlands. Therefore, the confined information provided for the project ‘VU Amsterdam site’ of Pieters Bouwtechniek is used for determining the characteristics of the road irregularity and the vehicle. In the documents of DGMR a soil layering is presented which is used by them for predicting the vibrations in the soil and the structure of this specific project (Table 15 in Appendix G: ‘Appendix: Extensive overview of Chapter 8 ‘Verification Projects’’). This soil layering is used to model the layered soil in FEMIX. Also, figures are presented for the soil response at some particular locations on site for the passage of a sand truck laden with 40 tonnes of sand (and Figure 59). It is stated that the soil response in vertical direction, with a distance of 30 m from the road, due to the passage of the truck is approximately 250 $\mu\text{m/s}$. The sand truck is of the type MAN TGS 10x8 WSA (Figure 6o).

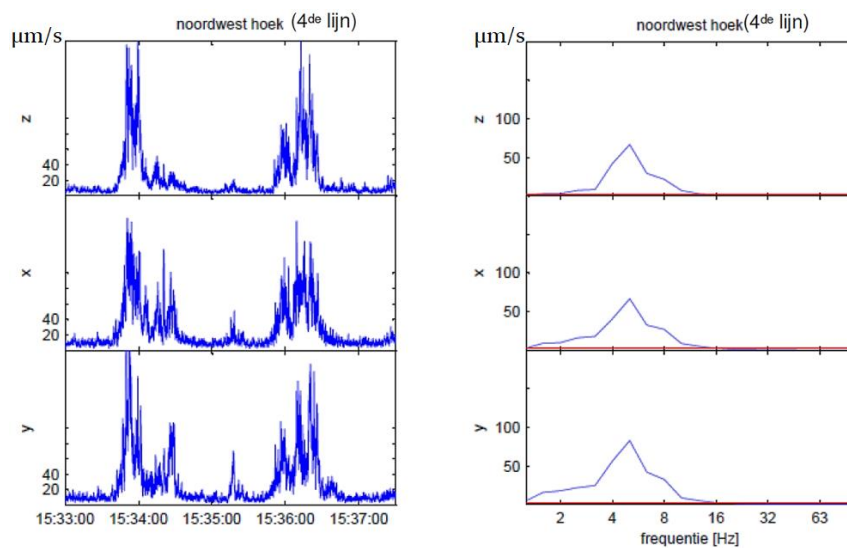


Figure 59. Soil response at the top left measurement point from Figure 172 at the VU Amsterdam site, taken from the documents of TNO (Koopman, 2012)



Figure 6o. MAN TGS 10x8 WSA sandtruck used for the measurements at the VU Amsterdam site (modderaandebanden.nl, 2019)

9. Source Modelling and Results in FEMIX

The possibilities of the computational tool will be limited in order to narrow the scope of this Master Thesis research. For the source-part (of the parts source, transmission, interaction, receiving structural system) only two specified vehicles will be considered: a light truck with two axles (for verification with the Degrande projects) or a heavy truck with five axles (for considering the excitation similar to the VU Amsterdam situation), which drives over a specified road irregularity: a speed bump with specific dimensions (height, length, slopes).

This section will describe what vehicle models are used, what the vehicle characteristics are and how the road irregularity is modelled. Additional explanatory text for this chapter can be found in Appendix H: ‘Appendix: Additions to Chapter 9 ‘Source Modelling and Results’,’ concerning the mathematical description of the road unevenness and the generated moving loads.

9.1. 2D Vehicle Model

Similar to the verification projects discussed in 8 ‘Verification Projects’ the vehicle that is implemented in the software FEMIX consists of a linear 2D 4DoF dynamical model (Figure 61). All the values for the vehicle characteristics are as specified in the verification projects (Appendix G ‘Appendix: Extensive overview of Chapter 8 ‘Verification Projects’’).

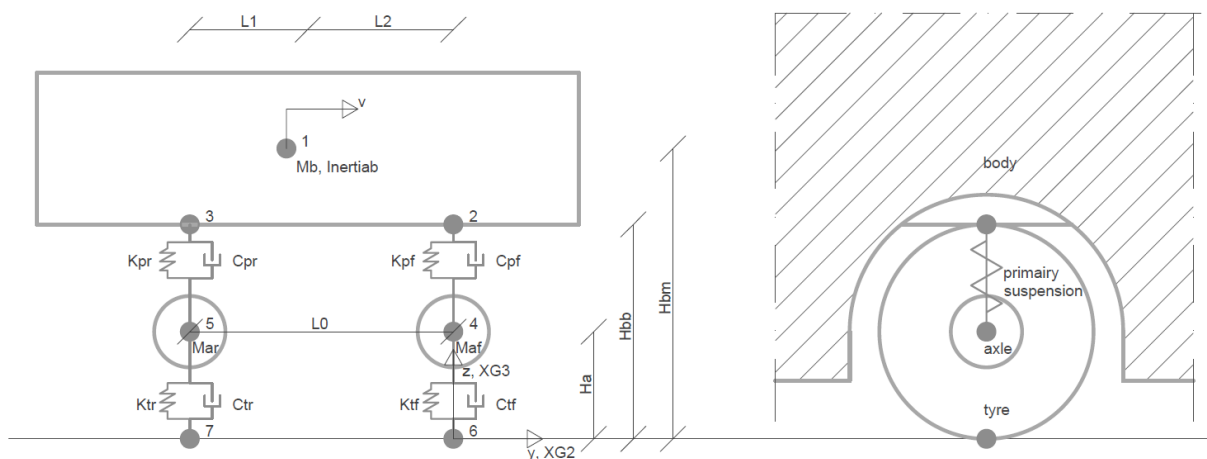


Figure 61. 2D 4 DoF dynamical vehicle model for the implementation in the FEMIX software (left) and a representation of the mass-dashpot-spring systems in a more reality-based representation in the form of the vehicle body, a spring-dashpot for the primary suspension, a mass for the axle and a spring-dashpot system for the tyre (right)

9.2. Road Unevenness

Also the characteristics of the road irregularity (Figure 62) over which the vehicle drives are similar to the verification projects discussed in 8 ‘Verification Projects’. Similar to what was discussed in 7.1.3 ‘Possibilities of FEMIX,’ the road irregularity is implemented by means of a Fourier expansion. The variables ‘ P ’ (period of the continuous function) and ‘ N ’ (number of summations in the expansion) for computing the Fourier expansion greatly influence the profile of the road irregularity and thus the generated loads. If P is chosen too small, multiple consecutive road bumps will influence the soil response at a specific location. Which value for P should be chosen depends on the vehicle speed and the distance to the receiver points, but for the verification projects it appears that a value for P equal to 50 m gives satisfying results (the generated loads are equal to those of the verification project).

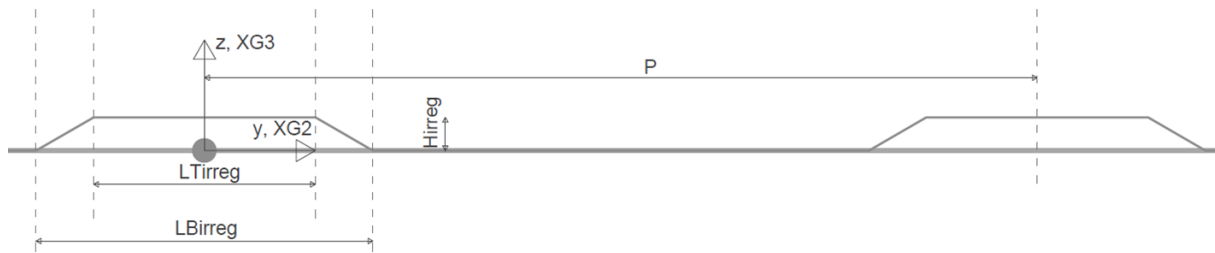


Figure 62. Representation of the road irregularity with specified variable input parameters (L_{Tirreg} , L_{Birreg} , H_{irreg} and P) for computing the road irregularity profile

The combination of the values for P and N determine how well the road irregularity approaches the actual desired road irregularity. Figure 63 presents the road irregularity profile for a specified value of P (equal to 50 m) and deviating values for N . A big difference can be observed when N is increased from $N = 50$ to $N = 200$. However, when further increasing the value for N (from $N = 200$ to $N = 600$) the profile of the road irregularity doesn't change that much. The more summation coefficients used, the more the Fourier expansion approaches the actual road irregularity profile. However, it will also increase the computational time for the soil response by a factor equal to the increase of N . For the verification projects it appears that, in combination with a value for P equal to 50 m, a value of ' N ' equal to 200 gives satisfying results. From this one could conclude that the combination of P and N being:

$$N = 4P \quad (9.1)$$

should give satisfying results for the problem under consideration in this Master thesis.

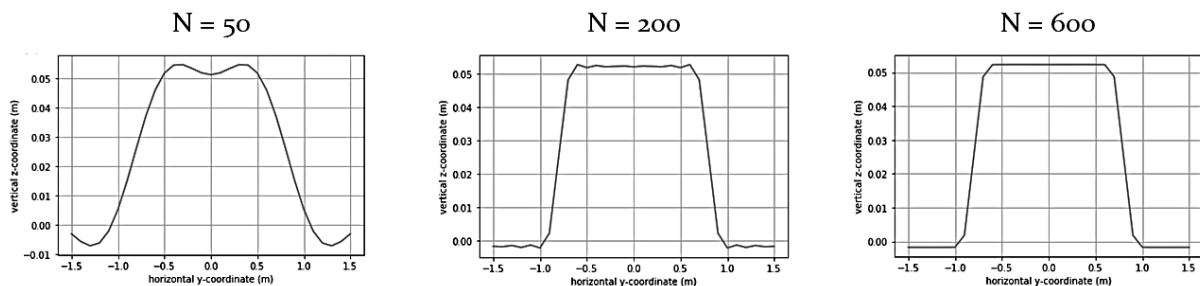


Figure 63. Representation of the road irregularity by means of a Fourier expansion with period ' P ' = 50 m and deviating values for the number of summations ' N '. Note that the height of the irregularity is equal to 0.054 m, the length at the bottom of the bump is equal to 1.9 m and the length at the top of the bump is equal to 1.3 m

9.3. Generated Moving Loads

The vehicle's response when driving over the road irregularity generates the moving axle loads that are applied to the road. These moving loads can be presented in the frequency domain and the time domain.

9.3.1. Loads in the frequency domain

The frequency spectrum of the vehicle's axles presents the frequency range at which the axle vibrates, i.e. what the loading frequencies are, and what load value is applied harmonically to the road at every frequency. The verification projects show only the frequency spectrum of the front axle of the vehicle. Figure 64 shows the frequency spectrum of the front axle computed by the software FEMIX (left) next to the frequency spectrum of the front axle of Verification Project Degrande et al. (1) – Free Field (right). The frequency spectrums are very similar and can be concluded to give the same results.

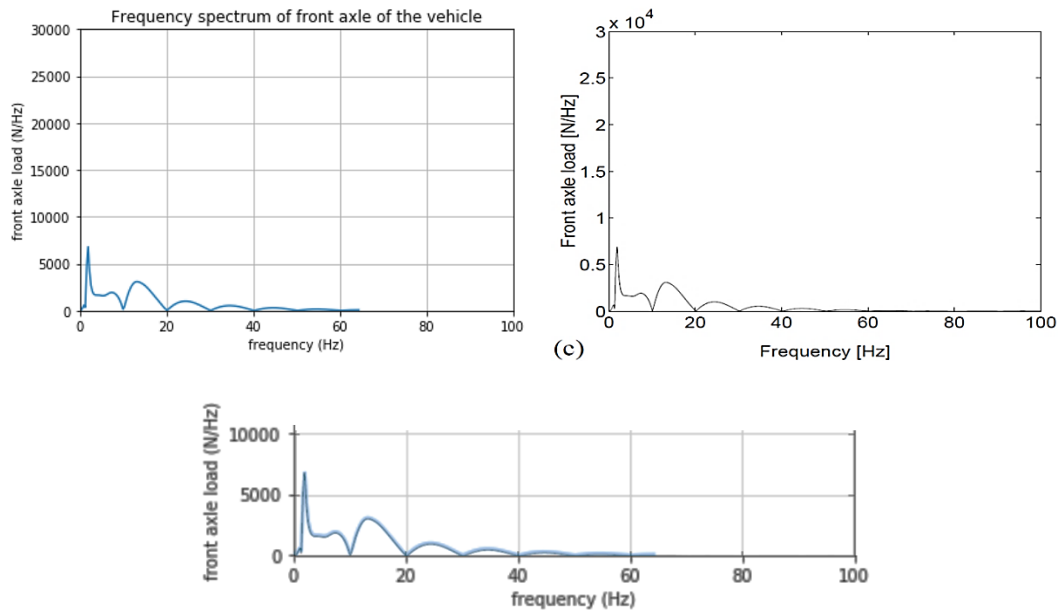


Figure 64. Computed front axle frequency spectrum by FEMIX (top left, blue) and the frequency spectrum of Verification Project Degrande et al. (1) – Free Field (top right, black) (Degrande & Lombaert, 2002). In the bottom figure the differences between both spectrums can be observed

9.3.2. Loads in the time domain

Next to the loads in the frequency domain also the loads in the time domain computed by FEMIX are compared with the loads in the time domain of the verification project (Figure 65). The loading in the time domain computed by FEMIX is very similar to that of the verification project and can be concluded to give the same results.

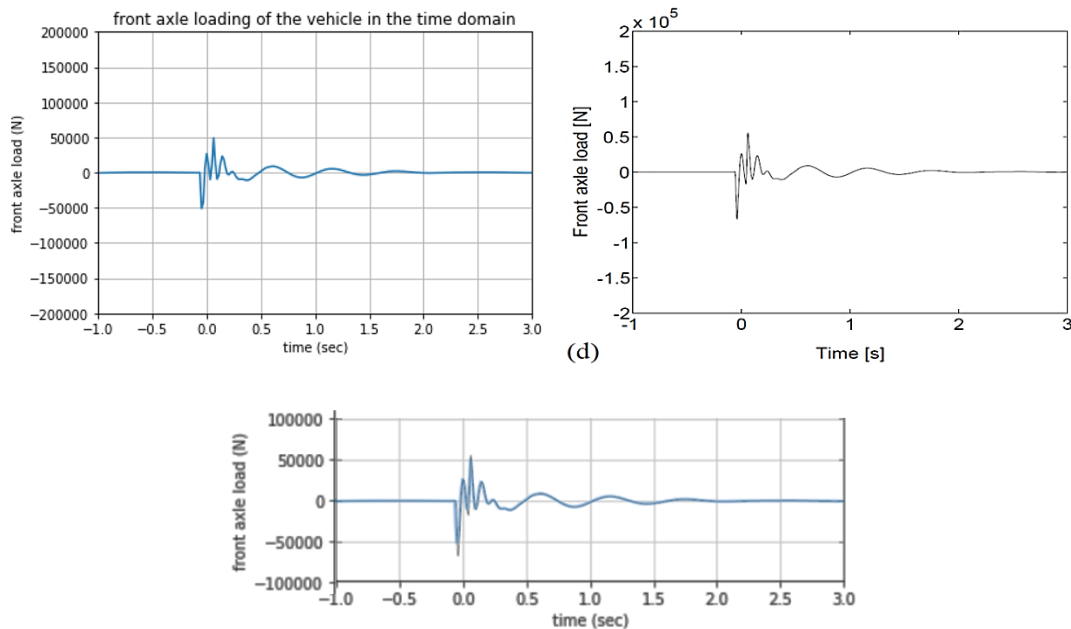


Figure 65. Computed front axle loading in the time domain by FEMIX (top left, blue) and the loading in the time domain of Verification Project Degrande et al. (1) – Free Field (top right, black) (Degrande & Lombaert, 2002). In the bottom figure the differences between both graphs can be observed

Since the differences between the computed results with FEMIX and the results of the verification project are very small, the generated loads by the software FEMIX are considered to be verified.

10. Transmission Modelling and Results in FEMIX

In the previous section the generation of the moving loads was considered and verified with the verification projects. The moving loads are applied to the elastic road which is supported by the elastic layered soil. This section describes how the road- and soil layering are taken into account by the computational tool and in what ways the receiver points in the soil are considered.

10.1. Road Layering

The moving loads are applied to the FEM-model of the road. The stiffness of the road makes that the moving point loads are distributed over a larger contact/ interface area between the road and the soil and therefore decreases the absolute impact loading onto the soil when comparing to the situation without the presence of a road.

The road can be modelled containing multiple layers with different materials (Figure 66). The FEM-model of the road is coupled to the soil (BEM) by means of a BEM-FEM coupling (see also 7.1 'FEMIX') at the interface between the road package and the soil. In this way the loads, altered by the stiffness of the road, are applied to the soil surface of the layered soil.

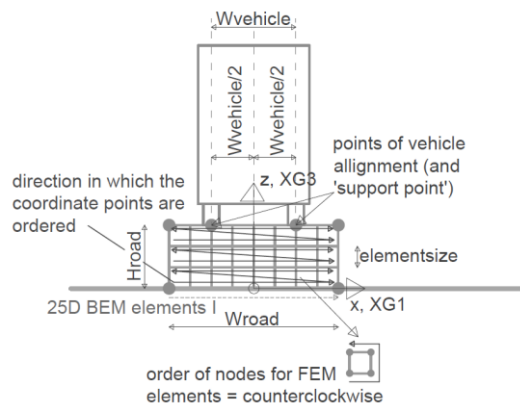


Figure 66. Representation of the vehicle on the layered FEM-model of the road which is connected to the soil surface by means of a BEM-FEM coupling. The order of the node-numbers is from left to right and from the bottom of the road to the top of the road

The road of the verification projects is modelled such that it is (partly) embedded in the soil and the bottom of the road is only connected to the soil vertically. This can also be modelled partly in FEMIX by modelling BEM-FEM elements only at the bottom of the road. However, the modelling is not exactly the same as in the verification project, because the BEM-FEM elements also account for coupling in the x - and y -direction (rather than in the z -direction only), which could cause some small discrepancies in the computed soil response.

10.2. Soil Layering

The layering of the soil can contain as many layers as desired by the user, however the deeper the soil domain gets (and therefore the more thin-layers have to be considered), the longer the computational time will be to compute the soil response. The verification projects of the KU Leuven have a maximum of five different soil layers with deviating depths, from which the bottom layer is the half-space (depth = infinity). Each layer is divided into the previously described thin-layers, therefore the soil layer heights have to be a multiple of the thin-layer thickness.

10.3. Receiver Points and Verification of Soil Response

The soil response by FEMIX can be computed for any point coordinate which is not part of a FEM-element and can be anywhere in the soil domain (any combination of x, y, z). The more points are specified for the soil response, the longer the computational time will be for computing the soil response.

First the soil response for ‘verification project Degrande et. al. (1) – Free Field’ is computed and compared to verify the free field soil response. Thereafter the soil response for ‘verification project Degrande et. al. (2) – Soil Building’ is computed and compared to verify the soil response with the presence of a building.

10.3.1. Soil response verification project Degrande et al. (1) – Free Field

Since the coupling of the road with the soil cannot be modelled in the exact same way as in the verification project, the free field soil response at a somewhat larger distance from the road will be compared (Figure 67 and Figure 68). This is because the influence of the different road-soil coupling is expected to be noticeable close to road but hardly noticeable further away.

Free Field soil response in the frequency domain

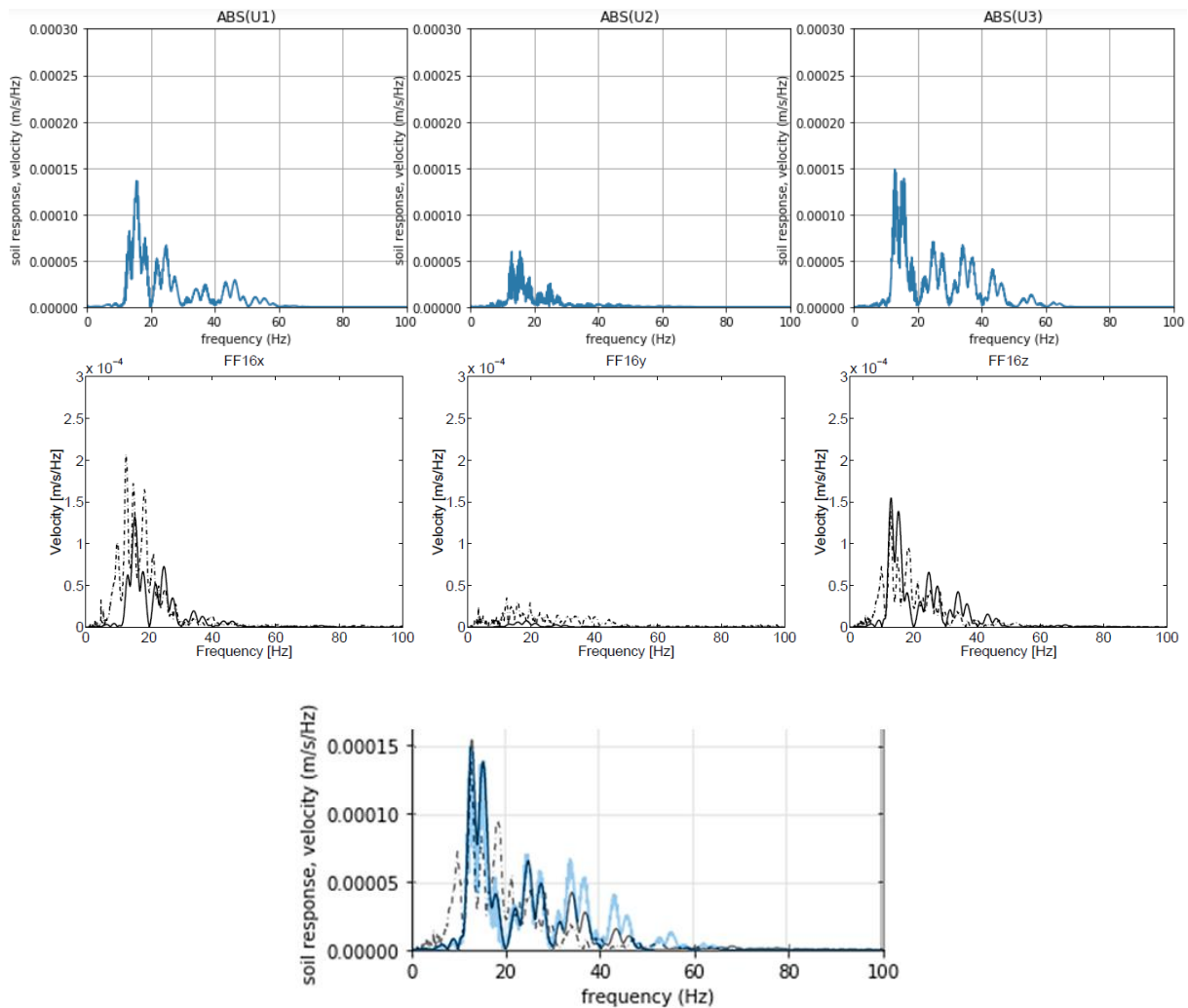


Figure 67. Computed frequency spectrum of the Free Field soil response (from left to right: x -, y -, z -direction) at 16 m from the middle of the road by FEMIX (top, blue) and of Verification Project Degrande et al. (1) – Free Field (middle, black) (Degrande & Lombaert, 2002), where the solid line is the predicted soil response and the dashed line is the measured soil response. In the bottom figure the differences between both spectrums of the vertical soil response can be observed

The frequency spectrums computed by FEMIX and of the verification project are very similar (Figure 67). However, the frequency spectrum computed by FEMIX slightly overestimates the soil response at higher frequencies ($f > 30$ Hz).

Free Field soil response in the time domain

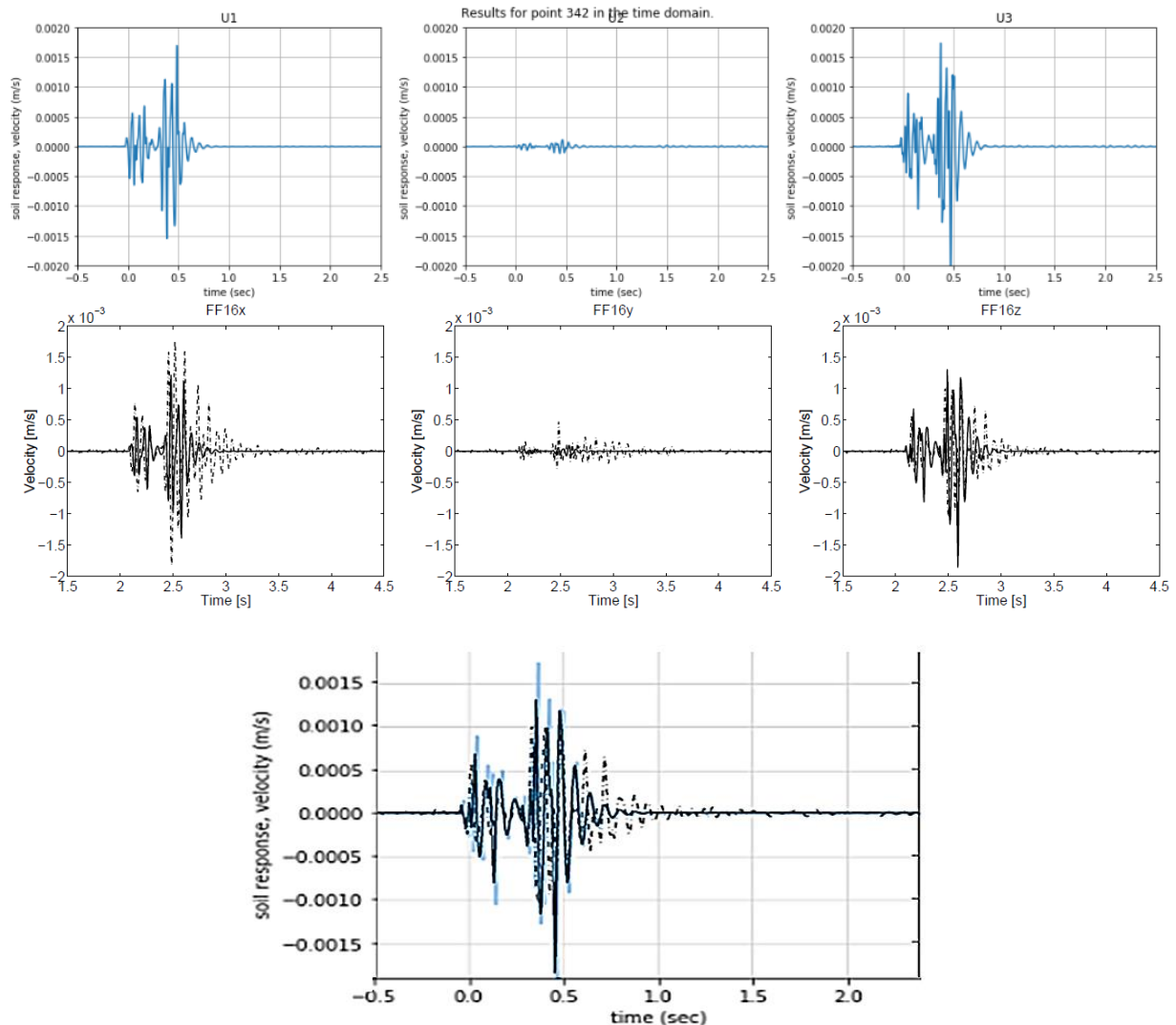


Figure 68. Computed time history of the Free Field soil response (from left to right: x-,y-,z-direction) at 16 m from the middle of the road by FEMIX (top) and of Verification Project Degrande et al. (1) – Free Field (middle) (Degrande & Lombaert, 2002), where the solid line is the predicted soil response and the dashed line is the measured soil response. In the bottom figure the differences between both time histories of the vertical soil response can be observed

The time histories computed by FEMIX and of the verification project are very similar (Figure 68). However, the amplitudes computed by FEMIX are slightly overestimated. This is a direct consequence of the overestimated soil response at the higher frequencies as described in the comparison of the frequency spectrums.

The differences between the computed results with FEMIX and the results of the verification project are very small and are probably a consequence of the difference in road-soil coupling. Therefore, the computed soil response by the software FEMIX is considered to be verified.

Free Field soil response in case the road is not embedded

The previous computations were for the situation where the road is embedded in the top soil layer in order to be in line with the model of Degrande et al. However when computing the same results for the situation where the road is on top of the soil surface, one can observe that the soil response has slightly larger amplitudes, but is very similar to the case with the embedded road (Figure 69). Also, for increasing distance from the road, the soil responses of both models get closer, indicating that the embedment of the road only influences the near field (close to the location of loading). Since the computational time of the soil response increases significantly for an embedded road, the situation for the road on top of the soil is more favourable for design practice.

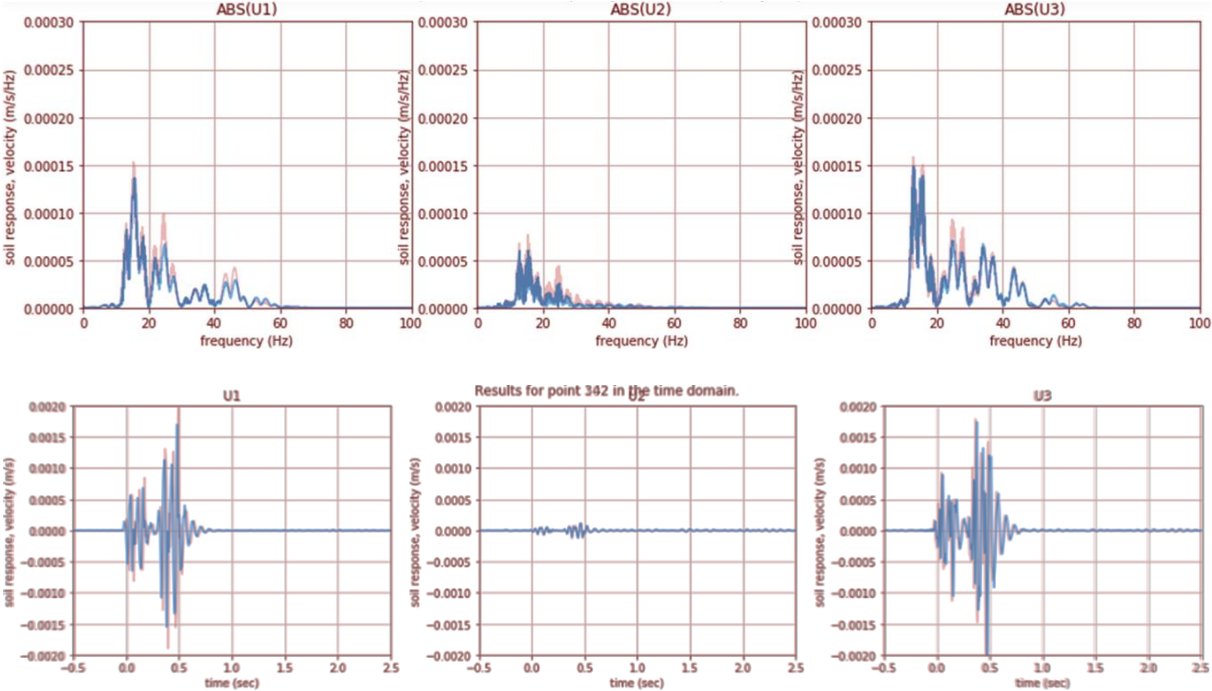


Figure 69. Difference of the frequency spectrums (top) and time histories (bottom) of the Free Field soil response (from left to right: x-,y-,z-direction) at 16 m from the middle of the road between the computation by FEMIX for the road embedded in the soil (blue lines) and the computation by FEMIX for the road on top of the soil surface (red lines).

10.3.2. Soil response verification project Degrande et al. (2) – Soil Building

The presence of the building might affect the soil response in the close proximity of the building. Due to the interference of the incoming waves (towards the building) and the reflected waves (away from the building), the soil response might be either amplified or attenuated. Due to the 2.5D approach of FEMIX the building can only be modelled as an infinitely long empty trench. However, the building of the verification project is rather narrow (only 5.6 m), therefore first the free field soil response is computed to compare with the measurement point of the verification project which is located close to the building (Figure 70).

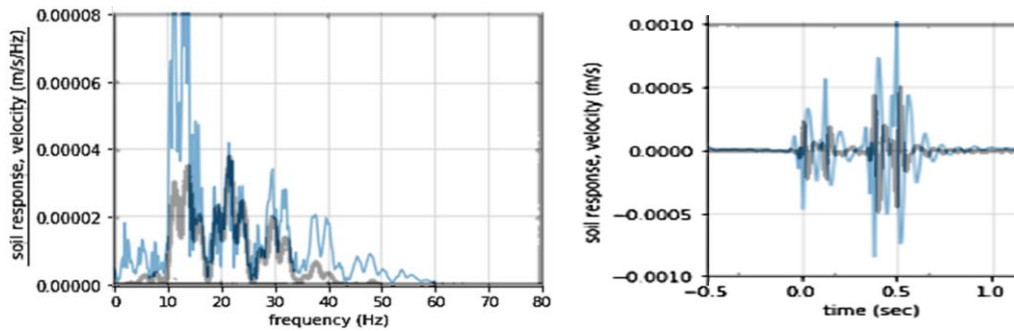


Figure 70. Difference of the frequency spectrum (left) and time history (right) of the vertical Free Field soil response between the computation by FEMIX (blue lines) and the results of the Verification Project Degrande et al. (2) – Soil Building (black lines) (Degrande, Pyl, Lombaert, & Haegeman, 2004)

As can be observed from Figure 70 the computed soil response by FEMIX has much higher amplitudes than the results of the verification project of Degrande et al. When including the building as an infinitely long empty trench, the soil response is even further amplified by a factor between 1.1 (soil approximated as a homogeneous halfspace) and 1.3 (layered soil). There might exist multiple reasons why the soil response computed by FEMIX has higher amplitudes than in the verification project. Among other things, it could be that:

- the road is modelled differently by Degrande et al. (the modelling of the road is not clearly specified), e.g. a stiffer road would decrease the amplitudes of the soil response;
- the soil properties are modelled differently by Degrande et al., perhaps taken into account the sloped soil and the pavement that is present at the particular building (Figure 71). Both the extra soil layer and the pavement would decrease the amplitudes of the soil response.



Figure 71. Picture taken from Google Maps (Google, 2019) at the specific site

Since both the modelling of the road and the modelling of the soil are not clearly specified in the literature, it can be concluded that the currently computed soil response by FEMIX comes close to the Degrande project but cannot be modelled the same due to lack of information. Therefore, the model of FEMIX is considered to be verified and is on the conservative side. To implement the results of FEMIX as excitation on the MDoF building system, the response will be factorized to come closer to the vibration amplitudes of the Degrande project. The computed response will be factorized in the frequency domain. The factor is frequency- and direction dependent (x -, y -, z -direction) and is used for both the soil response displacements and velocities (Figure 72). The modified soil response in the time domain is computed from the modified frequency spectrums (Figure 73) and is similar to the soil response of the verification project.

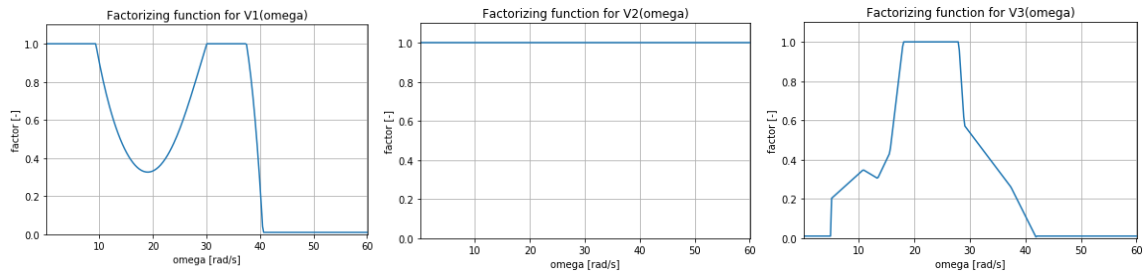


Figure 72. Factorizing functions for the computed soil response for Verification Project Degrande et al. (2) – Soil Building in the frequency domain for the soil response in the horizontal x-direction (left), the horizontal y-direction (middle) and the vertical z-direction (right)

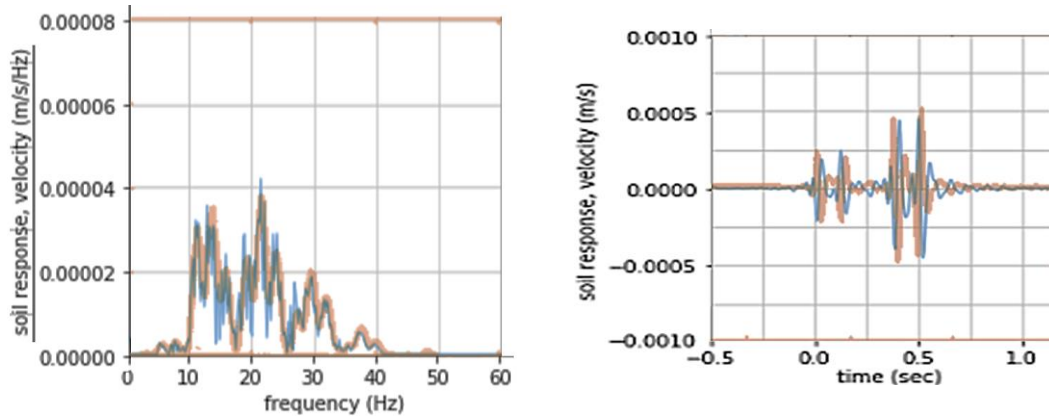


Figure 73. Difference of the frequency spectrum (left) and time history (right) of the vertical Free Field soil response between the modified computation by FEMIX (blue lines) and the results of the Verification Project Degrande et al. (2) – Soil Building (brown lines) (Degrande, Pyl, Lombaert, & Haegeman, 2004)

10.3.3. Soil response in Amsterdam

The soil layering and the (5-axled) vehicle model as stated in ‘8.2 VU Amsterdam’ are used to model the soil at a location similar to the VU in Amsterdam and to model the vehicle which generates the moving loads for this problem. Since the measurements performed at this location are done for the free field situation, all other model parameters (road layering and irregularity) are assumed to be equal to Verification Project Degrande et al. (1) – Free Field. It appears that the vertical soil response at 30 m from the road is much larger than the measured 250 $\mu\text{m/s}$ (see ‘8.2 VU Amsterdam’). Therefore the height of the road irregularity is decreased by a factor 0.083 (from 0.054 m to 0.0045 m) which makes that the vertical soil response computed by FEMIX is approximately equal to 250 $\mu\text{m/s}$ (Figure 74 and Figure 75) and is in line with the measurements performed at this particular site.

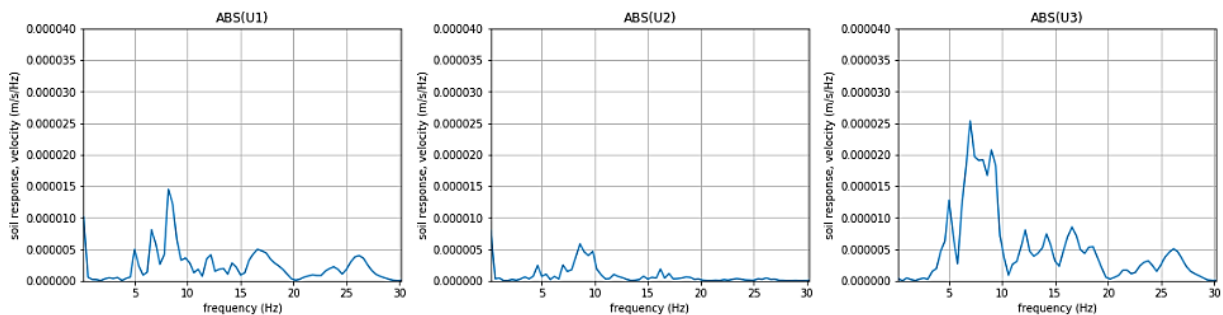


Figure 74. Frequency spectrums of the Free Field soil response for the soil similar to VU Amsterdam (from left to right: x-,y-,z-direction) at 30 m from the middle of the road, computed by FEMIX

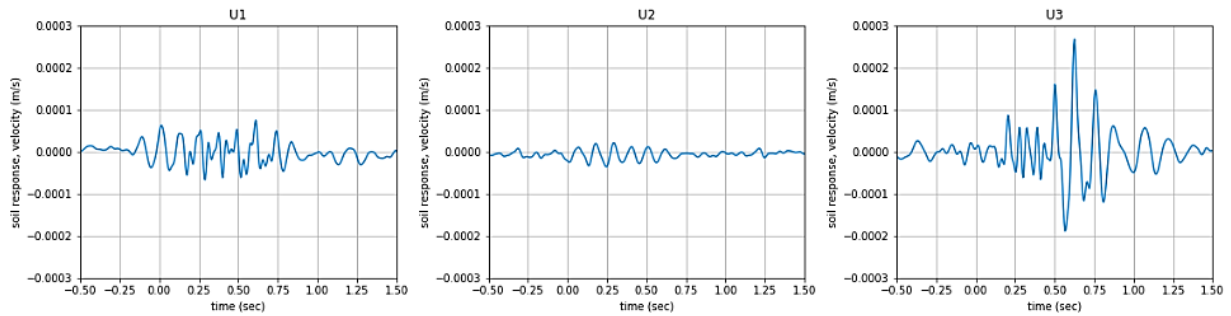


Figure 75. Time histories (bottom) of the Free Field soil response for the soil similar to VU Amsterdam (from left to right: x-,y-,z-direction) at 30 m from the middle of the road, computed by FEMIX

The soil response is computed over a distance of 100 m from the middle of the road with intervals of 2 m. The soil responses are also computed at a depth of -3 m. These soil responses are used as excitation input for the computational script of the practical engineering tool EDDABuS_{GS}. This makes that EDDABuS_{GS} is used for the situation of Amsterdam, which has a softer soil than the verification projects in Belgium. Note that the soil response holds for the free field, i.e. the influence of the presence of a building is not taken into account.

In order to compute the soil impedances (see 11.2 Derivation of Impedances) the layered soil of Amsterdam is approximated by a homogeneous halfspace. The parameters of the halfspace given in Table 2 give a similar soil response (similar PPV and dominant frequency range) as in the layered soil (Figure 76). The fact that the time domain representation of the soil response does not convert to zero before $t = -0.25$ s and after $t = 1.25$ s is due to a too large frequency step (0.4 Hz) for which the results are computed. A frequency step of 0.4 Hz means that the soil response repeats itself in opposite sign after $1/0.4$ Hz = 2.5 s.

Table 2. Simplification of the layered soil of Amsterdam into a homogeneous halfspace used for computing the dynamic soil impedances for the computational tool EDDABuS_{GS}

Layer	d (m)	ν (-)	ρ (kg/m ³)	$E \times 10^6$ (N/m ²)	$G \times 10^6$ (N/m ²)	C_s (m/s)	β (-)
1	∞	0.48	2000	22.2	7.5	61	0.0200

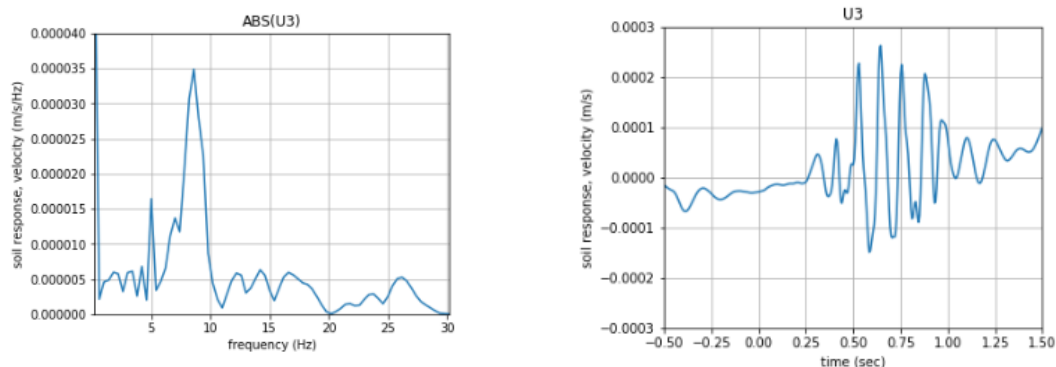


Figure 76. Frequency spectrum (left) and time history (right) of the Free Field soil response velocities for the approximated homogeneous halfspace for Amsterdam (z-direction) at 30 m from the middle of the road, computed by FEMIX

10.3.4. Soil response attenuation by wave barrier in soil of Amsterdam

Additionally, a small research was performed for comparing the free field soil responses for the location in Amsterdam after construction of a wave barrier with the free field soil response before construction of the wave barrier. The wave barrier is placed at 28 m from the middle of the road and has a thickness of 1.6 m. The depth of the wave barrier is 4 m only, because the

computational time of FEMIX increases significantly with increasing depth of the wave barrier. What is observed from the frequency domain is that the higher frequency range is attenuated for a much greater distance from the loading than the low frequency range (Figure 77). This is in line with what was found in the literature study and is caused by the fact that the wave barrier performs much better in attenuating the high frequency waves (short wavelengths) than the low frequency waves (long wavelengths).

For the time domain the PPV is computed for all distances from the middle of the road. The ratio $PPV_{WithBarrier}/PPV_{NoBarrier}$ is computed for all directions (x, y, z) and at both the soil surface and at a depth of 3 m in the soil (Figure 78). Also see the absolute PPV values in Appendix J: ‘Appendix: PPV with- and without wave barrier in soil Amsterdam’. At the soil surface the wave barrier with a depth of 4 m has effect on mitigating the soil response until a distance of 25 m behind the wave barrier (vertical direction of soil response, U_3), while this distance increases for the other two horizontal directions. However, at a depth of 3 m below soil surface the PPV is only decreased very close to the wave barrier. After this distance the wave reflections even cause an amplification of the soil responses at this depth (note that the absolute PPV values are still small).

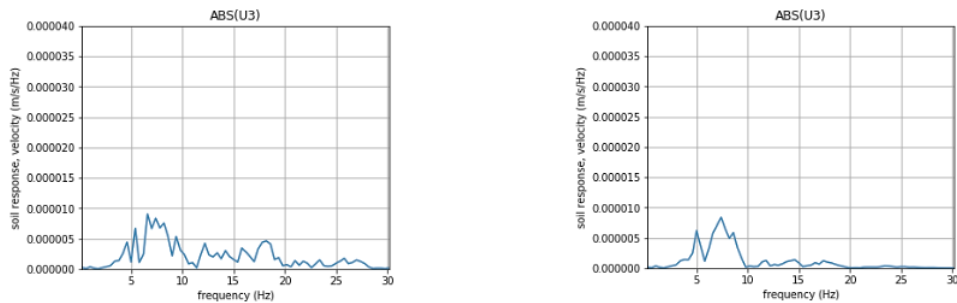


Figure 77. Frequency spectrum of soil response (velocities in vertical direction at soil surface) at 52 m from the middle of the road (or 24 m behind the wave barrier). Left: no wave barrier, right: wave barrier at 28 m from the middle of the road

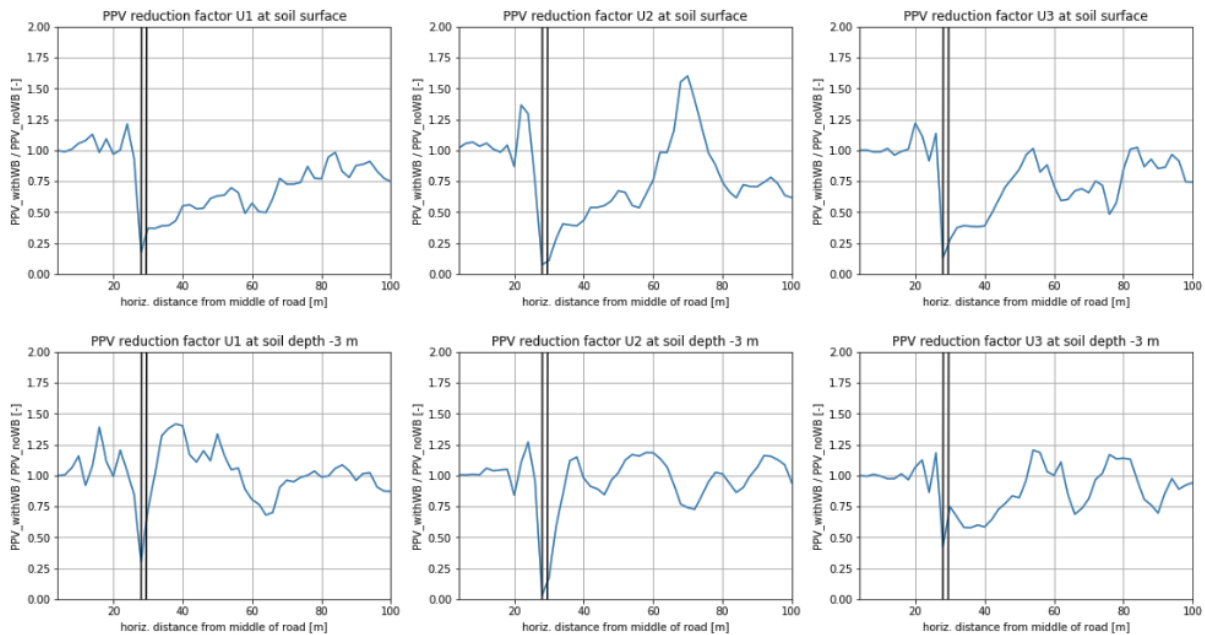


Figure 78. Effect on PPV (m/s) of the free field soil response with the realization of a wave barrier (width = 1.6 m, depth = 4 m) at 28 m from the middle of the road (represented by the two black vertical lines) for the 3 directions x (U_1), y (U_2) and z (U_3) at the soil surface (top) and at a depth of 3 m

11. Soil-Structure Interaction Modelling in EDDABu_{GS}

As described in chapter 6 ‘Soil-Structure Interaction’ of Part II ‘Literature Study’ there exist different approaches to compute the soil-structure interaction (SSI) between a given soil stratum and a specified structure. Since the subject of this thesis is about a practical engineering tool, the computational time of the tool should be kept low and therefore the most rigorous approach to compute the SSI, the ‘direct approach,’ is not convenient, because this approach asks for an elaborate modelling of the soil and the structure together by means of finite elements and asks for a long computational time. Instead the sub-structuring approach can be used to give reliable results for the computation of the SSI while still keeping the computational time relatively low. This sub-structuring approach has already been briefly introduced in chapter 6 ‘Soil-Structure Interaction’ of Part II ‘Literature Study’ and will be used for implementation in EDDABu_{GS}. The computation of the springs and dashpots that support the flexibly-supported building (the impedances) (Figure 49 c.) will be based on the tables of Gazetas (Gazetas G. , 1991).

Additional explanatory text for this chapter can be found in Appendix K: ‘Appendix: Additions to Chapter 11 ‘Soil-Structure Interaction Modelling,’ concerning the derivation of the impedances given in the tables of Gazetas and the assumptions needed for the practical use of the tables.

11.1. Background and Structural Simplifications in the Tables of Gazetas

In 1991 Mr G. Gazetas, Professor of Soil Mechanics at the National Technical University Athens, Greece and at the State University of New York, Buffalo, wrote the paper ‘Foundation vibrations’ (Gazetas G. , 1991) concerning the sub-structuring method for computing the impedances for SSI problems. This method estimates the dynamic ‘spring’ (stiffness) and ‘dashpot’ (damping) coefficients of flexibly-supported foundations. The research was performed for machine foundation vibrations which are generally small of size and move rigidly (Figure 79). Since machine foundations are constructed as rigid reinforced-concrete blocks, the response to the dynamic loads solely arises from the deformation of the supporting ground. Such foundations possess six degrees of freedom: three translational and three rotational (i.e. dynamic displacements along the axes x , y , z and dynamic rotation around the same axes).

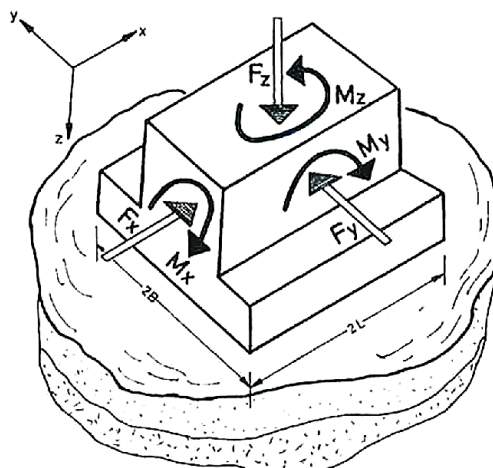


Figure 79. Rigid foundation block with its six degrees of freedom (Gazetas G. , 1991)

In the research of Gazetas the assumption is that the two bodies: the soil medium and the structure, remain always in contact, i.e. their displacements are identical and equal to the rigid body displacements of the foundation.

The type of structures under consideration within this thesis, the vibration sensitive laboratory building structures, are generally also made very stiff to minimize the dynamic response to the external excitation on the structure. This means that the simplification of a rigid structure is quite accurate for these kind of building structures and therefore the assumption of the global building to be rigid is used to determine the global dynamic response of the entire building.

The formulas and graphs given in the tables of Gazetas have been compiled from publications by Mr. Gazetas and his co-workers (Dobry and Fotopoulou). They are based on some simple physical models calibrated with results of rigorous boundary-element formulatates and data from other literature (Lysmer, Veletsos, Luco, Roesset and Kausel) (referred to as tables 15.1 and 15.2 in (Gazetas G. , 1991)). The tables 15.3 to 15.6 (Gazetas G. , 1991) are based on results of other research literature. An extensive overview of all the sources is given in the paper 'Foundation vibrations' (Gazetas G. , 1991).

11.2. Derivation of Impedances

Gazetas performed a lot of iterations to compute the impedances for a vast amount of different structural- and soil configurations. The impedances refer to axes passing through the foundation basemat-soil interface. The tables (Gazetas G. , 1991) used for this thesis are:

1. Table 15.1 and accompanying set of graphs refer to foundations of any solid shape resting on the surface of a homogeneous halfspace.
2. Table 15.2 and related graphs are for foundations with any solid basemat shape partially or fully embedded in a homogeneous halfspace.
3. Table 15.6 is mainly for laterally oscillating single floating piles in two inhomogeneous and a homogeneous stratum or halfspace. Some information is also given for vertical oscillations, and for pile-soil-pile dynamic interaction factors.

The layered soil stratum is approximated as a homogeneous halfspace (see 10.3.3 Soil response in Amsterdam). With this assumption the tables 15.1, 15.2 and 15.6 (Gazetas G. , 1991) and the accompanying graphs are used to determine the impedances of the rigid building structure. In symbols the impedance terms are computed as:

$$\mathbb{K}_j(\omega) = \bar{K}_j(\omega) + i\omega C_j(\omega) \quad (11.1)$$

$$\bar{K}_j(\omega) = K_{static} \cdot k(\omega) \quad (11.2)$$

$$C_j(\omega) = c(\omega) \cdot \rho \cdot f(C_s, v) \cdot g(B, L) + 2 \cdot \frac{\bar{K}_j(\omega)}{\omega} \cdot \beta \quad (11.3)$$

where $f(C_s, v)$ is a function of both C_s and v ($V_{La}(C_s, v)$) in case of the vertical- and rocking impedances or depends solely on C_s in case of the horizontal impedances and where $g(B, L)$ is equal to A_b (the effective surface area of the foundation basemat) in case of the translational impedances or is equal to I_{bj} where I_{bj} is the inertia of the soil, computed as: $\frac{1}{12} \cdot 2L \cdot (2B)^3$ (depending on the orientation of the building L and B should be interchanged) in case of the rocking impedances.

11.3. Practical Use of the Tables

The use of the graphs is bounded by a maximum value of $a_0 = \omega B / C_s = 2$, where ω is the excitation frequency, B is the half width of the building (shortest side) and C_s is the shear wave speed of the soil. The problem statement of this thesis concerns heavy road traffic induced

vibrations for laboratory buildings in The Netherlands. This means that values for the mentioned parameters might be within the following ranges:

$$\begin{aligned} 0 \text{ Hz} < f < 15 \text{ Hz}, \text{ thus: } 0 \text{ rad/s} < \omega < 95 \text{ rad/s} \\ 2 \text{ m} < B < 15 \text{ m} \\ 150 \text{ m/s} < C_s \end{aligned} \tag{11.4}$$

which might reasonably lead to values of a_0 up to $95 \text{ rad/s} \cdot 15 \text{ m} / 150 \text{ m/s} = 9.5 \text{ rad}$, which is far out of the bounds of the graphs. In order to make the tables of Gazetas applicable for the problems of interest for this thesis, the graphs accompanying the tables of Gazetas are extrapolated. Note that the extrapolation of these figures is a major simplification made for this thesis research.

Curve fitting for extrapolation of the graphs accompanying the tables of Gazetas

The numerical Python software will be used for the extrapolation of the graphs accompanying the tables of Gazetas in case of a homogeneous halfspace. Python has the possibility to use the function ‘curve fitting’. This method has been used to extrapolate most of the graphs. Two examples are given in Figure 80 and Figure 81. By using this method, a continuous function is derived which will give a value for the stiffness- or dashpot coefficient based on any possible input value a_0 .

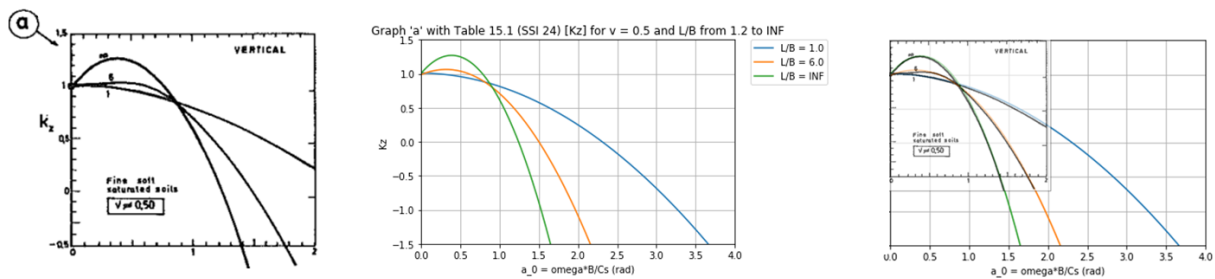


Figure 80. Graph a accompanying table 15.1, left: Gazetas (Gazetas G. , 1991), middle: extrapolated, right: both graphs in one

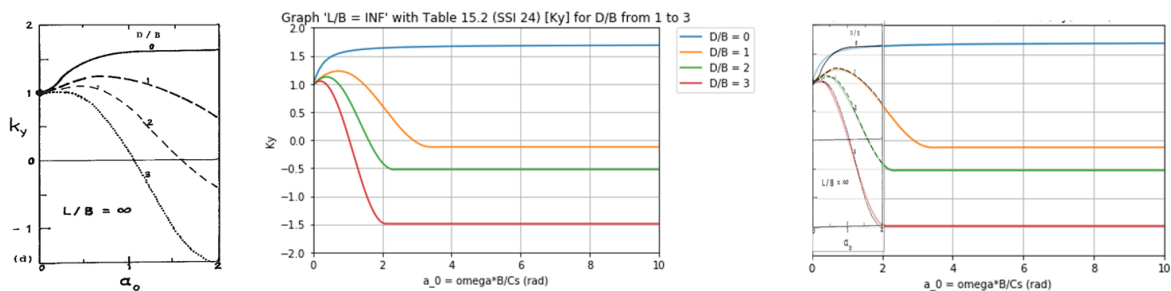


Figure 81. Graph k_y , $L/B = \infty$ accompanying table 15.2, left: Gazetas (Gazetas G. , 1991), middle: extrapolated, right: both graphs in one

Behaviour of pile groups in a homogeneous halfspace

The pile group interaction of the rigidly capped piles takes into account the arrival of vibrations at a particular pile that are induced by the oscillations of another pile in the pile-group (Figure 82). The greater the number of piles within the pile group, and the closer the piles are placed to each other, the more interaction that will take place. However, there is a limit to the total amount of piles in the group that affect each other due to the scattering of waves and the corresponding shadowing effect formed by the intermediate piles (Gazetas & Dobry, 1988). This number is yet unknown for this thesis, but an assumption has been made which is explained further on.

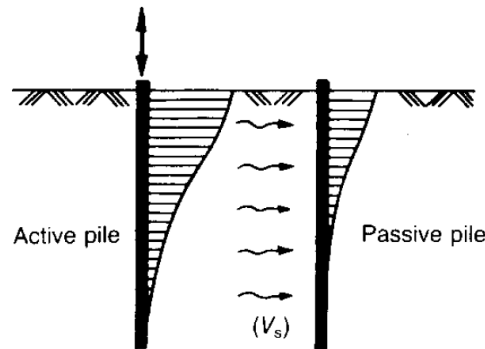


Figure 82. Distribution of displacement amplitudes of the soil along the shaft of an oscillating (active) pile and of a neighbouring (passive) pile (Gazetas & Dobry, 1988)

The ratio $K_j^G(\omega)/\sum_{i=1}^{P_{total}} K_{j,i}^S(\omega)$ (pile-group impedance / sum of single pile impedances) is approximated based on the graphs accompanying the paper of Gazetas et al. (Gazetas & Dobry, 1988). The following important assumptions have been made to come to this simplification:

- All piles are assumed to have the same axis-to-axis distance.
- The pile spacings (S) for the problems solved by the EDDABuSGS-tool are small (centre-to-centre distance of piles close to $2d$ and $< 4d$, where d is the pile diameter). This makes that the ratio $K_j^G(\omega)/\sum_{i=1}^{P_{total}} K_{j,i}^S(\omega)$ can be approximated by a parabolic function (group stiffness) or constant value (group damping) (Figure 83) which are dependent on the total number of piles in the pile group.

Note that the horizontal axis concerns a different value of the dimensionless frequency $a_0 = \omega d/C_s$, which, for The Netherlands, is generally below $15 \text{ Hz} \cdot 2\pi \cdot 0.6 \text{ m}/150 \text{ m/s} = 0.38 \text{ rad}$, meaning that the figures for pile-groups do not have to be extrapolated.

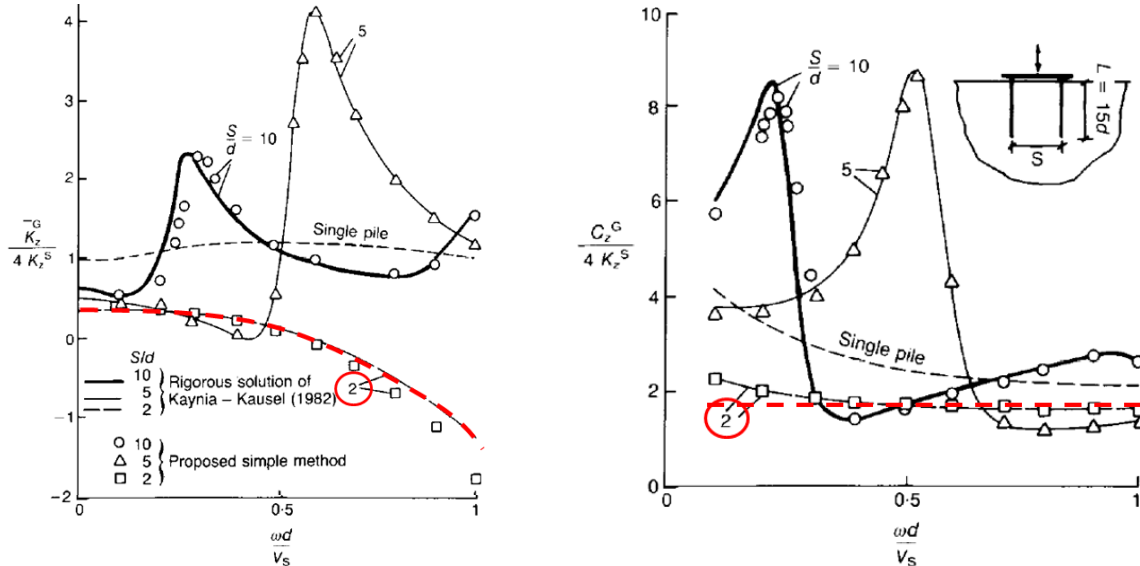


Figure 83. Principle of the assumptions made for the pile-group impedance terms based on the graphs accompanying the paper of Gazetas et al. (Gazetas & Dobry, 1988)

- The graphs are based on values $L/d = 15$ and $E_{pile}/E_{soil} = 1000$.
- Also, since only graphs are presented for a limited amount of piles in a pile group, the assumption has been made that the interaction between the piles does not change for pile-groups larger than 16 piles. This means that for pile-groups containing more than 16 piles in total, the interaction ratio $K_j^G(\omega)/\sum_{i=1}^{P_{total}} K_{j,i}^S(\omega)$ is based on the 4×4 pile group.

Now that the graphs for the embedded structure have been extrapolated and the graphs for the pile group impedance terms have been simplified, the tables of Gazetas can be used for the EDDABuSGS-tool of this thesis. For every calculation frequency the impedances have to be determined. Since the excitation on the structure is given as a Fourier expansion of the form:

$$U_i(t) = \sum_{j=1}^N [U_{i,c,j} \cos(k_{y_j} \cdot t) + U_{i,s,j} \sin(k_{y_j} \cdot t)] \quad (11.5)$$

with N summation terms, the impedances have to be determined N -times as well. After performing a Forward Fourier Transform of $U_i(t)$ (excitation in the time domain) to $\tilde{U}_i(\omega)$ (excitation in the frequency domain), the excitation frequencies ω for which the impedances have to be determined are known. With the values of the impedances known, the structural response of the 3DoF structure can be determined. The impedances due to the embedment of the structure and the impedances due to the pile foundation are summed to obtain the total impedance.

12. Receiving Structural System Modelling and Results in EDDABuSGS

In the previous chapters the excitation on the structural system is computed (by FEMIX) and the impedances are obtained that represent the flexibly supported structure on a flexible soil (and is applicable a pile foundation) (in EDDABuSGS). Now what remains is to determine the dynamic structural response of the structure itself (by EDDABuSGS). To this end the structural response is subdivided in the global dynamic response of the entire building which is assumed to be rigid and the local dynamic response of one particular flexible floor. The global dynamic response of the rigid building is used as excitation on the local flexible floor. The local dynamic response of the floor, RMS-velocities in the frequency domain, is the end result of EDDABuSGS and is in the same unit as the VC-curves (vibration requirements). This chapter will describe how the dynamic responses of both the global rigid building and the local flexible floor are computed.

Additional explanatory text for this chapter can be found in Appendix L: ‘Appendix: Additions to Chapter 12 ‘Receiving Structural System Modelling and Results’,’ concerning the derivation of the structural parameters of-, the excitation on- and the responsive motions of the 3DoF system. Also, the computation of the structural response of the flexible frame is considered more thoroughly.

12.1. Global Dynamic Response of the 3DoF Rigid Building

As described in chapter 11 ‘Soil-Structure Interaction’ the impedances of the flexibly supported building are based on the assumption that the global building motion can be simplified to a rigid volume with six degrees of freedom (three translational and three rotational). Since the buildings of interest of this master thesis concern vibration sensitive laboratory building structures, which are generally made relatively very stiff in order to minimize the vibrations in the building, the assumption of rigidity for the global building motion is justified. Therefore, the global building motion computed for this thesis research will also be considered as being rigid.

In order to minimize the computational time of the practical engineering tool EDDABuSGS only a 2D representation of the rigid building will be considered. This 2D plane is perpendicular to the longitudinal length of the road at which the heavy traffic induces the moving dynamic loads (Figure 2). This simplification makes that the global building response is computed for three degrees of freedom (3DoF) only: two translational and one rotational. The 3D computed impedances related to this 2D plane will be used for the flexible supports of the 2D rigid building. These impedances are $K_x(\omega)$, $K_z(\omega)$ and $K_{ry}(\omega)$ (Figure 85), where every $K_j(\omega)$ is composed of a real part (stiffness) and an imaginary part (damping), in line with the elaboration in chapter 11 ‘Soil-Structure Interaction’. The excitation on the 3DoF structure is composed of a horizontal excitation (in the x-direction), a vertical excitation (in the z-direction) and a rocking excitation (around the y-axis). The excitations follow from the soil response for one particular situation and are modified such that the point of application is at the same location as the springs- and dashpots of the flexible building supports.

12.1.1. Structural parameters

The structural properties of the 3DoF global building are gathered into two parameters: M_b (total mass of the building) and J_{CG} (total mass moment of inertia around the centre of gravity (CG) in the (x,z)-plane) (Figure 85). A simplification taken into account for the computation of the structural properties is that the building is symmetric around the two vertical planes and that all floor spans and wall thicknesses in one vertical plane are equal (Figure 84). M_b is composed of the masses of all structural floors, walls/columns, while J_{CG} is composed of the summation of the mass moment of inertia of all structural elements.

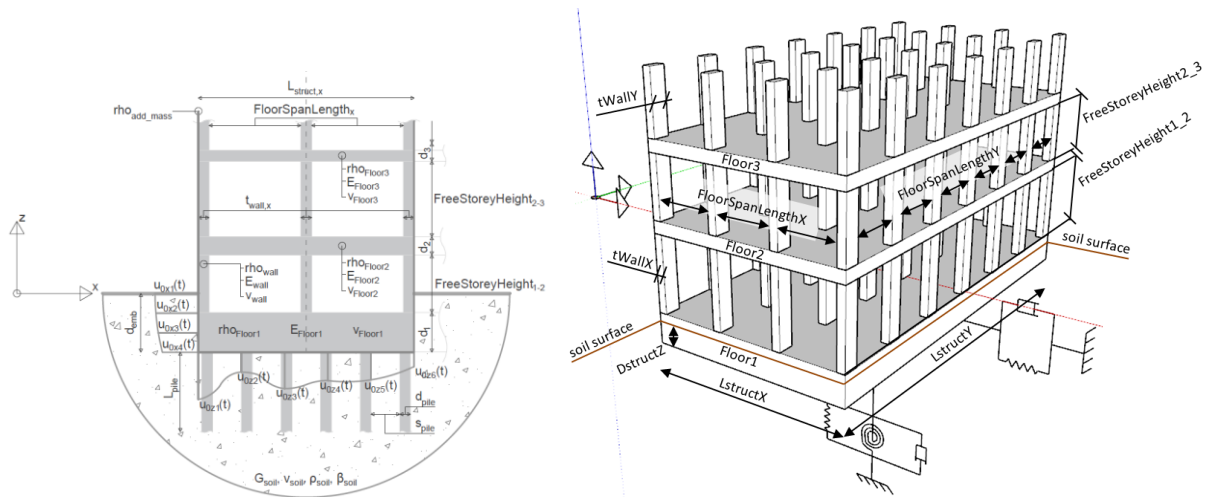


Figure 84. Simplified model for the computation of the parameters needed for the dynamic response of the 3DoF building

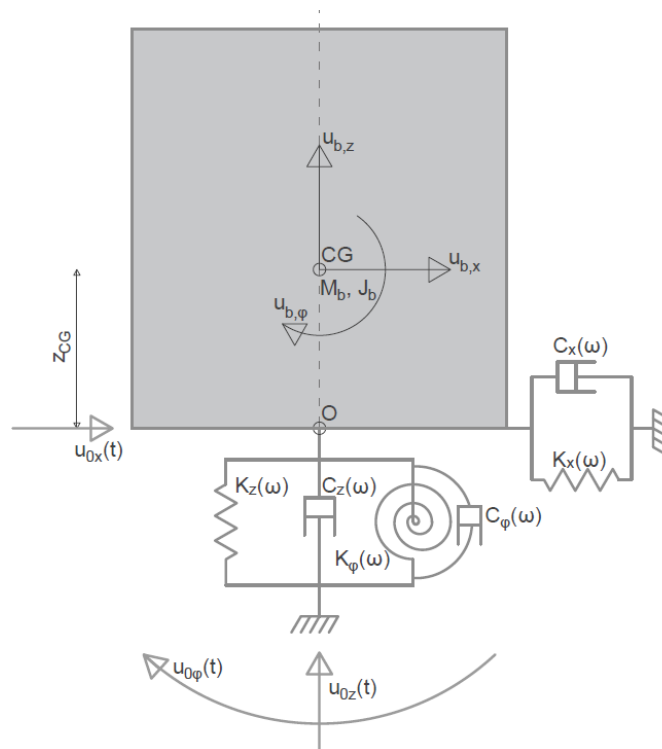


Figure 85. Simplified dynamical model which is used to set up the equations of motion for the rigid 3DoF building

12.1.2. Excitation

The excitation on the 3DoF system is derived from the soil response of one particular situation as described in chapter 10 ‘Transmission’. The excitations are taken as averages of the soil response at multiple points in the soil over the building length. These excitations (displacements/rotations and velocities) act on the springs and dashpots supporting the 3DoF system. The compression or extension of the springs and dashpots due to the imposed displacements and rotations causes dynamic forces to act on the 3DoF system.

12.1.3. Computation of the building response due to a harmonic loading term

As described before the loading on the 3DoF building is in the form of a summation of cosines and sines in the direction of every three degrees of freedom. Every pair consisting of a cosine- and sine term represent a dynamic harmonic loading with loading frequency k_{yj} (rad/s). The

building response due to the harmonic loading terms j ($j = 1, 2, \dots, N$) (either the cosine or sine-terms) with loading frequency $k_{y,j}$ (rad/s) is computed in line with Figure 85 and are added all together for the total building response. The equations of motions (derived by the aid of the Displacement Method), with the origin of the reference system at the center of gravity of the building, for every cosine- (or sine-) term with loading frequency $k_{y,j}$ (rad/s) then become:

$$\begin{aligned}
 & \begin{bmatrix} M_b & 0 & 0 \\ 0 & M_b & 0 \\ 0 & 0 & J_{CG} \end{bmatrix} \begin{bmatrix} \ddot{u}_{b,x,j} \\ \ddot{u}_{b,z,j} \\ \ddot{u}_{b,\varphi,j} \end{bmatrix} + \\
 & \begin{bmatrix} C_x(\omega) & 0 & -C_x(\omega) \cdot z_{CG} \\ 0 & C_z(\omega) & 0 \\ -C_x(\omega) \cdot z_{CG} & 0 & C_\varphi(\omega) + C_x(\omega) \cdot z_{CG}^2 \end{bmatrix} \begin{bmatrix} \dot{u}_{b,x,j} \\ \dot{u}_{b,z,j} \\ \dot{u}_{b,\varphi,j} \end{bmatrix} + \\
 & \begin{bmatrix} K_x(\omega) & 0 & -K_x(\omega) \cdot z_{CG} \\ 0 & K_z(\omega) & 0 \\ -K_x(\omega) \cdot z_{CG} & 0 & K_\varphi(\omega) + K_x(\omega) \cdot z_{CG}^2 \end{bmatrix} \begin{bmatrix} u_{b,x,j} \\ u_{b,z,j} \\ u_{b,\varphi,j} \end{bmatrix} \\
 & = \\
 & \begin{bmatrix} C_x(\omega) & 0 & 0 \\ 0 & C_z(\omega) & 0 \\ -C_x(\omega) \cdot z_{CG} & 0 & C_\varphi(\omega) \end{bmatrix} \begin{bmatrix} \dot{u}_{0,x,j} \\ \dot{u}_{0,z,j} \\ \dot{u}_{0,\varphi,j} \end{bmatrix} + \\
 & \begin{bmatrix} K_x(\omega) & 0 & 0 \\ 0 & K_z(\omega) & 0 \\ -K_x(\omega) \cdot z_{CG} & 0 & K_\varphi(\omega) \end{bmatrix} \begin{bmatrix} u_{0,x,j} \\ u_{0,z,j} \\ u_{0,\varphi,j} \end{bmatrix}
 \end{aligned} \tag{12.1}$$

Which can be represented in a more concise expression as:

$$\mathbf{M}\ddot{\underline{u}}_b(t) + \mathbf{C}(\omega)\dot{\underline{u}}_b(t) + \mathbf{K}(\omega)\underline{u}_b(t) = \underline{F}(t, \omega) \tag{12.2}$$

Note that the stiffness-, dashpot- and loading terms are frequency dependent. This is because the soil impedances are frequency dependent as was already discussed in chapter 11 ‘Soil-Structure Interaction’. The circular frequencies ω are the calculation frequencies for which the building response in the frequency domain is computed.

The eigenfrequencies of the 3DoF system are computed by solving the frequency dependent characteristic equation of the homogeneous equations of motions with aid of Maple (see Appendix M: ‘Appendix: Maple sheet for determining 3DoF eigenfrequencies’) and can be simplified to the following notation:

$$\det[-\omega^2 \mathbf{M} + \mathbf{K}(\omega)] = 0, \text{ i. e.:}$$

$$\begin{aligned}
 & K_x(\omega)M_b^2z_{CG}^2\omega^4 - J_{CG}M_b^2\omega^6 - K_x(\omega)K_z(\omega)M_bz_{CG}^2\omega^2 + J_{CG}K_x(\omega)M_b\omega^4 \\
 & + J_{CG}K_z(\omega)M_b\omega^4 + K_\varphi(\omega)M_b^2\omega^4 - J_{CG}K_x(\omega)K_z(\omega)\omega^2 - K_\varphi(\omega)K_x(\omega)M_b\omega^2 \\
 & - K_\varphi(\omega)K_z(\omega)M_b\omega^2 + K_\varphi(\omega)K_x(\omega)K_z(\omega) = 0
 \end{aligned} \tag{12.3}$$

The damping terms are left out of this computation because these terms significantly complexify the computation of the eigenfrequencies, while the damping terms only slightly

change the value of the eigenfrequencies (see the analogy with the SDoF system in 5.2 ‘Single Degree of Freedom system’).

The building response is computed in the frequency domain because this makes it easier to implement the frequency dependent stiffness and dashpot terms. A Forward Fourier Transform is used to find the building response in the frequency domain:

$$\tilde{\underline{u}}_b(\omega) = \int_{t=-\infty}^{\infty} \underline{u}_b(t) \cdot e^{-i\omega t} dt \quad (12.4)$$

Which transforms the equations of motion into:

$$(-\omega^2 \mathbf{M} + i\omega \mathbf{C}(\omega) + \mathbf{K}(\omega)) \tilde{\underline{u}}_b(\omega) = \underline{F}(\omega) \quad (12.5)$$

Where $(-\omega^2 \mathbf{M} + i\omega \mathbf{C}(\omega) + \mathbf{K}(\omega))$ is called the dynamic stiffness matrix (the impedance). The building response is computed by pre-multiplying both the left and right terms by the inverse of the dynamic stiffness matrix:

$$\tilde{\underline{u}}_b(\omega) = (-\omega^2 \mathbf{M} + i\omega \mathbf{C}(\omega) + \mathbf{K}(\omega))^{-1} \underline{F}(\omega) \quad (12.6)$$

The now computed building response $\tilde{\underline{u}}_b(\omega)$ is complex numbered and thus has a real- and an imaginary part ($\tilde{\underline{u}}_b(\omega) = Re(\tilde{\underline{u}}_b(\omega)) + Im(\tilde{\underline{u}}_b(\omega))$). The frequency spectrum of the building response (absolute values) is computed as:

$$|\tilde{\underline{u}}_b(\omega)| = \sqrt{Re(\tilde{\underline{u}}_b(\omega))^2 + Im(\tilde{\underline{u}}_b(\omega))^2} \quad (12.7)$$

The response of the building in the time domain is computed by performing the inverse Fourier Transform on the building response in the frequency domain:

$$\underline{u}_b(t) = \frac{1}{2\pi} \int_{\omega=-\infty}^{\infty} \tilde{\underline{u}}_b(\omega) \cdot e^{i\omega t} d\omega \quad (12.8)$$

Which is basically a summation of the form:

$$\underline{u}_b(t) = \frac{1}{2\pi} \cdot 2 \cdot d\omega \cdot \sum_{j=1}^N \left(Re(\tilde{\underline{u}}_b(\omega_j)) \cdot \cos(\omega_j \cdot t) + Im(\tilde{\underline{u}}_b(\omega_j)) \cdot \sin(\omega_j \cdot t) \right) \quad (12.9)$$

The now computed building response is only for the global rigid building motion. In case the structural design of the vibration sensitive structure only consists of a very rigid foundation block, this rigid building response can be used to compute the rms-velocities in the frequency domain (similar to the computation in 12.2.2 ‘Finding the response of the floor in the same form as the VC-curves’). The influence of changing a structural parameter can then be investigated. However, if one is interested in the dynamic response of a flexible (non-rigid) floor element, an additional computation is needed that takes into account the flexibility of the structural elements. The 3DoF rigid building motions (displacements) in the time domain are used as excitations on the flexible structural elements. This computation is elaborated in the next section 12.2 ‘Local Dynamic Response of Flexible Floor’.

12.2. Local Dynamic Response of Flexible Floor

The dynamic response of the bottom storey floor (or first floor) is of particular interest, because the vibration sensitive equipment is generally placed either on the foundation slab or the first floor. For this thesis a flexible frame is used to compute the dynamic response of the storey floor of interest, named ' w_1 ' (Figure 86 and Figure 87). The flexible frame takes into account the adjacent elements to w_1 as well to consider their influence on the dynamic response of w_1 (e.g. rotation stiffness at the boundaries of w_1 and the influence of the horizontal excitation on the vertical dynamic response of w_1). Since the response of interest of the local floor is the dynamic response, described more particular: the dynamic velocity, the gravity loading does not play a role, because the gravity loading is only static. Therefore, the gravity loading is not taken into account for the computation of the dynamic response of the flexible frame.

12.2.1. The composition of the flexible frame

The flexible frame is composed of four (undamped) Euler-Bernoulli beam floor elements: w_1, w_2, w_3, w_4 and four Euler-Bernoulli beam wall/column elements: u_1, u_2, u_3, u_4 . The principle of an Euler-Bernoulli beam (EB-beam) element was discussed in 5.5 'Continuous Systems'. Figure 86 is repeated from 5.5 'Continuous Systems' and gives a typical presentation of an EB-beam.

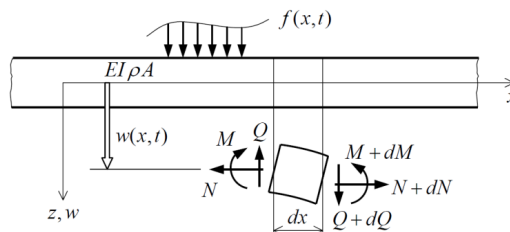


Figure 86. Typical representation of an EB-beam element

The dynamical properties of every EB-beam element consist of $EI_{i,j}$ (Nm^2), $\rho_{i,j}$ (kg/m^3) and $A_{i,j}$ (m^2) where: ($i = w, u$) and ($j = 1, 2, 3, 4$). The dynamic response of every EB-beam element is computed as its displacement (depending on time and the longitudinal coordinate of the element) perpendicular to the longitudinal axis of the element: $w_j(x,t)$ and $u_j(z,t)$ with ($j = 1, 2, 3, 4$). All EB-beam elements are assumed being inextensible (i.e. $EA = \infty$).

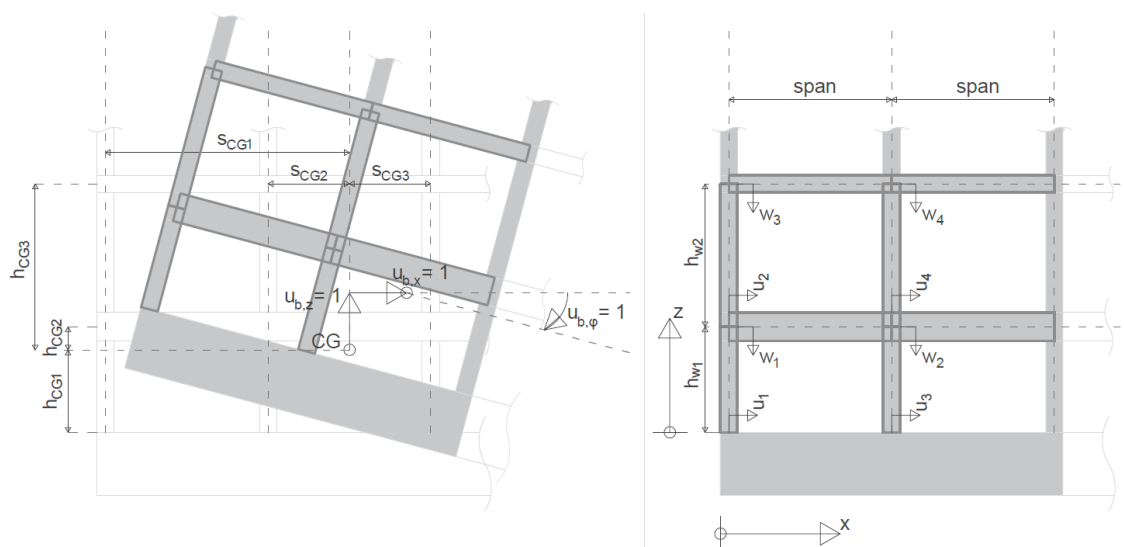


Figure 87. Principles for the flexible frame for computation of the local dynamic response of w_1 . Left: displaced flexible frame due to rigid building movement of 3DoF system. Right: flexible frame composed of four flexible Euler-Bernoulli beam floor elements w_1, w_2, w_3, w_4 and four flexible Euler-Bernoulli beam wall/column elements u_1, u_2, u_3, u_4

The equation of motion (EOM) of an EB-beam element consists of a fourth-order differential equation:

$$EI_{w,i} \frac{\delta^4 w_i(x,t)}{\delta x^4} + \rho A_{w,i} \frac{\delta^2 w_i(x,t)}{\delta t^2} = 0$$

or

$$EI_{u,i} \frac{\delta^4 u_i(z,t)}{\delta z^4} + \rho A_{u,i} \frac{\delta^2 u_i(z,t)}{\delta t^2} = 0$$
(12.10)

where ($i = 1, 2, 3, 4$).

The unknowns in the general solutions of the fourth-order differential equations need to be solved with the aid of the Boundary Conditions (BCs) of the element.

The flexible frame is rigidly fixed to the foundation slab which has a dynamical response equal to the 3DoF rigid building response computed in the previous section. This makes that the flexible frame for this thesis research is excited by the rigid building motion of the 3DoF system only. The BCs and ICs are such that they are compatible with the 3DoF rigid building motion and such that they make sure that the flexible frame is internally in equilibrium.

The dynamic response of the flexible EB-beam frame is solved as a summation of the dynamic responses of the frame due to all prescribed horizontal and vertical displacements and all prescribed rotations. In formula form this summation would look like:

$$Dyn_response = Dyn_response_{u_{b,x}} + Dyn_response_{u_{b,z}} + Dyn_response_{u_{b,\varphi}}$$
(12.11)

Where the BCs and ICs for every $Dyn_response_i$ ($i = u_{b,x}, u_{b,z}, u_{b,\varphi}$) can be different. All BCs and ICs per $Dyn_response_i$ are given in Appendices P to S (referenced as $Model_x$, $Model_z$ and $Model_\varphi$ respectively).

12.2.2. Finding the response of the floor in the same form as the VC-curves

In order to compare the dynamic response of w_1 with the VC-requirements, the dynamic response has to be transformed to velocities in the frequency domain. The expression of velocities of w_i is simply the computation of the time derivative: $\partial w_i(x,t)/\partial t$, which is numerically implemented in Python as:

$$\frac{\partial w_i(x,t)}{\partial t} = \frac{w_i(x,t+dt) - w_i(x,t)}{dt}$$
(12.12)

The representation of the dynamic response of w_1 (velocities, m/s), from here on called ' $v_{w1}(x,t)$ ' in the frequency domain is computed by a Forward Fourier Transform:

$$\tilde{v}_{w1}(x,\omega) = \int_{t=-\infty}^{\infty} v_{w1}(x,t) \cdot e^{-i\omega t} dt$$
(12.13)

and is numerically implemented in Python as:

$$\tilde{v}_{w1}(x,\omega) = \sum_{t=t_{min}}^{t_{max}} v_{w1}(x,t) \cdot e^{-i\omega t} dt$$
(12.14)

The result is a complex number (a real and an imaginary part). The absolute value is of interest to compare with the VC-requirement and is computed as:

$$|\tilde{v}_{w1}(x, \omega)| = \sqrt{\text{Re}(\tilde{v}_{w1}(x, \omega))^2 + \text{Im}(\tilde{v}_{w1}(x, \omega))^2} \quad (12.15)$$

Which gives the frequency spectrum of the dynamic floor response for a particular x -coordinate. The designing engineer (the user of the EDDABuSGS-tool) can give an array of x -coordinates for which the frequency spectrums need to be computed. However, the more x -coordinates, the longer the computational time for obtaining the results. Since the vibration sensitive equipment is often placed in the middle of the floor span, it is advised to compute the frequency spectrum at least for $x = \text{span}/2$. The VC-curves consider $1/3$ -octave bands and in every $1/3$ -octave band (j) the peak value of $|\tilde{v}_{w,i}(x, \omega)|$ is divided by $\sqrt{2}$, which gives the RMS-value of the frequency spectrum:

$$\tilde{v}_{w1,RMS,j}(x) = \frac{|\tilde{v}_{w1}(x)|_{peak,j}}{\sqrt{2}} \quad (12.16)$$

These RMS-spectrums are in the same unit as, and can be compared to, the VC-curve corresponding to the VC-requirement. Based on this the designing engineer can conclude whether or not the change in structural parameters is beneficial or not for reducing the vibration levels.

12.3. Verification of the Local Dynamic Response of the Flexible Floor

In order to verify EDDABuSGS the results are compared to the 'verification project Degrande et al. (3) – Building Response'. The 3DoF system is excited by the prescribed displaced soil (soil response) computed in 10.3.2 'Soil response verification project Degrande et al. (2) – Soil Building' for distances from the middle of the road from 16 m to 36 m with intervals of 2 m. The prescribed displacements and velocities of the soil excite the impedance springs and dashpots, which produces a force on the 3DoF system (Figure 88). The prescribed displacements and rotations are computed as averages of the soil response:

$$U_{x,avg}(t) = \left(\sum_i^N u_{x,i,z=0}(t) + u_{x,i,z=d_{emb}}(t) \right) / 2N \quad (12.17)$$

$$U_{z,avg}(t) = \left(\sum_i^N u_{z,i,z=d_{emb}}(t) \right) / N \quad (12.18)$$

$$U_{\phi,avg}(t) = \left(-\frac{U_{x,avg}(t)}{z_{CG} - d_{emb}/2} + \sum_i^N u_{z,i,z=d_{emb}}(t)/s_i \right) / (N + 1) \quad (12.19)$$

Where s_i is positive if the soil response point is located to the left of the vertical line of symmetry, and negative if the soil response point is located to the right of the vertical line of symmetry. The prescribed velocities ($V_{x,avg}$, and $V_{z,avg}$) and angular velocities ($V_{\phi,avg}$) are computed similarly. With the prescribed excitation the forces on the system are computed as:

$$\begin{aligned} F_{u,j,avg}(t, \omega) &= U_{j,avg}(t) \cdot K_j(\omega) \\ &\text{and} \\ F_{v,j,avg}(t, \omega) &= V_{j,avg}(t) \cdot C_j(\omega) \end{aligned} \quad (12.20)$$

where $j = x, z, \varphi$, which makes that the equations of motions: $M\ddot{u}_b(t) + C(\omega)\dot{u}_b(t) + K(\omega)u_b(t) = F(t, \omega)$ can be solved as described in 12.1 ‘Global Dynamic Response of the 3DoF Rigid Building’. The averaging of the soil responses as excitation to the 3DoF system can be justified for this thesis research since only low frequency soil responses, with a large wavelength (soft soils: $\lambda \geq 15$ m), are considered. Due to the large wavelength the soil response along the length- and the depth of the building deviates only for small amounts and can therefore be averaged out (Figure 89). Also, due to the assumption of rigidity of the structure, the structure cannot deform in the shape of the high frequency soil response (with small wavelengths), which makes that the structure reflects the high frequency soil responses for a great part back into the soil medium.

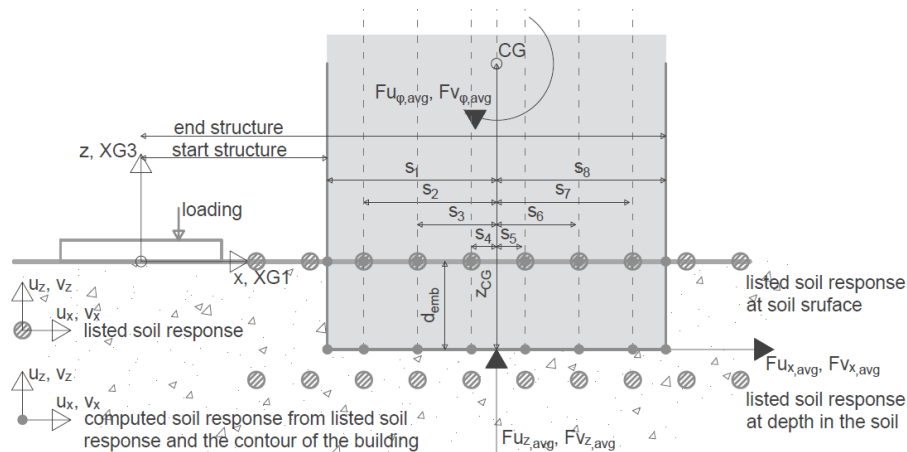


Figure 88. Principle of the computation of the excitation for the 3DoF rigid building system (displaced springs and dashpots)

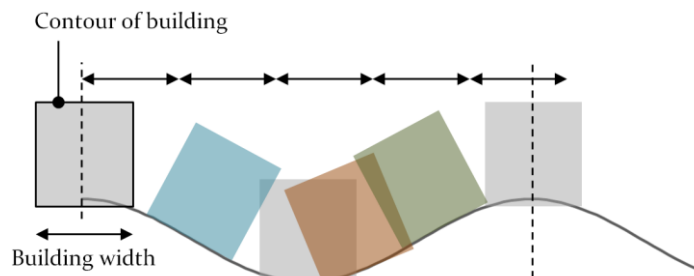


Figure 89. Principle of maximum building length which can be assumed to be rigid for a given wavelength of the soil response

The input parameters given for the computation of the structural response are included in Appendix N ‘Appendix: Input parameters for Verification Project Degrande et al. (3) – Building Response’. The entire building lengths are assumed to be rigid for the 3DoF system. The structural response of the global 3DoF system is represented in Figure 90. The local floor parameters are chosen in line with the figures that were given in the report of the verification project (Degrande, Pyl, & Clouteau, 2004). The prediction of the local floor response matches the measured floor response well. The prediction done in this Master thesis is more similar to the measured floor response than the prediction done in the verification project, therefore only the floor response computed by EDDABuS_{GS} and the measured floor response are compared in (Figure 91). The floor response computed by the EDDABuS_{GS} in the time domain has a peak velocity of approximately $1.0 \cdot 10^{-3}$ m/s, while the measurements show a peak velocity of approximately $0.75 \cdot 10^{-3}$ m/s.

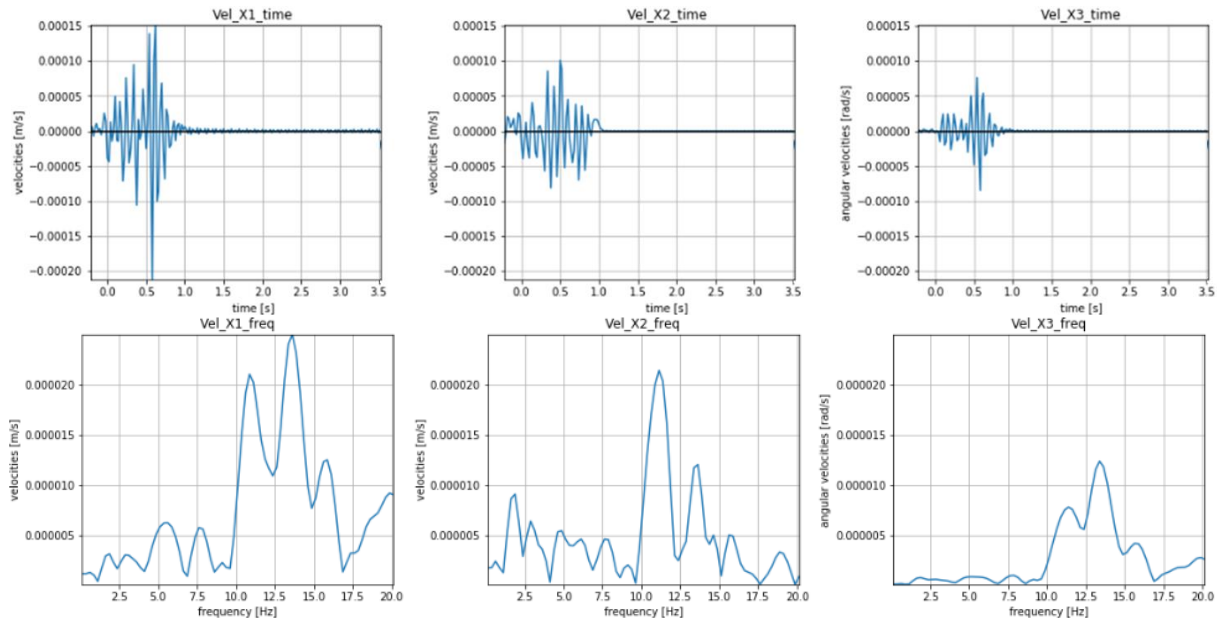


Figure 90. Structural response in the time domain (top) and the frequency domain (bottom) for all three DoF (x, z, φ) of the 3DoF system modelled for verification project Degrande et al. (3) – Building Response

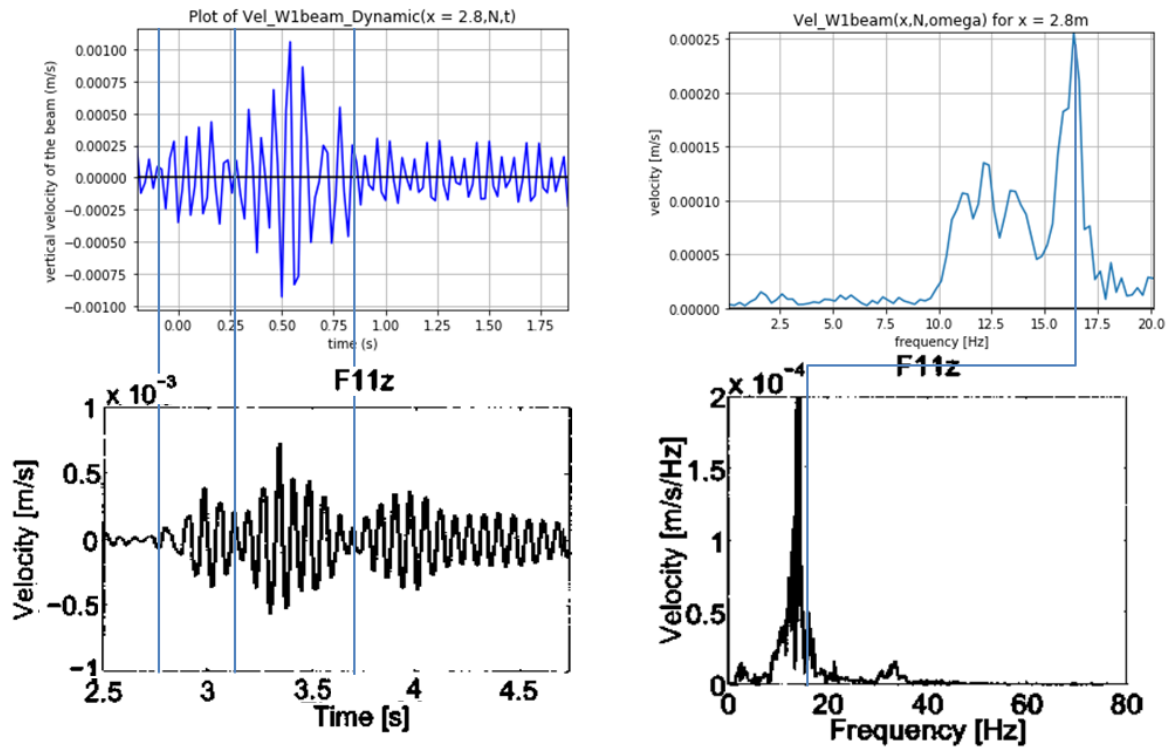


Figure 91. Predicted local EB-beam- (top) and measured- (bottom) structural response of the first floor in the time domain (left) and frequency domain (right) for verification project Degrande et al. (3) – Building Response

Since the computed structural response of the floor is very similar to the measured response of the floor, the computation of the structural response by EDDABuSGS is now assumed to be verified. The verified EDDABuSGS-tool will be used for performing several iterations for a vibration sensitive laboratory building located in Amsterdam, The Netherlands, to see the influence of changing certain parameters. This is done in the next chapter 13 ‘Results from Iterations by EDDABuSGS and Design Chart’.

12.4. Consequences for soil response and structural response when changing the Belgium soil into the Amsterdam soil

The structural response is also computed for the situation in which the building of the verification project is located in Amsterdam, The Netherlands. The only difference which is taken into account is the soil layering (softer soil).

First the free field soil response is compared between the case of the layered soil of Verification Project Degrande et al. (1) – Free Field (in Belgium, ‘stiffer’ soil) and the layered soil of Amsterdam (in The Netherlands, ‘soft’ soil). The results of this computation are included in Appendix O ‘Appendix: Results for Verification Project Degrande et al. (1) – Free Field and (3) – Building Response with layered soil of Amsterdam’. A different soil layering significantly influences the soil vibrations:

- Amplitudes of the soil velocities are amplified by a factor 2 to 3.
- The frequency content of the soil velocities around 5 Hz is amplified by a factor > 20
- The frequency content of the soil velocities between 10 and 17 Hz is amplified by a factor 2.5 to 3.

The principle of the altered soil response due to the softer soil layering also holds for Verification project Degrande et al. (3) – Building Response. The consequence for the computation of the building response is that the excitation on the building has larger amplitudes, with a lower frequency content, and the impedances of the flexible supported building are smaller. The results of this computation are also included in Appendix O ‘Appendix: Results for Verification Project Degrande et al. (1) – Free Field and (3) – Building Response with layered soil of Amsterdam’ and show that a different soil layering significantly influences the structural vibrations:

- Amplitudes of the structural vibration are amplified by a factor 2 to 3
- The lower frequency content (between 3 and 10 Hz) is much more excited (factor 10 around 5 Hz).

It is expected that the EDDABuS_{GS}-tool will perform better for the type of buildings that is aimed for when developing the tool, namely rather rigid and heavy vibration sensitive laboratory buildings, which can be assumed invariant in the y-direction. The building in the verification project, however, is more flexible and has a much smaller width in the y-direction than the length in the x-direction, and thus can only be modelled reliably to a certain extent. Measurements performed for rigid vibration sensitive buildings, which are specified such that they can also be modelled in EDDABuS_{GS}, are scarce. Therefore, future research should aim on performing measurements for structures that can be modelled by the computational model in order to verify the EDDABuS_{GS}-tool more thoroughly.

Part IV

Results & Conclusion

13. Results from Iterations by EDDABuS_{GS} and Design Chart

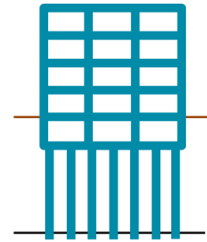
After verifying the computational tool EDDABuS_{GS} with the verification projects the tool has been used to perform iterations on the structural parameters to see what the influence of a parameter on the computed structural response is. A list of the computed iterations has been included in Appendix T ‘Appendix: Iterations of structural parameters to compute structural response’. A brief summary of the observations is given here and the design chart for vibration sensitive laboratory structures is computed from all knowledge gained by the literature study, the computations made for the verification projects and the iterations that were made with EDDABuS_{GS} (manual for tool included in Appendix U ‘Appendix: User manual of EDDABuS_{GS}’). It must be noted that the described observations only hold for the specific modelled situation. The excitation and structural response might be different for other cases.

13.1. Observations from Iterations

Reference case

The reference case is based on a fictional building in Amsterdam, The Netherlands. A brief description of the observations from the computations of the reference case has been included:

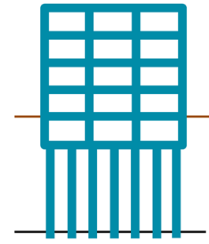
- Loading: dominant loading frequency content is in-between 3 and 10 Hz.
- 3DoF response: dominant 3DoF response frequency content is also in-between 3 and 10 Hz. The horizontal translational motion $u_{b,x}$ (X_1) has the greatest response and from the time domain one can observe that X_1 is approximately 4 times larger than X_2 (vertical translation $u_{b,z}$) and 10 times larger than X_3 (rotational motion $u_{b,\varphi}$).
- 3DoF response: the eigenfrequencies of the global 3DoF system in the range $0.2 \text{ Hz} \leq f \leq 20 \text{ Hz}$ are approximately 1.8 Hz, 1.95 Hz and 8.3 Hz.
- 3DoF response: The structural response amplitude is much larger for the horizontal translation than the vertical translation and rotation.
- 3DoF response: the damping-impedance terms for the horizontal translation are the smallest. The damping-impedance terms of the vertical translation are approximately 2 to 7 (depending on the frequency) times larger than the horizontal translational damping-impedance term. The rotational damping-impedance term is the highest and is approximately 100 to 200 (depending on frequency) times larger than the horizontal translational damping-impedance term.
- 3DoF response: The RMS values of the global 3DoF response are equal- or smaller than 15 $\mu\text{m/s}$.
- EB-beam floor response: the local structural response has no damping, therefore the response is never zero. After approximately 1.5 seconds, the floor is vibrating freely (without any excitation). Due to the numerical solution strategy (continuous Fourier expansion) the floor response is non-zero before $t = 0$ as well.
- EB-beam floor response: the local structural floor response has a maximum RMS value equal to 18.5 $\mu\text{m/s}$. The structural response has thus been amplified by a factor 1.23 when comparing the global structural response to the local structural response.
- Computational time for structural response results in the time domain: 42 mins.
- Computational time for structural response results in the time domain and frequency domain, including the RMS values of the velocities in the frequency domain: 342 mins.



Iteration: greater global building mass & stiffer local EB-beam floor

The greater global building mass ($2 \cdot M_b$) realizes a greater resistance against vibrations (impedance) for the 3DoF global building response. The eigenfrequencies have become smaller (factor 0.9), further away from the dominant loading frequencies, which makes that the structural response (globally and locally) has smaller amplitudes.

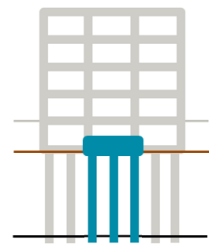
The stiffer local EB-beam floor element ($1.6 \cdot E$) realizes a greater resistance against vibrations (impedance) for the local EB-beam floor. The eigenfrequencies have shifted to the higher frequency range (> 10 Hz, further away from the dominant loading frequencies) which makes that the structural response (locally) has smaller amplitudes (factor 1.1 to 1.3).



Iteration: small rigid block

The structure is changed from large and heavy structure with flexible elements locally, into a smaller and very rigid structure. The following observations were made:

- Loading: lower forces (factor 10) and higher frequency content (dominant loading frequencies shifted to the right).
- 3DoF response: higher eigenfrequencies (5.85 Hz, 9.0 Hz, 11.95 Hz), smaller displacements and velocities X_1 (horiz. Translation, factor 0.4), but larger displacements and velocities X_2 (vert. translation, factor 2.4) and X_3 (rotation, factor 4.3). Lower supporting impedances (factor 5 to 100).
- EB-beam floor response: larger velocity peak in the time domain (factor 1.2). Smaller RMS value of velocities (factor 0.77).
- RMS value of EB-beam floor increased by factor 2.3 compared to RMS value of 3DoF.

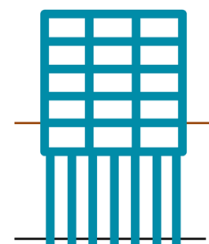


Conclusion: Due to the smaller dimensions of the structure, the stiffness impedance terms are mostly positive (while for the reference case, they become negative for a great frequency range) (see the tables of Gazetas and accompanying figures (Gazetas G. , 1991)). This means that the soil vibrations do not amplify the structural vibrations (which would be the case for negative stiffness terms), resulting in smaller RMS velocities eventually. However, it is expected that the stiffness impedance terms of the reference case are underestimated; they should attain lesser negative values or even positive values. Less negative impedance terms for the reference case would result in smaller RMS velocities as well.

Iteration: greater G value for (stiffer) soil impedances

The soil shear modulus is increased by a factor 5. This is only done in the impedance terms for the building supports. The excitation was remained unaffected (thus not taking into account the reduced excitation amplitudes and increased frequency content which would be the case in a real stiffer soil). The following observations were made:

- Loading: larger amplitudes (factor 1.75 to 3) and similar frequency content.
- 3DoF response: higher eigenfrequencies (2.85 Hz, 3.6 Hz, 11.85 Hz), larger amplitudes for displacements and velocities (factor 1 to 1.1). Greater supporting impedances (factor 2.5 to 3.5).
- EB-beam floor response: slightly larger amplitudes for (RMS) velocities (factor 1.1).
- RMS value of EB-beam floor increased by factor 1.3 compared to RMS value of 3DoF.



Conclusion: the greater stiffness of the soil (without taking into account the altered soil response) increases the impedance terms that support the 3DoF system. However due to the stiffening effect, the eigenfrequencies of the 3DoF system have come closer to the dominant excitation frequencies. The amplification of the vibration amplitude due to the higher

eigenfrequencies is greater than the decreasing effect of the vibration amplitude due to the increased impedance, which eventually results in a larger (RMS) value of the velocities.

This phenomenon can be explained from a more general approach, including all structural properties:

The mass distribution M_b and the mass moment of inertia J_{CG} of the structure influence the eigenfrequencies at which the structure vibrates. A larger value for both of these properties means an elongation of the natural period and thus lower eigenfrequencies. However, a greater stiffness K_j (which could be caused by a stiffer soil, a greater embedment depth and/or a stiffer pile foundation) creates a stiffening effect. The result is a shortening of the natural period and an increase of the eigenfrequencies.

Next to an influence on the eigenfrequencies, the mass, mass moment of inertia and the stiffness of the structural supports influence the resistance against vibrations (impedance, i.e. $\tilde{u}_b(\omega) = (-\omega^2 \mathbf{M} + i\omega \mathbf{C}(\omega) + \mathbf{K}(\omega))^{-1} \underline{F}(\omega)$) as well. A larger value for all of these properties means a greater impedance.

Whether or not a larger value of the mass, mass moment of inertia and the stiffness of the structural supports is beneficial depends on the ratio between the dominant frequencies of the loading and the eigenfrequencies of the structure ($f_{dom,load}/f_{n,str} \sim \omega/\omega_n$). The meaning of this can in principle be derived from the single degree of freedom system (Figure 92): in case ω/ω_n is close to 1 and an increase of the value K_j (or k_s in the figure) makes that this ratio is even closer to 1 (red arrow), the change in eigenfrequency makes that the response amplitude is raised to the power > 1 (parabolic, derivative ' r_c ' > 1), while the change in impedance makes that the response amplitude is only decreased to the power ≈ 1 (linearly, derivative ' r_c ' ≈ 1). In that case, the increase in stiffness is not beneficial in reducing the structural vibrations, because the amplification due to the change in eigenfrequency is greater than the reduction due to the increased impedance. However if ω/ω_n is approximately smaller than 0.4 or larger than 1.6 (green arrow) (these values are related to Figure 92 for a SDoF system and can differ for a specific situation), the change in eigenfrequency makes that the response amplitude is raised to the power $\ll 1$ ($r_c \ll 1$), while the impedance makes that the response amplitude is decreased to the power ≈ 1 ($r_c \approx 1$). In that case the increase of stiffness is beneficial in reducing the structural vibrations.

In the case of this specific iteration it thus appears that the increase of the eigenfrequencies has more influence on the amplitude of the vibrational response (amplification) than the increased impedance.

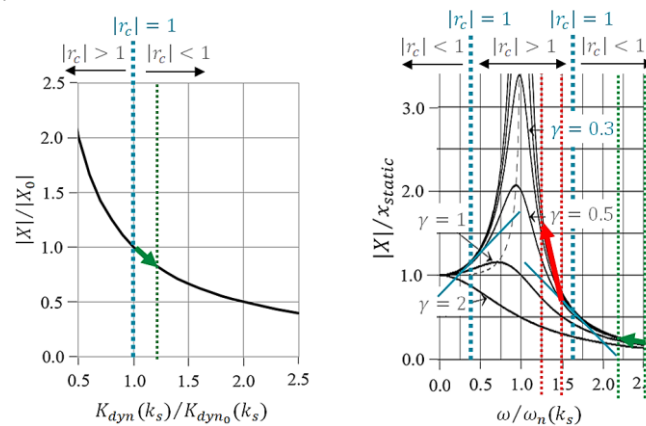
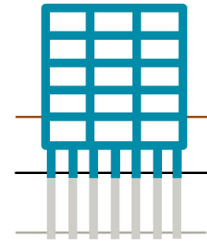


Figure 92. Principal of the effect on the amplitude of the structural response due to an increased impedance (left) and increased eigenfrequency (right) caused by a higher spring stiffness k_s . Green arrow: effect of increased impedance is greater than effect of increased eigenfrequency. Red arrow: effect of increased impedance is smaller than effect of increased eigenfrequency

Iteration: smaller pile length and raised sand layer

The pile length is reduced by a factor 3 and the load bearing sand layer has been lifted up together with the pile toes. Similar to the iteration with a greater shear modulus of the soil (G), the shorter pile lengths realize a stiffening effect for the global 3DoF system (mainly in the vertical and rotational direction: factor 10 increase of the vertical and rotational impedance stiffness terms). The eigenfrequencies have shifted to the right (higher eigenfrequencies: factor > 3). Both the global 3DoF- and local EB-beam floor response have slightly larger amplitudes (factor 1.1), while the resistance against vibrations (impedances) has increased. The reason for this is in principle similar to the previous iteration 'iteration: greater G value for (stiffer) soil impedances,' where the increase of the eigenfrequency has more influence on the amplitude of the vibrational response (amplification) than the increased impedance.

**Iteration: decreased computational time by changing computational parameters**

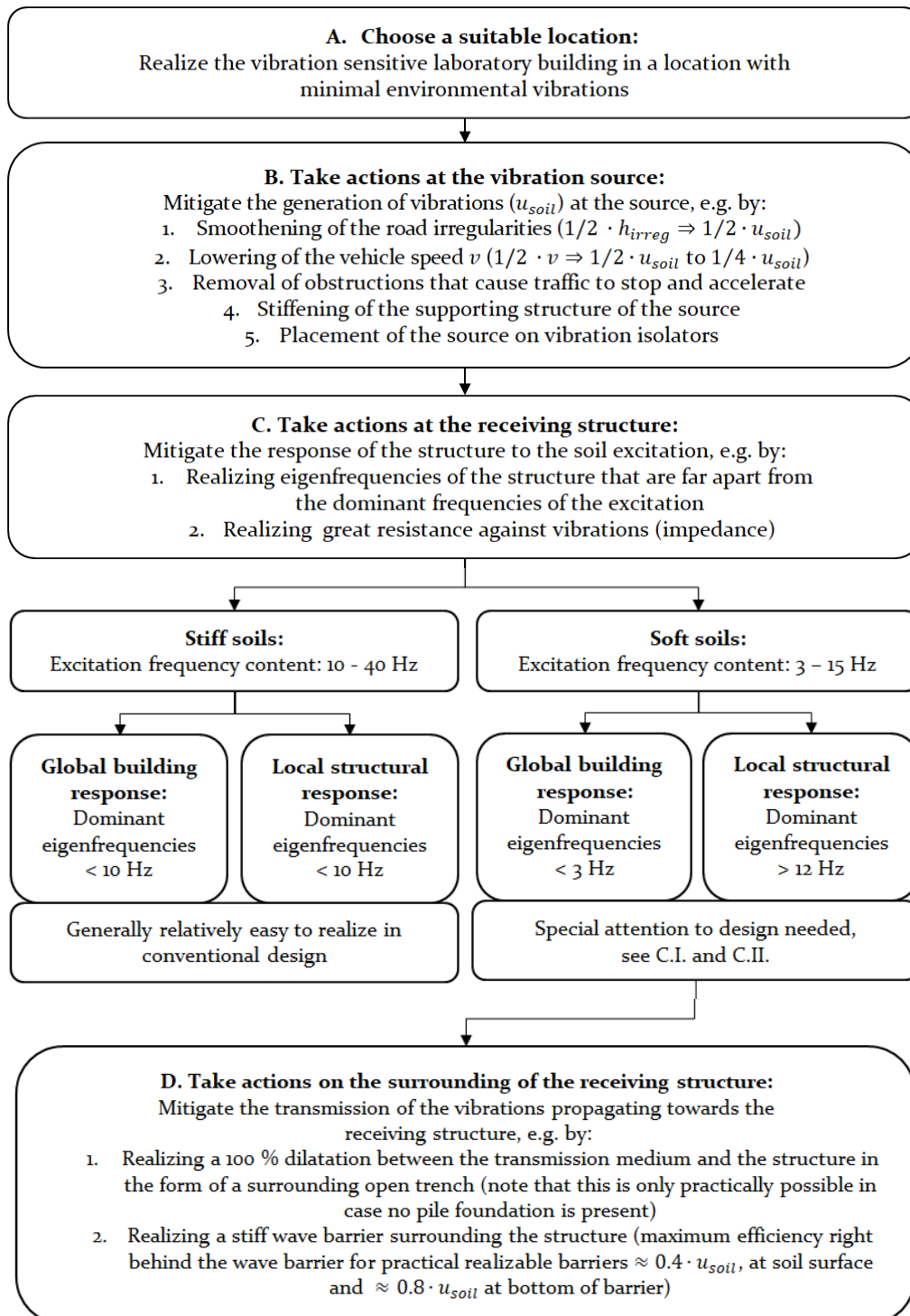
The iterations for changing the computational parameters t_{step} , t_{nr} , f_{step} and f_{nr} show that the computational time of EDDABuSGS can be decreased while still obtaining reliable results. However, taking too large steps and/or a too small range will result in unreliable results. It appears that, for the reference case (building in Amsterdam), the computational time can be reduced by a factor 0.35 (results in the time domain) to 0.55 (results in the time- and frequency domain), while still obtaining reliable results if the time- and frequency steps are unchanged, but the frequency range is decreased by a factor 2 (resulting in $f_{max} = 10.1$ Hz). The frequencies higher than 10 Hz do not significantly contribute to the structural response and can therefore be left out. The resulting computational times are:

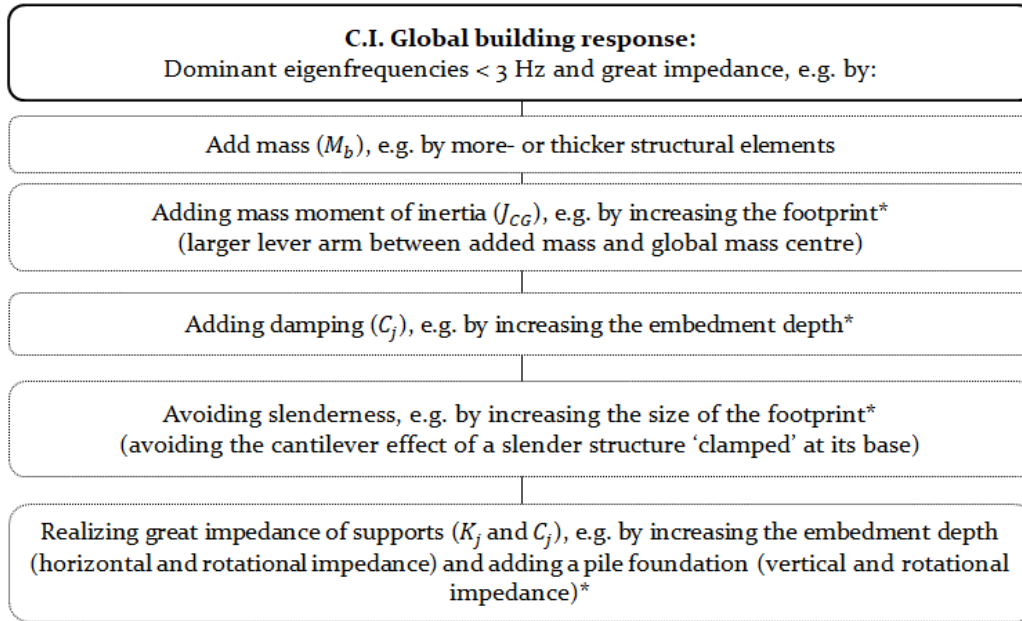
- Computational time for structural response results in the time domain: 24 mins.
- Computational time for structural response results in the time domain and frequency domain, including the RMS values of the velocities in the frequency domain: 118 mins.

13.2. Design Chart for Vibration Sensitive Laboratory Structures

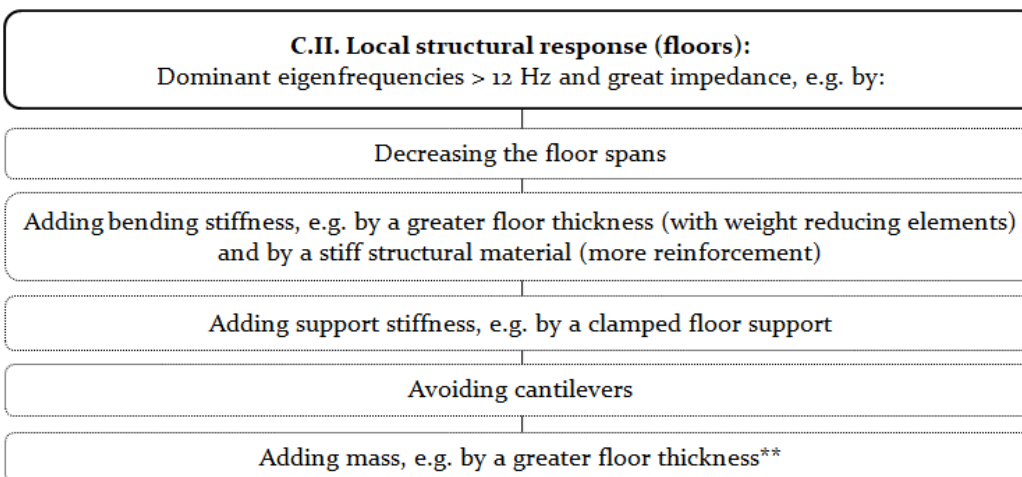
This section will briefly describe the particularities that need to be considered when designing a vibration sensitive laboratory structure which is excited by traffic induced vibrations, first in general and then more specific for the situation of soft soils in The Netherlands (Amsterdam). Note that the chart is limited to traffic induced vibrations and does not account for any other type of loading specifically. Also, no such elements as vibration isolating islands are mentioned because these are not part of the superstructure. The early design decisions based on this design chart should always be verified by a building physics/vibrations expert.

The representation of these particularities is done in the form of a design chart in top-down order:





* Be careful: this mitigation measure also increases the eigenfrequencies (*stiffening effect*). The eigenfrequencies thus come closer to the excitation frequencies. Always check whether the influence on the vibrations of increased impedance is greater than the influence of increased eigenfrequencies)



** Be careful: this mitigation measure also decreases the eigenfrequencies (*limbering effect*, which is the opposite of the *stiffening effect*). The eigenfrequencies thus come closer to the excitation frequencies. Always check whether the influence on the vibrations of increased impedance is greater than the influence of decreased eigenfrequencies)

14. Conclusions and Recommendations

The aim of this research was to create a practical engineering tool consisting of a computational part and a design chart which should give a structural engineer the ability to get insight into the influence of changing certain building parameters on the dynamic structural behaviour. This chapter concludes the research by answering the research questions that were derived at the start of this research, mentioned in 1.2 ‘Scope’. Thereafter recommendations will be given on how the EDDABuS_{GS}-tool should be used for designing purposes. Also, recommendations are considered for future work with the aim to further improve the EDDABuS_{GS}-tool.

Note that the conclusions made are based on the literature study and on the computed results (iterations in chapter 13) for a 2D building model, which is assumed to be rigid globally (entire building) and flexible locally (floor), located in a soft soil (more specific Amsterdam, The Netherlands), which is excited by heavy traffic induced soil vibrations only.

14.1. Discussion of Results

This section describes the relevant results for each of the research questions which are derived from the observations made by the iterations (described in 13.1 ‘Observations from Iterations’) and from the literature research.

How can *the* 2D model give reliable predictions for the 3D problem?

The 2D approximation

The 2D model considers the computation of the structural response in the (x,z)-plane. This means that the EDDABuS_{GS}-tool can only be expected to give reliable predictions for buildings that are not vulnerable to torsion, have dominant floor spans parallel to the x-direction (and thus can be assumed invariant in the y-direction) and are placed such that the (x,z)-plane is parallel to the dominant line of soil excitation.

The EDDABuS_{GS}-tool in general

First it is worth mentioning that the model in general is developed based on well-established mathematics and computational techniques and is verified with practical cases and examples that are relevant for this specific research.

- **Rigidity of the structure**

The 2D model assumes rigidity of the global structural response which is generally a simplification that can be made for vibration sensitive laboratory structures, because these buildings are often realized with a rigid structure. Flexible buildings, such as the one in the verification project of Degrande et al. can therefore be modelled less accurately and the vibration predictions are less reliable. Also due to rigidity of the structure, the excitation on the 3DoF system can be assumed as an average loading in the direction of every three degrees of freedom at a particular point of engagement. Flexible structures ask for a loading which is distributed along the building length. A similar reasoning applies to the soil impedances that are determined by the substructuring approach, assuming rigid body motions of the structure.

- **Low frequency content of the soil response**

Next to the rigidity of the structure itself, also the frequency content of the soil response, and thus the length of the dominant shear waves determines whether or not the assumption of global rigidity can be made. In case of traffic induced vibrations in soft soils, the dominant frequency content is generally low (< 10 Hz). Low frequency loadings have longer wavelengths (λ). The longer wavelengths make that larger building lengths (L_b) can be assumed to be rigid ($L_b \leq 1/4 \cdot \lambda_{\text{dominant}}$) (Figure 89).

- **Governing loading type is heavy traffic induced vibrations**

The type of loading for this computational tool considers the soil responses in Amsterdam due to heavy traffic only. This means that loading due to e.g. walking and machinery inside the

building and e.g. wind loading outside the building are not considered for this tool. The results obtained by this tool can only be reliable in the case that heavy traffic induced vibrations are the dominant loading type and in case the soil is similar to the modelled soil of Amsterdam.

- ***Small frequency- and time step but large frequency- and time range***

The requirements for a reliable computation of the results ask for a small time- (≤ 0.02 s) and frequency- (≤ 0.25 Hz) step, a small minimum value of the frequency range ($f_{step}/2$) and a large time- (e.g. $-0.2 \geq t \geq 1.5$ s) and frequency- (e.g. $0.125 \geq f \geq 20$ Hz) range. These requirements directly contradict the aim of a practical engineering tool which should compute the structural response within a couple of minutes. The smaller the step and the larger the range, the longer the computational time will be, which can add up to a day or even more. Therefore the frequency- and time step can be chosen bigger and a smaller range can be considered to make the computational time lower (see Appendix T: ‘Appendix: Iterations of structural parameters to compute structural response’). The dominant frequencies of the loading and the structural response are still reliable, however the amplitudes of both are generally overestimated (too large amplitudes, factor: 2 to 3.5) for a too coarse frequency domain and underestimated (too small amplitudes, factor: 0.75 to 1) for a too coarse time domain. Note that these values relate to the iterations made within this thesis research.

- ***Overestimation of eigenfrequencies local floor element***

An important note to make here is that the Euler-Bernoulli (clamped-clamped) representation of the local floor generally overestimates the floor’s eigenfrequencies (factor 1.5 – 3.4). Determining the influence factor of changing parameters can therefore be unreliable.

- ***Verification of the computed results***

Comparison of the computed results with the verification projects and the knowledge gained from the literature study show good agreement. The verification of the structural response could only partly be done because the type of building of the available verification project is not entirely suitable for the computational tool EDDABuS_{GS}.

How do the properties of the structure influence its vibrations?

- ***Influence on the eigenfrequencies of the structure***

From the iteration results performed by EDDABuS_{GS} the following conclusions can be made. The mass M_b and the mass moment of inertia J_{CG} of the structure influence the eigenfrequencies at which the structure vibrates. A larger value for both of these properties means an elongation of the natural period and thus (a) lower eigenfrequencies (or eigenfrequency). However, a greater embedment depth creates a larger value for damping and a stiffening effect. The structure can then be assumed to have stiffer structural supports (horizontal translation and rotational). The result is a shortening of the natural period and an increase of the eigenfrequencies (or eigenfrequency). End-bearing foundation piles also create a stiffening effect, however the amount of this effect depends on the excitation frequency and the axis-axis distance between the foundation piles. These conclusions are well in line with the applicable theory and therefore substantiate the reliability of the EDDABuS_{GS}-tool.

- ***Influence on the impedances of the structure***

Next to an influence on the eigenfrequencies, the mass, mass moment of inertia and the stiffness of the structural supports influence the resistance against vibrations (impedance, i.e. $\tilde{u}_b(\omega) = (-\omega^2 \mathbf{M} + i\omega \mathbf{C}(\omega) + \mathbf{K}(\omega))^{-1} \mathbf{F}(\omega)$) as well. A larger value for all of these properties means a greater impedance. This conclusion is well in line with the applicable theory and therefore substantiates the reliability of the EDDABuS_{GS}-tool.

- ***Reduction of vibration amplitude depends on both the shift in eigenfrequencies and the increase of the impedances***

Whether or not a larger value of the mass, mass moment of inertia and the stiffness of the building and the structural supports is beneficial for reducing the vibration amplitude depends on the change in ratio between the eigenfrequency of the structure and the dominant

frequency of the loading ($f_{n, str}/f_{dom, load}$) and on the increase of the impedance (see 13.1 'Observations from Iterations'). An increase in the values of mass and stiffness can be regarded to be beneficial for reducing the structural vibrations always if the ratio $f_{n, str}/f_{dom, load}$ gets further away from the value 1.0. This conclusion is well in line with the applicable theory and therefore substantiates the reliability of the EDDABuS_{GS}-tool.

- ***Damping always reduces the vibration amplitude***

Damping in the system appears to be beneficial always because it hardly affects the eigenfrequencies of the structure but does increase the resistance against vibrations.

In what ways do variations in built-ups of different soil layers influence the design of the structure?

- ***Frequency content of stiff soils is high, while for soft soils it is low***

The built-up of the different soil layers determines how stiff the soil reacts to the induced loads and how stiff the support of the soil towards the building is. Generally, a stiff soil has a relatively high frequency content (10 – 40 Hz excitation on the building), while soft soils have a lower frequency content (3 – 15 Hz excitation on the building).

- ***Stiff soils: conventional design, soft soils: special design attention needed***

This makes that in stiff soils the dominant eigenfrequencies of the structure should be lower than 10 Hz. This is generally quite well realisable in a conventional building design. However, in case of soft soils the dominant eigenfrequencies of the structure should be either very low (< 3 Hz) or relatively high (> 15 Hz). However, it is not easy to design a structure that has eigenfrequencies higher than 15 Hz (locally) or lower than 3 Hz (globally) while still realizing a large impedance of the structure.

How do sensitivities in the used models influence the structures design and how can these sensitivities be minimized?

- ***Simplifications made in the modelling***

The sensitivities in the model are introduced by simplifications made for the EDDABuS_{GS}-tool and by input parameters that can only be approximated to a limited extent. Also, the model is developed for one particular situation only: a soft soil (western part and northern of the Netherlands) which is excited by heavy traffic. The excitation is limited to one particular vehicle speed and induces loads on a very rigid building structure. The structure is not vulnerable to torsion and its structural vibrations are dominant the (x,z)-plane. Any deviation in these parameters brings an extra uncertainty to the reliability of the computed results.

- ***Approximation of the soil impedances based on extrapolation of existing results***

The main sensitivities of the EDDABuS_{GS}-tool consist of the simplification of the soil impedances based on the extrapolation of the tables of Gazetas which simplifies the soil to a non-layered homogeneous halfspace. It has not been verified whether this extrapolation is reliable. The expectation is that the vertical impedances are underestimated for $f \geq 3$ Hz (factor -4 to 1), thus underestimating the stiffness and damping of the supporting soil and overestimated for $f < 3$ Hz (factor 1 to 2). The horizontal impedances are, depending on the frequency, either underestimated or overestimated (factor 0.8 – 3). The underestimation of the stiffness impedance terms might be on the non-conservative side since the eigenfrequencies of the global building response can in reality come closer to the dominant loading frequencies.

- ***Approximation of the pile impedances based on extrapolation of existing results***

Also, the impedances generated by the pile foundation is greatly simplified by considering one particular situation and extrapolating this situation to all possible situations that can be modelled. First, the assumptions made for the geometry of the individual piles (L/d and E_{pile}/E_{soil}) and the pile groups (S) possibly bring a great sensitivity to the reliability of the computed results. Also, the fact that the pile group interaction factors are based on a limited

amount of information for already existing computations of pile groups might oversimplify the group interaction between the piles. The expectation is that the group interaction factors are underestimated for $f \leq 5$ Hz (factor 0.8 to 1), meaning that the stiffness and damping of the pile group is underestimated, and overestimated for $f > 5$ Hz (factor 1 to 4). The underestimation might be on the non-conservative side since the eigenfrequencies of the global building response can in reality come closer to the dominant loading frequencies.

- ***Computational parameters considering the frequency- and time instants***

For the computation of the results themselves a big sensitivity lies in the chosen computational parameters considering the time step, time range, frequency step and frequency range. The larger the time- and frequency step, the more unreliable the results will be. Also, a small time- and frequency range will make the results more unreliable. The expectation is that a larger frequency step will overestimate the response amplitude and is thus on the conservative side. However, a larger time step is expected to underestimate the response amplitude (see ‘Small frequency- and time step but large frequency- and time range’ in this section). Also, choosing a small step and a large range increases the computational time significantly, which makes that a large step and a small range is more preferred in the design phase.

- ***Results computed for limited amount of positions on the local floor***

In addition, to keep the computational time of the EDDABuS_{GS}-tool low, the structural response is only computed for a limited amount of x -coordinates along the length of the floor. It is not known in advance at which location the maximum RMS velocity in the frequency domain is going to occur. This makes that the reasoning whether or not a change in parameters is beneficial based on the limited amount of points can be unreliable (factor 0.6 to 1.5). A great amount of points should be considered for a reliable overview, however the problem then is the significantly increased computational time.

What is the influence of external interventions on the structure’s design?

In general, a decreased soil response results in a decreased excitation on the structure, thus allowing for less vibration mitigation measures in the (structural) design.

- ***Wave barriers reduce the soil vibrations only in the shadowing region***

From the literature study and the brief analysis in 10.3.4 ‘Soil response attenuation by wave barrier in soil of Amsterdam’ it can be concluded that the wave barrier always decreases the soil response in the shadowing region just behind the wave barrier (factor 0.2 to 1). However, the wave barrier needs to be thick enough (width $\geq 0.1 \cdot \lambda_R$) in order to give sufficient resistance to the vibration. Also, the depth of the wave barrier should be sufficiently large so that the receiving structure behind the wave barrier falls within the shadowing region of the wave barrier (depth barrier \geq depth of building and depth barrier $\geq 1/3 \cdot$ length building for a reduction factor approximately equal to 0.5 at soil surface). A drawback of the wave barrier is that it can significantly amplify the vibration amplitude at the side of the incoming waves (factor 1 to 2).

- ***Road on pile foundation decreases vibrations at soil surface but can cause a bridging effect (substantiated by literature research only)***

An external intervention in the form of making a pile foundation underneath the road on which the moving loads are generated assures a decreased soil response at the surface of the soil. However, if both the building and the road have a pile foundation and the pile toes are placed on the same sand layer, a bridging effect of the vibrations might occur. In that case the vibrations propagate through the piles underneath the road, continuing through the stiff soil layer at the pile toes, and eventually exciting the piles underneath the building. The result is a non-beneficial effect on the vibration mitigation.

- ***Cavities decrease the soil response in the shadowing region but also significantly lower the impedances of the building (substantiated by literature research only)***

A cavity surrounding the structure assures that no soil excitation on the building can take place at these locations. However, in soft clay soils, the buildings are generally placed on foundation piles and since the cavities can practically not be made longer than the pile length, the soil can still excite the foundation piles. Due to the cavity near the soil surface the building barely has any horizontal resistance against vibrations. This makes that only a dense and complex pile grid (inclined piles) can give sufficient horizontal resistance.

Overall conclusion

Due to the comprehensive approach of this Master thesis research, many factors influencing the design of a vibration sensitive laboratory structure have been considered, analysed, verified and implemented in the EDDABuS_{GS}-tool. Together, the computational EDDABuS_{GS}-tool and the design chart give an extensive overview of the influence of several important structural (and non-structural) parameters on the vibration levels inside the building. The computed results and the conclusions that are made from these results are in line with what is to be expected from the applicable theory. Therefore, the EDDABuS_{GS}-tool does what it is expected to do and the goal of this thesis, to develop a practical engineering tool for an early design phase of a project concerning vibration sensitive laboratory structures, is accomplished. However, the reliability of EDDABuS_{GS} can be improved by a more thorough verification of the simplifications made and by the implementation of more realistic, but computationally heavy, modelling of e.g. the structure and the soil medium.

14.2. Recommendations for Designing, Using EDDABuS_{GS}

- ***Use the EDDABuS_{GS}-tool for determining influences factors only***

It is advised to use the EDDABuS_{GS}-tool only for the purpose to see the effect of changing certain parameters on the structural response (ratios) and not to compute an absolute value on which will be based whether or not the design meets the vibration level requirements. This holds in general because due to all simplifications made the absolute value of the amplitudes cannot be predicted reliably.

- ***Model an equivalent local floor element with reliable dominant eigenfrequency***

First model a reference floor in a FEM software (e.g. Scia) and from that model obtain the dominant eigenfrequency (for heavy traffic induced vibrations, generally the first). Then model an equivalent Euler-Bernoulli beam in the EDDABuS_{GS}-tool with a similar dominant eigenfrequency. From this equivalent model the influence factor of changing parameters can be computed more reliably. Compute results at the x -coordinate along the length of the beam where the vibration sensitive equipment is expected to be located.

- ***Check the influence of affected eigenfrequencies and affected impedance***

In case the ratio $f_{dom,load}/f_{n,str}$ comes closer to 1 (see 13.1 'Observations from Iterations') the engineer should check whether or not the vibration amplitudes are decreased.

- ***Increase impedances, decrease eigenfrequencies of global structural response, increase eigenfrequencies of local structural response***

Generally, the global building response has low dominant eigenfrequencies (< 3 Hz), thus for the global building response for buildings in soft soils it is beneficial for decreasing the vibration amplitude to increase the mass and mass moment of inertia (decreasing the dominant eigenfrequencies). However, the local building response, e.g. stiff concrete floors, generally have dominant frequencies between 8 Hz and 12 Hz, thus for these elements the stiffness should be increased more than the increase in mass to come to higher dominant eigenfrequencies.

- ***Minimize sensitivities in results by performing a rigorous computation of a preliminary (reference) design first***

The sensitivity of the computed results can be minimized by performing first an extensive calculation by EDDABuS_{GS} for a reference case (preliminary design) and let this calculation run for a long computational time. Then the time- and frequency step can be made larger, while the time- and frequency ranges and the number of response points can be made smaller to see the influence of these simplifications on the computed vibration amplitude and the computational time. This influence factor can be taken into account for making iterations of the design with a large step, a small range and possibly only one response point.

- ***Design pile toes of adjacent structures on a less deep soil layer***

To avoid the bridging effect through the foundation piles of two adjacent structures, the structural design of the foundation piles should preferably be such that the pile toes of the building and the adjacent structure (e.g. the road) are not on the same stiff sand layer.

14.3. Recommendations for Future Research

- ***Verify computed results by measurements in practice***

Since the EDDABuS_{GS}-tool contains some simplifications which still need to be verified, it is highly recommended to verify the results of the tool by measurements in practice. The currently available measurements are scarce, therefore it is recommended to perform measurements in future research. The building type, soil layering, and load generation for which the verification is performed should be in line with the assumptions made for this tool in order for a fair comparison between the predictions by the tool and the measurements.

- ***Expand the applicability of the EDDABuS_{GS}-tool***

It is interesting for future research to expand the applicability of the EDDABuS_{GS}-tool for e.g. more types of soil layering, vehicle speeds, road irregularity profiles, vehicle characteristics, and even different types of loading (e.g. subways and wind or walking and machinery inside the building).

Implementing more types of soil excitation (due to heavy traffic, trams, trains etc.) can be done relatively easily by adding more sub-folders to the EDDABuS_{GS}-tool with pre-computed soil excitations.

- ***Verify the simplified soil- and pile foundation impedances by rigorous computational methods***

It is expected that the greatest sensitivity of the EDDABuS_{GS}-tool lays in the simplification of the soil- and pile foundation impedances. The values taken into account for the impedances should be verified, preferably by measurements in practice, but since that is hard to realize a verification with rigorous computational methods might also suffice (see 6.2 'Modelling of the Soil-Foundation System'). The computational time of these rigorous computational methods is generally very long, therefore it is recommended to tune the simplified functions for the impedances incorporated in the tool with the results of the rigorous computation. In this way the computational time of the EDDABuS_{GS}-tool still remains relatively low while the reliability of the results is increased.

- ***Implement a floor element instead of an Euler-Bernoulli beam***

Also, the implementation of a more reliable floor element is an aspect that can be interesting for future research. The current EDDABuS_{GS}-tool simplifies the floor to an Euler Bernoulli beam which spans in one direction only and has a continuous support on both sides, while in reality, floors can span in multiple directions and might be point-supported only, rather than a continuous support along an edge. By implementing a more reliable floor element, the computational time of the tool is expected to increase. Whether or not this weighs up against the more reliable results should be determined in that same future research.

References

- Abdelkarim, A., Vrouwenvelder, A., & Verweij, M. (1999). *Analysis of the dynamic response of layered, elastic media by means of the Fast Fourier Transform*. HERON, Vol. 44, No. 2 (1999) ISSN 0046-7316. Technical University Delft.
- Achenbach, J. (1975). *Wave Propagation in Elastic Solids*. Amsterdam: North-Holland Publishing Company.
- Al-Hussaini, T., & Ahmad, S. (1991, March 11-15). *Simple Design Methods for Vibration Isolation by Wave Barriers*. Proceeding: Second International Conference on Recent Advances in Geotechnical Earthquake Engineering and Soil Dynamics. Saint Louis, Missouri, United States: State University of New York.
- Al-Hunaidi, M., Rainer, J., & Tremblay, M. (1995, October 23). *Control of traffic-induced vibration in buildings using vehicle suspension systems*. Soil Dynamics and Earthquake Engineering 15. Canada: Elsevier Science Limited.
- Amick, H., Gendreau, M., Busch, T., & Gordon, C. (2005). *Evolving criteria for research facilities: vibration*. Proceedings of SPIE 5933, Buildings for Nanoscale Research and Beyond, 593303, (pp. 2, 4, 6, 10). San Diego, California.
- Azevedo, A. (2019, April 25). FEMIX. Opgehaald van alvaroazevedo: <http://www.alvaroazevedo.com/femix/>
- Barbosa, J. (2013). *Analysis and mitigation of vibrations induced by the passage of high-speed trains in nearby buildings*. Porto: Thesis presented to the Faculty of Engineering of the University of Porto for the Doctor Degree in Civil Engineering.
- Barbosa, J., Park, J., & Kausel, E. (2012). *Perfectly matched layers in the thin layer method*. Computer methods in applied mechanics and engineering 217-220(o): 262-274.
- Barkan, D. (1962). *Dynamics of Bases and Foundations*. New York, San Fransisco, Toronto, London: McGraw-Hill book company, inc.
- Bergmann, L., & Hatfield, H. (1938). *Ultrasonics and their scientific and technical applications*. New York: J. Wiley.
- Blauwendraad, J. (2016). *Dynamica van Systemen*. Collegedictaat CT2022. Technical University Delft, afdeling ConstructieMechanica.
- Braile, L. (2019, January 31). *Wave types*. Opgehaald van L. Braile, Earth and Atmospheric Sciences - Purdue University: <https://web.ics.purdue.edu/~braile/edumod/waves/>
- Cebon, D. (1993). *Interaction between heavy vehicles and roads*. SP-951, L. Ray Buckendale Lecture. SAE.
- de Zeeuw, A. (2018, June). *Topology Optimization of Wave Barriers*. Master Thesis. Technical University Delft.
- Degrande, G., & Lombaert, G. (2002, February 14). *The experimental validation of a numerical model for the prediction of the vibrations in the free field prodced by road traffic*. Journal of Sound and Vibration 262 (2003) 309-331.
- Degrande, G., Pyl, L., & Clouteau, D. (2004, December). *Validation of a Source-Receiver Model for Road Traffic-Induced Vibrations in Buildings. II: Receiver Model*. Journal of Engineering Mechanics ASCE 130(12): 1394-1406.
- Degrande, G., Pyl, L., Lombaert, G., & Haegeman, W. (2004, December). *Validation of a Source-Receiver Model for Road Traffic-Induced Vibrations in Buildings. I: Source Model*. Journal of Engineering Mechanics ASCE 130(12): 1377-1393.

- Deltares. (2019, June 7). Lesson Soil Dynamics. Environmental vibrations. Deltares.*
- Dorby, R., Oweis, I., & Urzua, A. (1976, August). Simplified procedure for estimating the fundamental period of a soil profile. Bulletin of the Seismological Society of America. Vol.66, No.4, pp. 1293-1321. Bulletin of the Seismological Society of America.*
- Eilders, L. (2015). Nieuwbouw TNW TU Delft Trillingmetingen HR- en MR-vloeren ten tijde van ruwbouwfase. Zoetermeer: Peutz.*
- FE Staff. (2017, April 4). The ups and downs of air spring, leaf spring truck suspension. Opgehaald van Fleet Equipment: <https://www.fleetequipmentmag.com/cooper-mixed-service-truck-drive-tire/>*
- Fennema, R. (2017). Trillingsbeheersing gebouwtechnische installaties. DGMR Bouw B.V.*
- Fennema, R. (2017). VU Onderzoekgebouw VO-fasedocument bouwfysica en brandveiligheid. DGMR Bouw B.V.*
- Fennema, R. (2018). Definitief Ontwerp bouwfysica, akoestiek, energiezuinigheid en trillingstechniek. DGMR Bouw B.V.*
- Fennema, R. (2018). Trillingsonderzoek WKO tussenstraat. DGMR Bouw B.V.*
- Fennema, R. (February 2018). Trillingsprognose labgebouw en uitvoeringsaspecten trillingsarme eilanden voor elektronenmicroscopen. DGMR Bouw B.V.*
- Fennema, R. (May 2018). Trillingen WKO en verkeer labgebouw "Schoolwerktuinen". DGMR Bouw B.V.*
- Foti, S. (2000). Multistation Methods for Geotechnical Characterization using Surface Waves. PhD Thesis in Geotechnical Engineering. Politecnico di Torino.*
- Gazetas, G. (1991). Foundation Vibrations. Foundation Engineering Handbook (p. 553-593). National Technical University Athens, Greece & State University of New York, Buffalo.*
- Gazetas, G., & Dobry, R. (1988). Simple method for dynamic stiffness and damping of floating pile groups. Geotechnique 38, No. 4.*
- Gillespie, T., Karamihias, S., Sayers, M., Nasim, M., Hansen, W., Ehsan, N., & Cebon, D. (1993). Effects of heavy vehicle characteristics on pavement response and performance. Technical Report 353. Washington, DC: NCHRP, Transportation Research Board.*
- Google. (2019, July 25). Google Maps. Opgehaald van Google Maps: <https://www.google.nl/>*
- Green, M., Cebon, D., & Cole, D. (1992, July 31). Effects of Vehicle Suspension Design on Dynamics of Highway Bridges. Journal of Structural Engineering. ASCE.*
- Hermens, M. (2012). Conclusies RHDHV n.a.v. metingen TNO. Royal HaskoningDHV.*
- Hölscher, P. (2014). Soil Dynamics. Course at the Technical University Delft. Delft, The Netherlands: Technical University Delft.*
- Hölscher, P. (2016). Soil dynamics in urban areas. Reader for part of the course CIE5430 at the Technical University Delft.*
- Hölscher, P. (2017). Soil Dynamics lecture 7. Soil Dynamics lectures TU Delft Master Geoen지니어ing CIE5340. Technical University Delft.*
- Hölscher, P. (2017). Soil Dynamics lectures. Soil Dynamics lectures TU Delft Master Geoen지니어ing CIE5340. Technical University Delft.*
- Hunaidi, O. (2000, June). Traffic Vibrations in Buildings. Construction Technology Update No. 39. Canada: Institute for Research in Construction.*
- Hunaidi, O., & Tremblay, M. (1997). Traffic-induced building vibrations in Montréal. Can. J. Civ. Eng. 24: 736-753. Canada: NRC Canada.*

- Infosteel. (2008, January 21). Trillingen van vloeren Ontwerprichtlijn. Retrieved from Infosteel: www.infosteel.be/hivoss/HIVOSS_NL/Floor_Guideline.pdf
- Janssen, S., & Ku, M. (2014). Nieuwbouw TNW Zuid - TU Delft Uitgangspunten constructief ontwerp. *Pieters Bouwtechniek*.
- Jia, J. (2018). *Soil Dynamics and Foundation Modeling*. Offshore and Earthquake Engineering. Norway: Springer ISBN 978-3-319-40357-1.
- Koopman, A. (2012). *Ambient trillingsmetingen t.b.v. locatieonderzoek Laserlab VU*. TNO.
- Kramer, S. (1996). *Geotechnical Earthquake Engineering*. Civil Engineering and Engineering Mechanics. Washington, United States: Prentice-Hall International Series.
- Lombaert, G., & Degrande, G. (2001, July). *Study of determining factors for traffic induced vibrations in buildings*. DWTC Research programme sustainable mobility research project MD/01/040. Leuven, Belgium: Katholieke Universiteit Leuven, Department of Civil Engineering, Structural Mechanics.
- Lombaert, G., Degrande, G., & Clouteau, D. (2000). Numerical modelling of free field traffic-induced vibrations. *Elsevier*.
- Lord Rayleigh, D. F. (1885, November). *On Waves Propagated along the Plane Surface of an Elastic Solid*. Proceedings of the London Mathematical Society / Volume s1-17, Issue 1.
- Lysmer, J. (1970, February). *Lumped Mass Method For Rayleigh Waves*. Bulletin of the Seismological Society of America. Vol. 60, No. 1, pp. 89-104. *Geoscienceworld*.
- MathIsFun.com. (2019, April 30). Calculus - Fourier Series. Opgehaald van MathIsFun: <https://www.mathsisfun.com/calculus/fourier-series.html>
- Metrikine, A. (2016). *Modes of undamped 2 DoF system*. Lectures Dynamics of Systems CTB 2300. Delft: Technical University Delft.
- Metrikine, A. (2018). *Dynamics, Slender Structures and an Introduction to Continuum Mechanics CT4145*. Module Dynamics of Mechanical Systems and Slender Structures. Delft: Technical University of Delft, Faculty of Civil Engineering and geosciences, section of Structural Mechanics.
- Metrikine, A., & Vrouwenvelder, A. (2018). *Part 2 Wave Dynamics*. Dynamics of Structures - CT4140. Delft University of Technology.
- Miura, k. (2016). *Dynamic Soil Structure Interaction*. Powerpoint presentation . Hiroshima University, Graduate School of Engineering.
- modderaandebanden.nl. (2019, July 17). MAN TGS 10x8 kippers. Opgehaald van Modder aan de Banden: <https://www.modderaandebanden.nl/index.php/man-10x8>
- Pap, Z., & Kollár, L. (2018). *Effect of Resonance in Soil-Structure Interaction for Finite Soil Layers*. OnlineFirst (2018) paper 11960 <https://doi.org/10.3311/PPci.11960> . Budapest University of Technology and Economics, Department of Structural Engineering.
- Papadopoulos, M. (2018, September). *Influence of dynamic soil-structure interaction on the building response to ground vibration*. PhD thesis in Civil Engineering. KU Leuven - Faculty of Engineering Science.
- Persson, N. (2016). *Predicting railway-induced ground vibrations*. Master's dissertation Structural Mechanics. Sweden: Lund University, Faculty of Engineering.
- PES Ltd. (2019, September 14). *Vibration Isolation Systems*. Opgehaald van PES Precise Solutions for Global Industries: http://www.pesukltd.com/products/vibration_isolation/cfm/vibration_isolation_systems/seismic_blocks/

- Pruiksma, J. (2015). *Validatie analytisch model en case berekeningen trillingsarm gebouw*. TNO.
- Python Software Foundation. (2019, April 26). *Opgehaald van python*: <https://www.python.org/>
- Richart, F., Hall, J., & Woods, R. (1970). *Vibrations of Soils and Foundations*. Theoretical and Applied Mechanics. Prentice-Hall International Series.
- Singh, J., Singh, S., & Joneson, E. (2006, April 19). *Measurement and Analysis of US Truck Vibration for Leaf Spring and Air Ride Suspensions, and Development of Test to Simulate these Conditions*. Packaging Technology and Science 2006: 309-323. Wiley InterScience.
- Snoeij, B. (2012, November 14). *TU Delft, nieuwbouw TNW-gebouw; beoordeling DO+ ten aanzien van trillingarme laboratoria*. Peutz.
- Snoeij, B. (2011). *TU Delft, nieuwbouw TNW-gebouw trillingonderzoek zuid-locatie*. Zoetermeer: Peutz.
- Snoeij, B. (2013). *TU Delft TNW trillingonderzoek zuid-locatie; centrum Logistiek & Milieu TU Delft*. Zoetermeer: Peutz.
- Spijkers, J., Vrouwenfelder, A., & Klaver, E. (2005, January). *Part I - Structural Vibrations*. Structural Dynamics CT 4140 . The Netherlands: Delft University of Technology, Faculty of Civil Engineering and Geosciences.
- Tsouvalas, A. (2018). *Structural Response to Earthquakes*. Lecture notes CIE5260 - Modules II & III. Delft: Technical University Delft, Faculty of Civil Engineering and Geosciences, Sections of Offshore Engineering & Dynamics of Structures.
- van der Poel, T. (1995, September). *The elastodynamic wavefield in horizontally layered media*. Master thesis in Technical Mathematics, Department of Applied Analysis. Technical University Delft & Delft Geotechnics.
- Verruijt, A. (2008). *Soil Dynamics*. Delft University of Technology.
- Versteegen, J., & Koekoek, M. (2018). *Onderzoeksgebouw VU Amsterdam DO rapport constructie*. Pieters Bouwtechniek.
- Vijayendra, K., Prasad, S., & Nayak, S. (2010, December). *Computation of Fundamental Period of Soil Deposit: A Comparative Study*. Indian Geotechnical Conference – 2010, GEOTrendz. IGS Mumbai Chapter & IIT Bombay.
- volvotrucks.nl. (2019, July 17). *Chassispecificaties voor de Volvo FL*. *Opgehaald van Volvo Trucks*: <https://www.volvotrucks.nl/nl-nl/trucks/volvo-fl/specifications/chassis.html>
- Watts, G. (1990). *Traffic induced vibrations in buildings*. Research report 246 . Crowthorne, Berkshire, United Kingdom: Transport and road research laboratory, Department of Transport.
- Woodrooffe, J., LeBlanc, P., & LePiane, K. (1986, July 25). *Effects of suspension variations on the dynamic wheel*. Vehicle Weights and Dimensions Study, Technical Report Volume 11. Canada: Roads and Transportation Association of Canada.
- Woods, R. (1968). *Screening of Surface Waves in Soils*. Journal of the Soil Mechanics and Foundations Division, Vol. 94, Issue 4, Pg. 951-980. American Society of Civil Engineers.

Appendices

A.	Appendix: application and interpretation of VC-curves	139
B.	Appendix: Additions to Chapter 3 ‘Source of Vibrations’	140
C.	Appendix: Extensive overview of Chapter 4 ‘Transmission of Vibrations’	143
D.	Appendix: Extensive overview of Chapter 5 ‘Structural System (Receiver of Vibrations)’	169
E.	Appendix: Additions to Chapter 6 ‘Soil-Structure Interaction’	190
F.	Appendix: Additions to Chapter 7 ‘Numerical Method for Computations’	193
G.	Appendix: Extensive overview of Chapter 8 ‘Verification Projects’	198
H.	Appendix: Additions to Chapter 9 ‘Source Modelling and Results’	214
I.	Appendix: table of computed vehicle axle load-frequency spectrums for changing parameter values	217
J.	Appendix: PPV with- and without wave barrier in soil Amsterdam.....	223
K.	Appendix: Additions to Chapter 11 ‘Soil-Structure Interaction Modelling’	224
L.	Appendix: Additions to Chapter 12 ‘Receiving Structural System Modelling and Results’	229
M.	Appendix: Maple sheet for determining 3DoF eigenfrequencies.....	239
N.	Appendix: Input parameters for Verification Project Degrande et al. (3) – Building Response	243
O.	Appendix: Results for Verification Project Degrande et al. (1) – Free Field and (3) – Building Response with layered soil of Amsterdam	257
P.	Appendix: Boundary- and Interface conditions of the three Modelx, z, φ	259
Q.	Appendix: Maple sheet for determining dynamic EB-beams response Modelx	261
R.	Appendix: Maple sheet for determining dynamic EB-beams response Modelz	280
S.	Appendix: Maple sheet for determining dynamic EB-beams response Modelφ	300
T.	Appendix: Iterations of structural parameters to compute structural response.....	318
U.	Appendix: User manual of EDDABuS _{GS}	349

A. Appendix: application and interpretation of VC-curves

Table 3. Application and interpretation of the generic vibration criterion (VC) curves (Amick, Gendreau, Busch, & Gordon, 2005).

Criterion Curve	Amplitude ¹ µm/s	Description of use
Workshop (ISO)	800	Distinctly perceptible vibration. Appropriate to workshops and non-sensitive areas.
Office (ISO)	400	Perceptible vibration. Appropriate to offices and non-sensitive areas.
Residential day (ISO)	200	Barely perceptible vibration. Appropriate to sleep areas in most instances. Usually adequate for computer equipment, hospital recovery rooms, semiconductor probe test equipment, and microscopes less than 40x.
Operating theatre (ISO)	100	Vibration not perceptible. Suitable in most instances for surgical suites, microscopes to 100x and for other equipment of low sensitivity.
VC-A	50	Adequate in most instances for optical microscopes to 400x, microbalances, optical balances, proximity and projection aligners, etc.
VC-B	25	Appropriate for inspection and lithography equipment (including steppers) to 3 µm line widths.
VC-C	12.5	Appropriate standard for optical microscopes to 1000x, lithography and inspection equipment (including moderately sensitive electron microscopes) to 1 µm detail size, TFT-LCD stepper/scanner processes.
VC-D	6.25	Suitable in most instances for demanding equipment, including many electron microscopes (SEM5 and TEM5) and E-Beam systems.
VC-E	3.12	A challenging criterion to achieve. Assumed to be adequate for the most demanding of sensitive systems including long path, laserbased, small target systems, E-Beam lithography systems working at nanometer scales, and other systems requiring extraordinary dynamic stability.
VC-F	1.56	Appropriate for extremely quiet research spaces; generally difficult to achieve in most instances, especially cleanrooms.
VC-G	0.78	Appropriate for extremely quiet research spaces; generally difficult to achieve in most instances, especially cleanrooms.

¹As measured in one-third octave bands of frequency

B. Appendix: Additions to Chapter 3 ‘Source of Vibrations’

1.1. Road Traffic Induced Vibrations - Empirical Prediction Model

A relatively simple prediction technique has been developed in order to make a first estimate on the peak vertical vibration levels at the foundation of buildings. This method is based on tests performed at the test track at the Transport and Road Research Laboratory (TRRL) in the UK with a wide range of heavy goods vehicles (HGVs). With these tests the trends in peak vibration levels, depending on vehicle speed, load and size of irregularity (Figure 93), have been established. The test results were then generalized to different site conditions by determining the amplitudes and attenuation rates of vibrations generated in different soils using a controlled impact method (with the aid of a hammer device).

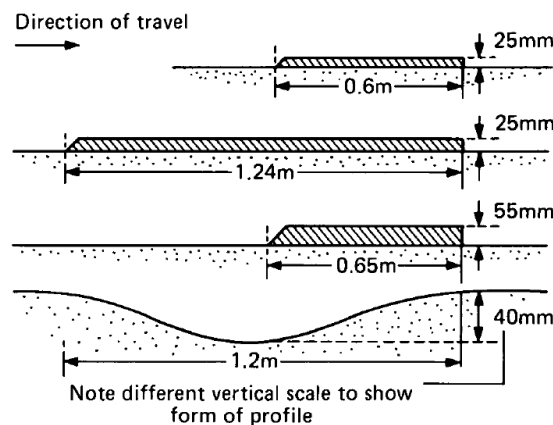


Figure 93. Test profiles used at the Transport and Road Research Laboratory (Watts, 1990)

Measurements had indicated that traffic vibrations generated in soft ground such as alluvium and peat soils were much greater than was the case for firmer soils under similar conditions. The expected PPV obtained from the tests at the test track were then factorized by the ratio $|H_s(f)| / |H_t(f)|$, where $|H_s(f)|$ and $|H_t(f)|$ are the moduli of the transfer function of mobilities at the site and on the track respectively and ‘ f ’ is the loading frequency. This frequency is typically between 10 – 12 Hz and results from the ‘wheel hop’ mode of vibrations of the heavy good vehicle (HGV) suspension (i.e. the vertical oscillatory motion of the wheels between the vehicle body and road surface). There is a large difference of up to two orders of magnitude between the response of a soft soil (peat) and very hard ground (chalk rock) (Figure 94).

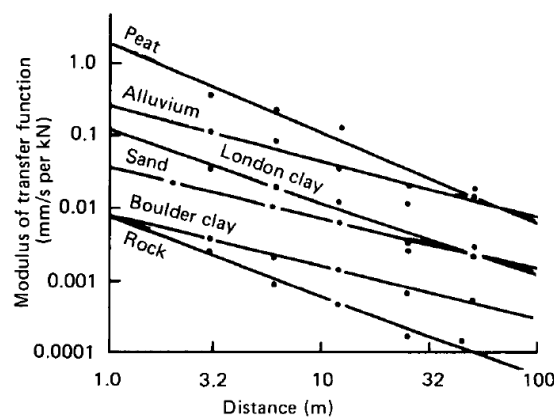


Figure 94. Transfer function for vertical PPV at 12 Hz by distance (Watts, 1990)

Obviously, it is difficult to model the generation of vibrations in these situations therefore the predictions developed by G.R. Watts are for the much more common situation only where a significant irregularity in the road surface is the cause of vibration effects.

The method is based on making predictions of vertical PPV at 6 m using the observed trends with amplitude of road surface irregularity and speed, and the most appropriate ground scaling factor. By combining these factors, the expected value of the maximum vertical PPV at a building foundation can be calculated as:

$$PPV_{foundation} = 0.028 \cdot a \cdot \frac{v}{48} \cdot t \cdot p \cdot \left(\frac{r}{6}\right)^x \quad (0.1)$$

where:

- PPV = peak particle velocity of the soil at the foundation (m/s)
- a = maximum height or depth of surface defect (mm)
- v = maximum expected speed of heavy good vehicles (HGVs) (km/h)
- t = ground scaling factor (see Table 4) (-)
- p = 0.75 in case surface defect occurs in one wheel path only (-)
- p = 1.00 in case surface defect occurs in both wheel path (-)
- r = distance of foundation from the defect (m)
- x = power factor for most appropriate soil type (see Table 4) (-)

Table 4. Effect of ground characteristics on transmission of vibration (Watts, 1990)

Ground type	Number of sites tested	Power coefficient for attenuation with distance 'x'***		Modulus of transfer function (x 10 ³) in mm/s per kN			Ground*** scaling factor $t = \frac{ H_s(f) }{ H_t(f) }$
		Range	Average	In ground at 6 m		Expected value at foundations 6 m	
				Range	Average		
Peat*	1	-	-1.19	-	189	41.9	3.84
Alluvium	2	-0.79 to -0.80	-0.79	72.5 to 82.0	77.3	77.3	7.07
London clay	3	-0.99 to -1.13	-1.06	20.9 to 56.3	33.8	33.8	3.10
Sand/gravel	3	-0.69 to -0.82	-0.74	9.92 to 11.0	10.3	10.3	0.94
Boulder clay	3	-0.71 to -1.18	-0.93	2.43 to 6.67	4.73	4.73	0.43
Chalk rock	1	-	-1.08	-	1.14	1.14	0.10

* For peat soil transfer function values and power coefficients are for 10 Hz.

** Power law for attenuation with distance is r^x where r is distance from source.

*** $|H_s(f)|$ and $|H_t(f)|$ are the moduli of the site and track transfer functions.

1.2. Road Traffic Induced Vibrations – Scientific Prediction Model

Influence of road stiffness on the vertical soil velocity

The road stiffness can influence the generated soil vibrations significantly. A stiffer road reduces the vibration levels of the dynamic axle loads, but when a soft road is applied the dynamic axle loads are hardly influenced. If one wants to incorporate this influence into the model the road-soil interaction needs to be taken into account. A predictive model can be created by modelling the road as an elastic beam with a rigid cross section, located at the surface of a horizontally layered halfspace. Both the road's bending and torsional deformations need to be accounted for. The soil's impedance is calculated by means of a boundary element method (Lombaert & Degrande, 2001).

In the past, the presence of the road has often been disregarded for the calculation of the free field road traffic induced vibrations. In this case, the dynamic axle loads are directly applied to

the soil. This assumption is only valid if the wavelength of the soil is large with respect to the area of the road-soil interface that accounts for the transmission of the forces to the soil. Also, in other studies it has been discovered that the effect of the pavement structure on the road-soil transfer function only affects the free field vibrations at small distances from the source and at high frequencies.

Influence of vehicle speed on the vertical soil velocity

Wave propagation induced by traffic driving over a traffic plateau has also been investigated in the lectures of Soil Dynamics at the TU Delft (Hölscher, 2014). Paul Holscher has shown that at relative small distance from the source the upgoing and the downgoing movement of the vehicle on the traffic plateau can be clearly distinguished (at 12 m: first a wave group initiated by the ascending- ($0.2 \leq t \leq 0.8$ s), then a pause ($0.8 \leq t \leq 1.0$ s), and finally another wave group for the descending ($1.0 \leq t \leq 1.6$ s) on the traffic plateau) (Figure 95). However, at larger distances this distinction is lost due to the fact that the different kind of waves propagate at different speeds and the faster reflected waves coincide with the slower non-reflected incident waves. The interfaces between the layers cause reflection and transmission of the incident waves. This phenomenon is very important when considering the wave propagation in a layered soil. Chapter 4. 'Transmission' introduces the propagation of waves first without soil layering (thus without layer interfaces) and thereafter considers the more realistic layered soil which accounts for the reflection and transmission of waves at the layer interfaces.

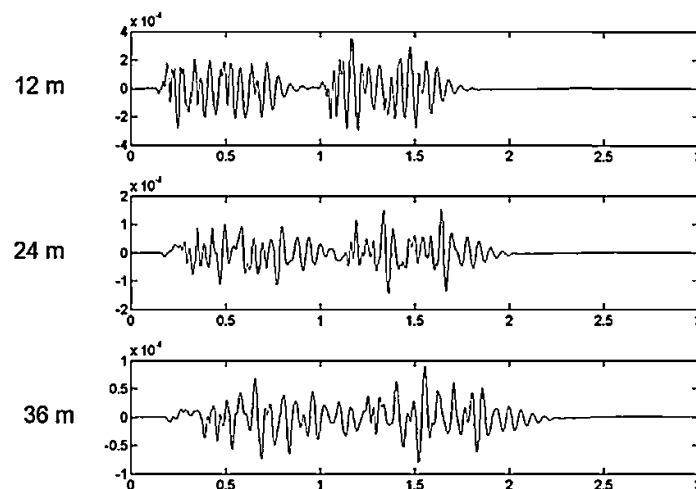


Figure 95. Propagation of waves in the soil ($m / m/s / m/s^2$) induced by a 2-axle vehicle driving over a traffic plateau at different distances from the plateau in the time domain (Hölscher, Soil Dynamics, 2014)

Additional concluding key factors influencing the free field traffic induced vibrations

- Compared to the use of simple empirical models, an elaborate numerical model, that is based on the physical nature of the problem, has the advantage that it provides physical insight and that it is well suited for a parametric study.
- A change of the characteristics of the suspension system or the tyres of a particular axle of the vehicle only affects the FRF of the same axle.

C. Appendix: Extensive overview of Chapter 4 ‘Transmission of Vibrations’

The vibrations generated by a source like road traffic can only reach a building’s structure once it is transmitted through a medium. This medium consists of the soil which is different for every site and can even differ within 1 m² at one site. The soil is often layered and consists of soil types of different densities and stiffness laying over each other. Also, in the Netherlands the soil is often layered where typically softer layers overly stiffer soil layers. The wavespeeds and the depth of the different layers influence the frequencies of the generated waves in the soil medium.

In the previous sections it was already discussed that determining the wave propagation for a certain soil layering is often difficult. However, several models have been created over the past half century which enables the prediction of wave propagation in layered media in a simplified manner. These approaches will be discussed in section 1.2 ‘Layered Elastic Soil Halfspace’. However first a simpler case will be discussed concerning a non-layered homogenous soil (1.1 ‘Homogeneous Elastic Soil’) to give a more general introduction to the soil dynamics of the transmission path.

1.1. Homogeneous Elastic Soil

Among many other authors (Verruijt, 2008), (Kramer, 1996), (Hölscher, 2016) and (Metrikine & Vrouwenvelder, 2018) give a comprehensive overview of the elastodynamics of a homogeneous elastic soil medium. A brief overview will be given in the present section, which is a confinement of the work of the previous mentioned authors. First let us consider waves in an infinite medium, in other words: a medium that has no bounds.

1.1.1. Waves in unbounded soil

Before hopping on to the three-dimensional medium, first the one-dimensional case will be briefly discussed in the form of an infinite long, linear elastic, rod. This representation should remind the reader of the fundamentals of soil dynamics but are not comprehensive. For more detailed derivations, please refer to the literature that is stated in the references.

For soil dynamics two important different types of vibrations can occur in a thin rod: longitudinal vibration (the axis of the rod extends and contracts) and torsional vibration (the rod rotates about its axis).

Longitudinal waves in an infinitely long rod

By using the basic requirements of equilibrium of forces and compatibility of displacements and using strain-displacement and stress-strain relationships, a one-dimensional wave equation can be derived and solved. Using Figure 96 the simplified governing equations can be derived.

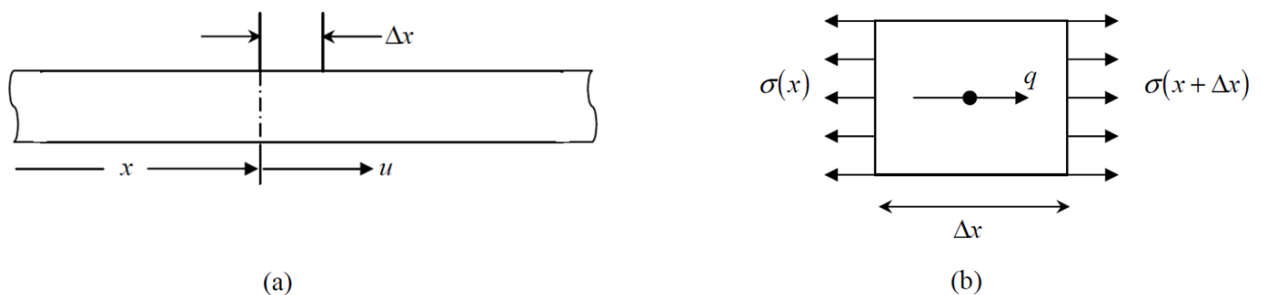


Figure 96. A thin rod (a) with co-ordinate x and displacement u of a section and (b) the stresses acting on element Δx of the rod (Metrikine & Vrouwenvelder, Part 2 Wave Dynamics, 2018)

In-line with Figure 96 the equation of the rod motion in the x -direction reads:

$$-\sigma(x)A + \sigma(x + \Delta x)A + qA\Delta x = \rho A \Delta x \frac{\delta^2 u}{\delta t^2} \quad (0.2)$$

where ρ is the mass density and A is the cross-sectional area of the rod. The latter is a constant in case of a prismatic rod. By taking into account the Taylor expansion of $\sigma(x + \Delta x) = \sigma(x) + (\delta\sigma/\delta x)\Delta x$ and assuming a homogeneous material for the rod (the Young's modulus E does not vary with x) and in the absence of body forces q , this equation reduces to:

$$\frac{\delta^2 u}{\delta x^2} = \frac{1}{c^2} \frac{\delta^2 u}{\delta t^2}, \quad c = \sqrt{\frac{E}{\rho}} \quad (0.3)$$

which is called the wave equation. In this partial differential equation u is the longitudinal displacement of the bar's cross-section, t represents time, x represents the special coordinate of a cross-section of the rod and c is a constant and represents the wave propagation velocity (or wave speed) and depends on the Young's modulus E and the density ρ of the bar's material. The wave propagation increases with increasing stiffness and with decreasing density.

The wave propagation velocity is not the same as the particle velocity while they both have the unit m/s. The wave speed is the speed at which an entire stress wave would travel along the rod. The particle velocity, however, is the velocity at which a single point within the rod would move as the wave passes through it (see also e.g. the differences between Figure 99 and Figure 100). The particle velocity can be shown to be related to the stress according to the expression (Metrikine & Vrouwenvelder, 2018):

$$v(x, t) = -\frac{c}{E} \sigma(x, t) = -\frac{1}{\rho c} \sigma(x, t) \quad (0.4)$$

The above equation shows that the particle velocity is proportional to the axial stress in the rod which generally changes continuously in dynamics. Wave speed in materials used in geotechnical and civil engineering range from 30 m/s to 10 000 m/s, while particle velocities range from 10^{-6} m/s to 10 m/s.

The coefficient of proportionality, (ρc) , is called the specific impedance of the material. This coefficient is another important property that influences the behaviour of waves at boundaries (Kramer, 1996).

Torsional waves in an infinitely long rod

For torsional waves the particle motion is constrained to planes perpendicular to the direction of wave propagation. However, the development of a wave equation for torsional vibrations follow the same steps as for longitudinal vibration and the following torsional wave equation can be derived (Kramer, 1996):

$$\frac{\delta^2 \theta}{\delta x^2} = \frac{1}{c^2} \frac{\delta^2 \theta}{\delta t^2} \quad (0.5)$$

where θ is the angle of twist of the rod and in this case $c = \sqrt{G/\rho}$ with G the shear modulus of the rod material.

The solution of the wave equations can be written in the general form, also referred to as the D' Alembert's solution:

$$u(x, t) = f(ct - x) + g(ct + x) \quad (0.6)$$

Where f and g can be any arbitrary functions of $(ct - x)$ and $(ct + x)$ that satisfy the wave equation. This solution describes a displacement wave $f(ct - x)$ traveling at velocity c in the positive x -direction and another displacement wave $g(ct + x)$ traveling at the same speed in the negative x -direction. It also implies that the shapes of the waves do not change with position or time.

In the case where the rod is subjected to an arbitrary steady-state harmonic stress, e.g. $\sigma(t) = \sigma_0 \cos(\omega t)$, where σ_0 is the stress wave amplitude and ω is the circular frequency of the applied loading, the solution can be expressed in the wavenumber $k = \omega/v$ in the form:

$$u(x, t) = A \cos(\omega t - kx) + B \cos(\omega t + kx) \tag{o.7}$$

Here the first term describes harmonic waves propagating in the positive x -direction and the second term described harmonic waves propagating in the negative x -direction. In case of an infinitely long rod no waves exist in the opposite direction of the incident wave (the radiation condition). In that situation the constant B has to be equal to zero, which results in an equation for the wave propagating in one direction only.

The wavenumber k is related to the wavelength, λ , of the motion by:

$$\lambda = cT = \frac{c}{f} = \frac{2\pi}{\omega} c = \frac{2\pi}{k} \tag{o.8}$$

Where T is the period of the applied loading and $f = 1/T$. Note that at a given frequency, the wavelength increases with increasing wave propagation speed. The wavenumber can be considered as having the same meaning to the wavelength as the meaning of the circular frequency has to the period of vibration (Figure 97).

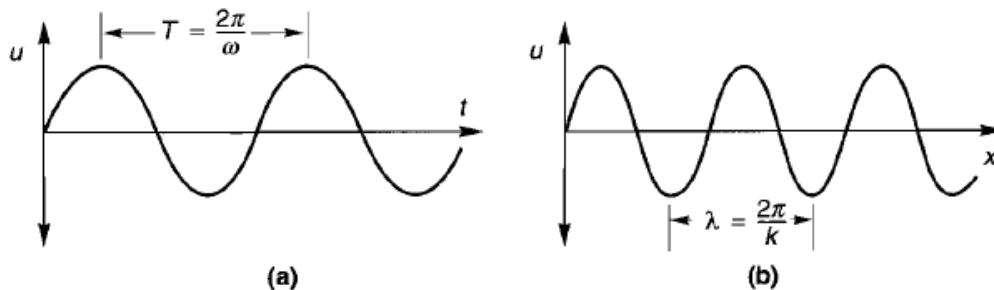


Figure 97. Particle displacement (a) as a function of time, and (b) as function of position along the rod (Kramer, 1996)

1.1.2. Waves in a three-dimensional infinite body

The described process for the one-dimensional case can be repeated for the case of wave propagation in a three-dimensional infinite medium. The derivation of three-dimensional equations of motion follows the same steps as those used for one-dimensional propagation. However, in the three-dimensional case the various relationships are more complex and derivation more cumbersome. The three-dimensional case will be briefly discussed.

In the derivation a Cartesian coordinate system is used (x, y, z) with corresponding displacements u, v, w (Figure 98).

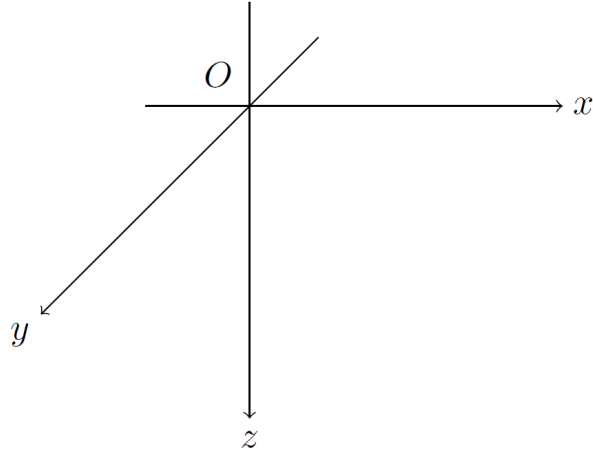


Figure 98. Cartesian coordinate system

The kinematic equations can then be given in the form:

$$\begin{aligned}
 \epsilon_{xx} &= \frac{\delta u}{\delta x}, & \epsilon_{yy} &= \frac{\delta v}{\delta y}, & \epsilon_{zz} &= \frac{\delta w}{\delta z}, \\
 \epsilon_{xy} &= \epsilon_{yx} = \frac{1}{2} \left(\frac{\delta u}{\delta y} + \frac{\delta v}{\delta x} \right), \\
 \epsilon_{yz} &= \epsilon_{zy} = \frac{1}{2} \left(\frac{\delta v}{\delta z} + \frac{\delta w}{\delta y} \right), \\
 \epsilon_{zx} &= \epsilon_{xz} = \frac{1}{2} \left(\frac{\delta w}{\delta x} + \frac{\delta u}{\delta z} \right)
 \end{aligned} \tag{0.9}$$

The constitutive equations can be given in matrix formulation as:

$$\begin{bmatrix} \sigma_{xx} \\ \sigma_{yy} \\ \sigma_{zz} \\ \sigma_{xy} \\ \sigma_{yz} \\ \sigma_{zx} \end{bmatrix} = \begin{bmatrix} \lambda + 2\mu & \lambda & \lambda & 0 & 0 & 0 \\ \lambda & \lambda + 2\mu & \lambda & 0 & 0 & 0 \\ \lambda & \lambda & \lambda + 2\mu & 0 & 0 & 0 \\ 0 & 0 & 0 & \mu & 0 & 0 \\ 0 & 0 & 0 & 0 & \mu & 0 \\ 0 & 0 & 0 & 0 & 0 & \mu \end{bmatrix} \begin{bmatrix} \epsilon_{xx} \\ \epsilon_{yy} \\ \epsilon_{zz} \\ 2\epsilon_{xy} \\ 2\epsilon_{yz} \\ 2\epsilon_{zx} \end{bmatrix} \tag{0.10}$$

with:

$$\lambda = \frac{Ev}{(1+v)(1-2v)}, \quad \mu = G = \frac{E}{2(1+v)} \tag{0.11}$$

Finally, the equilibrium equations can be given as:

$$\rho \frac{\delta^2 u}{dt^2} = \rho X + \frac{\delta \sigma_{xx}}{\delta x} + \frac{\delta \sigma_{yx}}{\delta y} + \frac{\delta \sigma_{zx}}{\delta z} \tag{0.12}$$

$$\rho \frac{\delta^2 v}{dt^2} = \rho Y + \frac{\delta \sigma_{xy}}{\delta x} + \frac{\delta \sigma_{yy}}{\delta y} + \frac{\delta \sigma_{zy}}{\delta z} \tag{0.13}$$

$$\rho \frac{\delta^2 w}{dt^2} = \rho Z + \frac{\delta \sigma_{xz}}{\delta x} + \frac{\delta \sigma_{yz}}{\delta y} + \frac{\delta \sigma_{zz}}{\delta z} \tag{0.14}$$

Neglecting body forces X , Y and Z gives the three-dimensional equations of motion for an isotropic, linear elastic solid:

$$\rho \frac{\delta^2 u}{\delta t^2} = (\lambda + \mu) \frac{\delta \epsilon_0}{\delta x} + \mu \nabla^2 u \quad (0.15)$$

$$\rho \frac{\delta^2 v}{\delta t^2} = (\lambda + \mu) \frac{\delta \epsilon_0}{\delta y} + \mu \nabla^2 v \quad (0.16)$$

$$\rho \frac{\delta^2 w}{\delta t^2} = (\lambda + \mu) \frac{\delta \epsilon_0}{\delta z} + \mu \nabla^2 w \quad (0.17)$$

with:

$$\epsilon_0 = \frac{\delta u_x}{\delta x} + \frac{\delta u_y}{\delta y} + \frac{\delta u_z}{\delta z} \quad (0.18)$$

and the Laplacian operator ∇^2 represents:

$$\nabla^2 = \frac{\delta^2}{\delta x^2} + \frac{\delta^2}{\delta y^2} + \frac{\delta^2}{\delta z^2} \quad (0.19)$$

These equations can be manipulated to produce two wave equations. Consequently, only two types of waves can travel through such an unbounded solid.

Compressional waves (P-waves)

The solution for the first type of wave can be obtained by differentiating each of the equations of motion (without body forces) with respect to x , y , and z and adding the results together (Kramer, 1996). Rearranging the solution yields the wave equation:

$$\frac{\delta^2 \epsilon_0}{\delta t^2} = \frac{\lambda + 2\mu}{\rho} \nabla^2 \epsilon_0 \quad (0.20)$$

This wave equation describes an irrotational, or dilatational, wave. It indicates that a dilatational wave will propagate through the body at a velocity:

$$c_p = \sqrt{\frac{\lambda + 2\mu}{\rho}} \quad (0.21)$$

This wave is called a P-wave (or primary wave) and c_p is referred to as the P-wave velocity of the material. The particle displacements are parallel to the direction of wave propagation (Figure 99). The longitudinal wave in the considered one-dimensional rod is actually a P-wave.

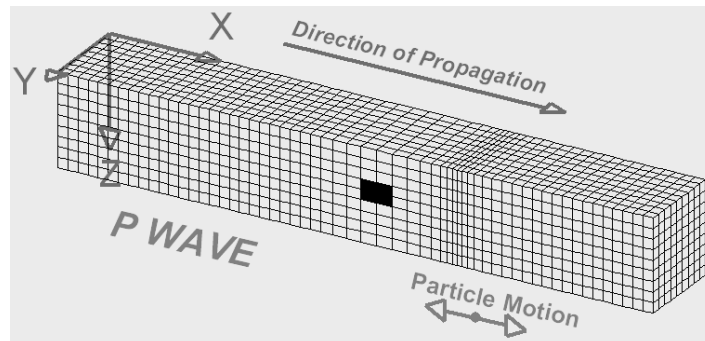


Figure 99. Representation of a P-wave. Alternating compression and dilation particle motion and parallel to direction of propagation (Braile, 2019)

Shear waves (S-waves)

To obtain the solution for the second type of wave, ϵ_0 is eliminated by differentiating the equation of motion with respect to (v, y) (equation (o.16)) with respect to z and the equation of motion with respect to (w, z) (equation (o.17)) with respect to y , and subtracting one from another (Kramer, 1996):

$$\rho \frac{\delta}{\delta t^2} \left(\frac{\delta w}{\delta y} - \frac{\delta v}{\delta z} \right) = \mu \nabla^2 \left(\frac{\delta w}{\delta y} - \frac{\delta v}{\delta z} \right) \quad (0.22)$$

With the definition of rotation:

$$\begin{aligned} \Omega_x &= \frac{1}{2} \left(\frac{dw}{dy} - \frac{dv}{dz} \right), \quad \Omega_y = \frac{1}{2} \left(\frac{du}{dz} - \frac{dw}{dx} \right), \quad \Omega_z \\ &= \frac{1}{2} \left(\frac{dv}{dx} - \frac{du}{dy} \right) \end{aligned} \quad (0.23)$$

equation (o.22) can be written in the form of the wave equation:

$$\frac{\delta^2 \Omega_x}{\delta t^2} = \frac{\mu}{\rho} \nabla^2 \Omega_x \quad (0.24)$$

which describes an equivoluminal, or distortional wave, of rotation about the x-axis. A similar expression can be obtained by the same procedure for rotation about the y- and z-axes. Equation (o.24) shows that the distortional wave will propagate through the solid at a velocity

$$c_s = \sqrt{\frac{\mu}{\rho}} = \sqrt{\frac{G}{\rho}} \quad (0.25)$$

This type of wave is commonly known as a S-wave (or shear wave) and c_s is referred to as shear wave velocity of the material. The particle motion is constrained to a plane perpendicular to the direction of wave propagation (Figure 100), just as it was in the case of the one-dimensional torsional wave.

S-waves are often divided into two types: SH-waves have particle motion occurring only in a horizontal plane and SV-waves have particle motion occurring only in a vertical plane.

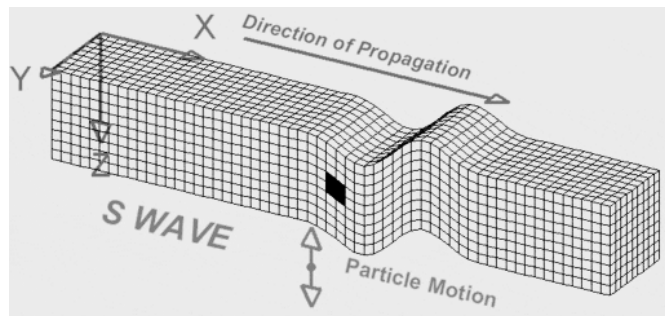


Figure 100. Representation of a S-wave. Alternating transverse particle motion in any plane (here in vertical plane) and perpendicular to direction of propagation (Braile, 2019)

For comparison of the wavespeeds of the different kind of waves in an unbounded solid the ratio between the wavespeeds is computed as:

$$\frac{c_p}{c_s} = \sqrt{\frac{2-2\nu}{1-2\nu}} \quad (0.26)$$

It becomes obvious that the Poisson's ratio is the only factor that affects the ratio. For a typical Poisson's ratio of 0.3 for geologic materials, the ratio $c_p/c_s = 1.87$ and for a Poisson's ratio of 0.49, the ratio $c_p/c_s = 7.14$. This shows that, depending on the soil material, the P-wave can arrive at a certain location much earlier than the S-wave.

1.1.3. Waves in a three-dimensional semi-infinite body

Till now it was assumed that the body had infinite dimensional length. However, a realistic soil body cannot be assumed to be infinite long in all directions. One dimension is restricted to the soil's surface where, generally speaking, no stresses occur. This surface is often referred to as the planar free surface (the effects of the earth's curvature are neglected) (Figure 101). New boundary conditions for the equations of motion are needed to account for this free surface. The additional solutions to the equations of motion obtained describe waves whose motion is concentrated in a shallow zone near the free surface. These waves are called surface waves and they attenuate with distance more slowly than body waves (P- and S-waves). Since laboratory buildings are placed at the free surface of the soil, the surface waves are very important, and they contain the largest part of energy that excites the objects at the free surface.

Two types of surface waves are of primary importance for buildings: the Rayleigh wave and the Love wave. The Love wave can only exist when the soil is layered and will therefore be discussed briefly in the next section 1.2 'Layered Elastic Soil Halfspace'. Other types of surface waves also exist but are much less significant for excitation to buildings at the free surface.

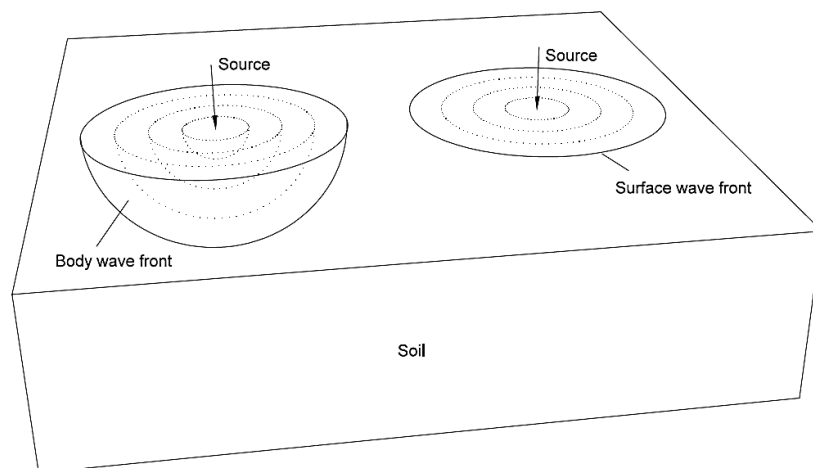


Figure 101. Geometrical attenuation for body waves (left) and surface waves (right) (Persson, 2016)

Rayleigh waves (R-waves)

The existence of elastodynamic waves propagating along the surface of an elastic half space was first considered by Rayleigh (Lord Rayleigh, 1885). This wave propagates near the free surface of an elastic half space and it strongly decreases exponentially with depth. The Rayleigh wave is generated by the interaction between the two body waves and the surface itself. Derivations of the Rayleigh wave solution can be found in many textbooks on soil dynamics and earthquake engineering (e.g. Kolsky (1963); Richart, Hall & Woods (1970); Das (1993); Kramer (1996)). A brief overview will be given of the characteristics of the Rayleigh wave.

The derivation of the Rayleigh wavespeed is a comprehensive procedure. When following the method used by Achenbach (Achenbach, 1975) referred to by (Verruijt, 2008) a very brief description can be given:

Consider the solution to the basic equations of elastodynamics in the form of expressions for the displacement in the (x,z) -plane. The solution is such that the displacement tends towards zero for $z \rightarrow \infty$ (the radiation condition). In this solution the amplitude of the displacement

components is independent of the lateral distance x . The two remaining unknown constants can be found by considering the boundary conditions at the free surface: $z = 0$: $\sigma_{zz} = 0$ & $\sigma_{zx} = 0$. After reformulating and rearranging the expressions it appears to be possible to approximate the Rayleigh wavespeed c_r by an analytical expression depending on the Poisson's ratio ν of the soil and the S-wave velocity c_s by the following expression (Bergmann & Hatfield, 1938):

$$c_r = \frac{0.87 + 1.12\nu}{1 + \nu} c_s \quad (0.27)$$

The above equation is only valid for values of $0 < \nu < 0.5$, a range that is valid for soils. From this equation it can be observed that the Rayleigh wave velocity is very close but a little smaller than the S-wave velocity in the same material. In the range of $0 < \nu < 0.5$, the Rayleigh wavespeed varies between $0.87c_s$ and $0.95c_s$ (Figure 102).

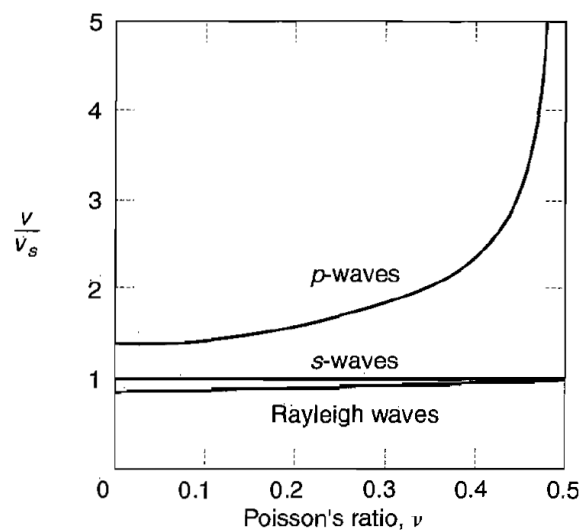


Figure 102. Variation of Rayleigh wave and body wave propagation velocities with poisson's ratio (Kramer, 1996)

Rayleigh waves can be thought of as combinations of P- and S-waves (SV-waves in the case of a vertical (x,z) -plane). In isotropic solids, the individual particles move in ellipses parallel to the direction of propagation (Figure 103).

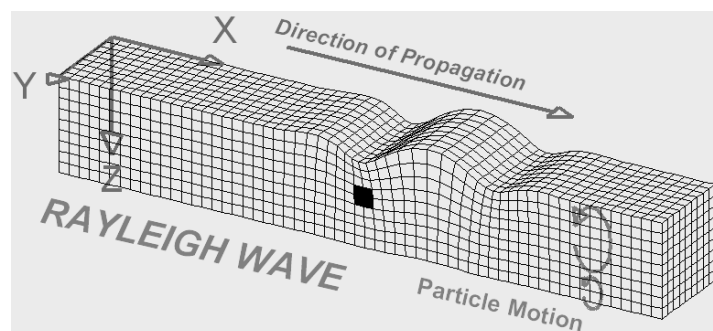


Figure 103. Representation of a Rayleigh wave. Elliptical particle motion in vertical plane and parallel to direction of propagation. Amplitude decreases with depth (Braille, 2019)

Also, the displacement amplitudes of the Rayleigh wave can be derived from the expression obtained when considering the velocity of the Rayleigh wave. The horizontal and vertical displacement amplitudes are illustrated for several values of Poisson's ratio (Figure 104) (Kramer, 1996).

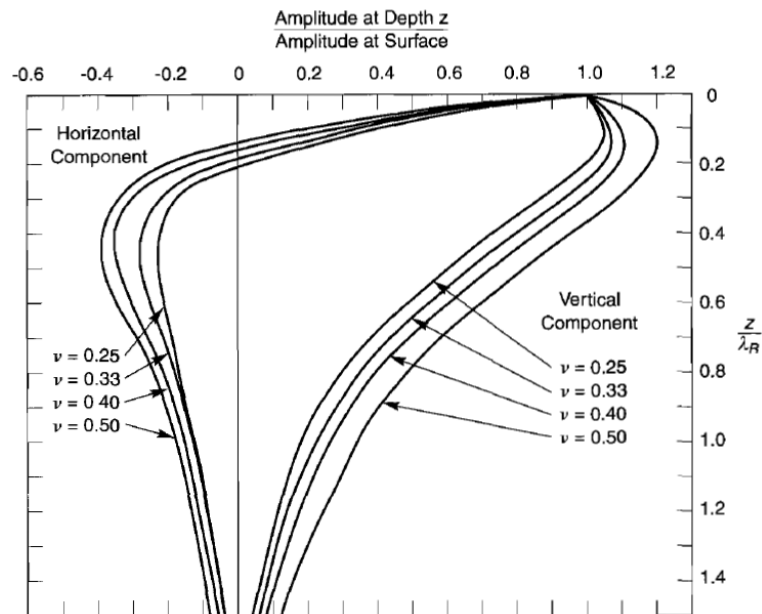


Figure 104. Horizontal and vertical motion of Rayleigh waves. A negative amplitude ratio indicates that the displacement deeper underneath the surface is in the opposite direction of the surface displacement (Kramer, 1996) after (Richart, Hall, & Woods, 1970)

From Figure 104 it appears that the horizontal displacement will be zero when the vertical displacement reaches its maximum (or minimum), and vice versa. Despite the fact that the amplitude decrease of the Rayleigh wave with depth is exponential, the superficial zone is still influenced by the soil material up to a depth of about a wavelength. In practice an absolute number for this wavelength is hard to determine since the soil is layered and damped and all soil layers influence the wavelength. Also, the excitation frequency influences the (Rayleigh) wave frequency, and thus the wavelength. To give an impression of this Rayleigh wavelength one can do a very rough estimate for road traffic induced vibrations by assuming an excitation frequency of 8 Hz (road traffic induced vibrations in The Netherlands are usually within the range of $3 \text{ Hz} < f < 15 \text{ Hz}$) and a Rayleigh-wave velocity of the soil about 120 m/s (soft soil, see 10.3.3 'Soil response in Amsterdam'). The wavelength would then be: $\lambda = c_r/f = 120/8 = 15 \text{ m}$.

1.1.4. Wave attenuation

The amplitude of a wave decreases as the wave travels through the soil medium. There are two primary mechanisms that cause this attenuation of wave amplitude: radiation damping and material damping.

Radiation damping

Radiation damping is the result from the spreading of wave energy over a larger volume of material as it travels away from its source. Since Rayleigh waves, generated by a line load, propagate as plane waves in the direction away from the line source, the Rayleigh waves don't have radiational damping. However, in the case of a point source the surface waves exhibit radiational damping in the form of plane surface circles in the direction away from the source (an annular wave field) (Figure 101).

Moreover, body waves (P- and S-waves), generated by a point source attenuate in all three-dimensional directions in the form of volumetric spheres in the direction away from the source (Figure 101).

In summary for a linear elastic homogeneous halfspace, excited by a point source, a simple power law of the following type can express the radiation damping consequences on waves amplitude (Foti, 2000):

$$\frac{1}{r^n} \text{ with } n = \begin{cases} 2 & \text{for longitudinal and shear waves on the surface} \\ 1 & \text{for body waves (P – and S – waves) in the solid} \\ 1/2 & \text{for Rayleigh waves} \end{cases} \quad (0.28)$$

where r is the distance from the point source. However, these radiation damping terms are for the far field only. Close to the source, the terms are more in line with $1/r^2$ for Rayleigh waves and $1/r^3$ for body waves in the solid.

Typically for elastic halfspaces the compressional wave (P-wave) arrives first at a particular location, before the arrival of the shear wave (S-wave). The Rayleigh wave arrives as last. This can also be observed in Figure 105 where Lamb has predicted the wavefield for a surface point force on an elastic homogeneous halfspace. Note also that the displacement caused by the arrival of the Rayleigh wave is much larger than the displacement caused by the arrival of the body waves.

However due to the much slower attenuation of the Rayleigh wave, most vibration energy at a particular distance from the source is carried by the Rayleigh wave. Lamb has predicted the wavefield for a surface point source on an elastic homogeneous halfspace which can be observed in Figure 105. Also an indication is given by R.D. Woods (Woods, 1968) for the energy ratio between the different kind of waves, generated by a point source at the surface of the elastic homogeneous soil medium. A visible representation is given in Figure 106.

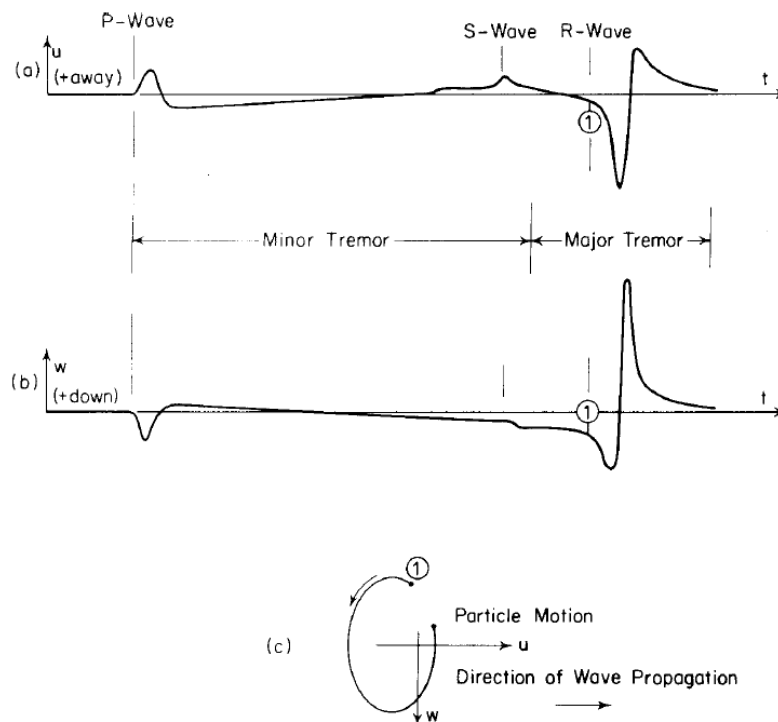


Figure 105. Complete wavefield predicted by Lamb (1904) for a surface point source on an elastic halfspace (a) horizontal radial motion; (b) vertical motion; (c) particle path of Rayleigh waves (Foti, 2000)

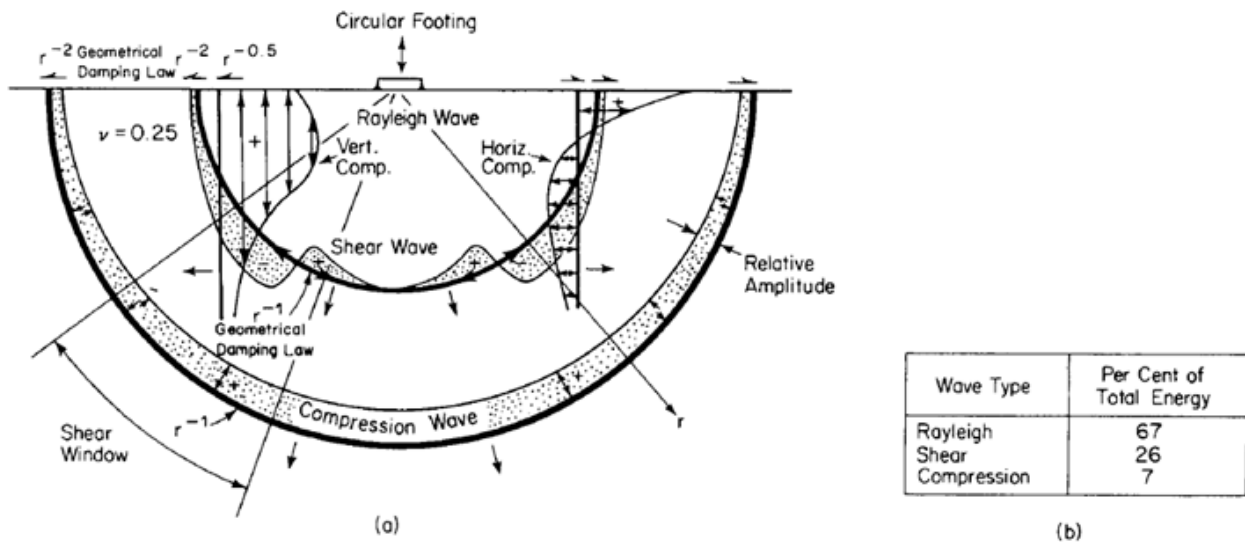


Figure 106. Harmonic vertical point source acting on the surface of a homogeneous, isotropic, linear elastic halfspace: (a) Complete displacements wave field; (b) partition of energy between different types of waves (Foti, 2000) from (Woods, 1968)

Material damping

Next to radiation damping the waves amplitudes also decay over distance because of material damping. Material damping occurs due to the absorption of energy by the materials the wave is travelling through. In the materials, part of the elastic energy of a travelling wave is converted to heat. The conversion is accompanied by a decrease in the amplitude of the wave. Material damping only plays a role when further away from the source (Hölscher, 2017). Different types of material have different kinds of damping, e.g. damping in peat is viscous, however, damping in sand is not viscous. Sand and clay have hysteric damping. When modelling the material damping an equivalent viscous damping based on stiffness (G) should be used. The equivalent viscous damping depends on amplitude, frequency and average static stress (Hölscher, 2017).

In order to include the effect of material damping, in addition to radiation damping, Bornitz (1931) has suggested to use a formula of the type (Verruijt, 2008):

$$\frac{w}{w_0} = \sqrt{\frac{r_0}{r}} e^{-\alpha(r-r_0)} \tag{0.29}$$

Where:

- w = amplitude of soil vibrations at distance r (-)
- w_0 = reference amplitude of soil vibrations at distance r_0 (-)
- r = observation distance from the load (m)
- r_0 = reference distance from the load (m)
- α = coefficient of wave energy absorption (see Table 5) (m^{-1})

Table 5. Approximate values of the coefficient of absorption of wave energy (damping constant) obtained as a result of investigations of wave propagation in different soils (Barkan, 1962)

No.	Soil	Coefficient of absorption α (m^{-1})
1	Yellow water-saturated fine-grained sand	0.100
2	Yellow water-saturated fine-grained sand in frozen state	0.060
3	Gray water-saturated sand with laminae of peat and organic silt	0.040
4	Clayey sands with laminae of more clayey sands and of clays with some sand and silt, above ground-water level	0.040
5	Heavy water-saturated brown clays with some sand and silt	0.040 - 0.120
6	Marly chalk	0.100
7	Loess and loessial soil	0.100

1.2. Layered Elastic Soil Halfspace

The existing waves just described were found for a homogeneous soil halfspace. However, this is rarely a realistic situation. The soil is composed of layers, e.g. softer layers near the surface and stiffer layers deeper down into the soil. The composition of the layers is different for every region and can even deviate significantly within one particular building site.

The waves that were found in the previous section still exist in the realistic stratified soil, however the differences between the layer properties causes the incident waves to reflect and refract at the interface between two layers. This makes that predicting the vibration propagation in a stratified soil becomes a difficult task. However, many studies have been done to this problem and several approaches exist for theoretical prediction models (see Part III Method).

This section will briefly describe the mechanisms that occur in a stratified soil halfspace. But first the one-dimensional problem will be extended to a case in which reflection and refraction occurs.

1.2.1. One dimensional wave propagation

Consider the rod from 1.1.1 'Waves in unbounded soil' again. However, this time the rod is composed of two semi-infinite rods, where there is a discontinuity in the cross-section, in the material properties, or both (Metrikine & Vrouwenvelder, 2018)(Figure 107). In the figure the incident wave is represented by an arbitrary shaped stress wave to the left of the junction of the two semi-infinite rods, propagating from left to right (in positive x – direction). The reflected wave is also to the left of the junction, however this wave propagates in the opposite direction (negative x – direction). The transmitted wave propagates from the left to the right (positive x – direction) at the right side of the junction.

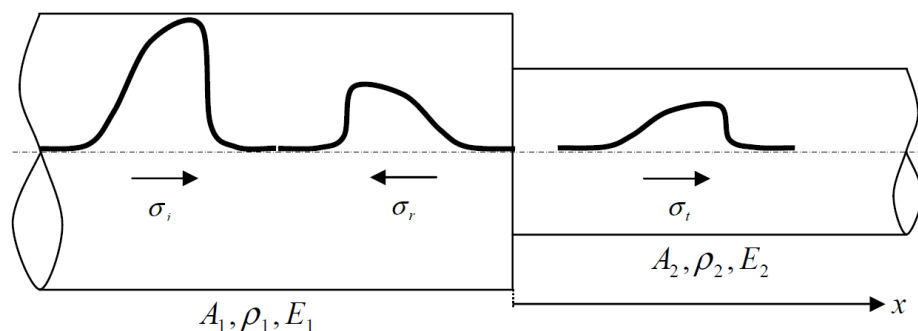


Figure 107. Incident (σ_i), reflected (σ_r) and transmitted (σ_t) stress waves at the junction of two rods ($Z_2 > Z_1$) (Metrikine & Vrouwenvelder, 2018)

Similar to what was presented in 1.1.1 ‘Waves in unbounded soil’ the solution can be expressed in terms of the D’Alembert’s solution. The rod displacements associated with these waves can then be described as:

$$u_i = f^+(t - x/c_1), \quad u_r = f^-(t + x/c_1), \quad u_t = f^+(t - x/c_2) \quad (0.30)$$

From these displacement solutions the stress and particle velocity associated with the waves can be computed. In the case the rods are free of external loading, the force field and the particle velocity field must be continuous at the junction.

Problems involving wave transmission across junctions are often spoken of in terms of an impedance (Z). This term expresses the ratio of a driving force to the resulting velocity at a given point of the structure (resistance against vibrations). For an elastic rod, the impedance is given by:

$$Z = \frac{F}{v} = \frac{\sigma A}{v} = \frac{EA}{c} = A\sqrt{\rho E} \quad (0.31)$$

Using the impedance, and substituting the stress-velocity relations into the continuity conditions of the particle velocity field at the junction, it is possible to write the stress fields of the transmitted and reflected waves in terms of the stress field of the incident wave as (Metrikine & Vrouwenvelder, 2018):

$$\sigma_t = \frac{2(Z_2/Z_1)(A_1/A_2)}{1 + Z_2/Z_1} \sigma_i, \quad \sigma_r = \frac{Z_2/Z_1 - 1}{1 + Z_2/Z_1} \sigma_i \quad (0.32)$$

where $Z_1 = A_1\sqrt{\rho_1 E_1}$, $Z_2 = A_2\sqrt{\rho_2 E_2}$.

These expressions show the following:

- If the impedances of the left and right rod are equal, no reflected waves occur at the junction.
- The transmitted stress pulse always keeps the sign of the incident stress pulse (compression is transmitted as compression and tension as tension).
- The sign of the reflected stress pulse depends on the ratio of Z_2 and Z_1 .

1.2.2. Three-dimensional wave propagation

A similar kind of mechanism of incident waves, reflected waves and transmitted waves occurs in a layered soil, where the previous example of the junction of two rods is similar to an interface between two soil layers. The free surface can be considered as a ‘free end’ (impedance ratio is zero). However, in general, the incident waves in a layered soil halfspace will not approach the interfaces at 90° angles as they do in the one-dimensional case. Also, the soil layers have different wave propagation speeds, depending on their material characteristics. As a consequence, both the reflected and transmitted waves have another propagating angle relative to the horizontal than the incident wave. Therefore, the transmitted waves are called refracted waves instead.

Fermat’s principle defines the propagation time of a seismic pulse between two arbitrary points A and B as the minimum travel time along any continuous path that connects the two points. The path that produces the minimum travel time is called a ray path, and its direction is often represented by a vector called a ray. A wavefront is defined as a surface of equal travel time, consequently, a ray path must (in an isotropic material) be perpendicular to the wavefront (Figure 108).

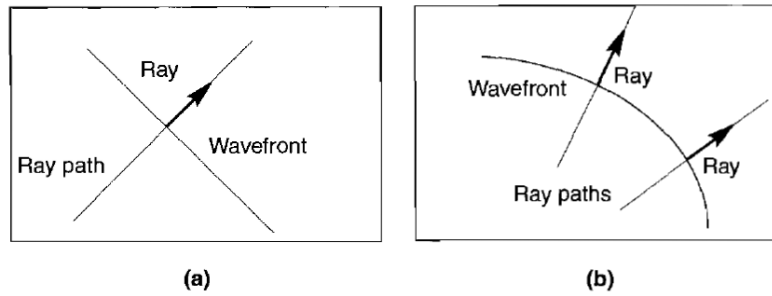


Figure 108. Ray path, ray, and wavefront for (a) plane wave and (b) curved wavefront (Kramer, 1996)

Snell considered the change of direction of ray paths at interfaces between materials with different wave propagation velocities. Using Fermat’s principle, Snell showed that

$$\frac{\sin i}{c} = \text{constant} \tag{0.33}$$

where i is the angle between the ray path and the normal to the interface and c is the velocity of the wave of interest. It indicates that the transmitted waves will be refracted (except when $i = 0$) when the wave propagation velocities are different on each side of the interface (Figure 109).

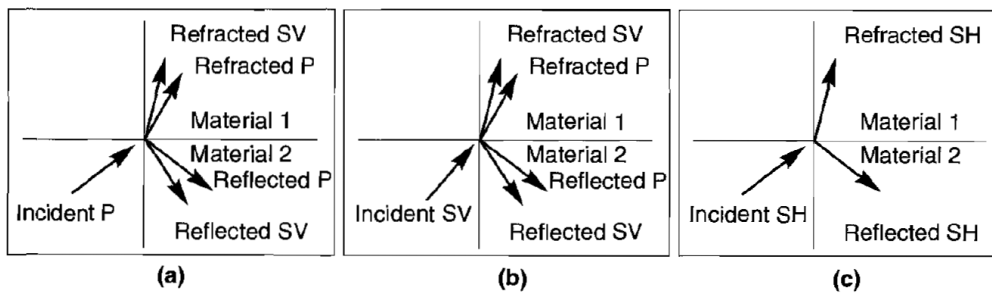


Figure 109. Reflected and refracted rays resulting from incident (a) p-wave, (b) SV-wave, and (c) SH-wave (Kramer, 1996)

The directions and relative amplitudes of the waves produced at the interface depend on both the direction and amplitude of the incident wave. Using Snell’s law and the requirements of equilibrium and compatibility, these directions and amplitudes can be determined.

The angle of incidence is equal to the angle of reflection for both P- and S-waves. The angle of refraction is uniquely related to the angle of incidence by the ratio of the wave velocities of the materials on each side of the interface. Snell’s law indicates that waves travelling from higher-velocity material into lower-velocity material will be refracted closer to the normal to the interfaces (Figure 110).

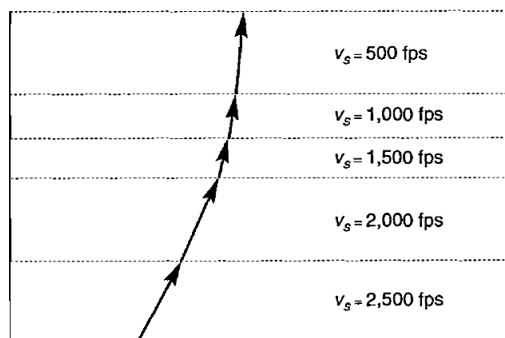


Figure 110. Refraction principle of an SH-wave ray path (reflected waves are not shown) (Kramer, 1996)

The creation of new waves and the reflection and refraction of the waves by these heterogeneities cause traffic induced vibration to reach a building by many different (ray) paths (Figure 111). Since the paths have different lengths and wavespeeds, the motion of the soil is spread out in time by this scattering effect (also see Figure 95 in Appendix B ‘Appendix: Additions to Chapter 3 ‘Source of Vibrations’’).

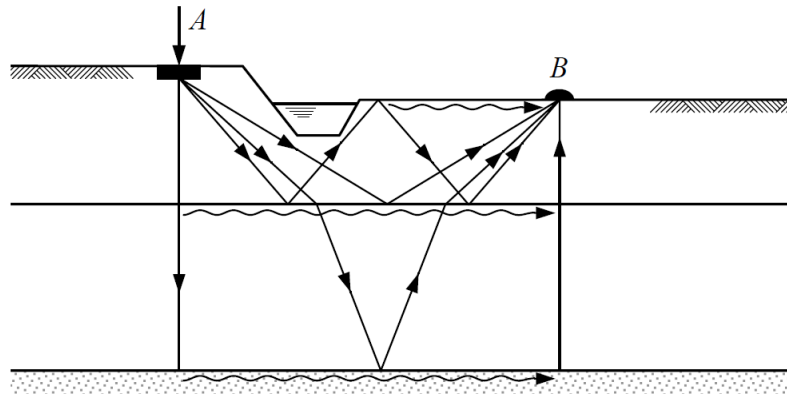


Figure 111. Simplified representation of possible paths along which energy is transferred (Spijkers, Vrouwenvelder, & Klaver, 2005)

Other waves

In a stratified soil medium also other waves can occur. One of these waves is the Love wave, which only exists in the situation when a surficial layer of lower S-wave velocity is overlying a half-space with a higher S-wave velocity. Love waves essentially consist of SH-waves (S-waves in the horizontal (x,y)-plane) that are trapped by multiple reflections within the surficial layer (Kramer, 1996) (Figure 112).

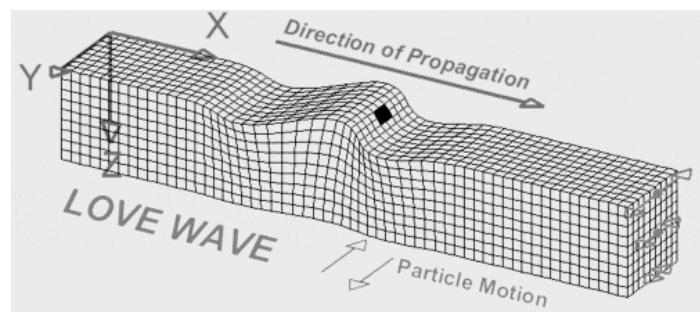


Figure 112. Representation of a Love wave (a horizontal S-wave). Particle motion perpendicular to direction of propagation. Amplitude decreases with depth (Braile, 2019)

For very low frequencies (and thus long wavelengths), the main part of the wavelength is within the underlying half-space. In that case the Love wave velocities are similar to the s-wave velocity of the underlying half-space. However, in case of high frequencies, the main part of the wavelength is within the surficial layer and barely reaches into the underlying half-space. In that case the Love wave velocities are similar to the S-wave velocity of the surficial layer. This frequency dependence indicates that Love waves are dispersive. This principle holds for all surface waves in a stratified soil medium. Therefore, also the Rayleigh waves are frequency dependent and characterised as being dispersive.

Also, a Stonely wave may be generated at the interface of two solids with certain properties. The wave propagates along the interface between the two solids. This resembles a Rayleigh wave in the sense that it is confined to the vicinity of the interface (Verruijt, 2008).

1.2.3. Conclusion layered soil medium

In a realistic stratified soil, a complex wave field is present, consisting of different kind of waves, propagating with different wavespeeds and different particle motion. For a prediction model which should give quite accurate results for the soil response a complex mathematical model is required. Several models have been created by different authors, relying on different kind of mathematics but all with the same aim: to predict the soil response in a stratified soil halfspace.

1.3. Dominant Frequencies Soil Medium

As waves propagate through soil media, their amplification or attenuation is mainly dependent on the fundamental natural period of the soil deposit. This fundamental natural period depends on mechanical and geometrical characteristics of the layered soil deposit.

Figure 113 presents an illustrative example of the soil response (soft soil) due to the passage of a truck at a distance of approximately 30 m from the receiver. The figure clearly shows an amplification of the soil response for the frequency range $4 \text{ Hz} < f < 7 \text{ Hz}$. This frequency range is generally within the frequency range of the eigenmodes of a truck, which are in the frequency range $1 \text{ Hz} < f < 15 \text{ Hz}$ (see 3.3 Road Traffic Induced Vibrations – Scientific Prediction Model). However, the strong peak at $f = 5 \text{ Hz}$ indicates some sort of resonance behaviour of the soil. This can be explained by the fact that for that particular frequency, the excitation frequency and the dominant frequency of the soil deposit are very close to each other, resulting in a strong magnification of the soil response. It is interesting to see in advance of the design process of a structure at which frequency the soil response is likely to be amplified strongly. The designer should then make sure that the eigenfrequencies of the structural system are far away from that dominant frequency of the soil deposit.

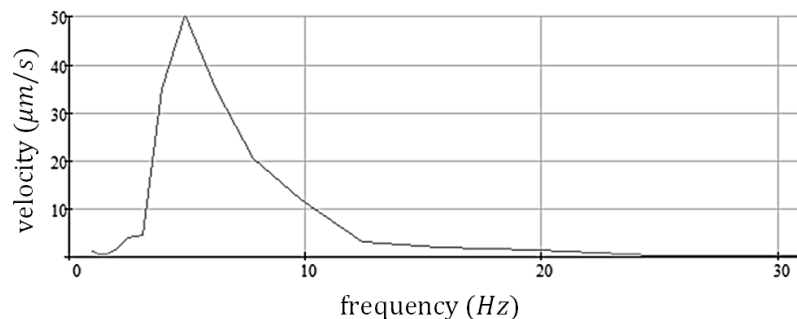


Figure 113. Illustrative soil response for soft soil deposits excited by a passing truck at a particular distance from the road

According to the paper ‘Computation of Fundamental Period of Soil Deposit: A Comparative Study’ (Vijayendra, Prasad, & Nayak, 2010), the fundamental period of a soil deposit is dependent on its thickness, low strain stiffness and density. The paper discusses different methods to determine an approximate value for the fundamental natural period of the soil. A very brief summary is given in this section.

Fundamental natural period of homogeneous soil deposits

For the case of homogeneous soil deposit overlying rigid bedrock, with a constant shear wave velocity profile throughout its depth H , the natural period T_n corresponding to the n^{th} mode of vibration is given by:

$$T_n = \frac{4H}{(2n - 1)c_s} \quad (0.34)$$

Hence, the natural period T corresponding to the fundamental mode ($n = 1$) is given by:

$$T_n = \frac{4H}{c_s} \quad (0.35)$$

Fundamental natural period of non-homogeneous soil deposits

Several procedures are discussed in the paper (Vijayendra, Prasad, & Nayak, 2010) for computing the fundamental natural period of a non-homogeneous soil deposit. The most simple method is less accurate than the other methods, but requires much less elaborated work. Therefore, only the simplest method is given here for use in preliminary design stages only.

In case of stratified soil deposits, made of several layers with different soil properties, the fundamental period of the entire deposit is usually computed using the equivalent shear wave velocity \bar{c}_s of the deposit which is calculated using weighted average of shear wave velocities of the individual layers. If h_i is the uniform thickness of the i^{th} layer and its average shear wave velocity is $(c_s)_i$, then the equivalent shear wave velocity of the deposit consisting of m layers is calculated as:

$$\frac{1}{\bar{c}_s} = \frac{1}{H} \left(\sum_{i=1}^m \frac{h_i}{(c_s)_i} \right) \quad (0.36)$$

Substituting \bar{c}_s in the equation of T_n , the fundamental natural period of the deposit can be computed as:

$$T = 4 \left(\sum_{i=1}^m \frac{h_i}{(c_s)_i} \right) = \sum_{i=1}^m \Delta T_i \quad (0.37)$$

where ΔT_i ($i = 1, 2, \dots, m$) are the natural periods of each of the layers in the deposit.

1.4. Wave Barriers

The rectangular wave barrier (open or infilled trenches), frequently used in engineering practice, reduces the ground vibration by interception, scattering and diffraction of the surface (Rayleigh) waves of relatively small wave lengths. Properly designed open or infilled trenches can be used for an effective vibration isolation (or screening) system.

This section describes the results of some researches performed concerning the effectiveness of the wave barrier as mitigation measure for ground-borne vibrations. First the research by T.M. Al-Hussaini and S. Ahmad concerning research of trenches in a 2D homogeneous soil halfspace will be considered. Thereafter the Master thesis research by A. de Zeeuw concerning wave barriers in layered soils is briefly discussed and finally the efficiency of wave barriers as subject of the research of J.M.O. Barbosa is regarded.

1.4.1. Simple design methods by T.M. Al-Hussaini and S. Ahmed

The following text summarizes the research performed by T.M. Al-Hussaini and S. Ahmad (Al-Hussaini & Ahmad, 1991) who presented models involving simple algebraic formulas for the design of rectangular wave barriers in homogeneous soil deposits. Vibration screening by open trenches in layered soils was also studied to identify the effects of layering on vibration screening. Since the research was performed for homogeneous soil deposits, with a relatively high excitation frequency (50 Hz), it must be noted that the algebraic formulas may not represent a realistic isolation behaviour for stratified soils excited by traffic induced vibrations.

For the research performed a rigorous 2D Direct Boundary Element method based on infinite-plane fundamental solution (in frequency domain) is used for the study. The depth, width and the distance of the trench are normalized with respect to the Rayleigh wavelength (Rayleigh wavelength = $\lambda_R = L_r$; $D = d/L_r$; $W = w/L_r$; $L = l/L_r$), see Figure 114.

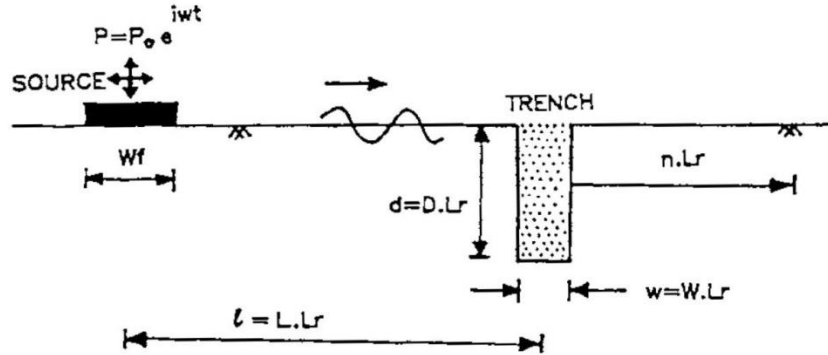


Figure 114. Schematic diagram of the problem studied: Passive vibration isolation by rectangular trenches in a viscoelastic halfspace (Al-Hussaini & Ahmad, 1991)

Screening of vertical vibration - open trench

The normalized width of the trench W is of very little importance except for shallow (normalized) depths ($D < 0.8$). For shallow depths, increase in width, in general, results in better performance of the trench. Considering narrow open trenches ($W = 0.1$ to 0.3), the simple expression:

$$A_r \cong \frac{1}{6}(D)^{-1.07} \quad (0.38)$$

may be used to represent the screening effectiveness of open trenches in the entire depth range of $D = 0.4$ to 2.0 .

Screening of vertical vibration - infilled trench

For an infilled trench both D and W appear to be equally important. For efficient design D should not be more than $1.2 \cdot L_r$ (Figure 115 and Figure 116). Vibration screening effectiveness of an infilled trench directly depends on the contrast (physical anomaly) in the material properties of the trench material and the soil. Increase in V_{st}/V_{ss} -ratio (= shear wave velocity of trench material / shear wave velocity of soil) results in better vibration screening. This means that a material of higher shear modulus provides greater resistance to the incoming wave. It is recommended that the V_{st}/V_{ss} -ratio should at least be 2.5. Also increased density of the trench material contributes to its screening efficiency. The simple model developed describes the average amplitude reduction ratio \bar{A}_{rv} due to an infilled trench, for $D < 1.2$, according to:

$$\bar{A}_{rv} = I_s I_v I_d I_a \quad (0.39)$$

where:

- I_s = shape factor (see Figure 116, a function of both D/W and A)
- I_v = velocity factor, for $V_{st}/V_{ss} > 2.5$, $I_v = [V_{st}/V_{ss}]^n$, where $n = 0.54 \cdot A$
- I_d = density factor: $I_d = [\rho_s/\rho_t]^m$, where $m = 0.94 \cdot A$
- I_a = area factor: $I_a = 0.57 \cdot (A)^{-0.25}$
- A = normalized cross-sectional area: $A = DW = dw/L_r^2$

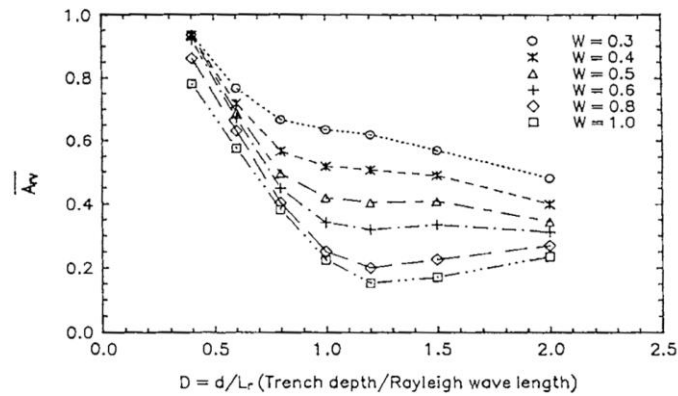


Figure 115. Influence of normalized trench depth and width for concrete (infilled) trench (Al-Hussaini & Ahmad, 1991)

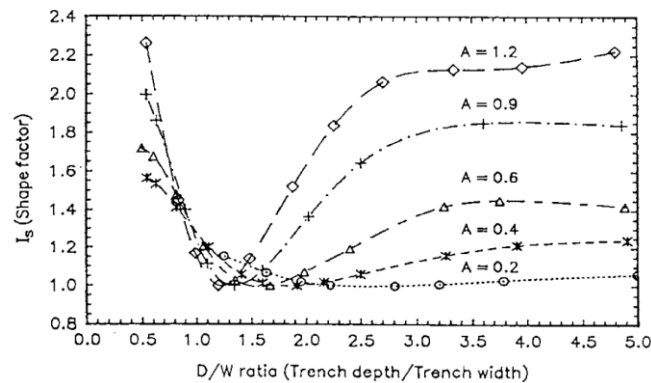


Figure 116. Influence of D/W ratio in the vibration screening by a concrete trench (Al-Hussaini & Ahmad, 1991)

Screening of vertical vibration - open trench in layered soil

A layered soil problem differs from the corresponding homogeneous half-space problem principally in two aspects. First, significant wave energy can be reflected from the layer interface back to the upper layer. Secondly, if the bottom layer is close to the ground surface, a significant part of the Rayleigh wave travels in the bottom layer. The conclusions may be summarized as follows:

- If the lower layer has a lower stiffness than the upper layer, the effect of layering can be ignored.
- If the lower layer has a higher stiffness than the upper layer, the effect of layering needs to be considered, because it reduces the screening effectiveness. However, at a H value of 8.0 (or more), the effect of layering is zero. In fact, the effect gets diminished drastically at a H value of around 6.0. Compared to a corresponding half-space problem, trenches need to be built deeper. Especially for V_{s1}/V_{s2} values (shear wave velocity ratio of top to bottom layer) smaller than around 0.7 – 0.75, trenches may have to be built deep down ($D = H + 1.0$) into the lower layer to achieve a good isolation effect (\bar{A}_{rv} value of 0.25 or less). When the top layer is shallow, such as $H = 0.5$, and the lower layer is much stiffer ($V_{s1}/V_{s2} = 0.25$), one needs to consider the trench depth in terms of the wavelength for the lower layer.

Screening of horizontal vibration – infilled trench

Similar to the case of vertical vibration screening, W and D appear to be equally important parameters. Considering design efficiency, depths greater than 1.5 or smaller than 0.6 are not considered. The amplitude reduction ratio for concrete infilled trenches can, be uniquely related to the cross-sectional area according to:

$$\bar{A}_{rh} \cong 0.4 \cdot (A)^{-0.33} \quad (0.40)$$

Increase in the ratio V_{rt}/V_{rs} of the Rayleigh wave velocity of the trench to that of the soil, results in better screening. The amplitude reduction ratio appears to decrease linearly with the density ratio ρ_t/ρ_s of the trench material and the soil. The simple model expresses the average amplitude reduction ratio for $0.6 < D < 1.5$ by:

$$\bar{A}_{rh} = I_a I_v I_d \quad (0.41)$$

where:

$$I_a = \text{area factor: } I_a = 0.4 \cdot (A)^{-0.33}$$

$$\text{for } V_{rt}/V_{rs} > 4.72, I_v = 1.0$$

$$\text{for } 2.63 < V_{rt}/V_{rs} < 4.72, I_v = 1.0 + m(4.72 - V_{rt}/V_{rs})/I_a$$

$$I_v = \text{velocity factor,}$$

$$\text{for } V_{rt}/V_{rs} < 2.63, I_v = 1.0 + (2.09m + 0.92 \left(V_{rt}/V_{rs} \right)^{-0.58} - 0.526)/I_a$$

$$\text{where, } m = 0.006 + 0.0382(A)$$

$$I_d = \text{density factor: } I_d = 1.0 - 0.24(\rho_t/\rho_s - 1.37)/I_a$$

$$A = \text{normalized cross-sectional area: } A = DW = dw/L_r^2$$

Conclusions by T.M. Al-Hussaini and S. Ahmed

The results predicted by the simple models, for trenches in homogeneous soils, compare favourably well with those obtained by rigorous numerical methods and available experimental data. The study identifies the important dimensionless parameters that control the effectiveness of a vibration screening system.

1.4.2. Optimization of wave barriers in layered soils by A. de Zeeuw

A. de Zeeuw performed a research for his Master thesis in Civil Engineering concerning the effectiveness of wave barriers in 2D layered soils when excited by a vertical harmonic point load at the surface. The soil is considered to be undamped.

Wave barrier in a two-layered soil

The 2D two-layered soils consist of a soft upper layer and a stiffer underlying halfspace (Figure 117 and Figure 118).

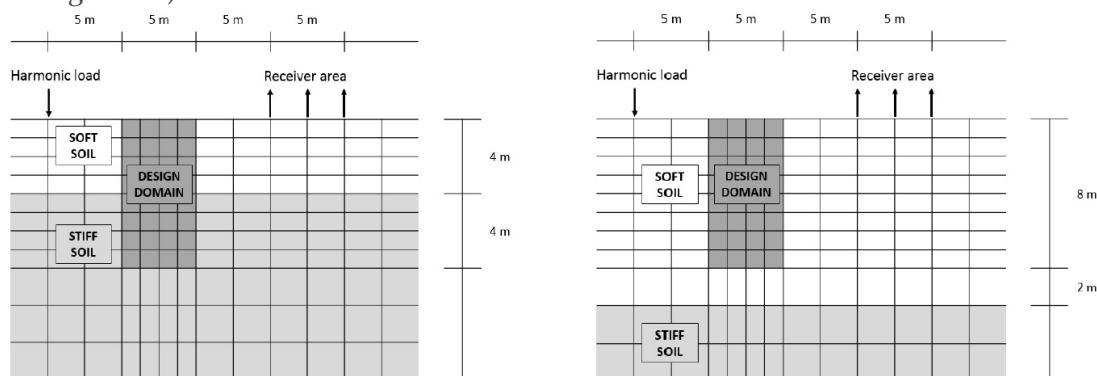


Figure 117. Inner FEM domain of the two-layered soil profiles. Left: shallow upper layer. Right: deep upper layer (de Zeeuw, 2018)

According to the research the following conclusions can be made regarding the effectiveness of wave barriers in 2D two-layered soils when excited by a vertical harmonic point load at the surface:

- The effectiveness of the wave barrier was sensitive to changes of the interface depth.

- Most of the energy from the loading is propagated in two wavetypes: a Rayleigh wave and a shear wave.
- The Rayleigh wave is propagating along the surface.
- Most energy of the shear wave is propagating at an angle of around 40 to 45 degrees.
- Much of the energy propagating as a shear wave is reflected from the interface upwards.
- The barrier shows a diminished effectiveness resulting from deviations in the interface depth.

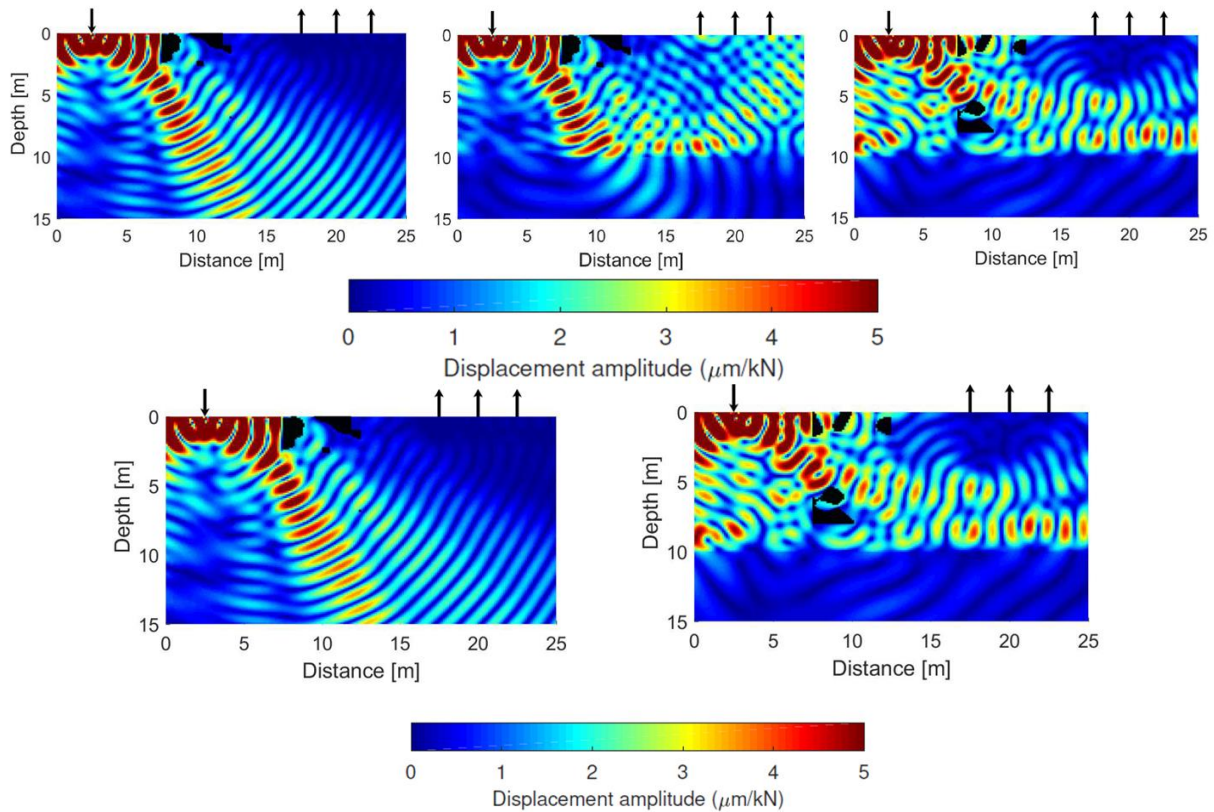


Figure 118. Displacement amplitude \hat{u}_{real} ($\mu\text{m}/\text{kN}$) for wave barrier optimized for 50 Hz. Left: \hat{u}_{real} for optimized wave barrier in homogeneous soil. Middle: \hat{u}_{real} for homogeneous-soil-optimized wave barrier in layered soil. Right: \hat{u}_{real} for optimized wave barrier in layered soil model (de Zeeuw, 2018)

Wave barrier in a three-layered soil

The 2D three-layered soils consist of a stiff top soil layer on a soft intermediate layer and a stiffer underlying halfspace (Figure 119 and Figure 120).

According to the research the following conclusions can be made regarding the effectiveness of wave barriers in 2D three-layered soils when excited by a vertical harmonic point load at the surface:

- An optimization objective function for a receiver at the surface only can result in a wave barrier that decreases the energy at the surface, while increasing the energy below the surface.
- For the optimized wave barrier, much of the energy appears to be continuously reflected within the softer layer, never reaching the surface (Figure 120). This is possible for shear waves approaching the interface at an angle lower than the critical angle, resulting in a full reflection as a shear wave.
- The diminishing effect of the barrier in a three-layered soil with deviation of the interface depth is larger than for a two-layered soil.

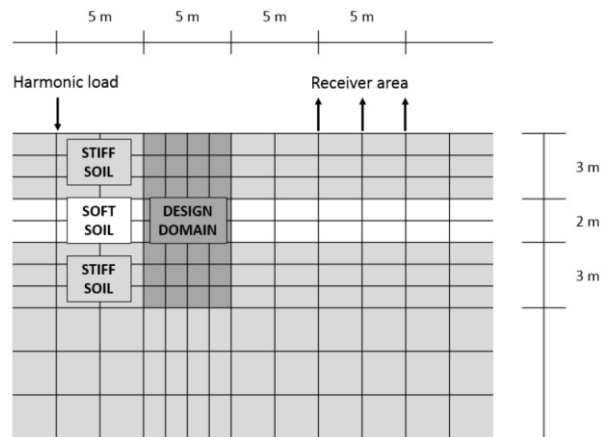


Figure 119. Inner FEM domain of the three-layered soil profile (de Zeeuw, 2018)

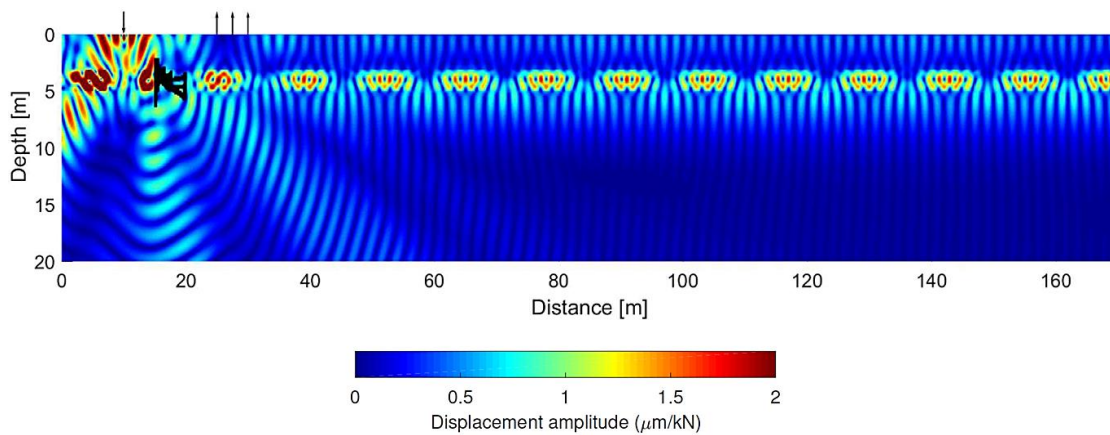


Figure 120. Displacement amplitude \hat{u}_{real} ($\mu\text{m}/\text{kN}$) for wave barrier optimized for 50 Hz. The embedded softer soil layer is used as a waveguide (de Zeeuw, 2018)

Optimized wave barrier in layered soil

Several optimization algorithms have been used to come to a new form of a wave barrier, optimized for the particular two-layered soil as described before. The final simplified wave barrier, which also takes manufacturability into account, has a relatively simple design while still providing a significant reduction of the vibration level at the receiver. The design is essentially a combination of two straight vertical barriers connected horizontally at the surface, see Figure 121, where F_{wAVG} indicates the vibration level reduction at receivers at the soil surface due to that specific wave barrier.

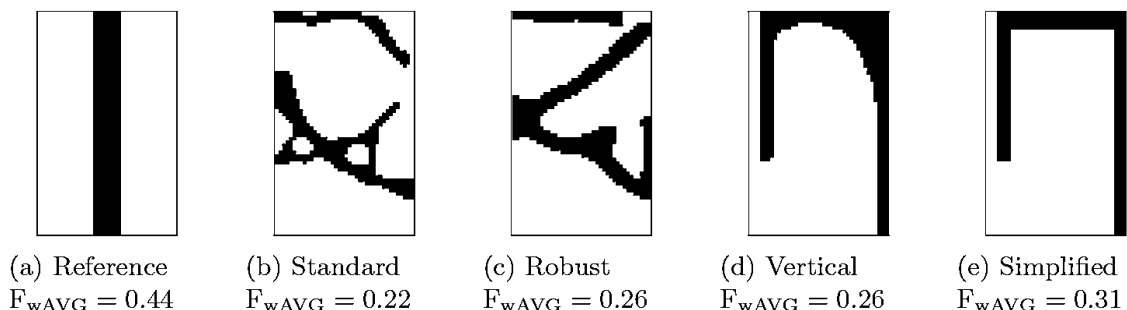


Figure 121. The shape of optimized wave barriers in a two-layered soil with increasing level of manufacturability with the soil interface at 10 m depth (de Zeeuw, 2018)

However, for the three-layer soil case it appears that, when taking into account the vertical optimization constraints, the reference barrier is in fact the optimal topology (Figure 122).

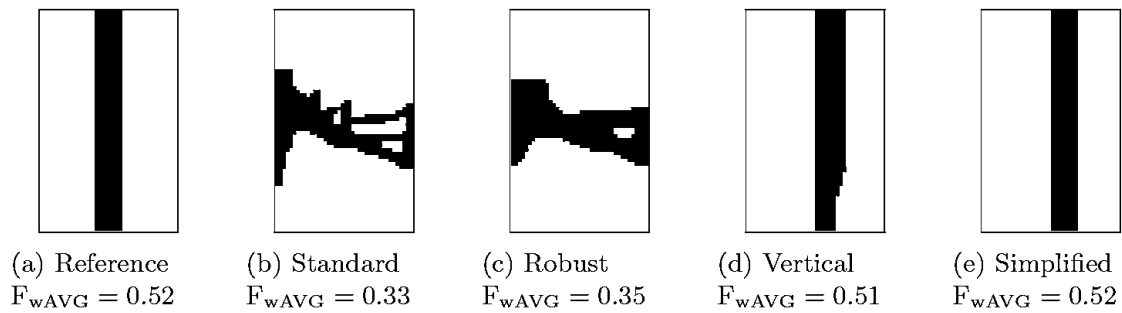


Figure 122. The shape of optimized wave barriers in a three-layered soil with increasing level of manufacturability (de Zeeuw, 2018)

1.4.3. Effectiveness of wave barriers by J.M.O. Barbosa

According to João Manuel de Oliveira Barbosa (Barbosa J. , 2013), who researched wave propagation induced by railway traffic, countermeasures at the propagation path have the goal to impede the waves of reaching a building, or at least, reducing the amplitude of the incident vibrations. The most common strategies are: subgrade stiffening; WIBs (wave impeding block); trenches and row of piles.

Subgrade stiffening consists of stiffening the soil in the proximity of the tracks, usually through jetgrouting or soil mixing techniques, which results in the reduction of the vibrations that are induced in the ground.

WIBs may be constructed beneath the track (active isolation) with the intention of replicating a rigid base, resulting in the decrease of the cut-off frequency of the foundation and in the attenuation of vibrations below this frequency, or under the building (passive isolation), with the purpose of deflecting waves that are about to impinge the building.

Trenches and row of piles are used to reflect surface waves and, like WIBs, can be bored or driven near the track (active isolation) or near the building that is going to be shielded (passive isolation). Their efficiency largely depends on the depth, and so, for moderate dimensions, they are merely suitable for reducing the vibrations at medium and high frequency ranges.

Several studied scenarios that focus on the reduction of vibrations through the use of trenches can be divided, according to the nature of the source, into mitigation of vibrations induced by standing loads or moving loads. The difference between the two resides in the vibration field that is induced in the ground. For a standing source, the ground responds with the same frequency as the excitation, while for moving loads the ground responds in a range of frequencies that depend on the speed of the source and on its frequency content (Doppler effect).

Vibrations induced by heavy traffic driving over an unevenness in the road are composed of both types. The standing source vibration field is induced by the impulsive load when the vehicle ascends and descends on the unevenness. However, the fact that the vehicle moves with a certain speed causes the creation of a vibration field of a moving load.

Works of (Ahmad and Al-Hussaini, 1991; Alzawi and Hesham El Nagggar, 2010; Celebi et al., 2009; Klein et al., 1997; Murillo et al., 2009; Ahmad et al., 1996; Beskos et al., 1986; Dasgupta et al., 1990; Hung and Ni, 2012; Leung et al., 1990; Shrivastava and Kameswara Rao, 2002; Yang and Hung, 1997; Celebi and Kirtel, 2012) indicate the following aspects as those that significantly influence the efficiency of trenches:

- Trench dimensions (depth and width): for open trenches only, the depth plays a role, while for in-filled trenches both dimensions matter.

- Properties of the in-fill material: open trenches perform better than in-filled trenches but their application in practical situations is complex due to the need of support of the trench walls.
- Properties and stratification of the soil: wave propagation in the soil depends on the stratification, and consequently so does the behaviour of trenches; nevertheless, the stratification of the soil can be neglected if the lower layers are softer than the upper layers.

Study linear homogenous halfspace

The study performed by Barbosa concerns the far field ($l = 5\lambda_R$, where l is the distance between the source and the trench).

For a study performed of a trench in a linear homogeneous halfspace with trench dimensions: $d = 1.0\lambda_R$ and $w = 0.1\lambda_R$, and the trench positioned at $l = 5\lambda_R$ from the source, the resulting reduction ratio for the soil vibration amplitude is given in Figure 123.

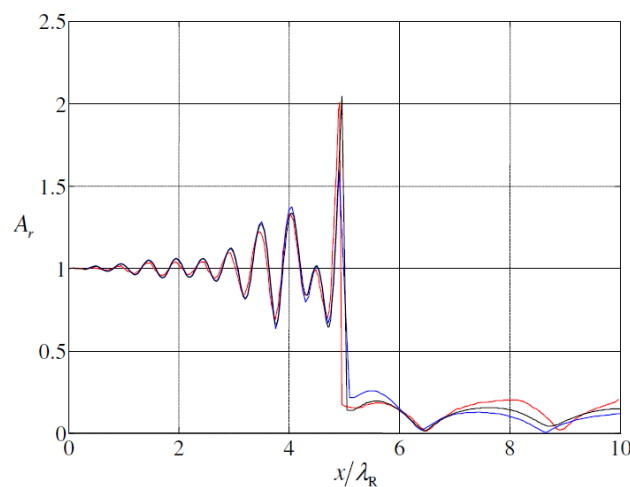


Figure 123. Reduction ratio A_r for an open trench as a function of the distance from the source. The different lines represent different calculation methods, but appear to be very similar (Barbosa J. , 2013)

It can clearly be observed that the vibration level just before the trench is significantly amplified due to reflections. However, for the field behind the trench the amplitude of the soil vibration is significantly reduced and is only 25 % compared to the case without a trench.

It was also concluded that, for an open trench, increasing the depth above $d = 1.0\lambda_R$ does not seem to result in a considerable change of the trench efficiency. For a trench filled with a soft material the maximum reduction is reached with a trench depth of about $d = 0.5\lambda_R$. For a trench filled with a stiff material the maximum reduction is reached with a trench depth deeper than $d = 1.5\lambda_R$.

When considering a change in the width of the trench it was concluded that for the open trench, the width does not have a significant influence, while for the in-filled trenches, the increase of the width leads, in general, to an increase of the trench performance. The optimal width is $w = 1.2\lambda_R$ for the soft in-fill material and $w = 1.0\lambda_R$ for the stiff in-fill material.

The stiffness of the in-fill material should preferably be lower than the soil stiffness. However also for in-fill materials that are stiffer than the soil it holds that the stiffer the material, the more reduction can be achieved (Figure 124). Also, the density of the in-fill material influences the behaviour of the trenches considerably. While for soft in-fill materials a lighter material is beneficial, for stiffer materials it is convenient to have high densities. The density has more influence on the behaviour of the stiff material than on the behaviour of the soft material.

Note that these conclusions are based on the case for a linear homogeneous halfspace with a very deep and wide trench ($\lambda_R \approx 15 m$), while in a realistic situation the soil is layered, and the trench will rarely be this (deep and) wide.

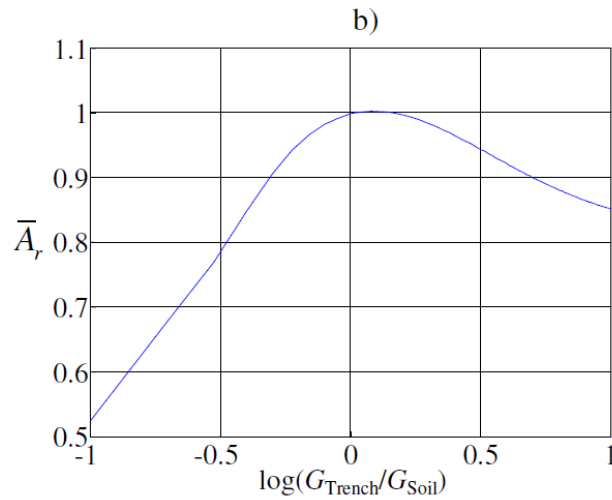


Figure 124. Reduction ratio \bar{A}_r as a function of the stiffness of the in-fill material over the stiffness of the soil (Barbosa J. , 2013)

Influence stratification of halfspace

The homogenous halfspace is replaced by a layer on top of a halfspace. The thickness of the layer is $H = \lambda_R$. When the lower halfspace is stiffer than the upper layer the stratification considerably changes the behaviour of the trenches. The influence of stratification is more noticeable for the open trench than for the in-filled trenches.

It must be noted that each parameter is studied independently of the others, and so, if more than one parameter varies in each study, different conclusions may be reached. Also, the studies performed concern standing line loads only. In the case of moving loads, the response of the ground is characterized by a wide frequency band and so the dimensionless study becomes difficult because the trench performs differently for every frequency.

Trenches for the mitigation of train induced vibrations

The following conclusions are achieved:

- Neglecting the train tracks leads to higher vibration levels in the soil surface (at least for short and medium distances) and to lower efficiency of trenches. Thus, its inclusion in the numerical model is necessary to assess the need for mitigation measures.
- The presence of the trench (causing wave reflections) does not influence the train-track interaction phenomenon.
- The behaviour of trenches when acted upon by moving loads is very different from their behaviour when acted upon by 2D line loads. In fact, 2D simulations tend to underestimate the efficiency of trenches, and that is more pronounced for concrete trenches than for geofoam trenches.
- Ranking the in-fill materials according to the efficiency of the trench, from the 2D simulations open trenches are placed first, geofoam trenches second, and concrete trenches in last place, while from the 3D simulations concrete trenches and open trenches come together in the first place, and geofoam trenches are placed last clearly.

The efficiency of trenches

The trench solutions are compared based on the insertion loss (IL) and on the running root mean square (RRMS) of the vertical velocity induced by the passage of the train. The IL curves show that above the frequency 10 Hz, the displacements are attenuated for all trench solutions (Figure 125). For this frequency the Rayleigh wavelength is 18 m, while the depth of the shallow trench (3 m) is only 1/6 of the Rayleigh wavelength. Still the shallow trenches are able to reduce the vibrations.

Also, based on the IL plots, the 6 m deep trenches tend to perform better than the 3 m deep trenches, as expected. For the ranking of the in-fill material it is concluded, based on the 3D analyses, that concrete trenches come first, empty trenches come second, though very close to the concrete trenches, and geofoam trenches come last, way below the other two. This ranking differs from the results of the 2D analyses, for which the open trenches come first, geofoam trenches come second, and concrete trenches get last place.

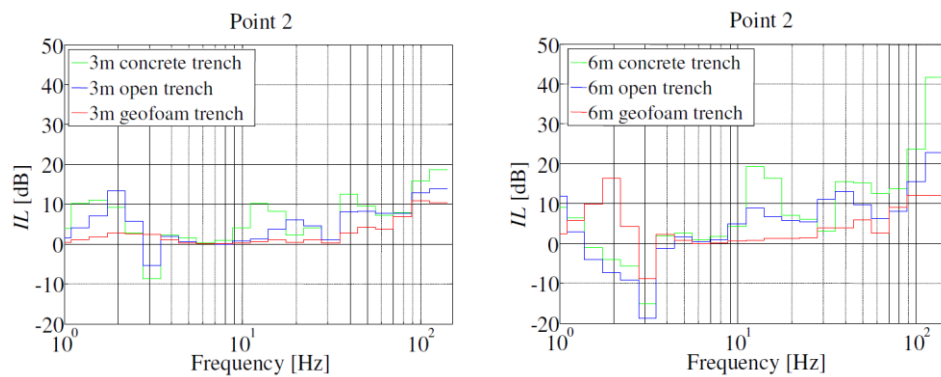


Figure 125. Typical figure for the insertion loss (IL) of the 3D analyses for different in-fill materials and depths of the trench (Barbosa J. , 2013)

The reason why the concrete trenches outperform the geofoam trenches when acted upon by moving loads (as opposed to what happens in the 2D simulations) is related to their high bending stiffness. The transmission of plane waves in the soil with a longitudinal wavelength smaller than the longitudinal bending wavelength of the barrier is hindered. In other words, when the longitudinal wavelength λ_y of a propagating wave is smaller than the free bending wavelength in the barrier λ_{yB} , but not shorter than the Rayleigh wavelength of the soil λ_R , then the waves are reflected at the barrier due to its bending stiffness. In plane strain conditions (2D), the wavelength is infinite and so the bending stiffness has no influence, but in 3D conditions, waves can propagate in all directions and so surface waves that propagate with an angle θ such that $\sin \theta > \lambda_R / \lambda_{yB}$ are reflected by the trench. The reflecting property supports the idea that 2D simulations are not sufficient to predict with enough accuracy the abatement of vibrations induced by moving loads, since the obtained results will tend to underestimate the actual reduction.

1.4.4. Conclusion wave barrier

The stratification of the soil makes that a wave barrier can perform very different from the case in which a wave barrier is used in a homogeneous soil halfspace. However, in all studies it is observed that the wave barrier does decrease the vibration levels in the soil in the close proximity behind the wave barrier. Since the vibration reduction holds for the soil right behind the wave barrier only, and since the vibration levels in the soil surrounding this 'shadowed' region can exhibit amplified vibration levels, it is advised to make the depth of the wave barrier always as deep, or deeper, than the toe of the foundation piles underneath the structure.

The reduction factor created by the wave barrier cannot easily be determined and depends on the situation.

D. Appendix: Extensive overview of Chapter 5 ‘Structural System (Receiver of Vibrations)’

The system to be considered for this thesis is a system with multiple degrees of freedom (MDoF). However, to remind the reader of the particularities of the dynamic response of a system, first a brief overview of the simple case of a single degree of freedom (SDoF) is presented. Thereafter the simple single degree of freedom case is extended to the case of a two degree of freedom system (which is already a multi-degrees of freedom system). After this introduction of a multi-degrees of freedom system, the two degree of freedom system is extended to a n -multi-degrees of freedom system. Finally, the case of continuous systems is briefly discussed. This system may be referred to as a n -multi-degrees of freedom system where n goes to infinity. All systems discussed in this thesis are supposed to be linear. This is justified by the fact that the vibration levels considered for vibration sensitive laboratory structures are relatively small so that all materials remain in their linear elastic state.

The structure considered in this thesis will then be simplified to a system which can be composed of the multi-degrees of freedom systems described in the preceding sections.

1.1. Simplification Laboratory Structure

The laboratory structure is simplified to a system that can be solved by established methods for structural dynamics. Since a laboratory structure has such strict vibration level criteria, the structure is often made very stiff in order to realize a system with natural frequencies higher than the fundamental excitation frequency. The most straightforward approximation one can make for such a structure is, therefore, a rigid slab or a rigid box volume (depending on the design) which has only three degrees of freedom: two translational (horizontal and vertical) and one rotational (rocking). This system is often referred to as a multi-degrees of freedom system (MDoF system).

However, due to this simplification, only the global modal shapes of the system can be determined. In reality, the floors and walls are not infinitely rigid, but are flexible, which causes these elements to undergo local modal shapes. These local modal shapes, for example, the natural frequencies of the floors and the walls are neglected, while these natural frequencies are often different than the natural frequencies of the global rigid system. Therefore, in order to make a proper estimation of the vibration levels of one floor, on which the laboratory equipment is placed, the local modal shapes should also be taken into account. Since these local modal shapes makes the interaction (chapter 6 Soil-Structure Interaction) between the structure and the soil mathematically very complicated, the interaction is only based on a rigid slab of rigid box volume. Then the response of this rigid structure is determined. Once the response of the rigid structure is known, the local elements, e.g. the floors are analysed separately. The excitation of these local elements is approximated by the response of the rigid structure, and this excitation is implemented as initial conditions for the local element.

1.2. Single Degree of Freedom system

Before hopping into the mathematics of the multi-degrees of freedom system (MDoF system), the simpler case of a single degree of freedom is briefly discussed to explain the fundamentals of the dynamic characteristics of a structure. The reader is expected to have some knowledge about the mathematical approach to such kind of systems, therefore only a brief explanation is given here. In case the reader wants to know more in-depth theory, he or she is kindly referred to the lecture notes of the Technical University Delft about Structural Dynamics, with course codes CT4140 (Spijkers, Vrouwenvelder, & Klaver, 2005), CT4145 (Metrikine, 2018) and CIE

5260 (Tsouvalas, 2018). The following text is a brief summary of the theory explained in these lecture notes.

1.2.1. Governing equations

To determine the dynamic response of a structural system, first the governing equations should be determined. This procedure can be done following different kind of methods. The most applicable methods for a single degree of freedom are the Displacement method and the Lagrangian formalism. For now, only the displacement method will be considered, since this method is very suitable for the structure subjected in this thesis and this method directly provides the stiffness matrix.

1.2.2. Undamped free vibration

First the most simple case of a single degree of freedom (SDoF) will be considered: the free vibration of an undamped system (Figure 126) where the loading term $F(t)$ is zero.

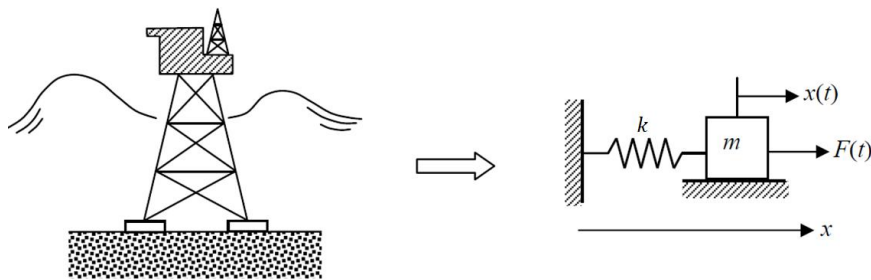


Figure 126. Idealization of horizontal motion of an offshore platform, excited by waves, by a mass-spring system with a translational degree of freedom (in x – direction) (Metrikine, 2018)

By applying the displacement method (displace the mass in the direction of the degree of freedom and write the equilibrium equations for the dynamic forces), the following equation of motion for the mass-spring system, which is a second ordinary linear differential equation, is obtained:

$$m\ddot{x} + kx = 0 \quad (0.42)$$

The system can only move if given an initial displacement or/and an initial velocity:

$$\begin{aligned} x(0) &= x_0 \\ \dot{x}(0) &= v_0 \end{aligned} \quad (0.43)$$

where the dot above the translational degree of freedom (displacement) means the first derivative of this DoF (two dots means the second derivative of this DoF), thus, in this case, velocity.

The general solution of an ordinary linear differential equation of N – th order with constant coefficients can be written as:

$$x(t) = \sum_{n=1}^N X_n \exp(s_n t) \quad (0.44)$$

Substitution of this general solution in the equation of motion, and simplifying the expression, one obtains the characteristic equation:

$$ms_n^2 + k = 0 \quad (0.45)$$

The characteristic exponents s_n are the roots of this equation and read for this case:

$$s_1 = i\sqrt{k/m}, \quad s_2 = -i\sqrt{k/m} \quad (0.46)$$

The general solution can then be written as:

$$x(t) = X_1 \exp(it\sqrt{k/m}) + X_2 \exp(-it\sqrt{k/m}) \quad (0.47)$$

and with the Euler formula:

$$\exp(i\alpha) = \cos \alpha + i \sin \alpha \quad (0.48)$$

the equation of the general solution can be written as:

$$x(t) = A \cos(\omega_n t) + B \sin(\omega_n t) \quad (0.49)$$

where

$$\omega_n = \sqrt{k/m} \quad (0.50)$$

is the natural frequency of the mass-spring system. This is the frequency, with which the mass-spring system would vibrate given arbitrary initial conditions.

The constants can be determined by substituting the general solution into the initial conditions. The expression then obtained is:

$$x(t) = x_0 \cos(\omega_n t) + \frac{v_0}{\omega_n} \sin(\omega_n t) \quad (0.51)$$

The free vibration looks like (Figure 127):

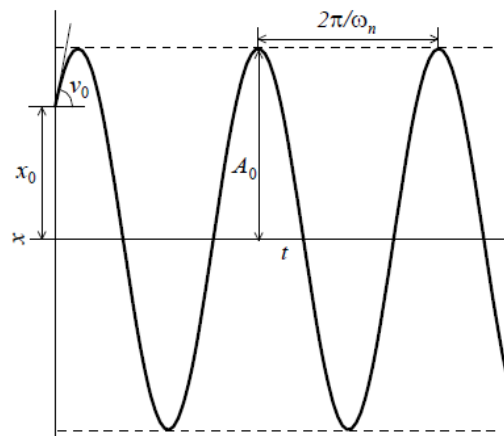


Figure 127. The free vibration of the undamped mass-spring system (Metrikine, 2018)

1.2.3. Undamped forced vibration

The previously considered case was a state of free vibration, i.e. the loading term was zero. The obtained results indicate the characteristics of the system, independent of any loading applied. However, when a force is applied the dynamic response of the system is altered. First the case of a harmonic loading is considered, since any time-dependent force can be represented as a superposition of harmonic forces with different amplitudes and phases. Thus, the dynamic behaviour of the mass-spring system under a harmonic force may be considered as a

fundamental knowledge, which facilitates understanding of the behaviour of the system under a force of arbitrary time signature. Thereafter, the more general loading case of arbitrary loading is considered.

Harmonic loading

Assume the external harmonic loading to be applied at the single degree of freedom as illustrated in Figure 126. The obtained equation of motion then is:

$$m\ddot{x} + kx = F_0 \cos(\omega t) \quad (0.52)$$

The general solution for this equation of motion is in the form of a homogeneous solution (the solution for the free vibration) plus a particular solution. Again, the unknown constants depend on the initial conditions. The finally obtained general solution is of the form:

$$x(t) = x_0 \cos(\omega_n t) + \frac{v_0}{\omega_n} \sin(\omega_n t) + \frac{F_0}{k} \frac{1}{1 - \omega^2/\omega_n^2} (\cos(\omega t) - \cos(\omega_n t)) \quad (0.53)$$

This expression shows that the mass-spring system vibrates at two frequencies, one being the natural frequency ω_n and the other being the frequency ω of the external force.

After a sufficiently long time, the dynamic behaviour of the mass-spring system subjected to a small damping (not yet taken into account here) is approximately described by the particular solution only. In this case the solution is called the steady-state solution and it is independent of the initial conditions. The steady-state solution for this problem reads:

$$x_{steady} = X \cos(\omega t) = \frac{F_0}{k} \frac{1}{1 - \omega^2/\omega_n^2} \cos(\omega t) \quad (0.54)$$

When plotting $X/x_{static} = \frac{1}{1 - \omega^2/\omega_n^2}$ as function of ω/ω_n one obtains the resonance diagram (Figure 128).

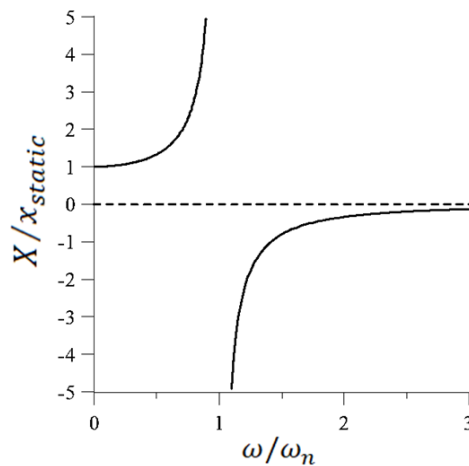


Figure 128. The resonance diagram of the forced single degree of freedom system (Metrikine, 2018)

The amplitude- and phase-frequency dependencies are shown in Figure 129.

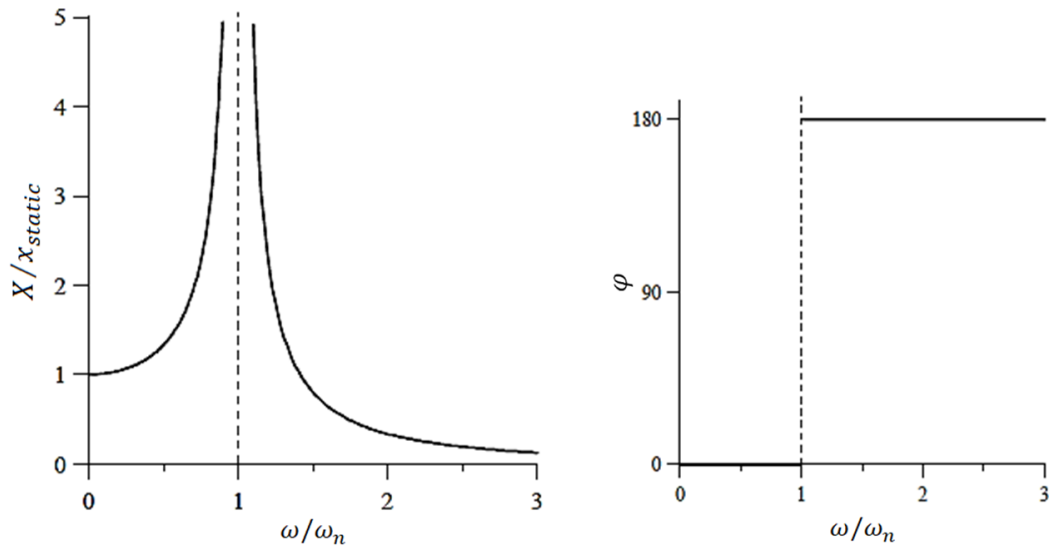


Figure 129. (left) Amplitude-frequency characteristic (magnification factor) and (right) phase-frequency characteristic (Metrikine, 2018)

These figures indicate that for ω close to $\omega = 0$, the loading frequency is extremely slow, and the mass will deflect by the force to its static deflection only.

For very high frequencies $\omega/\omega_n \gg 1$, the force changes its direction so fast that the mass simply has no time to follow and the amplitude of the response is very small.

At $\omega/\omega_n = 1$, the amplitude of the response becomes infinitely large. The frequency of the force coincides exactly with the natural frequency of the system, therefore, the force can push the mass always in the direction in which the mass moves itself, thereby increasing the amplitude of vibrations indefinitely. This phenomenon is known as resonance. The amplitude of resonant vibrations grows in time linearly and the displacement of the mass-spring system increases to infinity (in the undamped case) (Figure 130).

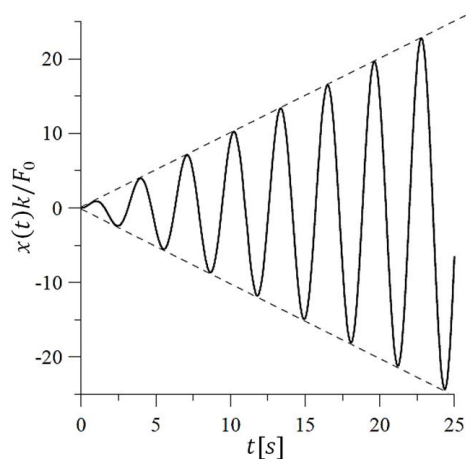


Figure 130. Development of resonance of the undamped forced single degree of freedom system in time (Metrikine, 2018)

General disturbing force

Next to a harmonic force, a general disturbing force can be taken into account in the mathematical formulation of the dynamical problem. This can be done by representing the force by Duhamel's integral in which the (non-periodic) force is represented as a sequence of short impulses. The total response is obtained by a continuous superposition (integral) of the system responses to these impulses:

$$x(t) = x_0 \cos(\omega_n t) + \frac{v_0}{\omega_n} \sin(\omega_n t) + \frac{1}{m\omega_n} \int_0^t F(t') \sin(\omega_n(t-t')) dt' \quad (0.55)$$

Another method is based on the application of the Laplace transform. The loading is represented as a continuous superposition (integral) of its harmonic components (instead of responses to the impulses) and the response to each of these harmonics can be found separately. The responses are then integrated by means of the inverse Laplace transform to give the dynamic response to the original non-harmonic load. This procedure is not further outlined here.

1.2.4. Damped free vibration

Every engineering system experiences damping that dissipates the energy of vibrations. Now the mass-spring system is considered to be subject to viscous damping, which is proportional to the velocity of the mass (Figure 131).

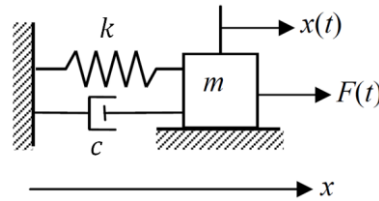


Figure 131. A mass-spring-dashpot system with a translational degree of freedom (in x – direction) (Metrikine, 2018)

Again, by applying the displacement method, and writing the balance of forces, one obtains the following scalar equation, which has one additional term compared to the undamped case:

$$m\ddot{x} + c\dot{x} + kx = F(t) \quad (0.56)$$

The procedure of finding the homogeneous solution (the loading term $F(t)$ is zero) of this damped system is similar to the undamped system. However, different notations are introduced:

$$\omega_n = \sqrt{k/m}, \quad c/m = 2n \quad (0.57)$$

Because of the damping parameter, the roots of the characteristic equation can become real ($n > \omega_n$), which represents a non-vibration (aperiodic) motion. The mass simply gradually creeps back towards the equilibrium position. However, in mechanics, more often the case is encountered in which ($n < \omega_n$), so that the roots are complex. The motion now is vibratory and the homogeneous solution, taking into account the initial conditions, is of the form:

$$x(t) = \exp(-nt) \left(x_0 \cos(\omega_1 t) + \left(\frac{v_0}{\omega_1} + \frac{nx_0}{\omega_1} \right) \sin(\omega_1 t) \right) \quad (0.58)$$

Due to the damping, the vibrations are attenuated over time (Figure 132). Thus, damping extracts energy from the system leading to a decay of the amplitude of vibrations.

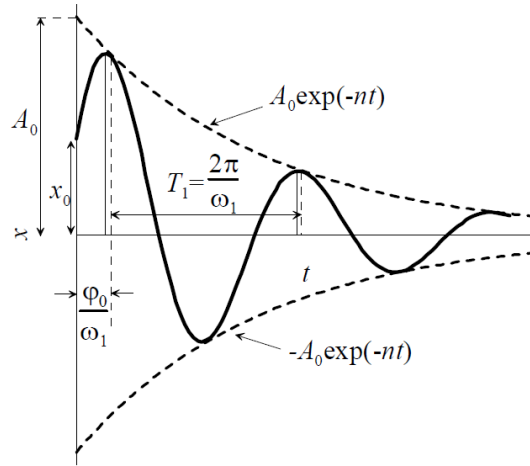


Figure 132. Free vibration of the mass-spring-dashpot system in the case $n < \omega_n$ (Metrikine, 2018)

The period of vibration T and its reciprocal, the frequency of vibration f_1 , depend on the damping parameter n :

$$f_1 = f_n \left(1 - \frac{n^2}{2\omega_n^2} \right), \quad \text{where } f_n = \frac{\omega_n}{2\pi} \quad (0.59)$$

1.2.5. Damped forced vibration

When taking into account the loading term, a similar approach is followed as for the undamped mass-spring system.

Harmonic loading

First the case of harmonic loading is considered again, and the equation of motion is:

$$m\ddot{x} + c\dot{x} + kx = F_0 \cos(\omega t) \quad (0.60)$$

Again, the general solution is the summation of the homogeneous solution (see the case of free vibration before) and a particular solution. The amount of damping is represented by the parameter $\gamma = 2n/\omega_n$. The particular solution, in case of the harmonic loading, is of the form:

$$x_{part} = \frac{f_0}{(\omega_n^2 - \omega^2) + 4n^2\omega^2} ((\omega_n^2 - \omega^2) \cos(\omega t) + 2n\omega \sin(\omega t)) \quad (0.61)$$

The particular solution is the steady-state solution. When rearranging this expression, the magnification factor:

$$\frac{|X|}{x_{static}} = \frac{1}{\sqrt{\left(1 - \frac{\omega^2}{\omega_n^2}\right)^2 + \gamma^2 \frac{\omega^2}{\omega_n^2}}} \quad (0.62)$$

and the phase lag can be plotted as function of ω/ω_n for different amounts of damping (Figure 133).

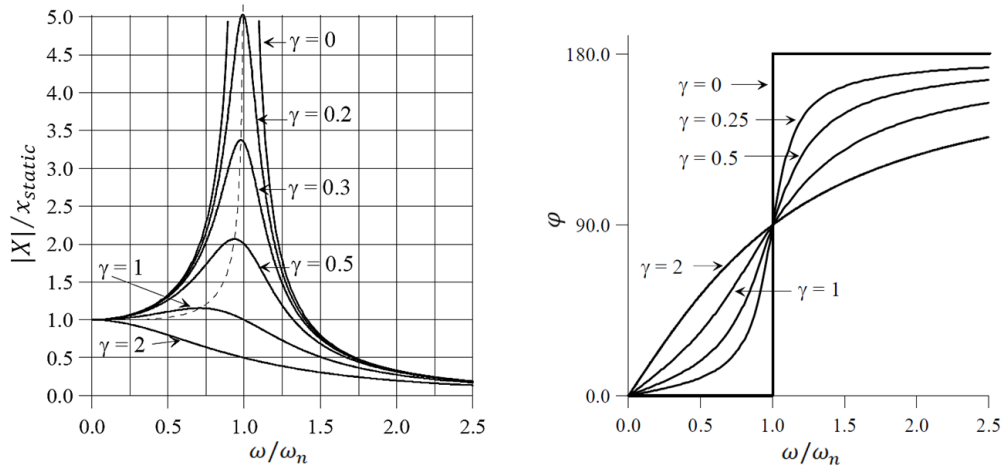


Figure 133. (left) Magnification factor and (right) Phase lag of the damped SDoF steady-state solution (Metrikine, 2018)

Note that, compared to the undamped SDoF-case (Figure 129), the peak at $\omega/\omega_n = 1$ for the damped SDoF system does not go towards infinity anymore, but is finite.

General disturbing force

When considering the case of an arbitrary time dependence of the external forces, the total solution can be obtained in exactly the same manner as it was done for the undamped mass-spring system, by using Dyhamel's integral. The total solution takes the form:

$$x(t) = \exp(-nt) \left(x_0 \cos(\omega_1 t) + \left(\frac{v_0}{\omega_1} + \frac{nx_0}{\omega_1} \right) \sin(\omega_1 t) \right) + \frac{1}{\omega_1} \int_0^t F(t') \exp(-n(t-t')) \sin(\omega_1(t-t')) dt' \quad (0.63)$$

As example the case of an external force suddenly applied to the mass:

$$F(t) = \begin{cases} 0 & t < 0 \\ F_0 & t \geq 0 \end{cases} \quad (0.64)$$

is considered. The obtained solution of the relative displacement x/x_{static} is represented in Figure 134 as function of the dimensionless time τ for three values of the damping (γ).

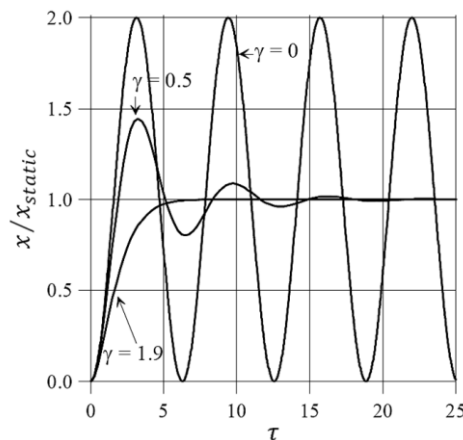


Figure 134. Response of a (damped) SDoF system to suddenly applied constant force (Metrikine, 2018)

1.3. Two Degrees of Freedom system

Before only single degree of freedom systems have been discussed. This system enables us to explain the resonance phenomenon and to calculate the natural frequencies of a number of structures. However, most realistic structures have multiple degrees of freedom. In order to explain additional phenomenon that occur in case of multiple degrees of freedom, the theory is developed to more complicated systems. As a first step, we consider a system with two degrees of freedom, which will yield the explanation of most ‘vibration dampers’ applied in practice. The most general undamped two degree of freedom system can be schematized as in Figure 135.

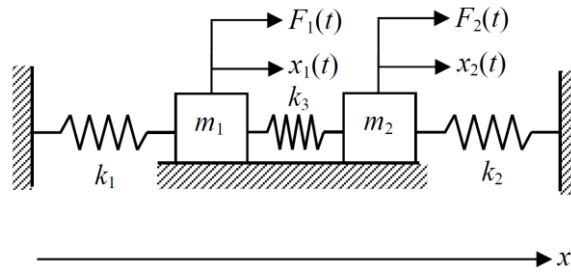


Figure 135. Undamped two degrees of freedom system with spring coupling (Metrikine, 2018)

Following the same principle as before, by applying the displacement method, two scalar equations are obtained:

$$\begin{aligned} m_1 \ddot{x}_1 + k_1 x_1 + k_3(x_1 - x_2) &= F_1(t) \\ m_2 \ddot{x}_2 + k_2 x_2 + k_3(x_2 - x_1) &= F_2(t) \end{aligned} \quad (0.65)$$

1.3.1. Undamped free vibration

Considering the undamped free vibrations of this system (the homogeneous solution), with the loading term $F_i(t) = 0$, where $i = 1, 2$, the general solution can be written in the form similar to the SDoF system, but then for both degrees of freedom:

$$x_1(t) = \sum_{n=1}^4 X_n^{(1)} \exp(s_n t), \quad x_2(t) = \sum_{n=1}^4 X_n^{(2)} \exp(s_n t) \quad (0.66)$$

Substituting the general solution into the equation of motion. The system of obtained equations has a non-trivial solution if the determinant of its coefficient matrix vanishes. This forms the characteristic equation of the two degrees of freedom system:

$$(m_1 s^2 + k_1 + k_3)(m_2 s^2 + k_2 + k_3) - k_3^2 = 0 \quad (0.67)$$

This characteristic equation has two values of s^2 as solutions. They are real and negative, so that the corresponding values of s are all imaginary. This implies that the motion of the two degree of freedom system is vibratory and takes place at two distinct frequencies.

The amplitudes of the free vibrations of the masses m_1 and m_2 are intrinsically related to each other. The free vibrations of the two degrees of freedom system are characterized by the natural frequencies and by the shapes of vibration at these frequencies, in case $k_1 = k_2 = k$, the natural frequencies are:

$$\omega_{n1} = \sqrt{k/m}, \quad \omega_{n2} = \sqrt{(k + 2k_3)/m} \quad (0.68)$$

These shapes are normally referred to as normal modes and imply a specific motion of the masses with respect to each other (Figure 136).

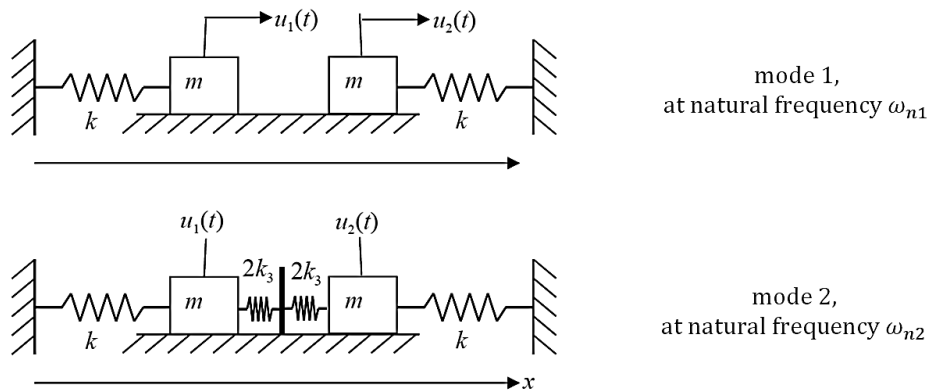


Figure 136. Normal modes of the undamped two degrees of freedom system. In mode 1, the two masses move in-phase with each other (k_3 is not stretched, nor compressed). In mode 2, the two masses move out-of-phase with each other (k_3 is stretched or compressed from both sides at the same time). (Metrikine, 2016)

Another example is the two degree of freedom shear frame in Figure 137 which is not further outlined here.

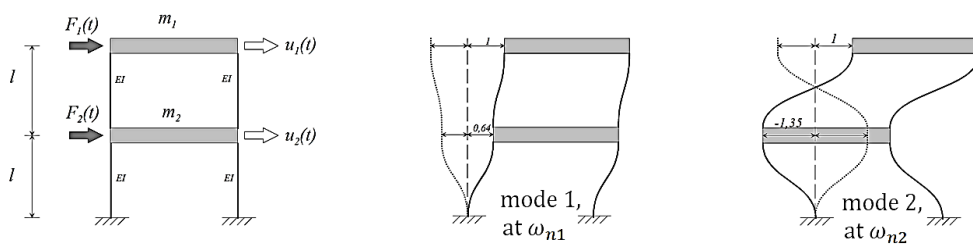


Figure 137. Normal modes of the undamped two degrees of freedom system: the shear frame (Blauwendraad, 2016)

The procedure can also be written in matrix notation, which is more convenient for the case in which more degrees of freedom in the system have to be considered:

$$\underline{M}\ddot{\underline{x}} + \underline{K}\underline{x} = 0 \tag{0.69}$$

And determining the determinant of this matrix:

$$\det[-\omega^2 \underline{M} + \underline{K}] = 0 \tag{0.70}$$

This is equivalent to finding the eigenvalues of the matrix $\underline{K}\underline{M}^{-1}$. The natural frequencies can be obtained in both ways. The normal modes of the free vibrations can be found by searching for the eigenvectors of the matrix $\underline{K}\underline{M}^{-1}$.

1.3.2. Undamped forced vibration

Now the case is considered in which a harmonic load is applied at one mass and the spring at the right-hand-side is not taken into account (Figure 138). The forced steady-state vibrations are considered. This vibration takes place at the frequency of the force.

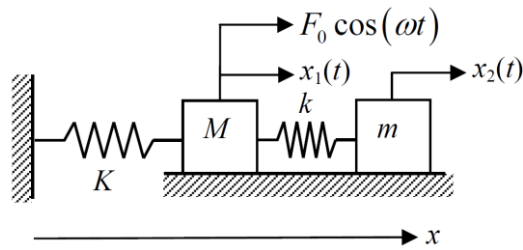


Figure 138. Forced two degrees of freedom system. The vibrations absorber k - m is attached to the main system K - M (Metrikine, 2018)

This auxiliary mass-spring system is normally referred to as an undamped dynamic vibration absorber. The parameters of the absorber (k, m) can be chosen such that the main system does not vibrate although it is subjected to the external harmonic force.

Compared to the scalar equations obtained before (in correspondence with Figure 135), the following terms are interchanged: $k_1 = K$, $m_1 = M$, $F_0^{(1)} = F_0$, $k_3 = k$, $k_2 = 0$, $m_2 = m$, $F_0^{(2)} = 0$.

Since no damping is considered in this steady-state-case, the masses vibrate with infinite amplitudes when the frequency of the force becomes equal to one of the two natural frequencies of the system (Figure 139). Furthermore, if the frequency of the force becomes equal to the natural frequency of the auxiliary system, the amplitude of the main system becomes zero.

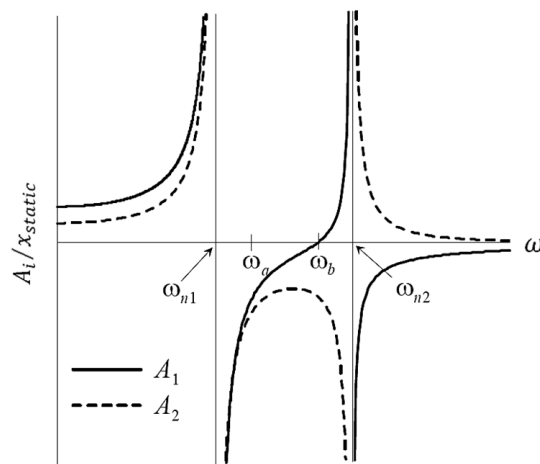


Figure 139. Displacement-frequency curves for the two degrees of freedom system (Metrikine, 2018)

1.4. Multi-Degrees of Freedom system

According to (Spijkers, Vrouwenvelder, & Klaver, 2005), many technical structures are so complicated that the dynamic behaviour of it cannot be described accurately with merely one or two degrees of freedom. Also, the structure to be considered in this thesis cannot be described by only one or two degrees of freedom. Therefore, in this section the two degrees of freedom system is expanded to the more general case of a n -multi-degrees of freedom system (MDoF system). The text is a brief summary of the very comprehensive explanation, given in the lecture notes Structural Dynamics CT 4140 – Part I Structural Vibrations of the Technical university Delft (Spijkers, Vrouwenvelder, & Klaver, 2005).

Different methods can be used to determine the solutions of these kind of systems. However, the Modal Analysis is mostly used as the basis of many computer programmes to determine the natural frequencies and eigenvectors of the system.

Due to the large number of degrees of freedom, it is more convenient to formulate the dynamic problem in matrix notation. However, when the number of degrees of freedom are limited (e.g. three DoF), the dynamic behaviour can be described quite accurately. This type of

structures will be applied to illustrate the theory with respect to the systems with n degrees of freedom. Also, the rigid slab or box volume considered for this thesis will also have only three degrees of freedom.

1.4.1. Differential equations (undamped case)

Again, the displacement method is used. As an example, a block foundation with three degrees of freedom (in the plane of the drawing) is considered (Figure 140). The degrees of freedom are two translations and a rotation about the centre of gravity, all three measured with respect to the state of static equilibrium, so that the deadweight load (mg) does not play a role in the dynamic analysis.

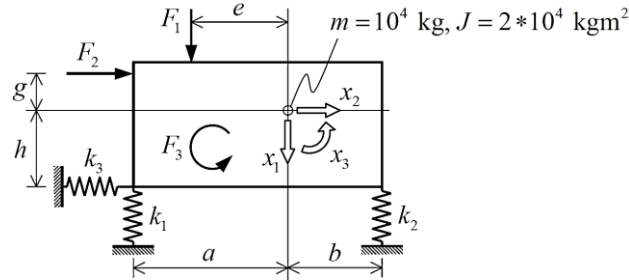


Figure 140. Foundation block with three degrees of freedom (Spijkers, Vrouwenvelder, & Klaver, 2005)

The equations of motion can be noted down in matrix notation:

$$\begin{bmatrix} m & 0 & 0 \\ 0 & m & 0 \\ 0 & 0 & J \end{bmatrix} \begin{bmatrix} \ddot{x}_1 \\ \ddot{x}_2 \\ \ddot{x}_3 \end{bmatrix} + \begin{bmatrix} k_1 + k_2 & 0 & ak_1 - bk_2 \\ 0 & k_3 & hk_3 \\ ak_1 - bk_2 & hk_3 & a^2k_1 + b^2k_2 + h^2k_3 \end{bmatrix} \begin{bmatrix} x_1 \\ x_2 \\ x_3 \end{bmatrix} = \begin{bmatrix} F_1 \\ F_2 \\ F_3 + eF_1 - gF_2 \end{bmatrix} \quad (0.71)$$

or symbolically:

$$\underline{M}\ddot{\underline{x}} + \underline{K}\underline{x} = \underline{F} \quad (0.72)$$

For this 3DoF-case the mass and stiffness matrices are both symmetrical (3×3) matrices in which the mass matrix is a diagonal matrix. However, for a n MDoF system, the matrices are of the size ($n \times n$).

1.4.2. Undamped free vibration of a n MDoF system

In the case the loading terms are zero, the n MDoF system undergoes only free vibrations. As homogeneous solution, a synchronic harmonic motion is assumed:

$$\underline{x}(t) = \underline{\hat{x}} \sin(\omega t + \varphi) \quad (0.73)$$

This solution implies that all degrees of freedom vary in time in the same manner. The free vibration is called a principal mode (or normal mode) of vibration. The unknown amplitude vector $\underline{\hat{x}}$ is called an eigenvector.

After substituting the proposed solution into the homogeneous system of equations, the generalized eigenvalue problem is obtained. A non-trivial solution will be found if the set of equations proves to be dependent, thus the determinant of the system should be equal to zero:

$$\det[-\omega^2 \underline{M} + \underline{K}] = 0 \quad (0.74)$$

with ω^2 representing the so-called eigenvalue. This leads to a polynomial of degree n in ω^2 , which is called the characteristic polynomial. The determination of the roots of the characteristic equation is often not possible without numerical methods. By the aid of the

computer the n natural frequencies and n associated eigenvectors of the system with n degrees of freedom can be found, but are only determined up to scalar multiples (Spijkers, Vrouwenvelder, & Klaver, 2005). The eigenvectors represent the principal modes of vibration and are therefore often displayed graphically. So, for system with n degrees of freedom, there appear to be n principal modes of vibration (eigenmodes). The free vibration of the system is the summation of all possible eigenmodes. The remaining unknown constant can be found from the prescribed initial conditions.

For the (forced) inhomogeneous problem. The vibrations are written in the more general form (no synchronous harmonic motion, but an arbitrary time function $u_i(t)$):

$$\underline{x}(t) = \sum_{i=1}^n \underline{\hat{x}}_i u_i(t) \quad (0.75)$$

The solutions for u_i are derived from the following set of uncoupled homogeneous differential equations:

$$\ddot{u}_i(t) + \omega_i^2 u_i(t) = 0, \quad (i = 1, 2, \dots, n) \quad (0.76)$$

The free vibration can be formulated symbolically by:

$$\underline{x}(t) = \underline{E} \underline{u}(t) \quad (0.77)$$

Where the square ($n \times n$) matrix \underline{E} is called the eigenmatrix and contains the eigenvectors as columns. This eigenmatrix plays an important role in solving the forced vibration (the inhomogeneous problem).

For the foundation block example ($n = 3$), three natural frequencies and three eigenvectors can be determined, from which the first natural frequency is called the ‘fundamental natural frequency’.

1.4.3. Undamped forced vibration of a n MDOF system by the Modal Analysis

For the forced vibration of the n MDOF system a particular solution, next to the homogeneous solution, is considered. The particular solution is similar to the homogeneous solution, however, now the time function $u_i(t)$ is unknown:

$$\underline{x}(t) = \underline{E} \underline{u}(t) \quad (0.78)$$

Here also a summation of synchronised motions is assumed. This assumption is the essence of the so-called Modal Analysis. In mathematical terminology, it is assumed that also in the case of forced vibration the response can be expanded in eigenvectors each weighed with an unknown time function.

The assumed particular solution is substituted in the inhomogeneous set of differential equations and the orthogonality condition is used to decouple the degrees of freedom.

Intermezzo: orthogonality conditions

Eigenvectors possess two characteristic properties, which are known as the orthogonality conditions. With the orthogonality conditions, the Modal Mass Matrix ($\underline{M}^* = \underline{E}^T \underline{M} \underline{E}$) and the Modal Stiffness Matrix ($\underline{K}^* = \underline{E}^T \underline{K} \underline{E}$) can be introduced, where \underline{E} is the eigenmatrix and \underline{E}^T the transposed eigenmatrix.

The following relation holds between the diagonal matrices \underline{M}^* and \underline{K}^* :

$\Omega^2 \mathbf{M}^* = \mathbf{K}^*$. Where Ω^2 is a diagonal matrix, with the eigenvalue ω_i^2 as elements on the main diagonal

The decoupled degrees of freedom $u_i(t)$, are also called Modal or Generalized degrees of freedom. A physical or geometrical interpretation of modal degrees of freedom is seldom available.

For a load function which is equal to zero when $t < 0$, a particular solution of the uncoupled set can be obtained by means of the integral of Duhamel. For the complete solution, the homogeneous solution and the particular solution are summed:

$$u_i(t) = C_i \sin(\omega_i t + \varphi_i) + \int_{\tau=0}^t \frac{\hat{x}_i^T F(\tau)}{\hat{x}_i^T \mathbf{M} \hat{x}_i} \frac{1}{\omega_i} \sin\{\omega_i(t - \tau)\} d\tau \quad (0.79)$$

The unknown constants are determined by the initial conditions. However, now the response is still described by the non-physical degrees of freedom $u_i(t)$. The response in the physical degrees of freedom $x_i(t)$ can be obtained by:

$$\begin{aligned} \underline{x}(t) &= \sum_{i=1}^n \hat{x}_i u_i(t) = \mathbf{E} \underline{u}(t) \\ &= \sum_{i=1}^n \left\{ \hat{x}_i C_i \sin(\omega_i t + \varphi_i) + \frac{\hat{x}_i \hat{x}_i^T}{\hat{x}_i^T \mathbf{M} \hat{x}_i} \frac{1}{\omega_i} \int_{\tau=0}^t F(\tau) \sin\{\omega_i(t - \tau)\} d\tau \right\} \end{aligned} \quad (0.80)$$

The method described is generally applicable and is more or less adapted for numerical computer applications. However, the procedure offers a structured method for hand calculations as well.

The expressions shown might not give a very clear overview, however, summarizing the modal analysis, it entails finding the solution of the inhomogeneous coupled system. This comes down to solving a decoupled set of differential equations formulated in the modal degrees of freedom. This uncoupled system is derived by assuming that the forced vibration can be written as a summation of eigenvectors; in other words: the response can be expanded in eigenvectors (the so-called Modal Analysis) (Spijkers, Vrouwenvelder, & Klaver, 2005).

1.4.4. Harmonic loads for a n MDOF system

When analysing the response of the system to a harmonic load function (with loading frequency Ω), the particular solution is assumed to be also a harmonic time function, having the same frequency as the load function. The amplitude of the particular solution can be determined by substitution into the decoupled system.

As example, it is considered that a harmonic loading is applied at one degree of freedom only, in this case, the degree of freedom x_p . The amplitude of the response \hat{u}_i can be obtained and the frequency response function $H_{u_i F_p}(\Omega)$ is introduced as:

$$\begin{aligned} H_{u_i F_p}(\Omega) &= \frac{u_i(t)}{F_p(t)} = \frac{\hat{u}_i}{F_p} = \frac{1}{1 - \left(\frac{\Omega}{\omega_i}\right)^2} \frac{1}{\omega_i^2} \frac{\hat{x}_{pi}}{\hat{x}_i^T \mathbf{M} \hat{x}_i} \\ &\text{where } (i = 1, 2, \dots, n) \ ; \ (p = 1, 2, \dots, n) \end{aligned} \quad (0.81)$$

Both i and p can assume values between 1 to n , therefore n^2 different frequency response functions are defined. All these frequency response functions are collected in the non-symmetrical frequency response matrix:

$$H_{u_i F_p} = \begin{bmatrix} H_{u_1 F_1} & H_{u_1 F_2} & \dots & H_{u_1 F_n} \\ H_{u_2 F_1} & H_{u_2 F_2} & \dots & H_{u_2 F_n} \\ \dots & \dots & \dots & \dots \\ H_{u_n F_1} & H_{u_n F_2} & \dots & H_{u_n F_n} \end{bmatrix} \quad (0.82)$$

In case of the synchronous loads (all loads vary according to the same harmonic time function) and concerning one specific degree of freedom $x_q(t)$, again a frequency response can be defined. This frequency response function possesses vertical asymptotes at the position of the (n) natural frequencies (Figure 141).

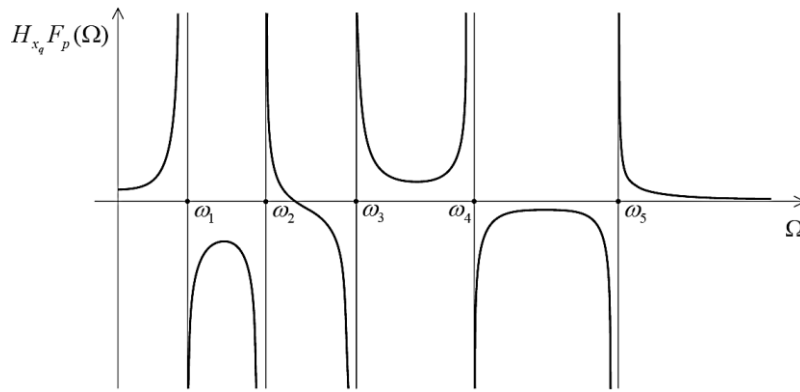


Figure 141. Frequency-response function for an undamped five degrees of freedom system for the degree of freedom $x_q(t)$ (Spijkers, Vrouwenvelder, & Klaver, 2005)

1.4.5. Viscous damped systems with n degrees of freedom

In case damping is taken into account for the system, the equations of motions have an additional term:

$$M\ddot{\underline{x}} + C\dot{\underline{x}} + K\underline{x} = \underline{F}(t) \quad (0.83)$$

Also, here the orthogonality condition is applied, introducing the modal damping matrix:

$$C^* = E^T C E \quad (0.84)$$

However, the modal damping matrix is not diagonal. The consequence is that the set of differential equations is only partly uncoupled; so-called damping coupling is present. This means that the modal analysis is not applicable for damped systems. However, there are techniques for these damped systems, where an uncoupled system is obtained and in which the modal analysis can be used in an altered (complex) form (complex modal analysis).

However, for now, the theory is restricted to a special class of damped systems, namely systems of which the modal damping matrix is forced to be a diagonal matrix.

Diagonal modal damping matrix

It is assumed that the damping matrix C is built up such that the eigenvectors with respect to this damping matrix also possess the characteristic orthogonality. In that case the modal

damping matrix \mathbf{C}^* is a diagonal matrix. The advantage of a diagonal modal damping matrix is that the set of differential equations is fully decoupled.

Also here a relative damping ratio ξ_i is defined per uncoupled degree of freedom. This term is called the modal damping ratio. The value for each of the modal damping ratios should be estimated based on insight and experience.

Most software packages, which are based on modal analysis, make the presumption of damping uncoupling. Generally, it can be said that damping uncoupling delivers reasonably accurate results for structures where the damping is reasonably uniformly distributed in the whole structure and moreover is not too large.

Proportional damping (Rayleigh damping)

An alternative for taking into account is by the method of proportional damping. In that case the modal damping matrix is a summation of two diagonal matrices and is therefore a diagonal matrix too:

$$\mathbf{C} = a_0 \mathbf{M} + a_1 \mathbf{K}, \quad \mathbf{C}^* = a_0 \mathbf{M}^* + a_1 \mathbf{K}^* \quad (0.85)$$

This procedure will not be elaborated any further.

1.4.6. Forced vibration of a damped n MDoF system

The general solution is again the summation of the homogeneous solution and a particular solution. A particular solution can be obtained by means of the integral of Duhamel for any given load function. The unknown constants are determined by the initial conditions. The solution formulated in the physical degrees of freedom, then is:

$$\begin{aligned} \underline{x}(t) = \sum_{i=1}^n \left\{ \hat{x}_i C_i e^{-\xi_i \omega_i t} \sin \left(\omega_i \left\{ \sqrt{1 - \xi_i^2} \right\} t + \varphi_i \right) \right. \\ \left. + \int_{\tau=0}^t \frac{\hat{x}_i \hat{x}_i^T \underline{F}(\tau)}{\hat{x}_i^T \mathbf{M} \hat{x}_i} \frac{1}{\omega_i \sqrt{1 - \xi_i^2}} e^{-\xi_i \omega_i t} \sin \left(\omega_i \left\{ \sqrt{1 - \xi_i^2} \right\} (t - \tau) \right) d\tau \right\} \end{aligned} \quad (0.86)$$

1.4.7. Harmonic loads for a damped n MDoF system

The harmonic function constitutes a basis for the analysis of all periodic loads. Here only the steady state solution is considered (the initial conditions, and thus the homogeneous vibration are damped out). Again, only the case is considered in which a harmonic load acts at one specific degree of freedom x_p . After obtaining the frequency-response function, it can be observed that the quotient \hat{u}_i / \hat{F}_p depends on the loading frequency Ω . As a result of the presence of damping, a phase shift occurs in the response $u_i(t)$ with respect to the load $F_p(t)$. Therefore, in the damped case the following applies:

$$H_{u_i F_p}(\Omega) = \frac{\hat{u}_i}{\hat{F}_p} \neq \frac{u_i(t)}{F_p(t)} \quad (0.87)$$

Figure 142 presents examples of both the frequency-response function $H_{u_i F_p}(\Omega)$ for particular values of i and p and the phase shift ϕ for the same particular values of i and p . Since i and p can both attain values between 1 and n , in total n^2 different frequency response functions can be obtained. Each frequency response function is of a simple type (similar to the damped SDOF case).

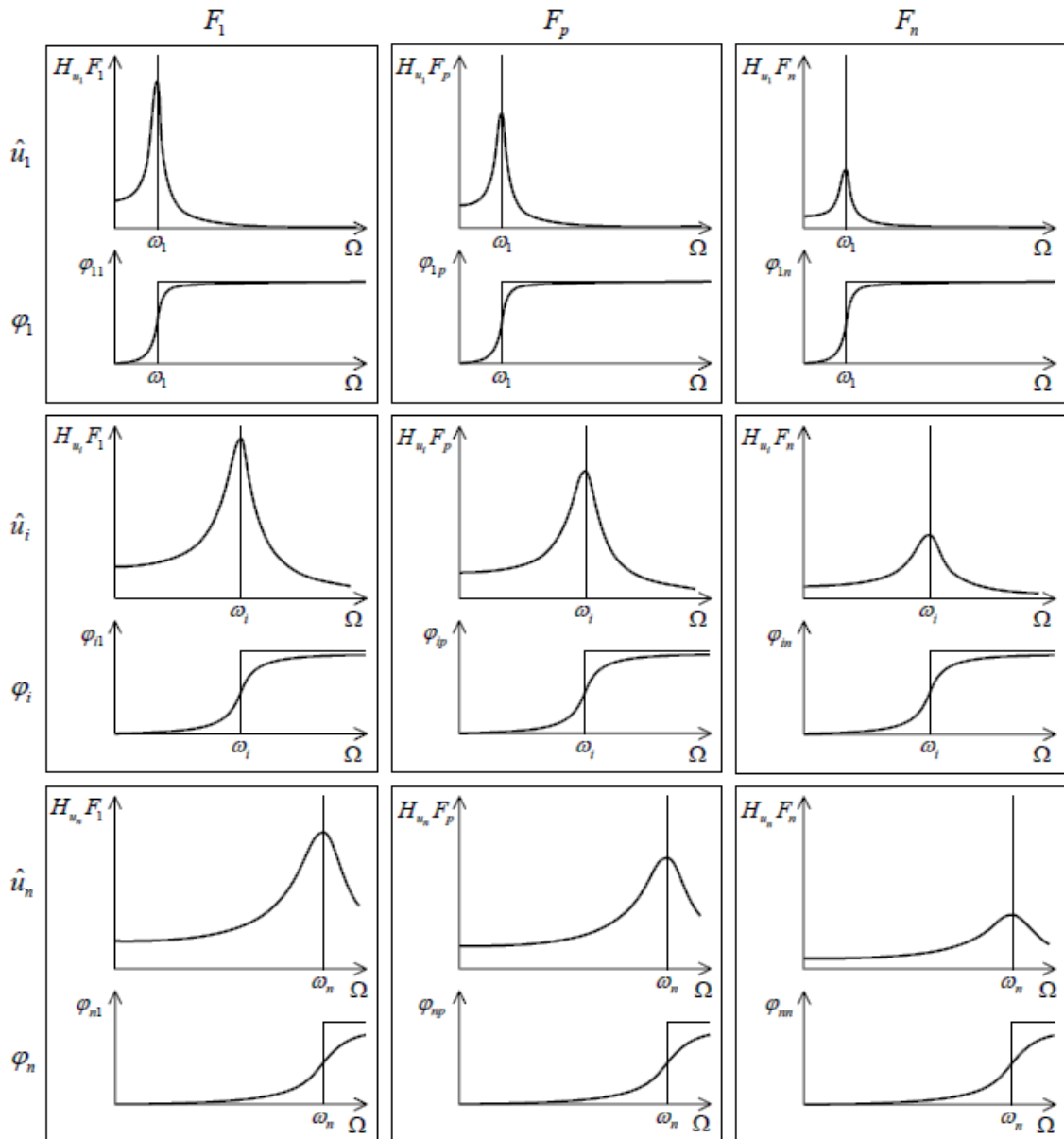


Figure 142. Frequency response function $H_{u_i F_p}(\Omega)$ for particular values of i and p (Spijkers, Vrouwenvelder, & Klaver, 2005)

The response is formulated in the physical degrees of freedom with the similar approach as described before.

In the case we are interested in one specific degree of freedom, for example the degree of freedom $x_q(t)$, the frequency response function for this degree of freedom due to a harmonic loading in the point x_p has the form as in Figure 143.

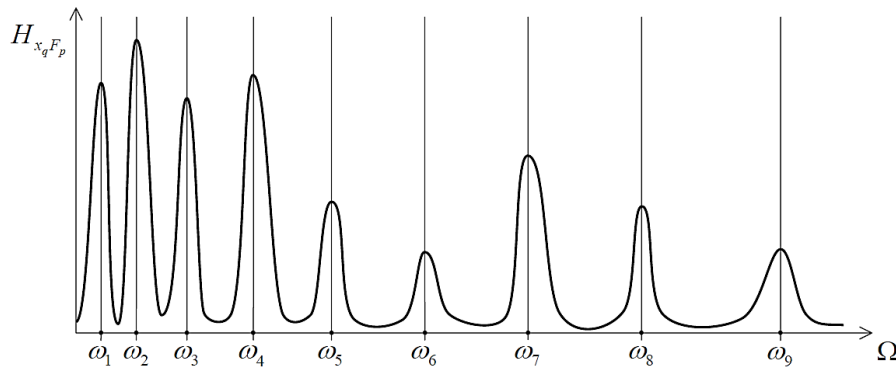


Figure 143. Example of a frequency response function for the degree of freedom $x_q(t)$ when a harmonic loading is applied in the point x_p (Spijkers, Vrouwenvelder, & Klaver, 2005)

1.5. Continuous Systems

The multi-degrees of freedom systems discussed before are classified as discrete systems. They are described by means of a coupled set of ordinary differential equations. However, when a system is analysed of which the mass is continuously distributed along a line, plane or volume, then also a continuous function should be chosen for the degree of freedom. These systems are typified as continuous systems. Their dynamic behaviour is described by means of partial differential equations (Spijkers, Vrouwenvelder, & Klaver, 2005). The soil, subject of the previous chapters, and described by an elastic half-space, is an example of a three-dimensional continuous system. In a linear structure two dimensions are small with regard to the third dimension, which is the case for example for the bending beam (or a floor slab).

1.5.1. Bending beam (Euler-Bernoulli beam model)

An example of linear structures which can be described by a continuous system is the bending beam. The bending beam is described by means of a fourth-order partial differential equation. The way a beam is supported (clamped, hinged, free, guided or movable end) is essential for its dynamic behaviour. The supports are not expressed in the differential equations describing its dynamic behaviour, but they are introduced by means of so-called boundary conditions, which are needed when solving the differential equations.

1.5.2. Governing differential equations

The displacement in the positive z -direction is indicated by the symbol $w(x, t)$ and it represents the degree of freedom, which is a continuous function of the position variable x , and naturally is a function of the time variable t too. The beam has a flexural stiffness EI (Nm^2), a cross-sectional area A (m^2) and a mass density ρ (kg/m^3). The displacement method will be used for the derivation of the equation of motion of an infinitesimal element dx of the beam (Figure 144).

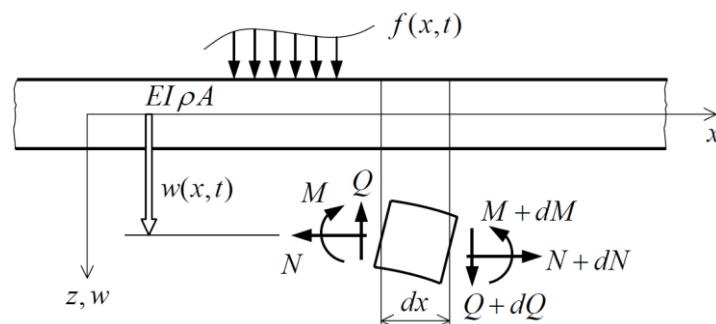


Figure 144. Sign convention and indication of the meaning of the symbols used for the prismatic beam (Spijkers, Vrouwenvelder, & Klaver, 2005)

The complete derivation of the problem is not included here. The reader is kindly referred to the lecture notes on Structural Vibrations CT 4140 part I of the Technical University Delft (Spijkers, Vrouwenvelder, & Klaver, 2005). A very brief overview is given here of the governing equations.

After substituting of the kinematic relations and the constitutive relation into Newton's second law, the following inhomogeneous partial differential equation of the fourth order is obtained:

$$EI \frac{\delta^4 w(x, t)}{\delta x^4} + \rho A \frac{\delta^2 w(x, t)}{\delta t^2} = f(x, t) \quad (0.88)$$

This is commonly referred to the Euler-Bernoulli beam.

1.5.3. Free vibration

In case the free vibrations are considered, again a solution $w(x)$ is sought for the eigenvalue problem. This solution is referred to as the eigenfunction. Eventually the solution is of the form:

$$\begin{aligned} w(x) &= C_1 e^{\beta x} + C_2 e^{-\beta x} + C_3 e^{i\beta x} + C_4 e^{-i\beta x} \\ &\text{or} \\ w(x) &= A \cosh(\beta x) + B \sinh(\beta x) + C \cos(\beta x) + D \sin(\beta x) \end{aligned} \quad (0.89)$$

in which:

$$\beta^4 = \frac{\rho A \omega^2}{EI} \quad (0.90)$$

This parameter β appears to be convenient for the further elaboration of the problem. The unknown constants are depending on the manner the beam is supported: the applied boundary conditions.

1.5.4. Boundary conditions

For the five unknown constants, only four boundary conditions exist: two at each end of the beam, thus one equation is missing. It appears, again, apart from a unknown constant the modal shapes of the structural system can be derived.

Boundary conditions concerning the deflection or slope are called kinematic boundary conditions. The boundary conditions concerning the bending moment and shear force are called dynamic boundary conditions. Two different types of, in practice often applied, boundary conditions will be briefly considered to illustrate the obtained results by applying the method for continuous systems: the simply support beam and the cantilevering beam.

Simply supported beam

Substituting the boundary conditions:

$$x = 0 \rightarrow \begin{cases} w(0) = 0 \\ M(0) = -EI \frac{d^2 w(0)}{dx^2} = 0 \end{cases}, \quad x = l \rightarrow \begin{cases} w(l) = 0 \\ M(l) = -EI \frac{d^2 w(l)}{dx^2} = 0 \end{cases} \quad (0.91)$$

into the expression for the eigenfunction $w(x)$ gives a set of algebraic equations. Further elaboration and substitution of β gives the following expression for the natural frequencies of the system:

$$\omega_n = n^2 \left(\frac{\pi}{l} \right)^2 \sqrt{\frac{EI}{\rho A}}, \quad (n = 1, 2, \dots \infty) \quad (0.92)$$

The bending beam appears to have an infinite number of natural frequencies (increasing quadratically with n). Since this result is neglecting the shear deformation and the rotation inertia, the formula derived for the natural frequencies gives only reliable results for low values of n .

For each natural frequency there appears to be a corresponding eigenfunction $w_n(x)$:

$$w_n(x) = D_n \sin\left(2\pi \frac{x}{\lambda_n}\right), \quad (n = 1, 2, \dots \infty) \quad (0.93)$$

in which $\lambda_n = 2l/n$ is the wavelength of the n^{th} eigenfunction. The three lowest eigenfunctions are displayed in Figure 145, each with an arbitrary (still undetermined) amplitude D_n .

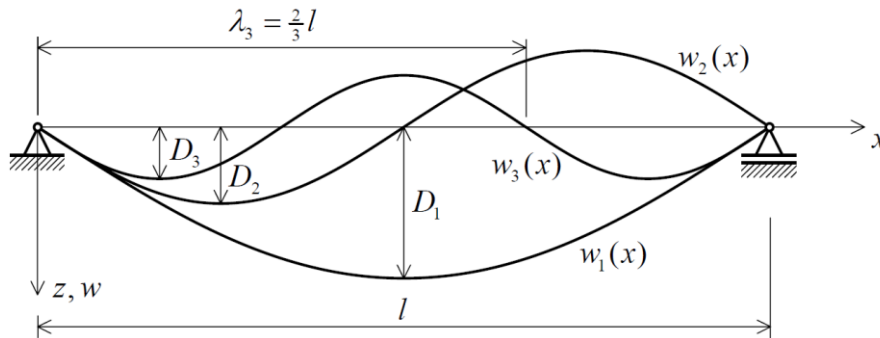


Figure 145. First three eigenmodes of the simply supported Euler-Bernoulli bending beam (Spijkers, Vrouwenvelder, & Klaver, 2005)

The remaining unknown constants are determined from the initial conditions at $t = 0$. This procedure is completely analogous with the way this occurs in discrete systems (the systems with a finite number of degrees of freedom described before). The eigenfunctions do have orthogonal properties with regard to the mass and the stiffness.

If the order of magnitude of the wavelength is equal to 10 times the height H of the beam, then the shear deformation starts to play a noticeable roll. Eigenfunctions with wavelengths smaller than 10 times the height of the beam must be approached with the utmost suspicion. For a reliable calculation of higher natural frequencies, the mechanical model must be elaborated with the shear deformation and rotation inertia. This approach delivers the much more complex Timoshenko beam model.

Cantilever beam

For the cantilever beam the boundary conditions are different from the simply supported beam:

$$x = 0 \rightarrow \begin{cases} w(0) = 0 \\ \frac{dw(0)}{dx} = 0 \end{cases}, \quad x = l \rightarrow \begin{cases} M(l) = -EI \frac{d^2 w(l)}{dx^2} = 0 \\ Q(l) = -EI \frac{d^3 w(l)}{dx^3} = 0 \end{cases} \quad (0.94)$$

Finding the natural frequencies of the cantilever beam gives more complicated expressions and eigenfunctions, but the procedure is similar as to the case of a simply supported beam. The

three lowest eigenfunctions are displayed in Figure 146, again, each with an arbitrary (still undetermined) amplitude D_n .

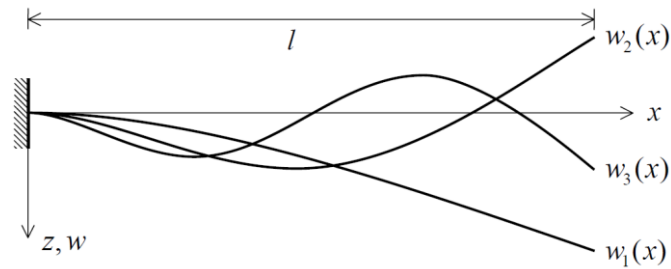


Figure 146. First three eigenmodes of the cantilever Euler-Bernoulli bending beam (Spijkers, Vrouwenvelder, & Klaver, 2005)

Natural frequencies beams - equivalent masses

The method of equivalent masses enables to find only the fundamental natural frequency in a simplified and approximate manner. Table 6 has been realized with which the first five natural frequencies of the Euler-Bernoulli beam can be approximated for specific boundary conditions. The natural frequencies can be determined, based on the value C , that is given in the table, by the formula:

$$\omega_n = C \sqrt{EI / (\rho A l^4)} \tag{0.95}$$

Table 6. First five natural frequencies and eigenmodes of Euler-Bernoulli beams with constant $EI/\rho A$ (Spijkers, Vrouwenvelder, & Klaver, 2005)

		$n = 1$	$n = 2$	$n = 3$	$n = 4$	$n = 5$
clamped	free	$C = 3.52$	$C = 22.4$	$C = 61.7$	$C = 121.0$	$C = 200.0$
simply supported	simply supported	$C = 9.87$	$C = 39.5$	$C = 88.9$	$C = 158.0$	$C = 247.0$
clamped	clamped	$C = 22.4$	$C = 61.7$	$C = 121.0$	$C = 200.0$	$C = 296.0$
free	free	$C = 22.4$	$C = 61.7$	$C = 121.0$	$C = 200.0$	$C = 298.0$
clamped	simply supported	$C = 15.4$	$C = 50.0$	$C = 104.0$	$C = 178.0$	$C = 272.0$
simply supported	free	$C = 15.4$	$C = 50.0$	$C = 104.0$	$C = 178.0$	$C = 272.0$

E. Appendix: Additions to Chapter 6 ‘Soil-Structure Interaction’

1.1. Effect of Soil-Structure Interaction on the Response of Structures

Effect on energy dissipation

Physically, the following happens according to K. Miura (Miura, 2016) when the ground and the building interact with each other (Figure 147): when the incident waves reach the bottom of the foundation, they are divided into two types: the waves entering into the building ($E_1 = \text{transmission waves}$) and the waves being reflected into the ground ($F_0 = \text{reflection waves}$).

The transmission waves E_1 , entering into the building, travel towards the top of the building which subject the building to vibration. Then, they are reflected at the top and travel back down to the foundation (F_1). Here, a crucial phenomenon occurs for consideration of the SSI. When the waves, that are reflected at the top of the building and are travelling downwards, reach the foundation, a part of them is transmitted into the ground ($R_1 = \text{radiation waves}$), while the rest is reflected back again into the building and starts to move upwards through the building. When the amount of radiation waves (R_1) is small, the waves once transmitted into the building, continue to remain in the building, and the building continues to vibrate for a long time. The apparent vibration condition becomes the same as that of the small damping of the building. The damping caused by escape of the (transmission) waves, from the building back into the ground, is called ‘radiation damping’.

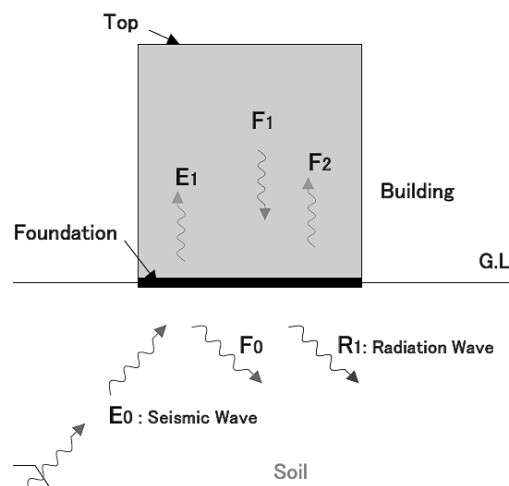


Figure 147. Physical representation of soil-structure interaction (Miura, 2016)

However, in case of a layered soil medium, the waves transmitted from the building are reflected at the layer interfaces and are returned to the building. Therefore, the radiation damping becomes normally smaller and the entire phenomenon becomes more complicated.

Non-linear soil response

Non-linear response of the soil can be caused by excessive structural deformation at the foundation level, or high-amplitude waves travelling through the soil caused by wave reflection at the interface with the structure (Tsouvalas, 2018). However, since this thesis focusses on rather stiff structures, excited by wavefields with relatively small amplitude, non-linear effects are disregarded from now on.

In conclusion, it is difficult to a priori decide whether neglecting SSI effects is generally conservative or not. However, it is clear that only through proper understanding of SSI effects,

one can adequately consider (or conservatively neglect) SSI effects in engineering design (Tsouvalas, 2018).

1.2. Modelling of the Soil-foundation System

At the initial stages of the design of a structure, simplified approaches are desired for taking into account SSI. When foundations are relatively rigid and/or of simple geometry, several methods exist to overcome the need for a full detailed description of the foundation-soil system (Figure 148). In principal, there are two main ways to solve dynamic SSI problems:

- Direct approach (suitable for both linear and non-linear formulations)
- Sub-structuring approach (limited to linear formulations)

Direct approach

In the direct approach, both soil and structure are modelled in a single step using a Finite Element model of the coupled system. This approach requires fewer assumptions compared to other approaches, yet the following issues limit its wide applicability by engineers:

- A large soil medium needs to be modelled and the boundaries of the truncated domain need to be properly defined (unwanted reflections of propagating waves may not occur).
- The mesh size should be adequately small (depending on the wavelength of the desired frequency range of the incident wavefield).
- The stability of the numerical integration scheme should be checked.
- The time step of the integration scheme should be small enough.

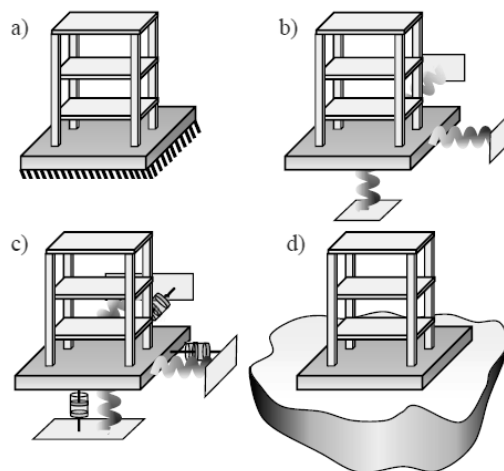


Figure 148. Levels of modelling the effect of the soil on the structure: (a) fixed support, (b) elastic support, (c) substructure approach, (d) direct approach (Pap & Kollár, 2018)

Due to the large computational effort of the direct approach and the computational efficiency of the sub-structuring approach in case of linear systems, the sub-structuring approach is the most practical approach for the initial design stages.

Sub-structuring approach

The idea of the sub-structuring method is very simple: since most of the difficulties in the FE formulation originate from the modelling of the soil domain. However, the engineer is mainly interested in the response of the structure and the response of the soil is of secondary importance. Then, an equivalent representation of the soil reaction with proper consideration of the incident wavefield usually suffices.

In this method the fully coupled system is treated as two separate systems joined at the common soil-structure interface by imposing force equilibrium conditions and kinematic compatibility at all times. The procedure for solving the problem is basically:

- Derivation of the impedance matrix (dynamic stiffness matrix) of the foundation-soil system.
- Formulation of the equations of motion (EOMs) of the structure in partitioned form, by separating the structural degrees of freedom from the foundation degrees of freedom.
- Formulation of the equilibrium conditions at the soil-structure interface (force equilibrium and displacement compatibility). This is usually formulated in the frequency domain for linear systems, because the soil impedance functions are obtained in the frequency domain as well.
- Solution of the coupled problem to determine the structural response and the motion of the soil at the interface (which is different from the free-field ground motion).

F. Appendix: Additions to Chapter 7 ‘Numerical Method for Computations’

1.1. FEMIX

1.1.1. Thin Layer Method

The Thin Layer Method (TLM) is a semi-discrete numerical technique used for the analysis of wave motion in layered media (Barbosa J. , 2013). The TLM discretizes the soil in perfect horizontal layers which are continuous in the horizontal direction but are discretized in several layers in the vertical direction (similar to a FEM-mesh, but only in the vertical direction). The horizontal directions are therefore described by analytical solutions, along which the material properties are assumed to be constant. Simply said the TLM is a Finite Element Method (FEM) (Figure 149) but with a mesh for which the horizontal dimensions of the mesh-elements are infinitesimal small ($\lim_{h \rightarrow 0}(h)$).

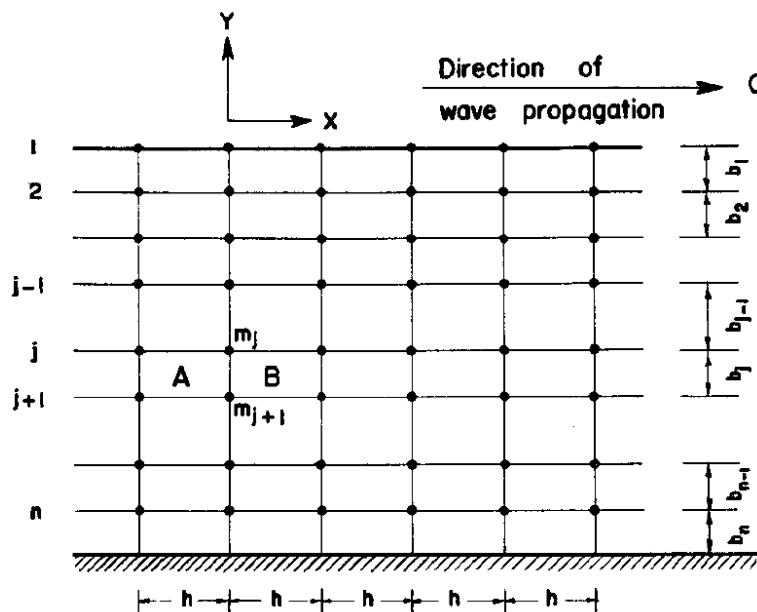


Figure 149. Finite Element mesh. As representation of the TLM the element width ‘h’ is infinitesimal small (Lysmer, 1970)

For obtaining the TLM, the wave equations are first expressed in matrix notation and are then discretized in the vertical direction. Therefore, the medium is subdivided into horizontal layers which are thin in the finite element sense, i.e., which are small in comparison with the expected wavelengths and strain gradients (Barbosa J. , 2013). In general, a Thin Layer Thickness of 0.1 m is a well-chosen division parameter.

The stresses (or tractions t) at the layer boundaries / interfaces need to be in equilibrium and the displacements (u) at the interfaces need to be compatible. Interpolation functions $N(z)$ in the vertical direction are used for accommodating these requirements. If the order of the interpolation function is equal to 2, the interpolation function is linear and thus gives a linear relation between the displacements at the top interface and the bottom interface of the Thin Layer. In case the interpolation order is higher than 2, inner surfaces are created inside one Thin Layer. Figure 150 presents an interpolation order $m = 3$, which corresponds to a quadratic interpolation with one internal nodal surface. FEMIX uses interpolation functions with order $m = 3$.

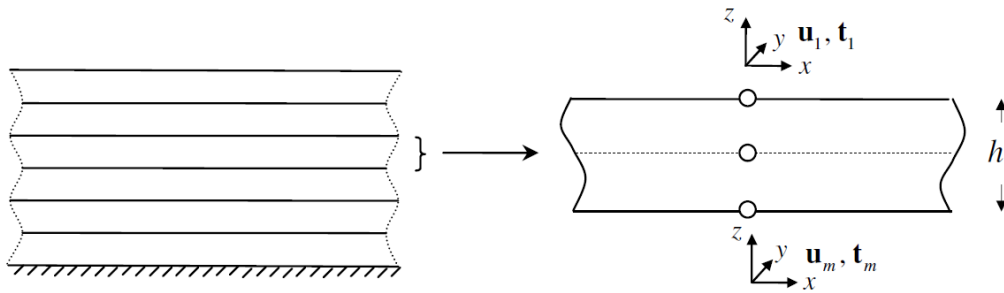


Figure 150. Discretization into thin-layers (left) and a thin-layer as a free body in space with the order of the interpolation function equal to 3 (Barbosa J. , 2013)

Similar to the Finite Element Method the thin-layer matrices (mass, stiffness,..) are overlapped layer by layer in the natural top down order of the interfaces, which results in a narrowly banded set of global system matrices and vectors that characterizes the complete stack of thin-layers. A system of linear partial differential equations is the result (Barbosa J. , 2013). The obtained results are exact for all three Cartesian coordinate directions (x, y, z).

1.1.2. Materials

Real soil behaves different when loaded in the horizontal directions than when loaded in the vertical direction. This is the case because the layers are formed by vertical sedimentation of particles and therefore, they present different mechanical characteristics in the vertical and horizontal directions (Barbosa J. , 2013). These types of materials are called cross-anisotropic materials and they can be included in the determination of the TLM. However, a drawback of considering cross-anisotropic materials is that they require the quantification of more elastic constant, thus requiring more experiments in order to obtain the corresponding parameters. Also, several studies (see for example the work of prof. Degrande et. al. of KU Leuven, discussed in section 8.1 'Projects KU Leuven') have shown that when considering isotropic materials only (the material behaves similar when loaded in all different directions) the predictions of the wave propagation and the soil response are well comparable to in-situ experiments and measurements. This indicates that considering isotropic materials for wave propagation in soils is a justified simplification and will therefore also be used for the research performed for this Master Thesis. The result is that only a limited number of parameters is needed to describe the soil material which makes the computation of the input parameters more practical.

1.1.3. Possibilities

2D structure embedded in the soil or 3D structure on the soil

It is also possible to implement a structure in or on the soil, next to or at some distance from, the track/road. This structure is implemented as a FEM-model and is coupled to the soil by means of a BEM-FEM coupling that takes into account the soil-structure interaction. The current version of FEMIX is built as such that the BEM-FEM coupling can only be taken into account in case the structure is either:

- A 2D structure embedded into the soil, which is invariant in the longitudinal (y -)direction (BEM-FEM coupling between the vertical walls of the structure and the layered soil) (Figure 151).
- A 3D structure resting on the soil (not embedded), which can be invariant in the longitudinal (y -)direction (BEM-FEM coupling between the horizontal foundation footings and the soil surface) (Figure 152).

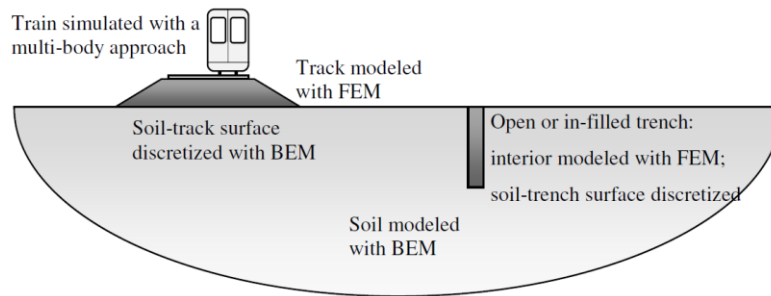


Figure 151. Example of a 2D structure (trench) in the soil (embedded) which is invariant in the longitudinal (3rd) direction (Barbosa J. , 2013)

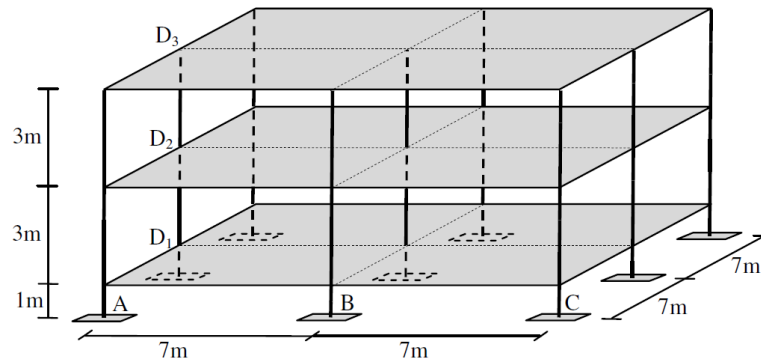


Figure 152. Example of a 3D structure on the soil (not embedded) for which the BEM-FEM coupling can be considered by FEMIX (Barbosa J. , 2013)

The dynamic structural behaviour is not computed within FEMIX but must be considered separately in a numerical computational script, such as Matlab or Python. The numerical computational script will use the output of FEMIX as input for the calculation (e.g. as excitation on the structure).

It must be noted that the BEM-FEM coupling between the track/road with the soil does not consider any coupling with a structure that might be present in the soil at some distance from the loading that could influence the deformation of the track/road and the soil underneath it, i.e. there is weak coupling between the track/road and the structure (Figure 153). This could be a relevant drawback in case the structure (e.g. a wave barrier, a building, ...) is close to the track/road and the waves propagating from the track/road towards the structure are reflected back to the track/road which influence the generation of the moving loads.

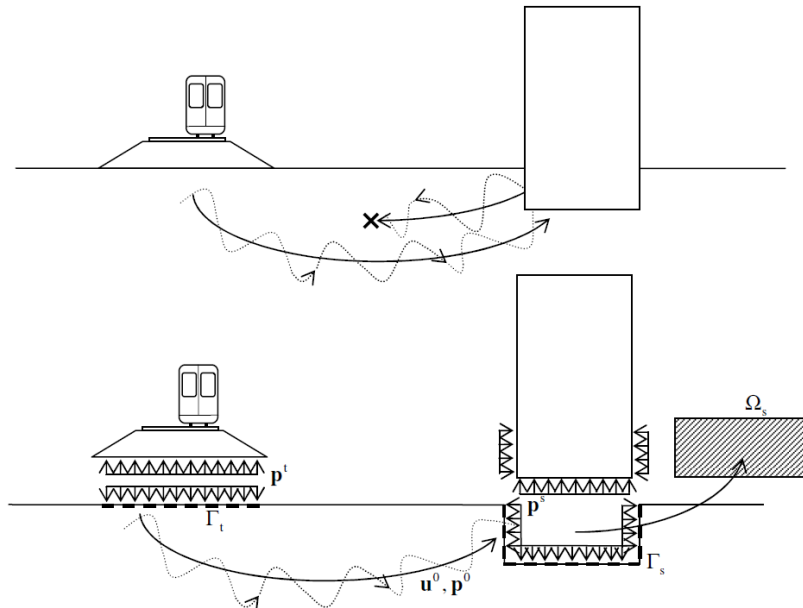


Figure 153. Weak coupling between track and structure (Barbosa J. , 2013)

1.1.4. Input files and computation

In order for FEMIX to start the computation of the soil response, the software needs input files in the form of .dat-files (data files). Separate data files are needed for:

- The vehicle model (MDoF system)
- The road irregularity
- The soil layering in the (y, z) -plane
- The geometry in the (x, z) -plane (point coordinates, calculation frequencies, and the BEM- & FEM geometries, such as a layered track/road, a wave barrier, and again the same soil layering)

An example of such a data-file is given in Figure 154.

```

26 <POINT_COORDINATES>
27 ## Point coordinates (global coordinate system)
28 COUNT = 71 ; # N. of points
29
30 ## Content of each column:
31 # A -> Counter
32 # B -> Coordinate - XG1
33 # C -> Coordinate - XG2
34 # D -> Coordinate - XG3
35 #
36 # A      B      C      D
37 1      -1.60000000  0.00000000  0.00000000 ;
38 2      -1.40000000  0.00000000  0.00000000 ;
39 3      -1.20000000  0.00000000  0.00000000 ;
40 4      -1.00000000  0.00000000  0.00000000 ;
41 5      -0.80000000  0.00000000  0.00000000 ;
42 6      -0.60000000  0.00000000  0.00000000 ;
43 7      -0.40000000  0.00000000  0.00000000 ;
44 8      -0.20000000  0.00000000  0.00000000 ;
45 ...
105 70      16.00000000  0.00000000  0.00000000 ;
106 71      24.00000000  0.00000000  0.00000000 ;
107 </POINT_COORDINATES>
108
144 <ELEMENT_NODES>
145 ## Nodes defining the elements
146 COUNT = 48 ; # N. of elements
147
148 ## Content of each column:
149 # A -> Counter
150 # B -> N. of nodes of the element
151 # C -> Nodes of the element
152 #
153 # A      B      C
154 1      4      1      2      19      18 ;
155 2      4      2      3      20      19 ;
156 3      4      3      4      21      20 ;
157 4      4      4      5      22      21 ;
158 5      4      5      6      23      22 ;
159 6      4      6      7      24      23 ;
160 7      4      7      8      25      24 ;
161 ...
199 47      4      49      50      67      66 ;
200 48      4      50      51      68      67 ;
201 </ELEMENT_NODES>
202

```

Figure 154. Example of data-file for the geometry in the (x, z) -plane, needed as input for the FEMIX software

The data-files used by FEMIX are rather cumbersome to fill-in manually after a parameter has been changed, therefore a Python script is created that computes the data-files automatically after a change in the input parameters. Python is a numerically programming language and is further explained in section 7.2 'Python'.

1.1.5. Execution of PREFEMIX, FEMIX and POSFEMIX

After all needed data-files are created the software FEMIX can be used. The software can be executed by calling it in the command prompt of the working computer. First the command 'prefemix' should be used. This part of the software takes only a couple of seconds for the computational time and it checks whether the necessary data-files are present for computing the 'femix' command and whether these data-files contain the right information (Figure 155). The 'femix' command performs the actual computation of the soil response. Depending on multiple input parameters (e.g. the road irregularity profile, the desired calculation frequencies, the number of points in the soil for which the soil response is wanted) the computational time can vary from a couple of minutes to a couple of days. FEMIX will indicate when the computation is complete. After the computation of 'femix,' the user should call 'posfemix' to generate the desired output for the soil response. Multiple options are available for the output of the soil response, but the most interesting options for this Master Thesis are `mlopt → fvcsv` and `mlopt → tvcsv`, which computes the soil response (particle velocity 'v') in the frequency domain ('f') and in the time domain ('t'). These options will generate the soil response for one specific point in the soil.

```

0Roadlayers=3Ptload=0.5\SoilProfile> prefemix
----- P R E F E M I X -----
                Finite Element Analysis
                Linear and nonlinear behavior

Version: 4.0 (Beta) (Build #1001)      Professional use not allowed
Date:    2019-02-18                    Language: C

More info: hppt://www.alvaroazevedo.com/femix
----- P R E F E M I X -----

Job name ? soilprofile
You answered: soilprofile
Reading file: soilprofile_g1.dat
Writing file: soilprofile_g1.bin
End of prefemix
### Success ###
    
```

Figure 155. Example of computing the command 'prefemix' of FEMIX for the data-file 'soilprofile' in the command prompt which describes the soil layering of the problem to be considered

G. Appendix: Extensive overview of Chapter 8 ‘Verification Projects’

The numerical software described in the previous chapter will be used to write a computational script for obtaining results for the soil response (soil vibrations in the free field) and for obtaining results for the structural response (vibrations in the structural elements). The results should be reliable in order to be used as indication of an educated guess about the vibration levels in the soil but mainly for the structure. Therefore, the results should be verified with experimental computed vibration levels for both the free field soil and the structural elements. Verification projects are needed for this verification work. Since the EDDABuS_{GS}-tool is aimed to be used for projects in The Netherlands at first, or more particularly, for projects of Pieters Bouwtechniek, it is desired to verify the tool (FEMIX and EDDABuS_{GS}) with experimental measurements performed for locations in The Netherlands. Pieters Bouwtechniek has already worked on projects with vibration sensitive structures in The Netherlands. These projects will be considered first (see 1.1 ‘Projects Pieters Bouwtechniek’).

The given measurement results for the projects of Pieters Bouwtechniek appear to be considered in a practical sense and not all information is provided that is needed for modelling the dynamic problem. Therefore, a more scientific approach is considered: after performing additional literature study, the scientific and experimental work of prof. Degrande et. al. of the KU Leuven seemed to be promising. Their work will be summarized in 8.1 ‘Projects KU Leuven’ together with figures to which the results of FEMIX and EDDABuS_{GS} can be compared, and eventually to which the results of the EDDABuS_{GS}-tool can be verified.

1.1. Projects Pieters Bouwtechniek

Since the EDDABuS_{GS}-tool is meant to be used in engineering practice and particularly for the use by Pieters Bouwtechniek, first a verification project is sought for in the projects done by Pieters Bouwtechniek. The following projects have been considered, however it appeared that the projects are not suitable to use as verification project for the tool (FEMIX and EDDABuS_{GS}). The reasons for this are also indicated for every project.

TNW Zuid	
Source	Bigbag used for measuring vibration levels just outside the building and inside the building. Weight of Bigbag and falling-height are unknown. Approximation for sand filling = 1500 kg and falling height is in-between 1.5 and 2.0 m. → Approximated loading can be modelled but cannot be verified.
Transmission	Soil layering (in terms of c_s) unknown but might possibly be approximated based on CPTs. Only one receiver point just outside the building. Reflection of vibrations due to the presence of the building have to be taken into account. → Soil layering can be modelled but cannot be verified.
Structure	Structural characteristics known. → Structural response can be verified when loading and soil layering are correct.
VU Amsterdam neighbourhood (Medical Faculty)	
Source	Small logistics vehicle on site: specifications are lacking completely. Dump truck driving by over the adjacent road: approximate infill mass is known. Vehicle characteristics (stiffness and damping of suspension and tyres and mass of axles unknown). → The loading cannot be modelled, no verification of generated loads possible.
Transmission	Soil layering unknown (might be possible to check with the aid of

	DinoLoket.nl). Not enough receiver points. Receiver point close to the building, reflection of vibrations due to presence building has to be taken into account. → No verification for free field soil vibrations possible.
Structure	One receiver point on foundation of structure. Structural specifications in a very broad sense known. → Limited verification of structural vibrations possible.
VU Amsterdam site	
Source	Dump truck driving by over the adjacent road: approximate infill mass is known. Vehicle characteristics (stiffness and damping of suspension and tyres and mass of axles unknown). → the loading cannot be modelled, no verification of generated loads possible.
Transmission	Soil layering (in terms of c_s) known approximately (given by DGMR). Many receiver points on site and no obstructing buildings. → The measurements can be used to verify the tool for the VU Amsterdam site (at least to see a similar shape of the frequency spectrum of the soil response).
Structure	No structure is present, so also no measurements. → No verification of structural vibrations possible.
Science Campus Leiden	
Source	No specification of the loading given / known. → Loading cannot be verified.
Transmission	No measurements performed outside the building. → Soil layering cannot be verified.
Structure	Measurements performed over a month at the 2 nd floor of the building. Structural characteristics are available. → Loading cannot be modelled. No verification of structural vibrations possible.
SRON Leiden	
Source	Measurements are performed for one location. Loading by traffic in the proximity of the location. → Loading cannot be verified.
Transmission	Location of measurement point unknown. Distance between loading and measurement point unknown. → Transmission cannot be verified.
Structure	No structure is present, so also no measurements. → No verification of structural vibrations possible.

1.2. Projects KU Leuven

Since the projects of Pieters Bouwtechniek are lacking specifications of one or more stages (source, transmission, interaction, receiver), they cannot be used for verification of the tool (FEMIX and EDDABuSGS): another verification project is needed. The KU Leuven has performed experimental measurements to validate their own numerical prediction model. Several projects were used to validate their numerical model.

The paper ‘The experimental validation of a numerical model for the prediction of the vibrations in the free field produced by road traffic’ (Degrande & Lombaert, 2002) describes the project concerning the validation of the predicted free field soil response due to the passage of a truck driving over an artificial road unevenness. This project will be referred to as ‘verification project Degrande et. al. (1) – Free Field’ from hereon.

The paper ‘Validation of a Source-Receiver Model for Road Traffic-Induced Vibrations in Buildings. I: Source Model’ (Degrande, Pyl, Lombaert, & Haegeman, 2004) describes the project concerning the validation of the predicted soil response in front of a building due to the passage of a truck driving over an artificial road unevenness. This project will be referred to as ‘verification project Degrande et. al. (2) – Soil Building’ from hereon.

The paper ‘Validation of a Source-Receiver Model for Road Traffic-Induced Vibrations in Buildings. II: Receiver Model’ (Degrande, Pyl, & Clouteau, 2004) describes the project concerning the validation of the predicted structural response of a building due to the passage of a truck driving over an artificial road unevenness. This project will be referred to as ‘verification project Degrande et. al. (3) – Building Response’ from hereon.

A brief summary will be given in the following subsections. The tool (FEMIX and EDDABuS_{GS}) will be verified by comparing the results from the tool to the results of the verification projects Degrande et. al. (1) to (3).

1.2.1. Verification Project Degrande et. al. (1) – Free Field

The verification project ‘The experimental validation of a numerical model for the prediction of the vibrations in the free field produced by road traffic’ (Degrande & Lombaert, 2002) will be used to verify the computed results by FEMIX for the free field soil response.

Source

In the verification project on-site measurements were computed for the passage of a Volvo FL6 truck at the ‘de Hemptinne site’ of the Belgian Army in Heverlee (Belgium). The truck drove with speeds between 23 and 58 km/h. The truck was modelled as a linear 2D four-degree-of-freedom system (Figure 10) and the artificial road unevenness consisted of plywood planks with a total height of 0.054 m in both wheel paths of the truck (Figure 156 and Figure 157).



Figure 156. The Volvo FL6 truck in front of the artificial road unevenness installed at the test site (Degrande & Lombaert, 2002)

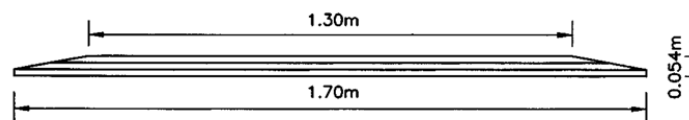


Figure 157. Artificial road unevenness with sizes indicated (Degrande, Pyl, Lombaert, & Haegeman, 2004)

The vehicle characteristics are given in Table 7. The deformation of the road due to the elasticity of the road material and the supporting soil is assumed to have no effect on the generated loads, i.e. the for the generation stage of the loads, the road is assumed to be

infinitely stiff. This simplification can be justified since the stiffness of the road is much greater than the stiffness of the tyres of the vehicle. The road is 6.2 m wide and is layered according to the specification in Table 8. The road is partly embedded in the soil and is connected to the bottom of the top soil layer (Figure 158).

Table 7. Specified vehicle characteristics for modelling the Volvo FL6 truck of the verification project (1) (Degrande & Lombaert, 2002)

$M_b = 9000 \text{ kg}$	$M_{ar} = 600 \text{ kg}$	$L_1 = -1.49 \text{ m}$	$K_{pr} = 610000 \text{ N/m}$	$C_{pr} = 16000 \text{ Ns/m}$
$I_b = 35000 \text{ kgm}^2$	$M_{af} = 400 \text{ kg}$	$L_2 = 3.72 \text{ m}$	$K_{pf} = 320000 \text{ N/m}$	$C_{pf} = 10050 \text{ Ns/m}$
			$K_{tr} = 3000000 \text{ N/m}$	$C_{tr} = 0 \text{ Ns/m}$
			$K_{tf} = 1500000 \text{ N/m}$	$C_{tf} = 0 \text{ Ns/m}$

Table 8. Specified road parameters of the verification project (1) (Degrande & Lombaert, 2002)

Layer type	$d \text{ (m)}$	$\nu \text{ (-)}$	$\rho \text{ (kg/m}^3\text{)}$	$E \times 10^6 \text{ (N/m}^2\text{)}$
1 Asphalt	0.15	0.33	2100	9150
2 Crushed stone	0.19	0.50	2000	500
3 Crushed concrete	0.25	0.50	1800	200

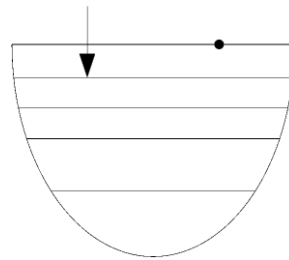


Figure 158. Road-soil interface at the bottom of the top soil layer (Lombaert & Degrande, 2001)

Transmission

The layering of the soil has been determined by the method ‘spectral analysis of surface waves’ (SASW) and seismic cone penetration tests (SCPT) on site and the specification is given in Table 9. The vibration levels are measured at several points in the free field next to the road (Figure 159). Three points are measured in all three (x-, y-, and z-) directions. For the other points the vibrations levels are only measured in vertical (z-) direction.

Table 9. Specified soil parameters of the verification project (1) (Degrande & Lombaert, 2002)

Layer	$d \text{ (m)}$	$\nu \text{ (-)}$	$\rho \text{ (kg/m}^3\text{)}$	$E \times 10^6 \text{ (N/m}^2\text{)}$	$C_s \text{ (m/s)}$	$C_p \text{ (m/s)}$	$\beta \text{ (-)}$
1	0.46	0.33	1900	57	106	212	0.0500
2	0.67	0.33	1900	133	162	324	0.0375
3	1.35	0.33	1900	223	210	420	0.0250
4	5.72	0.47	2000	322	234	984	0.0250
5	∞	0.47	2000	1288	468	1968	0.0250

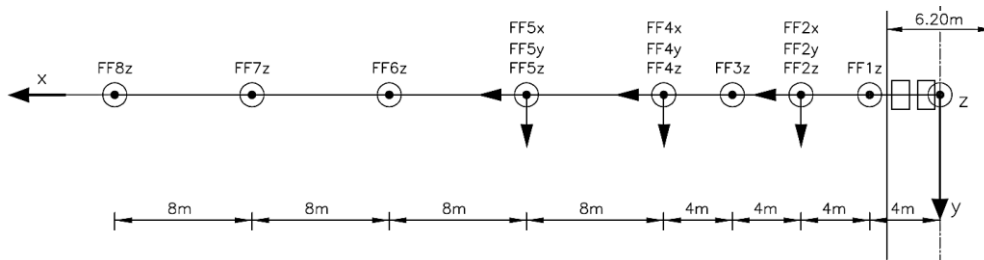


Figure 159. Position of the measurement points of the verification project (1) (Degrande & Lombaert, 2002)

Results

The generated loads due to the passage of the truck over the artificial unevenness are given in both the frequency- and time domain (Figure 160). The predicted accelerations of the front- and rear axle appear to be well comparably with the measured accelerations of the axles.

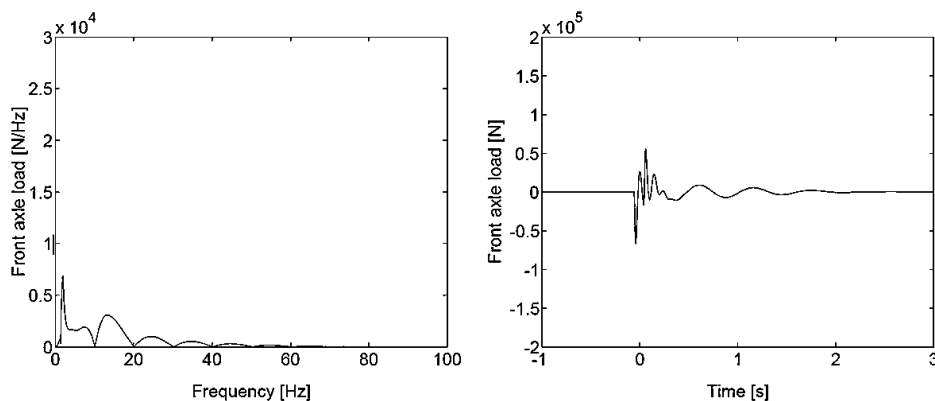


Figure 160. Frequency content (left) and time history (right) of the predicted front axle load of the Volvo FL6 truck when passing the artificial profile at a vehicle speed $v = 58$ km/h (Degrande & Lombaert, 2002)

The vibration levels (speed of the soil particle motion) have been determined for several receiver points. The most interesting points to verify with are points FF2, FF4 and FF5 since these are the points that are measured in all three directions. In this way the results of FEMIX can be compared for all three (x -, y - and z -) directions. The soil response results are given in Figure 161 and Figure 162.

Conclusions of the paper

A comparison between the predicted and measured response shows that the axle accelerations are well reproduced by the vehicle model. The most important difference is due to the loss of contact between the rear axle and the road. The influence of the loss of contact increases with increasing vehicle speed. The loss of contact cannot be modelled in the numerical model, because that would ask for a non-linear vehicle model.

The results of the validation are very satisfactory. The velocity components in the x - and z -direction are well predicted with a ratio of 0.5 to 1.5 between the predicted and the measured PPV. The experimental validation shows that the prediction model described the essential physical phenomena with very reasonable accuracy and is therefore well suited to perform a parametric study and to predict free field traffic-induced vibrations.

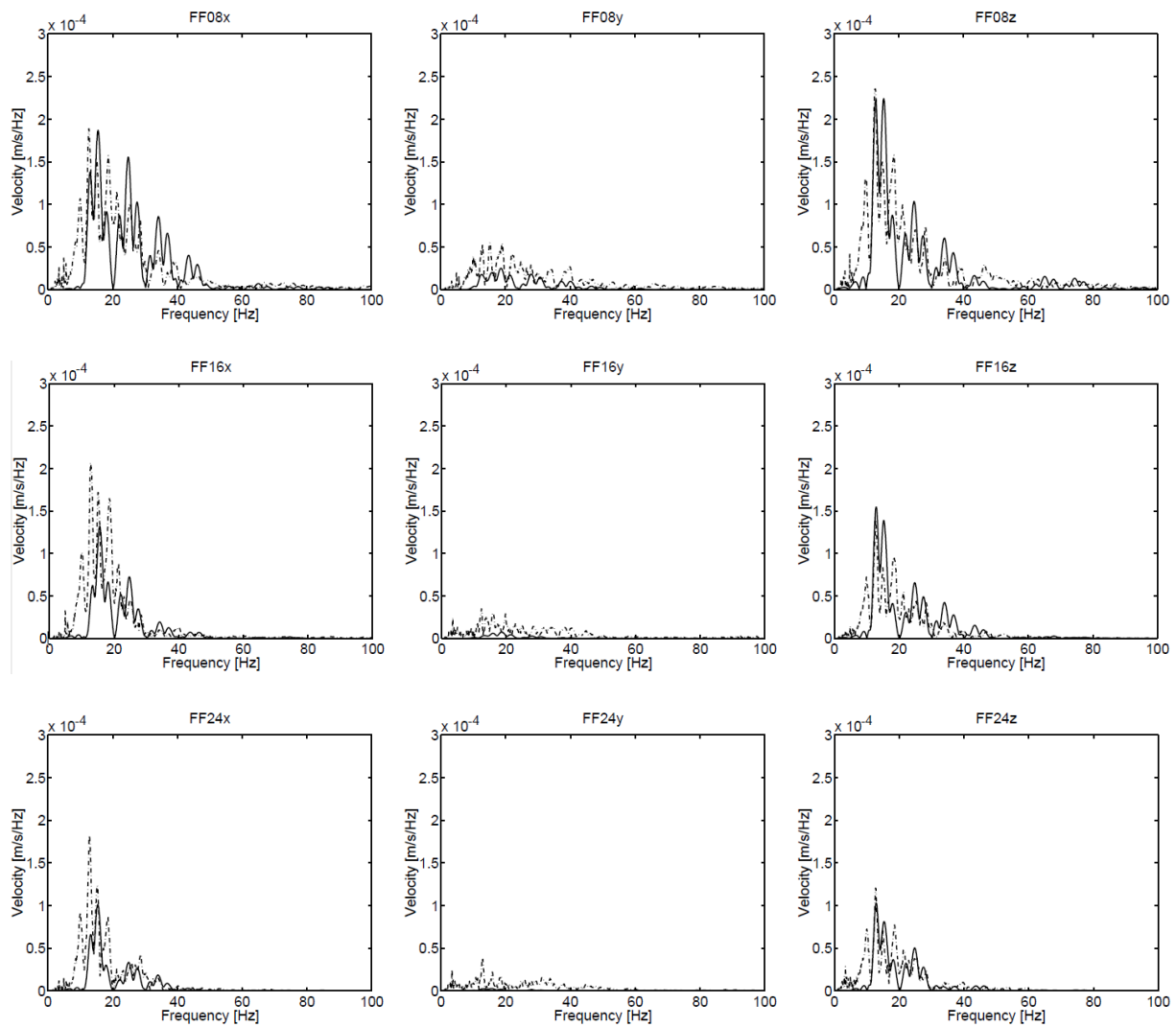


Figure 161. Frequency content of the predicted (solid line) and the measured (dash-dotted line) free field velocity at 8, 16 and 24 m for a vehicle speed $v = 58$ km/h (Degrande & Lombaert, 2002)

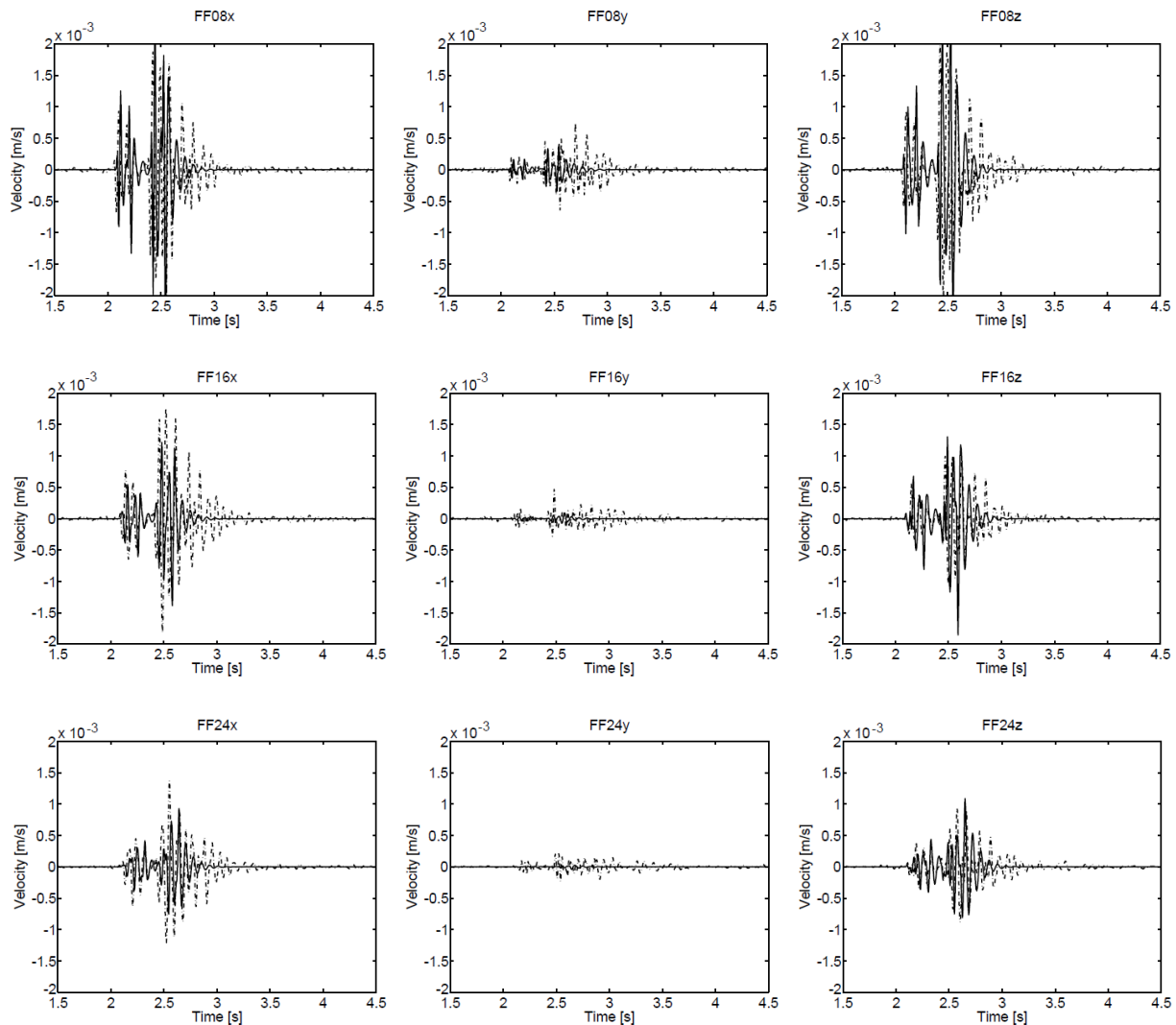


Figure 162. Time history of the predicted (solid line) and the measured (dash-dotted line) free field velocity at 8, 16 and 24 m for a vehicle speed $v = 58$ km/h (Degrande & Lombaert, 2002)

1.2.2. Verification Project Degrande et. al. (2) – Soil Building

The verification project ‘Validation of a Source-Receiver Model for Road Traffic-Induced Vibrations in Buildings. I: Source Model’ (Degrande, Pyl, Lombaert, & Haegeman, 2004) will be used to verify the computed results by FEMIX for the soil response. Note that this project cannot be used for the verification of the free field soil response because the presence of the building (reflection of vibrations) has to be taken into account for this project.

Source

Similar to verification project Degrande et. al. (1) – Free Field, as described before, also for the second verification project measurements have been performed on another site (in and around a single-family dwelling adjacent to a road connecting the Belgium municipalities Mol and Retie) for the passage of a Volvo FL6 truck (Figure 156) driving over the same artificial road unevenness (Figure 157). However, for this verification project the chosen vehicle characteristics are slightly different (Table 10) (possibly due to the fact that a different Volvo FL6 truck has been used for this site). Again, the generated loads are independent of the elastic deformation of the road and the supporting soil. The road is 3.5 m wide and is layered according to the specification in Table 11.

Table 10. Specified vehicle characteristics for modelling the Volvo FL6 truck of the verification projects (2) and (3) (Degrande, Pyl, Lombaert, & Haegeman, 2004)

$M_b = 7620 \text{ kg}$	$M_{ar} = 600 \text{ kg}$	$L_1 = -1.69 \text{ m}$	$K_{pr} = 610000 \text{ N/m}$	$C_{pr} = 16000 \text{ Ns/m}$
$I_b = 30000 \text{ kgm}^2$	$M_{af} = 400 \text{ kg}$	$L_2 = 3.51 \text{ m}$	$K_{pf} = 320000 \text{ N/m}$	$C_{pf} = 10050 \text{ Ns/m}$
			$K_{tr} = 3000000 \text{ N/m}$	$C_{tr} = 0 \text{ Ns/m}$
			$K_{tf} = 1500000 \text{ N/m}$	$C_{tf} = 0 \text{ Ns/m}$

Table 11. Specified road parameters of the verification projects (2) and (3) (Degrande, Pyl, Lombaert, & Haegeman, 2004)

Layer type	d (m)	ν (-)	ρ (kg/m ³)	$E \times 10^6$ (N/m ²)
1 Asphalt	0.15	0.33	2100	9150
2 Crushed stone	0.19	0.50	2000	500
3 Crushed concrete	0.25	0.50	1800	200

Transmission

The layering of the soil has been determined by a borehole experiment and SASW- and SCPT tests on site and the specification is given in Table 12. However this layered soil stratum has been simplified to a homogeneous halfspace (Table 13), because this would allow for a more computational-time efficient computation of the soil impedances used for the SSI between soil and structure. Note that the dynamic properties of the halfspace are equal to the second layer of the layered soil.

The vibration levels are measured at five points in the free field next to the road and the building (Figure 163). For point FF3 several figures are presented in the paper to which the results of the FEMIX can be compared. The measurements are in all three (x-, y-, and z-) directions.

Table 12. Specified soil parameters of the verification projects (2) and (3) (Degrande, Pyl, Lombaert, & Haegeman, 2004)

Layer	d (m)	ν (-)	ρ (kg/m ³)	$E \times 10^6$ (N/m ²)	C_s (m/s)	C_p (m/s)	β (-)
1	2.00	0.48	2000	116	140	714	0.0200
2	3.00	0.48	2000	237	200	1020	0.0200
3	∞	0.48	2000	370	250	1275	0.0200

Table 13. Simplification of the layered soil into a homogeneous halfspace used for computing the dynamic soil- and structural response of the verification projects (2) and (3) (Degrande, Pyl, Lombaert, & Haegeman, 2004)

Layer	d (m)	ν (-)	ρ (kg/m ³)	$E \times 10^6$ (N/m ²)	C_s (m/s)	C_p (m/s)	β (-)
1	∞	0.48	2000	237	200	1020	0.0200

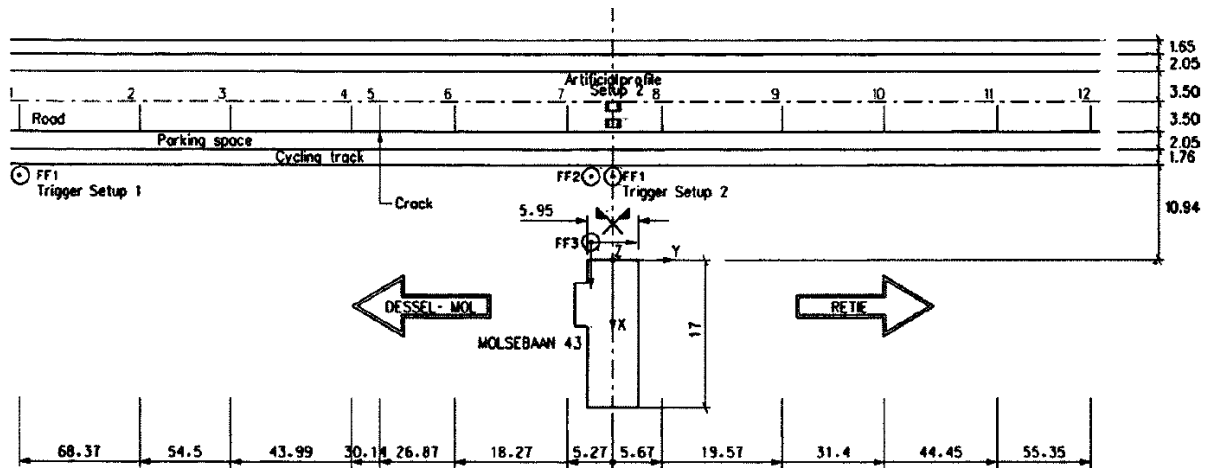


Figure 163. Position of the measurement points of the verification projects (2) and (3) (Degrande, Pyl, Lombaert, & Haegeman, 2004)

Results

The generated loads due to the passage of the truck over the artificial unevenness are given in both the frequency- and time domain (Figure 164). The predicted accelerations of the front- and rear axle appear to be well comparably with the measured accelerations of the axles.

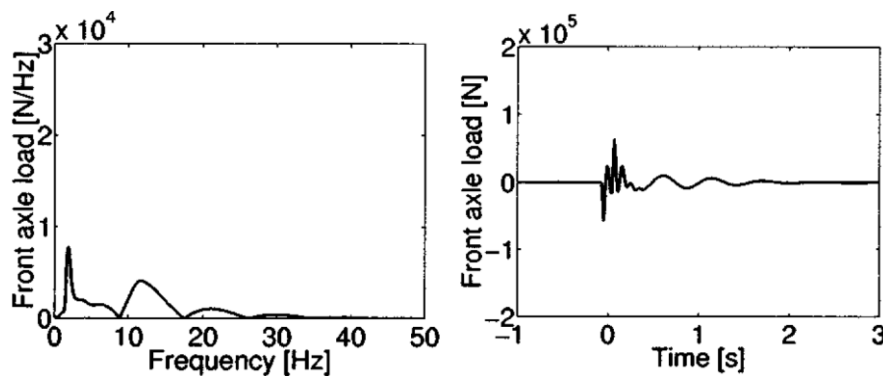


Figure 164. Frequency content (left) and time history (right) of the predicted front axle load of the Volvo FL6 truck when passing the artificial profile at a vehicle speed $v = 50$ km/h (Degrande, Pyl, Lombaert, & Haegeman, 2004)

The vibration levels (speed of the soil particle motion) for point FF3 are given in Figure 165 and Figure 166.

Conclusions of the paper

A comparison between the predicted and the measured vehicle responses has shown that the axle accelerations are well reproduced by the vehicle model.

For the passage on the plywood unevenness, the predicted free field response in the z-direction is overestimated, resulting in a ratio between the predicted and measured PPV equal to 1.6.

A homogeneous half-space with a uniform shear wave velocity $c_s = 200$ m/s has been assumed for the prediction of the free-field response. As a good correspondence between the predicted and measured free-field velocity has been obtained, the dynamic soil characteristics of this homogeneous half-space are used for part II of the paper, where the receiver model is validated.

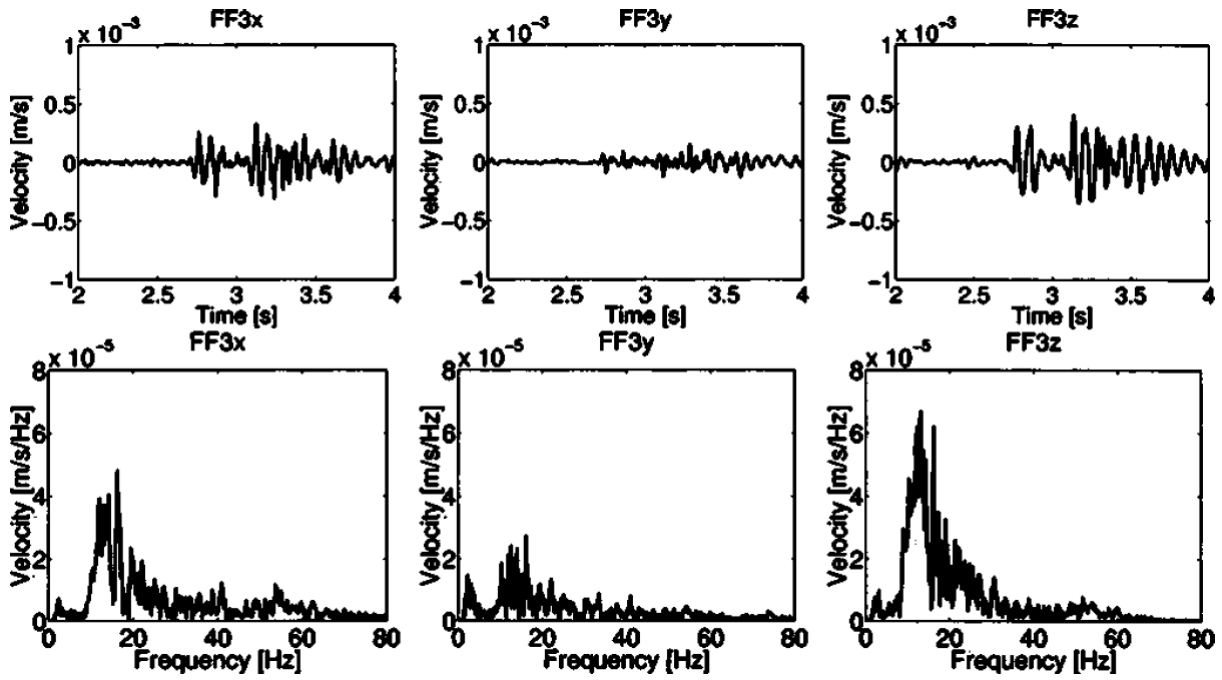


Figure 165. Time history and frequency content of the measured soil particle velocity in point FF3 for the passage of the truck at a speed $v = 50$ km/h on the plywood unevenness (Degrande, Pyl, Lombaert, & Haegeman, 2004)

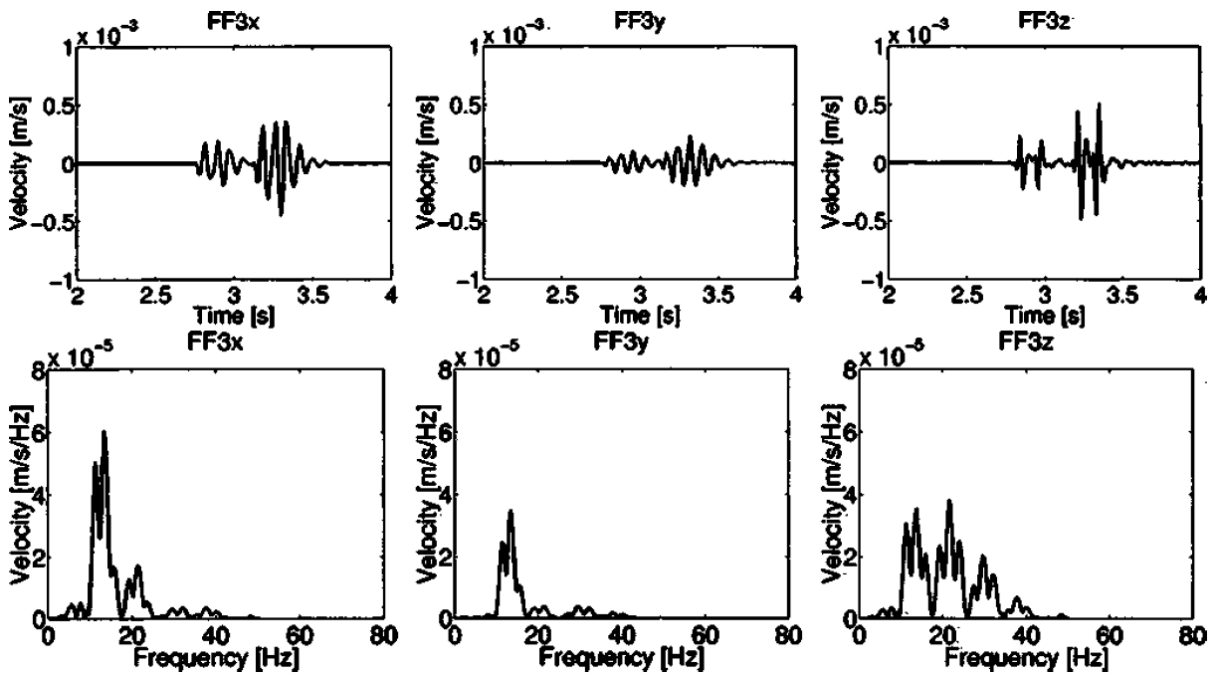


Figure 166. Time history and frequency content of the predicted soil particle velocity in point FF3 for the passage of the truck at a speed $v = 50$ km/h on the plywood unevenness (Degrande, Pyl, Lombaert, & Haegeman, 2004)

1.2.3. Verification Project Degrande et. al. (3) – Building Response

The verification project ‘Validation of a Source-Receiver Model for Road Traffic-Induced Vibrations in Buildings. I: Receiver Model’ (Degrande, Pyl, & Clouteau, 2004) will be used to verify the computed results by EDDABuS_{GS} for the structural response. For the source and transmission characteristics, see the Verification Project Degrande et. al. (2) – Soil Building, as described before.

Structure

The building is a two-storey structure with a rectangular plan and an embedded concrete box foundation. The structural building elements, their sizes and their material properties are specified in table Table 14. The dynamic soil-structure interaction is solved with a substructure method.

Table 14. Specified structural parameters of the verification project (3) (Degrande, Pyl, & Clouteau, 2004)

Element	Sizes	Material properties
Foundation / basement: embedded concrete box (Figure 167)	$L_x = 16.66$ m $L_y = 5.61$ m $d = 1.725$ m	$E = \text{unknown}$ N/mm ² $\nu_{xy} = \text{unknown}$ $\rho = \text{unknown}$ kg/m ³
Basement walls: concrete	$t = 0.30$ m	$E = \text{unknown}$ N/mm ² $\nu_{xy} = \text{unknown}$ $\rho = \text{unknown}$ kg/m ³
Basement floor (base slab): reinforced concrete	$d = 0.25$ m	$E = \text{unknown}$ N/mm ² $\nu_{xy} = \text{unknown}$ $\rho = \text{unknown}$ kg/m ³ (ρ includes non-structural layers)
1st and 2nd storey floors: prestressed Stalton beams with intermediate members of burnt clay (Figure 168)	$d = 0.11$ m	Equivalent orthotropic plate model: $E_x = 30.6 \times 10^3$ N/mm ² $E_y = 178.0 \times 10^3$ N/mm ² $G_{xy} = 19.4 \times 10^3$ N/mm ² $\nu_{xy} = 0.20$ $\rho = 5084$ kg/m ³
1st and 2nd storey floors: longitudinal concrete stiffening beam at mid-span	$d = 0.11$ m $w = 0.296$ m	$E_x = 32.6 \times 10^3$ N/mm ² $\rho = 3409$ kg/m ³
Internal cavity walls: brick	$t = 0.14$ m	$E = \text{unknown}$ N/mm ² $\nu_{xy} = \text{unknown}$ $\rho = \text{unknown}$ kg/m ³
Floor-wall connection in y-direction: rigid Floor-wall connection in x-direction: hinged External cavity walls are disregarded because they are self-supporting		
Roof: six longitudinal girders and transverse girders with a zinc covering		Equivalent orthotropic plate model: $E = \text{unknown}$ N/mm ² $\nu_{xy} = \text{unknown}$ $\rho = \text{unknown}$ kg/m ³

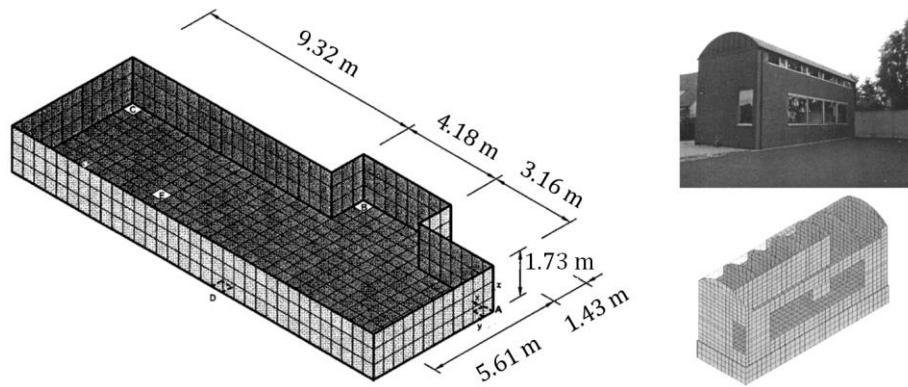


Figure 167. Embedded concrete box foundation with sizes (left) of the single-family dwelling (right) (Degrande, Pyl, & Clouteau, 2004)

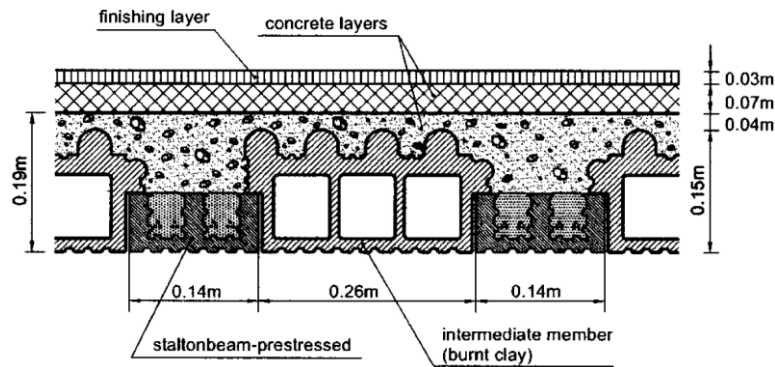


Figure 168. Cross section of the storey floors of verification project (3) (Degrande, Pyl, & Clouteau, 2004)

The vibration levels are measured at several points in the building (Figure 169). Point F11 is most interesting for comparison with the EDDABu_{GS}-tool, because the point is situated on the ground floor (1st floor) which has higher vibration amplitudes than in the basement due to the flexibility of the walls and the free span of the floor. Since the EDDABu_{GS}-tool includes a flexible frame on top of a rigid foundation, the prediction of the structural response of the ground floor (1st floor) is most interesting to verify all the computed results.

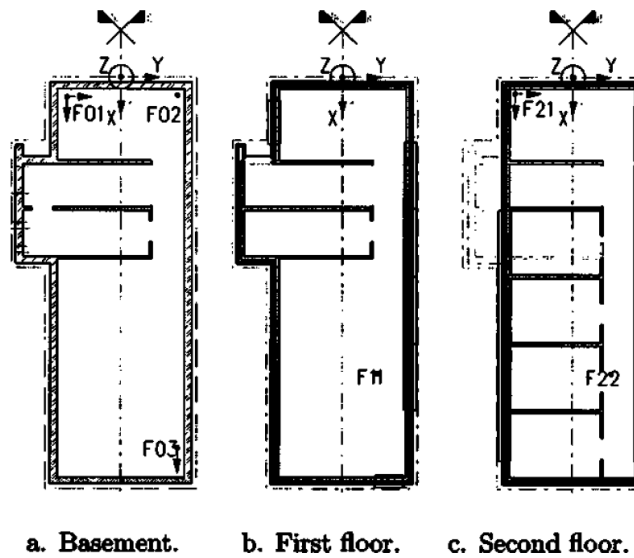


Figure 169. Position of the measurement points of the verification project (3) (Degrande, Pyl, & Clouteau, 2004)

Results

Figure 170 and Figure 171 show the predicted structural response (velocity) of point F11.

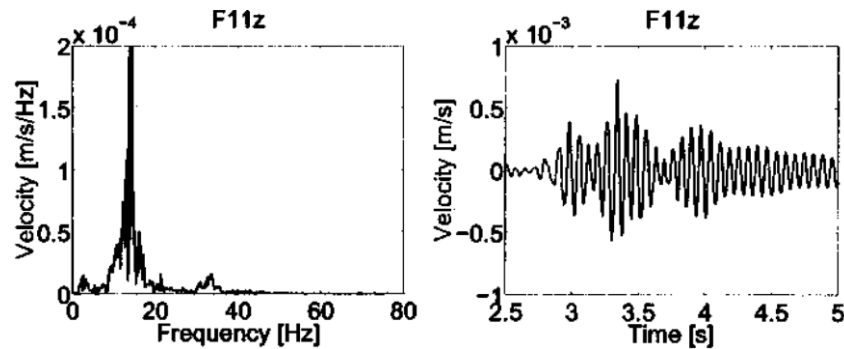


Figure 170. Frequency content (left) and time history (right) of the measured structural response (velocity) in point F11 for the passage of the truck at a speed $v = 50$ km/h on the plywood unevenness (Degrande, Pyl, & Clouteau, 2004)

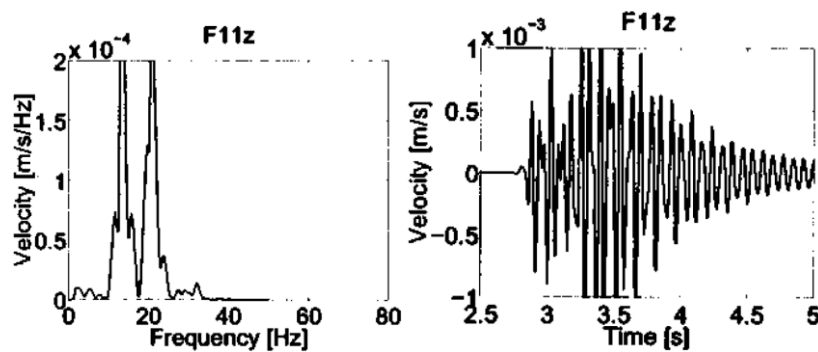


Figure 171. Frequency content (left) and time history (right) of the predicted structural response (velocity) in point F11 for the passage of the truck at a speed $v = 50$ km/h on the plywood unevenness (Degrande, Pyl, & Clouteau, 2004)

Conclusions of the paper

For the passage on a plywood unevenness, the results of the validation are very satisfactory. The time history and frequency content of the signals are well reproduced. The vertical response in the structure is slightly overestimated in the frequency range between 10 and 20 Hz, whereas for frequencies above 20 Hz, the overestimation of the vertical PPV is larger. Note that the dynamic floor response has larger amplitudes than the soil response just in front of the building.

1.3. Conclusion Verification Projects KU Leuven

The predictions of the numerical model of the verification projects Degrande et al. are verified to give reasonable accurate results. Therefore, the results of the verification projects will be compared with the results of the tool (FEMIX and EDDABuS_{GS}). First the results of the prediction model of the verification projects will be compared to the results of the tool since these results should be very similar because (almost) the exact same situations can be modelled (for the source- and transmission stage). However also a comparison will be made between the on-site performed measurements and the results of the tool, because the tool uses some other assumptions (e.g. a different numerical method for the soil vibrations and soil-structure interaction based on the tables of Gazetas) and could therefore give more or less accurate results for the soil response and the structural response.

1.4. VU Amsterdam

The EDDABuS_{GS}-tool eventually considers the dynamic response of the soil for locations in The Netherlands. Therefore, the confined information provided for the project 'VU Amsterdam site' of Pieters Bouwtechniek is used for determining the characteristics of the road irregularity and the vehicle. In the documents of DGMR a soil layering is presented which is used by them for predicting the vibrations in the soil and the structure of this specific project (Table 15). This soil layering is used to model the layered soil in FEMIX. Also figures are presented for the soil response at some particular locations on site for the passage of a sand truck laden with 40 tonnes of sand (Figure 172 and Figure 173). It is stated that the soil response in vertical direction, with a distance of 30 m from the road, due to the passage of the truck is approximately 250 μm/s.

Table 15. Dynamic specification of layered soil at the VU Amsterdam site as presented by DGMR (Fennema, May 2018)

Layer	d (m)	ν (-)	ρ (kg/m ³)	$E \times 10^6$ (N/m ²)	$G \times 10^6$ (N/m ²) $G = \frac{E}{2(1 + \nu)}$	C_s (m/s) $C_s = \sqrt{G/\rho}$	β (-)
1	1.00	0.25	1800	100	40,0	149	0.0100
2	0.30	0.30	1700	40	15,4	95	0.0200
3	1.50	0.45	1000	10	3,4	58	0.1000
4	0.70	0.40	1230	20	7,1	76	0.0400
5	2.90	0.40	1700	50	17,9	103	0.0400
6	0.80	0.25	1740	100	40,0	152	0.0100
7	2.30	0.40	1540	50	17,9	108	0.0100
8	0.40	0.45	1000	10	3,4	58	0.1000
9	5.50	0.25	2000	200	80,0	200	0.0100
10	2.00	0.40	1800	80	28,6	126	0.0400
11	∞	0.25	2000	450	180	300	0.0100

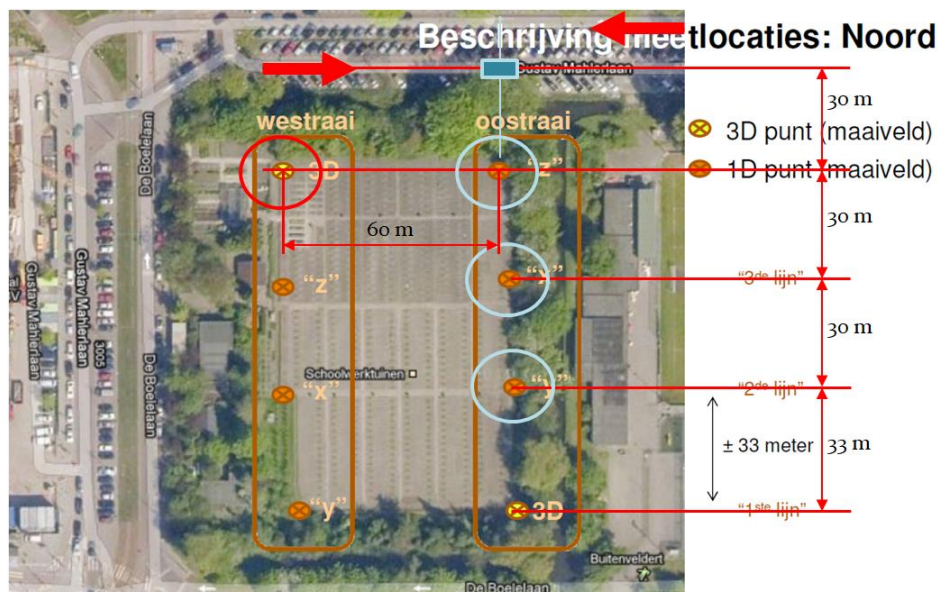


Figure 172. Situation of measurements at the VU Amsterdam site, taken from the documents of TNO (Koopman, 2012). The red arrows indicate the travelling path of the sand truck. The top left measurement point (x,y,z) and the top three measurement points on the right (z) are used to verify the result computed by FEMIX

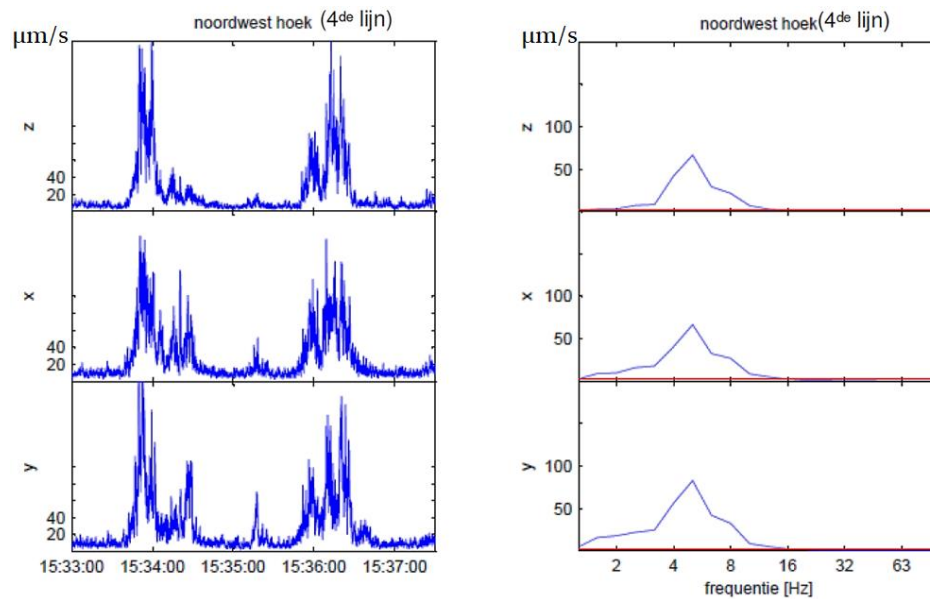


Figure 173. Soil response at the top left measurement point from Figure 172 at the VU Amsterdam site, taken from the documents of TNO (Koopman, 2012)

The sand truck is of the type MAN TGS 10x8 WSA (Figure 174), however the dynamic properties of the truck are unknown. Several experts (TU Delft, KU Leuven and the MAN manufacturer) have been contacted to ask for the dynamic properties (in a similar form as in Table 10), however no satisfying response was given yet. Therefore, the vehicle characteristics of the heavy-weighted MAN truck are approximated based on the vehicle characteristics of the light-weighted Volvo FL6 truck described before and the known gross weight and weight distribution of the MAN truck. Since the maximum axle loads of the MAN truck can be up to 11500 kg (modderaandebanden.nl, 2019) and the maximum axle loads of the Volvo FL6 truck is up to 7000 kg (volvotrucks.nl, 2019), the mass of the axles of the MAN truck are assumed to be $11500 / 7000 \cdot 600 \cdot 1.5 = 1500$ kg. The tyre stiffness of the MAN truck is approximated to be slightly lower than those of the Volvo FL6 truck because that brings the results more in line with the measurements performed at the VU Amsterdam site. The stiffness and damping of the suspension is unchanged. The approximated vehicle characteristics of the MAN truck are specified in Table 16. The vehicle speed at the time of the measurements on site was in-between 30 km/h and 50 km/h.



Figure 174. MAN TGS 10x8 WSA sandtruck used for the measurements at the VU Amsterdam site (modderaandebanden.nl, 2019)

Table 16. Assumed specified vehicle characteristics for modelling the MAN TGS 10x8 WSA truck

$M_b = 47000 \text{ kg}$	$M_a = 1500 \text{ kg}$		$K_p = 610000 \text{ N/m}$	$C_p = 16000 \text{ Ns/m}$
$I_b = 50000 \text{ kgm}^2$			$K_t = 2000000 \text{ N/m}$	$C_t = 0 \text{ Ns/m}$
$L_1 = -3.2 \text{ m}$ (rear axle)	$L_2 = -1.8 \text{ m}$	$L_3 = 0 \text{ m}$ (middle axle)	$L_4 = 1.8 \text{ m}$	$L_5 = 3.6 \text{ m}$ (front axle)

The remaining parameter that has to be tuned to meet the vibration amplitudes from the performed measurements is the road irregularity. Only the height of the road irregularity will be tuned (see 10.3.3 ‘Soil response in Amsterdam’) in order to narrow the number of parameters which can be tuned for this problem.

H. Appendix: Additions to Chapter 9 ‘Source Modelling and Results’

1.1. Road Unevenness

The characteristics of the road irregularity (Figure 62) over which the vehicle drives are similar to the verification projects discussed in 8 ‘Verification Projects’. As discussed in 7.1.3 ‘Possibilities,’ the road irregularity is implemented by means of a Fourier expansion. The functions $f(y)$ (where $y = XG2$) for the road irregularity are implemented, in line with (Lombaert, Degrande, & Clouteau, 2000), as:

$$f(y) = \begin{cases} 0 & -\frac{P}{2} \leq y < \frac{-LB_{irreg}}{2} \\ \frac{H_{irreg}}{2} \left[1 - \cos \left(\frac{2\pi \left(|y| - LT_{irreg} + \frac{(LB_{irreg} - LT_{irreg})}{2} \right)}{2(LB_{irreg} - LT_{irreg})} \right) \right] & \frac{-LB_{irreg}}{2} \leq y < \frac{-LT_{irreg}}{2} \\ H_{irreg} & \text{for } \frac{-LT_{irreg}}{2} \leq y < \frac{LT_{irreg}}{2} \\ \frac{H_{irreg}}{2} \left[1 - \cos \left(\frac{2\pi \left(|y| - LT_{irreg} + \frac{(LB_{irreg} - LT_{irreg})}{2} \right)}{2(LB_{irreg} - LT_{irreg})} \right) \right] & \frac{LT_{irreg}}{2} \leq y < \frac{LB_{irreg}}{2} \\ 0 & \frac{LB_{irreg}}{2} < y < \frac{P}{2} \end{cases} \quad (0.96)$$

and their exact representation for the ranges of the longitudinal coordinate ‘y’ for which the height of the road irregularity is larger than zero is given in Figure 175. Note that the scale of the horizontal- and vertical axes in the figure are not the same.

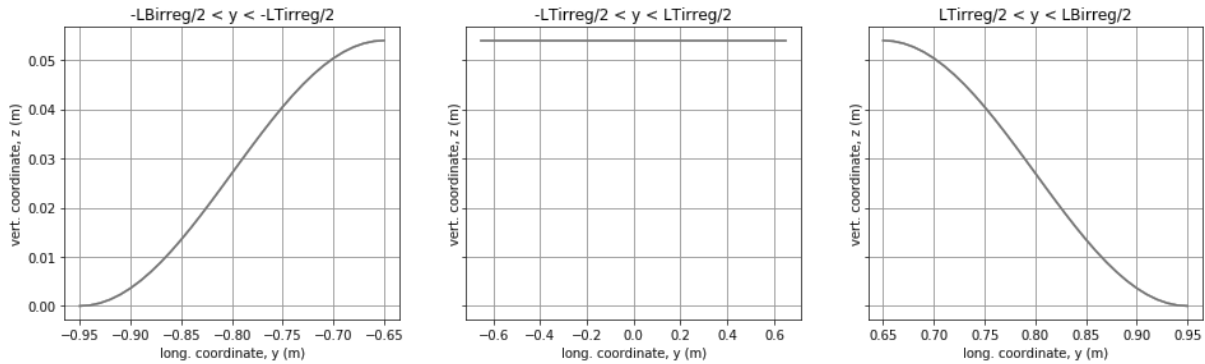


Figure 175. Exact representation of the functions $f(y)$ of the road irregularity for the ranges of the longitudinal coordinate ‘y’ for which the height of the road irregularity is larger than zero

1.2. Generated Moving Loads

In reality the road (and its irregularities) are elastic and might deform when the material is loaded. However, taking into account the affected loading by the coupling between the deformation of the road and the loads applied on it, increases the computational time. Therefore, decoupling the road deformation and the load generation simplifies the problem and decreases the computational time. According to Degrande et al. (Degrande & Lombaert, 2002) who refer to (Cebon, 1993) and (Gillespie, et al., 1993), this simplification can be satisfied since the stiffness of the road is much greater than the stiffness of the tyres and the suspension system of the vehicle, and thus the stiffness of the road can be assumed to be infinitely stiff compared to the tyres and suspension.

1.2.1. Loads by steel leaf suspension and air suspension

In section 3.1 ‘Road Traffic Induced Vibrations – Measurements’ the experiment of O. Hunaidi and M. Tremblay (Hunaidi & Tremblay, Traffic-induced buiding vibrations in Montréal, 1997) was described in which it was concluded that a city bus would generate greater vibration levels than a truck, while they had approximately the same total mass, but different suspension types. The truck had a steel leaf suspension and the bus had air suspension. Since air suspension damps out the vibrations more than a leaf suspension, that is for comfort purposes, one would not expect this vehicle to generate greater vibration levels than a truck with steel leaf suspension. Now this phenomenon can be investigated based on the vehicle model implemented in FEMIX.

The trucks of the verification projects have steel leaf suspensions, so the vehicle characteristics used for these projects are considered here to be the reference case (steel leaf suspension). No reliable values have been found for the suspension characteristics of a vehicle with air suspension, but one can argue that air suspension has more damping and might be less stiff. A simplified computational model has been created in the software ‘Maple’ to deviate values of the vehicle characteristics. The computation of this model is much quicker than with FEMIX, and therefore more convenient for performing many iterations. When deviating the values of the damping- and stiffness coefficient of the suspension and the tyres and deviating the mass distribution between axles and vehicle body, the following observations can be made (Figure 176):

- Decreasing the axle mass (μ) (and increasing the vehicle body mass, to have the same total mass) shifts the 2nd peak of the frequency spectrum to the right (stiffer response).
- Decreasing the stiffness of the suspension (k_p) shifts all peaks of the frequency spectrum to the left (less stiff response).
- Increasing the damping coefficient of the suspension (c_p) decreases the values of the frequency spectrum (smaller loads).
- Increasing the stiffness of the tyres (k_t) shifts the 2nd peak of the frequency spectrum to the right (stiffer response).
- Increasing the vehicle body mass (m_s) (without decreasing the axle masses) shifts the 1st peak of the frequency spectrum to the left (less stiff response).

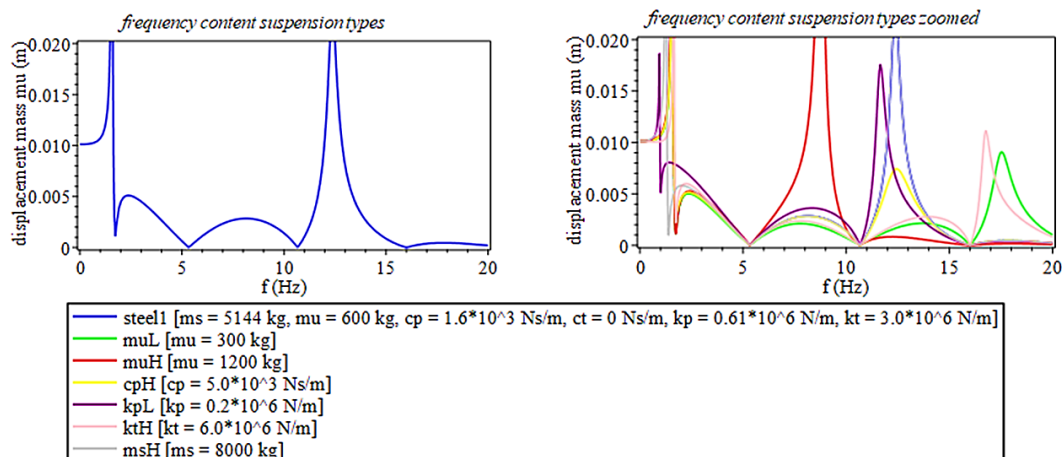


Figure 176. A frequency spectrum of an arbitrary heavy vehicle with steel leaf suspension vehicle characteristics (left) and frequency spectrums for deviating values of the vehicle characteristics (right)

Since the study of O. Hunaidi and M. Tremblay (Hunaidi & Tremblay, 1997) does not mention any values for the vehicle characteristics, a vehicle model for a bus with air suspension is approximated. Note that the values are chosen such that they are reasonable in line with what one would expect from this suspension system, but also make that the response of the vehicle

is in line with the experimental observations. Thus, the chosen values are not based on scientific experiments or literature.

When computing the frequency spectrum of the approximated bus with air suspension and stiffer tyres, one can observe that the 1st peak of the frequency spectrum decreases significantly but the 2nd peak increases and shifts somewhat to the right (stiffer response due to greater tyre stiffness) (Figure 177).

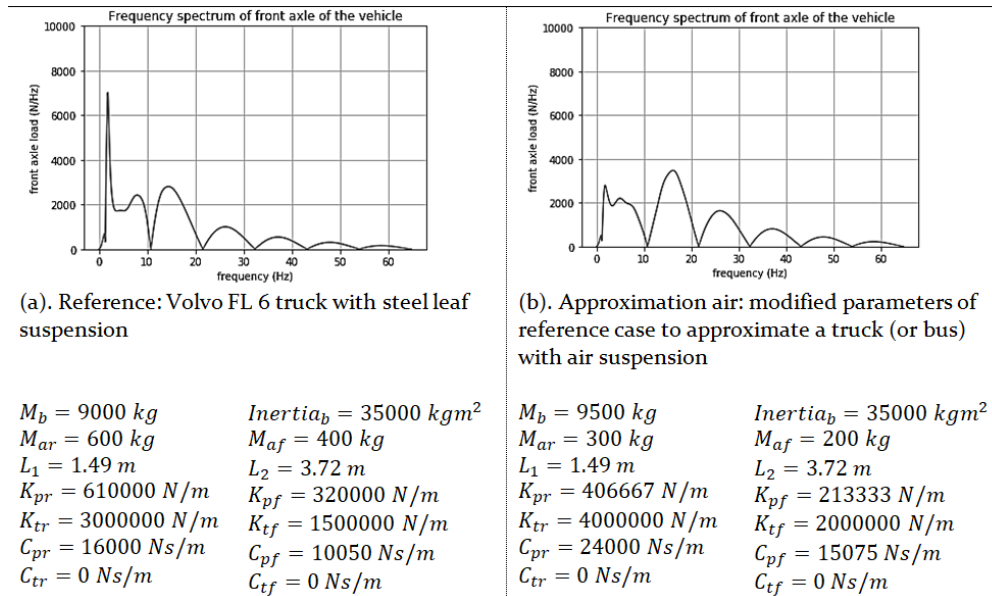


Figure 177. Frequency spectrum of the truck with steel leaf suspension of the verification project (left) and the approximated bus with air suspension (right). See Appendix I ‘Appendix: table of computed vehicle axle load-frequency spectrums for changing parameter values’ for frequency spectrums for deviating vehicle characteristics one-by-one

The experimental measurements of Al-Hunaidi were computed at sites in Montreal, which have a frequency spectrum of the soil response typically as in Figure 178. From this figure one can clearly observe that for the (low) frequency range, at which the vehicles generate loads (typically between 0 Hz and 25 Hz), the soil response increases rapidly with increasing frequency. Based on the frequency spectrums of the vehicles and the soil, one can conclude that the soil amplifies the vibrations for increasing frequencies and therefore the bus with air suspension and stiffer tyres generates greater soil vibrations (similar to the resonance effect, i.e. the dominant excitation frequency of the bus with air suspension is shifted towards the dominant natural frequency of the soil).

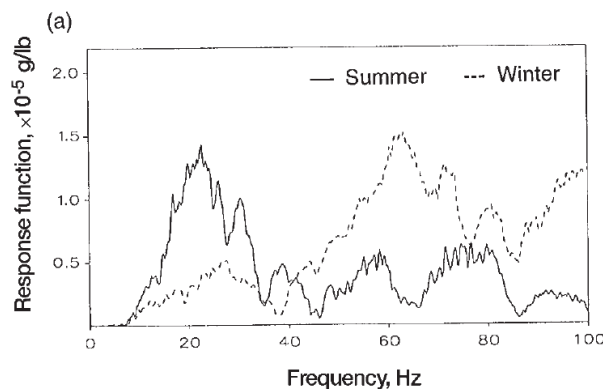
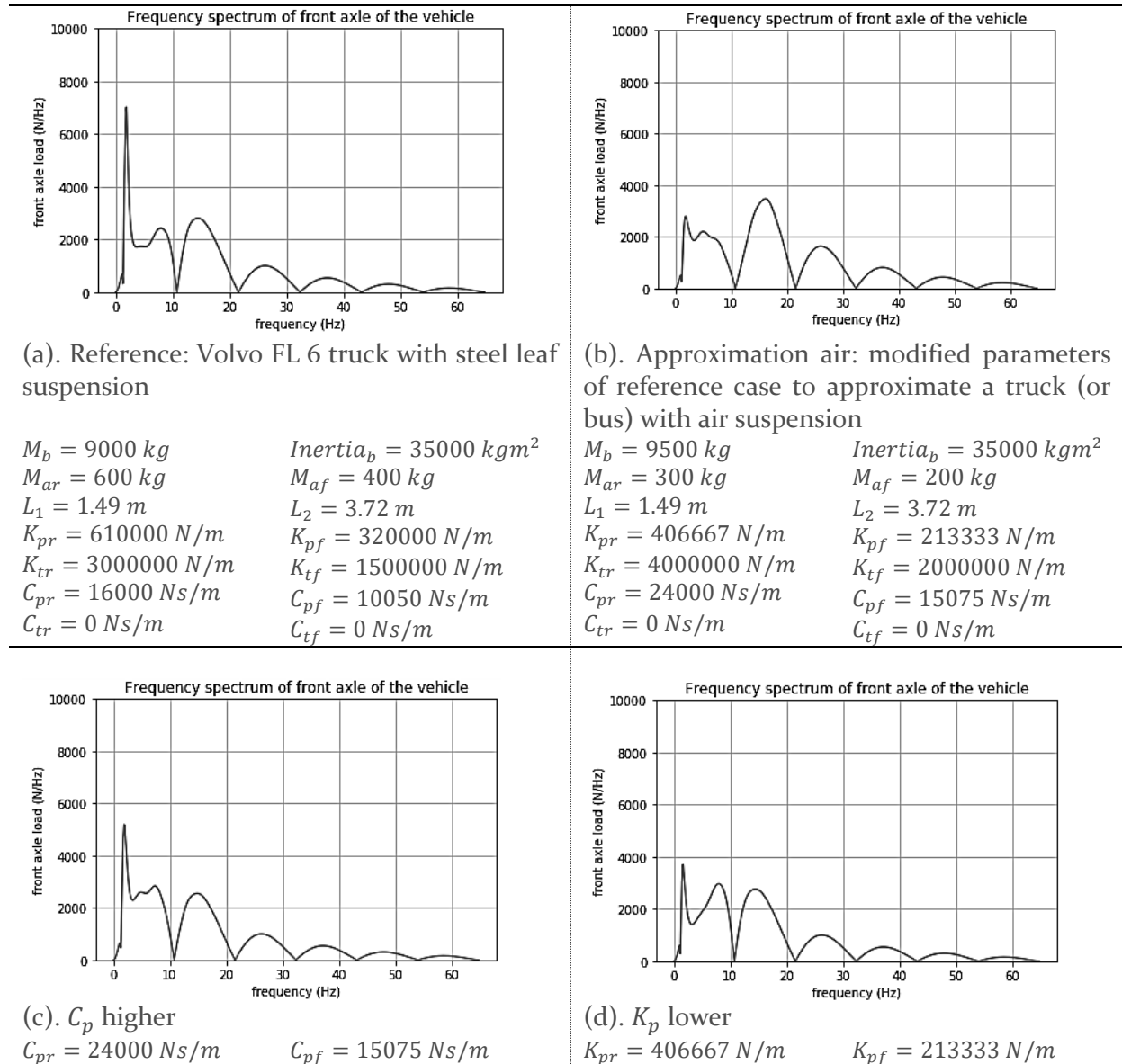
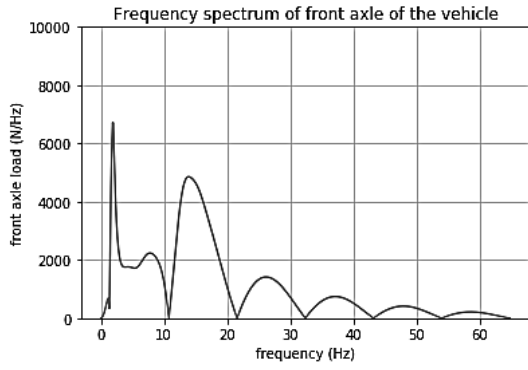


Figure 178. Vertical response (frequency spectrum) obtained with the drop weight device in summer and winter for the ground in front of a building at a particular site in Montreal (Hunaidi & Tremblay, Traffic-induced buiding vibrations in Montréal, 1997)

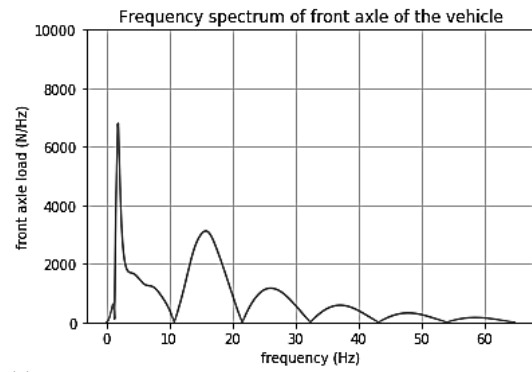
I. Appendix: table of computed vehicle axle load-frequency spectrums for changing parameter values

Table 17. Computed load-frequency spectrums of the 2D truck vehicle model when driving over the road unevenness as described in the verification project of Degrande et. al. for changing parameter values (Figures (a). – (h).)

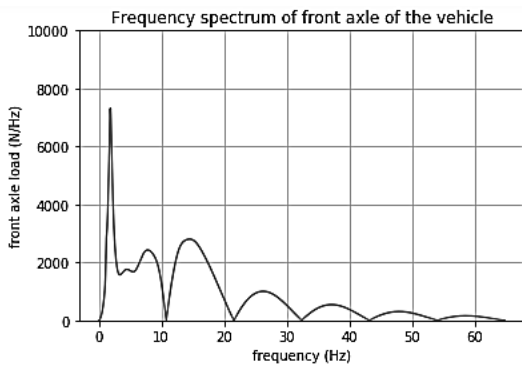




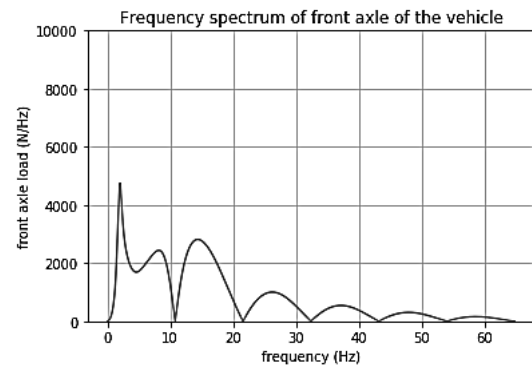
(e). K_t higher
 $K_{tr} = 4000000 \text{ N/m}$ $K_{tf} = 2000000 \text{ N/m}$



(f). M_a lower
 $M_{ar} = 300 \text{ kg}$ $M_{af} = 200 \text{ kg}$



(g). M_b higher
 $M_b = 13500 \text{ kg}$

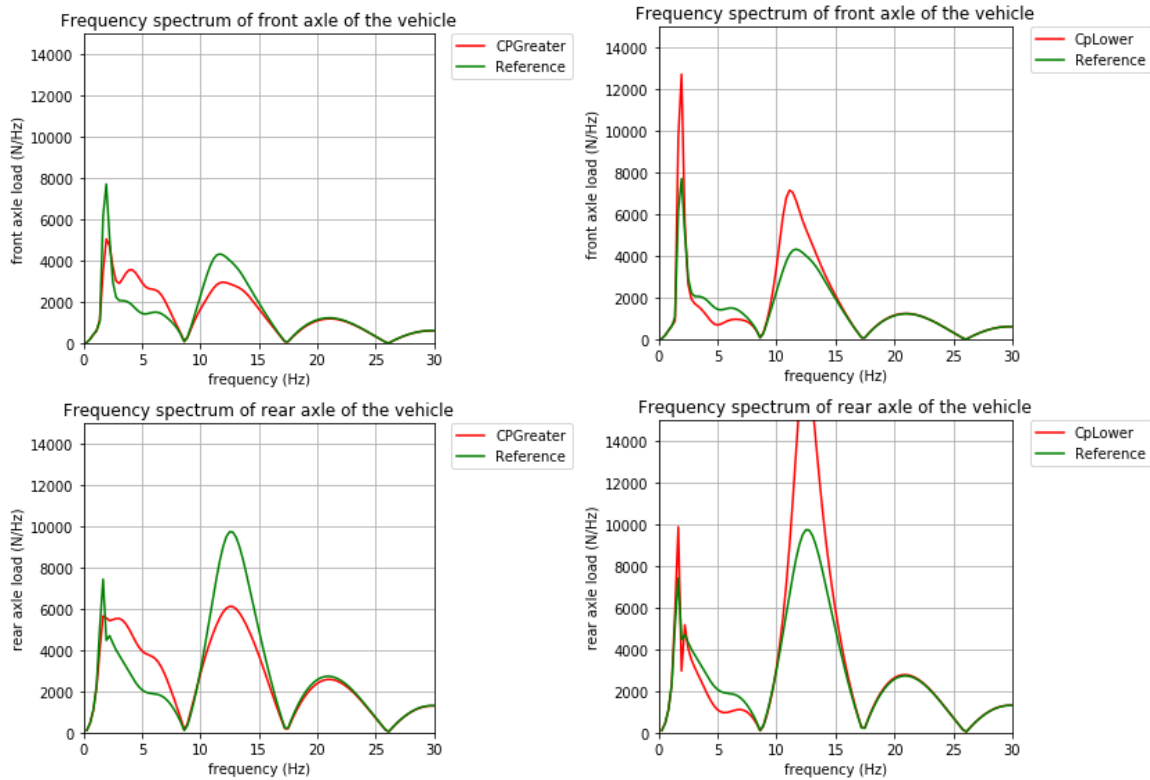


(h). M_b lower
 $M_b = 6000 \text{ kg}$

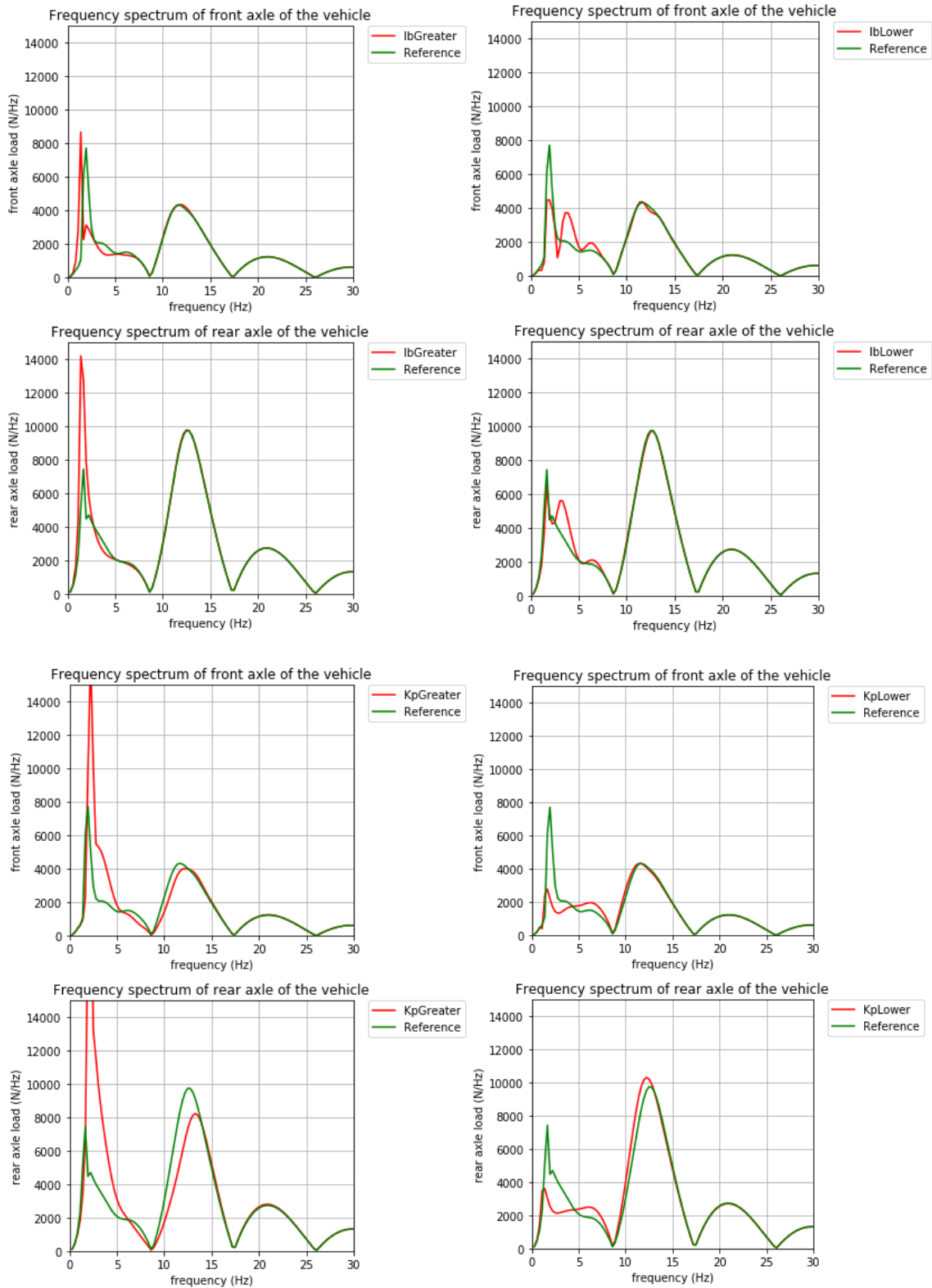
Additional iterations have been made for a slightly different reference vehicle. These iterations give an even more comprehensive overview of the influence of several parameters. In the iterations it is stated what parameter is made greater or lower. ‘Greater’ means that the reference value is factorized by 2 and ‘lower’ means that the reference value is factorized by 0.5. A very brief explanation is given for the observed changes.

Reference: Volvo FL 6 truck with greater inertia of the vehicle body and a lower weight

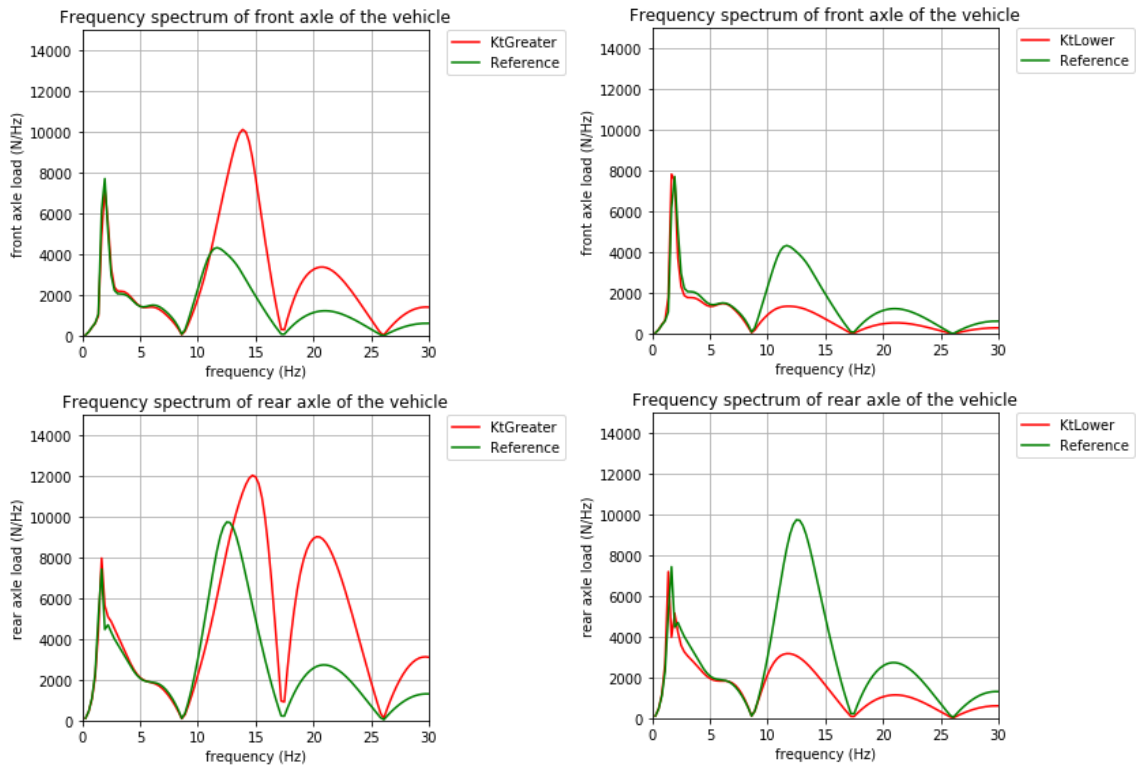
$M_b = 7620 \text{ kg}$	$Inertia_b = 300000 \text{ kgm}^2$
$M_{ar} = 600 \text{ kg}$	$M_{af} = 400 \text{ kg}$
$L_1 = 1.49 \text{ m}$	$L_2 = 3.72 \text{ m}$
$K_{pr} = 610000 \text{ N/m}$	$K_{pf} = 320000 \text{ N/m}$
$K_{tr} = 3000000 \text{ N/m}$	$K_{tf} = 1500000 \text{ N/m}$
$C_{pr} = 16000 \text{ Ns/m}$	$C_{pf} = 10050 \text{ Ns/m}$
$C_{tr} = 0 \text{ Ns/m}$	$C_{tf} = 0 \text{ Ns/m}$



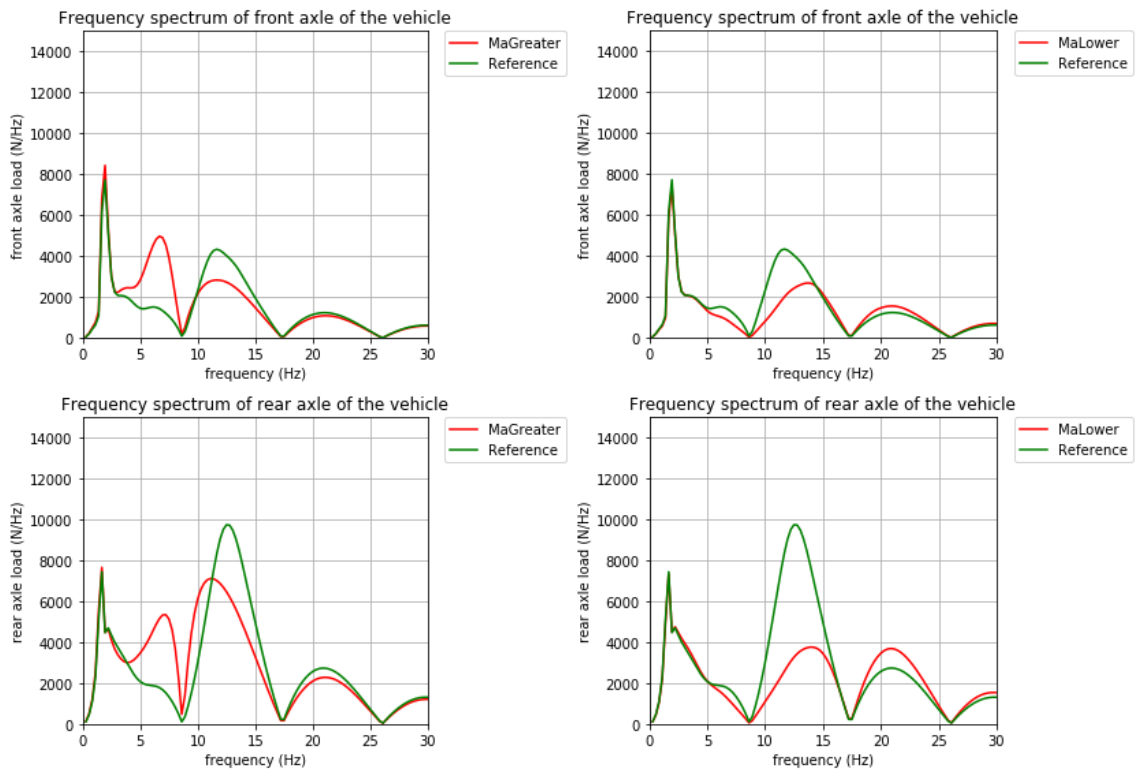
Explanation: more damping is lower amplitude.



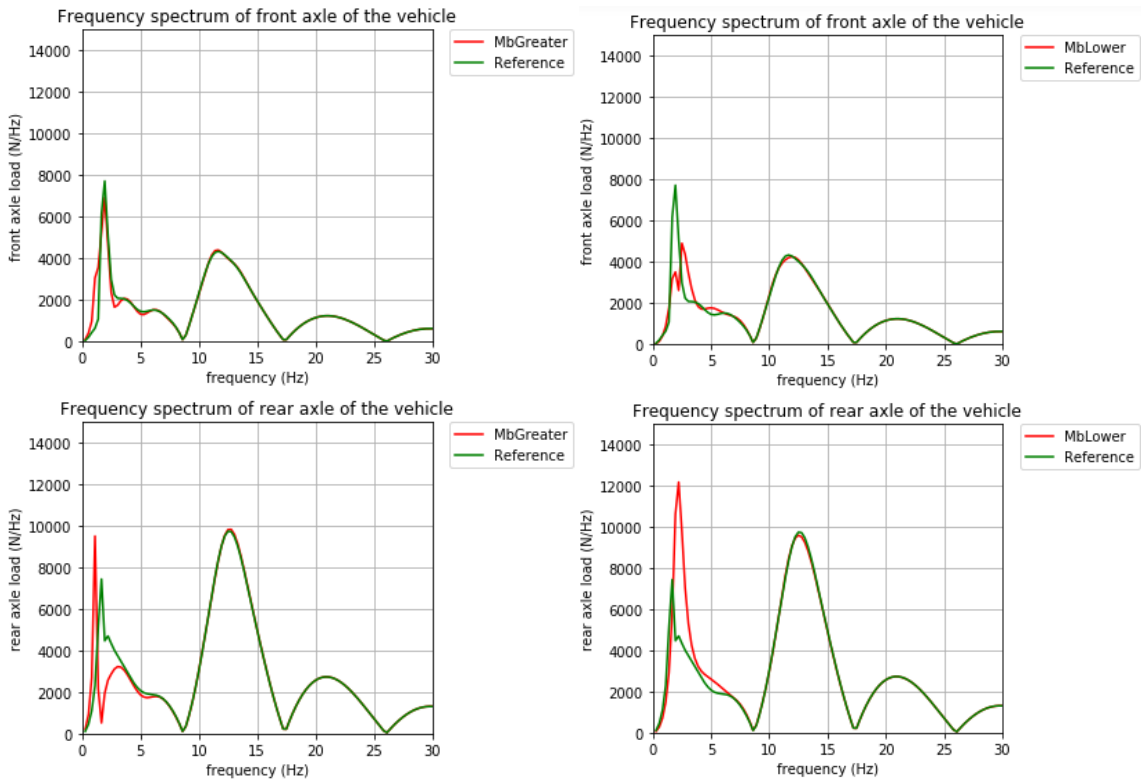
Explanation: greater suspension stiffness = less damping of impact (more direct impact with greater amplitude).



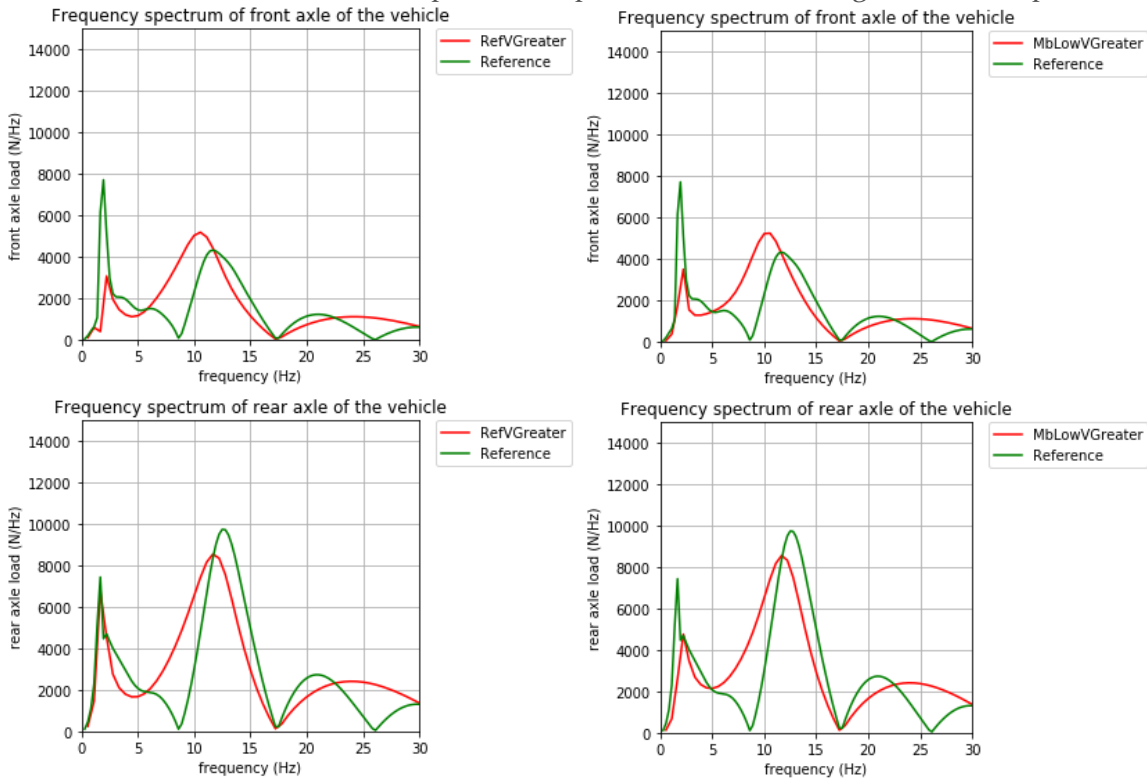
Explanation: greater tyre stiffness = less damping of impact (more direct impact with greater amplitude).



Explanation: greater axle mass gives a greater natural period = lower natural frequency, but increases the load amplitude at that lower frequency.

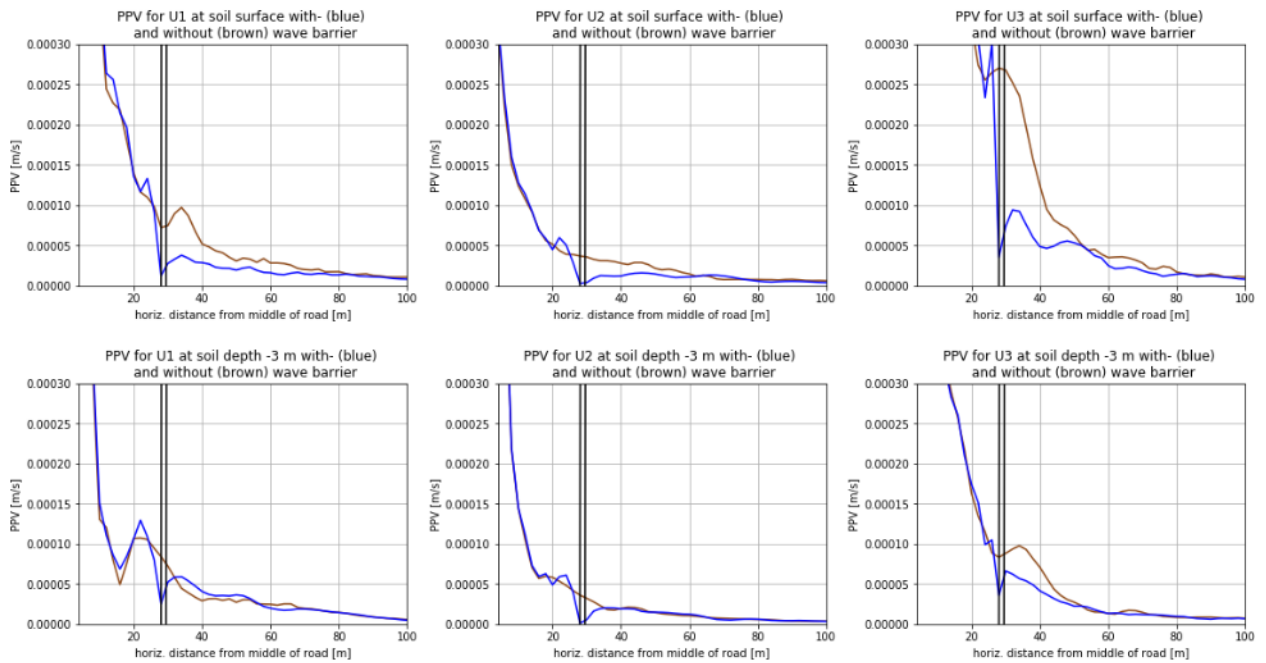


Explanation: greater body mass does not influence the spring loading, because it is already compressed quite a lot. Lower body mass elongates the natural period and matches the oscillations of the rear axle at this particular speed. When increasing the vehicle speed:



When increasing the vehicle speed the lower body mass decreases the amplitude of the loading oscillations at the rear axle. Also the higher frequency range (> 20 Hz) is more excited.

J. Appendix: PPV with- and without wave barrier in soil Amsterdam



The above figures contain the peak particle velocity (PPV) of the soil (soil similar to the Amsterdam case) at soil surface (top) and at soil depth -3 m (bottom) for the situation without the realization of the wave barrier (brown colour) and for the situation with the realization of the wave barrier (blue colour). The position of the wave barrier is indicated by the vertical black lines. The wave barrier has a width of 1.6 m and a depth of 4 m (x,z -plane) and is infinitely long in the y -direction.

K. Appendix: Additions to Chapter 11 ‘Soil-Structure Interaction Modelling’

1.1. Derivation of Impedances

In order to compute the impedances of the soil, what one basically needs to do is to imply a unit force or moment on the rigid foundation, supported by a specific soil with known parameters, in the direction of every degree of freedom and compute the flexibility matrix from the obtained dynamic displacements and rotations of the structure. Then by inverting the flexibility matrix, the dynamic stiffness matrix can be found. The dynamic stiffness matrix is composed of complex numbers (the impedances) and can be represented by a real part and an imaginary part ($\mathbb{K}_j(\omega) = \bar{K}_j(\omega) + i\omega C_j(\omega)$, where $j = x, y, z$ (swaying in 3 directions), rx, ry (rocking around two axes) or t (torsion around the vertical axis)) in which both \bar{K}_j and C_j are functions of the frequency ω . The real part \bar{K}_j is termed ‘dynamic stiffness’ and reflects the stiffness and inertia of the supporting soil. The imaginary part ωC_j is the product of circular frequency times the ‘dashpot coefficient,’ which reflects the radiation- (waves spreading away from the structure) and material damping (energy dissipation in the soil).

Moreover, in embedded foundations, and foundation on piles, the horizontal forces along the principal axes induce rotational in addition to translational oscillations, therefore, two more ‘cross-coupling’ horizontal-rocking impedances exist: $\mathbb{K}_{xry}(\omega)$ and $\mathbb{K}_{yrx}(\omega)$.

Gazetas performed a lot of iterations to compute the impedances for a vast amount of different structural- and soil configurations. The impedances refer to axes passing through the foundation basemat-soil interface. Once for a particular excitation frequency ω the eight dynamic impedances have been determined, the steady-state response of a rigid foundation block can be computed.

Gazetas developed an engineering approach of easy-to-use closed-form expression and graphs, based on the results of rigorous and approximate formulations. The errors encountered in a sensitivity analysis by Gazetas is well within an acceptable 15 percent.

The presentation of the tables and graphs of Gazetas is subdivided in different structural configurations (Gazetas G. , 1991):

4. Table 15.1 and accompanying set of graphs refer to foundations of any solid shape resting on the surface of a homogeneous halfspace.
5. Table 15.2 and related graphs are for foundations with any solid basemat shape partially or fully embedded in a homogeneous halfspace.
6. Table 15.3 refers mainly to circular and strip foundations on the surface of a homogeneous soil stratum underlain by bedrock.
7. Table 15.4 refers to circular and strip foundations partially or fully embedded in a homogeneous stratum underlain by bedrock.
8. Table 15.5 pertains to square and strip foundations on the surface of some inhomogeneous profiles, in which the shear modulus (G) increases smoothly with depth.
9. Table 15.6 is mainly for laterally oscillating single floating piles in two inhomogeneous and a homogeneous stratum or halfspace. Some information is also given for vertical oscillations, and for pile-soil-pile dynamic interaction factors.

Since it was observed in the verification projects of the KU Leuven (8.1.2 ‘Verification Project Degrande et al. (2) – Soil Building’) that estimating the layered soil stratum as a homogeneous halfspace can give reliable results, also the layered soil stratum used for the EDDABuSGS-tool is approximated as a homogeneous halfspace (see 10.3.3 Soil response in Amsterdam). With this assumption the tables 15.1, 15.2 and 15.6 and the accompanying graphs are used to determine the impedances of the rigid building structure.

Table 15.1: Arbitrary shaped foundation on the surface of a homogeneous halfspace

The tables of Gazetas are used first to find the static stiffness 'K' for every vibration mode of interest for a structure laying on top of a homogeneous halfspace, without pile foundation (most left figure of Figure 179). The other tables, to compute the impedances in case of an embedded structure or in case of a pile foundation (middle and right figures of Figure 179), refer to table 15.1 and perform certain computations on it (multiplication by or adding a factor). Then the dynamic stiffness coefficient 'k' and dynamic dashpot coefficient 'c' are computed based on the accompanying graphs (Figure 180).

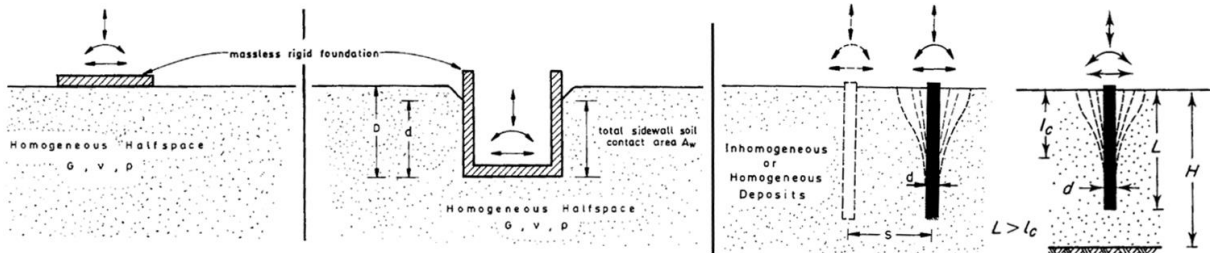


Figure 179. Geometrical assumptions for computing the SSI impedances for left: table 15.1, middle: table 15.2, right: table 15.6 (Gazetas G., 1991)

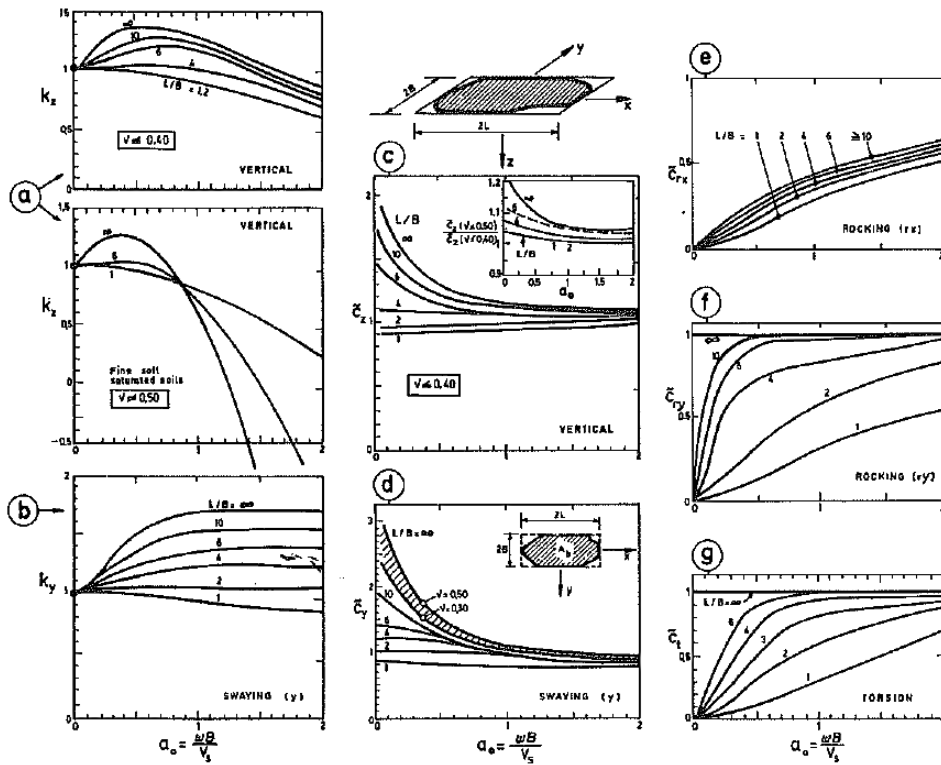


Figure 180. Graphs accompanying table 15.1, illustrating the frequency dependency (horizontal axes) of the stiffness- and dashpot coefficients (vertical axes) (Gazetas G., 1991)

The total dynamic stiffness ($\bar{K}_j(\omega)$) is computed by multiplying the dynamic stiffness coefficient with the static stiffness. The total dynamic damping ($C_j(\omega)$) is computed by multiplying the dashpot coefficient with the static properties of the soil (ρ, C_s, v) and the geometrical properties of the structure ($2B, 2L$) and by adding the term $2 \cdot \bar{K}_j(\omega) / \omega \cdot \beta$, where β is the damping ratio of the homogeneous soil. Thus in symbols the impedance terms are computed as:

$$\mathbb{K}_j(\omega) = \bar{K}_j(\omega) + i\omega C_j(\omega) \tag{0.97}$$

$$\bar{K}_j(\omega) = K_{static} \cdot k(\omega) \quad (0.98)$$

$$C_j(\omega) = c(\omega) \cdot \rho \cdot f(C_s, v) \cdot g(B, L) + 2 \cdot \frac{\bar{K}_j(\omega)}{\omega} \cdot \beta \quad (0.99)$$

where $f(C_s, v)$ is a function of both C_s and v ($V_{La}(C_s, v)$) in case of the vertical- and rocking impedances or depends solely on C_s in case of the horizontal impedances and where $g(B, L)$ is equal to A_b (the effective surface area of the foundation basemat) in case of the translational impedances or is equal to I_{bj} where I_{bj} is the inertia of the soil, computed as: $\frac{1}{12} \cdot 2L \cdot (2B)^3$ (depending on the orientation of the building L and B should be interchanged) in case of the rocking impedances.

Table 15.2: Arbitrary shaped foundation, partially or fully embedded in a homogeneous halfspace

The expressions given in table 15.2 refer to table 15.1 and perform certain multiplications on it to derive the impedances in case the structure is embedded in a homogeneous halfspace. The following computations are performed for the different stiffness and dashpot terms:

- The static stiffnesses of table 15.2 are computed by factorizing the static stiffness of table 15.1 (for zero embedment of the foundation).
- The dynamic stiffness coefficients in the vertical (z-) direction, for the rocking modes and for the torsional mode are computed by factorizing the dynamic stiffness coefficients of table 15.1.
- The dynamic stiffness coefficients in the horizontal (x- and y-) directions of table 15.2 are computed by using the accompanying graphs with this table.
- The dynamic dashpot coefficients of table 15.2 are computed by factorizing or adding (depending on which vibration mode) the dynamic dashpot coefficients of table 15.1.

Table 15.6: Flexible single piles (in this thesis considered within a homogeneous halfspace)

The expressions given are only for estimates of the stiffness of floating piles (so no end-bearing) in a homogeneous stratum of total thickness $H = 2L$ (where L is the length of the pile).

- The static axial-, lateral- and rocking stiffnesses computed with table 15.6 are based on the geometrical- and material properties of the pile and on the material properties of the soil.
- The dynamic axial stiffness coefficients are based on the geometrical properties of the pile.
- The dynamic axial radiation dashpot coefficients are based on the geometrical- and material properties of the pile and the material properties of the soil.
- For floating pile groups, interaction factors are given for axial in-phase oscillations of two piles. These factors depend on the frequency of excitation, the centre-to-centre distance of the piles, the geometrical properties of the piles and material properties of the soil.

1.2. Practical Use of the Tables

As one can see from the figures accompanying the tables of Gazetas (Figure 180), the use of the graphs are bounded by a maximum value of $a_0 = \omega B / C_s = 2$, where ω is the excitation frequency, B is the half width of the building (shortest side) and C_s is the shear wave speed of the soil. The problem statement of this thesis concerns heavy road traffic induced vibrations for laboratory buildings in The Netherlands. This means that values for the mentioned parameters might be within the following ranges:

$$\begin{aligned} 0 \text{ Hz} < f < 15 \text{ Hz}, \quad \text{thus: } 0 \text{ rad/s} < \omega < 95 \text{ rad/s} \\ 2 \text{ m} < B < 15 \text{ m} \\ 150 \text{ m/s} < C_s \end{aligned} \quad (0.100)$$

which might reasonably lead to values of a_0 up to $95 \text{ rad/s} \cdot 15 \text{ m} / 150 \text{ m/s} = 9.5 \text{ rad}$, which is far out of the bounds of the graphs. In order to make the tables of Gazetas applicable for the problems of interest for this thesis, the graphs accompanying the tables of Gazetas need to be extrapolated.

Assumptions needed for extrapolation of the graphs accompanying the tables of Gazetas

Before extrapolating the graphs accompanying the tables of Gazetas, first the graphs are addressed which accompany the tables concerning a soil layer overlaying a bedrock (Figure 181). Tables 15.3 and 15.4 consider the presence of a bedrock underneath a soil layer. The accompanying graphs clearly show the strong oscillations in the determination of the frequency dependent stiffness coefficients (Figure 182). These oscillations are due to resonance phenomena in the soil layer, at which the excitation frequency is very close to the natural frequency of the soil layer overlaying the bedrock. Due to reflections of the propagating waves at the interface between the overlaying soil layer and the bedrock, and between the bottom of the foundation and the soil, the dynamic stiffnesses vary greatly with the excitation frequency. This means that extrapolating these figures will bring unreliable results, since it is not known how the figures develop for higher excitation frequencies. However, in case of a homogeneous halfspace, no such resonances can occur, because no reflections take place at a bedrock, since no bedrock exists. Extrapolation of the figures for homogeneous halfspaces is therefore much easier and more intuitive: the figures reach a certain asymptote for higher values of excitation frequency.

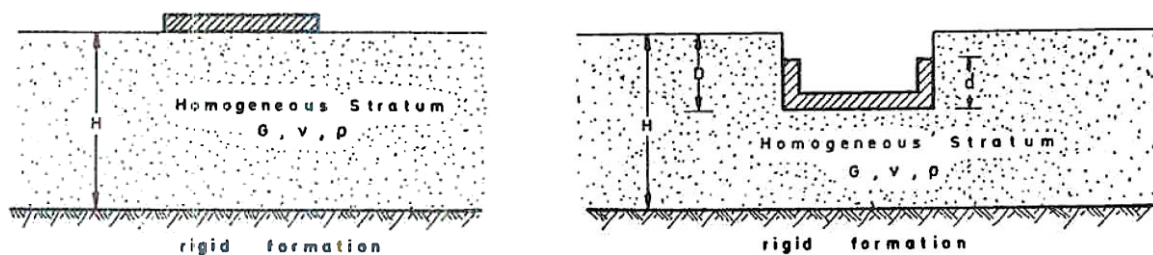


Figure 181. Structure with variable embedment in a soil layer overlaying a bedrock, left: table 15.3, right: table 15.4 (Gazetas G. , 1991)

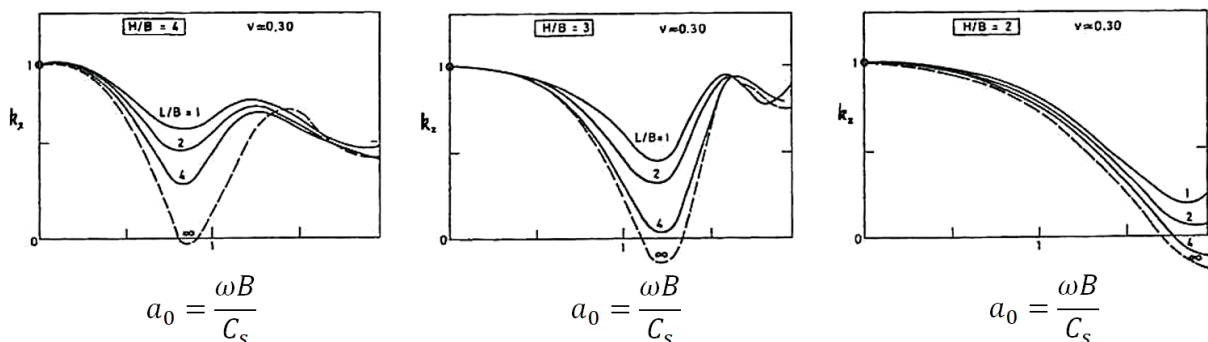


Figure 182. Part of the graphs accompanying table 15.3 for computing the dynamic stiffness coefficient in the vertical (z-) direction including the consideration of a bedrock underneath the soil layer with height H (Gazetas G. , 1991)

In the Netherlands, however, reality is in-between both extremes: no real bedrock is present (which would reflect all incoming waves), but soil layer interfaces are present within soil layers with different stiffness ratios which partly reflect the incoming waves. These partial reflections might also give rise to some kind of resonance phenomena. Therefore, if the engineer is looking for more reliable results for a specific soil layering, where the soil layer stiffness abruptly changes significantly, the engineer should compute the figures himself in a similar

manner as Gazetas did, but now for the particular layered soil stratum of interest. This will ask for a great amount of computations, and thus a long computational time. However, since the research of the present thesis is about a practical engineering tool, the assumption of a homogeneous halfspace for the soil in The Netherlands will be used which makes that extrapolation of the figures of Gazetas is possible.

Curve fitting for extrapolation of the graphs accompanying the tables of Gazetas

The numerical Python software will be used for the extrapolation of the graphs accompanying the tables of Gazetas in case of a homogeneous halfspace. Python has the possibility to use the function ‘curve fitting’ which sounds promising for extrapolating the tables of Gazetas. This function uses a given form of a function with certain unknown parameters, e.g. $a \cdot \tan^{-1}(b \cdot a_0 + c)$ (needs to be given by the script developer) and a set of point coordinates through which the graph needs to fit. The number of point coordinates should be equal to- or larger than number of unknown parameters in order for Python to find a solution for the unknowns. This method has been used to extrapolate most of the graphs. Two examples are given in Figure 183 and Figure 184. By using this method, a continuous function is derived which will give a value for the stiffness- or dashpot coefficient based on any possible input value a_0 .

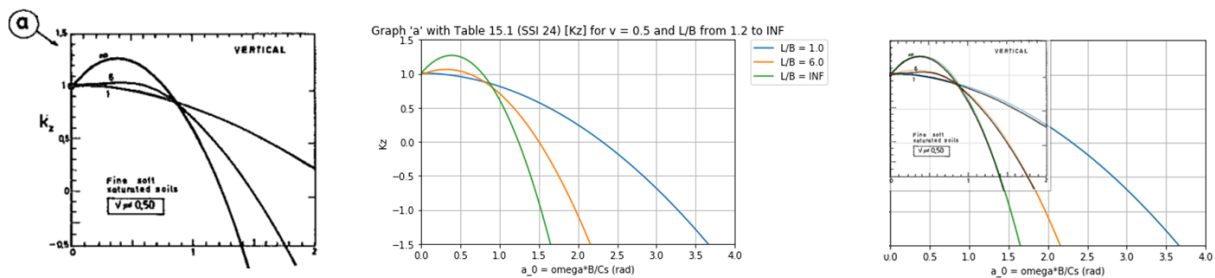


Figure 183. Graph a accompanying table 15.1, left: Gazetas (Gazetas G. , 1991), middle: extrapolated, right: both graphs in one

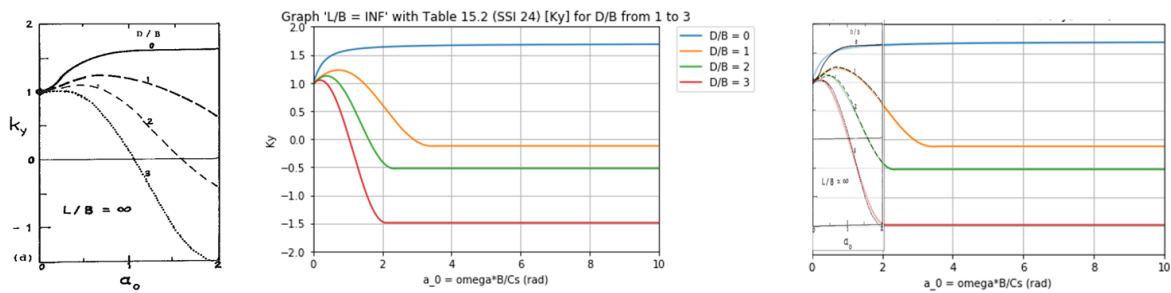


Figure 184. Graph k_y , $L/B = \infty$ accompanying table 15.2, left: Gazetas (Gazetas G. , 1991), middle: extrapolated, right: both graphs in one

L. Appendix: Additions to Chapter 12 ‘Receiving Structural System Modelling and Results’

1.1. Global Dynamic Response of the 3DoF Rigid Building

1.1.1. Structural parameters

The structural properties of the 3DoF global building are gathered into two parameters: M_b (total mass of the building) and J_{CG} (total mass moment of inertia around the centre of gravity (CG) in the (x,z) -plane) (Figure 186). A simplification taken into account for the computation of the structural properties is that the building is symmetric around the two vertical planes and that all floor spans and wall thicknesses in one plane are equal (Figure 185).

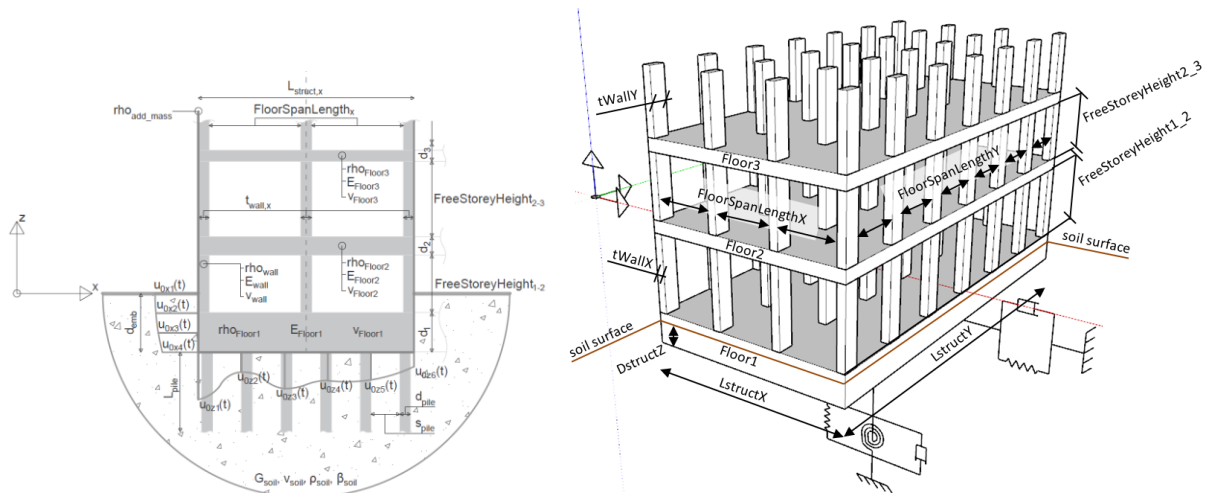


Figure 185. Simplified model for the computation of the parameters needed for the dynamic response of the 3DoF building

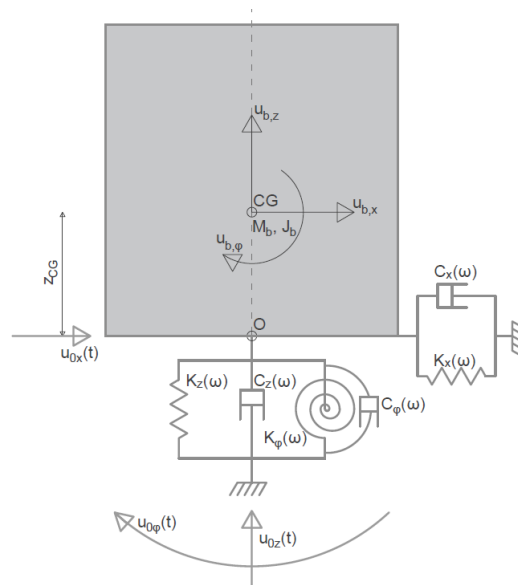


Figure 186. Simplified dynamical model which is used to set up the equations of motion for the rigid 3DoF building

M_b is composed of the masses of all structural floors, walls/columns and a mass component to take into account the extra mass of the non-structural elements (e.g. facades, internal walls):

$$M_b = \sum_{j=1}^{N_{fl}} \rho_{fl,j} \cdot l_{fl,j} \cdot w_{fl,j} \cdot h_{fl,j} + \sum_k^{N_w} \rho_{w,k} \cdot t_{w,x,k} \cdot t_{w,y,k} \cdot h_{w,k} + \rho_{add_mass} \cdot l_{struct,x} \cdot l_{struct,y} \cdot h_{struct,z} \quad (0.101)$$

where:

M_b	= total mass of building	[kg]
N_{fl}	= total number of floors	[-]
$\rho_{fl,j}$	= mass density of floor 'j'	[kg/m ³]
$l_{fl,j}$	= length of floor 'j' (or building length in x-direction)	[m]
$w_{fl,j}$	= width of floor 'j' (or building length in y-direction)	[m]
$h_{fl,j}$	= height of floor 'j' (in z-direction)	[m]
N_w	= total number of walls and columns	[-]
$\rho_{w,k}$	= mass density of wall 'k'	[kg/m ³]
$t_{w,x,k}$	= length (or thickness) of wall or column 'k' in x-direction	[m]
$t_{w,y,k}$	= length (or thickness) of wall or column 'k' in y-direction	[m]
$h_{w,k}$	= height of wall or column 'k' in z-direction	[m]
ρ_{add_mass}	= mass density of additional (non-structural) mass (total additional mass divided by total building volume)	[kg/m ³]
$l_{struct,x}$	= length of the building in x-direction	[m]
$l_{struct,y}$	= length of the building in y-direction	[m]
$h_{struct,z}$	= height of the building in z-direction	[m]

While J_{CG} is composed of the summation of the mass moment of inertias of all structural elements and a mass moment of inertia component of the additional non-structural mass. The numerical Python script is written in such a way that first all individual mass moments of inertia are taken around the rotation point 'O,' which is located at the basemat of the foundation, where the vertical line of symmetry passes through (at the centre of the foundation-soil interface). This computation will lead to the parameter J_O (mass moment of inertia around point 'O' and can be represented mathematically as:

$$J_O = \sum_{j=1}^{N_{fl}} \frac{1}{12} \cdot m_{fl,j} \cdot (l_{fl,j}^2 + h_{fl,j}^2) + m_{fl,j} \cdot (X_{O,fl,j}^2 + Z_{O,fl,j}^2) + \sum_{k=1}^{N_w} \frac{1}{12} \cdot m_{w,k} \cdot (t_{w,x,k}^2 + h_{w,k}^2) + m_{w,k} \cdot (X_{O,w,k}^2 + Z_{O,w,k}^2) + \frac{1}{12} \cdot m_{add_mass} \cdot (l_{struct,x}^2 + h_{struct,z}^2) + m_{add_mass} \cdot (X_{O,struct}^2 + Z_{O,struct}^2) \quad (0.102)$$

where:

J_O	= total mass moment of inertia of the building around point O	[kgm ²]
N_{fl}	= total number of floors	[-]
$m_{fl,j}$	= total mass of floor 'j' ($\rho_{fl,j} \cdot l_{fl,j} \cdot w_{fl,j} \cdot h_{fl,j}$)	[kg]
$l_{fl,j}$	= length of floor 'j' (or building length in x-direction)	[m]
$h_{fl,j}$	= height of floor 'j' (in z-direction)	[m]
$X_{O,fl,j}$	= horizontal distance (x-direction) between centre of gravity of floor 'j' and point O	[m]
$Z_{O,fl,j}$	= vertical distance (z-direction) between centre of gravity of floor 'j' and point O	[m]

N_w	= total number of walls and columns	[-]
$m_{w,k}$	= total mass of walls or columns 'k' where all elements on the same storey and on the same y-axis are summed ($\rho_{w,k} \cdot t_{w,x,k} \cdot (\sum_{s=1}^{N_{w,y}} t_{w,y,k,s}) \cdot h_{w,k}$)	[kg]
$t_{w,x,k}$	= length (or thickness) of wall or column 'k' in x-direction	[m]
$h_{w,k}$	= height of wall or column 'k' in z-direction	[m]
$X_{O,w,k}$	= horizontal distance (x-direction) between centre of gravity of wall or column 'k' and point O	[m]
$Z_{O,w,k}$	= vertical distance (z-direction) between centre of gravity of wall or column 'k' and point O	[m]
m_{add_mass}	= total additional (non-structural) mass ($\rho_{add_mass} \cdot l_{struct,x} \cdot l_{struct,y} \cdot h_{struct,z}$)	[kg/m ³]
$l_{struct,x}$	= length of the building in x-direction	[m]
$h_{struct,z}$	= height of the building in z-direction	[m]
$X_{O,struct}$	= horizontal distance (x-direction) between centre of gravity of the total additional mass and point O	[m]
$Z_{O,struct}$	= vertical distance (z-direction) between centre of gravity of the total additional mass and point O	[m]

After the computation of J_O the centre of gravity (CG) is computed for the total building. First all masses of every element are multiplied by their lever arm with respect to the point O . Then this value is divided by the summation of all masses. In a mathematical expression this looks as follows:

$$Z_{CG} = \frac{\sum_{j=1}^{N_{fl}} m_{fl,j} \cdot Z_{O,fl,j} + \sum_{k=1}^{N_w} m_{w,k} \cdot Z_{O,w,k} + m_{add_mass} \cdot Z_{O,struct}}{M_b = \sum_{j=1}^{N_{fl}} m_{fl,j} + \sum_{k=1}^{N_w} m_{w,k} + m_{add_mass}} \quad (0.103)$$

Since the assumption is that the building design is symmetrical around a vertical axis, the horizontal coordinate of the centre of gravity is on the line of symmetry. Now that the centre of gravity is determined, J_{CG} can be computed as:

$$J_{CG} = J_O - M_b \cdot Z_{CG}^2 \quad (0.104)$$

1.1.2. Excitation

The excitation on the 3DoF system is derived from the soil response of one particular situation as described in chapter 10 'Transmission'. The vertical excitation(s are taken as) is taken as an average of the vertical soil response at multiple points in the soil over the building length:

$$u_{0z} = \frac{\sum_i^{N_{uz}} u_{0z,i}}{N_{uz}} \quad (0.105)$$

Also for the horizontal excitations an average is taken of the horizontal soil responses at multiple points over the embedment depth of the building:

$$u_{0x} = \frac{\sum_i^{N_{ux}} u_{0x,i}}{N_{ux}} \quad (0.106)$$

The rocking excitation is taken as a rotation around the centre of gravity CG of the building and is computed as:

$$u_{0\varphi} = \frac{\sum_j^{N_{ux}} \frac{u_{0x,j}}{z_{CG,j}}}{N_{ux}} - \frac{\sum_i^{N_{uz,l}} \frac{u_{0z,i}}{x_{CG,i}}}{N_{uz,l}} + \frac{\sum_i^{N_{uz,r}} \frac{u_{0z,i}}{x_{CG,i}}}{N_{uz,r}} \quad (0.107)$$

where:

$u_{0\varphi}$	= rotational excitation	[kgm ²]
N_{ux}	= number of points of horizontal soil response over the embedment depth of the building	
$u_{0x,j}$	= horizontal soil response at point 'j'	
$z_{CG,j}$	= vertical distance between horizontal soil response at point 'j' and the centre of gravity	
$N_{uz,l}$	= number of points of vertical soil response over the length of the building at the left side from the vertical symmetry line	
$u_{0z,i}$	= vertical soil response at point 'i'	
$x_{CG,i}$	= horizontal distance between vertical soil response at point 'i' and the vertical symmetry line	
$N_{uz,r}$	= number of points of vertical soil response over the length of the building at the right side from the vertical symmetry line	

These excitations act on the springs and dashpots supporting the 3DoF system. The compression or extension of the springs and dashpots due to the imposed displacements and rotations causes dynamic forces to act on the 3DoF system. The dynamic forces are generally in the form of a Fourier expansion and are composed of a summation of cosines and sines:

$$F_i(t) = \sum_{j=1}^N [F_{i,c,j} \cos(k_{y_j} \cdot t) + F_{i,s,j} \sin(k_{y_j} \cdot t)] \quad (0.108)$$

1.1.3. Expressions of the building response in the direction of a degree of freedom

In chapter 5 'Structural System (Receiver of Vibrations)' it was already explained how the dynamic response of a multi-degrees of freedom system can be computed when the system is excited by a harmonic force in a particular direction. The computation of the dynamic response of the 3DoF rigid building motion due to a single harmonic force is in the exact same manner. In order to compute the total dynamic response of the 3DoF rigid building motion in every degree of freedom, the response of the degree of freedom due to all individual harmonic loading terms in the direction of all the degrees of freedom should be added:

$$\begin{aligned} u_{b,x}(t) &= \sum_{i=x,z,\varphi} u_{b,x,i}(t) = \sum_{i=x,z,\varphi} \left(\sum_{j=1}^N u_{b,x,i,j}(t) \right) \\ u_{b,z}(t) &= \sum_{i=x,z,\varphi} u_{b,z,i}(t) = \sum_{i=x,z,\varphi} \left(\sum_{j=1}^N u_{b,z,i,j}(t) \right) \\ u_{b,\varphi}(t) &= \sum_{i=x,z,\varphi} u_{b,\varphi,i}(t) = \sum_{i=x,z,\varphi} \left(\sum_{j=1}^N u_{b,\varphi,i,j}(t) \right) \end{aligned} \quad (0.109)$$

where:

$u_b(t)$	= the time-instant dependent building response given in the form as either displacements, velocities or accelerations	[m], [m/s] or [m/s ²]
$u_{b,x}(t)$	= total building response in the translational degree of freedom $u_{b,x}$	
$u_{b,x,i}(t)$	= building response in the translational degree of freedom $u_{b,x}$ due to all loading terms in the direction of the degree of freedom	

- $u_{b,i}$ ($i = x, z, \varphi$) = building response in the translational degree of freedom $u_{b,x}$ due to loading term j ($j = 1, 2, \dots, N$) in the direction of the degree of freedom $u_{b,i}$ ($i = x, z, \varphi$)
- $u_{b,x,i,j}(t)$ = total building response in the translational degree of freedom $u_{b,x}$ due to all loading terms in the direction of the degree of freedom $u_{b,i}$ ($i = x, z, \varphi$)
- $u_{b,z}(t)$ = building response in the translational degree of freedom $u_{b,z}$ due to loading term j ($j = 1, 2, \dots, N$) in the direction of the degree of freedom $u_{b,i}$ ($i = x, z, \varphi$)
- $u_{b,z,i,j}(t)$ = total building response in the translational degree of freedom $u_{b,z}$ due to all loading terms in the direction of the degree of freedom $u_{b,i}$ ($i = x, z, \varphi$)
- $u_{b,\varphi}(t)$ = building response in the translational degree of freedom $u_{b,\varphi}$ due to loading term j ($j = 1, 2, \dots, N$) in the direction of the degree of freedom $u_{b,i}$ ($i = x, z, \varphi$)
- $u_{b,\varphi,i,j}(t)$ = total building response in the translational degree of freedom $u_{b,\varphi}$ due to all loading terms in the direction of the degree of freedom $u_{b,i}$ ($i = x, z, \varphi$)

1.2. Local Dynamic Response of Flexible Floor

The dynamic response of the bottom storey floor is of particular interest, because the vibration sensitive equipment is generally placed either on the foundation slab or the first storey floor. For this thesis a flexible frame is used to compute the dynamic response of the storey floor of interest, named 'w₁' (Figure 187 and Figure 188). The flexible frame takes into account adjacent elements of w₁ as well to consider their influence on the dynamic response of w₁ (e.g. rotation stiffness at the boundaries of w₁ and the influence of the horizontal excitation on the vertical dynamic response of w₁). Since the response of interest of the local floor is the dynamic response, described more particular: the dynamic velocity, the gravity loading does not play a role, because the gravity loading is only static. Therefore, the gravity loading is not taken into account for the computation of the dynamic response flexible frame.

1.2.1. The composition of the flexible frame

The flexible frame is composed of four (undamped) Euler-Bernoulli beam floor elements: w₁, w₂, w₃, w₄ and four Euler-Bernoulli beam wall/column elements: u₁, u₂, u₃, u₄. The principle of an Euler-Bernoulli beam (EB-beam) element was discussed in 5.5 'Continuous Systems'. Figure 187 is repeated from 5.5 'Continuous Systems' and gives a typical presentation of an EB-beam.

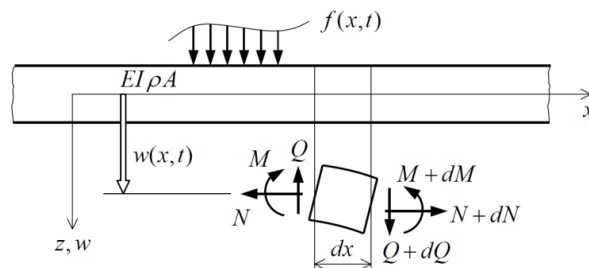


Figure 187. Typical representation of an EB-beam element

The dynamical properties of every EB-beam element consist of $EI_{i,j}$ (Nm²), $\rho_{i,j}$ (kg/m³) and $A_{i,j}$ (m²) where: ($i = w, u$) and ($j = 1, 2, 3, 4$). The dynamic response of every EB-beam element is computed as its displacement (depending on time and the longitudinal coordinate of the

element) perpendicular to the longitudinal axis of the element: $w_j(x, t)$ and $u_j(z, t)$ with ($j = 1, 2, 3, 4$). All EB-beam elements are assumed as being inextensible (i.e. $EA = \infty$).

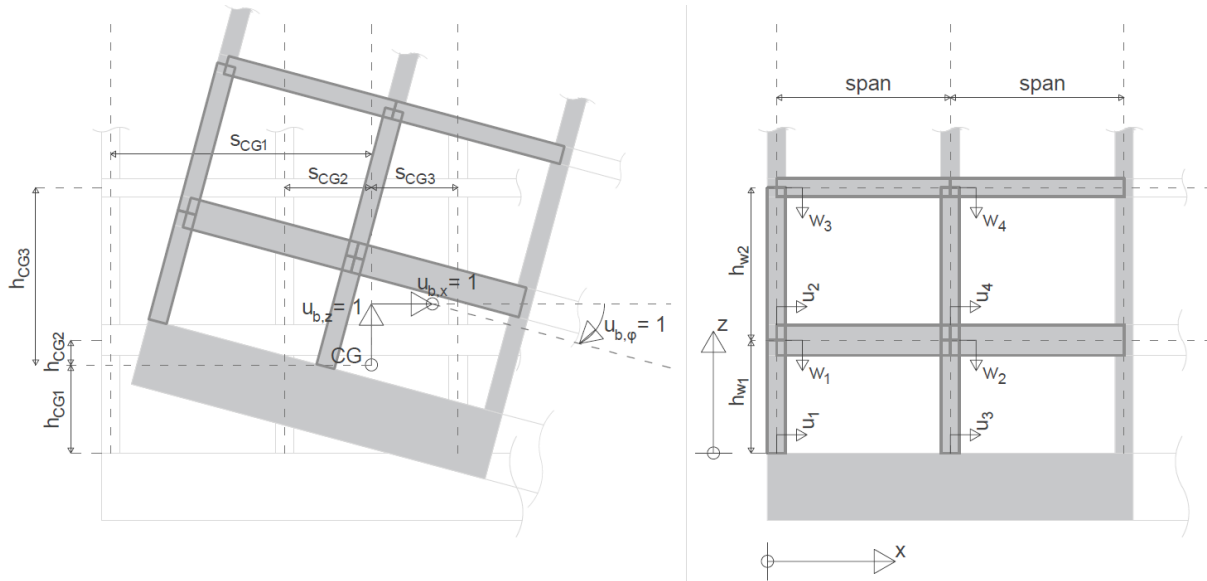


Figure 188. Principles for the flexible frame for computation of the local dynamic response of w_1 . Left: displaced flexible frame due to rigid building movement of 3DoF system. Right: flexible frame composed of four flexible Euler-Bernoulli beam floor elements w_1, w_2, w_3, w_4 and four flexible Euler-Bernoulli beam wall/column elements u_1, u_2, u_3, u_4

The equation of motion (EOM) of an EB-beam element consists of a fourth-order differential equation:

$$EI_{w,i} \frac{\delta^4 w_i(x, t)}{\delta x^4} + \rho A_{w,i} \frac{\delta^2 w_i(x, t)}{\delta t^2} = 0$$

or

$$EI_{u,i} \frac{\delta^4 u_i(z, t)}{\delta z^4} + \rho A_{u,i} \frac{\delta^2 u_i(z, t)}{\delta t^2} = 0$$

(0.110)

where ($i = 1, 2, 3, 4$).

The unknowns in the general solutions of the fourth-order differential equations (this will be further explained in 1.2.2 'Finding the response of the flexible frame') need to be solved with the aid of the Boundary Conditions (BCs) of the element. Every EB-beam element needs two BCs at the start-coordinate of the element and two BCs at the end-coordinate of the element. The BCs for a simply supported EB-beam element and for a cantilever EB-beam element were already given in 5.5 'Continuous Systems'. However, at the nodes where one EB-beam element is connected to another EB-beam element, Interface Conditions (ICs) are needed instead. The ICs make sure that the dynamic response of one EB-beam element is compatible with the dynamic response of the connecting EB-beam element(s). For example, in case two EB-beam elements are connected to each other, this interface needs 4 ICs (2 conditions for both element-ends).

The flexible frame is rigidly fixed to the foundation slab which has a dynamical response equal to the 3DoF rigid building response computed in the previous section. This makes that the flexible frame for this thesis research is excited by the rigid building motion of the 3DoF system only. The BCs and ICs are such that they are compatible with the 3DoF rigid building

motion and such that they make sure that the flexible frame is internally in equilibrium (Figure 189).

The dynamic response of the flexible EB-beam frame is solved as a summation of the dynamic responses of the frame due to all prescribed horizontal and vertical displacements and all prescribed rotations. In formula form this summation would look like:

$$\text{Dyn_response} = \text{Dyn_response}_{u_{b,x}} + \text{Dyn_response}_{u_{b,z}} + \text{Dyn_response}_{u_{b,\varphi}} \quad (o.111)$$

Where the BCs and ICs for every Dyn_response_i ($i = u_{b,x}, u_{b,z}, u_{b,\varphi}$) can be different. All BCs and ICs per Dyn_response_i are given in Appendix P ‘Appendix: Boundary- and Interface conditions of the three **Models**_{*x,z,φ*}’ (referenced as Model_{*x*}, Model_{*z*} and Model_{*φ*} respectively). A combination of them all, giving the most interesting BCs and ICs, is presented in Figure 189. Note that the combination of BCs and ICs given in Figure 189 is not correct for the computation of the dynamic response of the frame and should be subdivided as presented in Appendix P, otherwise a non-singular matrix needs to be solved which should not be the case for the current problem.

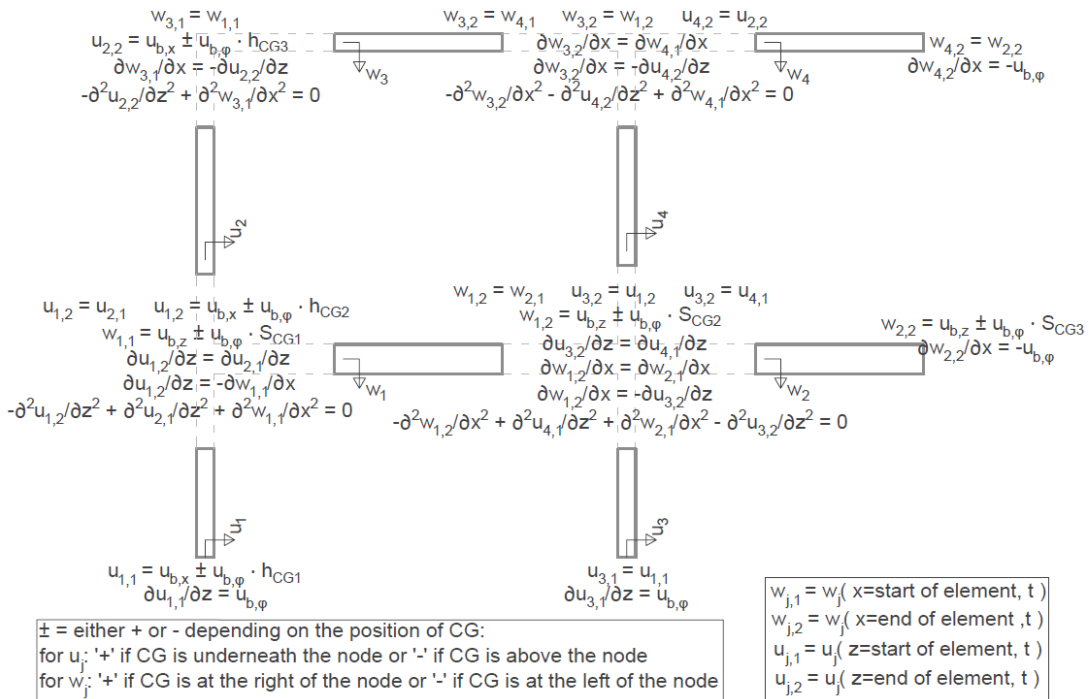


Figure 189. Combination of most interesting Interface- and Boundary Conditions of the flexible EB-beam frame, excited by the prescribed time dependent rigid building motion of the 3DoF system. The ICs and BCs per rigid body excitation (x, z, φ), as implemented in the Python script, can be found in Appendix P

Two BCs are needed at every node at which only one EB-beam element is connected. Four ICs are needed for the nodes with two EB-beam elements, six ICs for the nodes with three EB-beam elements and eight ICs for the nodes with four EB-beam elements. Some BCs and ICs are described with a ‘ \pm ’ sign. This means that either a ‘+’ or a ‘-’ needs to be considered here, based on the position of the centre of gravity (CG) of the global building with respect to the node of interest: the horizontal displacement due to the rocking motion is positive in case CG is underneath the node and is negative in case CG is above the node. The vertical displacement due to the rocking motion is positive in case CG is to the right of the node and is negative in case CG is to the left of the node. Some examples are presented in Figure 190.

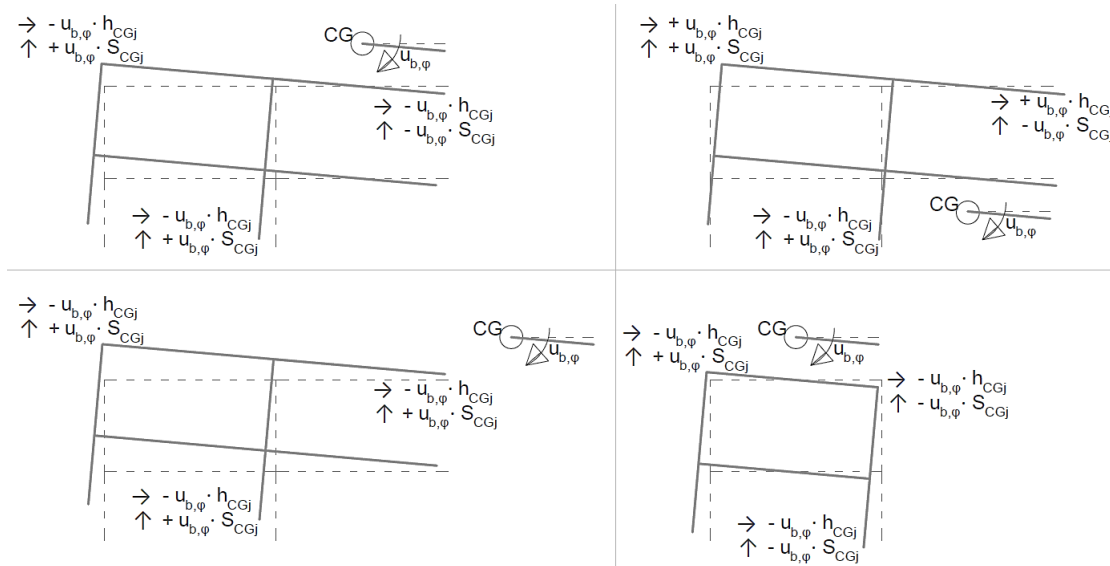


Figure 190. Some examples for determining whether the rocking motion generates a positive or negative horizontal and vertical displacement of a particular node in the frame based on the position of the centre of gravity (CG)

1.2.2. Finding the response of the flexible frame

The steady-state solution of the EB-beam has the same time signatures as that of the excitation and since the excitation (the rigid 3DoF building motion) is a summation of harmonics with time signatures $\cos(k_{y_j} \cdot t)$ and $\sin(k_{y_j} \cdot t)$, the steady-state solution of the EB-beams is also composed of these time signatures:

$$w_i(x, t) = \sum_{j=1}^N W_{i,c,j}(x) \cdot \cos(k_{y_j} \cdot t) + W_{i,s,j}(x) \cdot \sin(k_{y_j} \cdot t) \quad \text{or} \quad (0.112)$$

$$u_i(z, t) = \sum_{j=1}^N U_{i,c,j}(z) \cdot \cos(k_{y_j} \cdot t) + U_{i,s,j}(z) \cdot \sin(k_{y_j} \cdot t)$$

Where ($i = 1, 2, 3, 4$) and ($j = 1, 2, \dots, N$).

By inserting the steady-state solutions of the EB-beams into the EOMs, BCs and ICs and gathering the terms proportional to $\cos(k_{y_j} \cdot t)$ and $\sin(k_{y_j} \cdot t)$, $6N$ boundary-value problems are obtained: $3N$ boundary-value problems for all terms proportional to $\cos(k_{y_j} \cdot t)$ (N boundary-value problems for every Model_{*U*} ($U = x, z, \varphi$)) and $3N$ boundary-value problems for all terms proportional to $\sin(k_{y_j} \cdot t)$ (N boundary-value problems for every Model_{*U*} ($U = x, z, \varphi$)). The software 'Maple' is used to derive the boundary-value problems and to solve the typical boundary-value problems related to the $\cos(k_{y_j} \cdot t)$ terms for every Model_{*U*} (see Appendices Q, R and S for the elaboration of the boundary-value problem of the flexible EB-beam frame for the terms proportional to the $\cos(k_{y_1} \cdot t)$ terms). Every boundary-value problem is solved as a multiplication of the inversed coefficient matrix (derived from the BCs and ICs) and the loading vector. The procedure for each of the $6N$ boundary-value problems can be summarized as follows:

By substituting the steady-state solution into the EOM, the following remains:

The matrix and vectors can be written in letter-form as:

$$\underline{A}_{coeff} * \underline{B}_{coeff} = \underline{F} \quad (0.119)$$

where \underline{A}_{coeff} is the coefficient matrix, \underline{B}_{coeff} is the vector containing all 32 unknowns of one boundary-value problem and \underline{F} is the loading vector. The IC $\left(\frac{du_{3,2}}{dz} = \frac{du_{4,1}}{dz}\right)$ with substituted general solutions as described before can be written in line with the matrix notation as:

$$\begin{aligned} & (c_{15,25} \cdot A_{u,3,g,j} + c_{15,26} \cdot B_{u,3,g,j} + c_{15,27} \cdot C_{u,3,g,j} + c_{15,28} \cdot D_{u,3,g,j}) - \\ & (c_{15,29} \cdot A_{u,4,g,j} + c_{15,30} \cdot B_{u,4,g,j} + c_{15,31} \cdot C_{u,4,g,j} + c_{15,32} \cdot D_{u,4,g,j}) = f_{15} \end{aligned} \quad (0.120)$$

Where, for example, $c_{15,25} = \beta_{u3,g,j} \cdot \sinh(\beta_{u3,g,j} \cdot z)$ and $c_{15,31} = -\beta_{u4,g,j} \cdot \sin(\beta_{u4,g,j} \cdot z)$ and $f_{15} = 0$. The vector \underline{B}_{coeff} is solved by the multiplication of the inversed coefficient matrix with the loading vector:

$$\underline{B}_{coeff} = \underline{A}_{coeff}^{-1} * \underline{F} \quad (0.121)$$

This procedure is done (numerically in Python) for all $6N$ boundary-value problems which makes that all unknowns of $W_{i,g,j}(x)$ and $U_{i,g,j}(z)$ are known now and thus the steady-state solutions $w_i(x, t)$ and $u_i(z, t)$ (displacements) have been found ($i = 1, 2, 3, 4$). As already mentioned before, particular interest exists for the response $w_1(x, t)$, $0 < x < \text{span}$, which has a dynamic response with the same time signatures as the excitation (the 3DoF rigid building motion), however the amplitudes of the response are altered due to the structural properties of the flexible frame ($EI_{i,j}$ (Nm²), $\rho_{i,j}$ (kg/m³), $A_{i,j}$ (m²)).

1.2.3. Finding the response of the foundation slab in the same form as the VC-curves

The described procedure for computing the local dynamic response heavily focusses on the storey floor w_1 . However, also the local dynamic response of the foundation slab can be computed by this model. Depending on the stiffness of the foundation slab the dynamic response of the foundation slab is either equal to the dynamic response of the, in the previous section, computed 3DoF rigid building response (stiffness of foundation slab is very high) or can be derived from the flexible EB-beam frame by taking infinitely stiff wall/column elements ($EI_{u1} = \infty$ and $EI_{u3} = \infty$) and by choosing a floor span equal to a suitable centre-to-centre distance of the foundation piles (stiffness of foundation slab is not sufficient to be considered as being rigid). In this way the foundation slab is excited at its supports directly by the rigid 3DoF building response, without the influence of any deformations of u_1 and u_3 .

M. Appendix: Maple sheet for determining 3DoF eigenfrequencies


```

> restart;
> M_matrix := Matrix([
[M, 0, 0],
[0, M, 0],
[0, 0, J]
]);

> C_matrix := Matrix([
[Cx, 0, -Cx*z_CG],
[0, Cz, 0],
[-Cx*z_CG, 0, Cphi + Cx*z_CG^2],
]);

> K_matrix := Matrix([
[Kx, 0, -Kx*z_CG],
[0, Kz, 0],
[-Kx*z_CG, 0, Kphi + Kx*z_CG^2],
]);

> DynStiff_matrix := -omega_squared*M_matrix + K_matrix;

> with(LinearAlgebra);
> Determinant_DynStiff_matrix := Determinant(DynStiff_matrix);
Determinant_DynStiff_matrix := Kx*M^2*z_CG^2*omega_squared^2 - J*M^2*omega_squared^3 - Kx*Kz*Mz_CG^2*omega_squared^2 + J*Kz*Omega*omega_squared^2 + Kphi*M^2*omega_squared^2
- J*Kx*Kz*omega_squared - Kphi*Kx*Omega*omega_squared - Kphi*Kz*Omega*omega_squared + Kphi*Kx*Kz

> Determinant_DynStiff_matrix_v2 := Kx*M^2*z_CG^2*omega^4 - J*M^2*omega^4 - Kx*Kz*Mz_CG^2*omega^2 + J*Kz*Omega*omega^4 + Kphi*M^2*omega^4 - J*Kx*Kz*omega^2 - Kphi*Kz*M*omega^2 + Kphi*Kx*Kz;
> with(CodeGeneration);
> Python(Determinant_DynStiff_matrix_v2, resultname = "Determinant_DynStiff_matrix_v2");
Determinant_DynStiff_matrix_v2 = -J * M ** 2 * omega ** 6 + Kx * M ** 2 * z_CG ** 2 * omega ** 4 + J * Kx * M * omega ** 4 + J * Kz * M * omega *
* 4 + Kphi * M ** 2 * omega ** 4 - Kx * Kz * M * z_CG ** 2 * omega ** 2 - J * Kx * Kz * omega ** 2 - Kphi * Kx * omega ** 2 - Kphi * Kz * M *
omega ** 2 + Kphi * Kx * Kz

```

$$M_matrix := \begin{bmatrix} M & 0 & 0 \\ 0 & M & 0 \\ 0 & 0 & J \end{bmatrix} \quad (1)$$

$$C_matrix := \begin{bmatrix} Cx & 0 & -Cx_z_CG \\ 0 & Cz & 0 \\ -Cx_z_CG & 0 & Cx_z_CG^2 + Cphi \end{bmatrix} \quad (2)$$

$$K_matrix := \begin{bmatrix} Kx & 0 & -Kx_z_CG \\ 0 & Kz & 0 \\ -Kx_z_CG & 0 & Kx_z_CG^2 + Kphi \end{bmatrix} \quad (3)$$

$$DynStiff_matrix := \begin{bmatrix} -\omega^2 M + Kx & 0 & -Kx_z_CG \\ 0 & -\omega^2 M + Kz & 0 \\ -Kx_z_CG & 0 & Kx_z_CG^2 - \omega^2 J + Kphi \end{bmatrix} \quad (4)$$

$$Determinant_DynStiff_matrix := Determinant(DynStiff_matrix);$$

$$Determinant_DynStiff_matrix := Kx M^2 z CG^2 \omega^2 - J M^2 \omega^3 - Kx Kz Mz CG^2 \omega^2 + J Kz \Omega \omega^2 + Kphi M^2 \omega^2 - J Kx Kz \omega - Kphi Kx \Omega \omega - Kphi Kz \Omega \omega + Kphi Kx Kz$$

$$Determinant_DynStiff_matrix_v2 := Kx M^2 z CG^2 \omega^4 - J M^2 \omega^4 - Kx Kz Mz CG^2 \omega^2 + J Kz \Omega \omega^4 + Kphi M^2 \omega^4 - J Kx Kz \omega^2 - Kphi Kz M \omega^2 + Kphi Kx Kz;$$

$$with(CodeGeneration);$$

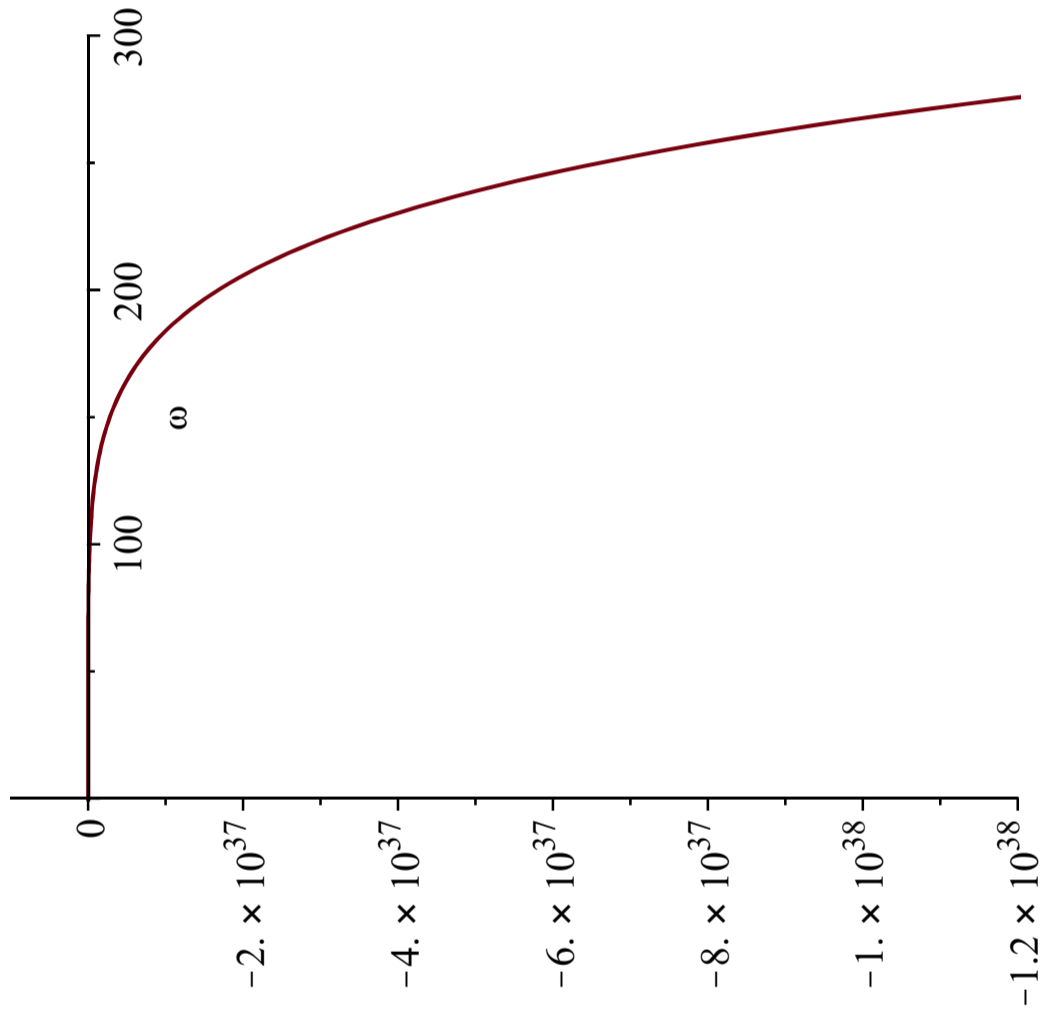
$$Python(Determinant_DynStiff_matrix_v2, resultname = "Determinant_DynStiff_matrix_v2");$$

$$Determinant_DynStiff_matrix_v2 = -J * M ** 2 * \omega ** 6 + Kx * M ** 2 * z_CG ** 2 * \omega ** 4 + J * Kx * M * \omega ** 4 + J * Kz * M * \omega *$$

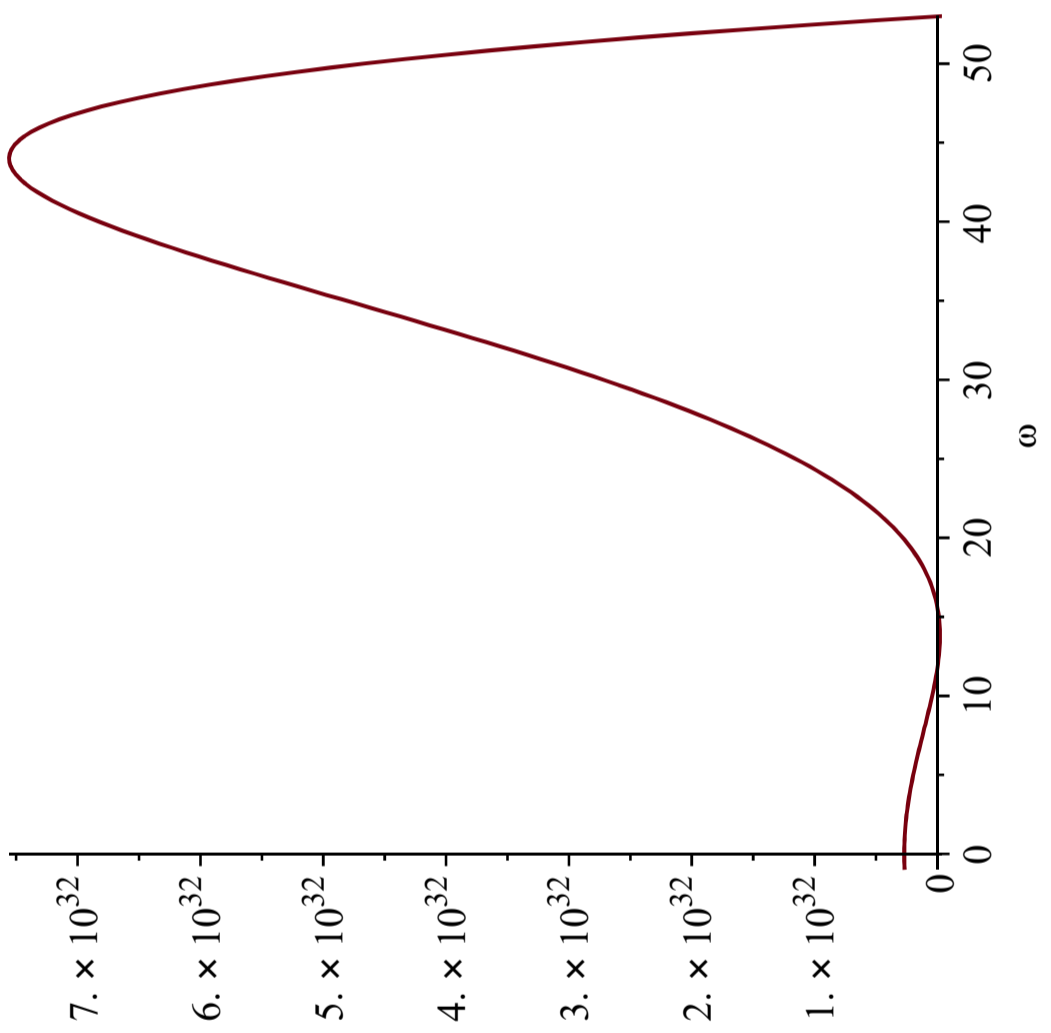
$$* 4 + Kphi * M ** 2 * \omega ** 4 - Kx * Kz * M * z_CG ** 2 * \omega ** 2 - J * Kx * Kz * \omega ** 2 - Kphi * Kx * \omega ** 2 - Kphi * Kz * M *$$

$$\omega ** 2 + Kphi * Kx * Kz$$

```
> plot( [subs(Kx = 1.5 · 1010, Kz = 0.3 · 1010, Kphi = 6 · 1011, M = 12348747, z_CG = 13.26, J = 1869944532, Determinant_DynStiff_matrix_v2)], omega = -1 .. 400);
```



```
> plot( [subs(Kx = 1.5 · 1010, Kz = 0.3 · 1010, Kphi = 6 · 1011, M = 12348747, z_CG = 13.26, J = 1869944532, Determinant_DynStiff_matrix_v2)], omega = -1 .. 53);
```



N. Appendix: Input parameters for Verification Project Degrande et al. (3) – Building Response

Input file for Python	Description
Author: Gerwin Schut	
Date: 2-9-2019	
Project: EV 5.2	

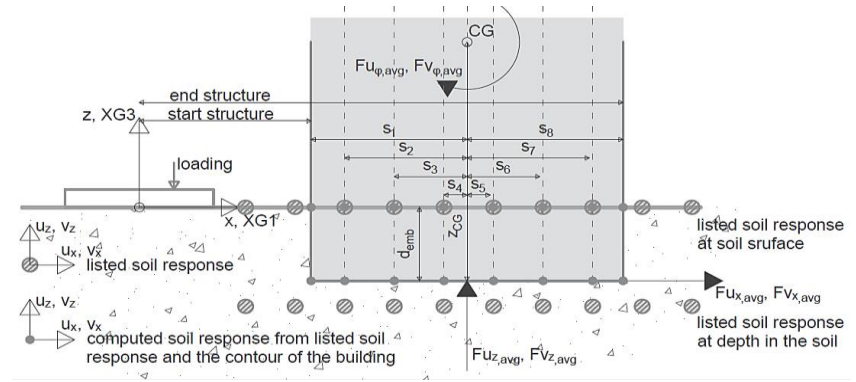
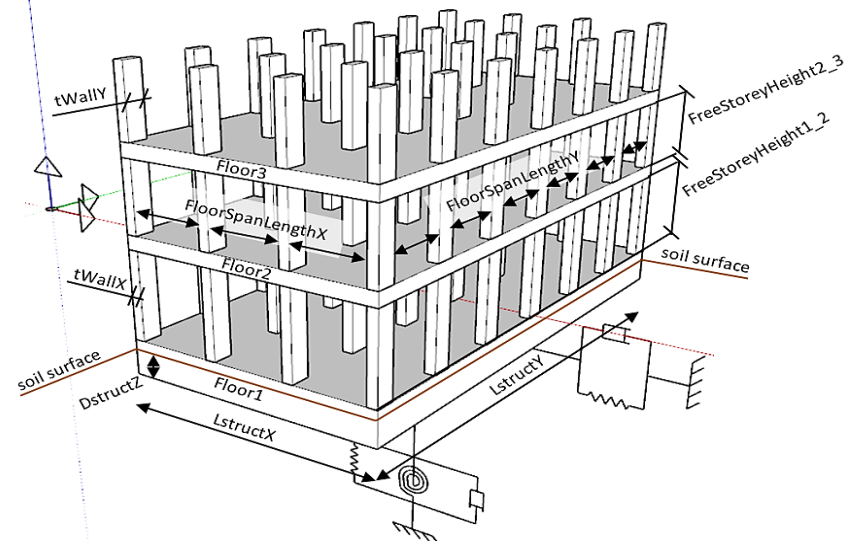
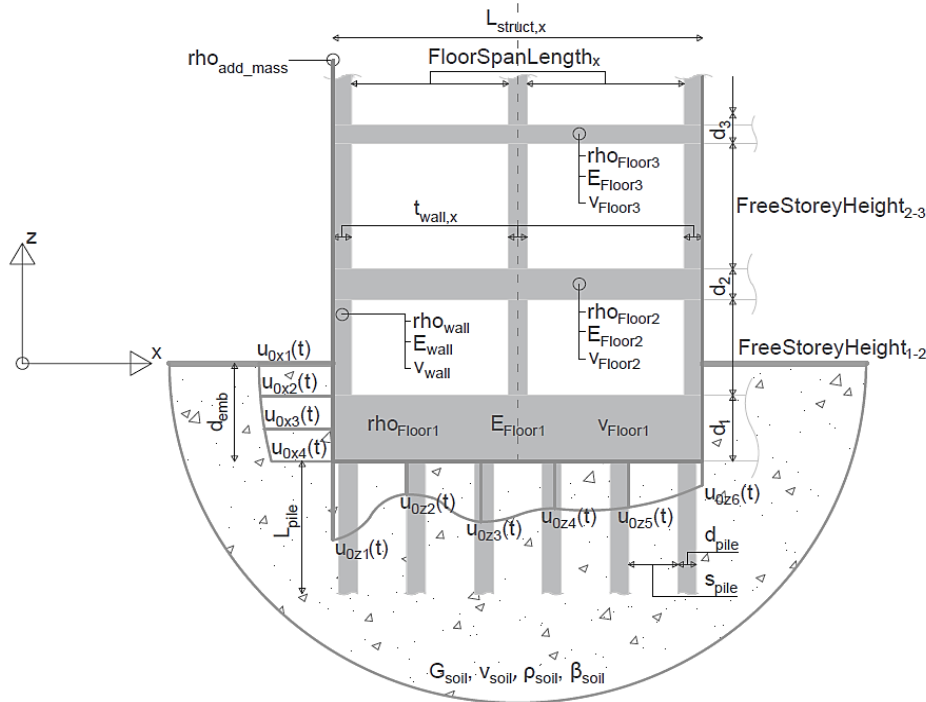
Parameters	Unit	Explanation	<i>← do not change this line</i>
-------------------	-------------	--------------------	----------------------------------

Python input requirements

Description	Parameters	Unit	Explanation
<i>do not change the descriptions in this column ↓</i>			

Script 0: 0.3DoFBuildingDesignParameters

Figures to explain several input parameters of Python scripts 0, 1 and 2



Input file for computing structural dynamic response

Date: 2-9-2019 | Author: Gerwin Schut

FLOORS for 3DoF system				
				properties of floor. Make sure that the text 'FloorProperties' + (the number of the wall), e.g. 'FloorProperties1' is present in the 'descriptions' column in case this floor has to be included in the computation. Otherwise delete the text 'FloorProperties'.
Floor 1	FloorProperties1			
	dFloor1	=	0.25 m	Thickness of floor
	MaterialFloor1	=	Concrete	Material name for the floor
	RhoFloor1	=	2500 kg/m3	density of floor material
	EFloor1	=	30000000000 N/m2	Young's modulus of floor material
	vFloor1	=	0.2	Poisson's ratio of floor material. Should be smaller than 0.5
Floor 2	FloorProperties2			
	dFloor2	=	0.26 m	Thickness of floor
	MaterialFloor2	=	Concrete	Material name for the floor
	RhoFloor2	=	2000 kg/m3	density of floor material
	EFloor2	=	30000000000 N/m2	Young's modulus of floor material
	vFloor2	=	0.2	Poisson's ratio of floor material. Should be smaller than 0.5
Floor 3	FloorProperties3			
	dFloor3	=	0.26 m	Thickness of floor
	MaterialFloor3	=	Concrete	Material name for the floor
	RhoFloor3	=	2000 kg/m3	density of floor material
	EFloor3	=	30000000000 N/m2	Young's modulus of floor material
	vFloor3	=	0.2	Poisson's ratio of floor material. Should be smaller than 0.5
Floor 4	FloorProperties4			
	dFloor4	=	0.1 m	Thickness of floor
	MaterialFloor4	=	Metal	Material name for the floor
	RhoFloor4	=	1000 kg/m3	density of floor material
	EFloor4	=	10000000000 N/m2	Young's modulus of floor material
	vFloor4	=	0.3	Poisson's ratio of floor material. Should be smaller than 0.5
FREE STOREY HEIGHTS for 3DoF system				
	FreeStoreyHeight1_2	=	1.47 m	Free storey height between floor 1 and 2
	FreeStoreyHeight2_3	=	2.74 m	Free storey height between floor 2 and 3
	FreeStoreyHeight3_4	=	3 m	Free storey height between floor 3 and 4

Input file for computing structural dynamic response

Date: 2-9-2019 | Author: Gerwin Schut

FLOORSPANS			
NrOfFloorSpansX	=	2	- number of floor spans in-plane (in the x-z-plane)
FloorSpanLengthX	=	8.25 m	length of floor spans in-plane (equal for all floor spans). Span in between the walls
NrOfFloorSpansY	=	1	- number of floor spans out-of-plane (in the y-z-plane)
FloorSpanLengthY	=	4.3 m	length of floor spans out-of-plane (equal for all floor spans). Span in between the walls
WALLS			
WallProperties			properties of wall. Make sure that the text 'WallProperties' + (the number of the wall), e.g. 'WallProperties1' is present in the 'descriptions' column in case this wall has to be included in the computation. Otherwise delete the text 'WallProperties'.
tWallX	=	0.15 m	Thickness of wall in-plane (in the x-z-plane)
tWallY	=	0.65 m	Thickness of wall out-of-plane (in the y-z-plane)
MaterialWall	=	Brickwork	- Material name for the wall
RhoWall	=	1400 kg/m ³	density of wall material
Ewall	=	8000000000 N/m ²	Young's modulus of wall material
vWall	=	0.14	- Poisson's ratio of wall material. Should be smaller than 0.5
LstructX	=	16.95 m	total length of structure (in-plane) in x-direction
LstructY	=	5.6 m	total depth of structure (out-of-plane) in y-direction
HstructZ	=	7.98 m	total height of structure in z-direction
AdditionalMass	=	47.513 kg/m ³	additional mass that needs to be taken into account for the total mass of the building and the mass moment inertia of the building which acts as resistance against vibrations (impedance). Divide the total mass to be added by the total volume of the structure (LstructX x LstructY x HstructZ)
Continue on next page with script 1			

Script 1: 1.ScriptToCompute3DoFExcitation			
Structure for 3DoF system			
pos_StartStructure	=	18.25 m	distance along the x-axis from the middle of the road to the start of the building
pos_EndStructure	=	35.2 m	distance along the x-axis from the middle of the road to the end of the building
DstructZ	=	1.73 m	depth of structure (e.g. box or slab) without pile foundation
Excitation 3DoF system			
Exc_factor	=	0 -	0: the excitation is not factorized 1: the excitation is factorized according to EV5.2 by factorizing the frequency domain and computing the time domain from there
tmin_exc	=	-0.2 s	start time-instant for the excitation input (preferably Excitation(tmin_exc) = 0)
tmax_exc	=	1 s	end time-instant for the excitation input (preferably Excitation(tmax_exc) = 0)
tstep_exc	=	0.02 s	time step for the excitation input (should be sufficiently small for reliable excitation input)
t_nr_exc	=	61	nr of time instants considered to compute the excitation in the time domain
Continue on next page with script 2			

Script 2: 2.ImpedancesAnd3DoFStructuralResponse				
Soil approximation for impedances 3DoF system				
	G_HS	=	120000000	N/m2 shear modulus of soil approximation as homogeneous HalfSpace
	rho_HS	=	2000	kg/m3 material mass density of soil approximation as homogeneous HalfSpace
	v_HS	=	0.48	- Poisson's ratio of soil approximation as homogeneous HalfSpace
	Beta_HS	=	0.02	- damping ratio of soil approximation as homogeneous HalfSpace
<i>in case of piles only</i>	Esoil0	=	237000000	N/m2 Young's modulus of soil material at the pile head (top of the pile, underneath the foundation slab)
<i>in case of piles only</i>	rho_L	=	2000	kg/m3 material mass density of soil approximation at pile-length of the foundation pile (pile tip)
<i>in case of piles only</i>	v_L	=	0.48	- Poisson's ratio of soil approximation at pile-length of foundation pile (pile tip)
<i>in case of piles only</i>	Cs_L	=	200	m/s shear wave speed of soil approximation at pile-length of the foundation pile (pile tip)
<i>in case of piles only</i>	Cs_Lm	=	100	m/s shear wave speed of soil approximation at mid-length of the foundation pile
<i>in case of piles only</i>	Cs_H	=	400	m/s shear wave speed of soil approximation at twice the pile-length of the foundation pile (pile tip + pile length)
<i>in case of piles only</i>	Beta_L	=	0.01	- damping ratio of soil approximation at pile-length of the foundation pile (pile tip)
<i>in case of piles only</i>	HsoilZ	=	36	m depth of H (which is taken as twice the pile length)
Structure for 3DoF system				
	DstructZeff	=	1.73	m effective depth of structural wall-soil interface
	AbReducingFactor	=	1	- reducing factor for contact area Ab between bottom of structure and soil to take into account loss of contact due to e.g. rocking of the structure.
	AwReducingFactor	=	1	- reducing factor for contact area Aw between structural walls and soil to take into account loss of contact due to e.g. rocking of the structure.
	presence_piles	=	0	0: no foundation piles are included 1: the foundation piles are included as specified below:
<i>in case of piles only</i>	Dpile	=	0.7	m diameter of a single foundation pile
<i>in case of piles only</i>	LpileZ	=	18	m length of a single foundation pile (underneath bottom of foundation slab to pile tip)
<i>in case of piles only</i>	nrPilesX	=	9	- nr of foundation piles on the same axis parallel to the x-axis (symmetrically divided)
<i>in case of piles only</i>	nrPilesY	=	26	- nr of foundation piles on the same axis parallel to the y-axis (symmetrically divided)
<i>in case of piles only</i>	Ptot	=	234	- total nr of foundation piles (minimum amount is 4)
<i>in case of piles only</i>	Spiles	=	2.1	m axis-to-axis distance foundation piles
<i>in case of piles only</i>	Epile	=	30000000000	N/m2 Young's Modulus of foundation pile material (e.g. concrete)

Input file for computing structural dynamic response

Date: 2-9-2019 | Author: Gerwin Schut

Computational options 3DoF system			
freq_step_str	=	0.25 Hz	frequency step used to compute the 3DoF soil impedances and the 3DoF structural response and the EB-beam flexible frame structural response in the frequency domain. Also: freq_min_str = freq_step_str/2
freq_nr_str	=	81	nr of frequencies considered to compute the freq_max_str
freq_max_str	=	20.125 Hz	maximum frequency considered for computing the 3DoF soil impedances and the 3DoF structural response and the EB-beam flexible frame structural response in the frequency domain.
tmin_resp	=	-0.22 s	minimum time instant to consider for the computation of the structural response
tstep_resp	=	0.02 s	time step to consider for the computation of the structural response
t_nr_resp	=	211	nr of time instants to consider for the computation of the structural response
tmax_resp	=	3.98 s	maximum time instant to consider for the computation of the structural response
freq_plot_forcings	=	7 Hz	specific frequency for which the frequency dependent forcings are plotted (compressed springs)
Plotting parameters 3DoF system			
plot_3DoF_velocities_time	=	1	0: do not plot the 3DoF response velocities in the time domain 1: plot the 3DoF response velocities in the time domain
plot_3DoF_velocities_freq	=	1	0: do not plot the 3DoF response velocities in the frequency domain 1: plot the 3DoF response velocities in the frequency domain
plot_3DoF_RMSvelocities_freq	=	1	0: do not plot the 3DoF response RMS velocities in the frequency domain 1: plot the 3DoF response RMS velocities in the frequency domain
Excitation 3DoF system (in case a simpler excitation is wanted than the stored excitation lists in the folder 'SoilResponses')			
overwrite_exc_3DoF	=	0	0: the excitation will be taken from the excitation.csv-files, computed by script 1. 1: the excitation will not be taken from the excitation.csv-files. Instead a more simple excitation can be constructed with the parameters specified below this parameter.
Harmonic excitation term 1			
Freq_3DoF_exc1	=	5 Hz	The frequency of the harmonic excitation: $U(t) = A_{ucj} \cdot \cos(\text{Freq_excj} \cdot t) + A_{usj} \cdot \sin(\text{Freq_excj} \cdot t)$
Au1cj_3DoF_exc1	=	0.00001 m	Amplitude of the harmonic excitation corresponding to the cosine term of the displacements (u)

Input file for computing structural dynamic response
Date: 2-9-2019 | Author: Gerwin Schut

Au1sj_3DoF_exc1	=	0.00001	m	Amplitude of the harmonic excitation corresponding to the sine term of the displacements (u)
Au3cj_3DoF_exc1	=	0.00001	m	Amplitude of the harmonic excitation corresponding to the cosine term of the displacements (u)
Au3sj_3DoF_exc1	=	0.00001	m	Amplitude of the harmonic excitation corresponding to the sine term of the displacements (u)
AuPHIcj_3DoF_exc1	=	0.00001	rad	Amplitude of the harmonic excitation corresponding to the cosine term of the displacements (u)
AuPHIsj_3DoF_exc1	=	0.00001	rad	Amplitude of the harmonic excitation corresponding to the sine term of the displacements (u)
Av1cj_3DoF_exc1	=	0.0001	m/s	Amplitude of the harmonic excitation corresponding to the cosine term of the velocities (v)
Av1sj_3DoF_exc1	=	0.0001	m/s	Amplitude of the harmonic excitation corresponding to the sine term of the velocities (v)
Av3cj_3DoF_exc1	=	0.0001	m/s	Amplitude of the harmonic excitation corresponding to the cosine term of the velocities (v)
Av3sj_3DoF_exc1	=	0.0001	m/s	Amplitude of the harmonic excitation corresponding to the sine term of the velocities (v)
AvPHIcj_3DoF_exc1	=	0.0001	rad/s	Amplitude of the harmonic excitation corresponding to the cosine term of the velocities (v)
AvPHIsj_3DoF_exc1	=	0.0001	rad/s	Amplitude of the harmonic excitation corresponding to the sine term of the velocities (v)
Harmonic excitation term 2				
Freq_3DoF_exc2	=	10	Hz	The frequency of the harmonic excitation: $U(t) = A_{ucj} \cdot \cos(\text{Freq_excj} \cdot t) + A_{usj} \cdot \sin(\text{Freq_excj} \cdot t)$
Au1cj_3DoF_exc2	=	0.00001	m	Amplitude of the harmonic excitation corresponding to the sine term of the displacements (u)
Au1sj_3DoF_exc2	=	0.00001	m	Amplitude of the harmonic excitation corresponding to the sine term of the displacements (u)
Au3cj_3DoF_exc2	=	0.00001	m	Amplitude of the harmonic excitation corresponding to the cosine term of the displacements (u)
Au3sj_3DoF_exc2	=	0.00001	m	Amplitude of the harmonic excitation corresponding to the sine term of the displacements (u)

Input file for computing structural dynamic response

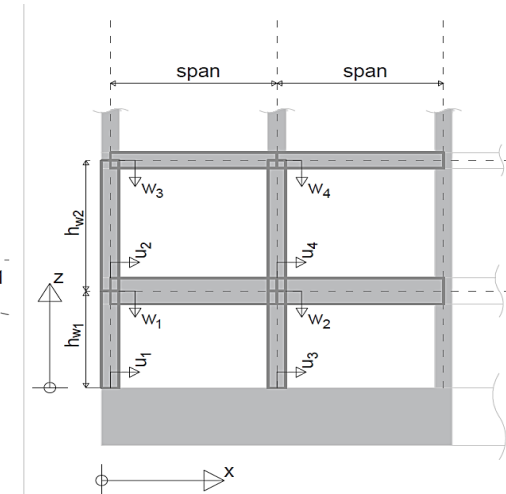
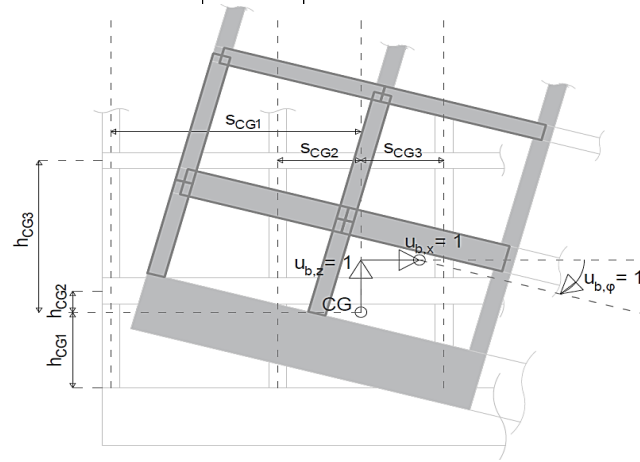
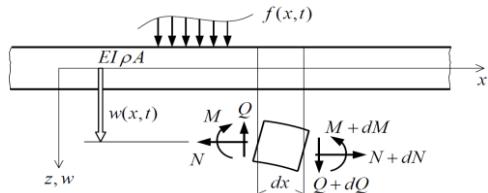
Date: 2-9-2019 | Author: Gerwin Schut

AuPHIcj_3DoF_exc2	=	0.00001	rad	Amplitude of the harmonic excitation corresponding to the cosine term of the displacements (u)
AuPHIsj_3DoF_exc2	=	0.00001	rad	Amplitude of the harmonic excitation corresponding to the sine term of the displacements (u)
Av1cj_3DoF_exc2	=	0.0001	m/s	Amplitude of the harmonic excitation corresponding to the cosine term of the velocities (v)
Av1sj_3DoF_exc2	=	0.0001	m/s	Amplitude of the harmonic excitation corresponding to the sine term of the velocities (v)
Av3cj_3DoF_exc2	=	0.0001	m/s	Amplitude of the harmonic excitation corresponding to the cosine term of the velocities (v)
Av3sj_3DoF_exc2	=	0.0001	m/s	Amplitude of the harmonic excitation corresponding to the sine term of the velocities (v)
AvPHIcj_3DoF_exc2	=	0.0001	rad/s	Amplitude of the harmonic excitation corresponding to the cosine term of the velocities (v)
AvPHIsj_3DoF_exc2	=	0.0001	rad/s	Amplitude of the harmonic excitation corresponding to the sine term of the velocities (v)
Insert additional excitation terms here				

Continue on next page with script 3

Script 3: 3.EB-beam frame matrix_allExcitations

Figures to explain several input parameters of Python script 3



EB-beam frame additional (or more detailed / free to pick) properties. Otherwise refer input cell to structural properties of script 0

Structure for EB-beam frame			
EB_span	=	5.6	m length (span) of all EB-beam floor elements
EB_hw1	=	1.6	m length (storey height) of the EB-beam wall elements u1 and u3
EB_hw2	=	3	m length (storey height) of the EB-beam wall elements u2 and u4
wj_width	=	3.1	m width of the EB-beam floor elements (factorized out in the computation)
w1_height	=	0.26	m floor height or thickness of EB-beam floor element w1
w2_height	=	0.26	m floor height or thickness of EB-beam floor element w2
w3_height	=	0.26	m floor height or thickness of EB-beam floor element w3
w4_height	=	0.26	m floor height or thickness of EB-beam floor element w4
uj_width	=	0.65	m width of the EB-beam wall elements (factorized out in the computation)
u1_height	=	0.3	m wall height or thickness of EB-beam wall element u1
u2_height	=	0.14	m wall height or thickness of EB-beam wall element u2
u3_height	=	0.3	m wall height or thickness of EB-beam wall element u3
u4_height	=	0.14	m wall height or thickness of EB-beam wall element u4
rho_structure	=	2500	kg/m3 material mass density of the EB-beam frame structure
E_mod_structure	=	8700000000	N/m2 Young's Modulus of the EB-beam frame structure

Input file for computing structural dynamic response
Date: 2-9-2019 | Author: Gerwin Schut

Computation of EB-beam frame			
freq_step_str_EB	=	0.25	Hz
freq_nr_str_EB	=	81	-
freq_max_str_EB	=	20.125	Hz
tmin_resp_EB	=	-0.2	
tstep_resp_EB	=	0.02	s
t_nr_resp_EB	=	105	
tmax_resp_EB	=	1.88	s
Plotting parameters EB-beam frame			
plot_displaced_frames_UxWzPHly	=	0	0: do not plot the displaced EB-beam frame due to the excitations Ux, Wz and PHly for a particular time instant 1: plot the displaced EB-beam frame due to the excitations Ux, Wz and PHly for the time instants specified below:
plot_displaced_frame_tot	=	0	0: do not plot the displaced EB-beam frame due to all excitation types for a particular time instant 1: plot the displaced EB-beam frame due to all excitation types for the time instants specified below:
time_instant_frame_plot_1	=	0.5	s time instant at which the results of the EB-beam frame are computed and plotted
<i>time_instant_frame_plot_2</i>	=	0.1	s time instant at which the results of the EB-beam frame are computed and plotted
plot_max_defl_factor	=	0.1	factor multiplied with min(hw, hw2, span) to obtain a limit displacement in the EB-beam frame plots. This limit is used to obtain a scalingfactor for plotting the displaced EB-beam frames. Advised is to keep this value equal to 0.1
applying_scaling_factor	=	0	- 0: no scalingfactor will be applied to the plots of the deformed EB-beam frame 1: the scalingfactor for the plots will be determined by the script (computational heavy) 2: the scaling factor will be chosen from the specified factors below:
apply_ScalingFactorUx	=	600	- Scaling factor applied when '2' is chosen above (for the response due to excitation Ux only), refers to plot_displaced_frames_UxWzPHly
apply_ScalingFactorWz	=	600	- Scaling factor applied when '2' is chosen above (for the response due to excitation Wz only), refers to plot_displaced_frames_UxWzPHly

Input file for computing structural dynamic response

Date: 2-9-2019 | Author: Gerwin Schut

apply_ScalingFactorPHly	=	600	-	Scaling factor applied when '2' is chosen above (for the response due to excitation PHly only), refers to plot_displaced_frames_UxWzPHly
apply_ScalingFactor	=	600	-	Scaling factor applied when '2' is chosen above (for the response due to all excitations), refers to plot_displaced_frames_tot
Plotting parameters EB-beam element w1				
plot_w1_displ_time		0		0: do not plot the displaced beam element w1 along the length of the element for a particular time instant 1: plot the displaced beam element w1 along the length of the element for a the particular time instants specified below:
time_instant_w1_displ_plot_1	=	0	s	time instant at which the displacements of the EB-beam element w1 are computed and plotted
<i>time_instant_w1_displ_plot_2</i>	=	0.1	s	time instant at which the displacements of the EB-beam element w1 are computed and plotted
plot_w1_displ_coord		0		0: do not plot the displaced beam element w1 over the time domain of the forcing for a particular x-coordinate along the element 1: plot the displaced beam element w1 over the time domain of the forcing for a particular x-coordinate along the element as specified below:
x_coord_w1_displ_plot_1	=	2.8	m	x-coordinate at which the displacements of the EB-beam element w1 are computed and plotted
<i>x_coord_w1_displ_plot_2</i>	=	1.4	m	x-coordinate at which the displacements of the EB-beam element w1 are computed and plotted
plotting velocities of w1 in the space-time domain				
plot_w1_veloc_time		0		0: do not plot the velocities of the beam element w1 along the length of the element for a particular time instant 1: plot the velocities of the beam element w1 along the length of the element for a the particular time instants specified below:
time_instant_w1_veloc_plot_1	=	0	s	time instant at which the velocities of the EB-beam element w1 are computed and plotted
<i>time_instant_w1_veloc_plot_2</i>	=	0.1	s	time instant at which the velocities of the EB-beam element w1 are computed and plotted

Input file for computing structural dynamic response

Date: 2-9-2019 | Author: Gerwin Schut

plot_w1_veloc_coord	=	1		0: do not plot the velocities of the beam element w1 over the time domain of the forcing for a particular x-coordinate along the element 1: plot the velocities of the beam element w1 over the time domain of the forcing for a particular x-coordinate along the element as specified below:
x_coord_w1_veloc_plot_1	=	2.8	m	x-coordinate at which the velocities of the EB-beam element w1 are computed and plotted
<i>x_coord_w1_veloc_plot_2</i>	=	1.4	m	x-coordinate at which the velocities of the EB-beam element w1 are computed and plotted
plotting velocities of w1 in the space-frequency domain				
plot_w1_velocFreq_coord	=	1		0: do not plot the velocities of the beam element w1 over the specified calculation-frequency domain for a particular x-coordinate along the element 1: plot the velocities of the beam element w1 over the specified calculation-frequency domain for a particular x-coordinate along the element as specified below:
x_coord_w1_velocFreq_plot_1	=	2.8	m	position in floor w1 to compute the frequency response spectrum
<i>x_coord_w1_velocFreq_plot_1</i>	=	1.4	m	position in floor w1 to compute the frequency response spectrum
plotting RMS-velocities of w1 in the space-frequency domain				
plot_w1_RMSvelocFreq_coord	=	1		0: do not plot the velocities of the beam element w1 over the specified calculation-frequency domain for a particular x-coordinate along the element 1: plot the velocities of the beam element w1 over the specified calculation-frequency domain for a particular x-coordinate along the element as specified below:
x_coord_w1_RMSvelocFreq_plot_1	=	2.8	m	position in floor w1 to compute the frequency response spectrum
Excitation EB-beam frame (in case a simpler excitation is wanted than the stored excitation lists in the csv-files '3DoF_Building_Response')				
overwrite_exc_EB	=	0	-	0: the excitation will be taken from the excitation.csv-files. 1: the excitation will not be taken from the excitation.csv-files. Instead a more simple excitation can be constructed with the parameters specified below this parameter.
Harmonic excitation term 1				
Freq_EB_exc1	=	30	Hz	The frequency of the harmonic excitation: $U(t) = A_{ucj} \cdot \cos(\text{Freq_excj} \cdot t) + A_{usj} \cdot \sin(\text{Freq_excj} \cdot t)$
Ax1cj_EB_exc1	=	0.0003	m	Amplitude of the harmonic excitation corresponding to the cosine term of the displacements (u)

Input file for computing structural dynamic response

Date: 2-9-2019 | Author: Gerwin Schut

Ax1sj_EB_exc1	=	0.0003	m	Amplitude of the harmonic excitation corresponding to the sine term of the displacements (u)
Ax2cj_EB_exc1	=	0.0003	m	Amplitude of the harmonic excitation corresponding to the cosine term of the displacements (u)
Ax2sj_EB_exc1	=	0.0003	m	Amplitude of the harmonic excitation corresponding to the sine term of the displacements (u)
Ax3cj_EB_exc1	=	0.00002	rad	Amplitude of the harmonic excitation corresponding to the cosine term of the displacements (u)
Ax3sj_EB_exc1	=	0.00002	rad	Amplitude of the harmonic excitation corresponding to the sine term of the displacements (u)
Harmonic excitation term 2				
Freq_EB_exc2	=	8	Hz	The frequency of the harmonic excitation: $U(t) = Aucj \cdot \cos(\text{Freq_excj} \cdot t) + Ausj \cdot \sin(\text{Freq_excj} \cdot t)$
Ax1cj_EB_exc2	=	0.0003	m	Amplitude of the harmonic excitation corresponding to the sine term of the displacements (u)
Ax1sj_EB_exc2	=	0.0003	m	Amplitude of the harmonic excitation corresponding to the sine term of the displacements (u)
Ax2cj_EB_exc2	=	0.0003	m	Amplitude of the harmonic excitation corresponding to the cosine term of the displacements (u)
Ax2sj_EB_exc2	=	0.0003	m	Amplitude of the harmonic excitation corresponding to the sine term of the displacements (u)
Ax3cj_EB_exc2	=	0.00002	rad	Amplitude of the harmonic excitation corresponding to the cosine term of the displacements (u)
Ax3sj_EB_exc2	=	0.00002	rad	Amplitude of the harmonic excitation corresponding to the sine term of the displacements (u)
Insert additional excitation terms here				
End of input parameters				

O. Appendix: Results for Verification Project Degrande et al. (1) – Free Field and (3) – Building Response with layered soil of Amsterdam

Verification Project Degrande et al. (1) – Free Field with layered soil of Amsterdam

Another computation has been performed for the modelled situation as in ‘Verification Project Degrande et al. (1) – Free Field’. However, in this case the soil layering has been adjusted to the soil layering as described in 10.3.3 ‘Soil response in Amsterdam,’ which, compared to the original verification project, entails a softer soil. All other parameters are unchanged.

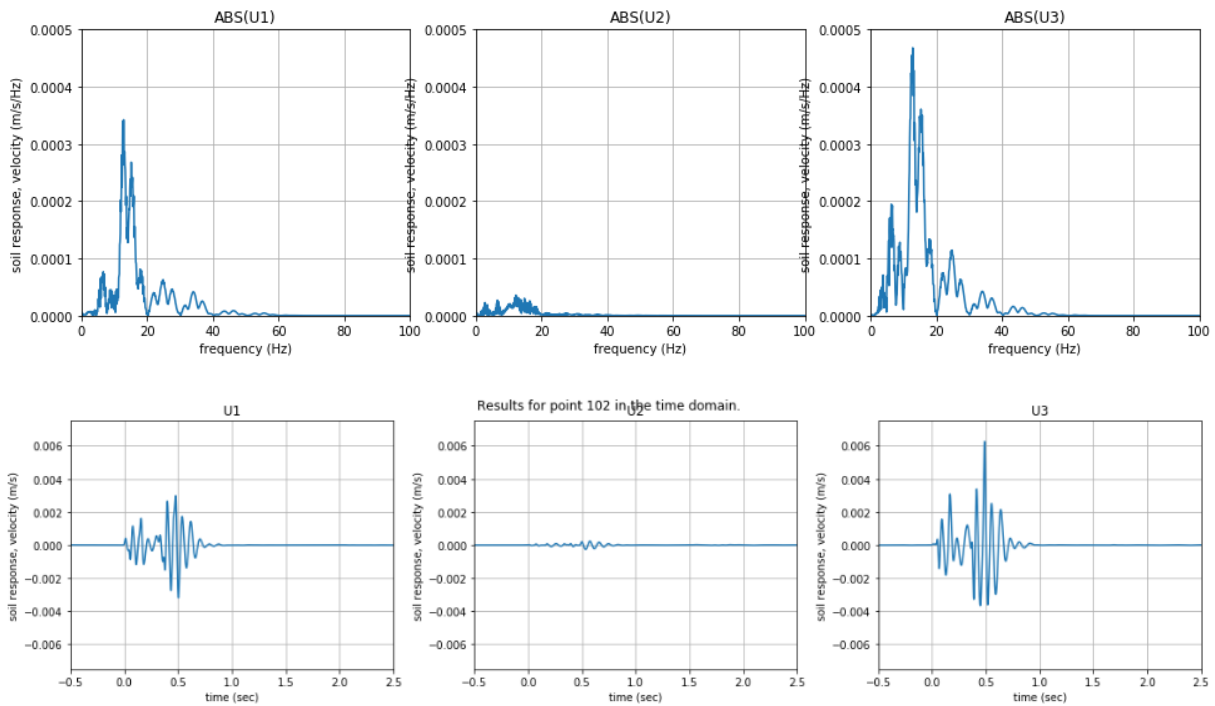


Figure 191. Frequency spectrum (top) and time history (bottom) of the Free Field soil response (from left to right: x-,y-,z-direction) at 16 m from the middle of the road by FEMIX

Comparison with original verification project:

Larger amplitudes of the free field soil response velocities (factor 2 to 3). The frequency content around 5 Hz is amplified by a factor > 20 and the frequency content between 10 and 17 Hz is amplified by a factor 2.5 to 3.

Verification Project Degrande et al. (3) – Building Response with layered soil of Amsterdam

Another computation has been performed for the modelled situation as in ‘Verification Project Degrande et al. (3) – Building Response’. However, in this case the soil layering has been adjusted to the soil layering as described in 10.3.3 ‘Soil response in Amsterdam,’ which, compared to the original verification project, entails a softer soil. All other parameters are unchanged.

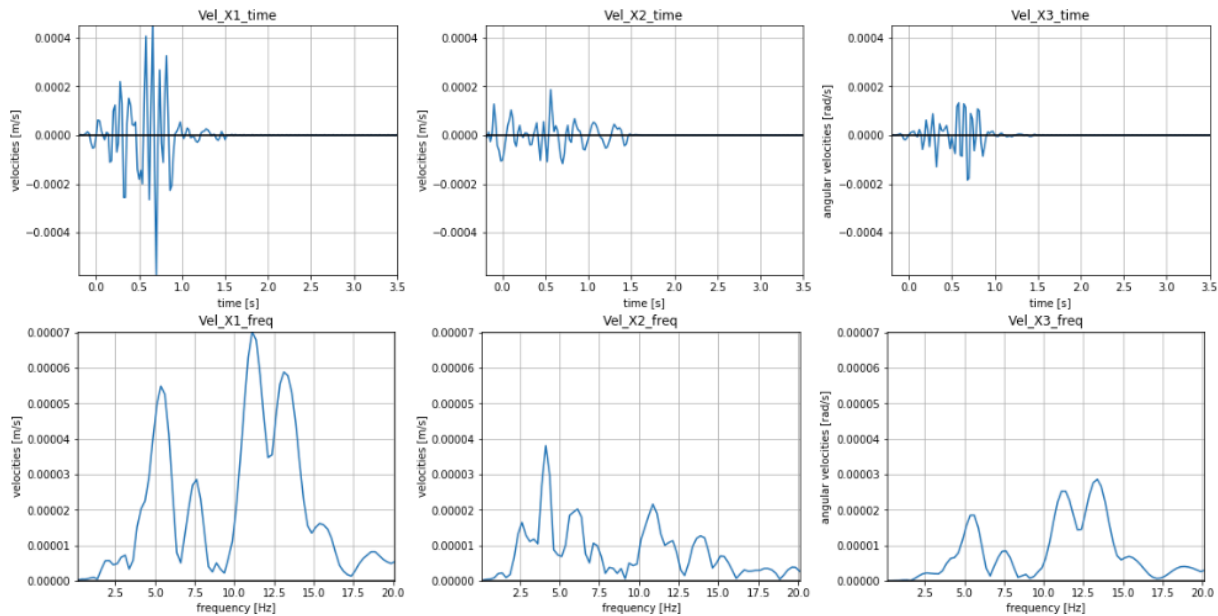


Figure 192. Structural response in the time domain (top) and the frequency domain (bottom) for all three DoF (x,z,φ) of the 3DoF system modelled for verification project Degrande et al. (3) – Building Response with the layered soil of Amsterdam

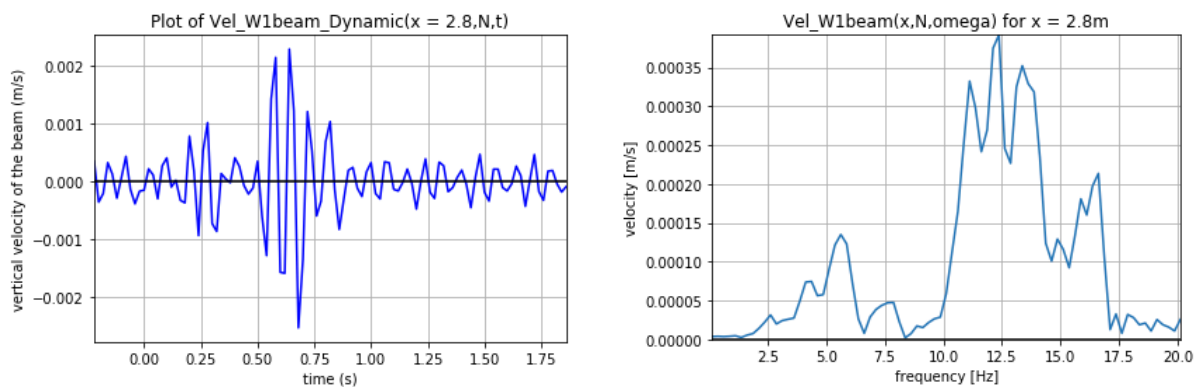


Figure 193. Predicted local EB-beam structural response of the first floor in the time domain (left) and frequency domain (right) for verification project Degrande et al. (3) – Building Response with the layered soil of Amsterdam

Comparison with original verification project:

Larger amplitudes of the 3DoF response (factor 2 to 3). The frequency content around 5 Hz is amplified by a factor 8 to 10 and the frequency content between 10 and 17 Hz is amplified by a factor 1 to 2.5.

Larger amplitudes of the local EB-beam floor (factor 2). The frequency content around 5 Hz is amplified by a factor 10 and the frequency content between 10 and 17 Hz is amplified by a factor 1 to 2.5.

P. Appendix: Boundary- and Interface conditions of the three Models_{x,z,φ}

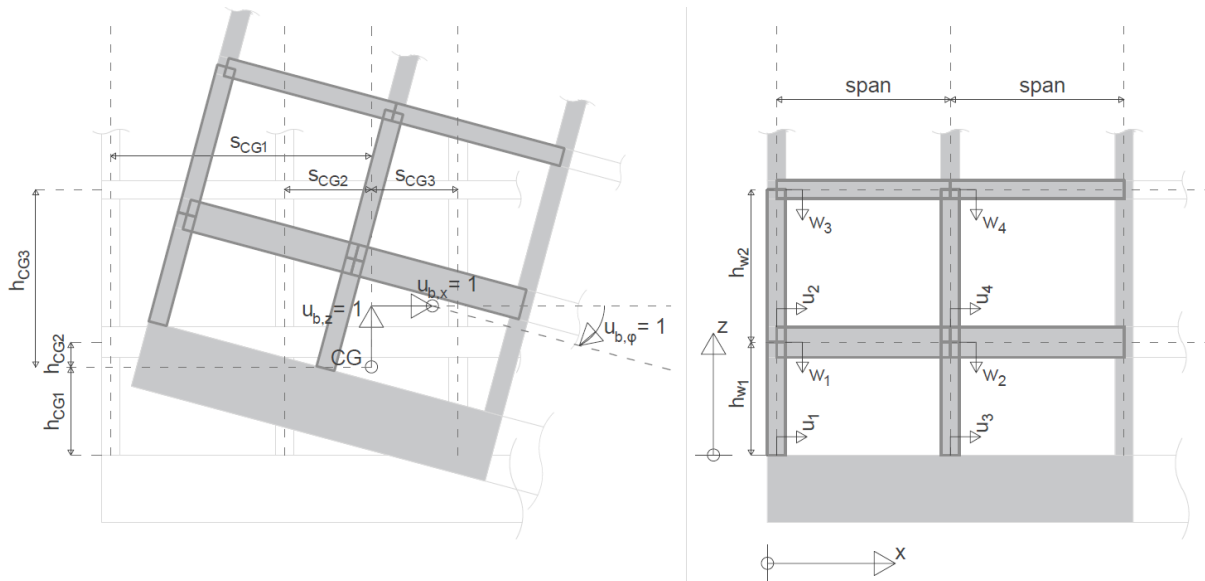


Figure 194. Reference system and lever-arms within the EB-beam frame

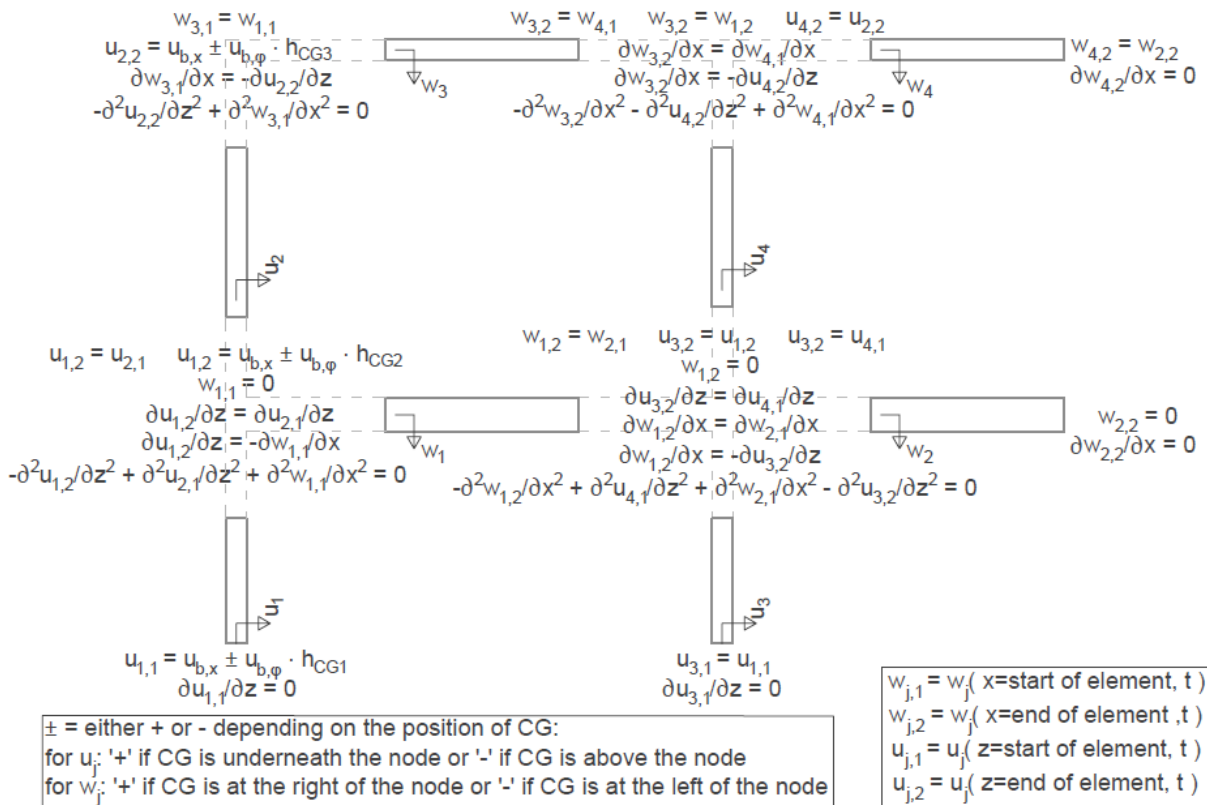


Figure 195. Model_x representing the BCs and ICs for computing the dynamic response due to all horizontal excitations

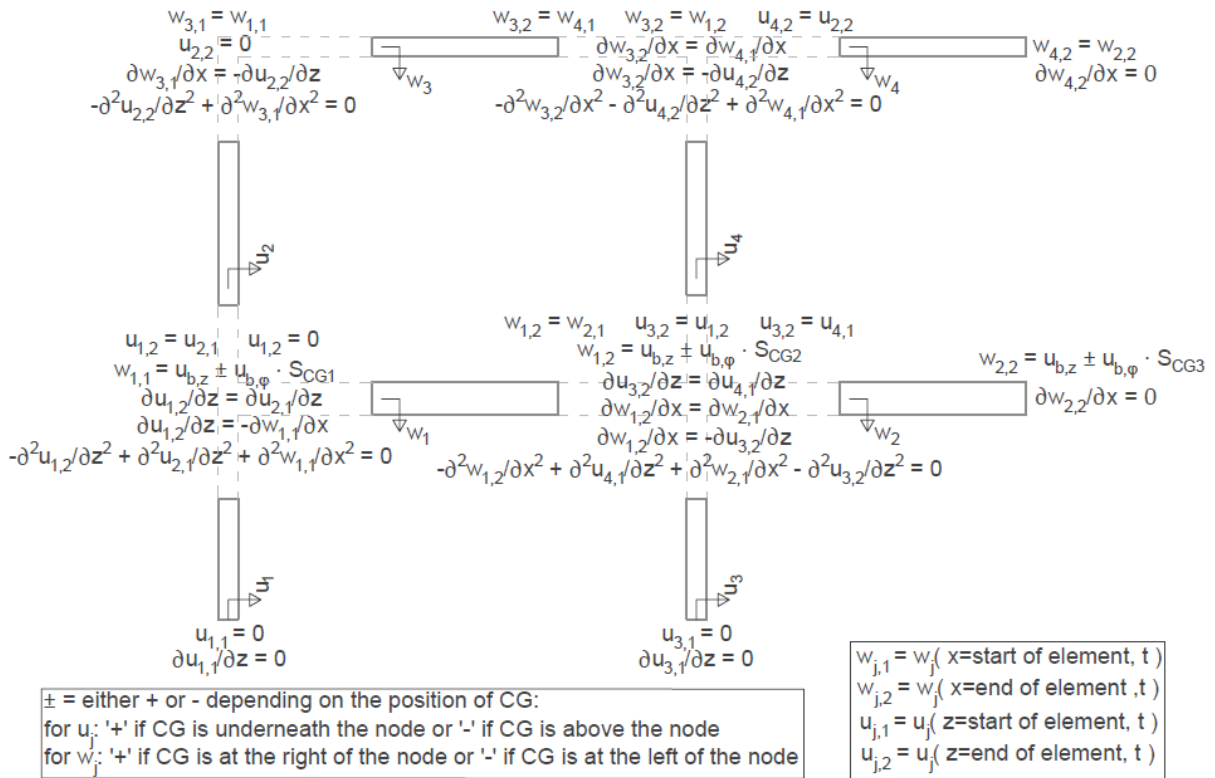


Figure 196. Model_z representing the BCs and ICs for computing the dynamic response due to all vertical excitations

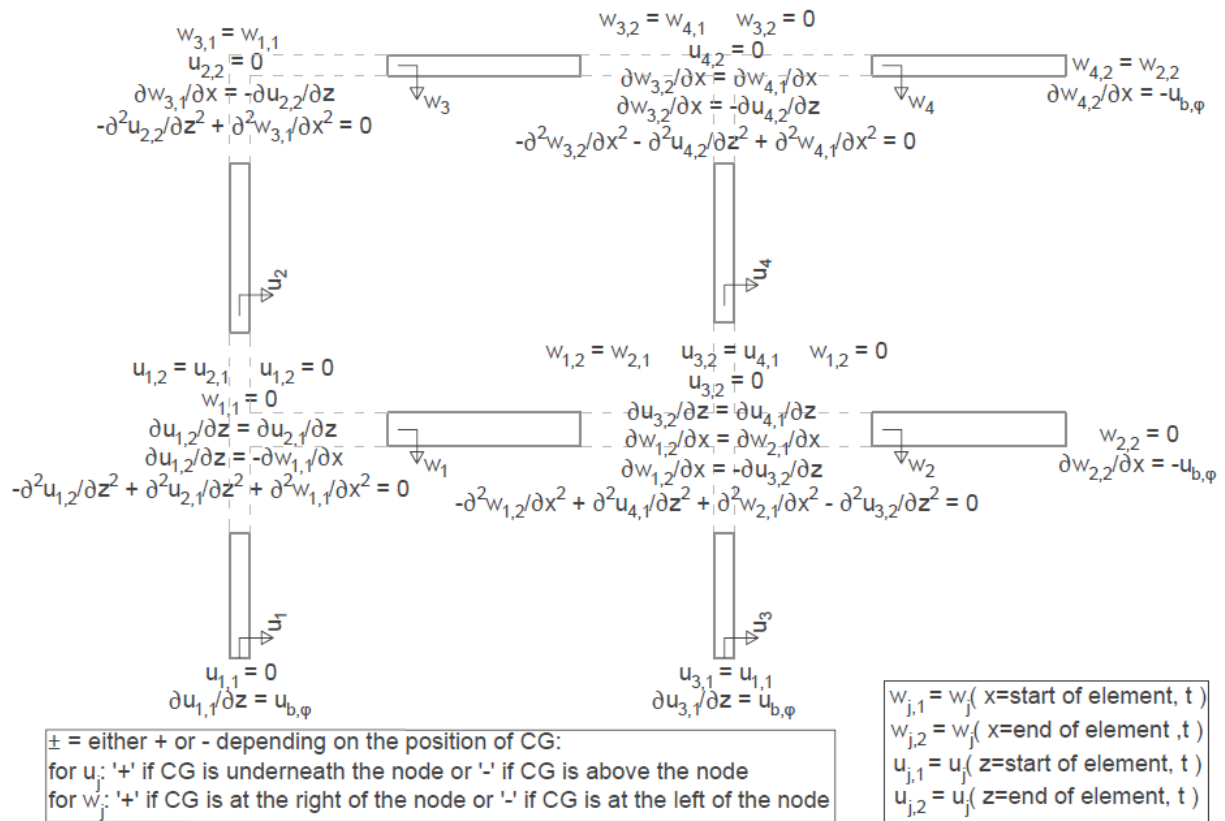


Figure 197. Model_φ representing the BCs and ICs for computing the dynamic response due to all rotational excitations

Q. Appendix: Maple sheet for determining dynamic EB-beams response Model_x

> restart;

>

Model_x (horizontal excitation at bottom of frame only)

Excitation

> $ux := Uxc_j \cdot \cos(\Omega_j \cdot t) + Uxs_j \cdot \sin(\Omega_j \cdot t);$ $ux := Uxc_j \cos(\Omega_j t) + Uxs_j \sin(\Omega_j t)$ (1)

>

Steady-State solutions of every element in the Model

> $w1 := W1c_1 \cdot \cos(\Omega_j \cdot t) + W1s_1 \cdot \sin(\Omega_j \cdot t);$ $w1 := W1c_1 \cos(\Omega_j t) + W1s_1 \sin(\Omega_j t)$ (2)

> $w2 := W2c_1 \cdot \cos(\Omega_j \cdot t) + W2s_1 \cdot \sin(\Omega_j \cdot t);$ $w2 := W2c_1 \cos(\Omega_j t) + W2s_1 \sin(\Omega_j t)$ (3)

> $w3 := W3c_1 \cdot \cos(\Omega_j \cdot t) + W3s_1 \cdot \sin(\Omega_j \cdot t);$ $w3 := W3c_1 \cos(\Omega_j t) + W3s_1 \sin(\Omega_j t)$ (4)

> $w4 := W4c_1 \cdot \cos(\Omega_j \cdot t) + W4s_1 \cdot \sin(\Omega_j \cdot t);$ $w4 := W4c_1 \cos(\Omega_j t) + W4s_1 \sin(\Omega_j t)$ (5)

> $u1 := U1c_1 \cdot \cos(\Omega_j \cdot t) + U1s_1 \cdot \sin(\Omega_j \cdot t);$ $u1 := U1c_1 \cos(\Omega_j t) + U1s_1 \sin(\Omega_j t)$ (6)

> $u2 := U2c_1 \cdot \cos(\Omega_j \cdot t) + U2s_1 \cdot \sin(\Omega_j \cdot t);$ $u2 := U2c_1 \cos(\Omega_j t) + U2s_1 \sin(\Omega_j t)$ (7)

> $u3 := U3c_1 \cdot \cos(\Omega_j \cdot t) + U3s_1 \cdot \sin(\Omega_j \cdot t);$ $u3 := U3c_1 \cos(\Omega_j t) + U3s_1 \sin(\Omega_j t)$ (8)

> $u4 := U4c_1 \cdot \cos(\Omega_j \cdot t) + U4s_1 \cdot \sin(\Omega_j \cdot t);$ $u4 := U4c_1 \cos(\Omega_j t) + U4s_1 \sin(\Omega_j t)$ (9)

>

Substituting the steady-state solutions into the EOM of every element and gathering for the $\cos(\Omega_j \cdot t)$ - (c_j) and $\sin(\Omega_j \cdot t)$ - (s_j) terms gives the following EOM's and corresponding general solutions:

> $EOMw1c_1 := -rhoA_w1 \cdot \Omega_j^2 \cdot W1c_1 + EI_w1 \cdot diff(W1c_1, x^4) = 0 :$

> $W1c_1 := Aw1c_1 \cdot \cosh(\beta_{aw1} \cdot j \cdot x) + Bw1c_1 \cdot \sinh(\beta_{aw1} \cdot j \cdot x) + Cw1c_1 \cdot \cos(\beta_{aw1} \cdot j \cdot x) + Dw1c_1 \cdot \sin(\beta_{aw1} \cdot j \cdot x);$ (10)

$W1c_1 := Aw1c_1 \cosh(\beta_{aw1} j x) + Bw1c_1 \sinh(\beta_{aw1} j x) + Cw1c_1 \cos(\beta_{aw1} j x) + Dw1c_1 \sin(\beta_{aw1} j x)$

> $EOMw1s_1 := -rhoA_w1 \cdot \Omega_j^2 \cdot W1s_1 + EI_w1 \cdot diff(W1s_1, x^4) = 0 :$

> $W1s_1 := Aw1s_1 \cdot \cosh(\beta_{aw1} \cdot j \cdot x) + Bw1s_1 \cdot \sinh(\beta_{aw1} \cdot j \cdot x) + Cw1s_1 \cdot \cos(\beta_{aw1} \cdot j \cdot x) + Dw1s_1 \cdot \sin(\beta_{aw1} \cdot j \cdot x);$ (11)

$W1s_1 := Aw1s_1 \cosh(\beta_{aw1} j x) + Bw1s_1 \sinh(\beta_{aw1} j x) + Cw1s_1 \cos(\beta_{aw1} j x) + Dw1s_1 \sin(\beta_{aw1} j x)$

> $EOMw2c_1 := -rhoA_w2 \cdot \Omega_j^2 \cdot W2c_1 + EI_w2 \cdot diff(W2c_1, x^4) = 0 :$

> $W2c_1 := Aw2c_1 \cdot \cosh(\beta_{aw2} \cdot j \cdot x) + Bw2c_1 \cdot \sinh(\beta_{aw2} \cdot j \cdot x) + Cw2c_1 \cdot \cos(\beta_{aw2} \cdot j \cdot x) + Dw2c_1 \cdot \sin(\beta_{aw2} \cdot j \cdot x);$ (12)

$W2c_1 := Aw2c_1 \cosh(\beta_{aw2} j x) + Bw2c_1 \sinh(\beta_{aw2} j x) + Cw2c_1 \cos(\beta_{aw2} j x) + Dw2c_1 \sin(\beta_{aw2} j x)$

> $EOMw2s_1 := -rhoA_w2 \cdot \Omega_j^2 \cdot W2s_1 + EI_w2 \cdot diff(W2s_1, x^4) = 0 :$

> $W2s_1 := Aw2s_1 \cdot \cosh(\beta_{aw2} \cdot j \cdot x) + Bw2s_1 \cdot \sinh(\beta_{aw2} \cdot j \cdot x) + Cw2s_1 \cdot \cos(\beta_{aw2} \cdot j \cdot x) + Dw2s_1 \cdot \sin(\beta_{aw2} \cdot j \cdot x);$ (13)

$W2s_1 := Aw2s_1 \cosh(\beta_{aw2} j x) + Bw2s_1 \sinh(\beta_{aw2} j x) + Cw2s_1 \cos(\beta_{aw2} j x) + Dw2s_1 \sin(\beta_{aw2} j x)$

> $EOMw3c_1 := -rhoA_w3 \cdot \Omega_j^2 \cdot W3c_1 + EI_w3 \cdot diff(W3c_1, x^4) = 0 :$

> $W3c_1 := Aw3c_1 \cdot \cosh(\beta_{aw3} \cdot j \cdot x) + Bw3c_1 \cdot \sinh(\beta_{aw3} \cdot j \cdot x) + Cw3c_1 \cdot \cos(\beta_{aw3} \cdot j \cdot x) + Dw3c_1 \cdot \sin(\beta_{aw3} \cdot j \cdot x);$ (14)

$W3c_1 := Aw3c_1 \cosh(\beta_{aw3} j x) + Bw3c_1 \sinh(\beta_{aw3} j x) + Cw3c_1 \cos(\beta_{aw3} j x) + Dw3c_1 \sin(\beta_{aw3} j x)$

> $EOMw3s_1 := -rhoA_w3 \cdot \Omega_j^2 \cdot W3s_1 + EI_w3 \cdot diff(W3s_1, x^4) = 0 :$

> $W3s_1 := Aw3s_1 \cdot \cosh(\beta_{aw3} \cdot j \cdot x) + Bw3s_1 \cdot \sinh(\beta_{aw3} \cdot j \cdot x) + Cw3s_1 \cdot \cos(\beta_{aw3} \cdot j \cdot x) + Dw3s_1 \cdot \sin(\beta_{aw3} \cdot j \cdot x);$ (15)

$W3s_1 := Aw3s_1 \cosh(\beta_{aw3} j x) + Bw3s_1 \sinh(\beta_{aw3} j x) + Cw3s_1 \cos(\beta_{aw3} j x) + Dw3s_1 \sin(\beta_{aw3} j x)$

$$\begin{aligned}
&> EOMw4c_1 := -rhoA_w4 \cdot \Omega I^2 \cdot W4c_1 + EI_w4 \cdot diff(W4c_1, x\$4) = 0 : \\
&> W4c_1 := Aw4c_1 \cdot cosh(Betaw4_j \cdot x) + Bw4c_1 \cdot sinh(Betaw4_j \cdot x) + Cw4c_1 \cdot cos(Betaw4_j \cdot x) + Dw4c_1 \cdot sin(Betaw4_j \cdot x); \\
&\quad W4c_1 := Aw4c_1 \cosh(Betaw4_j x) + Bw4c_1 \sinh(Betaw4_j x) + Cw4c_1 \cos(Betaw4_j x) + Dw4c_1 \sin(Betaw4_j x)
\end{aligned} \tag{16}$$

$$\begin{aligned}
&> EOMw4s_1 := -rhoA_w4 \cdot \Omega I^2 \cdot W4s_1 + EI_w4 \cdot diff(W4s_1, x\$4) = 0 : \\
&> W4s_1 := Aw4s_1 \cdot cosh(Betaw4_j \cdot x) + Bw4s_1 \cdot sinh(Betaw4_j \cdot x) + Cw4s_1 \cdot cos(Betaw4_j \cdot x) + Dw4s_1 \cdot sin(Betaw4_j \cdot x); \\
&\quad W4s_1 := Aw4s_1 \cosh(Betaw4_j x) + Bw4s_1 \sinh(Betaw4_j x) + Cw4s_1 \cos(Betaw4_j x) + Dw4s_1 \sin(Betaw4_j x)
\end{aligned} \tag{17}$$

$$\begin{aligned}
&> EOMulc_1 := -rhoA_u1 \cdot \Omega I^2 \cdot U1c_1 + EI_u1 \cdot diff(U1c_1, z\$4) = 0 : \\
&> U1c_1 := Au1c_1 \cdot cosh(Betau1_j \cdot z) + Bu1c_1 \cdot sinh(Betau1_j \cdot z) + Cu1c_1 \cdot cos(Betau1_j \cdot z) + Du1c_1 \cdot sin(Betau1_j \cdot z); \\
&\quad U1c_1 := Au1c_1 \cosh(Betau1_j z) + Bu1c_1 \sinh(Betau1_j z) + Cu1c_1 \cos(Betau1_j z) + Du1c_1 \sin(Betau1_j z)
\end{aligned} \tag{18}$$

$$\begin{aligned}
&> EOMuls_1 := -rhoA_u1 \cdot \Omega I^2 \cdot U1s_1 + EI_u1 \cdot diff(U1s_1, z\$4) = 0 : \\
&> U1s_1 := Au1s_1 \cdot cosh(Betau1_j \cdot z) + Bu1s_1 \cdot sinh(Betau1_j \cdot z) + Cu1s_1 \cdot cos(Betau1_j \cdot z) + Du1s_1 \cdot sin(Betau1_j \cdot z); \\
&\quad U1s_1 := Au1s_1 \cosh(Betau1_j z) + Bu1s_1 \sinh(Betau1_j z) + Cu1s_1 \cos(Betau1_j z) + Du1s_1 \sin(Betau1_j z)
\end{aligned} \tag{19}$$

$$\begin{aligned}
&> EOMu2c_1 := -rhoA_u2 \cdot \Omega I^2 \cdot U2c_1 + EI_u2 \cdot diff(U2c_1, z\$4) = 0 : \\
&> U2c_1 := Au2c_1 \cdot cosh(Betau2_j \cdot z) + Bu2c_1 \cdot sinh(Betau2_j \cdot z) + Cu2c_1 \cdot cos(Betau2_j \cdot z) + Du2c_1 \cdot sin(Betau2_j \cdot z); \\
&\quad U2c_1 := Au2c_1 \cosh(Betau2_j z) + Bu2c_1 \sinh(Betau2_j z) + Cu2c_1 \cos(Betau2_j z) + Du2c_1 \sin(Betau2_j z)
\end{aligned} \tag{20}$$

$$\begin{aligned}
&> EOMu2s_1 := -rhoA_u2 \cdot \Omega I^2 \cdot U2s_1 + EI_u2 \cdot diff(U2s_1, z\$4) = 0 : \\
&> U2s_1 := Au2s_1 \cdot cosh(Betau2_j \cdot z) + Bu2s_1 \cdot sinh(Betau2_j \cdot z) + Cu2s_1 \cdot cos(Betau2_j \cdot z) + Du2s_1 \cdot sin(Betau2_j \cdot z); \\
&\quad U2s_1 := Au2s_1 \cosh(Betau2_j z) + Bu2s_1 \sinh(Betau2_j z) + Cu2s_1 \cos(Betau2_j z) + Du2s_1 \sin(Betau2_j z)
\end{aligned} \tag{21}$$

$$\begin{aligned}
&> EOMu3c_1 := -rhoA_u3 \cdot \Omega I^2 \cdot U3c_1 + EI_u3 \cdot diff(U3c_1, z\$4) = 0 : \\
&> U3c_1 := Au3c_1 \cdot cosh(Betau3_j \cdot z) + Bu3c_1 \cdot sinh(Betau3_j \cdot z) + Cu3c_1 \cdot cos(Betau3_j \cdot z) + Du3c_1 \cdot sin(Betau3_j \cdot z); \\
&\quad U3c_1 := Au3c_1 \cosh(Betau3_j z) + Bu3c_1 \sinh(Betau3_j z) + Cu3c_1 \cos(Betau3_j z) + Du3c_1 \sin(Betau3_j z)
\end{aligned} \tag{22}$$

$$\begin{aligned}
&> EOMu3s_1 := -rhoA_u3 \cdot \Omega I^2 \cdot U3s_1 + EI_u3 \cdot diff(U3s_1, z\$4) = 0 : \\
&> U3s_1 := Au3s_1 \cdot cosh(Betau3_j \cdot z) + Bu3s_1 \cdot sinh(Betau3_j \cdot z) + Cu3s_1 \cdot cos(Betau3_j \cdot z) + Du3s_1 \cdot sin(Betau3_j \cdot z); \\
&\quad U3s_1 := Au3s_1 \cosh(Betau3_j z) + Bu3s_1 \sinh(Betau3_j z) + Cu3s_1 \cos(Betau3_j z) + Du3s_1 \sin(Betau3_j z)
\end{aligned} \tag{23}$$

$$\begin{aligned}
&> EOMu4c_1 := -rhoA_u4 \cdot \Omega I^2 \cdot U4c_1 + EI_u4 \cdot diff(U4c_1, z\$4) = 0 : \\
&> U4c_1 := Au4c_1 \cdot cosh(Betau4_j \cdot z) + Bu4c_1 \cdot sinh(Betau4_j \cdot z) + Cu4c_1 \cdot cos(Betau4_j \cdot z) + Du4c_1 \cdot sin(Betau4_j \cdot z); \\
&\quad U4c_1 := Au4c_1 \cosh(Betau4_j z) + Bu4c_1 \sinh(Betau4_j z) + Cu4c_1 \cos(Betau4_j z) + Du4c_1 \sin(Betau4_j z)
\end{aligned} \tag{24}$$

$$\begin{aligned}
&> EOMu4s_1 := -rhoA_u4 \cdot \Omega I^2 \cdot U4s_1 + EI_u4 \cdot diff(U4s_1, z\$4) = 0 : \\
&> U4s_1 := Au4s_1 \cdot cosh(Betau4_j \cdot z) + Bu4s_1 \cdot sinh(Betau4_j \cdot z) + Cu4s_1 \cdot cos(Betau4_j \cdot z) + Du4s_1 \cdot sin(Betau4_j \cdot z); \\
&\quad U4s_1 := Au4s_1 \cosh(Betau4_j z) + Bu4s_1 \sinh(Betau4_j z) + Cu4s_1 \cos(Betau4_j z) + Du4s_1 \sin(Betau4_j z)
\end{aligned} \tag{25}$$

Substitute the general solutions into the IC's and BC's (4*8 EB-elements = 32 needed IC's + BC's) and gather for the cos(Omega_1) terms

$$\begin{aligned}
&BC @ x = 0, z = 0 [2 BC's] \\
&> BC1c_1M := simplify(subs(z=0, U1c_1)) - Uxc_j - PHlyc_j \cdot hcgl : BC1c_1 := BC1c_1M = 0; \\
&\quad BC1c_1 := -PHlyc_j hcgl + Au1c_1 + Cu1c_1 - Uxc_j = 0
\end{aligned} \tag{26}$$

$$\begin{aligned}
&> BC2c_1M := simplify(subs(z=0, diff(U1c_1, z))) : BC2c_1 := BC2c_1M = 0; \\
&\quad BC2c_1 := Betau1_j (Bu1c_1 + Du1c_1) = 0
\end{aligned} \tag{27}$$

$$\begin{aligned}
&BC @ x = span, z = 0 [2 BC's] \\
&> BC3c_1M := simplify(subs(z=0, U3c_1)) - Uxc_j - PHlyc_j \cdot hcgl : BC3c_1 := BC3c_1M = 0; \\
&\quad BC3c_1 := -PHlyc_j hcgl + Au3c_1 + Cu3c_1 - Uxc_j = 0
\end{aligned} \tag{28}$$

$$\begin{aligned}
&> BC4c_1M := simplify(subs(z=0, diff(U3c_1, z))) : BC4c_1 := BC4c_1M = 0; \\
&\quad BC4c_1 := Betau3_j (Bu3c_1 + Du3c_1) = 0
\end{aligned} \tag{29}$$

BC @ x = 2*span, z = hw1 [2 BC's]

$$\begin{aligned} > BC5c_1M := \text{simplify}(\text{subs}(x=2\cdot\text{span}, W2c_1)) : BC5c_1 := BC5c_1M=0; \\ & BC5c_1 := Aw2c_1 \cosh(2 \text{ Betaw2_j span}) + Bw2c_1 \sinh(2 \text{ Betaw2_j span}) + Cw2c_1 \cos(2 \text{ Betaw2_j span}) + Dw2c_1 \sin(2 \text{ Betaw2_j span}) = 0 \end{aligned} \quad (30)$$

$$\begin{aligned} > BC6c_1M := \text{simplify}(\text{subs}(x=2\cdot\text{span}, \text{diff}(W2c_1, x))) : BC6c_1 := BC6c_1M=0; \\ & BC6c_1 := \text{Betaw2_j} (Aw2c_1 \sinh(2 \text{ Betaw2_j span}) + Bw2c_1 \cosh(2 \text{ Betaw2_j span}) - Cw2c_1 \sin(2 \text{ Betaw2_j span}) + Dw2c_1 \cos(2 \text{ Betaw2_j span})) = 0 \end{aligned} \quad (31)$$

BC @ x = 2*span, z = hw1+hw2 [2 BC's]

$$\begin{aligned} > BC7c_1M := \text{simplify}(\text{subs}(x=2\cdot\text{span}, W4c_1)) : BC7c_1 := BC7c_1M=0; \\ & BC7c_1 := Aw4c_1 \cosh(2 \text{ Betaw4_j span}) + Bw4c_1 \sinh(2 \text{ Betaw4_j span}) + Cw4c_1 \cos(2 \text{ Betaw4_j span}) + Dw4c_1 \sin(2 \text{ Betaw4_j span}) = 0 \end{aligned} \quad (32)$$

$$\begin{aligned} > BC8c_1M := \text{simplify}(\text{subs}(x=2\cdot\text{span}, \text{diff}(W4c_1, x))) : BC8c_1 := BC8c_1M=0; \\ & BC8c_1 := \text{Betaw4_j} (Aw4c_1 \sinh(2 \text{ Betaw4_j span}) + Bw4c_1 \cosh(2 \text{ Betaw4_j span}) - Cw4c_1 \sin(2 \text{ Betaw4_j span}) + Dw4c_1 \cos(2 \text{ Betaw4_j span})) = 0 \end{aligned} \quad (33)$$

IC @ x = 0, z = hw1 [6 IC's]

$$\begin{aligned} > IC1c_1M := \text{simplify}(\text{subs}(z=hw1, U1c_1)) - \text{simplify}(\text{subs}(z=hw1, U2c_1)) : IC1c_1 := IC1c_1M=0; \\ & IC1c_1 := Au1c_1 \cosh(\text{Betau1_j hw1}) + Bu1c_1 \sinh(\text{Betau1_j hw1}) + Cu1c_1 \cos(\text{Betau1_j hw1}) + Du1c_1 \sin(\text{Betau1_j hw1}) - Au2c_1 \cosh(\text{Betau2_j hw1}) - Bu2c_1 \sinh(\text{Betau2_j hw1}) \\ & \quad - Cu2c_1 \cos(\text{Betau2_j hw1}) - Du2c_1 \sin(\text{Betau2_j hw1}) = 0 \end{aligned} \quad (34)$$

$$\begin{aligned} > IC2c_1M := \text{simplify}(\text{subs}(x=0, W1c_1)) : IC2c_1 := IC2c_1M=0; \\ & IC2c_1 := Aw1c_1 + Cw1c_1 = 0 \end{aligned} \quad (35)$$

$$\begin{aligned} > IC3c_1M := \text{simplify}(\text{subs}(z=hw1, \text{diff}(U1c_1, z))) - \text{simplify}(\text{subs}(z=hw1, \text{diff}(U2c_1, z))) : IC3c_1 := IC3c_1M=0; \\ & IC3c_1 := \text{Betau1_j} (Au1c_1 \sinh(\text{Betau1_j hw1}) + Bu1c_1 \cosh(\text{Betau1_j hw1}) - Cu1c_1 \sin(\text{Betau1_j hw1}) + Du1c_1 \cos(\text{Betau1_j hw1})) - \text{Betau2_j} (Au2c_1 \sinh(\text{Betau2_j hw1}) \\ & \quad + Bu2c_1 \cosh(\text{Betau2_j hw1}) - Cu2c_1 \sin(\text{Betau2_j hw1}) + Du2c_1 \cos(\text{Betau2_j hw1})) = 0 \end{aligned} \quad (36)$$

$$\begin{aligned} > IC4c_1M := \text{simplify}(\text{subs}(z=hw1, \text{diff}(U1c_1, z))) + \text{simplify}(\text{subs}(x=0, \text{diff}(W1c_1, x))) : IC4c_1 := IC4c_1M=0; \\ & IC4c_1 := \text{Betau1_j} (Au1c_1 \sinh(\text{Betau1_j hw1}) + Bu1c_1 \cosh(\text{Betau1_j hw1}) - Cu1c_1 \sin(\text{Betau1_j hw1}) + Du1c_1 \cos(\text{Betau1_j hw1})) + \text{Betaw1_j} (Bw1c_1 + Dw1c_1) = 0 \end{aligned} \quad (37)$$

$$\begin{aligned} > IC5c_1M := \text{simplify}(\text{subs}(z=hw1, U1c_1)) - Uxc_j - PHlyc_j \cdot hcg2 : IC5c_1 := IC5c_1M=0; \\ & IC5c_1 := Au1c_1 \cosh(\text{Betau1_j hw1}) + Bu1c_1 \sinh(\text{Betau1_j hw1}) + Cu1c_1 \cos(\text{Betau1_j hw1}) + Du1c_1 \sin(\text{Betau1_j hw1}) - Uxc_j - PHlyc_j \cdot hcg2 = 0 \end{aligned} \quad (38)$$

$$\begin{aligned} > IC6c_1M := -\text{simplify}(\text{subs}(z=hw1, \text{diff}(U1c_1, z^2))) + \text{simplify}(\text{subs}(z=hw1, \text{diff}(U2c_1, z^2))) + \text{simplify}(\text{subs}(x=0, \text{diff}(W1c_1, x^2))) : IC6c_1 := IC6c_1M=0; \\ & IC6c_1 := -\text{Betau1_j}^2 (Au1c_1 \cosh(\text{Betau1_j hw1}) + Bu1c_1 \sinh(\text{Betau1_j hw1}) - Cu1c_1 \cos(\text{Betau1_j hw1}) - Du1c_1 \sin(\text{Betau1_j hw1})) + \text{Betau2_j}^2 (Au2c_1 \cosh(\text{Betau2_j hw1}) \\ & \quad + Bu2c_1 \sinh(\text{Betau2_j hw1}) - Cu2c_1 \cos(\text{Betau2_j hw1}) - Du2c_1 \sin(\text{Betau2_j hw1})) + \text{Betaw1_j}^2 (Aw1c_1 - Cw1c_1) = 0 \end{aligned} \quad (39)$$

IC @ x = 0, z = hw1+hw2 [6 IC's]

$$\begin{aligned} > IC7c_1M := \text{simplify}(\text{subs}(x=0, W3c_1)) : IC7c_1 := IC7c_1M=0; \\ & IC7c_1 := Aw3c_1 + Cw3c_1 = 0 \end{aligned} \quad (40)$$

$$\begin{aligned} > IC8c_1M := \text{simplify}(\text{subs}(z=hw1 + hw2, \text{diff}(U2c_1, z))) + \text{simplify}(\text{subs}(x=0, \text{diff}(W3c_1, x))) : IC8c_1 := IC8c_1M=0; \\ & IC8c_1 := \text{Betau2_j} (Au2c_1 \sinh(\text{Betau2_j} (hw1 + hw2)) + Bu2c_1 \cosh(\text{Betau2_j} (hw1 + hw2)) - Cu2c_1 \sin(\text{Betau2_j} (hw1 + hw2)) + Du2c_1 \cos(\text{Betau2_j} (hw1 + hw2))) + \text{Betaw3_j} (Bw3c_1 \\ & \quad + Dw3c_1) = 0 \end{aligned} \quad (41)$$

$$\begin{aligned} > IC9c_1M := \text{simplify}(\text{subs}(z=hw1 + hw2, U2c_1)) - Uxc_j - PHlyc_j \cdot hcg3 : IC9c_1 := IC9c_1M=0; \\ & IC9c_1 := Au2c_1 \cosh(\text{Betau2_j} (hw1 + hw2)) + Bu2c_1 \sinh(\text{Betau2_j} (hw1 + hw2)) + Cu2c_1 \cos(\text{Betau2_j} (hw1 + hw2)) + Du2c_1 \sin(\text{Betau2_j} (hw1 + hw2)) - Uxc_j - PHlyc_j \cdot hcg3 = 0 \end{aligned} \quad (42)$$

$$\begin{aligned} > IC10c_1M := -\text{simplify}(\text{subs}(z=hw1 + hw2, \text{diff}(U2c_1, z^2))) + \text{simplify}(\text{subs}(x=0, \text{diff}(W3c_1, x^2))) : IC10c_1 := IC10c_1M=0; \\ & IC10c_1 := -\text{Betau2_j}^2 (Au2c_1 \cosh(\text{Betau2_j} (hw1 + hw2)) + Bu2c_1 \sinh(\text{Betau2_j} (hw1 + hw2)) - Cu2c_1 \cos(\text{Betau2_j} (hw1 + hw2)) - Du2c_1 \sin(\text{Betau2_j} (hw1 + hw2))) + \text{Betaw3_j}^2 (Aw3c_1 \\ & \quad - Cw3c_1) = 0 \end{aligned} \quad (43)$$

IC @ x = span, z = hw1 [8 IC's]

$$\begin{aligned} > IC11c_1M := \text{simplify}(\text{subs}(x=\text{span}, W1c_1)) - \text{simplify}(\text{subs}(x=\text{span}, W2c_1)) : IC11c_1 := IC11c_1M=0; \\ & IC11c_1 := Aw1c_1 \cosh(\text{Betaw1_j span}) + Bw1c_1 \sinh(\text{Betaw1_j span}) + Cw1c_1 \cos(\text{Betaw1_j span}) + Dw1c_1 \sin(\text{Betaw1_j span}) - Aw2c_1 \cosh(\text{Betaw2_j span}) - Bw2c_1 \sinh(\text{Betaw2_j span}) \\ & \quad - Cw2c_1 \cos(\text{Betaw2_j span}) - Dw2c_1 \sin(\text{Betaw2_j span}) = 0 \end{aligned} \quad (44)$$

$$\begin{aligned} > IC12c_1M := \text{simplify}(\text{subs}(x=\text{span}, W1c_1)) : IC12c_1 := IC12c_1M=0; \\ & IC12c_1 := Aw1c_1 \cosh(\text{Betaw1_j span}) + Bw1c_1 \sinh(\text{Betaw1_j span}) + Cw1c_1 \cos(\text{Betaw1_j span}) + Dw1c_1 \sin(\text{Betaw1_j span}) = 0 \end{aligned} \quad (45)$$

$$\begin{aligned} > IC13c_1M := \text{simplify}(\text{subs}(z=hw1, U3c_1)) - \text{simplify}(\text{subs}(z=hw1, U4c_1)) : IC13c_1 := IC13c_1M=0; \\ & IC13c_1 := Au3c_1 \cosh(\text{Betau3_j hw1}) + Bu3c_1 \sinh(\text{Betau3_j hw1}) + Cu3c_1 \cos(\text{Betau3_j hw1}) + Du3c_1 \sin(\text{Betau3_j hw1}) - Au4c_1 \cosh(\text{Betau4_j hw1}) - Bu4c_1 \sinh(\text{Betau4_j hw1}) \\ & \quad - Cu4c_1 \cos(\text{Betau4_j hw1}) - Du4c_1 \sin(\text{Betau4_j hw1}) = 0 \end{aligned} \quad (46)$$

$$\begin{aligned} > IC14c_1M := \text{simplify}(\text{subs}(x=\text{span}, \text{diff}(W1c_1, x))) - \text{simplify}(\text{subs}(x=\text{span}, \text{diff}(W2c_1, x))) : IC14c_1 := IC14c_1M=0; \end{aligned} \quad (47)$$

$$IC14c_1 := Betaw1_j (Aw1c_1 \sinh(Betaw1_j \text{span}) + Bw1c_1 \cosh(Betaw1_j \text{span}) - Cw1c_1 \sin(Betaw1_j \text{span}) + Dw1c_1 \cos(Betaw1_j \text{span})) - Betaw2_j (Aw2c_1 \sinh(Betaw2_j \text{span}) + Bw2c_1 \cosh(Betaw2_j \text{span}) - Cw2c_1 \sin(Betaw2_j \text{span}) + Dw2c_1 \cos(Betaw2_j \text{span})) = 0 \quad (47)$$

$$\begin{aligned} &> IC15c_1M := \text{simplify}(\text{subs}(z=hw1, \text{diff}(U3c_1, z))) - \text{simplify}(\text{subs}(z=hw1, \text{diff}(U4c_1, z))) : IC15c_1 := IC15c_1M=0; \\ IC15c_1 &:= Betaw3_j (Au3c_1 \sinh(Betaw3_j hw1) + Bu3c_1 \cosh(Betaw3_j hw1) - Cu3c_1 \sin(Betaw3_j hw1) + Du3c_1 \cos(Betaw3_j hw1)) - Betaw4_j (Au4c_1 \sinh(Betaw4_j hw1) + Bu4c_1 \cosh(Betaw4_j hw1) - Cu4c_1 \sin(Betaw4_j hw1) + Du4c_1 \cos(Betaw4_j hw1)) = 0 \end{aligned} \quad (48)$$

$$\begin{aligned} &> IC16c_1M := \text{simplify}(\text{subs}(x=\text{span}, \text{diff}(W1c_1, x))) + \text{simplify}(\text{subs}(z=hw1, \text{diff}(U3c_1, z))) : IC16c_1 := IC16c_1M=0; \\ IC16c_1 &:= Betaw1_j (Aw1c_1 \sinh(Betaw1_j \text{span}) + Bw1c_1 \cosh(Betaw1_j \text{span}) - Cw1c_1 \sin(Betaw1_j \text{span}) + Dw1c_1 \cos(Betaw1_j \text{span})) + Betaw3_j (Au3c_1 \sinh(Betaw3_j hw1) + Bu3c_1 \cosh(Betaw3_j hw1) - Cu3c_1 \sin(Betaw3_j hw1) + Du3c_1 \cos(Betaw3_j hw1)) = 0 \end{aligned} \quad (49)$$

$$\begin{aligned} &> IC17c_1M := -\text{simplify}(\text{subs}(x=\text{span}, \text{diff}(W1c_1, x\$2))) + \text{simplify}(\text{subs}(z=hw1, \text{diff}(U4c_1, z\$2))) + \text{simplify}(\text{subs}(x=\text{span}, \text{diff}(W2c_1, x\$2))) - \text{simplify}(\text{subs}(z=hw1, \text{diff}(U3c_1, z\$2))) : IC17c_1 := IC17c_1M=0; \end{aligned}$$

$$IC17c_1 := -Betaw1_j^2 (Aw1c_1 \cosh(Betaw1_j \text{span}) + Bw1c_1 \sinh(Betaw1_j \text{span}) - Cw1c_1 \cos(Betaw1_j \text{span}) - Dw1c_1 \sin(Betaw1_j \text{span})) + Betaw4_j^2 (Au4c_1 \cosh(Betaw4_j hw1) + Bu4c_1 \sinh(Betaw4_j hw1) - Cu4c_1 \cos(Betaw4_j hw1) - Du4c_1 \sin(Betaw4_j hw1)) + Betaw2_j^2 (Aw2c_1 \cosh(Betaw2_j \text{span}) + Bw2c_1 \sinh(Betaw2_j \text{span}) - Cw2c_1 \cos(Betaw2_j \text{span}) - Dw2c_1 \sin(Betaw2_j \text{span})) - Betaw3_j^2 (Au3c_1 \cosh(Betaw3_j hw1) + Bu3c_1 \sinh(Betaw3_j hw1) - Cu3c_1 \cos(Betaw3_j hw1) - Du3c_1 \sin(Betaw3_j hw1)) = 0 \quad (50)$$

$$\begin{aligned} &> IC18c_1M := \text{simplify}(\text{subs}(z=hw1, U3c_1)) - Uxc_j - PHlyc_j \cdot hcg2 : IC18c_1 := IC18c_1M=0; \\ IC18c_1 &:= Au3c_1 \cosh(Betaw3_j hw1) + Bu3c_1 \sinh(Betaw3_j hw1) + Cu3c_1 \cos(Betaw3_j hw1) + Du3c_1 \sin(Betaw3_j hw1) - Uxc_j - PHlyc_j \cdot hcg2 = 0 \end{aligned} \quad (51)$$

>

IC @ x = span, z = hw1+hw2 [6 IC's]

$$\begin{aligned} &> IC19c_1M := \text{simplify}(\text{subs}(x=\text{span}, W3c_1)) - \text{simplify}(\text{subs}(x=\text{span}, W4c_1)) : IC19c_1 := IC19c_1M=0; \\ IC19c_1 &:= Aw3c_1 \cosh(Betaw3_j \text{span}) + Bw3c_1 \sinh(Betaw3_j \text{span}) + Cw3c_1 \cos(Betaw3_j \text{span}) + Dw3c_1 \sin(Betaw3_j \text{span}) - Aw4c_1 \cosh(Betaw4_j \text{span}) - Bw4c_1 \sinh(Betaw4_j \text{span}) - Cw4c_1 \cos(Betaw4_j \text{span}) - Dw4c_1 \sin(Betaw4_j \text{span}) = 0 \end{aligned} \quad (52)$$

$$\begin{aligned} &> IC20c_1M := \text{simplify}(\text{subs}(x=\text{span}, W3c_1)) : IC20c_1 := IC20c_1M=0; \\ IC20c_1 &:= Aw3c_1 \cosh(Betaw3_j \text{span}) + Bw3c_1 \sinh(Betaw3_j \text{span}) + Cw3c_1 \cos(Betaw3_j \text{span}) + Dw3c_1 \sin(Betaw3_j \text{span}) = 0 \end{aligned} \quad (53)$$

$$\begin{aligned} &> IC21c_1M := \text{simplify}(\text{subs}(x=\text{span}, \text{diff}(W3c_1, x))) - \text{simplify}(\text{subs}(x=\text{span}, \text{diff}(W4c_1, x))) : IC21c_1 := IC21c_1M=0; \\ IC21c_1 &:= Betaw3_j (Aw3c_1 \sinh(Betaw3_j \text{span}) + Bw3c_1 \cosh(Betaw3_j \text{span}) - Cw3c_1 \sin(Betaw3_j \text{span}) + Dw3c_1 \cos(Betaw3_j \text{span})) - Betaw4_j (Aw4c_1 \sinh(Betaw4_j \text{span}) + Bw4c_1 \cosh(Betaw4_j \text{span}) - Cw4c_1 \sin(Betaw4_j \text{span}) + Dw4c_1 \cos(Betaw4_j \text{span})) = 0 \end{aligned} \quad (54)$$

$$\begin{aligned} &> IC22c_1M := \text{simplify}(\text{subs}(x=\text{span}, \text{diff}(W3c_1, x))) + \text{simplify}(\text{subs}(z=hw1 + hw2, \text{diff}(U4c_1, z))) : IC22c_1 := IC22c_1M=0; \\ IC22c_1 &:= Betaw3_j (Aw3c_1 \sinh(Betaw3_j \text{span}) + Bw3c_1 \cosh(Betaw3_j \text{span}) - Cw3c_1 \sin(Betaw3_j \text{span}) + Dw3c_1 \cos(Betaw3_j \text{span})) + Betaw4_j (Au4c_1 \sinh(Betaw4_j (hw1 + hw2)) + Bu4c_1 \cosh(Betaw4_j (hw1 + hw2)) - Cu4c_1 \sin(Betaw4_j (hw1 + hw2)) + Du4c_1 \cos(Betaw4_j (hw1 + hw2))) = 0 \end{aligned} \quad (55)$$

$$\begin{aligned} &> IC23c_1M := -\text{simplify}(\text{subs}(x=\text{span}, \text{diff}(W3c_1, x\$2))) - \text{simplify}(\text{subs}(z=hw1 + hw2, \text{diff}(U4c_1, z\$2))) + \text{simplify}(\text{subs}(x=\text{span}, \text{diff}(W4c_1, x\$2))) : IC23c_1 := IC23c_1M=0; \\ IC23c_1 &:= -Betaw3_j^2 (Aw3c_1 \cosh(Betaw3_j \text{span}) + Bw3c_1 \sinh(Betaw3_j \text{span}) - Cw3c_1 \cos(Betaw3_j \text{span}) - Dw3c_1 \sin(Betaw3_j \text{span})) - Betaw4_j^2 (Au4c_1 \cosh(Betaw4_j (hw1 + hw2)) + Bu4c_1 \sinh(Betaw4_j (hw1 + hw2)) - Cu4c_1 \cos(Betaw4_j (hw1 + hw2)) - Du4c_1 \sin(Betaw4_j (hw1 + hw2))) + Betaw4_j^2 (Aw4c_1 \cosh(Betaw4_j \text{span}) + Bw4c_1 \sinh(Betaw4_j \text{span}) - Cw4c_1 \cos(Betaw4_j \text{span}) - Dw4c_1 \sin(Betaw4_j \text{span})) = 0 \end{aligned} \quad (56)$$

$$\begin{aligned} &> IC24c_1M := \text{simplify}(\text{subs}(z=hw1 + hw2, U4c_1)) - Uxc_j - PHlyc_j \cdot hcg3 : IC24c_1 := IC24c_1M=0; \\ IC24c_1 &:= Au4c_1 \cosh(Betaw4_j (hw1 + hw2)) + Bu4c_1 \sinh(Betaw4_j (hw1 + hw2)) + Cu4c_1 \cos(Betaw4_j (hw1 + hw2)) + Du4c_1 \sin(Betaw4_j (hw1 + hw2)) - Uxc_j - PHlyc_j \cdot hcg3 = 0 \end{aligned} \quad (57)$$

>

> interface(rtables=35);

>

>

Coefficient matrix

> Mc_j := Matrix([
 [coeff(BC1c_1M, Aw1c_1), coeff(BC1c_1M, Bw1c_1), coeff(BC1c_1M, Cw1c_1), coeff(BC1c_1M, Dw1c_1),
 coeff(BC1c_1M, Aw2c_1), coeff(BC1c_1M, Bw2c_1), coeff(BC1c_1M, Cw2c_1), coeff(BC1c_1M, Dw2c_1),
 coeff(BC1c_1M, Aw3c_1), coeff(BC1c_1M, Bw3c_1), coeff(BC1c_1M, Cw3c_1), coeff(BC1c_1M, Dw3c_1),
 coeff(BC1c_1M, Aw4c_1), coeff(BC1c_1M, Bw4c_1), coeff(BC1c_1M, Cw4c_1), coeff(BC1c_1M, Dw4c_1),
 coeff(BC1c_1M, Au1c_1), coeff(BC1c_1M, Bu1c_1), coeff(BC1c_1M, Cu1c_1), coeff(BC1c_1M, Du1c_1),
 coeff(BC1c_1M, Au2c_1), coeff(BC1c_1M, Bu2c_1), coeff(BC1c_1M, Cu2c_1), coeff(BC1c_1M, Du2c_1),


```
Uxc_j + PHlyc_j·hcg1,  
0,  
0,  
0,  
0,  
0,  
0,  
0,  
0,  
0,  
0,  
Uxc_j + PHlyc_j·hcg2,  
0,  
0,  
0,  
Uxc_j + PHlyc_j·hcg3,  
0,  
0,  
0,  
0,  
0,  
0,  
0,  
0,  
Uxc_j + PHlyc_j·hcg2,  
0,  
0,  
0,  
0,  
0,  
Uxc_j + PHlyc_j·hcg3  
]);
```

$$F_c_j := \begin{bmatrix} \text{PHIyc}_j \text{ hcg1} + \text{Uxc}_j \\ 0 \\ \text{PHIyc}_j \text{ hcg1} + \text{Uxc}_j \\ 0 \\ 0 \\ 0 \\ 0 \\ 0 \\ 0 \\ 0 \\ 0 \\ 0 \\ \text{PHIyc}_j \text{ hcg2} + \text{Uxc}_j \\ 0 \\ 0 \\ 0 \\ \text{PHIyc}_j \text{ hcg3} + \text{Uxc}_j \\ 0 \\ 0 \\ 0 \\ 0 \\ 0 \\ 0 \\ 0 \\ 0 \\ \text{PHIyc}_j \text{ hcg2} + \text{Uxc}_j \\ 0 \\ 0 \\ 0 \\ 0 \\ 0 \\ \text{PHIyc}_j \text{ hcg3} + \text{Uxc}_j \end{bmatrix}$$

```
> Python(Fc_j, resultname="F_vector_c_j");
F_vector_c_j = numpy.mat([PHIyc_j * hcg1 + Uxc_j,0,PHIyc_j * hcg1 + Uxc_j,0,0,0,0,0,0,0,0,0,0,PHIyc_j * hcg2 + Uxc_j,0,0,0,PHIyc_j * hcg3 + Uxc_j,
0,0,0,0,0,0,0,0,PHIyc_j * hcg2 + Uxc_j,0,0,0,0,0,PHIyc_j * hcg3 + Uxc_j])
>
> #test_vector:=vector
>
```

> *Coeff_vector* := subs(*Uxc_j*=1, *Uxs_j*=1, *PHIyc_j*=1, *Omega_j*=1, *rhoA_w1*=1, *rhoA_w2*=1, *rhoA_w3*=1, *rhoA_w4*=1, *rhoA_u1*=1, *rhoA_u2*=1, *rhoA_u3*=1, *rhoA_u4*=1, *EI_w1*=1, *EI_w2*=1, *EI_w3*=1, *EI_w4*=1, *EI_u1*=1, *EI_u2*=1, *EI_u3*=1, *EI_u4*=1, *Betaw1_j*=1, *Betaw2_j*=1, *Betaw3_j*=1, *Betaw4_j*=1, *Betau1_j*=1, *Betau2_j*=1, *Betau3_j*=1, *Betau4_j*=1, *span*=1, *hw1*=1, *hw2*=1, *hcg1*=1, *hcg2*=1, *hcg3*=1, *LinearAlgebra*[*Multiply*](*LinearAlgebra*[*MatrixInverse*](*Mc_j_comp*), *Fc_j*));

Coeff_vector :=

1.25339703571085 10⁸
-1.24366775577511 10⁸
-1.25339703571088 10⁸
2.43241240701675 10⁷
-5.29952510941048 10⁸
5.70204863660217 10⁸
2.33824006862509 10⁸
2.53346470730038 10⁷
-4.44096913240416 10⁸
6.46311237633327 10⁸
4.44096913240423 10⁸
-3.73411541479704 10⁸
7.16423506397987 10⁸
-7.70839196635300 10⁸
-3.16098162416494 10⁸
-3.42489870595529 10⁷
-1.00400733016008 10⁸
3.01679852282316 10⁸
1.00400735016008 10⁸
-3.01679852282316 10⁸
6.73301148080738 10⁸
-8.20871843793083 10⁸
-5.24351679186132 10⁸
2.48422149976392 10⁸
7.42683921800327 10⁷
-2.23158501216791 10⁸
-7.42683901800327 10⁷
2.23158501216791 10⁸
2.04915608165207 10⁷
1.33025364648323 10⁷
7.42775845011559 10⁷
-1.03848661658868 10⁸

```
> Awlc_1_comp := Coeff_vector(1); Bwlc_1_comp := Coeff_vector(2); Cwlc_1_comp := Coeff_vector(3); Dwlc_1_comp := Coeff_vector(4);
      Awlc_1_comp := 1.25339703571085 108
      Bwlc_1_comp := -1.24366775577511 108
      Cwlc_1_comp := -1.25339703571088 108
      Dwlc_1_comp := 2.43241240701675 107
```

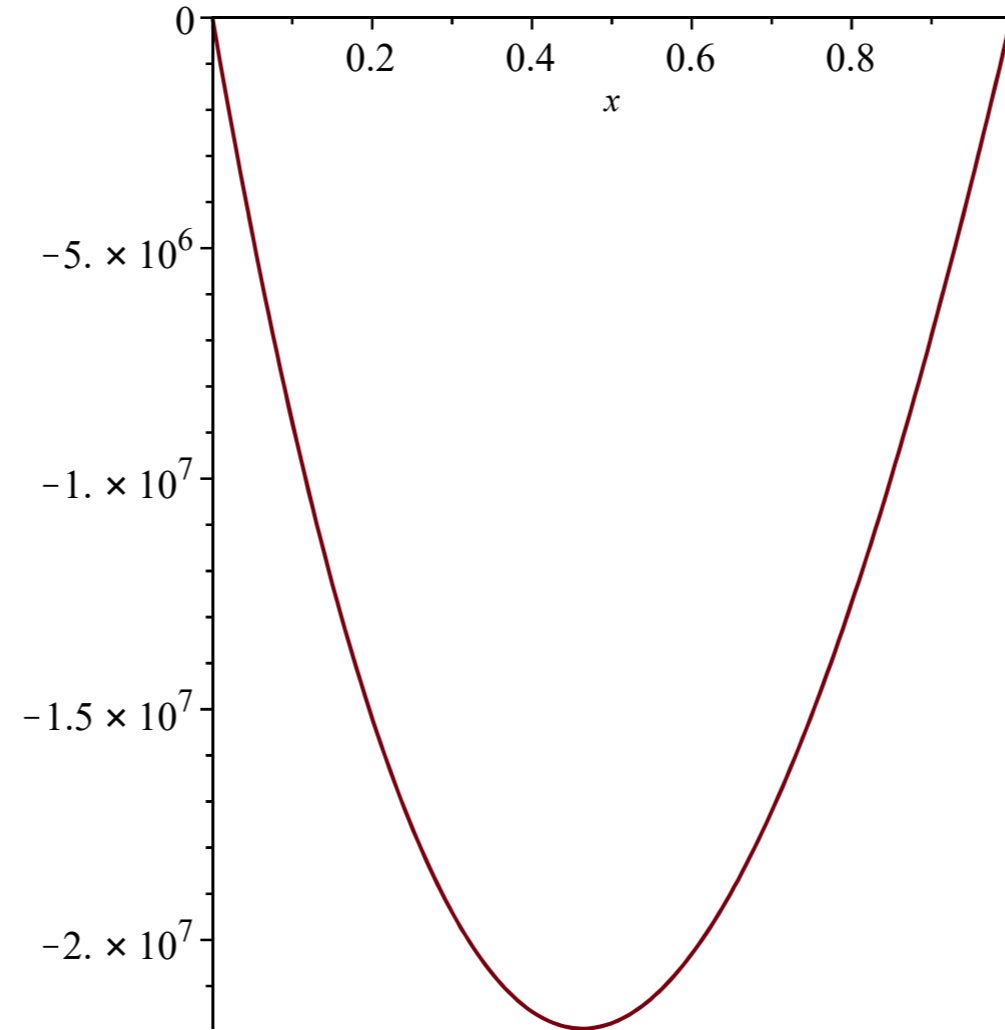
(62)

```
> Wlc_1_comp := subs(Awlc_1=Awlc_1_comp, Bwlc_1=Bwlc_1_comp, Cwlc_1=Cwlc_1_comp, Dwlc_1=Dwlc_1_comp, Betaw1_j=1, Wlc_1);
      Wlc_1_comp := 1.25339703571085 108 cosh(x) - 1.24366775577511 108 sinh(x) - 1.25339703571088 108 cos(x) + 2.43241240701675 107 sin(x)
```

(63)

```
> with(plots) :
```

```
> plotWlc_1_comp := plot(Wlc_1_comp, x=0..1) : display([plotWlc_1_comp]);
```



```
> Uxc_j := 1 : Uxs_j := 1 : PHyc_j := 1 : Omega_j := 10 : Omega_1 := Omega_j : hcg1 := 1 : hcg2 := 1 : hcg3 := 1 :
```

```
> rhoA_w1 := 1 : rhoA_w2 := 1 : rhoA_w3 := 1 : rhoA_w4 := 1 : rhoA_u1 := 1 : rhoA_u2 := 1 : rhoA_u3 := 1 : rhoA_u4 := 1 :
```

```
> EI_w1 := 1 : EI_w2 := 1 : EI_w3 := 1 : EI_w4 := 1 : EI_u1 := 1 : EI_u2 := 1 : EI_u3 := 1 : EI_u4 := 1 :
```

```
> Betaw1_j :=  $\left(\frac{\rho A_w1}{EI_w1} \cdot \Omega_j^2\right)^{\left(\frac{1}{4}\right)}$  : Betaw2_j :=  $\left(\frac{\rho A_w2}{EI_w2} \cdot \Omega_j^2\right)^{\left(\frac{1}{4}\right)}$  : Betaw3_j :=  $\left(\frac{\rho A_w3}{EI_w3} \cdot \Omega_j^2\right)^{\left(\frac{1}{4}\right)}$  : Betaw4_j :=  $\left(\frac{\rho A_w4}{EI_w4} \cdot \Omega_j^2\right)^{\left(\frac{1}{4}\right)}$  :
```

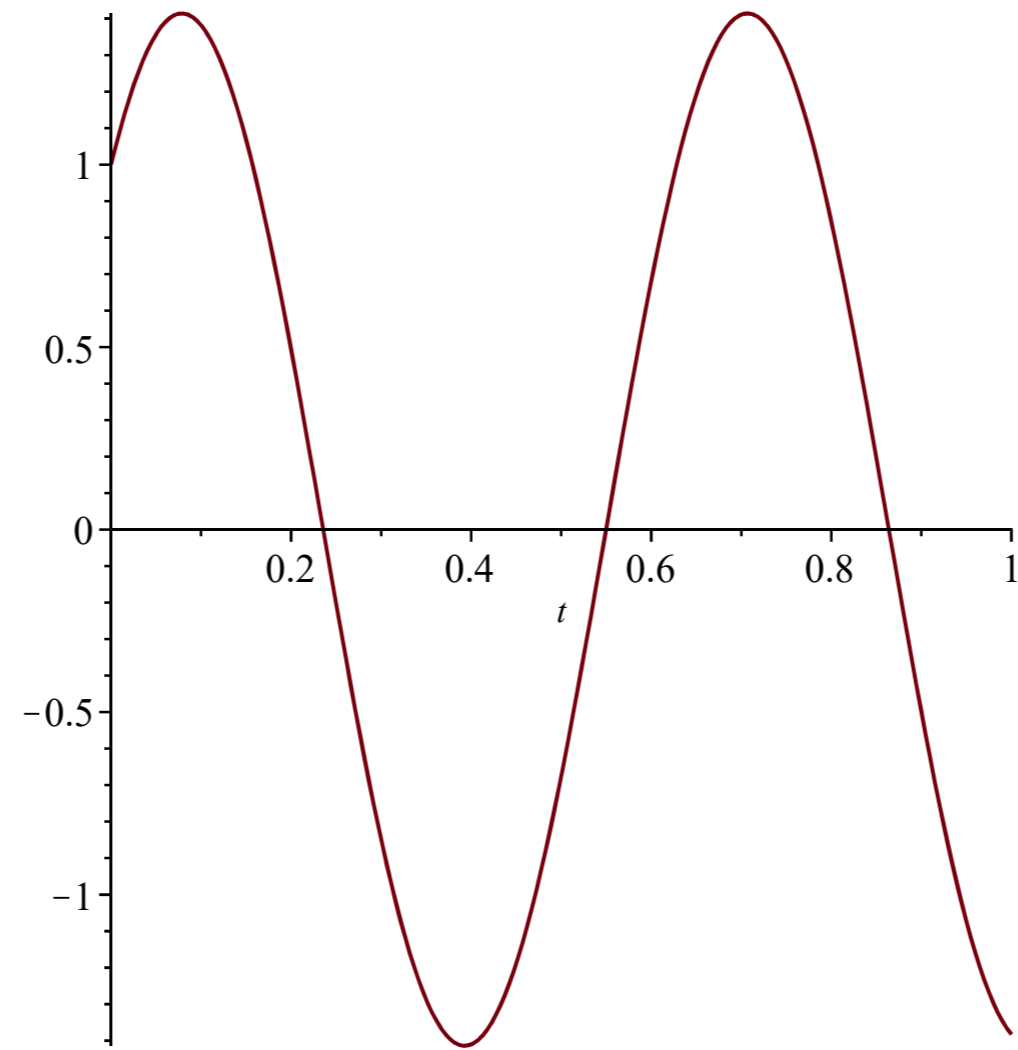
```
> Betau1_j :=  $\left(\frac{\rho A_u1}{EI_u1} \cdot \Omega_j^2\right)^{\left(\frac{1}{4}\right)}$  : Betau2_j :=  $\left(\frac{\rho A_u2}{EI_u2} \cdot \Omega_j^2\right)^{\left(\frac{1}{4}\right)}$  : Betau3_j :=  $\left(\frac{\rho A_u3}{EI_u3} \cdot \Omega_j^2\right)^{\left(\frac{1}{4}\right)}$  : Betau4_j :=  $\left(\frac{\rho A_u4}{EI_u4} \cdot \Omega_j^2\right)^{\left(\frac{1}{4}\right)}$  :
```

```
> span := 1 : hw1 := 1 : hw2 := 1 :
```

```
>
```

```
> ux;  
└─┬─  
> plotUx_1_comp := plot(ux, t=0..1) : display([plotUx_1_comp]);
```

$$\cos(10 t) + \sin(10 t)$$



R. Appendix: Maple sheet for determining dynamic EB-beams response Model_z

```

> restart;
>
Model_z (vertical excitation at bottom of frame only)
Excitation
> wz1 := Wz1c_j*cos(Omega_j*t);
wz1 := Wz1c_j cos(Omega_j t) (1)
> wz2 := wz1; Wz2cj := Wz1c_j:
wz2 := Wz1c_j cos(Omega_j t) (2)
>
Steady-State solutions of every element in the Model
> w1 := W1c_1*cos(Omega_j*t) + W1s_1*sin(Omega_j*t);
w1 := W1c_1 cos(Omega_j t) + W1s_1 sin(Omega_j t) (3)
> w2 := W2c_1*cos(Omega_j*t) + W2s_1*sin(Omega_j*t);
w2 := W2c_1 cos(Omega_j t) + W2s_1 sin(Omega_j t) (4)
> w3 := W3c_1*cos(Omega_j*t) + W3s_1*sin(Omega_j*t);
w3 := W3c_1 cos(Omega_j t) + W3s_1 sin(Omega_j t) (5)
> w4 := W4c_1*cos(Omega_j*t) + W4s_1*sin(Omega_j*t);
w4 := W4c_1 cos(Omega_j t) + W4s_1 sin(Omega_j t) (6)
> u1 := U1c_1*cos(Omega_j*t) + U1s_1*sin(Omega_j*t);
u1 := U1c_1 cos(Omega_j t) + U1s_1 sin(Omega_j t) (7)
> u2 := U2c_1*cos(Omega_j*t) + U2s_1*sin(Omega_j*t);
u2 := U2c_1 cos(Omega_j t) + U2s_1 sin(Omega_j t) (8)
> u3 := U3c_1*cos(Omega_j*t) + U3s_1*sin(Omega_j*t);
u3 := U3c_1 cos(Omega_j t) + U3s_1 sin(Omega_j t) (9)
> u4 := U4c_1*cos(Omega_j*t) + U4s_1*sin(Omega_j*t);
u4 := U4c_1 cos(Omega_j t) + U4s_1 sin(Omega_j t) (10)
>
Substituting the steady-state solutions into the EOM of every element and gathering for the cos(Omega_1)- (c_1) and sin(Omega_1)- (s_1) terms gives the following EOM's and corresponding general solutions:
> EOMw1c_1 := -rhoA_w1*Omega^2*W1c_1 + EI_w1*diff(W1c_1, x$4) = 0 :
> W1c_1 := Aw1c_1*cosh(Betaw1_j*x) + Bw1c_1*sinh(Betaw1_j*x) + Cw1c_1*cos(Betaw1_j*x) + Dw1c_1*sin(Betaw1_j*x);
W1c_1 := Aw1c_1 cosh(Betaw1_j x) + Bw1c_1 sinh(Betaw1_j x) + Cw1c_1 cos(Betaw1_j x) + Dw1c_1 sin(Betaw1_j x) (11)
> EOMw1s_1 := -rhoA_w1*Omega^2*W1s_1 + EI_w1*diff(W1s_1, x$4) = 0 :
> W1s_1 := Aw1s_1*cosh(Betaw1_j*x) + Bw1s_1*sinh(Betaw1_j*x) + Cw1s_1*cos(Betaw1_j*x) + Dw1s_1*sin(Betaw1_j*x);
W1s_1 := Aw1s_1 cosh(Betaw1_j x) + Bw1s_1 sinh(Betaw1_j x) + Cw1s_1 cos(Betaw1_j x) + Dw1s_1 sin(Betaw1_j x) (12)
> EOMw2c_1 := -rhoA_w2*Omega^2*W2c_1 + EI_w2*diff(W2c_1, x$4) = 0 :
> W2c_1 := Aw2c_1*cosh(Betaw2_j*x) + Bw2c_1*sinh(Betaw2_j*x) + Cw2c_1*cos(Betaw2_j*x) + Dw2c_1*sin(Betaw2_j*x);
W2c_1 := Aw2c_1 cosh(Betaw2_j x) + Bw2c_1 sinh(Betaw2_j x) + Cw2c_1 cos(Betaw2_j x) + Dw2c_1 sin(Betaw2_j x) (13)
> EOMw2s_1 := -rhoA_w2*Omega^2*W2s_1 + EI_w2*diff(W2s_1, x$4) = 0 :
> W2s_1 := Aw2s_1*cosh(Betaw2_j*x) + Bw2s_1*sinh(Betaw2_j*x) + Cw2s_1*cos(Betaw2_j*x) + Dw2s_1*sin(Betaw2_j*x);
W2s_1 := Aw2s_1 cosh(Betaw2_j x) + Bw2s_1 sinh(Betaw2_j x) + Cw2s_1 cos(Betaw2_j x) + Dw2s_1 sin(Betaw2_j x) (14)
> EOMw3c_1 := -rhoA_w3*Omega^2*W3c_1 + EI_w3*diff(W3c_1, x$4) = 0 :
> W3c_1 := Aw3c_1*cosh(Betaw3_j*x) + Bw3c_1*sinh(Betaw3_j*x) + Cw3c_1*cos(Betaw3_j*x) + Dw3c_1*sin(Betaw3_j*x);
W3c_1 := Aw3c_1 cosh(Betaw3_j x) + Bw3c_1 sinh(Betaw3_j x) + Cw3c_1 cos(Betaw3_j x) + Dw3c_1 sin(Betaw3_j x) (15)
> EOMw3s_1 := -rhoA_w3*Omega^2*W3s_1 + EI_w3*diff(W3s_1, x$4) = 0 :
> W3s_1 := Aw3s_1*cosh(Betaw3_j*x) + Bw3s_1*sinh(Betaw3_j*x) + Cw3s_1*cos(Betaw3_j*x) + Dw3s_1*sin(Betaw3_j*x);

```

$$W3s_1 := Aw3s_1 \cosh(\text{Betaw3_j}x) + Bw3s_1 \sinh(\text{Betaw3_j}x) + Cw3s_1 \cos(\text{Betaw3_j}x) + Dw3s_1 \sin(\text{Betaw3_j}x) \quad (16)$$

$$\text{> } EOMw4c_1 := -\rho A_{w4} \cdot \Omega I^2 \cdot W4c_1 + EI_{w4} \cdot \text{diff}(W4c_1, x\$4) = 0 :$$

$$\text{> } W4c_1 := Aw4c_1 \cdot \cosh(\text{Betaw4_j}x) + Bw4c_1 \cdot \sinh(\text{Betaw4_j}x) + Cw4c_1 \cdot \cos(\text{Betaw4_j}x) + Dw4c_1 \cdot \sin(\text{Betaw4_j}x);$$

$$W4c_1 := Aw4c_1 \cosh(\text{Betaw4_j}x) + Bw4c_1 \sinh(\text{Betaw4_j}x) + Cw4c_1 \cos(\text{Betaw4_j}x) + Dw4c_1 \sin(\text{Betaw4_j}x) \quad (17)$$

$$\text{> } EOMw4s_1 := -\rho A_{w4} \cdot \Omega I^2 \cdot W4s_1 + EI_{w4} \cdot \text{diff}(W4s_1, x\$4) = 0 :$$

$$\text{> } W4s_1 := Aw4s_1 \cdot \cosh(\text{Betaw4_j}x) + Bw4s_1 \cdot \sinh(\text{Betaw4_j}x) + Cw4s_1 \cdot \cos(\text{Betaw4_j}x) + Dw4s_1 \cdot \sin(\text{Betaw4_j}x);$$

$$W4s_1 := Aw4s_1 \cosh(\text{Betaw4_j}x) + Bw4s_1 \sinh(\text{Betaw4_j}x) + Cw4s_1 \cos(\text{Betaw4_j}x) + Dw4s_1 \sin(\text{Betaw4_j}x) \quad (18)$$

$$\text{> } EOMu1c_1 := -\rho A_{u1} \cdot \Omega I^2 \cdot U1c_1 + EI_{u1} \cdot \text{diff}(U1c_1, z\$4) = 0 :$$

$$\text{> } U1c_1 := Au1c_1 \cdot \cosh(\text{Betau1_j}z) + Bu1c_1 \cdot \sinh(\text{Betau1_j}z) + Cu1c_1 \cdot \cos(\text{Betau1_j}z) + Du1c_1 \cdot \sin(\text{Betau1_j}z);$$

$$U1c_1 := Au1c_1 \cosh(\text{Betau1_j}z) + Bu1c_1 \sinh(\text{Betau1_j}z) + Cu1c_1 \cos(\text{Betau1_j}z) + Du1c_1 \sin(\text{Betau1_j}z) \quad (19)$$

$$\text{> } EOMu1s_1 := -\rho A_{u1} \cdot \Omega I^2 \cdot U1s_1 + EI_{u1} \cdot \text{diff}(U1s_1, z\$4) = 0 :$$

$$\text{> } U1s_1 := Au1s_1 \cdot \cosh(\text{Betau1_j}z) + Bu1s_1 \cdot \sinh(\text{Betau1_j}z) + Cu1s_1 \cdot \cos(\text{Betau1_j}z) + Du1s_1 \cdot \sin(\text{Betau1_j}z);$$

$$U1s_1 := Au1s_1 \cosh(\text{Betau1_j}z) + Bu1s_1 \sinh(\text{Betau1_j}z) + Cu1s_1 \cos(\text{Betau1_j}z) + Du1s_1 \sin(\text{Betau1_j}z) \quad (20)$$

$$\text{> } EOMu2c_1 := -\rho A_{u2} \cdot \Omega I^2 \cdot U2c_1 + EI_{u2} \cdot \text{diff}(U2c_1, z\$4) = 0 :$$

$$\text{> } U2c_1 := Au2c_1 \cdot \cosh(\text{Betau2_j}z) + Bu2c_1 \cdot \sinh(\text{Betau2_j}z) + Cu2c_1 \cdot \cos(\text{Betau2_j}z) + Du2c_1 \cdot \sin(\text{Betau2_j}z);$$

$$U2c_1 := Au2c_1 \cosh(\text{Betau2_j}z) + Bu2c_1 \sinh(\text{Betau2_j}z) + Cu2c_1 \cos(\text{Betau2_j}z) + Du2c_1 \sin(\text{Betau2_j}z) \quad (21)$$

$$\text{> } EOMu2s_1 := -\rho A_{u2} \cdot \Omega I^2 \cdot U2s_1 + EI_{u2} \cdot \text{diff}(U2s_1, z\$4) = 0 :$$

$$\text{> } U2s_1 := Au2s_1 \cdot \cosh(\text{Betau2_j}z) + Bu2s_1 \cdot \sinh(\text{Betau2_j}z) + Cu2s_1 \cdot \cos(\text{Betau2_j}z) + Du2s_1 \cdot \sin(\text{Betau2_j}z);$$

$$U2s_1 := Au2s_1 \cosh(\text{Betau2_j}z) + Bu2s_1 \sinh(\text{Betau2_j}z) + Cu2s_1 \cos(\text{Betau2_j}z) + Du2s_1 \sin(\text{Betau2_j}z) \quad (22)$$

$$\text{> } EOMu3c_1 := -\rho A_{u3} \cdot \Omega I^2 \cdot U3c_1 + EI_{u3} \cdot \text{diff}(U3c_1, z\$4) = 0 :$$

$$\text{> } U3c_1 := Au3c_1 \cdot \cosh(\text{Betau3_j}z) + Bu3c_1 \cdot \sinh(\text{Betau3_j}z) + Cu3c_1 \cdot \cos(\text{Betau3_j}z) + Du3c_1 \cdot \sin(\text{Betau3_j}z);$$

$$U3c_1 := Au3c_1 \cosh(\text{Betau3_j}z) + Bu3c_1 \sinh(\text{Betau3_j}z) + Cu3c_1 \cos(\text{Betau3_j}z) + Du3c_1 \sin(\text{Betau3_j}z) \quad (23)$$

$$\text{> } EOMu3s_1 := -\rho A_{u3} \cdot \Omega I^2 \cdot U3s_1 + EI_{u3} \cdot \text{diff}(U3s_1, z\$4) = 0 :$$

$$\text{> } U3s_1 := Au3s_1 \cdot \cosh(\text{Betau3_j}z) + Bu3s_1 \cdot \sinh(\text{Betau3_j}z) + Cu3s_1 \cdot \cos(\text{Betau3_j}z) + Du3s_1 \cdot \sin(\text{Betau3_j}z);$$

$$U3s_1 := Au3s_1 \cosh(\text{Betau3_j}z) + Bu3s_1 \sinh(\text{Betau3_j}z) + Cu3s_1 \cos(\text{Betau3_j}z) + Du3s_1 \sin(\text{Betau3_j}z) \quad (24)$$

$$\text{> } EOMu4c_1 := -\rho A_{u4} \cdot \Omega I^2 \cdot U4c_1 + EI_{u4} \cdot \text{diff}(U4c_1, z\$4) = 0 :$$

$$\text{> } U4c_1 := Au4c_1 \cdot \cosh(\text{Betau4_j}z) + Bu4c_1 \cdot \sinh(\text{Betau4_j}z) + Cu4c_1 \cdot \cos(\text{Betau4_j}z) + Du4c_1 \cdot \sin(\text{Betau4_j}z);$$

$$U4c_1 := Au4c_1 \cosh(\text{Betau4_j}z) + Bu4c_1 \sinh(\text{Betau4_j}z) + Cu4c_1 \cos(\text{Betau4_j}z) + Du4c_1 \sin(\text{Betau4_j}z) \quad (25)$$

$$\text{> } EOMu4s_1 := -\rho A_{u4} \cdot \Omega I^2 \cdot U4s_1 + EI_{u4} \cdot \text{diff}(U4s_1, z\$4) = 0 :$$

$$\text{> } U4s_1 := Au4s_1 \cdot \cosh(\text{Betau4_j}z) + Bu4s_1 \cdot \sinh(\text{Betau4_j}z) + Cu4s_1 \cdot \cos(\text{Betau4_j}z) + Du4s_1 \cdot \sin(\text{Betau4_j}z);$$

$$U4s_1 := Au4s_1 \cosh(\text{Betau4_j}z) + Bu4s_1 \sinh(\text{Betau4_j}z) + Cu4s_1 \cos(\text{Betau4_j}z) + Du4s_1 \sin(\text{Betau4_j}z) \quad (26)$$

Substitute the general solutions into the IC's and BC's (4*8 EB-elements = 32 needed IC's + BC's) and gather for the cos(Omega_1) terms

BC @ x = 0, z = 0 [2 BC's]

$$\text{> } BC1c_1M := \text{simplify}(\text{subs}(z=0, U1c_1)) : BC1c_1 := BC1c_1M=0;$$

$$BC1c_1 := Au1c_1 + Cu1c_1 = 0 \quad (27)$$

$$\text{> } BC2c_1M := \text{simplify}(\text{subs}(z=0, \text{diff}(U1c_1, z))) : BC2c_1 := BC2c_1M=0;$$

$$BC2c_1 := \text{Betau1_j} (Bu1c_1 + Du1c_1) = 0 \quad (28)$$

BC @ x = span, z = 0 [2 BC's]

$$\text{> } BC3c_1M := \text{simplify}(\text{subs}(z=0, U3c_1)) : BC3c_1 := BC3c_1M=0;$$

$$BC3c_1 := Au3c_1 + Cu3c_1 = 0 \quad (29)$$

$$\text{> } BC4c_1M := \text{simplify}(\text{subs}(z=0, \text{diff}(U3c_1, z))) : BC4c_1 := BC4c_1M=0;$$

$$BC4c_1 := \text{Betaw3_j} (Bu3c_1 + Du3c_1) = 0 \quad (30)$$

BC @ x = 2*span, z = hw1 [2 BC's]

$$\begin{aligned} > BC5c_1M := \text{simplify}(\text{subs}(x=2 \cdot \text{span}, W2c_1)) - Wzc_j - PHlyc_j \cdot \text{scg3} : BC5c_1 := BC5c_1M = 0; \\ BC5c_1 &:= Aw2c_1 \cosh(2 \text{ Betaw2_j span}) + Bw2c_1 \sinh(2 \text{ Betaw2_j span}) + Cw2c_1 \cos(2 \text{ Betaw2_j span}) + Dw2c_1 \sin(2 \text{ Betaw2_j span}) - Wzc_j - PHlyc_j \cdot \text{scg3} = 0 \end{aligned} \quad (31)$$

$$\begin{aligned} > BC6c_1M := \text{simplify}(\text{subs}(x=2 \cdot \text{span}, \text{diff}(W2c_1, x))) : BC6c_1 := BC6c_1M = 0; \\ BC6c_1 &:= \text{Betaw2_j} (Aw2c_1 \sinh(2 \text{ Betaw2_j span}) + Bw2c_1 \cosh(2 \text{ Betaw2_j span}) - Cw2c_1 \sin(2 \text{ Betaw2_j span}) + Dw2c_1 \cos(2 \text{ Betaw2_j span})) = 0 \end{aligned} \quad (32)$$

BC @ x = 2*span, z = hw1+hw2 [2 BC's]

$$\begin{aligned} > BC7c_1M := \text{simplify}(\text{subs}(x=2 \cdot \text{span}, W4c_1)) - \text{simplify}(\text{subs}(x=2 \cdot \text{span}, W2c_1)) : BC7c_1 := BC7c_1M = 0; \\ BC7c_1 &:= Aw4c_1 \cosh(2 \text{ Betaw4_j span}) + Bw4c_1 \sinh(2 \text{ Betaw4_j span}) + Cw4c_1 \cos(2 \text{ Betaw4_j span}) + Dw4c_1 \sin(2 \text{ Betaw4_j span}) - Aw2c_1 \cosh(2 \text{ Betaw2_j span}) - Bw2c_1 \sinh(2 \text{ Betaw2_j span}) \\ &\quad - Cw2c_1 \cos(2 \text{ Betaw2_j span}) - Dw2c_1 \sin(2 \text{ Betaw2_j span}) = 0 \end{aligned} \quad (33)$$

$$\begin{aligned} > BC8c_1M := \text{simplify}(\text{subs}(x=2 \cdot \text{span}, \text{diff}(W4c_1, x))) : BC8c_1 := BC8c_1M = 0; \\ BC8c_1 &:= \text{Betaw4_j} (Aw4c_1 \sinh(2 \text{ Betaw4_j span}) + Bw4c_1 \cosh(2 \text{ Betaw4_j span}) - Cw4c_1 \sin(2 \text{ Betaw4_j span}) + Dw4c_1 \cos(2 \text{ Betaw4_j span})) = 0 \end{aligned} \quad (34)$$

IC @ x = 0, z = hw1 [6 IC's]

$$\begin{aligned} > IC1c_1M := \text{simplify}(\text{subs}(z=hw1, U1c_1)) - \text{simplify}(\text{subs}(z=hw1, U2c_1)) : IC1c_1 := IC1c_1M = 0; \\ IC1c_1 &:= Au1c_1 \cosh(\text{Betaw1_j hw1}) + Bu1c_1 \sinh(\text{Betaw1_j hw1}) + Cu1c_1 \cos(\text{Betaw1_j hw1}) + Du1c_1 \sin(\text{Betaw1_j hw1}) - Au2c_1 \cosh(\text{Betaw2_j hw1}) - Bu2c_1 \sinh(\text{Betaw2_j hw1}) \\ &\quad - Cu2c_1 \cos(\text{Betaw2_j hw1}) - Du2c_1 \sin(\text{Betaw2_j hw1}) = 0 \end{aligned} \quad (35)$$

$$\begin{aligned} > IC2c_1M := \text{simplify}(\text{subs}(x=0, W1c_1)) - Wzc_j - PHlyc_j \cdot \text{scg1} : IC3c_1 := IC3c_1M = 0; \\ IC3c_1 &:= IC3c_1M = 0 \end{aligned} \quad (36)$$

$$\begin{aligned} > IC3c_1M := \text{simplify}(\text{subs}(z=hw1, U1c_1)) : IC2c_1 := IC2c_1M = 0; \\ IC2c_1 &:= -PHlyc_j \cdot \text{scg1} + Aw1c_1 + Cw1c_1 - Wzc_j = 0 \end{aligned} \quad (37)$$

$$\begin{aligned} > IC4c_1M := \text{simplify}(\text{subs}(z=hw1, \text{diff}(U1c_1, z))) - \text{simplify}(\text{subs}(z=hw1, \text{diff}(U2c_1, z))) : IC4c_1 := IC4c_1M = 0; \\ IC4c_1 &:= \text{Betaw1_j} (Au1c_1 \sinh(\text{Betaw1_j hw1}) + Bu1c_1 \cosh(\text{Betaw1_j hw1}) - Cu1c_1 \sin(\text{Betaw1_j hw1}) + Du1c_1 \cos(\text{Betaw1_j hw1})) - \text{Betaw2_j} (Au2c_1 \sinh(\text{Betaw2_j hw1}) \\ &\quad + Bu2c_1 \cosh(\text{Betaw2_j hw1}) - Cu2c_1 \sin(\text{Betaw2_j hw1}) + Du2c_1 \cos(\text{Betaw2_j hw1})) = 0 \end{aligned} \quad (38)$$

$$\begin{aligned} > IC5c_1M := \text{simplify}(\text{subs}(z=hw1, \text{diff}(U1c_1, z))) + \text{simplify}(\text{subs}(x=0, \text{diff}(W1c_1, x))) : IC5c_1 := IC5c_1M = 0; \\ IC5c_1 &:= \text{Betaw1_j} (Au1c_1 \sinh(\text{Betaw1_j hw1}) + Bu1c_1 \cosh(\text{Betaw1_j hw1}) - Cu1c_1 \sin(\text{Betaw1_j hw1}) + Du1c_1 \cos(\text{Betaw1_j hw1})) + \text{Betaw1_j} (Bw1c_1 + Dw1c_1) = 0 \end{aligned} \quad (39)$$

$$\begin{aligned} > IC6c_1M := -\text{simplify}(\text{subs}(z=hw1, \text{diff}(U1c_1, z^2))) + \text{simplify}(\text{subs}(z=hw1, \text{diff}(U2c_1, z^2))) + \text{simplify}(\text{subs}(x=0, \text{diff}(W1c_1, x^2))) : IC6c_1 := IC6c_1M = 0; \\ IC6c_1 &:= -\text{Betaw1_j}^2 (Au1c_1 \cosh(\text{Betaw1_j hw1}) + Bu1c_1 \sinh(\text{Betaw1_j hw1}) - Cu1c_1 \cos(\text{Betaw1_j hw1}) - Du1c_1 \sin(\text{Betaw1_j hw1})) + \text{Betaw2_j}^2 (Au2c_1 \cosh(\text{Betaw2_j hw1}) \\ &\quad + Bu2c_1 \sinh(\text{Betaw2_j hw1}) - Cu2c_1 \cos(\text{Betaw2_j hw1}) - Du2c_1 \sin(\text{Betaw2_j hw1})) + \text{Betaw1_j}^2 (Aw1c_1 - Cw1c_1) = 0 \end{aligned} \quad (40)$$

IC @ x = 0, z = hw1+hw2 [6 IC's]

$$\begin{aligned} > IC7c_1M := \text{simplify}(\text{subs}(x=0, W3c_1)) - \text{simplify}(\text{subs}(x=0, W1c_1)) : IC7c_1 := IC7c_1M = 0; \\ IC7c_1 &:= Aw3c_1 + Cw3c_1 - Aw1c_1 - Cw1c_1 = 0 \end{aligned} \quad (41)$$

$$\begin{aligned} > IC8c_1M := \text{simplify}(\text{subs}(z=hw1 + hw2, \text{diff}(U2c_1, z))) + \text{simplify}(\text{subs}(x=0, \text{diff}(W3c_1, x))) : IC8c_1 := IC8c_1M = 0; \\ IC8c_1 &:= \text{Betaw2_j} (Au2c_1 \sinh(\text{Betaw2_j} (hw1 + hw2)) + Bu2c_1 \cosh(\text{Betaw2_j} (hw1 + hw2)) - Cu2c_1 \sin(\text{Betaw2_j} (hw1 + hw2)) + Du2c_1 \cos(\text{Betaw2_j} (hw1 + hw2))) + \text{Betaw3_j} (Bw3c_1 \\ &\quad + Dw3c_1) = 0 \end{aligned} \quad (42)$$

$$\begin{aligned} > IC9c_1M := \text{simplify}(\text{subs}(z=hw1 + hw2, U2c_1)) - \text{simplify}(\text{subs}(z=hw1 + hw2, U4c_1)) : IC9c_1 := IC9c_1M = 0; \\ IC9c_1 &:= Au2c_1 \cosh(\text{Betaw2_j} (hw1 + hw2)) + Bu2c_1 \sinh(\text{Betaw2_j} (hw1 + hw2)) + Cu2c_1 \cos(\text{Betaw2_j} (hw1 + hw2)) + Du2c_1 \sin(\text{Betaw2_j} (hw1 + hw2)) - Au4c_1 \cosh(\text{Betaw4_j} (hw1 + hw2)) \\ &\quad - Bu4c_1 \sinh(\text{Betaw4_j} (hw1 + hw2)) - Cu4c_1 \cos(\text{Betaw4_j} (hw1 + hw2)) - Du4c_1 \sin(\text{Betaw4_j} (hw1 + hw2)) = 0 \end{aligned} \quad (43)$$

$$\begin{aligned} > IC10c_1M := -\text{simplify}(\text{subs}(z=hw1 + hw2, \text{diff}(U2c_1, z^2))) + \text{simplify}(\text{subs}(x=0, \text{diff}(W3c_1, x^2))) : IC10c_1 := IC10c_1M = 0; \\ IC10c_1 &:= -\text{Betaw2_j}^2 (Au2c_1 \cosh(\text{Betaw2_j} (hw1 + hw2)) + Bu2c_1 \sinh(\text{Betaw2_j} (hw1 + hw2)) - Cu2c_1 \cos(\text{Betaw2_j} (hw1 + hw2)) - Du2c_1 \sin(\text{Betaw2_j} (hw1 + hw2))) + \text{Betaw3_j}^2 (Aw3c_1 \\ &\quad - Cw3c_1) = 0 \end{aligned} \quad (44)$$

IC @ x = span, z = hw1 [8 IC's]

$$\begin{aligned} > IC11c_1M := \text{simplify}(\text{subs}(x=\text{span}, W1c_1)) - \text{simplify}(\text{subs}(x=\text{span}, W2c_1)) : IC11c_1 := IC11c_1M = 0; \\ IC11c_1 &:= Aw1c_1 \cosh(\text{Betaw1_j span}) + Bw1c_1 \sinh(\text{Betaw1_j span}) + Cw1c_1 \cos(\text{Betaw1_j span}) + Dw1c_1 \sin(\text{Betaw1_j span}) - Aw2c_1 \cosh(\text{Betaw2_j span}) - Bw2c_1 \sinh(\text{Betaw2_j span}) \\ &\quad - Cw2c_1 \cos(\text{Betaw2_j span}) - Dw2c_1 \sin(\text{Betaw2_j span}) = 0 \end{aligned} \quad (45)$$

$$\begin{aligned} > IC12c_1M := \text{simplify}(\text{subs}(x=\text{span}, W1c_1)) - Wzc_j - PHlyc_j \cdot \text{scg2} : IC12c_1 := IC12c_1M = 0; \\ IC12c_1 &:= Aw1c_1 \cosh(\text{Betaw1_j span}) + Bw1c_1 \sinh(\text{Betaw1_j span}) + Cw1c_1 \cos(\text{Betaw1_j span}) + Dw1c_1 \sin(\text{Betaw1_j span}) - Wzc_j - PHlyc_j \cdot \text{scg2} = 0 \end{aligned} \quad (46)$$

$$\begin{aligned} &> IC13c_1M := \text{simplify}(\text{subs}(z = hw1, U3c_1)) - \text{simplify}(\text{subs}(z = hw1, U4c_1)) : IC13c_1 := IC13c_1M = 0; \\ IC13c_1 &:= Au3c_1 \cosh(\text{Betaw3}_j hw1) + Bu3c_1 \sinh(\text{Betaw3}_j hw1) + Cu3c_1 \cos(\text{Betaw3}_j hw1) + Du3c_1 \sin(\text{Betaw3}_j hw1) - Au4c_1 \cosh(\text{Betaw4}_j hw1) - Bu4c_1 \sinh(\text{Betaw4}_j hw1) \\ &\quad - Cu4c_1 \cos(\text{Betaw4}_j hw1) - Du4c_1 \sin(\text{Betaw4}_j hw1) = 0 \end{aligned} \quad (47)$$

$$\begin{aligned} &> IC14c_1M := \text{simplify}(\text{subs}(x = span, \text{diff}(W1c_1, x))) - \text{simplify}(\text{subs}(x = span, \text{diff}(W2c_1, x))) : IC15c_1 := IC15c_1M = 0; \\ IC15c_1 &:= IC15c_1M = 0 \end{aligned} \quad (48)$$

$$\begin{aligned} &> IC15c_1M := \text{simplify}(\text{subs}(z = hw1, \text{diff}(U3c_1, z))) - \text{simplify}(\text{subs}(z = hw1, \text{diff}(U4c_1, z))) : IC16c_1 := IC16c_1M = 0; \\ IC16c_1 &:= IC16c_1M = 0 \end{aligned} \quad (49)$$

$$\begin{aligned} &> IC16c_1M := \text{simplify}(\text{subs}(x = span, \text{diff}(W1c_1, x))) + \text{simplify}(\text{subs}(z = hw1, \text{diff}(U3c_1, z))) : IC17c_1 := IC17c_1M = 0; \\ IC17c_1 &:= IC17c_1M = 0 \end{aligned} \quad (50)$$

$$\begin{aligned} &> IC17c_1M := -\text{simplify}(\text{subs}(x = span, \text{diff}(W1c_1, x\$2))) + \text{simplify}(\text{subs}(z = hw1, \text{diff}(U4c_1, z\$2))) + \text{simplify}(\text{subs}(x = span, \text{diff}(W2c_1, x\$2))) - \text{simplify}(\text{subs}(z = hw1, \text{diff}(U3c_1, z\$2))) : IC18c_1 := \\ IC18c_1 &:= IC18c_1M = 0; \\ IC18c_1 &:= IC18c_1M = 0 \end{aligned} \quad (51)$$

$$\begin{aligned} &> IC18c_1M := \text{simplify}(\text{subs}(z = hw1, U1c_1)) - \text{simplify}(\text{subs}(z = hw1, U3c_1)) : IC14c_1 := IC14c_1M = 0; \\ IC14c_1 &:= \text{Betaw1}_j (Aw1c_1 \sinh(\text{Betaw1}_j span) + Bw1c_1 \cosh(\text{Betaw1}_j span) - Cw1c_1 \sin(\text{Betaw1}_j span) + Dw1c_1 \cos(\text{Betaw1}_j span)) - \text{Betaw2}_j (Aw2c_1 \sinh(\text{Betaw2}_j span) \\ &\quad + Bw2c_1 \cosh(\text{Betaw2}_j span) - Cw2c_1 \sin(\text{Betaw2}_j span) + Dw2c_1 \cos(\text{Betaw2}_j span)) = 0 \end{aligned} \quad (52)$$

$$\begin{aligned} &> \\ IC @ x = span, z = hw1+hw2 [6 IC's] \end{aligned}$$

$$\begin{aligned} &> IC19c_1M := \text{simplify}(\text{subs}(x = span, W3c_1)) - \text{simplify}(\text{subs}(x = span, W4c_1)) : IC19c_1 := IC19c_1M = 0; \\ IC19c_1 &:= Aw3c_1 \cosh(\text{Betaw3}_j span) + Bw3c_1 \sinh(\text{Betaw3}_j span) + Cw3c_1 \cos(\text{Betaw3}_j span) + Dw3c_1 \sin(\text{Betaw3}_j span) - Aw4c_1 \cosh(\text{Betaw4}_j span) - Bw4c_1 \sinh(\text{Betaw4}_j span) \\ &\quad - Cw4c_1 \cos(\text{Betaw4}_j span) - Dw4c_1 \sin(\text{Betaw4}_j span) = 0 \end{aligned} \quad (53)$$

$$\begin{aligned} &> IC20c_1M := \text{simplify}(\text{subs}(x = span, W3c_1)) - \text{simplify}(\text{subs}(x = span, W1c_1)) : IC24c_1 := IC24c_1M = 0; \\ IC24c_1 &:= IC24c_1M = 0 \end{aligned} \quad (54)$$

$$\begin{aligned} &> IC21c_1M := \text{simplify}(\text{subs}(x = span, \text{diff}(W3c_1, x))) - \text{simplify}(\text{subs}(x = span, \text{diff}(W4c_1, x))) : IC21c_1 := IC21c_1M = 0; \\ IC21c_1 &:= \text{Betaw3}_j (Aw3c_1 \sinh(\text{Betaw3}_j span) + Bw3c_1 \cosh(\text{Betaw3}_j span) - Cw3c_1 \sin(\text{Betaw3}_j span) + Dw3c_1 \cos(\text{Betaw3}_j span)) - \text{Betaw4}_j (Aw4c_1 \sinh(\text{Betaw4}_j span) \\ &\quad + Bw4c_1 \cosh(\text{Betaw4}_j span) - Cw4c_1 \sin(\text{Betaw4}_j span) + Dw4c_1 \cos(\text{Betaw4}_j span)) = 0 \end{aligned} \quad (55)$$

$$\begin{aligned} &> IC22c_1M := \text{simplify}(\text{subs}(x = span, \text{diff}(W3c_1, x))) + \text{simplify}(\text{subs}(z = hw1 + hw2, \text{diff}(U4c_1, z))) : IC22c_1 := IC22c_1M = 0; \\ IC22c_1 &:= \text{Betaw3}_j (Aw3c_1 \sinh(\text{Betaw3}_j span) + Bw3c_1 \cosh(\text{Betaw3}_j span) - Cw3c_1 \sin(\text{Betaw3}_j span) + Dw3c_1 \cos(\text{Betaw3}_j span)) + \text{Betaw4}_j (Au4c_1 \sinh(\text{Betaw4}_j (hw1 + hw2)) \\ &\quad + Bu4c_1 \cosh(\text{Betaw4}_j (hw1 + hw2)) - Cu4c_1 \sin(\text{Betaw4}_j (hw1 + hw2)) + Du4c_1 \cos(\text{Betaw4}_j (hw1 + hw2))) = 0 \end{aligned} \quad (56)$$

$$\begin{aligned} &> IC23c_1M := -\text{simplify}(\text{subs}(x = span, \text{diff}(W3c_1, x\$2))) - \text{simplify}(\text{subs}(z = hw1 + hw2, \text{diff}(U4c_1, z\$2))) + \text{simplify}(\text{subs}(x = span, \text{diff}(W4c_1, x\$2))) : IC23c_1 := IC23c_1M = 0; \\ IC23c_1 &:= -\text{Betaw3}_j^2 (Aw3c_1 \cosh(\text{Betaw3}_j span) + Bw3c_1 \sinh(\text{Betaw3}_j span) - Cw3c_1 \cos(\text{Betaw3}_j span) - Dw3c_1 \sin(\text{Betaw3}_j span)) - \text{Betaw4}_j^2 (Au4c_1 \cosh(\text{Betaw4}_j (hw1 + hw2)) \\ &\quad + Bu4c_1 \sinh(\text{Betaw4}_j (hw1 + hw2)) - Cu4c_1 \cos(\text{Betaw4}_j (hw1 + hw2)) - Du4c_1 \sin(\text{Betaw4}_j (hw1 + hw2))) + \text{Betaw4}_j^2 (Aw4c_1 \cosh(\text{Betaw4}_j span) + Bw4c_1 \sinh(\text{Betaw4}_j span) \\ &\quad - Cw4c_1 \cos(\text{Betaw4}_j span) - Dw4c_1 \sin(\text{Betaw4}_j span)) = 0 \end{aligned} \quad (57)$$

$$\begin{aligned} &> IC24c_1M := \text{simplify}(\text{subs}(z = hw1 + hw2, U4c_1)) : IC20c_1 := IC20c_1M = 0; \\ IC20c_1 &:= Aw3c_1 \cosh(\text{Betaw3}_j span) + Bw3c_1 \sinh(\text{Betaw3}_j span) + Cw3c_1 \cos(\text{Betaw3}_j span) + Dw3c_1 \sin(\text{Betaw3}_j span) - Aw1c_1 \cosh(\text{Betaw1}_j span) - Bw1c_1 \sinh(\text{Betaw1}_j span) \\ &\quad - Cw1c_1 \cos(\text{Betaw1}_j span) - Dw1c_1 \sin(\text{Betaw1}_j span) = 0 \end{aligned} \quad (58)$$

$$\begin{aligned} &> \\ &> \text{interface}(rtablesiz = 35); \end{aligned} \quad (59)$$

$$\begin{aligned} &> \\ &> \end{aligned}$$

Coefficient matrix

$$\begin{aligned} &> Mc_j := \text{Matrix}([\\ &\quad [\text{coeff}(BC1c_1M, Aw1c_1), \text{coeff}(BC1c_1M, Bw1c_1), \text{coeff}(BC1c_1M, Cw1c_1), \text{coeff}(BC1c_1M, Dw1c_1), \\ &\quad \text{coeff}(BC1c_1M, Aw2c_1), \text{coeff}(BC1c_1M, Bw2c_1), \text{coeff}(BC1c_1M, Cw2c_1), \text{coeff}(BC1c_1M, Dw2c_1), \\ &\quad \text{coeff}(BC1c_1M, Aw3c_1), \text{coeff}(BC1c_1M, Bw3c_1), \text{coeff}(BC1c_1M, Cw3c_1), \text{coeff}(BC1c_1M, Dw3c_1), \\ &\quad \text{coeff}(BC1c_1M, Aw4c_1), \text{coeff}(BC1c_1M, Bw4c_1), \text{coeff}(BC1c_1M, Cw4c_1), \text{coeff}(BC1c_1M, Dw4c_1), \\ &\quad \text{coeff}(BC1c_1M, Au1c_1), \text{coeff}(BC1c_1M, Bu1c_1), \text{coeff}(BC1c_1M, Cu1c_1), \text{coeff}(BC1c_1M, Du1c_1), \end{aligned}$$

> *Coeff_vector* := subs(*Wz1c_j*=1, *Wz1s_j*=1, *Wz2c_j*=1, *Wz2s_j*=1, *Wzc_j*=1, *PHIyc_j*=1, *Omega_j*=1, *rhoA_w1*=1, *rhoA_w2*=1, *rhoA_w3*=1, *rhoA_w4*=1, *rhoA_u1*=1, *rhoA_u2*=1, *rhoA_u3*=1, *rhoA_u4*=1, *EI_w1*=1, *EI_w2*=1, *EI_w3*=1, *EI_w4*=1, *EI_u1*=1, *EI_u2*=1, *EI_u3*=1, *EI_u4*=1, *Betaw1_1*=1, *Betaw2_1*=1, *Betaw3_1*=1, *Betaw4_1*=1, *Betau1_1*=1, *Betau2_1*=1, *Betau3_1*=1, *Betau4_1*=1, *span*=1, *hw1*=1, *hw2*=1, *scg3*=1, *scg1*=1, *scg2*=1, LinearAlgebra[Multiply](LinearAlgebra[MatrixInverse](*Mc_j_comp*), *Fc_j*));

Coeff_vector :=

$$\begin{bmatrix} -1.25341537869434 \cdot 10^8 \\ 1.24369631453323 \cdot 10^8 \\ 1.25341539869432 \cdot 10^8 \\ -2.43259255756979 \cdot 10^7 \\ 5.29954427902908 \cdot 10^8 \\ -5.70206925838154 \cdot 10^8 \\ -2.33824851587322 \cdot 10^8 \\ -2.53347375645275 \cdot 10^7 \\ 4.44100572232361 \cdot 10^8 \\ -6.46316269494225 \cdot 10^8 \\ -4.44100570232353 \cdot 10^8 \\ 3.73414209676882 \cdot 10^8 \\ -7.16431054673820 \cdot 10^8 \\ 7.70847318623734 \cdot 10^8 \\ 3.16101493914547 \cdot 10^8 \\ 3.42493490584903 \cdot 10^7 \\ 1.00401792243676 \cdot 10^8 \\ -3.01683032249632 \cdot 10^8 \\ -1.00401792243676 \cdot 10^8 \\ 3.01683032249632 \cdot 10^8 \\ -6.73305632094109 \cdot 10^8 \\ 8.20877503985481 \cdot 10^8 \\ 5.24355627216568 \cdot 10^8 \\ -2.48424364907938 \cdot 10^8 \\ -7.42686594258785 \cdot 10^7 \\ 2.23159306980653 \cdot 10^8 \\ 7.42686594258790 \cdot 10^7 \\ -2.23159306980653 \cdot 10^8 \\ -2.04881039429607 \cdot 10^7 \\ -1.33066280844345 \cdot 10^7 \\ -7.42799867752457 \cdot 10^7 \\ 1.03849581709403 \cdot 10^8 \end{bmatrix}$$

```

> Awlc_1_comp := Coeff_vector(1); Bwlc_1_comp := Coeff_vector(2); Cwlc_1_comp := Coeff_vector(3); Dwlc_1_comp := Coeff_vector(4);
    Awlc_1_comp := -1.25341537869434 108
    Bwlc_1_comp := 1.24369631453323 108
    Cwlc_1_comp := 1.25341539869432 108
    Dwlc_1_comp := -2.43259255756979 107

```

(63)

```

> Wlc_1_comp := subs(Awlc_1=Awlc_1_comp, Bwlc_1=Bwlc_1_comp, Cwlc_1=Cwlc_1_comp, Dwlc_1=Dwlc_1_comp, Betaw1_j=1, Wlc_1);
    Wlc_1_comp := -1.25341537869434 108 cosh(x) + 1.24369631453323 108 sinh(x) + 1.25341539869432 108 cos(x) - 2.43259255756979 107 sin(x)

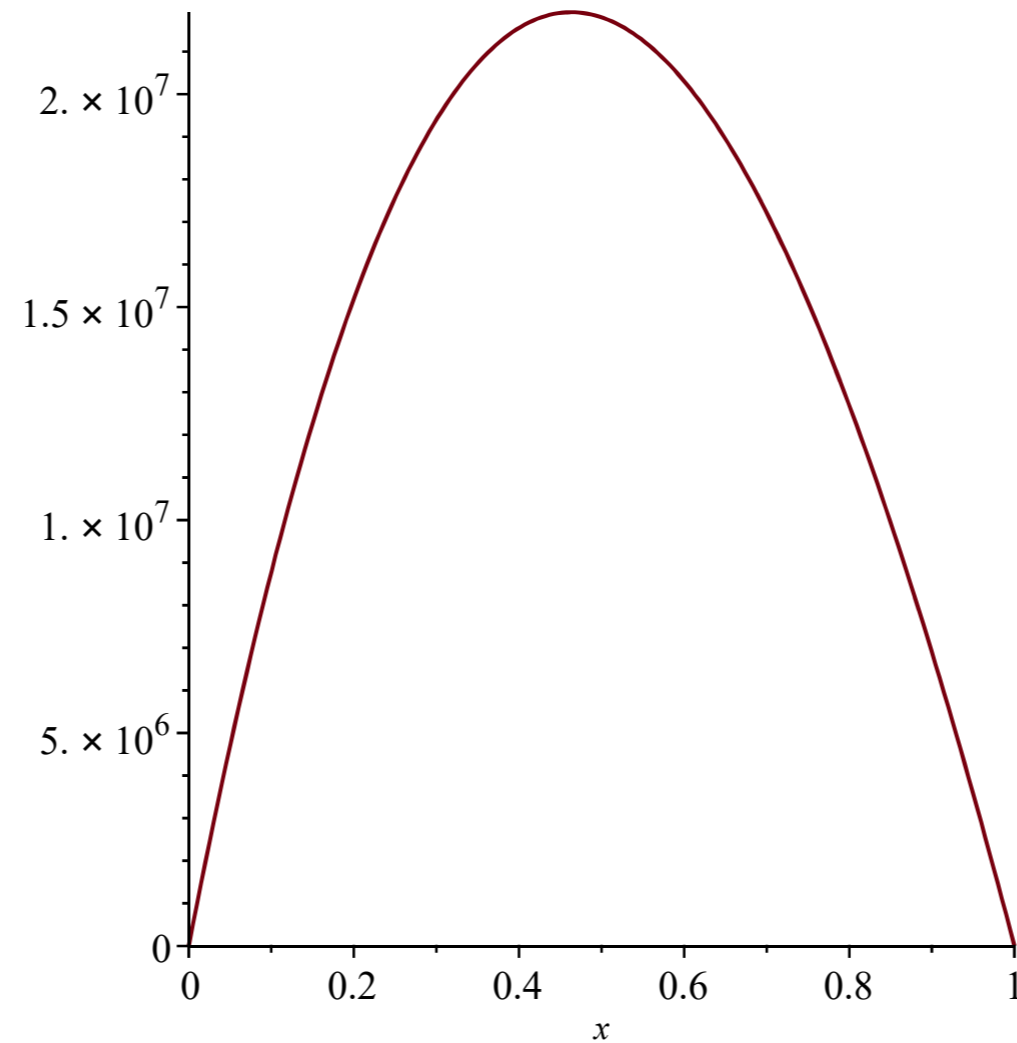
```

(64)

```

> with(plots) :
> plotWlc_1_comp := plot(Wlc_1_comp, x=0..1) : display([plotWlc_1_comp]);

```



```

>
> Wz1c_j := 1 : Wz1s_j := 1 : Wz2c_j := 1 : Wz2s_j := 1 : Omega_j := 10 : Omega_1 := Omega_j :
> Wzc_j := 1 : PHyc_j := 1 : scg3 := 1 : scg1 := 1 : scg2 := 1 :
> rhoA_w1 := 1 : rhoA_w2 := 1 : rhoA_w3 := 1 : rhoA_w4 := 1 : rhoA_u1 := 1 : rhoA_u2 := 1 : rhoA_u3 := 1 : rhoA_u4 := 1 :
> EI_w1 := 1 : EI_w2 := 1 : EI_w3 := 1 : EI_w4 := 1 : EI_u1 := 1 : EI_u2 := 1 : EI_u3 := 1 : EI_u4 := 1 :

```

```

> Betaw1_j :=  $\left(\frac{\rho A_w1}{EI_w1} \cdot \Omega_j^2\right)^{\left(\frac{1}{4}\right)}$  : Betaw2_j :=  $\left(\frac{\rho A_w2}{EI_w2} \cdot \Omega_j^2\right)^{\left(\frac{1}{4}\right)}$  : Betaw3_j :=  $\left(\frac{\rho A_w3}{EI_w3} \cdot \Omega_j^2\right)^{\left(\frac{1}{4}\right)}$  : Betaw4_j :=  $\left(\frac{\rho A_w4}{EI_w4} \cdot \Omega_j^2\right)^{\left(\frac{1}{4}\right)}$  :
> Betau1_j :=  $\left(\frac{\rho A_u1}{EI_u1} \cdot \Omega_j^2\right)^{\left(\frac{1}{4}\right)}$  : Betau2_j :=  $\left(\frac{\rho A_u2}{EI_u2} \cdot \Omega_j^2\right)^{\left(\frac{1}{4}\right)}$  : Betau3_j :=  $\left(\frac{\rho A_u3}{EI_u3} \cdot \Omega_j^2\right)^{\left(\frac{1}{4}\right)}$  : Betau4_j :=  $\left(\frac{\rho A_u4}{EI_u4} \cdot \Omega_j^2\right)^{\left(\frac{1}{4}\right)}$  :

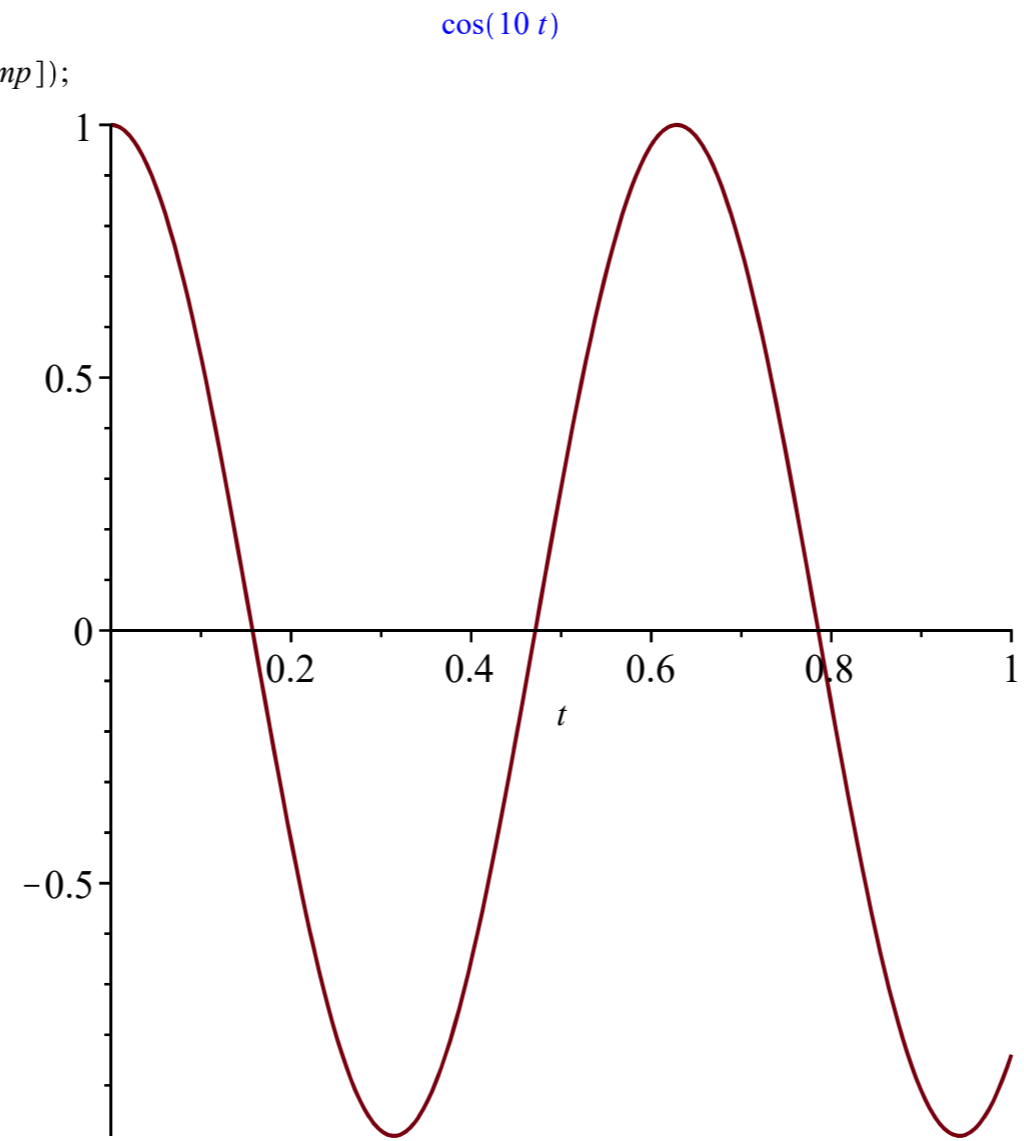
```

```

> span := 1 : hw1 := 1 : hw2 := 1 :

```

```
>  
wz1;  
plotWz1_1_comp := plot(wz1, t=0..1) : display([plotWz1_1_comp]);
```

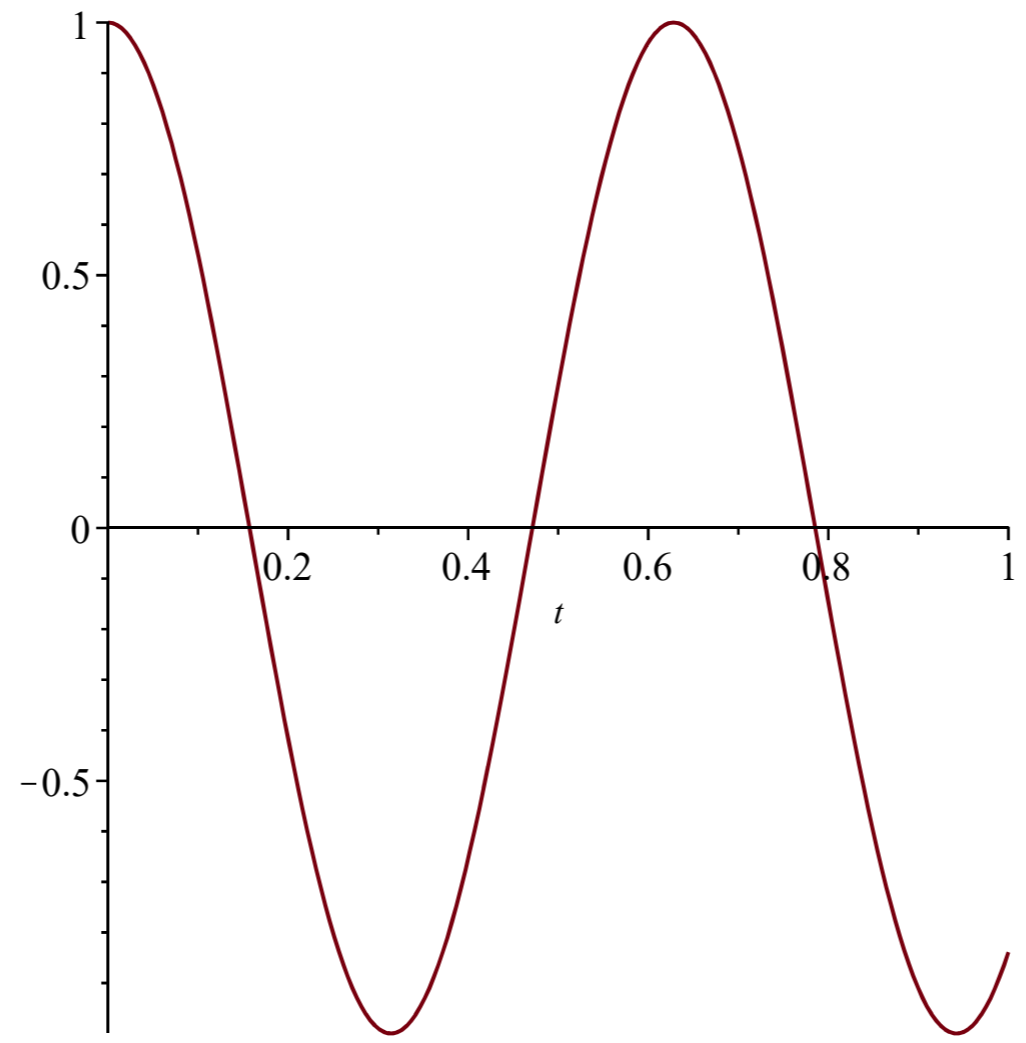


(65)

```
> wz2;  
plotWz2_1_comp := plot(wz2, t=0..1) : display([plotWz2_1_comp]);
```

cos(10 t)

(66)



S. Appendix: Maple sheet for determining dynamic EB-beams response Model _{φ}

```

> restart;
>
Model_phi (rotational excitation at bottom of frame only)
Excitation
> phiy := PHIyc_j*cos(Omega_j*t) + PHIys_j*sin(Omega_j*t);
                                phiy := PHIyc_j cos(Omega_j t) + PHIys_j sin(Omega_j t)
                                (1)
>
Steady-State solutions of every element in the Model
> w1 := W1c_1*cos(Omega_j*t) + W1s_1*sin(Omega_j*t);
                                w1 := W1c_1 cos(Omega_j t) + W1s_1 sin(Omega_j t)
                                (2)
> w2 := W2c_1*cos(Omega_j*t) + W2s_1*sin(Omega_j*t);
                                w2 := W2c_1 cos(Omega_j t) + W2s_1 sin(Omega_j t)
                                (3)
> w3 := W3c_1*cos(Omega_j*t) + W3s_1*sin(Omega_j*t);
                                w3 := W3c_1 cos(Omega_j t) + W3s_1 sin(Omega_j t)
                                (4)
> w4 := W4c_1*cos(Omega_j*t) + W4s_1*sin(Omega_j*t);
                                w4 := W4c_1 cos(Omega_j t) + W4s_1 sin(Omega_j t)
                                (5)
> u1 := U1c_1*cos(Omega_j*t) + U1s_1*sin(Omega_j*t);
                                u1 := U1c_1 cos(Omega_j t) + U1s_1 sin(Omega_j t)
                                (6)
> u2 := U2c_1*cos(Omega_j*t) + U2s_1*sin(Omega_j*t);
                                u2 := U2c_1 cos(Omega_j t) + U2s_1 sin(Omega_j t)
                                (7)
> u3 := U3c_1*cos(Omega_j*t) + U3s_1*sin(Omega_j*t);
                                u3 := U3c_1 cos(Omega_j t) + U3s_1 sin(Omega_j t)
                                (8)
> u4 := U4c_1*cos(Omega_j*t) + U4s_1*sin(Omega_j*t);
                                u4 := U4c_1 cos(Omega_j t) + U4s_1 sin(Omega_j t)
                                (9)
>
Substituting the steady-state solutions into the EOM of every element and gathering for the cos(Omega_1)- (c_1) and sin(Omega_1)- (s_1) terms gives the following EOM's and corresponding general solutions:
> EOMw1c_1 := -rhoA_w1*Omega^2*W1c_1 + EI_w1*diff(W1c_1, x$4) = 0 :
> W1c_1 := Aw1c_1*cosh(Betaw1_j*x) + Bw1c_1*sinh(Betaw1_j*x) + Cw1c_1*cos(Betaw1_j*x) + Dw1c_1*sin(Betaw1_j*x);
                                W1c_1 := Aw1c_1 cosh(Betaw1_j x) + Bw1c_1 sinh(Betaw1_j x) + Cw1c_1 cos(Betaw1_j x) + Dw1c_1 sin(Betaw1_j x)
                                (10)
> EOMw1s_1 := -rhoA_w1*Omega^2*W1s_1 + EI_w1*diff(W1s_1, x$4) = 0 :
> W1s_1 := Aw1s_1*cosh(Betaw1_j*x) + Bw1s_1*sinh(Betaw1_j*x) + Cw1s_1*cos(Betaw1_j*x) + Dw1s_1*sin(Betaw1_j*x);
                                W1s_1 := Aw1s_1 cosh(Betaw1_j x) + Bw1s_1 sinh(Betaw1_j x) + Cw1s_1 cos(Betaw1_j x) + Dw1s_1 sin(Betaw1_j x)
                                (11)
> EOMw2c_1 := -rhoA_w2*Omega^2*W2c_1 + EI_w2*diff(W2c_1, x$4) = 0 :
> W2c_1 := Aw2c_1*cosh(Betaw2_j*x) + Bw2c_1*sinh(Betaw2_j*x) + Cw2c_1*cos(Betaw2_j*x) + Dw2c_1*sin(Betaw2_j*x);
                                W2c_1 := Aw2c_1 cosh(Betaw2_j x) + Bw2c_1 sinh(Betaw2_j x) + Cw2c_1 cos(Betaw2_j x) + Dw2c_1 sin(Betaw2_j x)
                                (12)
> EOMw2s_1 := -rhoA_w2*Omega^2*W2s_1 + EI_w2*diff(W2s_1, x$4) = 0 :
> W2s_1 := Aw2s_1*cosh(Betaw2_j*x) + Bw2s_1*sinh(Betaw2_j*x) + Cw2s_1*cos(Betaw2_j*x) + Dw2s_1*sin(Betaw2_j*x);
                                W2s_1 := Aw2s_1 cosh(Betaw2_j x) + Bw2s_1 sinh(Betaw2_j x) + Cw2s_1 cos(Betaw2_j x) + Dw2s_1 sin(Betaw2_j x)
                                (13)
> EOMw3c_1 := -rhoA_w3*Omega^2*W3c_1 + EI_w3*diff(W3c_1, x$4) = 0 :
> W3c_1 := Aw3c_1*cosh(Betaw3_j*x) + Bw3c_1*sinh(Betaw3_j*x) + Cw3c_1*cos(Betaw3_j*x) + Dw3c_1*sin(Betaw3_j*x);
                                W3c_1 := Aw3c_1 cosh(Betaw3_j x) + Bw3c_1 sinh(Betaw3_j x) + Cw3c_1 cos(Betaw3_j x) + Dw3c_1 sin(Betaw3_j x)
                                (14)
> EOMw3s_1 := -rhoA_w3*Omega^2*W3s_1 + EI_w3*diff(W3s_1, x$4) = 0 :
> W3s_1 := Aw3s_1*cosh(Betaw3_j*x) + Bw3s_1*sinh(Betaw3_j*x) + Cw3s_1*cos(Betaw3_j*x) + Dw3s_1*sin(Betaw3_j*x);
                                W3s_1 := Aw3s_1 cosh(Betaw3_j x) + Bw3s_1 sinh(Betaw3_j x) + Cw3s_1 cos(Betaw3_j x) + Dw3s_1 sin(Betaw3_j x)
                                (15)

```

$$\begin{aligned}
&> EOMw4c_1 := -rhoA_w4 \cdot \Omega I^2 \cdot W4c_1 + EI_w4 \cdot diff(W4c_1, x\$4) = 0 : \\
&> W4c_1 := Aw4c_1 \cdot \cosh(Betaw4_j \cdot x) + Bw4c_1 \cdot \sinh(Betaw4_j \cdot x) + Cw4c_1 \cdot \cos(Betaw4_j \cdot x) + Dw4c_1 \cdot \sin(Betaw4_j \cdot x); \\
&\quad W4c_1 := Aw4c_1 \cosh(Betaw4_j x) + Bw4c_1 \sinh(Betaw4_j x) + Cw4c_1 \cos(Betaw4_j x) + Dw4c_1 \sin(Betaw4_j x)
\end{aligned} \tag{16}$$

$$\begin{aligned}
&> EOMw4s_1 := -rhoA_w4 \cdot \Omega I^2 \cdot W4s_1 + EI_w4 \cdot diff(W4s_1, x\$4) = 0 : \\
&> W4s_1 := Aw4s_1 \cdot \cosh(Betaw4_j \cdot x) + Bw4s_1 \cdot \sinh(Betaw4_j \cdot x) + Cw4s_1 \cdot \cos(Betaw4_j \cdot x) + Dw4s_1 \cdot \sin(Betaw4_j \cdot x); \\
&\quad W4s_1 := Aw4s_1 \cosh(Betaw4_j x) + Bw4s_1 \sinh(Betaw4_j x) + Cw4s_1 \cos(Betaw4_j x) + Dw4s_1 \sin(Betaw4_j x)
\end{aligned} \tag{17}$$

$$\begin{aligned}
&> EOMulc_1 := -rhoA_u1 \cdot \Omega I^2 \cdot U1c_1 + EI_u1 \cdot diff(U1c_1, z\$4) = 0 : \\
&> U1c_1 := Au1c_1 \cdot \cosh(Betau1_j \cdot z) + Bu1c_1 \cdot \sinh(Betau1_j \cdot z) + Cu1c_1 \cdot \cos(Betau1_j \cdot z) + Du1c_1 \cdot \sin(Betau1_j \cdot z); \\
&\quad U1c_1 := Au1c_1 \cosh(Betau1_j z) + Bu1c_1 \sinh(Betau1_j z) + Cu1c_1 \cos(Betau1_j z) + Du1c_1 \sin(Betau1_j z)
\end{aligned} \tag{18}$$

$$\begin{aligned}
&> EOMuls_1 := -rhoA_u1 \cdot \Omega I^2 \cdot U1s_1 + EI_u1 \cdot diff(U1s_1, z\$4) = 0 : \\
&> U1s_1 := Au1s_1 \cdot \cosh(Betau1_j \cdot z) + Bu1s_1 \cdot \sinh(Betau1_j \cdot z) + Cu1s_1 \cdot \cos(Betau1_j \cdot z) + Du1s_1 \cdot \sin(Betau1_j \cdot z); \\
&\quad U1s_1 := Au1s_1 \cosh(Betau1_j z) + Bu1s_1 \sinh(Betau1_j z) + Cu1s_1 \cos(Betau1_j z) + Du1s_1 \sin(Betau1_j z)
\end{aligned} \tag{19}$$

$$\begin{aligned}
&> EOMu2c_1 := -rhoA_u2 \cdot \Omega I^2 \cdot U2c_1 + EI_u2 \cdot diff(U2c_1, z\$4) = 0 : \\
&> U2c_1 := Au2c_1 \cdot \cosh(Betau2_j \cdot z) + Bu2c_1 \cdot \sinh(Betau2_j \cdot z) + Cu2c_1 \cdot \cos(Betau2_j \cdot z) + Du2c_1 \cdot \sin(Betau2_j \cdot z); \\
&\quad U2c_1 := Au2c_1 \cosh(Betau2_j z) + Bu2c_1 \sinh(Betau2_j z) + Cu2c_1 \cos(Betau2_j z) + Du2c_1 \sin(Betau2_j z)
\end{aligned} \tag{20}$$

$$\begin{aligned}
&> EOMu2s_1 := -rhoA_u2 \cdot \Omega I^2 \cdot U2s_1 + EI_u2 \cdot diff(U2s_1, z\$4) = 0 : \\
&> U2s_1 := Au2s_1 \cdot \cosh(Betau2_j \cdot z) + Bu2s_1 \cdot \sinh(Betau2_j \cdot z) + Cu2s_1 \cdot \cos(Betau2_j \cdot z) + Du2s_1 \cdot \sin(Betau2_j \cdot z); \\
&\quad U2s_1 := Au2s_1 \cosh(Betau2_j z) + Bu2s_1 \sinh(Betau2_j z) + Cu2s_1 \cos(Betau2_j z) + Du2s_1 \sin(Betau2_j z)
\end{aligned} \tag{21}$$

$$\begin{aligned}
&> EOMu3c_1 := -rhoA_u3 \cdot \Omega I^2 \cdot U3c_1 + EI_u3 \cdot diff(U3c_1, z\$4) = 0 : \\
&> U3c_1 := Au3c_1 \cdot \cosh(Betau3_j \cdot z) + Bu3c_1 \cdot \sinh(Betau3_j \cdot z) + Cu3c_1 \cdot \cos(Betau3_j \cdot z) + Du3c_1 \cdot \sin(Betau3_j \cdot z); \\
&\quad U3c_1 := Au3c_1 \cosh(Betau3_j z) + Bu3c_1 \sinh(Betau3_j z) + Cu3c_1 \cos(Betau3_j z) + Du3c_1 \sin(Betau3_j z)
\end{aligned} \tag{22}$$

$$\begin{aligned}
&> EOMu3s_1 := -rhoA_u3 \cdot \Omega I^2 \cdot U3s_1 + EI_u3 \cdot diff(U3s_1, z\$4) = 0 : \\
&> U3s_1 := Au3s_1 \cdot \cosh(Betau3_j \cdot z) + Bu3s_1 \cdot \sinh(Betau3_j \cdot z) + Cu3s_1 \cdot \cos(Betau3_j \cdot z) + Du3s_1 \cdot \sin(Betau3_j \cdot z); \\
&\quad U3s_1 := Au3s_1 \cosh(Betau3_j z) + Bu3s_1 \sinh(Betau3_j z) + Cu3s_1 \cos(Betau3_j z) + Du3s_1 \sin(Betau3_j z)
\end{aligned} \tag{23}$$

$$\begin{aligned}
&> EOMu4c_1 := -rhoA_u4 \cdot \Omega I^2 \cdot U4c_1 + EI_u4 \cdot diff(U4c_1, z\$4) = 0 : \\
&> U4c_1 := Au4c_1 \cdot \cosh(Betau4_j \cdot z) + Bu4c_1 \cdot \sinh(Betau4_j \cdot z) + Cu4c_1 \cdot \cos(Betau4_j \cdot z) + Du4c_1 \cdot \sin(Betau4_j \cdot z); \\
&\quad U4c_1 := Au4c_1 \cosh(Betau4_j z) + Bu4c_1 \sinh(Betau4_j z) + Cu4c_1 \cos(Betau4_j z) + Du4c_1 \sin(Betau4_j z)
\end{aligned} \tag{24}$$

$$\begin{aligned}
&> EOMu4s_1 := -rhoA_u4 \cdot \Omega I^2 \cdot U4s_1 + EI_u4 \cdot diff(U4s_1, z\$4) = 0 : \\
&> U4s_1 := Au4s_1 \cdot \cosh(Betau4_j \cdot z) + Bu4s_1 \cdot \sinh(Betau4_j \cdot z) + Cu4s_1 \cdot \cos(Betau4_j \cdot z) + Du4s_1 \cdot \sin(Betau4_j \cdot z); \\
&\quad U4s_1 := Au4s_1 \cosh(Betau4_j z) + Bu4s_1 \sinh(Betau4_j z) + Cu4s_1 \cos(Betau4_j z) + Du4s_1 \sin(Betau4_j z)
\end{aligned} \tag{25}$$

Substitute the general solutions into the IC's and BC's (4*8 EB-elements = 32 needed IC's + BC's) and gather for the cos(Omega_1) terms

$$\begin{aligned}
&BC @ x = 0, z = 0 [2 BC's] \\
&> BC1c_1M := simplify(subs(z=0, U1c_1)) : BC1c_1 := BC1c_1M=0; \\
&\quad BC1c_1 := Au1c_1 + Cu1c_1 = 0
\end{aligned} \tag{26}$$

$$\begin{aligned}
&> BC2c_1M := simplify(subs(z=0, diff(U1c_1, z))) - PHIyc_j : BC2c_1 := BC2c_1M=0; \\
&\quad BC2c_1 := Betau1_j (Bu1c_1 + Du1c_1) - PHIyc_j = 0
\end{aligned} \tag{27}$$

$$\begin{aligned}
&BC @ x = span, z = 0 [2 BC's] \\
&> BC3c_1M := simplify(subs(z=0, U3c_1)) : BC3c_1 := BC3c_1M=0; \\
&\quad BC3c_1 := Au3c_1 + Cu3c_1 = 0
\end{aligned} \tag{28}$$

$$\begin{aligned}
&> BC4c_1M := simplify(subs(z=0, diff(U3c_1, z))) - PHIyc_j : BC4c_1 := BC4c_1M=0; \\
&\quad BC4c_1 := Betau3_j (Bu3c_1 + Du3c_1) - PHIyc_j = 0
\end{aligned} \tag{29}$$

BC @ x = 2*span, z = hw1 [2 BC's]

$$\begin{aligned} > BC5c_{1M} := \text{simplify}(\text{subs}(x=2 \cdot \text{span}, W2c_1)) : BC5c_1 := BC5c_{1M}=0; \\ & \quad BC5c_1 := Aw2c_1 \cosh(2 \text{ Betaw2}_j \text{ span}) + Bw2c_1 \sinh(2 \text{ Betaw2}_j \text{ span}) + Cw2c_1 \cos(2 \text{ Betaw2}_j \text{ span}) + Dw2c_1 \sin(2 \text{ Betaw2}_j \text{ span}) = 0 \end{aligned} \quad (30)$$

$$\begin{aligned} > BC6c_{1M} := \text{simplify}(\text{subs}(x=2 \cdot \text{span}, \text{diff}(W2c_1, x))) + \text{PHIyc}_j : BC6c_1 := BC6c_{1M}=0; \\ & \quad BC6c_1 := \text{Betaw2}_j (Aw2c_1 \sinh(2 \text{ Betaw2}_j \text{ span}) + Bw2c_1 \cosh(2 \text{ Betaw2}_j \text{ span}) - Cw2c_1 \sin(2 \text{ Betaw2}_j \text{ span}) + Dw2c_1 \cos(2 \text{ Betaw2}_j \text{ span})) + \text{PHIyc}_j = 0 \end{aligned} \quad (31)$$

BC @ x = 2*span, z = hw1+hw2 [2 BC's]

$$\begin{aligned} > BC7c_{1M} := \text{simplify}(\text{subs}(x=2 \cdot \text{span}, W4c_1)) : BC7c_1 := BC7c_{1M}=0; \\ & \quad BC7c_1 := Aw4c_1 \cosh(2 \text{ Betaw4}_j \text{ span}) + Bw4c_1 \sinh(2 \text{ Betaw4}_j \text{ span}) + Cw4c_1 \cos(2 \text{ Betaw4}_j \text{ span}) + Dw4c_1 \sin(2 \text{ Betaw4}_j \text{ span}) = 0 \end{aligned} \quad (32)$$

$$\begin{aligned} > BC8c_{1M} := \text{simplify}(\text{subs}(x=2 \cdot \text{span}, \text{diff}(W4c_1, x))) + \text{PHIyc}_j : BC8c_1 := BC8c_{1M}=0; \\ & \quad BC8c_1 := \text{Betaw4}_j (Aw4c_1 \sinh(2 \text{ Betaw4}_j \text{ span}) + Bw4c_1 \cosh(2 \text{ Betaw4}_j \text{ span}) - Cw4c_1 \sin(2 \text{ Betaw4}_j \text{ span}) + Dw4c_1 \cos(2 \text{ Betaw4}_j \text{ span})) + \text{PHIyc}_j = 0 \end{aligned} \quad (33)$$

IC @ x = 0, z = hw1 [6 IC's]

$$\begin{aligned} > IC1c_{1M} := \text{simplify}(\text{subs}(z=hw1, U1c_1)) - \text{simplify}(\text{subs}(z=hw1, U2c_1)) : IC1c_1 := IC1c_{1M}=0; \\ IC1c_1 := Au1c_1 \cosh(\text{Betau1}_j \text{ hw1}) + Bu1c_1 \sinh(\text{Betau1}_j \text{ hw1}) + Cu1c_1 \cos(\text{Betau1}_j \text{ hw1}) + Du1c_1 \sin(\text{Betau1}_j \text{ hw1}) - Au2c_1 \cosh(\text{Betau2}_j \text{ hw1}) - Bu2c_1 \sinh(\text{Betau2}_j \text{ hw1}) \\ - Cu2c_1 \cos(\text{Betau2}_j \text{ hw1}) - Du2c_1 \sin(\text{Betau2}_j \text{ hw1}) = 0 \end{aligned} \quad (34)$$

$$\begin{aligned} > IC2c_{1M} := \text{simplify}(\text{subs}(x=0, W1c_1)) : IC2c_1 := IC2c_{1M}=0; \\ & \quad IC2c_1 := Aw1c_1 + Cw1c_1 = 0 \end{aligned} \quad (35)$$

$$\begin{aligned} > IC3c_{1M} := \text{simplify}(\text{subs}(z=hw1, \text{diff}(U1c_1, z))) - \text{simplify}(\text{subs}(z=hw1, \text{diff}(U2c_1, z))) : IC3c_1 := IC3c_{1M}=0; \\ IC3c_1 := \text{Betau1}_j (Au1c_1 \sinh(\text{Betau1}_j \text{ hw1}) + Bu1c_1 \cosh(\text{Betau1}_j \text{ hw1}) - Cu1c_1 \sin(\text{Betau1}_j \text{ hw1}) + Du1c_1 \cos(\text{Betau1}_j \text{ hw1})) - \text{Betau2}_j (Au2c_1 \sinh(\text{Betau2}_j \text{ hw1}) \\ + Bu2c_1 \cosh(\text{Betau2}_j \text{ hw1}) - Cu2c_1 \sin(\text{Betau2}_j \text{ hw1}) + Du2c_1 \cos(\text{Betau2}_j \text{ hw1})) = 0 \end{aligned} \quad (36)$$

$$\begin{aligned} > IC4c_{1M} := \text{simplify}(\text{subs}(z=hw1, \text{diff}(U1c_1, z))) + \text{simplify}(\text{subs}(x=0, \text{diff}(W1c_1, x))) : IC4c_1 := IC4c_{1M}=0; \\ IC4c_1 := \text{Betau1}_j (Au1c_1 \sinh(\text{Betau1}_j \text{ hw1}) + Bu1c_1 \cosh(\text{Betau1}_j \text{ hw1}) - Cu1c_1 \sin(\text{Betau1}_j \text{ hw1}) + Du1c_1 \cos(\text{Betau1}_j \text{ hw1})) + \text{Betaw1}_j (Bw1c_1 + Dw1c_1) = 0 \end{aligned} \quad (37)$$

$$\begin{aligned} > IC5c_{1M} := \text{simplify}(\text{subs}(z=hw1, U1c_1)) - \text{simplify}(\text{subs}(z=hw1, U3c_1)) : IC5c_1 := IC5c_{1M}=0; \\ IC5c_1 := Au1c_1 \cosh(\text{Betau1}_j \text{ hw1}) + Bu1c_1 \sinh(\text{Betau1}_j \text{ hw1}) + Cu1c_1 \cos(\text{Betau1}_j \text{ hw1}) + Du1c_1 \sin(\text{Betau1}_j \text{ hw1}) - Au3c_1 \cosh(\text{Betau3}_j \text{ hw1}) - Bu3c_1 \sinh(\text{Betau3}_j \text{ hw1}) \\ - Cu3c_1 \cos(\text{Betau3}_j \text{ hw1}) - Du3c_1 \sin(\text{Betau3}_j \text{ hw1}) = 0 \end{aligned} \quad (38)$$

$$\begin{aligned} > IC6c_{1M} := -\text{simplify}(\text{subs}(z=hw1, \text{diff}(U1c_1, z\$2))) + \text{simplify}(\text{subs}(z=hw1, \text{diff}(U2c_1, z\$2))) + \text{simplify}(\text{subs}(x=0, \text{diff}(W1c_1, x\$2))) : IC6c_1 := IC6c_{1M}=0; \\ IC6c_1 := -\text{Betau1}_j^2 (Au1c_1 \cosh(\text{Betau1}_j \text{ hw1}) + Bu1c_1 \sinh(\text{Betau1}_j \text{ hw1}) - Cu1c_1 \cos(\text{Betau1}_j \text{ hw1}) - Du1c_1 \sin(\text{Betau1}_j \text{ hw1})) + \text{Betau2}_j^2 (Au2c_1 \cosh(\text{Betau2}_j \text{ hw1}) \\ + Bu2c_1 \sinh(\text{Betau2}_j \text{ hw1}) - Cu2c_1 \cos(\text{Betau2}_j \text{ hw1}) - Du2c_1 \sin(\text{Betau2}_j \text{ hw1})) + \text{Betaw1}_j^2 (Aw1c_1 - Cw1c_1) = 0 \end{aligned} \quad (39)$$

IC @ x = 0, z = hw1+hw2 [6 IC's]

$$\begin{aligned} > IC7c_{1M} := \text{simplify}(\text{subs}(x=0, W3c_1)) : IC7c_1 := IC7c_{1M}=0; \\ & \quad IC7c_1 := Aw3c_1 + Cw3c_1 = 0 \end{aligned} \quad (40)$$

$$\begin{aligned} > IC8c_{1M} := \text{simplify}(\text{subs}(z=hw1 + hw2, \text{diff}(U2c_1, z))) + \text{simplify}(\text{subs}(x=0, \text{diff}(W3c_1, x))) : IC8c_1 := IC8c_{1M}=0; \\ IC8c_1 := \text{Betau2}_j (Au2c_1 \sinh(\text{Betau2}_j (hw1 + hw2)) + Bu2c_1 \cosh(\text{Betau2}_j (hw1 + hw2)) - Cu2c_1 \sin(\text{Betau2}_j (hw1 + hw2)) + Du2c_1 \cos(\text{Betau2}_j (hw1 + hw2))) + \text{Betaw3}_j (Bw3c_1 \\ + Dw3c_1) = 0 \end{aligned} \quad (41)$$

$$\begin{aligned} > IC9c_{1M} := \text{simplify}(\text{subs}(z=hw1 + hw2, U2c_1)) - \text{simplify}(\text{subs}(z=hw1 + hw2, U4c_1)) : IC9c_1 := IC9c_{1M}=0; \\ IC9c_1 := Au2c_1 \cosh(\text{Betau2}_j (hw1 + hw2)) + Bu2c_1 \sinh(\text{Betau2}_j (hw1 + hw2)) + Cu2c_1 \cos(\text{Betau2}_j (hw1 + hw2)) + Du2c_1 \sin(\text{Betau2}_j (hw1 + hw2)) - Au4c_1 \cosh(\text{Betau4}_j (hw1 + hw2)) \\ - Bu4c_1 \sinh(\text{Betau4}_j (hw1 + hw2)) - Cu4c_1 \cos(\text{Betau4}_j (hw1 + hw2)) - Du4c_1 \sin(\text{Betau4}_j (hw1 + hw2)) = 0 \end{aligned} \quad (42)$$

$$\begin{aligned} > IC10c_{1M} := -\text{simplify}(\text{subs}(z=hw1 + hw2, \text{diff}(U2c_1, z\$2))) + \text{simplify}(\text{subs}(x=0, \text{diff}(W3c_1, x\$2))) : IC10c_1 := IC10c_{1M}=0; \\ IC10c_1 := -\text{Betau2}_j^2 (Au2c_1 \cosh(\text{Betau2}_j (hw1 + hw2)) + Bu2c_1 \sinh(\text{Betau2}_j (hw1 + hw2)) - Cu2c_1 \cos(\text{Betau2}_j (hw1 + hw2)) - Du2c_1 \sin(\text{Betau2}_j (hw1 + hw2))) + \text{Betaw3}_j^2 (Aw3c_1 \\ - Cw3c_1) = 0 \end{aligned} \quad (43)$$

IC @ x = span, z = hw1 [8 IC's]

$$\begin{aligned} > IC11c_{1M} := \text{simplify}(\text{subs}(x=\text{span}, W1c_1)) - \text{simplify}(\text{subs}(x=\text{span}, W2c_1)) : IC11c_1 := IC11c_{1M}=0; \\ IC11c_1 := Aw1c_1 \cosh(\text{Betaw1}_j \text{ span}) + Bw1c_1 \sinh(\text{Betaw1}_j \text{ span}) + Cw1c_1 \cos(\text{Betaw1}_j \text{ span}) + Dw1c_1 \sin(\text{Betaw1}_j \text{ span}) - Aw2c_1 \cosh(\text{Betaw2}_j \text{ span}) - Bw2c_1 \sinh(\text{Betaw2}_j \text{ span}) \\ - Cw2c_1 \cos(\text{Betaw2}_j \text{ span}) - Dw2c_1 \sin(\text{Betaw2}_j \text{ span}) = 0 \end{aligned} \quad (44)$$

$$\begin{aligned} > IC12c_{1M} := \text{simplify}(\text{subs}(x=\text{span}, W1c_1)) : IC12c_1 := IC12c_{1M}=0; \\ & \quad IC12c_1 := Aw1c_1 \cosh(\text{Betaw1}_j \text{ span}) + Bw1c_1 \sinh(\text{Betaw1}_j \text{ span}) + Cw1c_1 \cos(\text{Betaw1}_j \text{ span}) + Dw1c_1 \sin(\text{Betaw1}_j \text{ span}) = 0 \end{aligned} \quad (45)$$

$$\begin{aligned} > IC13c_{1M} := \text{simplify}(\text{subs}(z=hw1, U3c_1)) - \text{simplify}(\text{subs}(z=hw1, U4c_1)) : IC13c_1 := IC13c_{1M}=0; \\ IC13c_1 := Au3c_1 \cosh(\text{Betau3}_j \text{ hw1}) + Bu3c_1 \sinh(\text{Betau3}_j \text{ hw1}) + Cu3c_1 \cos(\text{Betau3}_j \text{ hw1}) + Du3c_1 \sin(\text{Betau3}_j \text{ hw1}) - Au4c_1 \cosh(\text{Betau4}_j \text{ hw1}) - Bu4c_1 \sinh(\text{Betau4}_j \text{ hw1}) \end{aligned} \quad (46)$$


```

- Cu4c_1 cos(Betau4_j hw1) - Du4c_1 sin(Betau4_j hw1) = 0
> IC14c_1M := simplify(subs(x=span, diff(W1c_1, x))) - simplify(subs(x=span, diff(W2c_1, x))) : IC14c_1 := IC14c_1M=0;
IC14c_1 := Betaw1_j (Aw1c_1 sinh(Betaw1_j span) + Bw1c_1 cosh(Betaw1_j span) - Cw1c_1 sin(Betaw1_j span) + Dw1c_1 cos(Betaw1_j span)) - Betaw2_j (Aw2c_1 sinh(Betaw2_j span)
+ Bw2c_1 cosh(Betaw2_j span) - Cw2c_1 sin(Betaw2_j span) + Dw2c_1 cos(Betaw2_j span)) = 0 (47)
> IC15c_1M := simplify(subs(z=hw1, diff(U3c_1, z))) - simplify(subs(z=hw1, diff(U4c_1, z))) : IC15c_1 := IC15c_1M=0;
IC15c_1 := Betau3_j (Au3c_1 sinh(Betau3_j hw1) + Bu3c_1 cosh(Betau3_j hw1) - Cu3c_1 sin(Betau3_j hw1) + Du3c_1 cos(Betau3_j hw1)) - Betau4_j (Au4c_1 sinh(Betau4_j hw1)
+ Bu4c_1 cosh(Betau4_j hw1) - Cu4c_1 sin(Betau4_j hw1) + Du4c_1 cos(Betau4_j hw1)) = 0 (48)
> IC16c_1M := simplify(subs(x=span, diff(W1c_1, x))) + simplify(subs(z=hw1, diff(U3c_1, z))) : IC16c_1 := IC16c_1M=0;
IC16c_1 := Betaw1_j (Aw1c_1 sinh(Betaw1_j span) + Bw1c_1 cosh(Betaw1_j span) - Cw1c_1 sin(Betaw1_j span) + Dw1c_1 cos(Betaw1_j span)) + Betau3_j (Au3c_1 sinh(Betau3_j hw1)
+ Bu3c_1 cosh(Betau3_j hw1) - Cu3c_1 sin(Betau3_j hw1) + Du3c_1 cos(Betau3_j hw1)) = 0 (49)
> IC17c_1M := -simplify(subs(x=span, diff(W1c_1, x$2))) + simplify(subs(z=hw1, diff(U4c_1, z$2))) + simplify(subs(x=span, diff(W2c_1, x$2))) - simplify(subs(z=hw1, diff(U3c_1, z$2))) : IC17c_1 :=
IC17c_1M=0;
IC17c_1 := -Betaw1_j^2 (Aw1c_1 cosh(Betaw1_j span) + Bw1c_1 sinh(Betaw1_j span) - Cw1c_1 cos(Betaw1_j span) - Dw1c_1 sin(Betaw1_j span)) + Betau4_j^2 (Au4c_1 cosh(Betau4_j hw1)
+ Bu4c_1 sinh(Betau4_j hw1) - Cu4c_1 cos(Betau4_j hw1) - Du4c_1 sin(Betau4_j hw1)) + Betaw2_j^2 (Aw2c_1 cosh(Betaw2_j span) + Bw2c_1 sinh(Betaw2_j span) - Cw2c_1 cos(Betaw2_j span)
- Dw2c_1 sin(Betaw2_j span)) - Betau3_j^2 (Au3c_1 cosh(Betau3_j hw1) + Bu3c_1 sinh(Betau3_j hw1) - Cu3c_1 cos(Betau3_j hw1) - Du3c_1 sin(Betau3_j hw1)) = 0 (50)
> IC18c_1M := simplify(subs(z=hw1, U3c_1)) : IC18c_1 := IC18c_1M=0;
IC18c_1 := Au3c_1 cosh(Betau3_j hw1) + Bu3c_1 sinh(Betau3_j hw1) + Cu3c_1 cos(Betau3_j hw1) + Du3c_1 sin(Betau3_j hw1) = 0 (51)
IC @ x = span, z = hw1+hw2 [6 IC's]
> IC19c_1M := simplify(subs(x=span, W3c_1)) - simplify(subs(x=span, W4c_1)) : IC19c_1 := IC19c_1M=0;
IC19c_1 := Aw3c_1 cosh(Betaw3_j span) + Bw3c_1 sinh(Betaw3_j span) + Cw3c_1 cos(Betaw3_j span) + Dw3c_1 sin(Betaw3_j span) - Aw4c_1 cosh(Betaw4_j span) - Bw4c_1 sinh(Betaw4_j span)
- Cw4c_1 cos(Betaw4_j span) - Dw4c_1 sin(Betaw4_j span) = 0 (52)
> IC20c_1M := simplify(subs(x=span, W3c_1)) : IC20c_1 := IC20c_1M=0;
IC20c_1 := Aw3c_1 cosh(Betaw3_j span) + Bw3c_1 sinh(Betaw3_j span) + Cw3c_1 cos(Betaw3_j span) + Dw3c_1 sin(Betaw3_j span) = 0 (53)
> IC21c_1M := simplify(subs(x=span, diff(W3c_1, x))) - simplify(subs(x=span, diff(W4c_1, x))) : IC21c_1 := IC21c_1M=0;
IC21c_1 := Betaw3_j (Aw3c_1 sinh(Betaw3_j span) + Bw3c_1 cosh(Betaw3_j span) - Cw3c_1 sin(Betaw3_j span) + Dw3c_1 cos(Betaw3_j span)) - Betaw4_j (Aw4c_1 sinh(Betaw4_j span)
+ Bw4c_1 cosh(Betaw4_j span) - Cw4c_1 sin(Betaw4_j span) + Dw4c_1 cos(Betaw4_j span)) = 0 (54)
> IC22c_1M := simplify(subs(x=span, diff(W3c_1, x))) + simplify(subs(z=hw1 + hw2, diff(U4c_1, z))) : IC22c_1 := IC22c_1M=0;
IC22c_1 := Betaw3_j (Aw3c_1 sinh(Betaw3_j span) + Bw3c_1 cosh(Betaw3_j span) - Cw3c_1 sin(Betaw3_j span) + Dw3c_1 cos(Betaw3_j span)) + Betau4_j (Au4c_1 sinh(Betau4_j (hw1 + hw2))
+ Bu4c_1 cosh(Betau4_j (hw1 + hw2)) - Cu4c_1 sin(Betau4_j (hw1 + hw2)) + Du4c_1 cos(Betau4_j (hw1 + hw2))) = 0 (55)
> IC23c_1M := -simplify(subs(x=span, diff(W3c_1, x$2))) - simplify(subs(z=hw1 + hw2, diff(U4c_1, z$2))) + simplify(subs(x=span, diff(W4c_1, x$2))) : IC23c_1 := IC23c_1M=0;
IC23c_1 := -Betaw3_j^2 (Aw3c_1 cosh(Betaw3_j span) + Bw3c_1 sinh(Betaw3_j span) - Cw3c_1 cos(Betaw3_j span) - Dw3c_1 sin(Betaw3_j span)) - Betau4_j^2 (Au4c_1 cosh(Betau4_j (hw1 + hw2))
+ Bu4c_1 sinh(Betau4_j (hw1 + hw2)) - Cu4c_1 cos(Betau4_j (hw1 + hw2)) - Du4c_1 sin(Betau4_j (hw1 + hw2))) + Betaw4_j^2 (Aw4c_1 cosh(Betaw4_j span) + Bw4c_1 sinh(Betaw4_j span)
- Cw4c_1 cos(Betaw4_j span) - Dw4c_1 sin(Betaw4_j span)) = 0 (56)
> IC24c_1M := simplify(subs(z=hw1 + hw2, U4c_1)) : IC24c_1 := IC24c_1M=0;
IC24c_1 := Au4c_1 cosh(Betau4_j (hw1 + hw2)) + Bu4c_1 sinh(Betau4_j (hw1 + hw2)) + Cu4c_1 cos(Betau4_j (hw1 + hw2)) + Du4c_1 sin(Betau4_j (hw1 + hw2)) = 0 (57)
>
> interface(rtables=35);
10 (58)
>
>
Coefficient matrix
> Mc_j := Matrix([
[coeff(BC1c_1M, Aw1c_1), coeff(BC1c_1M, Bw1c_1), coeff(BC1c_1M, Cw1c_1), coeff(BC1c_1M, Dw1c_1),
coeff(BC1c_1M, Aw2c_1), coeff(BC1c_1M, Bw2c_1), coeff(BC1c_1M, Cw2c_1), coeff(BC1c_1M, Dw2c_1),
coeff(BC1c_1M, Aw3c_1), coeff(BC1c_1M, Bw3c_1), coeff(BC1c_1M, Cw3c_1), coeff(BC1c_1M, Dw3c_1),
coeff(BC1c_1M, Aw4c_1), coeff(BC1c_1M, Bw4c_1), coeff(BC1c_1M, Cw4c_1), coeff(BC1c_1M, Dw4c_1),
coeff(BC1c_1M, Au1c_1), coeff(BC1c_1M, Bu1c_1), coeff(BC1c_1M, Cu1c_1), coeff(BC1c_1M, Du1c_1),

```


= 1, EI_u1 = 1, EI_u2 = 1, EI_u3 = 1, EI_u4 = 1, Betaw1_j = 1, Betaw2_j = 1, Betaw3_j = 1, Betaw4_j = 1, Betau1_j = 1, Betau2_j = 1, Betau3_j = 1, Betau4_j = 1, span = 1, hw1 = 1, hw2 = 1, LinearAlgebra[Multiply](LinearAlgebra[MatrixInverse](Mc_j_comp), Fc_j));

Coeff_vector :=

```

-7.11157989501953
 10.7497632503510
  7.11158007383347
 -6.53830409049988
 14.3062858581543
-15.7462692260742
 -7.14500904083252
  0.344332665205002
 13.0511498451233
-17.3814001083374
-13.0511491298676
  8.72190523147583
-25.0665607452393
 26.6171300411224
 10.2269580364227
  2.22657164186239
  2.23130059242249
 -9.22592681646347
 -2.23130068182945
 10.2259268164635
-13.9389300346375
 18.0575294494629
 13.3620028495789
 -8.23778378963470
 -3.28647398948669
  7.35364580154419
  3.28647339344025
 -6.35364580154419
 12.2327308654785
-14.6499977111816
 -8.90472364425659
  3.74564635753632

```

(61)

> Awlc_1_comp := Coeff_vector(1); Bwlc_1_comp := Coeff_vector(2); Cwlc_1_comp := Coeff_vector(3); Dwlc_1_comp := Coeff_vector(4);

```

Awlc_1_comp := -7.11157989501953
Bwlc_1_comp := 10.7497632503510
Cwlc_1_comp := 7.11158007383347
Dwlc_1_comp := -6.53830409049988

```

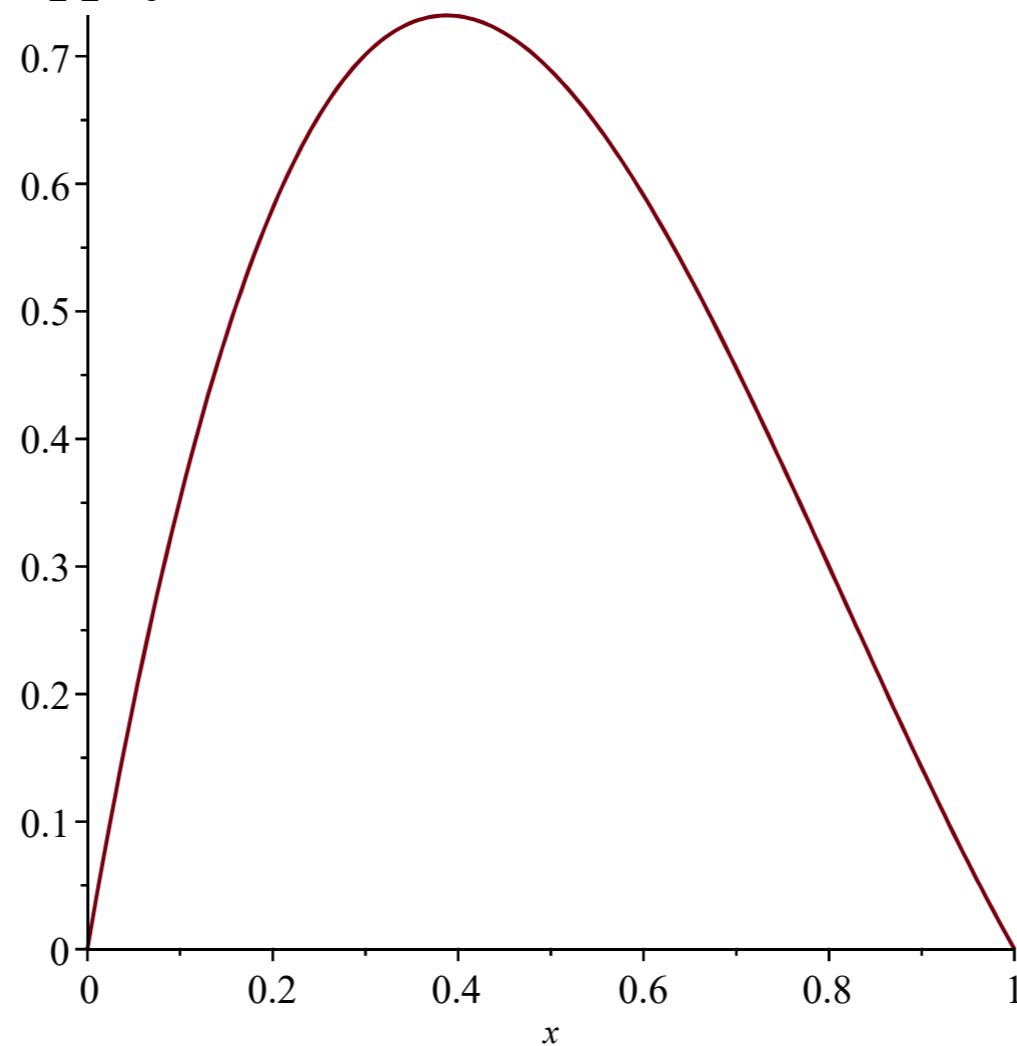
(62)

```
> Wlc_1_comp := subs(Awlc_1=Awlc_1_comp, Bwlc_1=Bwlc_1_comp, Cwlc_1=Cwlc_1_comp, Dwlc_1=Dwlc_1_comp, Betaw1_j=1, Wlc_1);
Wlc_1_comp := -7.11157989501953 cosh(x) + 10.7497632503510 sinh(x) + 7.11158007383347 cos(x) - 6.53830409049988 sin(x)
```

(63)

```
> with(plots):
```

```
> plotWlc_1_comp := plot(Wlc_1_comp, x=0..1) : display([plotWlc_1_comp]);
```



```
>
> PHlyc_j := 1 : PHlys_j := 1 : Omega_j := 10 : Omega_1 := Omega_j :
> rhoA_w1 := 1 : rhoA_w2 := 1 : rhoA_w3 := 1 : rhoA_w4 := 1 : rhoA_u1 := 1 : rhoA_u2 := 1 : rhoA_u3 := 1 : rhoA_u4 := 1 :
> EI_w1 := 1 : EI_w2 := 1 : EI_w3 := 1 : EI_w4 := 1 : EI_u1 := 1 : EI_u2 := 1 : EI_u3 := 1 : EI_u4 := 1 :
```

```
> Betaw1_j :=  $\left(\frac{\rho A_w1}{EI_w1} \cdot \Omega_j^2\right)^{\left(\frac{1}{4}\right)}$  : Betaw2_j :=  $\left(\frac{\rho A_w2}{EI_w2} \cdot \Omega_j^2\right)^{\left(\frac{1}{4}\right)}$  : Betaw3_j :=  $\left(\frac{\rho A_w3}{EI_w3} \cdot \Omega_j^2\right)^{\left(\frac{1}{4}\right)}$  : Betaw4_j :=  $\left(\frac{\rho A_w4}{EI_w4} \cdot \Omega_j^2\right)^{\left(\frac{1}{4}\right)}$  :
```

```
> Betau1_j :=  $\left(\frac{\rho A_u1}{EI_u1} \cdot \Omega_j^2\right)^{\left(\frac{1}{4}\right)}$  : Betau2_j :=  $\left(\frac{\rho A_u2}{EI_u2} \cdot \Omega_j^2\right)^{\left(\frac{1}{4}\right)}$  : Betau3_j :=  $\left(\frac{\rho A_u3}{EI_u3} \cdot \Omega_j^2\right)^{\left(\frac{1}{4}\right)}$  : Betau4_j :=  $\left(\frac{\rho A_u4}{EI_u4} \cdot \Omega_j^2\right)^{\left(\frac{1}{4}\right)}$  :
```

```
> span := 1 : hw1 := 1 : hw2 := 1 :
```

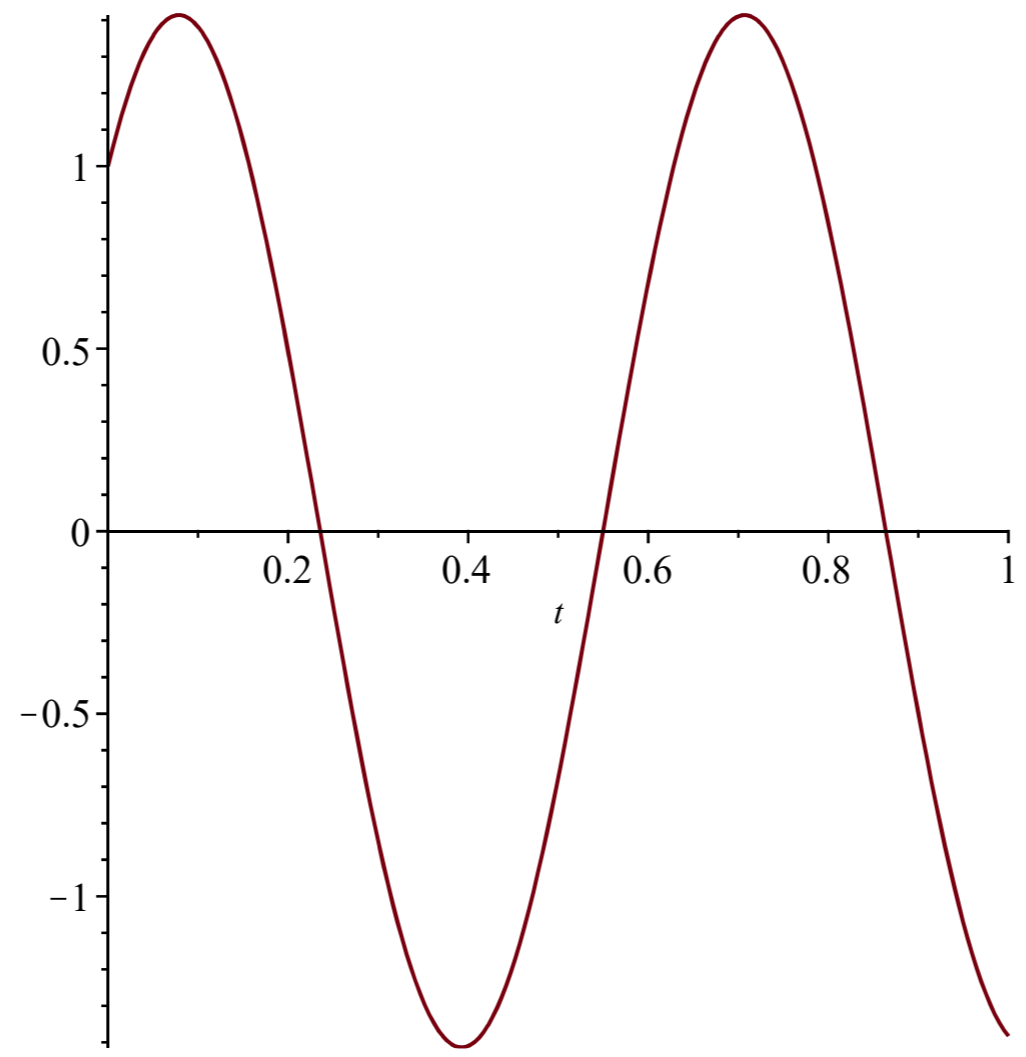
```
>
```

```
> phiy;
```

$\cos(10 t) + \sin(10 t)$

(64)

```
> plotPHly_1_comp := plot(phiy, t=0..1) : display([plotPHly_1_comp]);
```



T. Appendix: Iterations of structural parameters to compute structural response

1. Reference case

The input parameters are as in the input-Excel file on the following pages. An additional mass has been considered to take into account the weight of the façade which is assumed to have a weight equal to 1 kN/m^2 façade area. The middle of the structure is located at 30 m from the middle of the road. The soil is assumed to be soft.

The computational results are given after the input parameters. The iterations made from this reference case only show the relevant results that are influenced by the change in parameter(s).

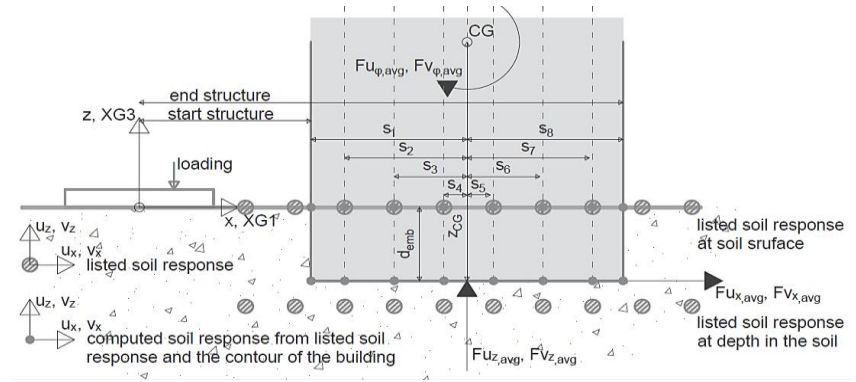
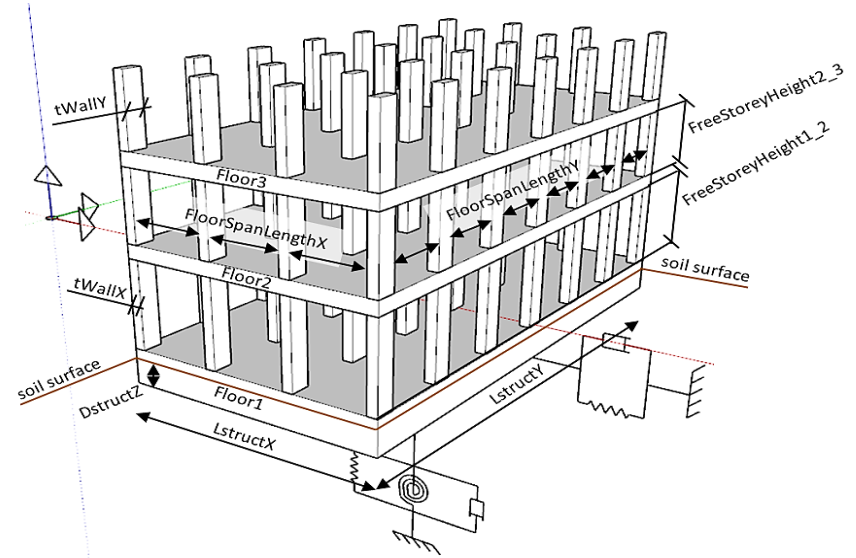
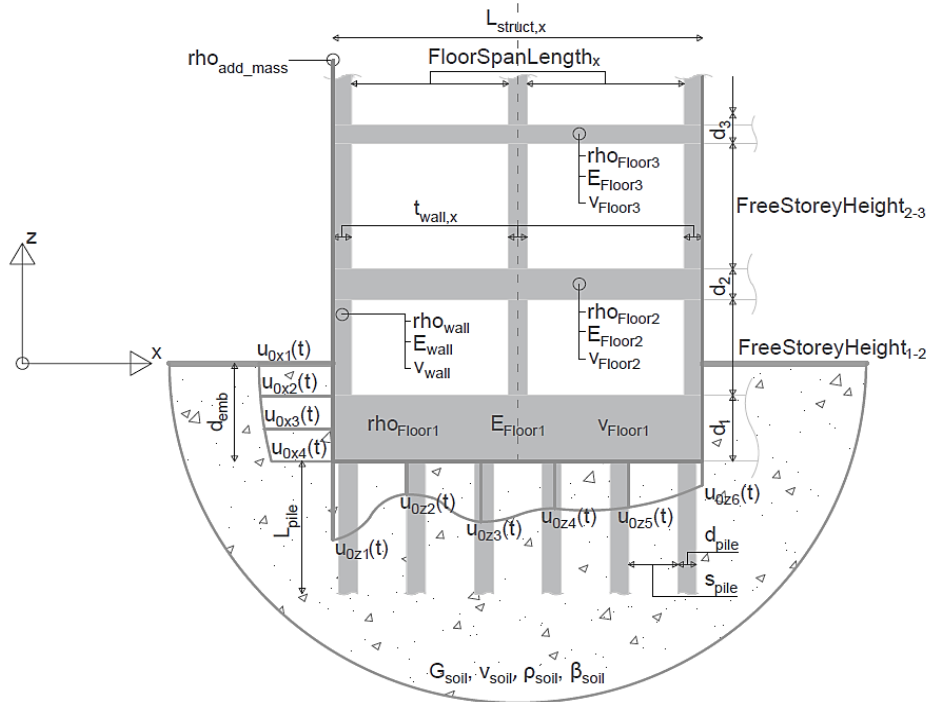
Input file for Python	Description
Author: Gerwin Schut	
Date: 5-9-2019	
Project: Building in Amsterdam	

Python input requirements

Description	Parameters	Unit	Explanation
<i>do not change the descriptions in this column</i> ↓			

Script 0: 0.3DoFBuildingDesignParameters

Figures to explain several input parameters of Python scripts 0, 1 and 2



Input file for computing structural dynamic response

Date: 5-9-2019 | Author: Gerwin Schut

FLOORS for 3DoF system				
				properties of floor. Make sure that the text 'FloorProperties' + (the number of the wall), e.g. 'FloorProperties1' is present in the 'descriptions' column in case this floor has to be included in the computation. Otherwise delete the text 'FloorProperties'.
Floor 1	FloorProperties1			
	dFloor1	=	1 m	Thickness of floor
	MaterialFloor1	=	Concrete	Material name for the floor
	RhoFloor1	=	2500 kg/m3	density of floor material
	EFloor1	=	30000000000 N/m2	Young's modulus of floor material
	vFloor1	=	0.2	Poisson's ratio of floor material. Should be smaller than 0.5
Floor 2	FloorProperties2			
	dFloor2	=	0.6 m	Thickness of floor
	MaterialFloor2	=	Concrete	Material name for the floor
	RhoFloor2	=	2500 kg/m3	density of floor material
	EFloor2	=	30000000000 N/m2	Young's modulus of floor material
	vFloor2	=	0.2	Poisson's ratio of floor material. Should be smaller than 0.5
Floor 3	FloorProperties3			
	dFloor3	=	0.4 m	Thickness of floor
	MaterialFloor3	=	Concrete	Material name for the floor
	RhoFloor3	=	2500 kg/m3	density of floor material
	EFloor3	=	30000000000 N/m2	Young's modulus of floor material
	vFloor3	=	0.2	Poisson's ratio of floor material. Should be smaller than 0.5
Floor 4	FloorProperties4			
	dFloor4	=	0.4 m	Thickness of floor
	MaterialFloor4	=	Concrete	Material name for the floor
	RhoFloor4	=	2500 kg/m3	density of floor material
	EFloor4	=	30000000000 N/m2	Young's modulus of floor material
	vFloor4	=	0.2	Poisson's ratio of floor material. Should be smaller than 0.5
Floor 5	FloorProperties5			
	dFloor5	=	0.5 m	Thickness of floor
	MaterialFloor5	=	Concrete	Material name for the floor
	RhoFloor5	=	2000 kg/m3	density of floor material
	EFloor5	=	30000000000 N/m2	Young's modulus of floor material

Input file for computing structural dynamic response

Date: 5-9-2019 | Author: Gerwin Schut

	vFloor5	=	0.2	-	Poisson's ratio of floor material. Should be smaller than 0.5
Floor 6	FloorProperties6				properties of floor.
	dFloor6	=	0.5	m	Thickness of floor
	MaterialFloor6	=	Concrete	-	Material name for the floor
	RhoFloor6	=	2000	kg/m3	density of floor material
	EFloor6	=	30000000000	N/m2	Young's modulus of floor material
	vFloor6	=	0.2	-	Poisson's ratio of floor material. Should be smaller than 0.5
Floor 7	FloorProperties7				properties of floor.
	dFloor7	=	0.5	m	Thickness of floor
	MaterialFloor7	=	Concrete	-	Material name for the floor
	RhoFloor7	=	2000	kg/m3	density of floor material
	EFloor7	=	30000000000	N/m2	Young's modulus of floor material
	vFloor7	=	0.2	-	Poisson's ratio of floor material. Should be smaller than 0.5
Floor 8	FloorProperties8				properties of floor.
	dFloor8	=	0.4	m	Thickness of floor
	MaterialFloor8	=	Concrete	-	Material name for the floor
	RhoFloor8	=	2000	kg/m3	density of floor material
	EFloor8	=	30000000000	N/m2	Young's modulus of floor material
	vFloor8	=	0.2	-	Poisson's ratio of floor material. Should be smaller than 0.5
FREE STOREY HEIGHTS for 3DoF system					
	FreeStoreyHeight1_2	=	3.9	m	Free storey height between floor 1 and 2
	FreeStoreyHeight2_3	=	4.1	m	Free storey height between floor 2 and 3
	FreeStoreyHeight3_4	=	4.1	m	Free storey height between floor 3 and 4
	FreeStoreyHeight4_5	=	3.8	m	Free storey height between floor 3 and 4
	FreeStoreyHeight5_6	=	3.8	m	Free storey height between floor 3 and 4
	FreeStoreyHeight6_7	=	3.8	m	Free storey height between floor 3 and 4
	FreeStoreyHeight7_8	=	3.9	m	Free storey height between floor 3 and 4
FLOORSPANS					
	NrOfFloorSpansX	=	3	-	number of floor spans in-plane (in the x-z-plane)
	FloorSpanLengthX	=	6.6	m	length of floor spans in-plane (equal for all floor spans). Span in between the walls
	NrOfFloorSpansY	=	7	-	number of floor spans out-of-plane (in the y-z-plane)

Input file for computing structural dynamic response

Date: 5-9-2019 | Author: Gerwin Schut

FloorSpanLengthY	=	6.6	m	length of floor spans out-of-plane (equal for all floor spans). Span in between the walls
WALLS				
WallProperties				properties of wall. Make sure that the text 'WallProperties' + (the number of the wall), e.g. 'WallProperties1' is present in the 'descriptions' column in case this wall has to be included in the computation. Otherwise delete the text 'WallProperties'.
tWallX	=	0.6	m	Thickness of wall in-plane (in the x-z-plane)
tWallY	=	0.6	m	Thickness of wall out-of-plane (in the y-z-plane)
MaterialWall	=	Concrete	-	Material name for the wall
RhoWall	=	2500	kg/m3	density of wall material
Ewall	=	30000000000	N/m2	Young's modulus of wall material
vWall	=	0.2	-	Poisson's ratio of wall material. Should be smaller than 0.5
LstructX	=	22.2	m	total length of structure (in-plane) in x-direction
LstructY	=	51	m	total depth of structure (out-of-plane) in y-direction
HstructZ	=	29.4	m	total height of structure in z-direction
AdditionalMass	=	12.93	kg/m3	additional mass that needs to be taken into account for the total mass of the building and the mass moment inertia of the building which acts as resistance against vibrations (impedance). Divide the total mass to be added by the total volume of the structure (LstructX x LstructY x HstructZ)
Continue on next page with script 1				

Script 1: 1.ScriptToCompute3DoFExcitation			
Structure for 3DoF system			
pos_StartStructure	=	18.9 m	distance along the x-axis from the middle of the road to the start of the building
pos_EndStructure	=	41.1 m	distance along the x-axis from the middle of the road to the end of the building
DstructZ	=	5.5 m	depth of structure (e.g. box or slab) without pile foundation
Excitation 3DoF system			
Exc_factor	=	0 -	0: the excitation is not factorized 1: the excitation is factorized according to EV5.2 by factorizing the frequency domain and computing the time domain from there
tmin_exc	=	-0.1 s	start time-instant for the excitation input (preferably Excitation(tmin_exc) = 0)
tmax_exc	=	1.5 s	end time-instant for the excitation input (preferably Excitation(tmax_exc) = 0)
tstep_exc	=	0.02 s	time step for the excitation input (should be sufficiently small for reliable excitation input)
t_nr_exc	=	81	nr of time instants considered to compute the excitation in the time domain
Continue on next page with script 2			

Script 2: 2.ImpedancesAnd3DoFStructuralResponse				
Soil approximation for impedances 3DoF system				
	G_HS	=	7500000	N/m2 shear modulus of soil approximation as homogeneous HalfSpace
	rho_HS	=	2000	kg/m3 material mass density of soil approximation as homogeneous HalfSpace
	v_HS	=	0.48	- Poisson's ratio of soil approximation as homogeneous HalfSpace
	Beta_HS	=	0.02	- damping ratio of soil approximation as homogeneous HalfSpace
<i>in case of piles only</i>	Esoil0	=	50000000	N/m2 Young's modulus of soil material at the pile head (top of the pile, underneath the foundation slab)
<i>in case of piles only</i>	rho_L	=	2000	kg/m3 material mass density of soil approximation at pile-length of the foundation pile (pile tip)
<i>in case of piles only</i>	v_L	=	0.25	- Poisson's ratio of soil approximation at pile-length of foundation pile (pile tip)
<i>in case of piles only</i>	Cs_L	=	200	m/s shear wave speed of soil approximation at pile-length of the foundation pile (pile tip)
<i>in case of piles only</i>	Cs_Lm	=	100	m/s shear wave speed of soil approximation at mid-length of the foundation pile
<i>in case of piles only</i>	Cs_H	=	400	m/s shear wave speed of soil approximation at twice the pile-length of the foundation pile (pile tip + pile length)
<i>in case of piles only</i>	Beta_L	=	0.01	- damping ratio of soil approximation at pile-length of the foundation pile (pile tip)
<i>in case of piles only</i>	HsoilZ	=	36	m depth of H (which is taken as twice the pile length)
Structure for 3DoF system				
	DstructZeff	=	5.5	m effective depth of structural wall-soil interface
	AbReducingFactor	=	1	- reducing factor for contact area Ab between bottom of structure and soil to take into account loss of contact due to e.g. rocking of the structure.
	AwReducingFactor	=	1	- reducing factor for contact area Aw between structural walls and soil to take into account loss of contact due to e.g. rocking of the structure.
	presence_piles	=	1	0: no foundation piles are included 1: the foundation piles are included as specified below:
<i>in case of piles only</i>	Dpile	=	0.7	m diameter of a single foundation pile
<i>in case of piles only</i>	LpileZ	=	18	m length of a single foundation pile (underneath bottom of foundation slab to pile tip)
<i>in case of piles only</i>	nrPilesX	=	9	- nr of foundation piles on the same axis parallel to the x-axis (symmetrically divided)
<i>in case of piles only</i>	nrPilesY	=	26	- nr of foundation piles on the same axis parallel to the y-axis (symmetrically divided)
<i>in case of piles only</i>	Ptot	=	234	- total nr of foundation piles (minimum amount is 4)
<i>in case of piles only</i>	Spiles	=	2.1	m axis-to-axis distance foundation piles
<i>in case of piles only</i>	Epile	=	30000000000	N/m2 Young's Modulus of foundation pile material (e.g. concrete)

Input file for computing structural dynamic response

Date: 5-9-2019 | Author: Gerwin Schut

Computational options 3DoF system			
freq_step_str	=	0.25 Hz	frequency step used to compute the 3DoF soil impedances and the 3DoF structural response and the EB-beam flexible frame structural response in the frequency domain. Also: freq_min_str = freq_step_str/2
freq_nr_str	=	81	nr of frequencies considered to compute the freq_max_str
freq_max_str	=	20.125 Hz	maximum frequency considered for computing the 3DoF soil impedances and the 3DoF structural response and the EB-beam flexible frame structural response in the frequency domain.
tmin_resp	=	-0.12 s	minimum time instant to consider for the computation of the structural response
tstep_resp	=	0.02 s	time step to consider for the computation of the structural response
t_nr_resp	=	137	nr of time instants to consider for the computation of the structural response
tmax_resp	=	2.6 s	maximum time instant to consider for the computation of the structural response
freq_plot_forcings	=	7 Hz	specific frequency for which the frequency dependent forcings are plotted (compressed springs)
Plotting parameters 3DoF system			
plot_3DoF_velocities_time	=	1	0: do not plot the 3DoF response velocities in the time domain 1: plot the 3DoF response velocities in the time domain
plot_3DoF_velocities_freq	=	1	0: do not plot the 3DoF response velocities in the frequency domain 1: plot the 3DoF response velocities in the frequency domain
plot_3DoF_RMSvelocities_freq	=	1	0: do not plot the 3DoF response RMS velocities in the frequency domain 1: plot the 3DoF response RMS velocities in the frequency domain
Excitation 3DoF system (in case a simpler excitation is wanted than the stored excitation lists in the folder 'SoilResponses')			
overwrite_exc_3DoF	=	0	0: the excitation will be taken from the excitation.csv-files, computed by script 1. 1: the excitation will not be taken from the excitation.csv-files. Instead a more simple excitation can be constructed with the parameters specified below this parameter.
Harmonic excitation term 1			
Freq_3DoF_exc1	=	5 Hz	The frequency of the harmonic excitation: $U(t) = A_{ucj} \cdot \cos(\text{Freq_excj} \cdot t) + A_{usj} \cdot \sin(\text{Freq_excj} \cdot t)$
Au1cj_3DoF_exc1	=	0.00001 m	Amplitude of the harmonic excitation corresponding to the cosine term of the displacements (u)

Input file for computing structural dynamic response
Date: 5-9-2019 | Author: Gerwin Schut

Au1sj_3DoF_exc1	=	0.00001	m	Amplitude of the harmonic excitation corresponding to the sine term of the displacements (u)
Au3cj_3DoF_exc1	=	0.00001	m	Amplitude of the harmonic excitation corresponding to the cosine term of the displacements (u)
Au3sj_3DoF_exc1	=	0.00001	m	Amplitude of the harmonic excitation corresponding to the sine term of the displacements (u)
AuPHIcj_3DoF_exc1	=	0.00001	rad	Amplitude of the harmonic excitation corresponding to the cosine term of the displacements (u)
AuPHIsj_3DoF_exc1	=	0.00001	rad	Amplitude of the harmonic excitation corresponding to the sine term of the displacements (u)
Av1cj_3DoF_exc1	=	0.0001	m/s	Amplitude of the harmonic excitation corresponding to the cosine term of the velocities (v)
Av1sj_3DoF_exc1	=	0.0001	m/s	Amplitude of the harmonic excitation corresponding to the sine term of the velocities (v)
Av3cj_3DoF_exc1	=	0.0001	m/s	Amplitude of the harmonic excitation corresponding to the cosine term of the velocities (v)
Av3sj_3DoF_exc1	=	0.0001	m/s	Amplitude of the harmonic excitation corresponding to the sine term of the velocities (v)
AvPHIcj_3DoF_exc1	=	0.0001	rad/s	Amplitude of the harmonic excitation corresponding to the cosine term of the velocities (v)
AvPHIsj_3DoF_exc1	=	0.0001	rad/s	Amplitude of the harmonic excitation corresponding to the sine term of the velocities (v)
Harmonic excitation term 2				
Freq_3DoF_exc2	=	10	Hz	The frequency of the harmonic excitation: $U(t) = A_{ucj} \cdot \cos(\text{Freq_excj} \cdot t) + A_{usj} \cdot \sin(\text{Freq_excj} \cdot t)$
Au1cj_3DoF_exc2	=	0.00001	m	Amplitude of the harmonic excitation corresponding to the sine term of the displacements (u)
Au1sj_3DoF_exc2	=	0.00001	m	Amplitude of the harmonic excitation corresponding to the sine term of the displacements (u)
Au3cj_3DoF_exc2	=	0.00001	m	Amplitude of the harmonic excitation corresponding to the cosine term of the displacements (u)
Au3sj_3DoF_exc2	=	0.00001	m	Amplitude of the harmonic excitation corresponding to the sine term of the displacements (u)

Input file for computing structural dynamic response

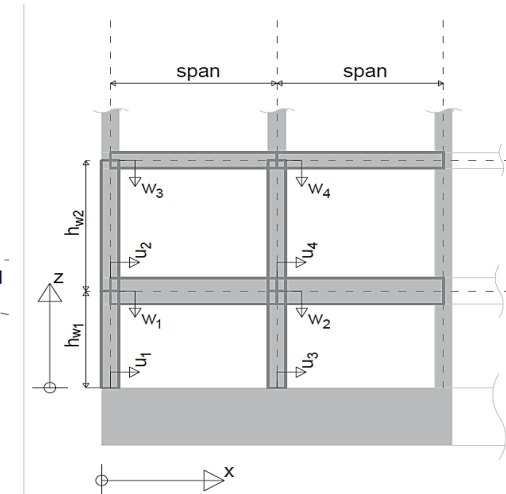
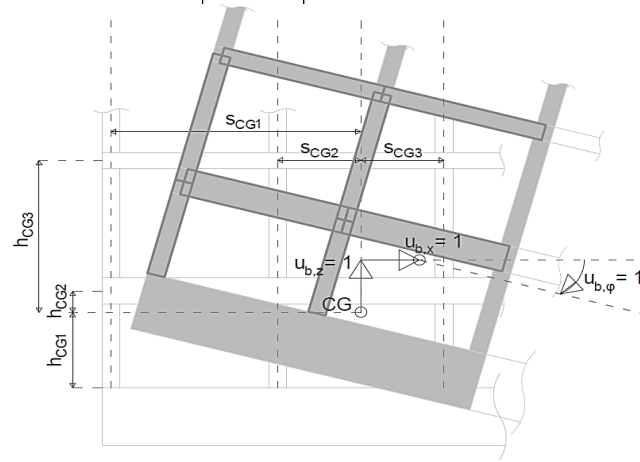
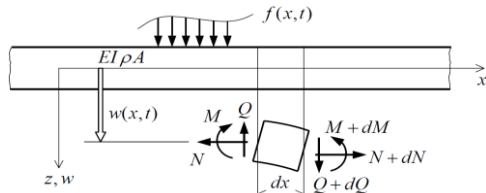
Date: 5-9-2019 | Author: Gerwin Schut

AuPHIcj_3DoF_exc2	=	0.00001	rad	Amplitude of the harmonic excitation corresponding to the cosine term of the displacements (u)
AuPHIsj_3DoF_exc2	=	0.00001	rad	Amplitude of the harmonic excitation corresponding to the sine term of the displacements (u)
Av1cj_3DoF_exc2	=	0.0001	m/s	Amplitude of the harmonic excitation corresponding to the cosine term of the velocities (v)
Av1sj_3DoF_exc2	=	0.0001	m/s	Amplitude of the harmonic excitation corresponding to the sine term of the velocities (v)
Av3cj_3DoF_exc2	=	0.0001	m/s	Amplitude of the harmonic excitation corresponding to the cosine term of the velocities (v)
Av3sj_3DoF_exc2	=	0.0001	m/s	Amplitude of the harmonic excitation corresponding to the sine term of the velocities (v)
AvPHIcj_3DoF_exc2	=	0.0001	rad/s	Amplitude of the harmonic excitation corresponding to the cosine term of the velocities (v)
AvPHIsj_3DoF_exc2	=	0.0001	rad/s	Amplitude of the harmonic excitation corresponding to the sine term of the velocities (v)
Insert additional excitation terms here				

Continue on next page with script 3

Script 3: 3.EB-beam frame matrix_allExcitations

Figures to explain several input parameters of Python script 3



EB-beam frame additional (or more detailed / free to pick) properties. Otherwise refer input cell to structural properties of script 0

Structure for EB-beam frame			
EB_span	=	10.18233765	m length (span) of all EB-beam floor elements
EB_hw1	=	4.5	m length (storey height) of the EB-beam wall elements u1 and u3
EB_hw2	=	4.5	m length (storey height) of the EB-beam wall elements u2 and u4
wj_width	=	1	m width of the EB-beam floor elements (factorized out in the computation)
w1_height	=	0.5	m floor height or thickness of EB-beam floor element w1
w2_height	=	0.5	m floor height or thickness of EB-beam floor element w2
w3_height	=	0.4	m floor height or thickness of EB-beam floor element w3
w4_height	=	0.4	m floor height or thickness of EB-beam floor element w4
uj_width	=	1	m width of the EB-beam wall elements (factorized out in the computation)
u1_height	=	0.55	m wall height or thickness of EB-beam wall element u1
u2_height	=	0.55	m wall height or thickness of EB-beam wall element u2
u3_height	=	0.3	m wall height or thickness of EB-beam wall element u3
u4_height	=	0.3	m wall height or thickness of EB-beam wall element u4
rho_structure	=	4000	kg/m3 material mass density of the EB-beam frame structure
E_mod_structure	=	19000000000	N/m2 Young's Modulus of the EB-beam frame structure

Computation of EB-beam frame			
freq_step_str_EB	=	0.25	Hz
freq_nr_str_EB	=	81	-
freq_max_str_EB	=	20.125	Hz
tmin_resp_EB	=	-0.14	
tstep_resp_EB	=	0.02	s
t_nr_resp_EB	=	138	
tmax_resp_EB	=	2.6	s
Plotting parameters EB-beam frame			
plot_displaced_frames_UxWzPHly	=	0	0: do not plot the displaced EB-beam frame due to the excitations Ux, Wz and PHly for a particular time instant 1: plot the displaced EB-beam frame due to the excitations Ux, Wz and PHly for the time instants specified below:
plot_displaced_frame_tot	=	0	0: do not plot the displaced EB-beam frame due to all excitation types for a particular time instant 1: plot the displaced EB-beam frame due to all excitation types for the time instants specified below:
time_instant_frame_plot_1	=	0.5	s time instant at which the results of the EB-beam frame are computed and plotted
<i>time_instant_frame_plot_2</i>	=	0.1	s time instant at which the results of the EB-beam frame are computed and plotted
plot_max_defl_factor	=	0.1	factor multiplied with min(hw,hw2,span) to obtain a limit displacement in the EB-beam frame plots. This limit is used to obtain a scalingfactor for plotting the displaced EB-beam frames. Advised is to keep this value equal to 0.1
applying_scaling_factor	=	0	- 0: no scalingfactor will be applied to the plots of the deformed EB-beam frame 1: the scalingfactor for the plots will be determined by the script (computational heavy) 2: the scaling factor will be chosen from the specified factors below:
apply_ScalingFactorUx	=	600	- Scaling factor applied when '2' is chosen above (for the response due to excitation Ux only), refers to plot_displaced_frames_UxWzPHly
apply_ScalingFactorWz	=	600	- Scaling factor applied when '2' is chosen above (for the response due to excitation Wz only), refers to plot_displaced_frames_UxWzPHly

Input file for computing structural dynamic response

Date: 5-9-2019 | Author: Gerwin Schut

apply_ScalingFactorPHly	=	600	-	Scaling factor applied when '2' is chosen above (for the response due to excitation PHly only), refers to plot_displaced_frames_UxWzPHly
1300273914 apply_ScalingFactor	=	600	-	Scaling factor applied when '2' is chosen above (for the response due to all excitations), refers to plot_displaced_frames_tot
Plotting parameters EB-beam element w1				
plot_w1_displ_time		0		0: do not plot the displaced beam element w1 along the length of the element for a particular time instant 1: plot the displaced beam element w1 along the length of the element for a the particular time instants specified below:
time_instant_w1_displ_plot_1	=	0	s	time instant at which the displacements of the EB-beam element w1 are computed and plotted
<i>time_instant_w1_displ_plot_2</i>	=	0.1	s	time instant at which the displacements of the EB-beam element w1 are computed and plotted
plot_w1_displ_coord		0		0: do not plot the displaced beam element w1 over the time domain of the forcing for a particular x-coordinate along the element 1: plot the displaced beam element w1 over the time domain of the forcing for a particular x-coordinate along the element as specified below:
x_coord_w1_displ_plot_1	=	5.091168825	m	x-coordinate at which the displacements of the EB-beam element w1 are computed and plotted
<i>x_coord_w1_displ_plot_2</i>	=	2.545584412	m	x-coordinate at which the displacements of the EB-beam element w1 are computed and plotted
plotting velocities of w1 in the space-time domain				
plot_w1_veloc_time		0		0: do not plot the velocities of the beam element w1 along the length of the element for a particular time instant 1: plot the velocities of the beam element w1 along the length of the element for a the particular time instants specified below:
time_instant_w1_veloc_plot_1	=	0	s	time instant at which the velocities of the EB-beam element w1 are computed and plotted
<i>time_instant_w1_veloc_plot_2</i>	=	0.1	s	time instant at which the velocities of the EB-beam element w1 are computed and plotted

Input file for computing structural dynamic response

Date: 5-9-2019 | Author: Gerwin Schut

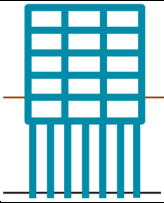
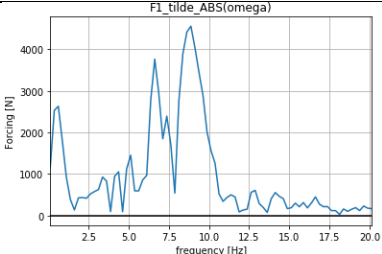
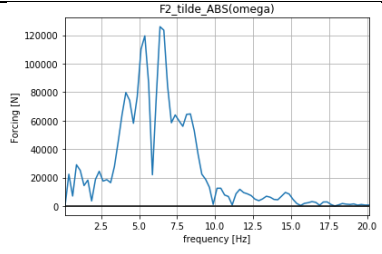
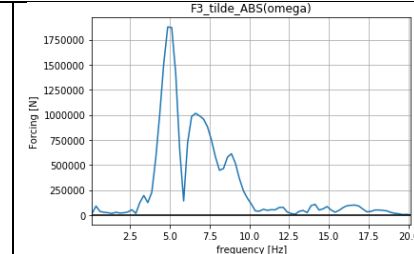
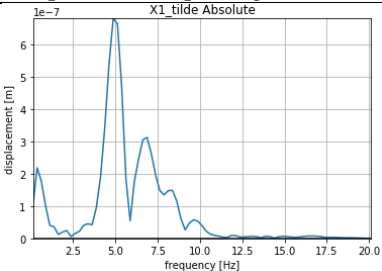
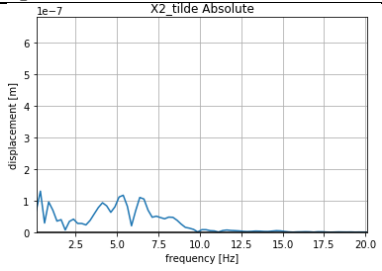
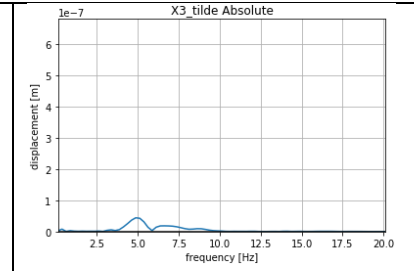
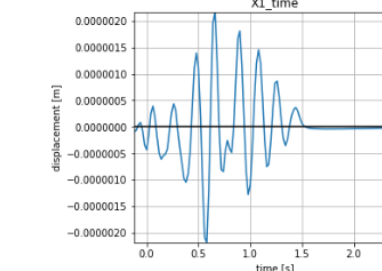
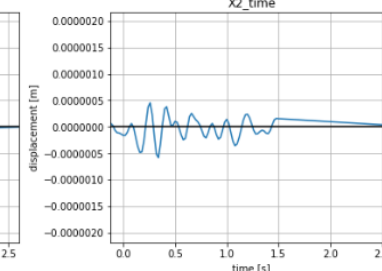
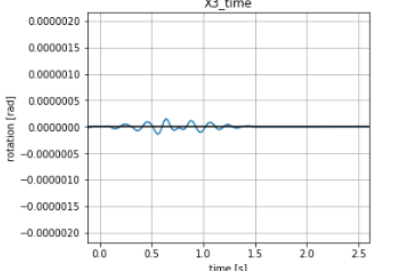
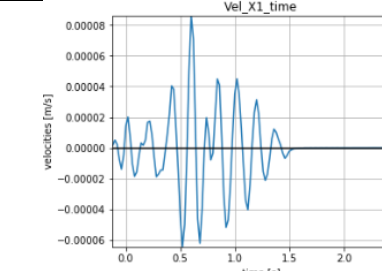
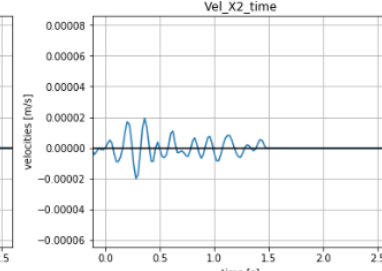
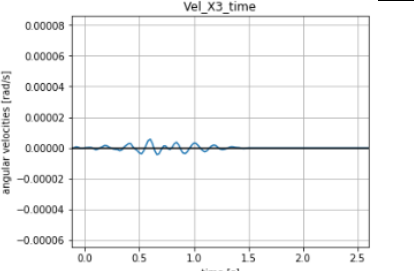
plot_w1_veloc_coord	=	1		0: do not plot the velocities of the beam element w1 over the time domain of the forcing for a particular x-coordinate along the element 1: plot the velocities of the beam element w1 over the time domain of the forcing for a particular x-coordinate along the element as specified below:
x_coord_w1_veloc_plot_1	=	5.091168825	m	x-coordinate at which the velocities of the EB-beam element w1 are computed and plotted
<i>x_coord_w1_veloc_plot_2</i>	=	2.545584412	m	x-coordinate at which the velocities of the EB-beam element w1 are computed and plotted
plotting velocities of w1 in the space-frequency domain				
plot_w1_velocFreq_coord	=	1		0: do not plot the velocities of the beam element w1 over the specified calculation-frequency domain for a particular x-coordinate along the element 1: plot the velocities of the beam element w1 over the specified calculation-frequency domain for a particular x-coordinate along the element as specified below:
x_coord_w1_velocFreq_plot_1	=	5.091168825	m	position in floor w1 to compute the frequency response spectrum
<i>x_coord_w1_velocFreq_plot_1</i>	=	2.545584412	m	position in floor w1 to compute the frequency response spectrum
plotting RMS-velocities of w1 in the space-frequency domain				
plot_w1_RMSvelocFreq_coord	=	1		0: do not plot the velocities of the beam element w1 over the specified calculation-frequency domain for a particular x-coordinate along the element 1: plot the velocities of the beam element w1 over the specified calculation-frequency domain for a particular x-coordinate along the element as specified below:
x_coord_w1_RMSvelocFreq_plot_1	=	5.091168825	m	position in floor w1 to compute the frequency response spectrum
Excitation EB-beam frame (in case a simpler excitation is wanted than the stored excitation lists in the csv-files '3DoF_Building_Response')				
overwrite_exc_EB	=	0	-	0: the excitation will be taken from the excitation.csv-files. 1: the excitation will not be taken from the excitation.csv-files. Instead a more simple excitation can be constructed with the parameters specified below this parameter.
Harmonic excitation term 1				
Freq_EB_exc1	=	30	Hz	The frequency of the harmonic excitation: $U(t) = A_{ucj} \cdot \cos(\text{Freq_excj} \cdot t) + A_{usj} \cdot \sin(\text{Freq_excj} \cdot t)$
Ax1cj_EB_exc1	=	0.0003	m	Amplitude of the harmonic excitation corresponding to the cosine term of the displacements (u)

Input file for computing structural dynamic response

Date: 5-9-2019 | Author: Gerwin Schut

Ax1sj_EB_exc1	=	0.0003	m	Amplitude of the harmonic excitation corresponding to the sine term of the displacements (u)
Ax2cj_EB_exc1	=	0.0003	m	Amplitude of the harmonic excitation corresponding to the cosine term of the displacements (u)
Ax2sj_EB_exc1	=	0.0003	m	Amplitude of the harmonic excitation corresponding to the sine term of the displacements (u)
Ax3cj_EB_exc1	=	0.00002	rad	Amplitude of the harmonic excitation corresponding to the cosine term of the displacements (u)
Ax3sj_EB_exc1	=	0.00002	rad	Amplitude of the harmonic excitation corresponding to the sine term of the displacements (u)
Harmonic excitation term 2				
Freq_EB_exc2	=	8	Hz	The frequency of the harmonic excitation: $U(t) = A_{ucj} \cdot \cos(\text{Freq_excj} \cdot t) + A_{usj} \cdot \sin(\text{Freq_excj} \cdot t)$
Ax1cj_EB_exc2	=	0.0003	m	Amplitude of the harmonic excitation corresponding to the sine term of the displacements (u)
Ax1sj_EB_exc2	=	0.0003	m	Amplitude of the harmonic excitation corresponding to the sine term of the displacements (u)
Ax2cj_EB_exc2	=	0.0003	m	Amplitude of the harmonic excitation corresponding to the cosine term of the displacements (u)
Ax2sj_EB_exc2	=	0.0003	m	Amplitude of the harmonic excitation corresponding to the sine term of the displacements (u)
Ax3cj_EB_exc2	=	0.00002	rad	Amplitude of the harmonic excitation corresponding to the cosine term of the displacements (u)
Ax3sj_EB_exc2	=	0.00002	rad	Amplitude of the harmonic excitation corresponding to the sine term of the displacements (u)
Insert additional excitation terms here				
End of input parameters				

Results:

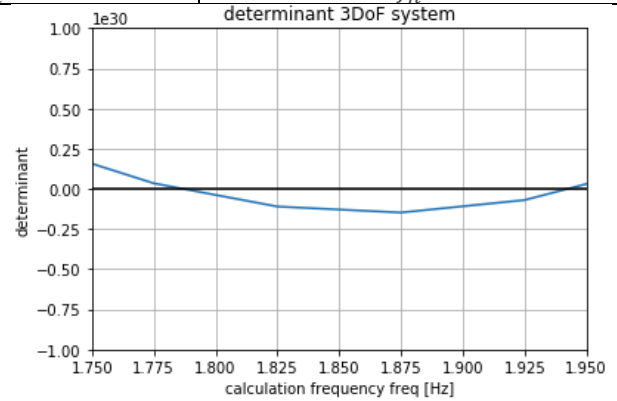
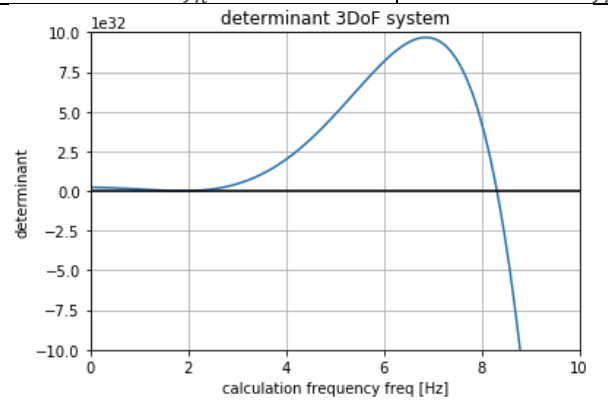
Title: Building in Amsterdam 'Reference' Date: 2019-9-6		
Computational parameters 3DoF and EB-beam frame		
$t_{step_exc} = 0.02\ s$	$t_{nr_exc} = 81$	$t_{max_exc} = 1.5\ s$
$f_{step_resp} = 0.25\ Hz$	$f_{nr_resp} = 81$	$f_{max_resp} = 20.125\ Hz$
$t_{step_resp} = 0.02\ s$	$t_{nr_resp} = 137$	$t_{max_resp} = 2.6\ s$
3DoF system:		
$M_b = 12348747\ kg$	$J_{CG} = 1869944533\ kgm^2$	$z_{CG} = 13.26\ m$
Excitation (frequency dependent forces):		
		
$peak = 4.5\ kN$	$peak = 120\ kN$	$peak = 1800\ kNm$
Response (frequency domain displacements):		
		
Response (time domain displacements):		
		
$peak = -2.0 \cdot 10^{-6}\ m$	$peak = -0.5 \cdot 10^{-6}\ m$	$peak = -0.2 \cdot 10^{-6}\ rad$
Response (time domain velocities):		
		
$peak = 8.0 \cdot 10^{-5}\ m/s$	$peak = 2.0 \cdot 10^{-5}\ m/s$	$peak = 0.5 \cdot 10^{-5}\ rad/s$

Eigenfrequencies (range of $f = \omega/2\pi$ for which $\det[-\omega^2 \mathbf{M} + \mathbf{K}(\omega)] = 0$):

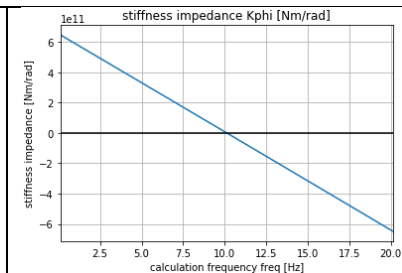
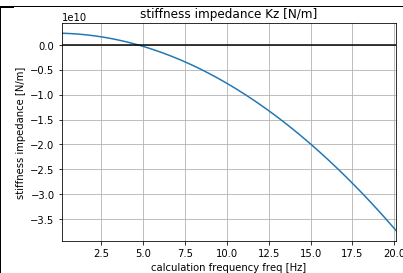
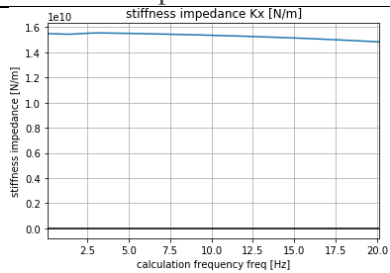
$$1.775 \leq f_n \leq 1.825$$

$$1.925 \leq f_n \leq 1.975$$

$$8.275 \leq f_n \leq 8.325$$



Stiffness impedance terms:

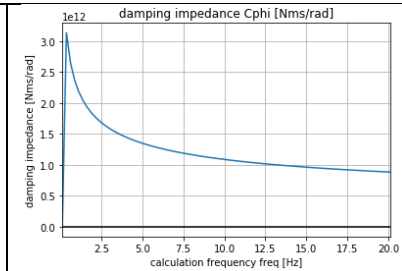
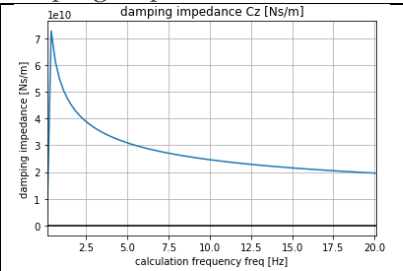
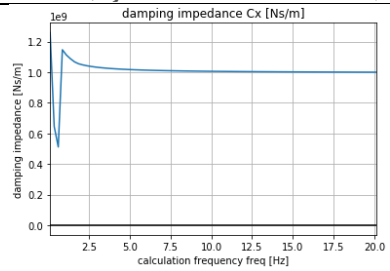


$$peak = 1.55 \cdot 10^{10} \text{ N/m}$$

$$peak = 0.25 \cdot 10^{10} \text{ N/m}$$

$$peak = 63 \cdot 10^{10} \text{ Nm/rad}$$

Total (hysteric and radiation) damping impedance terms:

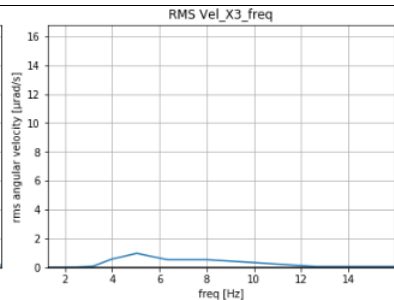
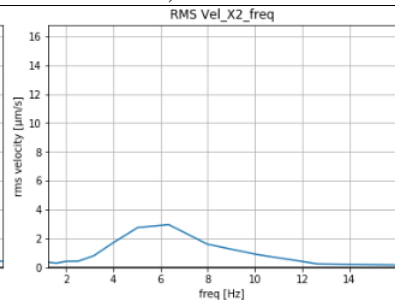
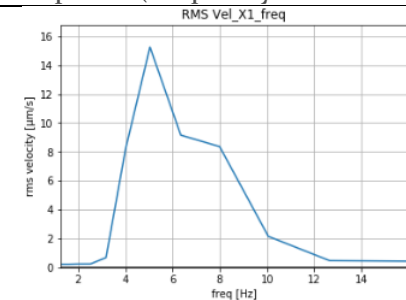


$$peak = 0.12 \cdot 10^{10} \text{ Ns/m}$$

$$peak = 7.0 \cdot 10^{10} \text{ Ns/m}$$

$$peak = 300 \cdot 10^{10} \text{ Nms/rad}$$

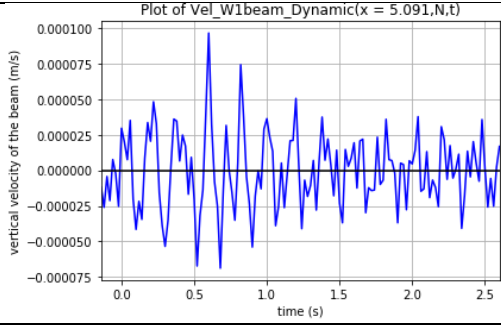
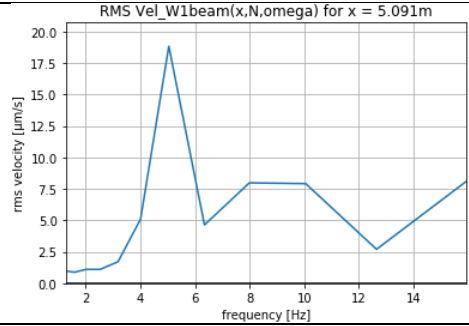
Response (frequency domain RMS velocities)



$$peak = 15 \mu\text{m/s}$$

$$peak = 3 \mu\text{m/s}$$

$$peak = 1 \mu\text{m/s}$$

EB-beam frame element w1:		
 <p>Plot of Vel_W1beam_Dynamic(x = 5.091,N,t)</p>		 <p>RMS Vel_W1beam(x,N,omega) for x = 5.091m</p>
$peak = 1 \cdot 10^{-4} \text{ m/s}$		$peak = 18.5 \text{ } \mu\text{m/s}$
Script 0 & 1		
$t_{comp} = 1 \text{ mins}$		
Script 2		
$v(t): t_{comp} = 40 \text{ mins}$		$v(f) + v_{RMS}(f): t_{comp} = +8 \text{ mins}$
Script 3		
$v(t): t_{comp} = 1 \text{ mins}$	$v(f): t_{comp} = +140 \text{ mins}$	$v_{RMS}(f): t_{comp} = +152 \text{ mins}$
Total comp. time for time domain only: $1 + 40 + 1 = 42 \text{ mins} = REF$		
Total comp. time incl. freq. domain RMS: $1 + 48 + 1 + 140 + 152 = 342 \text{ mins} = REF$		

2. Iteration: greater global building mass (42 - 342 mins)

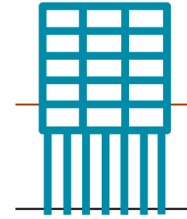
Changed input:

3DoF system:

$$M_b = 24697495 \text{ kg}$$

Results:

Title: Building in Amsterdam 'Greater global building mass'
Date: 2019-9-6



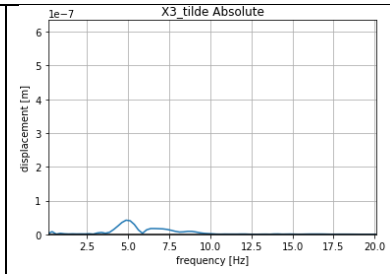
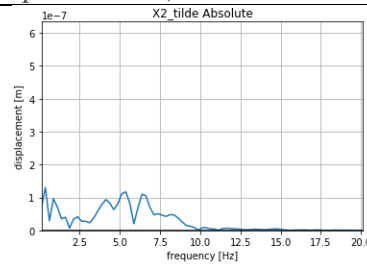
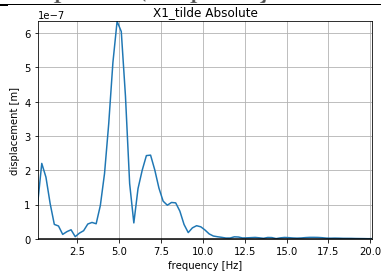
3DoF system:

$$M_b = 24697495 \text{ kg}$$

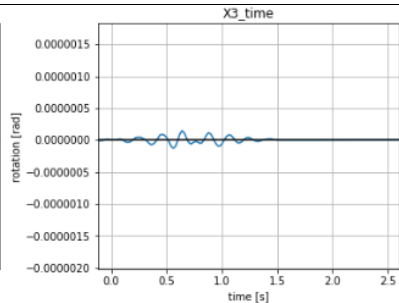
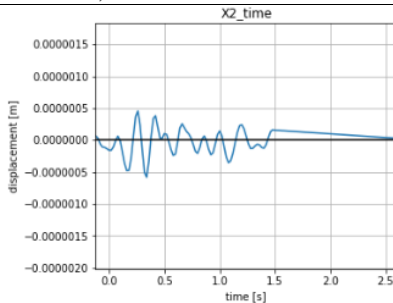
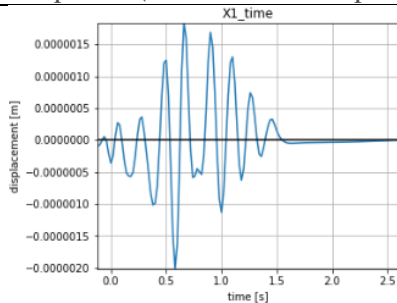
$$J_{CG} = 2972255 \text{ kgm}^2$$

$$z_{CG} = 0.55 \text{ m}$$

Response (frequency domain displacements):



Response (time domain displacements):



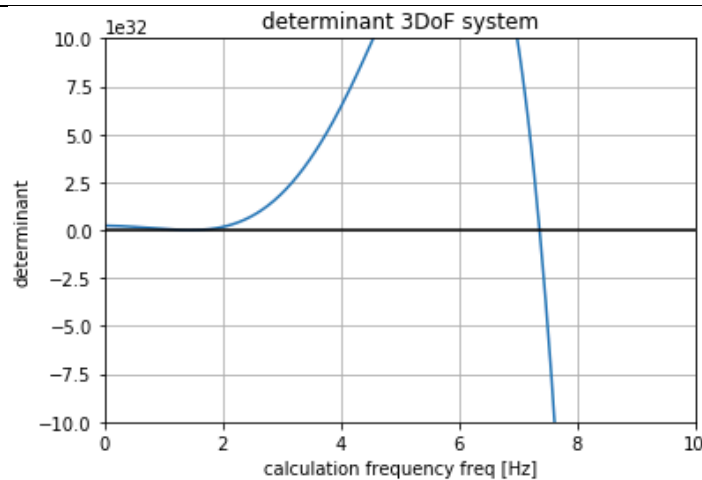
$$\text{peak} = -2.0 \cdot 10^{-6} \text{ m}$$

$$\text{peak} = -0.5 \cdot 10^{-6} \text{ m}$$

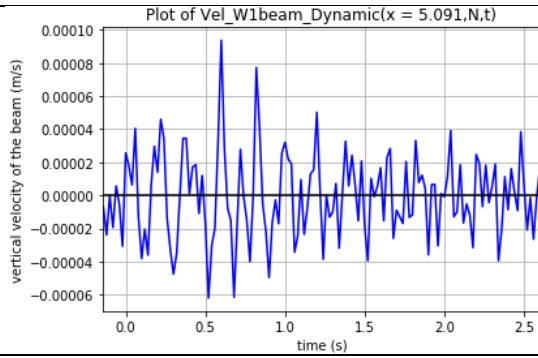
$$\text{peak} = -0.2 \cdot 10^{-6} \text{ rad}$$

Observed eigenfrequencies in range of $0.375 \text{ Hz} \leq f (= \omega/2\pi) \leq 20.125 \text{ Hz}$ for which $\det[-\omega^2 \mathbf{M} + \mathbf{K}(\omega)] = 0$:

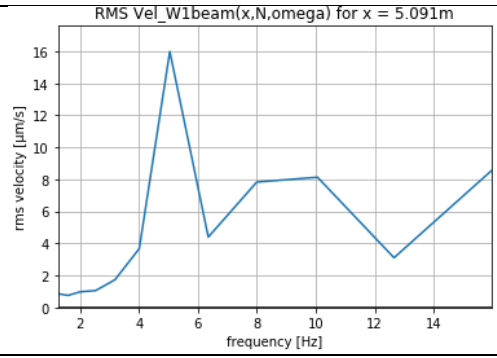
$$7.325 \leq f_n \leq 7.375$$



EB-beam frame element w1:



$peak = 0.95 \cdot 10^{-4} \text{ m/s}$



$peak = 16 \mu\text{m/s}$

3. Iteration: small rigid block (42 - 342 mins)

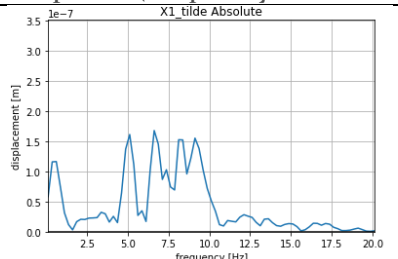
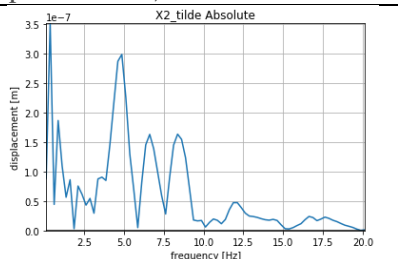
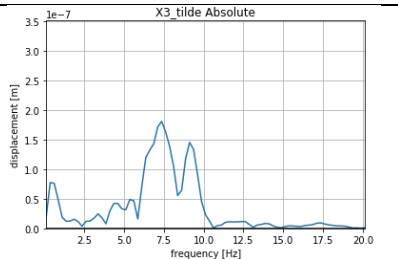
Changed input:

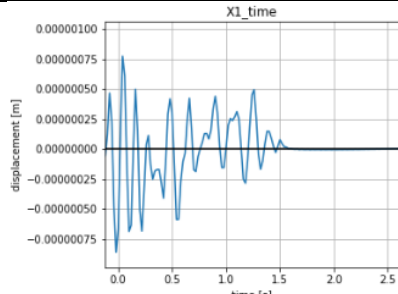
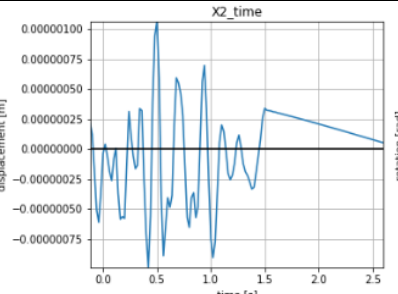
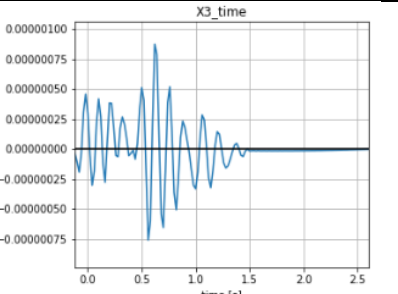
3DoF system:
<ul style="list-style-type: none"> 1 rigid floor / slab only. Dimensions: $L_{structX} = 8.1$ m, $L_{structY} = 20$ m, $H_{strcutZ} = 0.8$ m $D_{pile} = 0.47$ m, $L_{pileZ} = 18$ m, $nrPilesX = 4$, $nrPilesY = 8$, $Spiles = 2.6$ m
EB-beam frame:
<ul style="list-style-type: none"> Span = 3.68 m, $w_1_{height} = 0.8$ m, $w_3_{height} = 0.01$ m, $EB_{hw1} = 0.2$ m

Results:

Title: Building in Amsterdam 'Small rigid block' Date: 2019-9-6	
--	---

3DoF system:	$M_b = 324084$ kg	$J_{CG} = 1793899$ kgm ²	$z_{CG} = 0.4$ m
--------------	-------------------	-------------------------------------	------------------

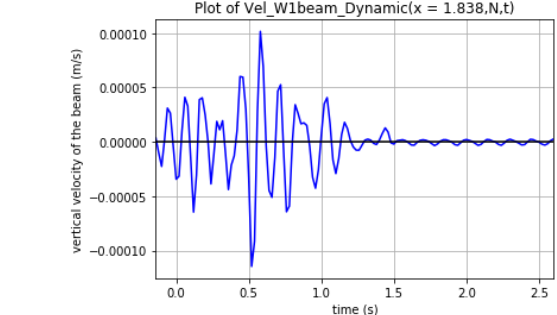
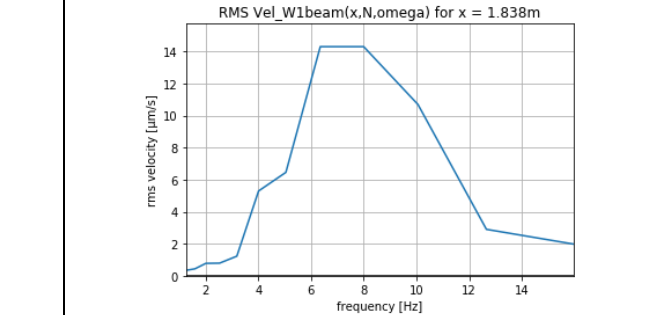
Response (frequency domain displacements):		
		

Response (time domain displacements):		
		

$peak = -0.80 \cdot 10^{-6}$ m	$peak = 1.2 \cdot 10^{-6}$ m	$peak = -0.85 \cdot 10^{-6}$ rad
--------------------------------	------------------------------	----------------------------------

Observed eigenfrequencies in range of $0.375 \text{ Hz} \leq f (= \omega/2\pi) \leq 20.125 \text{ Hz}$ for which $\det[-\omega^2 \mathbf{M} + \mathbf{K}(\omega)] = 0$:

$5.825 \leq f_n \leq 5.875$	$8.975 \leq f_n \leq 9.025$	$11.925 \leq f_n \leq 11.975$
-----------------------------	-----------------------------	-------------------------------

EB-beam frame element w1:	
	
$peak = -1.2 \cdot 10^{-4}$ m/s	$peak = 14.2$ µm/s

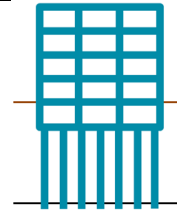
4. Iteration: greater G value for (stiffer) soil impedances (42 - 342 mins)

Changed input:

3DoF system:
<ul style="list-style-type: none"> • $G_{HS} = 37.5 \times 10^6 \text{ N/m}^2$, $\rho_{HS} = 2000 \text{ kg/m}^3$, $\nu_{HS} = 0.48$, $\beta_{HS} = 0.02$, • $E_{soil} = 250 \times 10^6 \text{ N/m}^2$, $C_{sL} = 447 \text{ m/s}$, $C_{sLm} = 224 \text{ m/s}$, $C_{sH} = 895 \text{ m/s}$

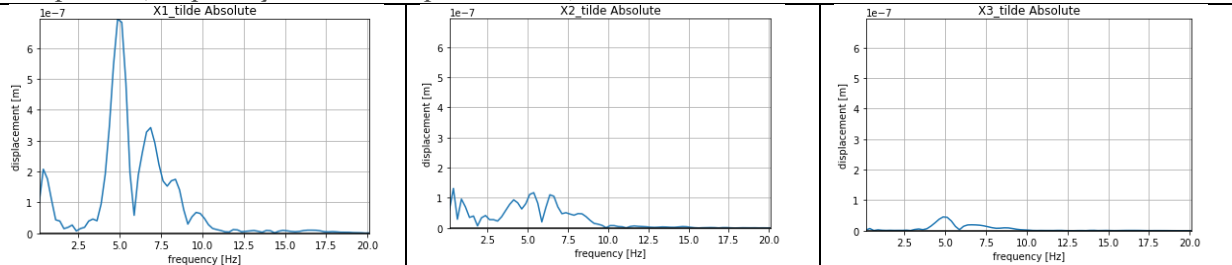
Results:

Title: Building in Amsterdam 'Increased stiffness soil impedance'
Date: 2019-9-6

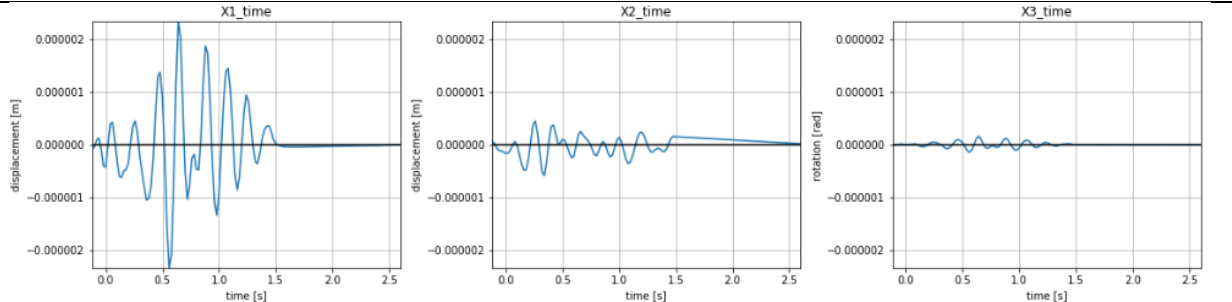


3DoF system:

Response (frequency domain displacements):



Response (time domain displacements):



$peak = -2.2 \cdot 10^{-6} \text{ m}$

$peak = -0.5 \cdot 10^{-6} \text{ m}$

$peak = -0.2 \cdot 10^{-6} \text{ rad}$

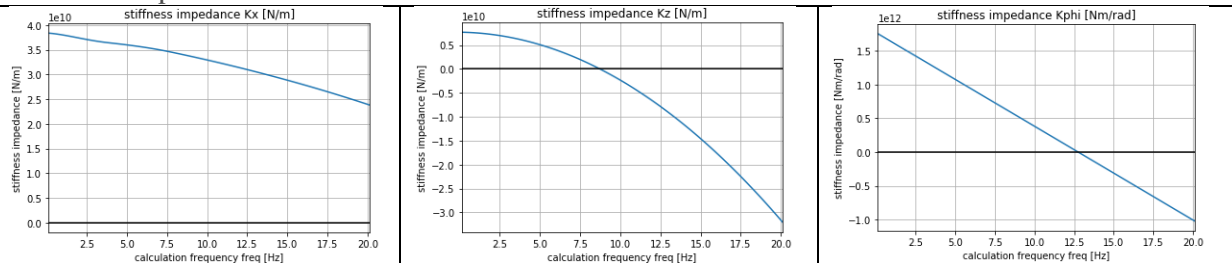
Observed eigenfrequencies in range of $0.375 \text{ Hz} \leq f (= \omega/2\pi) \leq 20.125 \text{ Hz}$ for which $\det[-\omega^2 \mathbf{M} + \mathbf{K}(\omega)] = 0$:

$2.825 \leq f_n \leq 2.875$

$3.575 \leq f_n \leq 3.625$

$11.825 \leq f_n \leq 11.875$

Stiffness impedance terms:

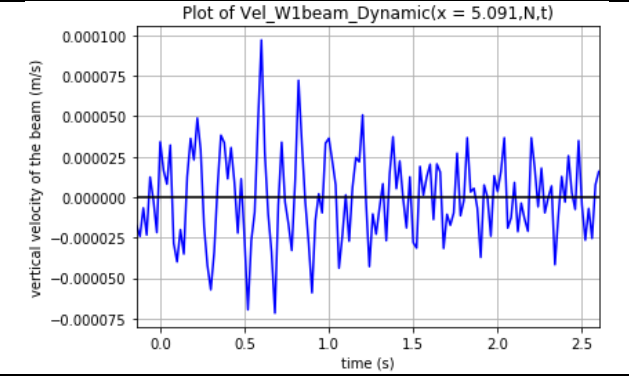


$peak = 3.9 \cdot 10^{10} \text{ N/m}$

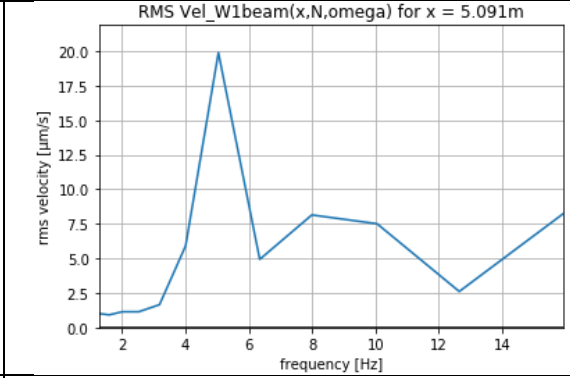
$peak = 0.8 \cdot 10^{10} \text{ N/m}$

$peak = 180 \cdot 10^{10} \text{ Nm/rad}$

EB-beam frame element w1:



$peak = 1.0 \cdot 10^{-4} \text{ m/s}$



$peak = 20 \mu\text{m/s}$

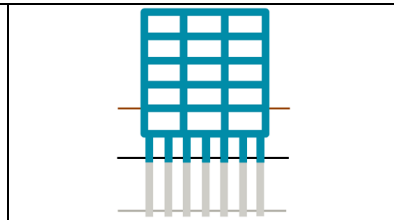
5. Iteration: smaller pile length and raised sand layer (42 - 342 mins)

Changed input:

3DoF system:
<ul style="list-style-type: none"> LpileZ = 6 m

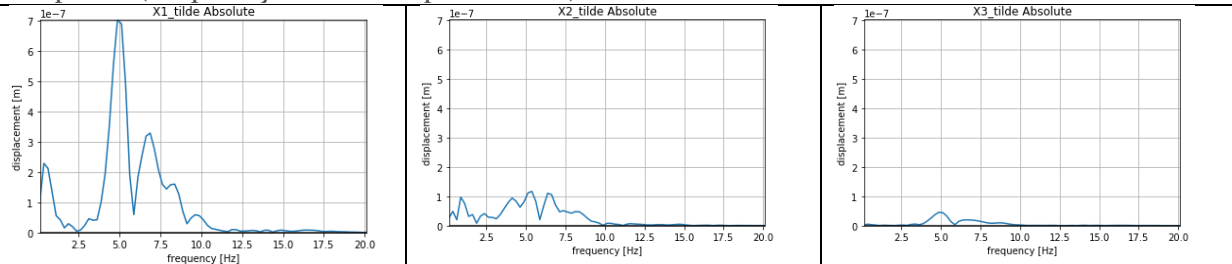
Results:

Title: Building in Amsterdam 'Increased stiffness pile foundation'
Date: 2019-9-6

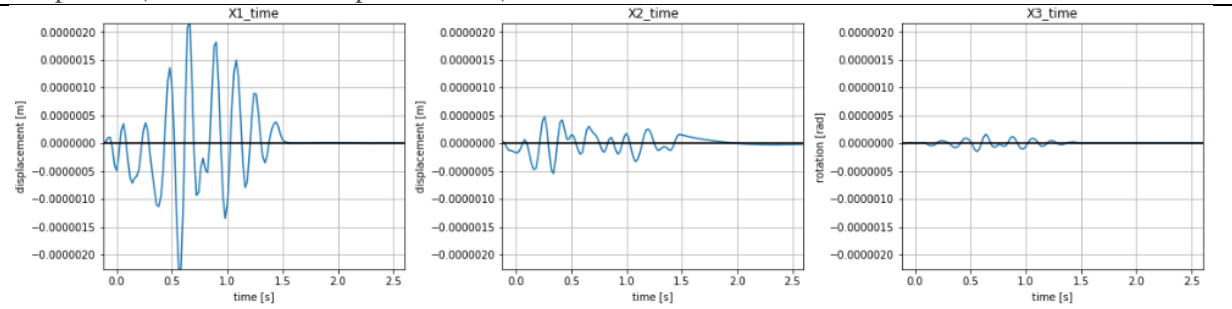


3DoF system:

Response (frequency domain displacements):



Response (time domain displacements):



$peak = -2.2 \cdot 10^{-6} m$

$peak = -0.5 \cdot 10^{-6} m$

$peak = -0.2 \cdot 10^{-6} rad$

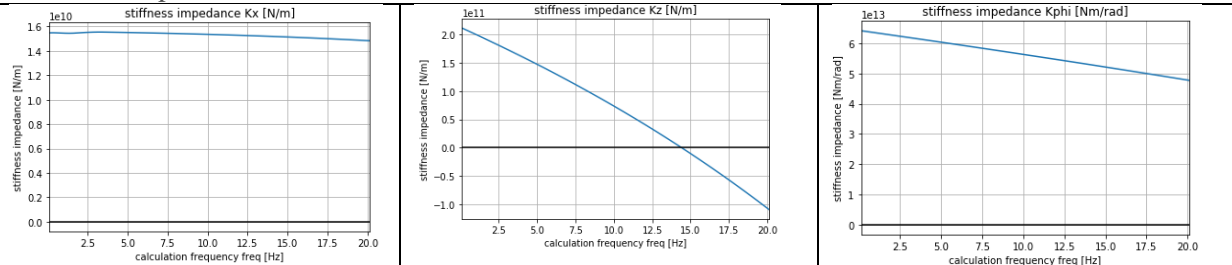
Observed eigenfrequencies in range of $0.375 Hz \leq f (= \omega/2\pi) \leq 20.125 Hz$ for which $\det[-\omega^2 M + K(\omega)] = 0$:

$5.475 \leq f_n \leq 5.525$

$10.925 \leq f_n \leq 10.975$

$20.125 \leq f_n$

Stiffness impedance terms:

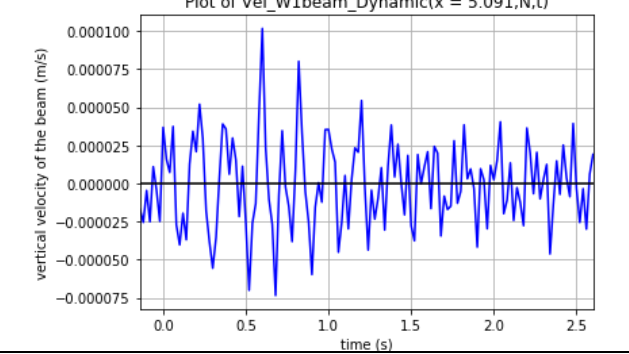


$peak = 1.55 \cdot 10^{10} N/m$

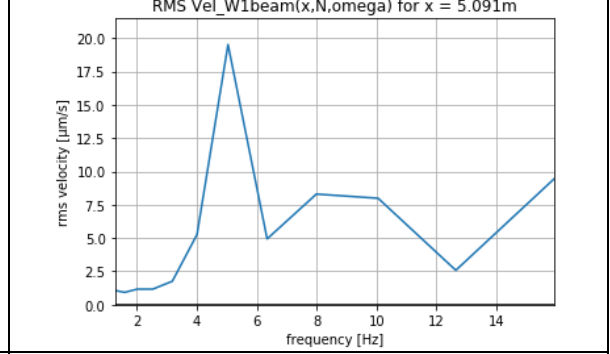
$peak = 22.0 \cdot 10^{10} N/m$

$peak = 650 \cdot 10^{10} Nm/rad$

EB-beam frame element w1:



$peak = 1.0 \cdot 10^{-4} \text{ m/s}$



$peak = 19.5 \mu\text{m/s}$

6. Iteration: stiffer equivalent local EB-beam floor (42 - 342 mins)

Changed input:

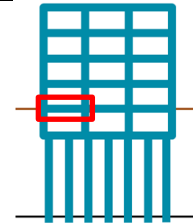
EB-beam frame element w1:

- span = 10.18 m, w1_height = w2_height = 0.5 m
- rho_structure = 4000 kg/m³, Emod = 30 x 10⁹ N/m²

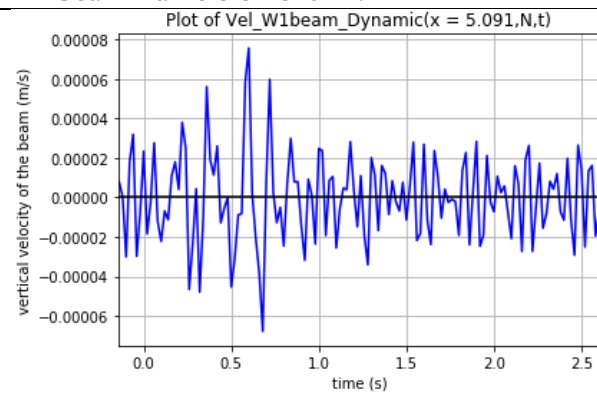
Results:

Title: Building in Amsterdam 'Stiffer equivalent local EB-beam floor'

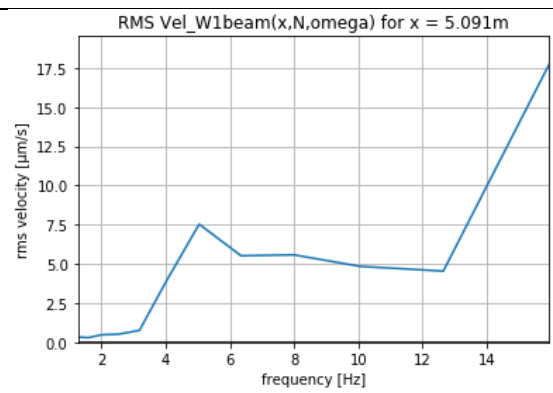
Date: 2019-9-6



EB-beam frame element w1:



peak = 0.75 · 10⁻⁴ m/s



peak = 17.5 µm/s

7. Iteration: more coordinates along local EB-beam floor (42 - 950 mins)

Changed input:

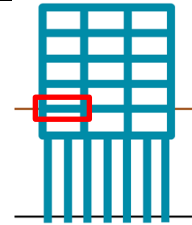
EB-beam frame element w1:

- 4 more point coordinates along length of beam (5 coordinates in total)
- $(1/4, 1/3, 1/2, 2/3, 3/4) \cdot span$

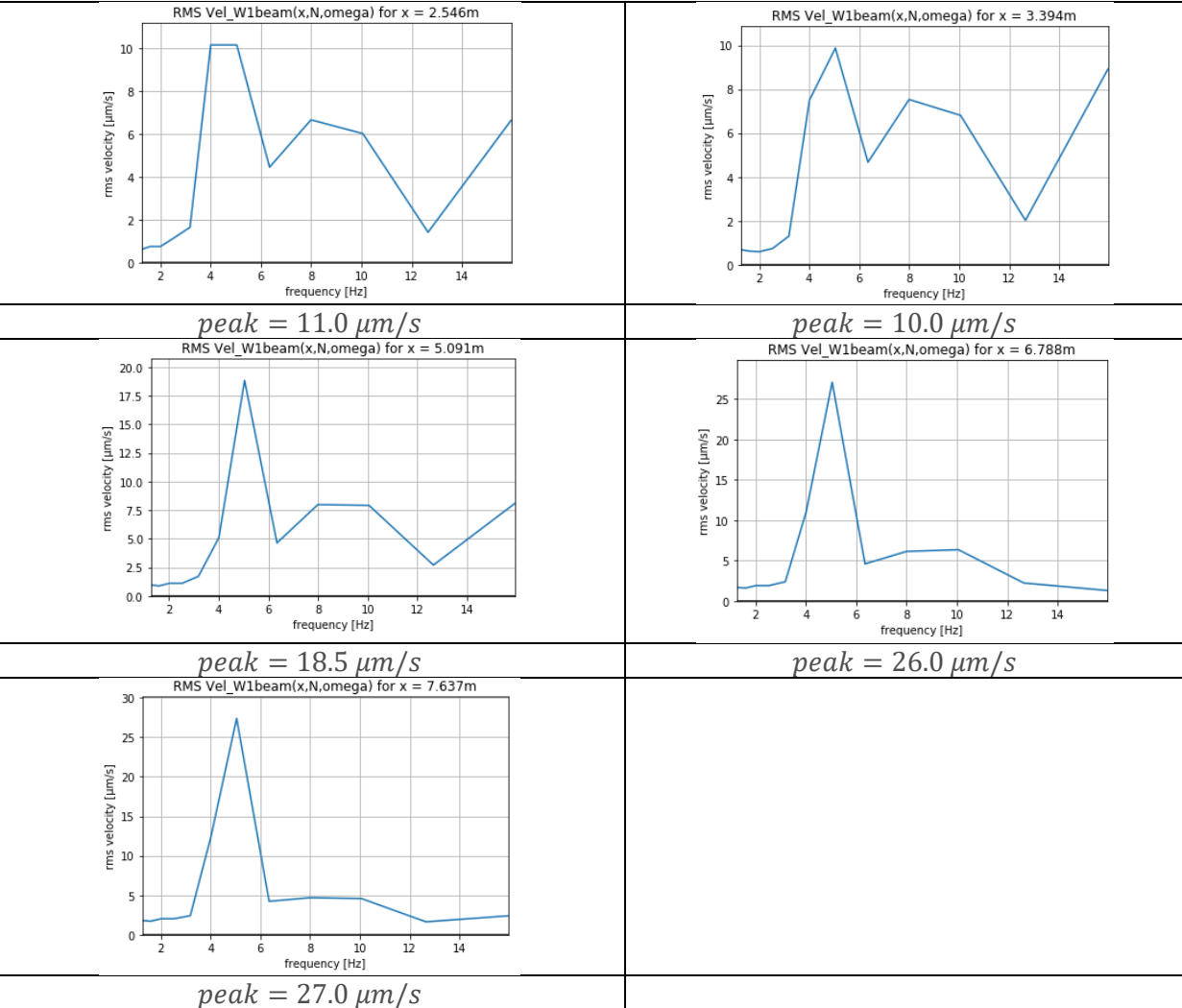
Results:

Title: Building in Amsterdam 'More coordinates local EB-beam floor'

Date: 2019-9-6



EB-beam frame element w1:

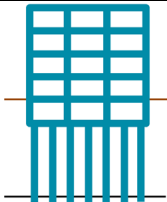


8. Iteration: reference optimized computational time 1 (24 - 118 mins)

Changed input:

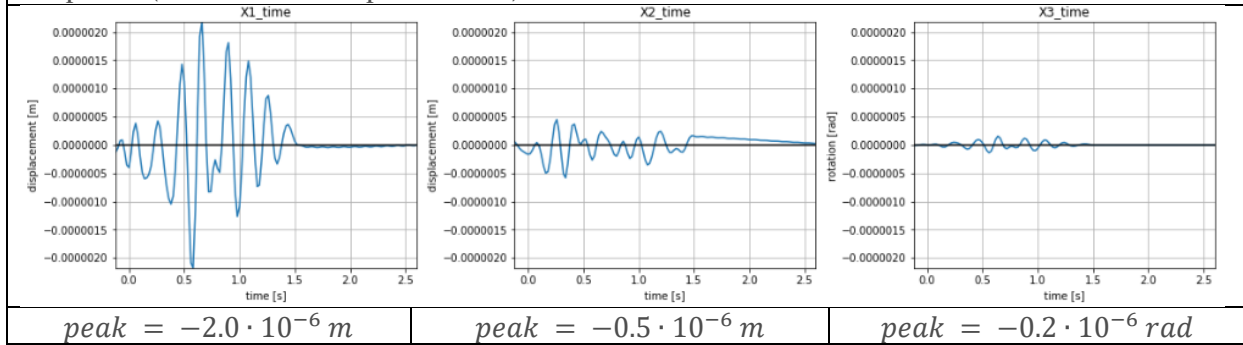
Computational parameters 3DoF and EB-beam frame		
$t_{step_exc} = 0.02 \text{ s}$	$t_{nr_exc} = 81$	$t_{max_exc} = 1.5 \text{ s}$
$f_{step_resp} = 0.25 \text{ Hz}$	$f_{nr_resp} = 41$	$f_{max_resp} = 10.125 \text{ Hz}$
$t_{step_resp} = 0.02 \text{ s}$	$t_{nr_resp} = 137$	$t_{max_resp} = 2.6 \text{ s}$

Results:

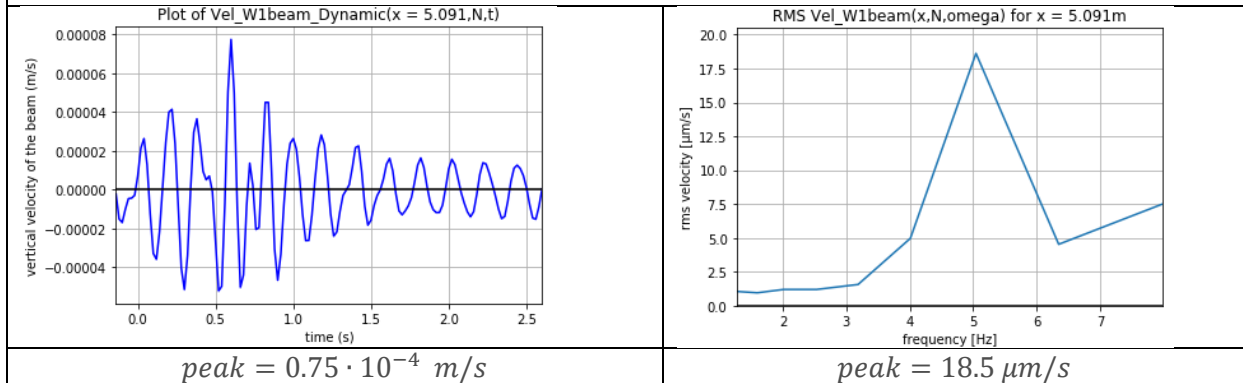
Title: Building in Amsterdam 'Iteration: reference optimized computational time 1' Date: 2019-9-6	
--	---

3DoF system:

Response (time domain displacements):



EB-beam frame element w1:



Script 0 & 1		
$t_{comp} = 1 \text{ mins}$		
Script 2		
$v(t): t_{comp} = 22 \text{ mins}$		$v(f) + v_{RMS}(f): t_{comp} = +4 \text{ mins}$
Script 3		
$v(t): t_{comp} = 1 \text{ mins}$	$v(f): t_{comp} = +36 \text{ mins}$	$v_{RMS}(f): t_{comp} = +58 \text{ mins}$
Total comp. time for time domain only: $1 + 22 + 1 = 24 \text{ mins} = \frac{24}{42} = 0.55 \cdot REF$		
Underestimation of EB-beam floor in time domain = $0.75/1 = 0.75$		
Total comp. time incl. freq. domain RMS: $1 + 22 + 1 + 36 + 58 = 118 \text{ mins} = \frac{118}{342} = 0.35 \cdot REF$		
Underestimation of EB-beam floor in freq. domain RMS = $18.5/18.5 = 1$		

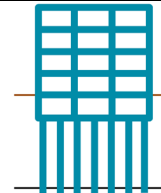
9. Iteration: reference optimized computational time 2 (13 - 49 mins)

Changed input:

Computational parameters 3DoF and EB-beam frame		
$t_{step_exc} = 0.04 \text{ s}$	$t_{nr_exc} = 41$	$t_{max_exc} = 1.5 \text{ s}$
$f_{step_resp} = 0.25 \text{ Hz}$	$f_{nr_resp} = 41$	$f_{max_resp} = 10.125 \text{ Hz}$
$t_{step_resp} = 0.04 \text{ s}$	$t_{nr_resp} = 69$	$t_{max_resp} = 2.6 \text{ s}$

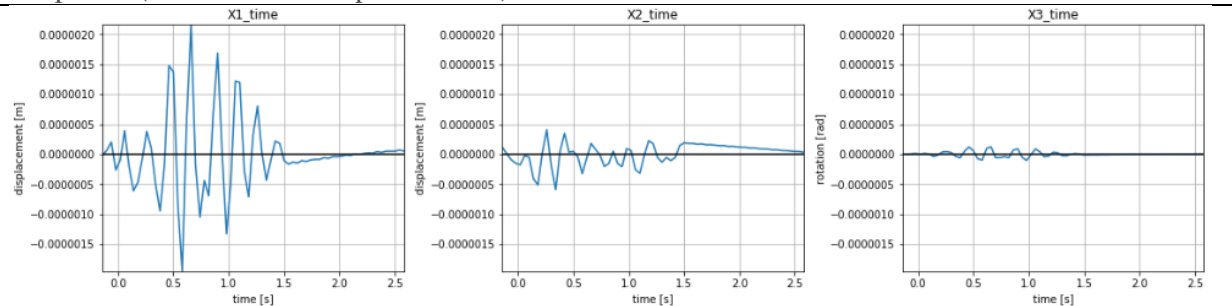
Results:

Title: Building in Amsterdam 'Iteration: reference optimized computational time 2'
Date: 2019-9-6



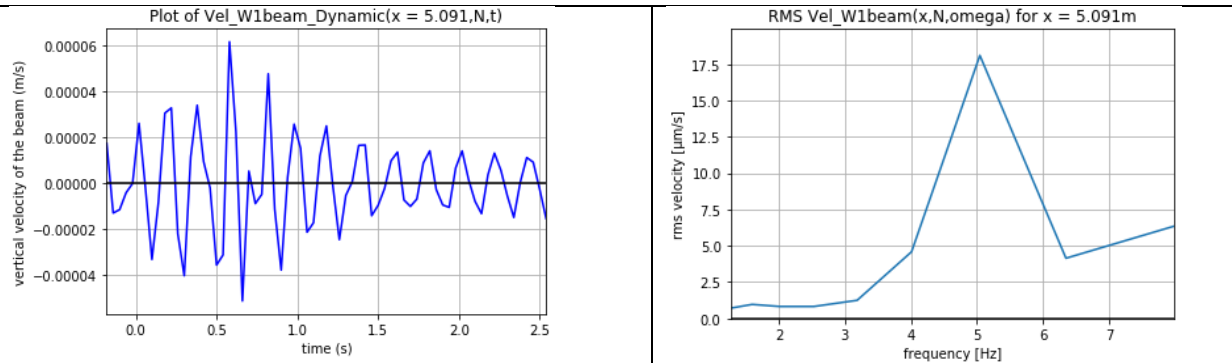
3DoF system:

Response (time domain displacements):



$peak = -2.2 \cdot 10^{-6} \text{ m}$ $peak = -0.51 \cdot 10^{-6} \text{ m}$ $peak = -0.2 \cdot 10^{-6} \text{ rad}$

EB-beam frame element w1:



$peak = 0.61 \cdot 10^{-4} \text{ m/s}$ $peak = 18.0 \text{ } \mu\text{m/s}$

Script 0 & 1

$t_{comp} = 1 \text{ mins}$

Script 2

$v(t) + v(f) + v_{RMS}(f): t_{comp} = 11 \text{ mins}$

Script 3

$v(t): t_{comp} = 1 \text{ mins}$ $v(f): t_{comp} = +17 \text{ mins}$ $v_{RMS}(f): t_{comp} = +19 \text{ mins}$

Total comp. time for time domain only: $1 + 11 + 1 = 13 \text{ mins} = \frac{13}{42} = 0.3 \cdot REF$

Underestimation of EB-beam floor in time domain = $0.61/1 = 0.61$

Total comp. time incl. freq. domain RMS: $1 + 11 + 1 + 17 + 19 = 49 \text{ mins} = \frac{49}{342} = 0.14 \cdot REF$

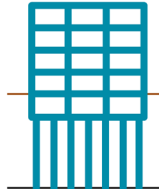
Underestimation of EB-beam floor in freq. domain RMS = $18.0/18.5 = 0.97$

10. Iteration: reference optimized computational time 2, variant 2 (8 - 25 mins)

Changed input:

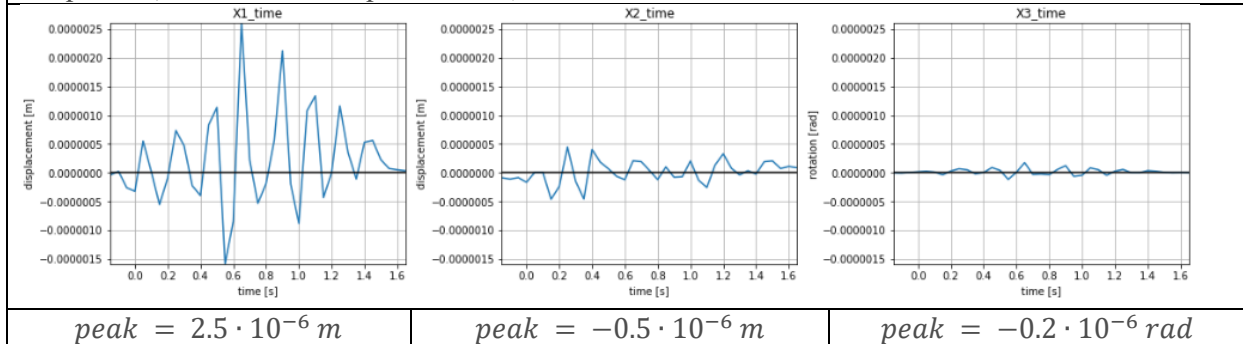
Computational parameters 3DoF and EB-beam frame		
$t_{step_exc} = 0.05 \text{ s}$	$t_{nr_exc} = 33$	$t_{max_exc} = 1.5 \text{ s}$
$f_{step_resp} = 0.375 \text{ Hz}$	$f_{nr_resp} = 28$	$f_{max_resp} = 10.3125 \text{ Hz}$
$t_{step_resp} = 0.05 \text{ s}$	$t_{nr_resp} = 37$	$t_{max_resp} = 1.65 \text{ s}$

Results:

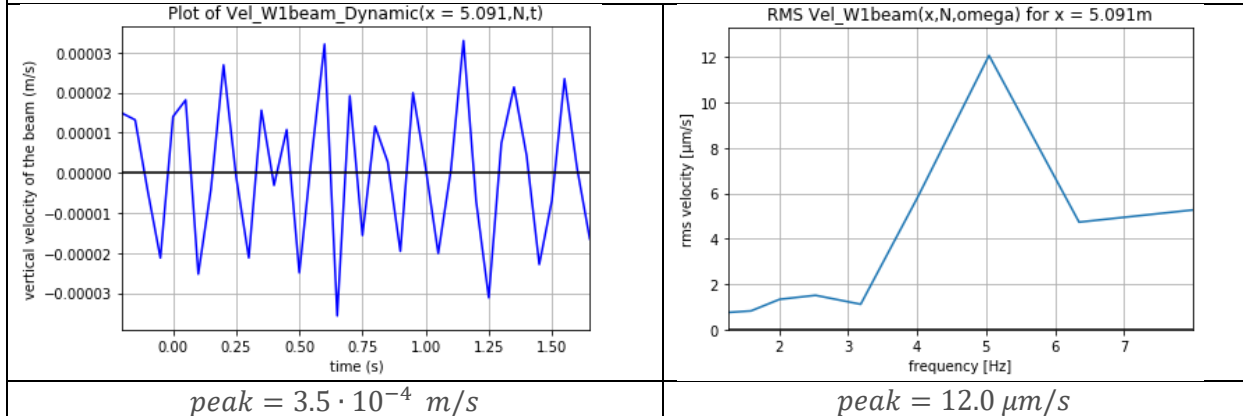
Title: Building in Amsterdam 'Iteration: reference optimized computational time 2, variant 2' Date: 2019-9-6	
---	---

3DoF system:

Response (time domain displacements):



EB-beam frame element w1:



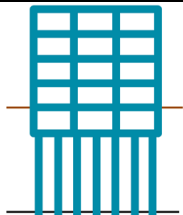
Script 0 & 1		
$t_{comp} = 1 \text{ mins}$		
Script 2		
$v(t) + v(f) + v_{RMS}(f): t_{comp} = 6 \text{ mins}$		
Script 3		
$v(t): t_{comp} = 1 \text{ mins}$	$v(f): t_{comp} = +5 \text{ mins}$	$v_{RMS}(f): t_{comp} = +12 \text{ mins}$
Total comp. time for time domain only: $1 + 6 + 1 = 8 \text{ mins} = \frac{8}{42} = 0.2 \cdot REF$		
Overestimation of EB-beam floor in time domain = $3.5/1 = 3.5$		
Total comp. time incl. freq. domain RMS: $1 + 6 + 1 + 5 + 12 = 25 \text{ mins} = \frac{25}{342} = 0.07 \cdot REF$		
Underestimation of EB-beam floor in freq. domain RMS = $12.0/18.5 = 0.65$		

11. Iteration: reference optimized computational time 3 (8 - 24 mins)

Changed input:

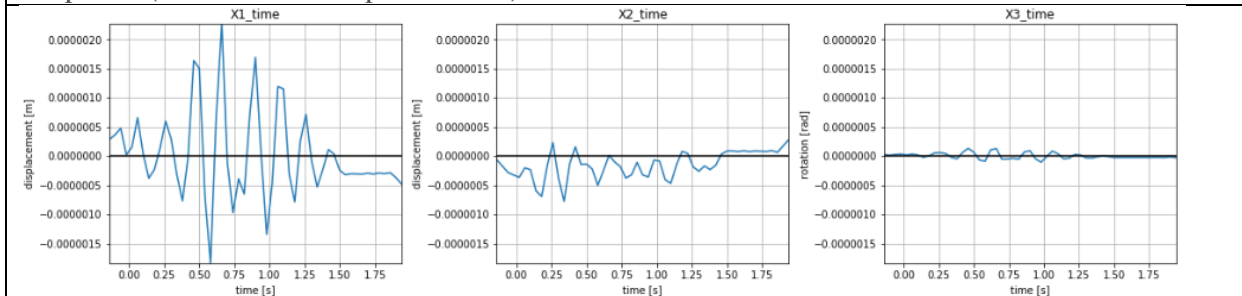
Computational parameters 3DoF and EB-beam frame		
$t_{step_exc} = 0.04 \text{ s}$	$t_{nr_exc} = 41$	$t_{max_exc} = 1.5 \text{ s}$
$f_{step_resp} = 0.5 \text{ Hz}$	$f_{nr_resp} = 21$	$f_{max_resp} = 10.25 \text{ Hz}$
$t_{step_resp} = 0.04 \text{ s}$	$t_{nr_resp} = 53$	$t_{max_resp} = 1.94 \text{ s}$

Results:

<p>Title: Building in Amsterdam 'Iteration: reference optimized computational time 3'</p> <p>Date: 2019-9-6</p>	
---	---

3DoF system:

Response (time domain displacements):

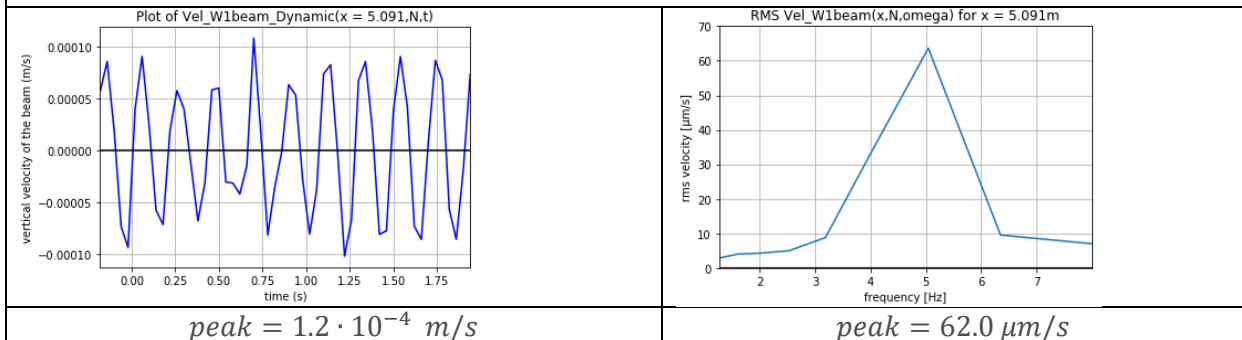


$peak = -2.2 \cdot 10^{-6} \text{ m}$

$peak = -0.7 \cdot 10^{-6} \text{ m}$

$peak = -0.2 \cdot 10^{-6} \text{ rad}$

EB-beam frame element w1:



$peak = 1.2 \cdot 10^{-4} \text{ m/s}$

$peak = 62.0 \text{ µm/s}$

Script 0 & 1	
$t_{comp} = 1 \text{ mins}$	
Script 2	
$v(t) + v(f) + v_{RMS}(f): t_{comp} = 6 \text{ mins}$	
Script 3	
$v(t): t_{comp} = 1 \text{ mins}$	$v(f) + v_{RMS}(f): t_{comp} = +16 \text{ mins}$
Total comp. time for time domain only: $1 + 6 + 1 = 8 \text{ mins} = \frac{8}{42} = 0.2 \cdot REF$	
Overestimation of EB-beam floor in time domain = $1.2/1 = 1.2$	
Total comp. time incl. freq. domain RMS: $1 + 6 + 1 + 16 = 24 \text{ mins} = \frac{24}{342} = 0.07 \cdot REF$	
Overestimation of EB-beam floor in freq. domain RMS = $62.0/18.5 = 3.4$	

U. Appendix: User manual of EDDABuS_{GS}

EDDABuS_{GS} stands for ‘Early Design Dynamic Analysis of Building Structures by Gerwin Schut’

A brief manual is included in this appendix to guide the user of the EDDABuS_{GS}-tool through the steps to take for computing the dynamic structural response. EDDABuS_{GS} uses the programming software ‘Python’.

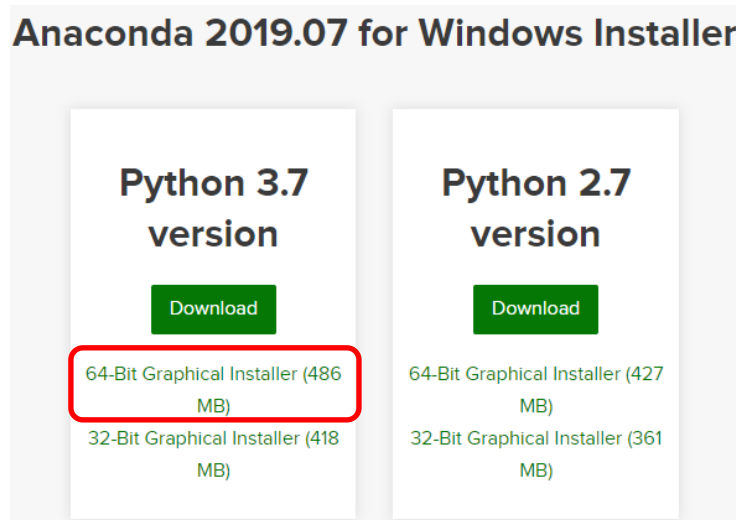
The images shown in this manual are partly derived from the computer at Pieters Bouwtechniek, which is set-up in the Dutch language and in Windows, because this is the environment for which the tool has been developed.

Downloading Python

1. Go to the website ‘<https://www.anaconda.com/distribution/>’
2. Select your operating system (e.g. Windows, default selection is macOS)



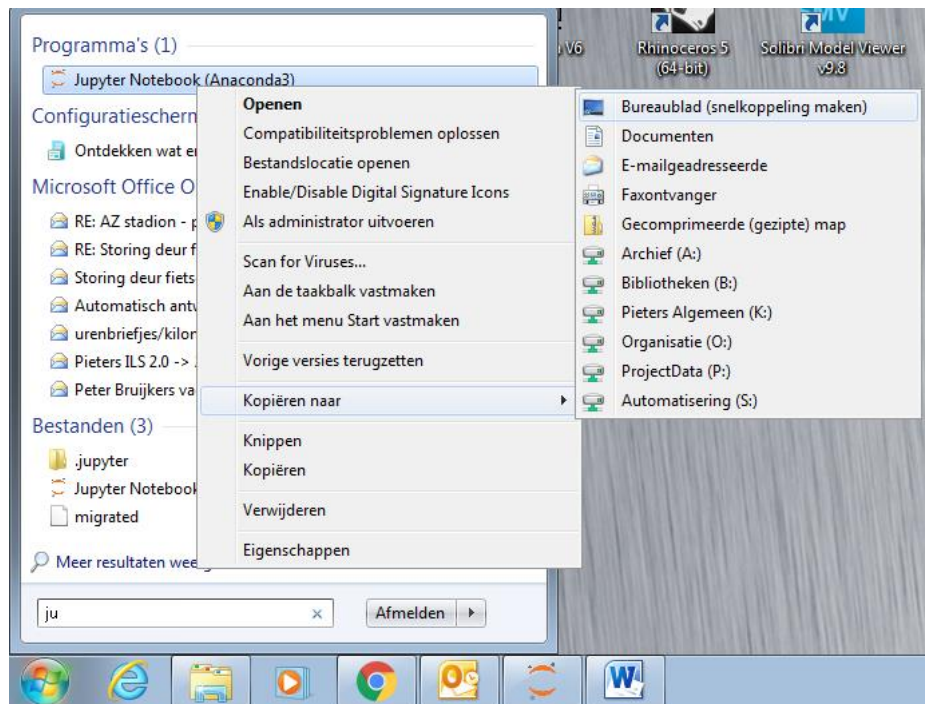
3. Download the graphical installer for Python 3.7 (64 bit version) or a later version if available



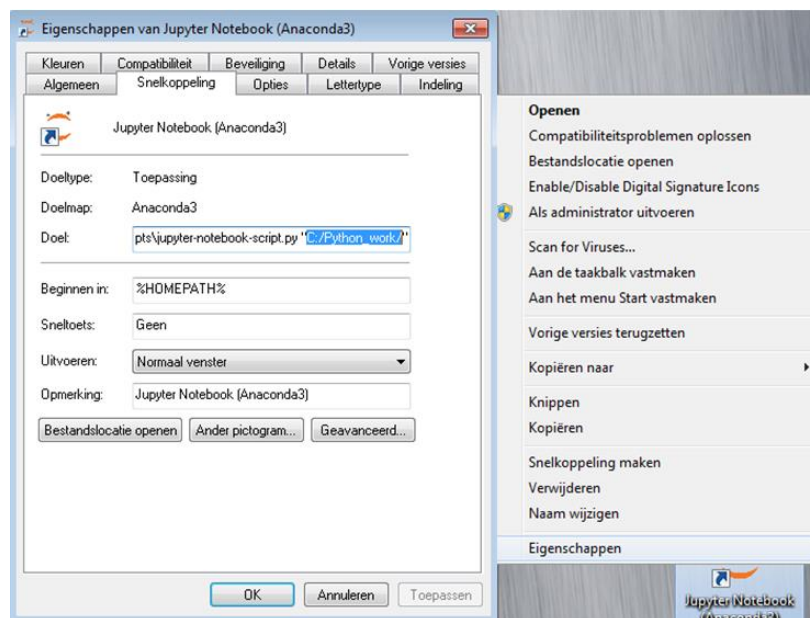
4. Run the installation program and choose the default options

Set-up the Python working directory (after installing Python on the pc):

1. Create a folder called ‘Python_work’ (or any other desired name) at any desired location in the pc-environment (e.g. at the C-disk of the pc)
2. Type ‘Jupyter’ in the search option of windows
3. Right-click on ‘Jupyter Notebook’
4. Left-click on ‘copy to’
5. Left-click on ‘desktop’ (a short-cut to ‘Jupyter Notebook’ has been created on the desktop of this pc).



6. Right-click on the short-cut icon
7. Left-click on 'properties'
8. Go to the tab 'short-cuts'
9. In the third cell ('Doel'), change "%USERPROFILE%/" into the directory-path created at 1. (e.g. "C:/Python_work/")



Now every time the user opens Python by the just created Jupyter Notebook short-cut, the correct Python environment is opened. This environment is opened in a webbrowser. In this particular manual, the Python Notebook is opened in the webbrowser Google Chrome (but it might also be e.g. Internet Explorer).

Using the tool after set-up

In windows explorer:

1. Copy the folder 'EDDABuS_start' and rename it any desired name (e.g. '2019Sep9ProjectName_subject')

The folder should at least contain the four IPYNB-files, one excel-file 'InputFileXLS' and a folder with saved soil responses (e.g. 'SoilResponsesStartVUams'). Note that any desired soil excitation can be implemented in the tool by adding more subfolders with pre-computed soil responses (e.g. 'SoilResponsesStartArbitraryLocationByArbitrarySource').

Naam	Gewijzigd op	Type
SoilResponsesStartVUams	9-9-2019 14:59	Bestandsmap
0.3DoFBuildingDesignParameters.ipynb	6-9-2019 12:18	IPYNB-bestand
1.ScriptToCompute3DoFExcitation.ipynb	6-9-2019 12:18	IPYNB-bestand
2.ImpedancesAnd3DoFStructuralRespons...	7-9-2019 10:58	IPYNB-bestand
3.EB-beam frame matrix_allExcitations.ip...	7-9-2019 11:42	IPYNB-bestand
InputFileXLS	6-9-2019 12:18	Microsoft Excel-w...

2. Copy the folder with the desired saved soil responses and rename it to 'SoilResponses'
3. Open the excel file 'InputFileXLS' and fill in all parameters (additional explanation of the parameters is given in the next section)

In the Jupyter Notebook environment:

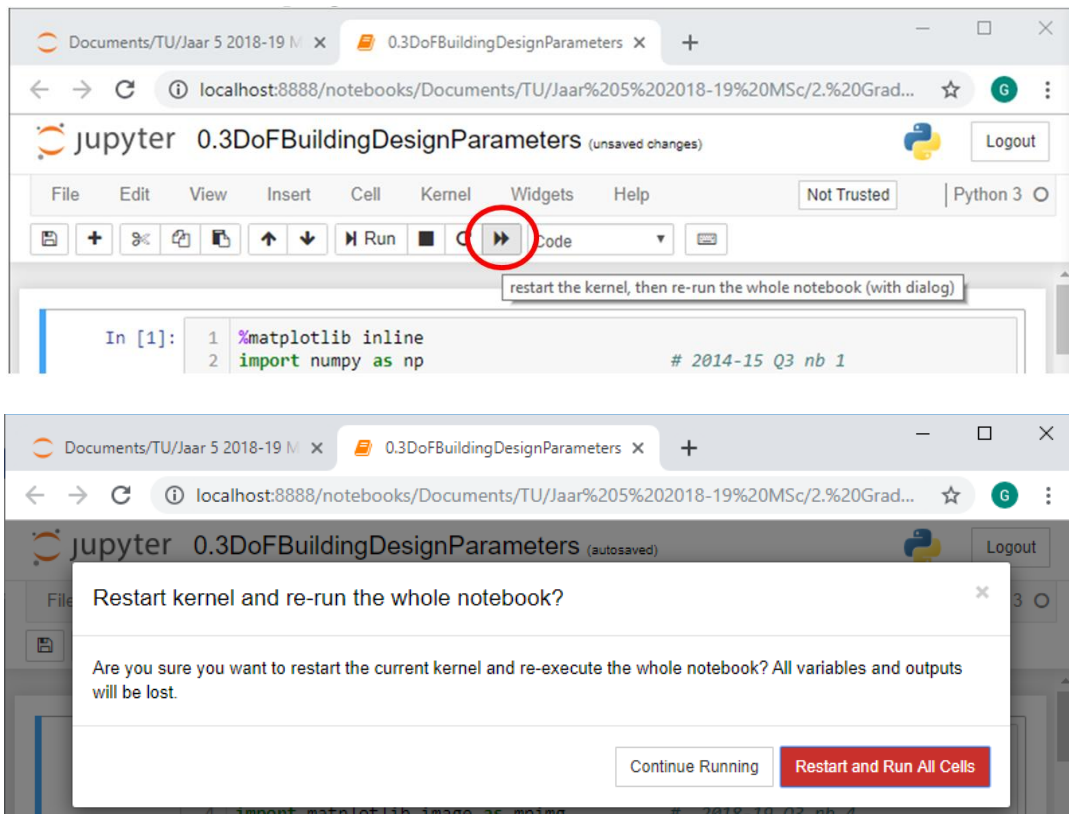
4. Open the created folder '2019Sep9ProjectName_subject' through the Python Notebook environment (after left-clicking the short-cut icon 'Jupyter Notebook' at the desktop of the pc)

The screenshot shows a web browser window displaying the Jupyter Notebook interface. The address bar shows the URL: localhost:8888/tree/Documents/TU/Jaar%205%202018-19%20MSc/2.%20Graduation... The Jupyter logo and 'Quit' and 'Logout' buttons are visible. Below the navigation tabs (Files, Running, Clusters), there is a file browser view showing the directory structure: Documents / TU / Jaar 5 2018-19 MSc / 2. Graduation Thesis / 1. Graduation Thesis MSc 2018-2019 / Computations / Python iterations / EDTVA_start_2019Sep9. The file list includes folders like SoilResponses and SoilResponsesStartVUams, and files like 0.3DoFBuildingDesignParameters.ipynb, 1.ScriptToCompute3DoFExcitation.ipynb, 2.ImpedancesAnd3DoFStructuralResponse.ipynb, 3.EB-beam frame matrix_allExcitations.ipynb, and InputFileXLS.xlsx.

5. Here, again the four IPYNB-files and at least one excel file are visible. Check whether you have created the folder with the name 'SoilResponses'. In this environment only the IPYNB-files are important (these are the four Python scripts)

Running the 1st script: Script o

6. Open (left-click) script '0.3DoFBuildingDesignParameters.ipynb'. The notebook will be opened in a new tab of the web browser. This notebook contains the script for computing the global 3DoF structural properties.
7. Left-click the 'run' icon in the tool-bar and left-click 'Restart and Run All Cells' (this icon will run the entire script again):



8. Wait for the text 'computation of sheet complete' to appear at the bottom-line of the script

```

62         writer.writerow(lines[i])
63
In [ ]: 1
In [8]: 1 print('computation of sheet complete')
        computation of sheet complete

```

9. A new Excel-file '3DoFBuildingProperties' has been created. This file will be used by the other scripts.

Running the 2nd script: Script 1

10. Open (left-click) script '1.ScriptToCompute3DoFExcitation.ipynb'. The notebook will be opened in a new tab of the webbrowser. This notebook contains the script for computing the global 3DoF excitation.
11. Left-click the 'run' icon in the tool-bar and left-click 'Restart and Run All Cells' (this icon will run the entire script again)
12. Wait for the text 'computation of sheet complete' to appear at the bottom-line of the script
13. Two new Excel-files 'excitation_displacements_td' and 'excitation_velocities_tv' have been created. These files will be used by the next script.

Running the 3rd script: Script 2

14. Open (left-click) script '2.ImpedancesAnd3DoFStructuralResponse.ipynb'. The notebook will be opened in a new tab of the webbrowser. This notebook contains the script for computing the global 3DoF structural response.
15. Left-click the 'run' icon in the tool-bar and left-click 'Restart and Run All Cells' (this icon will run the entire script again)

16. The script first computes the 3DoF structural response in the time domain and puts these results in two new Excel-files: '3DoF_Building_Response_TIME' and '3DoF_Building_Response_FourierExp'. These files are used by the next script. Once these two new Excel-files have been created, the user can continue by running script '3.EB-beam frame matrix_allExcitations.ipynb' (step number 17).

However, script '2.ImpedancesAnd3DoFStructuralResponse.ipynb' continues running to also compute the 3DoF structural response in the frequency domain, but these results are not needed for running script '3.EB-beam frame matrix_allExcitations.ipynb'. Script '2.ImpedancesAnd3DoFStructuralResponse.ipynb' has finished computing once the text 'computation of sheet completed' appears.

After the computation of the script has been completed all figures of interest for the global 3DoF structural response can be found throughout the script (from cell 44 onwards). All plotted time- and frequency instants are only to make clear at which stage the computation is. This gives the user the ability to estimate the computational time remaining.

Running the 4th script: Script 3

17. Open (left-click) script '3.EB-beam frame matrix_allExcitations.ipynb'. The notebook will be opened in a new tab of the webbrowser. This notebook contains the script for computing the local (flexible) structural EB-beam floor response.
18. Left-click the 'run' icon in the tool-bar and left-click 'Restart and Run All Cells' (this icon will run the entire script again)
19. After the text 'computation of sheet completed' has appeared, all figures of interest for the local structural EB-beam floor response can be found throughout the script (from cell 20 onwards, depending on the chosen plotting-options in the Excel-file 'InputFileXLS'). All plotted time- and frequency instants are only to make clear at which stage the computation is. This gives the user the ability to estimate the computational time remaining.

Optimize the computational time of iterations

Note that computing the local EB-beam floor response in the time domain is completed relatively quick (approximately 1 to 2 minutes). However, the structural response in the frequency domain takes (much) longer, depending on the computational parameters given in the Excel-file 'InputFileXLS'. In the situation where the user wants to make a lot of iterations in a short amount of time, looking at the time domain response is sufficient for getting insight into what influence changing a particular parameter has on the structural vibrations.

The same principle holds for computing the global 3DoF response, where the time domain already gives sufficient insight into what the influence of changing a particular parameter is on the structural vibrations.

Additional explanation Excel-file 'InputFileXLS'

The input-excel-file 'InputFileXLS' has been set-up such that first the parameters that concern script 0 need to be filled in (indicated by the light-blue colour). Then the parameters of script 1 (light-orange colour), script 2 (light-green colour) and eventually script 3 (light-purple colour) need to be filled in.

Input parameters script 0 (light-blue |||| colour).

Here the structural properties of the global 3DoF system need to be given (floors, walls, spans, heights, etc.). An additional mass can be given that needs to be taken into account in the computation of the structural response (e.g. the mass of the façade).

Note that the structural properties of the local EB-beam frame (script 3) does not necessarily need to have the same properties as given in script 0.

Input parameters script 1 (light-orange |||| colour).

Here the parameters are given concerning the excitation on the 3DoF system. The position of the structure determines which csv-files from the folder 'SoilResponses' are used to compute the excitation. The time-input parameters indicate at which time-range the soil response needs to be considered as non-zero. This time range should become clear after running the script first for a broad time range. Then the user can see at which time instants the excitation is approximately zero. The user can then adjust the time instants in 'InputFileXLS' and can then re-run script 1.

Input parameters script 2 (light-green |||| colour).

Here the parameters are given for the impedance terms of the 3DoF system (soil and pile foundation). The dynamic soil parameters need to become clear from measurements and experiments at the particular site of the project.

Computational input parameters

The input parameters for the frequency instants determine the frequency range that needs to be considered for computing the structural response, but also determine the maximum time-range that can be considered: $t_{max} = 1/(f_{step})$. After this t_{max} the structural response is repeated in opposite sign. This is due to the numerical solution method (concerning the Fourier expansion). Thus, f_{step} should be small enough to make sure that the structural response has damped out before t_{max} has been reached.

The input parameters for the time instants determine the time range that needs to be considered for computing the structural response, but also determine the maximum frequency-range that can be considered: $f_{max} = 1/(2 \cdot t_{step})$. After this f_{max} the structural response in the frequency domain is mirrored. This is due to the numerical solution method (concerning the Fourier expansion). Thus, t_{step} should be small enough to make sure that the structural response in the frequency domain considers all frequencies of interest before reaching f_{max} .

The computational parameters can be optimized (fastest computation) after first a rigorous computation has been performed. From the rigorous computation, the user can see what the dominant frequency range is that needs to be considered for computing the structural response. Also, the maximum time that needs to be considered can be obtained from the rigorous computation. This is the time at which the structural response has either damped out (global 3DoF system) or has reached its steady-state vibration (local EB-beam floor). Appendix T 'Appendix: Iterations of structural parameters to compute structural response' shows that for the computation of the reference case of 'Building in Amsterdam' in this thesis, the following computational parameters can be considered as optimized:

Computational parameters 3DoF and EB-beam frame		
$t_{step_exc} = 0.02 \text{ s}$	$t_{nr_exc} = 81$	$t_{max_exc} = 1.5 \text{ s}$
$f_{step_resp} = 0.25 \text{ Hz}$	$f_{nr_resp} = 41$	$f_{max_resp} = 10.125 \text{ Hz}$
$t_{step_resp} = 0.02 \text{ s}$	$t_{nr_resp} = 137$	$t_{max_resp} = 2.6 \text{ s}$
Computational time: $(v(t)) - (v(t) + v_{RMS}(f)) = (24) \text{ mins} - (118) \text{ mins}$		

Overwriting the excitation on the 3DoF system

The excitation is computed from the saved soil responses (csv-files) in the folder 'SoilResponses'. However, in case the user desires to consider a different kind of excitation, or a more simple excitation, then the tool gives the option to overwrite the excitation. The new excitation should be given in the form of a Fourier expansion (thus a summation of sines and cosines with particular radial frequencies and amplitudes).

Input parameters script 3 (light-purple ||||| colour).

Here the parameters are given for the local flexible EB-beam frame. The structural properties given here can be similar to- or different from the structural properties given for scripts 0 to 2.

The computational input parameters for this script have the same meaning as in script 2, but now for the computation of the structural response of the local EB-beam frame. It is advised to use the same time- and frequency input parameters as in script 2.

Also, for script 3 the option is given to overwrite the excitation to the local EB-beam frame. Similar to script 2, this can be done by giving a new excitation in the form of a Fourier expansion.

